



Sustainable Transportation Systems

Plan, Design, Build,
Manage, and Maintain



**Proceedings of the 9th Asia Pacific Transportation
Development Conference**

Edited by Yong Bai, Ph.D., P.E., Wei-Chou Virgil Ping, Ph.D., P.E.,
L. David Shen, Ph.D., P.E., and Xiaohu Chen, Ph.D.

ASCE



**TRANSPORTATION
& DEVELOPMENT
INSTITUTE**

SUSTAINABLE TRANSPORTATION SYSTEMS

PLAN, DESIGN, BUILD, MANAGE, AND MAINTAIN

PROCEEDINGS OF THE NINTH ASIA PACIFIC TRANSPORTATION
DEVELOPMENT CONFERENCE

June 29–July 1, 2012
Chongqing, China

SPONSORED BY

International Chinese Transportation Professionals Association
T. Y. Lin International Group, China
Chongqing Urban Planning Bureau, China
Chongqing Jiaotong University
Chongqing Rail Transit (Group) Co. Ltd.
Chongqing Transport Planning Institute
The Transportation & Development Institute (T&DI)
of the American Society of Civil Engineers

EDITED BY

Yong Bai, Ph.D., P.E., F.ASCE
Wei-Chou Virgil Ping, Ph.D., P.E.
L. David Shen, Ph.D., P.E., T.E.
Xiaohu Chen, Ph.D.

ASCE



TRANSPORTATION
& DEVELOPMENT
INSTITUTE

Published by the American Society of Civil Engineers

Cataloging-in-Publication Data on file with the Library of Congress.

American Society of Civil Engineers
1801 Alexander Bell Drive
Reston, Virginia, 20191-4400

www.pubs.asce.org

Any statements expressed in these materials are those of the individual authors and do not necessarily represent the views of ASCE, which takes no responsibility for any statement made herein. No reference made in this publication to any specific method, product, process, or service constitutes or implies an endorsement, recommendation, or warranty thereof by ASCE. The materials are for general information only and do not represent a standard of ASCE, nor are they intended as a reference in purchase specifications, contracts, regulations, statutes, or any other legal document. ASCE makes no representation or warranty of any kind, whether express or implied, concerning the accuracy, completeness, suitability, or utility of any information, apparatus, product, or process discussed in this publication, and assumes no liability therefore. This information should not be used without first securing competent advice with respect to its suitability for any general or specific application. Anyone utilizing this information assumes all liability arising from such use, including but not limited to infringement of any patent or patents.

ASCE and American Society of Civil Engineers—Registered in U.S. Patent and Trademark Office.

Photocopies and permissions. Permission to photocopy or reproduce material from ASCE publications can be obtained by sending an e-mail to permissions@asce.org or by locating a title in ASCE's online database (<http://cedb.asce.org>) and using the "Permission to Reuse" link. *Bulk reprints.* Information regarding reprints of 100 or more copies is available at <http://www.asce.org/reprints>.

Copyright © 2012 by the American Society of Civil Engineers.
All Rights Reserved.
ISBN 978-0-7844-1229-9
Manufactured in the United States of America.

Preface

We would like to welcome you to the 9th Asia Pacific Transportation Development Conference sponsored by the International Chinese Transportation Professionals Association (ICTPA), T.Y. Lin International Group, Chongqing Urban Planning Bureau, and the Transportation and Development Institute of the American Society of Civil Engineers (ASCE) and hosted by T.Y. Lin International China, Chongqing Jiaotong University, Chongqing Rail Transit (Group) Co. Ltd, and Chongqing Transport Planning Institute. The theme of the conference is “Sustainable Transportation System.”

Transportation professionals are facing continuous challenges including endless traffic congestion, ever-worsening environmental impacts, rising energy cost and deteriorating quality of life. To meet these challenges requires new innovations to develop sustainable transportation systems through planning, design, build, management, and maintenance. This special publication produced by the ASCE is one of several official proceedings of the conference. The ASCE proceedings include 81 peer-reviewed papers addressing nine major areas including: 1) Sustainable Transportation Development; 2) Low Carbon Emissions and Energy Saving in Transportation, 3) Multi-modal Transportation System, 4) Intelligent Transportation Systems, 5) Advancements in Traffic Control Technologies, 6) Transportation and Work Zone Safety, 7) Design and Construction of Bridges and Tunnels, 8) Pavement Materials, Design and Construction, and 9) Geotechnical Design and Construction. Recent advances in new strategies, new methods, and new technologies are presented to address topics relating to funding, planning, design, construction, maintenance, and management of transportation facilities including aviation, port, harbor, highway, bridge, tunnels, rapid transit, and railroad.

One of the conference organizers is the ICTPA, a 25-year-old professional organization that has conducted conferences throughout North America and Asia to examine local and global transportation development issues. With the rapid growth in the recent years, China has become one of the largest transportation infrastructure markets in the world. Many authors studied transportation development in China have showcased new ideas and approaches emerged from some of the world’s largest transportation projects in that country. On the other hand, practitioners and scholars from the United States and other developed countries and regions have presented latest advances in transportation system management and maintenance. The unique combination of these two main streams presented by a distinguished group of international recognized practitioners and scholars has provided a wide range of stimulation and inspiration in solving global transportation problems.

We believe that the proceedings will be invaluable to transportation professionals in advancing their career. In closing, we hope that you enjoy the conference and the City of Chongqing and catch up with old friends and colleagues and make new ones.

Man-Chung Tang, Ph.D., P.E., Hon.M.ASCE
Honorary Conference Chairman
Chairman of the TY Lin International Group

Endi Zhai, Ph.D., P.E., G.E.
Conference Chairman
President of the ICTPA

Acknowledgments

The organizers of the 9th Asia Pacific Transportation Development Conference would like to thank the T.Y. Lin International Group, China to provide financial support for the production of the ASCE proceedings. The Conference Organizing Committee, the Technical Committee, and the International Advisory Committee should be acknowledged for their dedication and contributions to the success of the conference programs.

Organizing Committee Members

Dr. Man-Chung Tang, Honorary Chair, T.Y. Lin International Group
Dr. Endi Zhai, Chair, International Chinese Transportation Professionals Association
Mr. Yuan Zhang, Co-chair, Chongqing Urban Planning Bureau
Mr. Jin Yang, Co-chair, T.Y. Lin International Group, China
Prof. Boming Tang, Co-chair, Chongqing Jiaotong University
Mr. Jianhua Zhong, Co-chair, Chongqing Rail Transit (Group) Co. Ltd.
Mr. Yong Yu, Co-chair, Chongqing Transport Planning Institute

Technical Committee Members

Prof. Yong Bai, Chair, The University of Kansas
Dr. Xiaohu Chen, Co-chair, T. Y. Lin International Group, China
Dr. Alice Ming-Hsiang Kuo, Co-Chair, ICTPA
Ms. Li Lin, Co-chair, Chongqing Rail Transit (Group) Co. Ltd.
Prof. Jing Shi, Co-chair, Tsinghua University
Ms. Chwen Siripocanont, Co-chair, T. Y. Lin International Group
Prof. Zhongfu Xiang, Co-chair, Chongqing Jiaotong University
Mr. Tao Zhou, Co-chair, Chongqing Transport Planning Institute

Prof. Baabak Ashuri, Georgia Institute of Technology
Prof. S. K. Jason Chang, National Taiwan University
Prof. Steven I. Chien, New Jersey Institute of Technology
Prof. Chia-Pei Chou, National Taiwan University
Prof. Gerardo Flintsch, Virginia Tech
Prof. Tien-Fang Fwa, National University of Singapore
Prof. Bham Ghulam, Missouri University of Science & Technology
Prof. Shanglong Gong, Chongqing Jiaotong University
Prof. Anbang Gu, Chongqing Jiaotong University
Prof. Jie Han, University of Kansas
Prof. Kevin Heaslip, Utah State University
Prof. Mustaque Hossain, Kansas State University
Dr. Amy Y. Hu, THI Consultants
Prof. Helai Huang, Central South University

Prof. Wei-Hsing Huang, National Central University, Taiwan
Prof. Xudong Jia, California State Polytechnic University
Prof. Xinguo Jiang, Southwest Jiaotong University
Prof. Phil Lewis, Oklahoma State University
Mr. Dennis Li, MetroSolutions Limited
Dr. Yingfeng Li, Texas Transportation Institute
Prof. Pei-Sung Lin, University of South Florida
Prof. Han-bing Liu, Jilin University
Dr. Hua Liu, Kleinfelder, Inc.
Prof. Yanfeng Ouyang, University of Illinois
Prof. W. Virgil Ping, Florida State University
Prof. Steven D. Schrock, University of Kansas
Prof. Joel Shon, Tainan University of Technology
Prof. Reginald R. Souleyrette, Iowa State University
Prof. Limin Sun, Tongji University
Dr. W.Y. Szeto, University of Hong Kong
Prof. Kevin C. Wang, University of Arkansas
Prof. Zhijun Wang, Chongqing University
Prof. S. C. Wong, University of Hong Kong
Prof. Zhanmin Zhang, University of Texas
Prof. Xizhao Zhou, Shanghai Maritime University

International Advisory Committee Members

Dr. Joe Lee
Mr. Jerry Cheng
Mr. Jimmy Lin
Dr. Charles Liu
Dr. L. David Shen
Mr. Peter Lai
Mr. Chi-Hsin Shao
Dr. Mike Houh
Prof. J. P. Bardet

The organizers would also like to acknowledge many people, whose names are not shown above, have contributed their knowledge, time, and energy to make the conference successful.

Contents

Sustainable Transportation Development

Cost Benefit Analysis of Freeway Service Patrol Programs: A Case Study in Florida	1
Pei-Sung Lin, Aldo Fabregas, and Hongyun Chen	
San Leandro 2010 Bicycle and Pedestrian Master Plan Update	9
Reh-Lin N. Chen, Carol R. Levine, Keith R. Cooke, and Uche Udemezue	
China's Transportation Balancing Development Strategy Discussion	16
Rui Geng	
Comprehensive Evaluation Model for Programming Projects of Traffic Infrastructure Based on Rough Set	22
Shan Jiang, Weiming Liu, and Ling Shi	
Travel Characteristics of Different Social Groups in Large Scale Residential Areas in the Periphery of Shanghai: A Case Study of Jinhexincheng	29
Jinping Guan	
The Research of the Eco-Port Group's Assessment System Based on ANP	38
Cui-lian Liu, Jian-mei Liu, Tiao-lan Yu, and Bao-jun Gong	
Mechanism of Urban Spatial Structure Evolution under the Influence of Port Function Upgrading: A Case Study of Dalian	47
C. Liang and N. Wang	
Chongqing Urban Traffic Congestion Solution Method and Strategy	55
Xingzhong Gao	
TOD Mode and the Interface between the Urban Groups	60
Jin Nan	
The Social Cost of Traffic Congestion and Countermeasures in Beijing	68
Li-zeng Mao, Hong-ge Zhu, and Li-ren Duan	
An Analysis of Airport Runway Designs to Maximize New Airport Throughput to Meet China's Long-Term Air Travel Demand	77
William F. Yim	
Comparison of Software Packages for Life Cycle Cost and Benefit Analysis of Highway Projects	85
Yi Jiang, Guangyuan Zhao, and Shuo Li	
Coordination between Comprehensive Transportation and Social Development at the Regional Level in China	101
Jing Shi, Nian Zhou, and Zhaozhang Wu	
Service Excellence: Road Tunnel Safety	110
William Cheung	

City Development and Public Transportation Planning: A Case Study of Taichung City	119
Chao-Fu Yeh and Ying-Chih Lu	
Car Parking in China—Issues and Solutions	130
Vincent Au	
<i>Low Carbon Emissions and Energy Saving in Transportation</i>	
Evaluation of Construction Equipment Fleets through Fuel Use and Emissions Inventories	138
Phil Lewis and Apif Hajji	
Developing a Sustainable Freight Transportation Framework with the Consideration of Improving Safety and Minimizing Carbon Emissions.....	146
Rita Neff and Yong Bai	
Application of the Theory of Minimum Rate of Energy Dissipation to River Regulation	154
Jun-hong Zhang, Guo-xiang Gong, Jia-an Luo, and Yang-fei Ou	
Low Carbon Management Concepts in TOD Planning.....	160
Chia-Nung Li	
Characteristics of Fuel Consumption and Vehicular Operation of Buses in Taipei’s Exclusive Bus Lanes	168
Y. C. Hu, W. T. Lin, G. P. Chen, and Y. W. Yang	
Developing a Time-Based Model for Buses for Integration with Planning Model for Greenhouse Gas Analyses	176
P. C. Wen, Y. C. Hu, S. Y. Chen, H. H. Chen, and C. W. Chang	
<i>Multi-Model Transportation System</i>	
A Sustainable Multi-User Multi-Criteria Transportation Network Equilibrium Model.....	184
Wenjun Hu and Xizhao Zhou	
Transfer Mode Selection of High-Speed Rail Passengers Based on Travel Time Variability.....	193
Ling Jiang, Shijun Yu, and Yandong Zhu	
Miami Intermodal Center: Airport Connection for the Future.....	201
L. David Shen	
Driverless Medium-Capacity Transit As an Airport Connector: Taipei’s Experience	209
Jiun-Jia Hsu and L. David Shen	
Research on Urban Bus Stop Parking Capacity Reliability	217
Chenghui Chen, Cong Cong, and Yongneng Xu	
The Planning Strategy of Combination Mode of Slow Traffic Ways in Central City of Chongqing.....	226
Xia Chen, Wei Liu, Dan Huang, and Jianjie Gao	

Comparison of BRT Systems in Four Chinese Cities: Beijing, Changzhou, Xiamen, and Jinan	234
Ying-Chih Lu, S. K. Jason Chang, and Ming Yu	
Research on Travel Behaviors of High Speed Trains' Passengers Based on Frequency and Distance of Trip.....	248
Xin Zou, Wang Ji Feng, and Hongbin Zhao	
Fleet Size Metamodel for Dial-a-Ride Services with Time Constraints	257
Ying Luo and Paul Schonfeld	
Development of Intercity through Train Services between Mainland China and Hong Kong	268
Carmen Li	

Intelligent Transportation Systems

Chongqing Intelligent Transport System Plan	274
Fu Yan	
A Practical Intelligent Method to Quickly Screen Pedestrian Related Potential Conflicts with Motor Vehicles	282
F. Qiao, P.-H. Kuo, and L. Yu	
Spatial Approaches for Conflating GIS Roadway Datasets	290
Yingfeng Li, and Chunxiao Liu	
Bus and Metro Integration Improvements in Beijing.....	299
Mingzheng Sun, Lijing Song, Feng Chen, and Kai Xian	
An Iterative Procedure for the Estimation of Dynamic Toll Demand, Toll, and Level-of-Service on Toll Facilities.....	308
Jinghua Xu and Steven Ruegg	
Experience of Radio Taxis in Algeria.....	316
H. Bencherif and F. Boubakour	

Advancements in Traffic Control Technologies

Vehicle Speed Determination Based on Front Windshield Glass Rupture Area	324
Chuanjiao Sun, Jie Zhang, and Xiaojing Ban	
The Timing to Retime and Maintain Traffic Signal Systems	332
Pei-Sung Lin, Aldo Fabregas, and Hongyun Chen	
Assessment of a Flashing Yellow Arrow Signal Implementation Using Gap Acceptance Measures.....	341
Pei-Sung Lin, Aldo Fabregas, and Enrique Gonzalez-Velez	
Traffic Signal Control of Fuzzy Neural Network Based on Line Length of Cars in Waiting	349
Xue Li, Bai-chuan Lu, and Yi Li	
Study of Carpool User Behaviors and Route Characteristics in Taiwan	356
C. L. Chung, J. Y. Jeng, Z. Y. Lee, and June-Shian Lee	

Transportation and Work Zone Safety

Characteristics of Truck-Related Crashes in Highway Work Zones.....	364
Yue Li, Feifei Cheng, and Yong Bai	
Evaluation on the Effectiveness of Sideview Video Systems to Reduce Transit Bus Side Crashes	372
Pei-Sung Lin, Achilleas Kourtellis, and Chanyoung Lee	
A Study of Steady State for Distance Headway	380
Hsueh-Heng Chen and Tsung-Chin Lin	
Determining Drivers' Acceptance of Using Graphics on Portable Changeable Message Signs in Highway Work Zones.....	387
Yilei Huang and Yong Bai	
Transportation Infrastructure Disaster Impact and Lessons Learned after Typhoon MORAKOT	395
Min-Cheng Teng, Jau-Lang Su, and Shen-Wen Chien	
Reliability Analysis of Highway Evacuation Network Post-Earthquake Disaster	404
Sai-ni Yang, Xue-chi Zhang, Jia-yuan Ye, and Jian-lin Wu	
A Comprehensive Evaluation Model for Earthquake Emergency Shelter	412
Huan Cheng and X. K. Yang	
Key Concepts in the Development of a Transit Safety Management System	423
Dennis Y. N. Li	

Design and Construction of Bridges and Tunnels

Application of Variable Weight Grey Clustering Method in Tunnel Collapse Risk Evaluation	429
Zhenyu Yi	
Analysis of the Influence upon the Beijing-Tianjin Intercity High Speed Railway by a Subway Shield Tunnel Crossing Below	438
Gancheng Xu, Chengxue Li, and Houyu Wang	
Design of the SR522 Snohomish River Bridge under Multiple Hazards.....	447
Hongzhi Zhang	
Model Test Studies on Ground Subsidence and Cracks Induced by Tunneling in Weak Rock Mass with High Water Content.....	455
X. Wei and G. Wang	
Application of Story Isolation Technique in the Seismic Reduction of Integrated Building-Bridge Station.....	464
W. Guo, Z. Yu, and H. S. Zhang	
Network Arches: The World's Lightest Arch Bridges	473
Per Tveit	
Seismic Failure Analysis of Huilan Flyover in Wenchuan Earthquake.....	481
Jie Meng, Jiandong Zhang, and Zhao Liu	

Fatigue Considerations in the Design of Cable-Stayed Road-Rail Bridges with Orthotropic Steel Deck.....	491
Xiaohu Chen, Delan Yin, Yaping Lai, and Xiaofei Liu	
Waterproofing Solutions for Metro Tunnels.....	500
Francis Lung	
Experimental Study of the Bearing Capacity of Double CFST Member.....	508
Zhongfu Xiang and Yang Yu	
Seismic Design of Dillon Road Grade Separation Bridge.....	515
Jian Lan	
A Study on the Application of Resin Composite Sleeper in the Design of Long-Span Rail Bridges	523
An-shuang Liu, Delan Yin, and Guoxiang Liu	
<i>Pavement Materials, Design, and Construction</i>	
Research on the Technique of Utilizing River Sludge As Road Fill.....	532
Fanyi Bai, Haiyun Song, Lei Cao, and Baowei Zhang	
The Key Technologies for Construction Quality Control of Cement Emulsified Asphalt Mortar of CRTS Ballastless Slab Track for High-Speed Railway.....	541
Liangwei Lou, Yan Cheng, Changhua Zhu, and Xinhua Zhong	
Preliminary Analysis of AASHO Road Test Rigid Pavement Data Using Linear Mixed-Effects Models	549
H. W. Ker, Y. H. Lee, T. C. Huang, and K. Lin	
Research on Strength Developing Procedure of Epoxy Asphalt Mixture	558
L. L. Chen, Z. D. Qian, and C. L. Jiang	
Research on Flexural Strength of Asphalt Mixture in Cold Highlands	567
Youpo Wei, Yunxiang Song, and Yumei Li	
Long-Life Pavement Design and Construction—A Case Study.....	574
George Wang, Yuhong Wang, Russell Thompson, and Yong Han Ahn	
A Rational Approach for Estimating the Resilient Modulus of Constructed Granular Subgrade Materials.....	583
W. Virgil Ping and Biqing Sheng	
The Effect of Groundwater Base Clearance on Constructability of Florida Pavements	591
W. Virgil Ping and Biqing Sheng	
Effect of Polymer Binder Content on Fracture Mechanics Properties of Hot Mix Asphalt Concrete	599
W. Virgil Ping and Yuan Xiao	
Pavement Noise Investigation in North Carolina.....	608
George C. Wang	
Precast Prestressed Concrete Pavement Construction	616
Luh-Maan Chang and Yu-Tzu Chen	

Geotechnical Design and Construction

Performances of Vibro Compaction Gravel-Concrete Composite Pile	624
G. Q. Kong	
Time-Frequency Analysis of Seismic Response of a High Steep Hill with Two Side Slopes When Subjected to Ground Shaking by Using HHT	632
Changwei Yang, Jianjing Zhang, Gang Fan, Zhiyi Huang, and Cheng Zhang	
Experimental and Numerical Investigation of the Influence of Dilatancy on a Shallow Anchor Plate in Sand	644
Jinyuan Liu	
Seismic Analysis of Lateral Loaded Pile under Strong Shaking: A Case Study from the 2008 Wenchuan Earthquake.....	652
Jianjing Zhang, Chun-Xiao Nie, Qiang Liu, and Changwei Yang	
Numerical Modeling of Strike-Slip Fault Rupture Propagation through Soft Soil Deposit and Embankment.....	662
Qi Chen, Qiang Liu, Chun-Xiao Nie, and Changwei Yang	
Research on Assessment Method of High, Large, Steeply Inclined, and Accumulation Slope Stability in Southeast Region of Chongqing.....	672
Wei Huang, Xiao Feng, Jianting Zhou, and Guanghuai Yang	
Dynamic Response of High-Speed Rail Roadbed under Harmonic Moving Loads	686
Fu-Chun Xue, Liping Yan, Jian-Min Zhang, and Jian-Lin Ma	

Indexes

Author Index.....	695
Subject Index	697

Cost Benefit Analysis of Freeway Service Patrol Programs: A Case Study in Florida

Pei-Sung Lin¹, Ph.D., P.E., PTOE, Aldo Fabregas², and Hongyun Chen³, Ph.D.

¹Program Director, ITS, Traffic Operations and Safety Program, Center for Urban Transportation Research (CUTR), University of South Florida, 4202 E. Fowler Ave., CUT 100, Tampa, FL 33620; PH: (813) 974-4910; FAX: (813) 974-5168; Email: lin@cutr.usf.edu

²Research Associate, ITS, Traffic Operations and Safety Program, Center for Urban Transportation Research (CUTR), University of South Florida, 4202 E. Fowler Ave., CUT 100, Tampa, FL 33620; PH: (813) 974-3296; FAX: (813) 974-5168; Email: fabregas@cutr.usf.edu

³Research Assistant, ITS, Traffic Operations and Safety Program, Center for Urban Transportation Research (CUTR), University of South Florida, 4202 E. Fowler Ave., CUT 100, Tampa, FL 33620; PH: (813) 974-9795; FAX: (813) 974-5168; Email: egonzal@cutr.usf.edu

ABSTRACT: Florida's Road Rangers provide free highway assistance services during incidents on Florida's roadways to reduce delay and improve safety for the motoring public and responders. This paper presents the research results from a recent completed study to describe and quantify the benefits derived from the Road Ranger program. The Freeway Service Patrol Evaluation (FSPE) model, developed by the University of California at Berkeley, was used to quantify the benefit-cost (B/C) ratio using a variety of data from Florida SunGuide[®] database for the year 2010. The benefits (delay and fuel saving) of the Road Ranger program were about \$135.3 million in total, and the costs (contract) were about \$19.9 million. Overall, the program achieved a B/C ratio of 6.78 in 2010. This paper will be informative for any agency looking to identify opportunities to improve the allocation of available funding for similar incident response programs.

INTRODUCTION

According to the latest Urban Mobility Report published by Texas Transportation Institute (TTI), 4.8 billion hours of extra time were wasted due to the traffic congestion in 2010 with 1.9 billion extra gallons of fuel used (Schrank et al.). Transportation agencies are striving to mitigate traffic congestion and the effects due to the congestion. Non-recurring congestions account for almost half of the congestion which might be crashes, hazardous weather change, and any unexpected events (Kimley-Horn 2011). To reduce non-recurring delays caused by incidents, many states run freeway service patrols (FSP) to quickly respond to incidents.

In Florida, the FSP service is provided under the Florida's Road Ranger (RR) program funded by the Florida Department of Transportation (FDOT). The Florida's

RR program is one of the most effective elements of the FDOT Traffic Incident Management (TIM) Program. It supports emergency first responder personnel and disabled/stranded motorists to clear the roadway as quickly as possible, and prevents potential secondary incidents. FDOT began funding the program in 1999 and by 2010, the number of incidents assisted ascended to more than 3.1 million.

Current, FSP are present in at least 40 states nationwide under different names and responsible agencies. A national survey of 19 agencies showed that the benefit-cost (B/C) ratios for FSP program ranged from 4.6:1 to 42:1, as shown in Table 1. The average B/C was 12.4 and the median was 9.45:1(Baird). The study performed in 2005 by FDOT estimated that the B/C ratio for the Florida's RR program was 25.8:1(Hagen and Zhou) which also proved the importance of having the program and success in congestion mitigation.

Table 1 States' Benefit and Cost Analysis Results

Location	Name	Year	Results
AL (Statewide)	Service and Assistance Patrol	2009	1.7:1 to 23.4:1
Charlotte, NC	Incident Management	1993	3:1 to 7:1
Chicago, IL	Emergency Traffic Patrol	1990	17:1
Dallas, TX	Courtesy Patrol	1995	3.3:1 to 36.2:1
Denver, CO	Mile High Courtesy Patrol	1996	20:1 to 23:1
Detroit, MI	Freeway Courtesy Patrol	1995	14:1
Fresno, CA	Freeway Service Patrol	1995	12.5:1
FL (Statewide)	Road Ranger Program	2005	2:1 to 40:1
Houston, TX	Motorist Assistance Program	1994	6.6:1 to 23.3:1
Los Angeles, CA	Metro Freeway Service Patrol	1993	11:1
Minneapolis, MN	Highway Helper	1995	5:1
New York, NY	Highway Emergency Local	1995	23.5:1
Norfolk, VA	Safety Service Patrol	1995	2:1 to 2.5:1
Oakland, CA	Freeway Service Patrol	1991	3.5:1
Orange Co., CA	Freeway Service Patrol	1995	3:1
Riverside Co., CA	Freeway Service Patrol	1995	3:1
Sacramento, CA	Freeway Service Patrol	1995	5.5:1

However, recent budget hardships in Florida have forced legislature to reduce the availability of funding for the Florida's RR program by half. Thus, it is necessary to develop a comprehensive analysis to inform legislators in a clear and concise manner about the updated benefits of the Florida's RR program ensuring their support for the program in the future. Also, it is important to perform analyses aiming at identifying opportunities for improvement and cost efficiencies. In this way, the program can be expanded or improved without incurring additional budget expenses. Hence, the main objective of this study was to perform an updated B/C analysis of the Florida's Road Ranger program. The paper will present the methodology used in the study, data collection, B/C analysis, result and recommendations.

METHODOLOGY

The Freeway Service Patrol Evaluation (FSPE) model was used to quantify the amount of savings due to reductions in traffic delay, fuel, and emissions; the contract costs of the RR program were used in this model.

Delay saving. Delay savings is one of the major benefits of a freeway service patrol program. The difference in delay with and without the Florida's RR program is one of the main components of the net benefit calculations. Figure 1 shows the differences in delays due to the presence of the program. The horizontal axis and the vertical axis represent the time and the cumulative volume for a freeway segment, respectively.

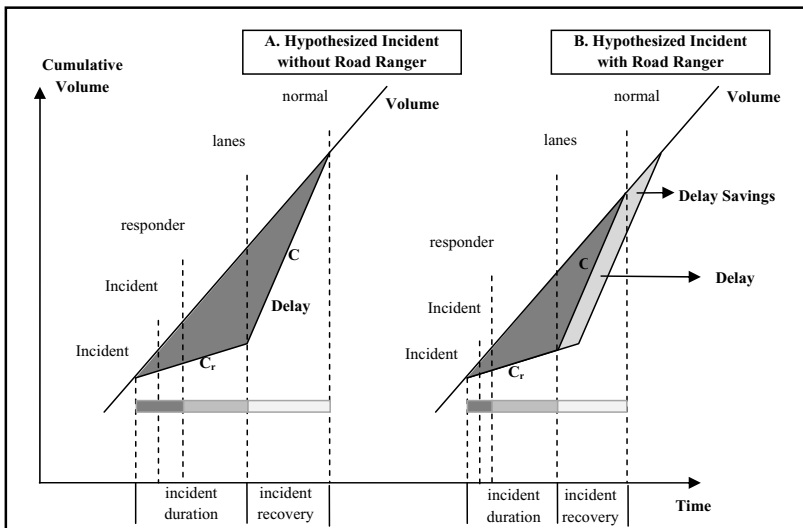


Figure 1 Delay comparison with and without the Florida's RR program

Part A of Figure 1 presents the delay without Road Rangers and part B presents the same incident with the assistance from Road Rangers. It is assumed that the freeway is working at or near full capacity. When an incident occurs, the capacity is reduced to C_r and it will take some time to recover and return to the initial conditions which is presented as C , after the incident is cleared. Since Road Rangers are patrolling the freeway, the detection and arrival times in part B (assisted by RRs) are less than in part A (without RRs). Thus, the total delay saving is highlighted in light grey as the total time in delay for the condition B is relatively shorter than that in the condition A. The direct measurements of delay were performed by an FSPE model mainly consisting of reduced response time in incidents assisted by the Florida's RR program. The FSPE model uses the capacity reduction factors to calculate the remaining capacity during an incident recommended by the Highway Capacity Manual (HCM 2000). The values are presented in Table 2.

Fuel and emission savings. Fuel consumption and excess of emissions occur during the incident-induced delays are also important to include the total benefits to have the

Florida's RR program. The FSPE model uses the Emissions FACTor (EMFAC) model with the latest mobile source emission rates published by the California Air Resource Board (CARB) for measuring fuel and emission savings. Emissions rates and fuel consumption rates in the selected model were implemented as lookup tables based on average speed. The pollutants considered in the model were carbon monoxide (CO), hydrocarbons (HC), and oxides of nitrogen (NOx). The air pollutant emissions are calculated based on the following formula:

$$F_i = D \times e_i \quad (1)$$

where, $i=1$ is the fuel consumption in gallons; $i=2$ is the HC emissions in Kg; $i=3$ is CO emission in Kg; $i=4$ is NOx emission in Kg; F_i is fuel consumption or emissions; D is incident-induced delay; and e_i represents the fuels or emission factor.

Table 2: Remaining Freeway Capacity under Incident Conditions in HCM 2000

Incident Type	Location	No. of Freeway Lanes/Direction			
		2	3	4	5+
Accident	Right Shoulder	81%	83%	85%	87%
	Median	81%	83%	85%	87%
	1-Lane	35%	49%	58%	65%
Breakdown	Right Shoulder	95%	98%	98%	98%
	Median	95%	98%	98%	98%
	1-Lane	35%	49%	58%	65%
Debris	Right Shoulder	95%	98%	98%	98%
	Median	95%	98%	98%	98%
	1-Lane	35%	49%	58%	65%

Costs of the RR program. The Florida's RR program service covers a total of 1,321 centerline miles of the interstates and toll roads in Florida for FDOT Districts 1, 2, 4, 5, 6, 7, and the Florida's Turnpike Enterprise (FTE) in 2010. The service was divided into zones, and each zone was assigned the Road Ranger truck(s) with a service schedule by weekends and weekdays, respectively. The total cost of RR services for a particular zone were calculated by the updated hourly cost (contract cost) provided by local agencies in each district, truck types, the hours of operation, and the number of truck in that particular zone. The hours of operation may range from 24 hours to peak service hours only.

DATA COLLECTION

The FSPE model was generated for each zone by weekday and weekend respectively. Table 3 lists main input parameters for the FSPE model including service description, roadway design characteristics, traffic characteristics, and incident data. Only those incidents which caused lane blockage, right shoulder blockage, or left shoulder blockage, were used in the FSPE model. Incidents were grouped into nine categories under three incident types (accident, breakdown, and debris) and three types of lane-blockage (one lane blockage, left shoulder, and right shoulder). SunGuide[®] software was used as the data resource to collect the Florida's RR operations data, mean time

spent per incident type, mean response time without RR service, traffic profile (weekday, Saturday, and Sunday), geometric profile, and filed speed.

Table 3: Data Inputs and Data Sources for the FSPE Model

Data Sheet	Variables	Type
Service Description	District and Beat Name, Date, Hours of Operation, Number of Trucks;	Input
	Cost of Service	Input
Design Characteristics	Direction, Geometric Design, Number of Lanes, Length, Number of Mixed Flow Lanes, HOV lane (if any), Presence of Right Shoulders/Median	Input
Traffic Characteristics	Average Annual Daily Traffic, percentage of trucks, directionality Factors (AM, Midday, and PM peak periods)	Input
Incident Characteristics	Mean Time and Percentage of Incidents at Right Shoulder, Median and In-lane by Each Type (Accidents, Breakdowns, and Debris)	Input
Additional Parameters	Capacity Values	Default
	Remaining Freeway Capacity Factors	Default
	Fuel/emission Base Rates	Default
	Travel Time Value, and Fuel Costs	Input
Traffic Profiles	Occupancy Rates	Input
	Percentage of Hourly Volume (in a 24hr day without incidents)	Optional Input
	Percentage of Hourly Volumes by Directions	Optional Input

To level out those differences for the analysis, the same response time without RRs was used. This time will be set at 30 minutes based on studies developed by California (Skabardonis and Mauch) and the open roads policy by FDOT (FDOT 2002). The travel time values for each person hour of travel and truck hour were obtained from the Urban Mobility Report 2009. Average vehicle occupancy can be found from the National Household Travel Survey (NHTS). The percentage of trucks in total traffic can be found in the FDOT traffic information CD. The Travel Time Value (TTV) for the FSPE model can be calculated as:

$$TTV_n = V_{Pn} \times O_{vn} \times (1 - P_{Tn}) + V_{Tn} \times P_{Tn} \quad (2)$$

where, n is the service zone number, V_{Pn} is the value of person hour in the zone; O_{vn} is the average vehicle occupancy rate in the zone n; P_{Tn} is the percentage of truck in zone n; and V_{Tn} is the value of truck hour in the zone.

A total of 204 scenarios were completed in the final database. To effectively generate the models, the research team developed the FSPE model generator, scenario generator, and model runner software which can systematically, automatically, and effectively run the FSPE model.

DATA ANALYSIS

The distribution of incident types and mean time spent were compiled and summarized in Figure 2 and **Error! Reference source not found.**, respectively. The right shoulder blockage due to vehicle breakdowns constitute of the majority of the incidents, 68.56% for weekdays and 71.09% for the weekends. The vehicle breakdown on the left shoulder and lane blockage of accidents are the second and third demanding incidents in Florida, respectively. The mean time spent was defined as the difference between the departure time and the arrival time of a responder during a particular incident. The lane blockage of accidents is the most time consuming incident type which last 50.93 min for weekdays and 52.52 min for weekends in average. Overall statistics for Florida showed an average of 45 to 52 minutes for mean time spent on accidents, 18 to 33 minutes for breakdowns, and 11 to 18 minutes for debris.

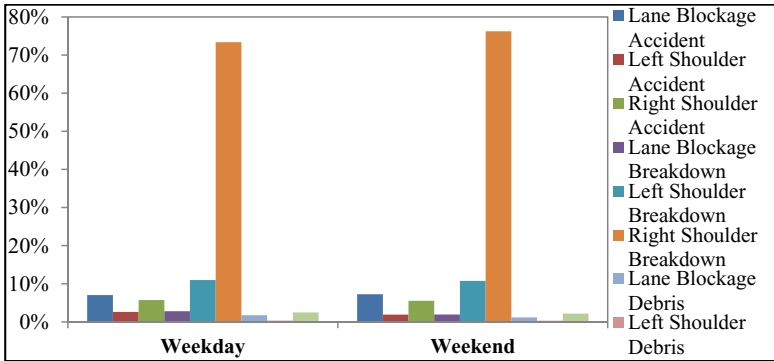


Figure 2 Distributions of incident types in Florida in 2010

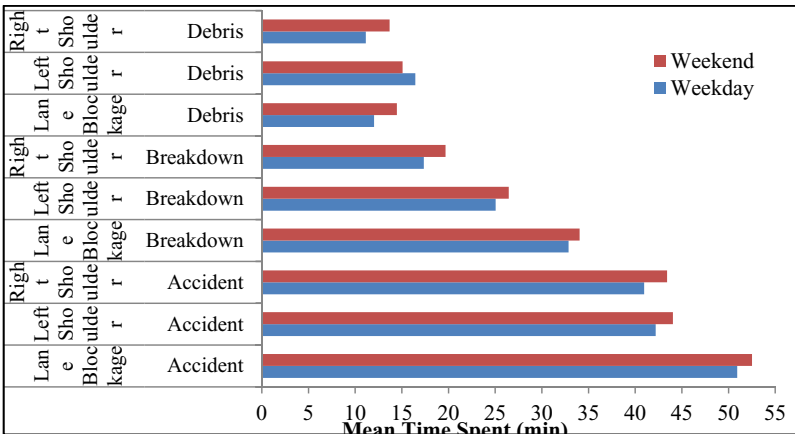


Figure 3 Distribution and incident clearance time by the Florida's RR program

The B/C ratios for the service zones were aggregated by weekday and weekends correspondingly and the overall B/C for the whole state are presented in Table 4. It can be observed that the B/C ratio for the state is 6.93 for weekdays and 6.20 for weekends. Overall, a 6.78:1 ratio was achieved for the Road Ranger program in 2010. The benefits (delay and fuel saving) of the Road Ranger program were about \$135.3 million in total, and the costs (contract cost) were about \$19.9 million. This indicates an overall positive effect of the Florida's Road Ranger program in alleviating delays caused by accidents, vehicle breakdowns, and debris.

Table 4: Road Ranger Program B/C Ratio Summary

District	Delay Saving (\$)	Fuel Saving (\$)	Total Benefits (\$)	Cost (\$)	B/C Ratio
Weekend	106,623,059	4,168,332	110,791,391	15,989,643	6.93
Weekday	23,877,834	938,339	24,479,730	3,949,446	6.20
Overall	130,500,893	5,106,671	135,271,121	19,939,089	6.78

Figure 3 shows a scatterplot of B/C ratios plotted against the average speed (mph) and proportion of lane blockages. The figure shows that those segments with higher speeds tends to have lower B/C ratios while the higher total percentage or probability of lane blockage per zone shows the opposite trend. Zones with increased probability of lane blockages tend to have higher B/C ratios. This is consistent with the assumptions and the data used to build the FSPE model in this study. In Florida, a significant proportion of the freeways have wide shoulders facilitating moving some of the incidents away from the travel lanes.

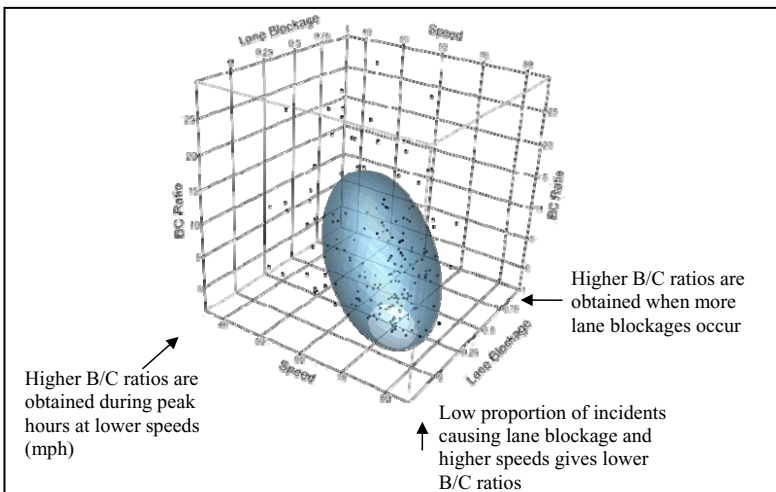


Figure 3: Three-dimensional scatter plot of B/C ratios of zones in Florida

CONCLUSION AND RECOMMENDATION

In this study, a benefit-cost analysis of the Road Ranger program in Florida was performed by using the FSPE models. Overall statistics for Florida showed an average of 45 to 52 minutes for mean time spent on accidents, 18 to 33 minutes for breakdowns, and 11 to 18 minutes for debris. The overall B/C ratio for the Road Ranger program in 2010 was estimated at 6.93 for weekdays, 6.20 for weekends, and 6.78 in average. The benefits (delay and fuel saving) of the Florida's Road Ranger program were about \$135.3 million in total, and the costs (contract) were about \$19.9 million. This indicates that the benefits of the Florida's Road Ranger program will exceed the overall cost.

The Florida's Road Ranger program has a positive impact in alleviating congestion on Florida's highways due to traffic incidents. The detailed B/C information by highway segments will be informative for any agency looking to identify opportunities to improve the allocation of available funding for similar incident response programs. The research team suggested that similar reviews should be conducted annually to effectively manage the program based on the up-to-date B/C ratios. However, it is noticed that current evaluation tools rely on capacity reduction factors calculated in contexts, so this may not be applicable to all the regions in Florida or other states. Also, a consistent effort to improve the data collection/processing may be necessary to adequately collect, process, and store information to evaluate any incident response programs in a more efficient and effective manner.

REFERENCES

- Schrank, D., T. Lomax, B. Eisele. (2011). "TTI's 2011 Urban Mobility Report- Powered by INRIX Traffic Data". Texas Transportation Institute, The Texas A&M University System, College Station, TX.
- Kimley-Horn and Associates, Inc. (2011). "SHRP 2 Report S2-L010RR-2: Guide to Integrating Business Processes to Improve Travel Time Reliability". Transportation Research Board (TRB), Washington, D.C.
- Baird, M.E. Vanderbilt University. (2008). "Overview of Freeway Service Patrols in the United States: Final Report". Southeastern Transportation Center.
- Hagen, L., H. Zhou, and Singh. (2005). "Benefit and Cost Analysis of the Freeway Service Patrol Program in Florida", Florida Department of Transportation, Tallahassee, 2005.
- Transportation Research Board of the National Academies. (2000). "Highway Capacity Manual". Washington, D.C..
- Skabardonis A. and M. Mauch. (2005). "FSP Beat Evaluation and Predictor Models: Users Manual". Research. Report No. UCB-ITS-RR-2005-XX, Institute of Transportation Studies, University of California-Berkeley, California.
- Florida Department of Transportation. (2002). "State of Florida 'OPEN ROADS POLICY': Quick Clearance for Safety and Mobility". FDOT Intelligent Transportation System.

San Leandro 2010 Bicycle and Pedestrian Master Plan Update

Reh-Lin N. Chen, P.E., PTOE¹, Carol R. Levine², Keith R. Cooke, P.E.³
Uche Udemezue, P.E.⁴

¹Senior Transportation Engineer, Engineering & Transportation Department, City of San Leandro, 835 East 14th Street, San Leandro, CA, 94577; PH (510) 577-3438; FAX (510) 577-3294; email: rchen@sanleandro.org

²Principal, Spokemore Consulting, 734 Mandana Blvd., Oakland, CA 94610, PH (510) 507-1681; email: CarolLevine@peoplepc.com

³Principal Engineer, Engineering & Transportation Department, City of San Leandro, 835 East 14th Street, San Leandro, CA, 94577; PH (510) 577-3439; FAX (510) 577-3294; email: kcooke@sanleandro.org

⁴Director, Engineering & Transportation Department, City of San Leandro, 835 East 14th Street, San Leandro, CA, 94577; PH (510) 577-3402; FAX (510) 577-3294; email: uudemezue@sanleandro.org

ABSTRACT:

In 1997, the City of San Leandro adopted the *Bikeway Plan of the Circulation Element of the City's General Plan* which provided policies and programs and guided the planning and development of bikeways throughout the city. In 2004, a pedestrian component was added to address both bicycle and pedestrian issues in a similar and consistent fashion and to allow the City to be more competitive in obtaining grant funding. To reflect demographic changes and new policies and design standards for bicyclists and pedestrians, this document was updated in 2010.

The *2010 Bicycle and Pedestrian Master Plan Update* (Master Plan) is the official policy document guiding the development of facilities to enhance bicycling and walking as additional and appropriate transportation choices for residents.

The Master Plan included the guidance of a City Council-appointed Bicycle and Pedestrian Advisory Committee (BPAC). The BPAC was composed of 13 members and three alternates. BPAC members, who represented both bicycle and pedestrian interests, were selected from each of the City's Council districts. The BPAC met five times over nine months and was effective in providing valuable insight into the Master Plan. The Master Plan was adopted by the City Council in February 2011.

The Master Plan Update includes the following chapters: Introduction; Goals and Policies; Bicycle Network; Pedestrian Network; Safety, Education and Enforcement; and Implementation.

A companion document, *The Bicycle and Pedestrian Design Guidelines*, was also developed with the guidance of the BPAC. It provides details that assist with the design of bicycle and pedestrian facilities recommended for the City of San Leandro.

INTRODUCTION

The City of San Leandro adopted the *Bikeway Plan of the Circulation Element of the City's General Plan* in 1997. The document provided policies and programs, and guided the planning and development of bikeways throughout the city. In 2004 the Bikeway Plan was further expanded to address both bicycle and pedestrian issues in a similar and consistent fashion. By incorporating pedestrian policies, programs, and proposed improvements, the City improved its competitiveness in applying for grant funding to construct pedestrian-related and bicycle-related improvements. To reflect demographic changes and new policies and design standards for bicyclists and pedestrians, this document was updated in 2010.

The *2010 Bicycle and Pedestrian Master Plan Update* (Master Plan) is the official policy document guiding the development of facilities to enhance bicycling and walking as additional and appropriate transportation choices for San Leandro residents. The Planning Commission conducted a public hearing of the draft Master Plan in November 2010 and recommended adoption of the document to City Council. The Master Plan was adopted by City Council in February 2011.

The Master Plan was developed with the input and guidance of a City Council-appointed Bicycle and Pedestrian Advisory Committee (BPAC) which was convened to guide the update of the Master Plan. In response to the invitation for BPAC members, City staff received 26 applications from interested parties throughout the City. The BPAC, composed of 13 full members and three alternates, were selected from each of the Council districts and represented both bicycle and pedestrian interests. The BPAC met five times over nine months and was extremely effective in providing valuable insights. Although the BPAC was considered a short-term Ad hoc committee for input on updating the Master Plan, community and city staff interest prompted the formation of a permanent BPAC to advise on the plan's implementation.

Analysis

Relationship to the General Plan

The Master Plan is a comprehensive update of the 1997 and 2004 plans that allows the City to remain competitive for Regional, State and Federal grant monies. The Master Plan is wholly consistent with the goals and policies of the *San Leandro General Plan*. The Master Plan will remain as part of the Circulation Element and will help implement General Plan policies related to land use, circulation and recreation.

Specifically, the City's vision is for:

A city where walking and bicycling are fully integrated into daily life, providing environmentally-friendly transportation alternatives that are both safe and convenient for people of all ages and abilities.

Updated Bicycle and Pedestrian Master Plan

The Master Plan Update includes the following chapters: Introduction; Goals and Policies; Bicycle Network; Pedestrian Network; Safety, Education and Enforcement; and Implementation.

The Introduction chapter identifies relationships with other plans, conformance with funding requirements, community involvement in development of the plan, and project setting, including identifying major activity centers (e.g., schools, community and senior centers, public libraries, parks, city government services, retail destinations, major employment centers), and multimodal connections (e.g., BART, AC Transit).

The Goals and Policies chapter provides guidance for promoting and enhancing bicycle and pedestrian activity and safety in San Leandro. Highlights of this chapter include:

- Goal #3 – Develop a bicycle system that meets the needs of utilitarian and recreation users, helps reduce vehicle trips, and links residential neighborhoods with local and regional destinations
 - Policy 3.1 – Develop a bikeway system that connects residential neighborhoods to employment and shopping areas, multi-modal terminals, schools, recreational facilities and other destinations
 - Policy 3.5 – Address barriers to bicycling, such as the lack of secure bicycle parking, signals that do not detect bicycles, difficulty in carrying significant baggage by bicycle, and bicycle prohibitions on transit
- Goal #4 – Create a well-connected pedestrian environment by improving the walkability of all streets in San Leandro through the planning, implementing, and maintaining of pedestrian-supportive infrastructure that meets the needs of all users
 - Policy 4.2 – Ensure safe pedestrian connections between important community destinations, such as residential areas, transit locations, schools, senior centers and other community facilities
 - Policy 4.3 - Increase connectivity and access across barriers to walking such as incomplete or uneven sidewalks, sidewalk obstructions, including cars parked on sidewalks, trail gaps, wide intersections, and poor connections to transit stops

The Bicycle Network chapter identifies the existing and proposed bicycle network. Much of the bicycle network identified in the 1997 and 2004 plans is maintained in the 2010 update, with additional bicycle facilities proposed to expand coverage to previously underserved areas of the city. A total of 63 miles of bicycle facilities are proposed in the Master Plan. Bikeway selection criteria include: coverage; system rational; avoidance of arterials; connection to employment centers; connection to schools, libraries and parks; connection to regional bikeways; and suitability of bikeway type. Figure 11 on Page 35 of the Master Plan provides a map of the entire bicycle network including:

- BART Trail (East Bay Greenway)
- San Leandro Boulevard Bike Lanes
- Doolittle Drive Bike Lanes
- Proposed Estudillo Canal Trail

The Pedestrian Network chapter identifies various locations where pedestrian improvements are desired. The locations are identified either as Pedestrian Improvement Areas that encompass a large area of high pedestrian activity, or Key Pedestrian Locations that identify a specific focused location of pedestrian activity. Figure 12 on Page 44 of the updated Master Plan provides a map of the Pedestrian Improvement Areas and Key Pedestrian Locations. Example Pedestrian Improvement Areas and Key Pedestrian Locations include:

- San Leandro Marina Pedestrian Improvement Area
- Kaiser Development Area Pedestrian Improvement Area
- Downtown San Leandro BART Station Pedestrian Improvement Area
- East 14th Street Corridor Pedestrian Improvement Area
- Garfield Elementary School
- Wicks Boulevard at the Marina Community Center
- Bancroft Middle School
- 150th Avenue/Hesperian Boulevard/Bancroft Avenue/East 14th Street Intersection

The recommended pedestrian improvements addressed the needs of all pedestrians. Recommendations include:

- Assess and Repair Sidewalk Surface
- Ensure All Curb Ramps Meet Americans with Disabilities Act (ADA) Standards
- Update Signals within the City to Meet Accessible Pedestrian Signal Guidelines
- Safety and Accessibility Improvements at the Railroad Crossings
- Improve Crosswalks at Uncontrolled Intersections

The Safety Education chapter discusses existing safety conditions for bicycling and walking in San Leandro, including an evaluation of recent collision activity and current safety and education programs available to San Leandro residents. Additional education and enforcement programs are recommended to improve safety for bicyclists and pedestrians.

During the 4-year period between 2006 and 2009, there were 79 reported collisions in San Leandro involving bicycles, with a total of 59 reported injuries. No fatalities occurred during this period. This reflects an average of approximately 20 bicycle collisions annually. The number indicates a reduction in the average of 23 annual collisions reported in the 2004 Plan and the average of 32 annual collisions reported in the 1997 Plan. Wrong-way riding and right-of-way violations by either the cyclist or motorist continue to be the most common causes of motor vehicle-bicycle collisions. These collisions can be reduced by improving bicycle safety education emphasizing teaching current and potential bicyclists of all ages about the fundamentals of bicycle riding. Bicycle safety education should also target motorists, law enforcement officers and the general public.

During the same 4-year period of this analysis, there were 109 reported pedestrian collisions in San Leandro with a total of 86 reported injuries. No fatalities occurred during this period. This reflects an average of approximately 27 pedestrian-involved collisions annually. The number indicates a reduction in the average 33 annual collisions reported in the 2004 Plan. Motorists were at fault a majority of the time, and the most common collision factor was the motorist violating pedestrian right-of-way. Pedestrian safety education programs targeted at all road users is an important means for promoting safe interactions between pedestrians, motorists, and cyclists.

The Implementation Chapter identifies various grant funding sources that can be pursued to implement the proposed bicycle and pedestrian programs/projects. Coordination with multiple agencies both inside and outside the city is also essential. To facilitate implementation efforts, this chapter presents the project prioritization methodologies, a summary of past expenditures, and conceptual cost estimates. Funding and implementation strategies are also described.

Since there are more projects than can be completed at any given time, it is necessary to prioritize the projects to provide guidance as to which projects are to be developed first. Full lists of these bicycle and pedestrian projects can be seen in Tables 5, 6, 7, and 8 on pages 76-91. Additionally, high priority bicycle and pedestrian projects for the 5-year expenditure plan are also listed in Table 9 on page 95.

A companion document, *The Bicycle and Pedestrian Design Guidelines* (Guidelines), was also developed with the guidance of the BPAC. The Guidelines provide details that will assist with the detailed design of various bicycle and pedestrian facilities, such as bike parking, curb bulb-outs, and enhanced crosswalks. The Guidelines is a working document that can be easily updated by staff as new guidelines and methods become available. Additionally, a San Leandro Bicycle Map with Safety Brochure was prepared for distribution to the general public.

Establishment of a Permanent BPAC

San Leandro has a comprehensive multi-modal transportation system with established and informal bicycle/pedestrian networks. However, to maximize the use of bicycle and pedestrian travel, it is essential that planning for these modes be integrated in all City transportation improvement projects whenever feasible. The numerous transportation improvement projects that are either proposed, programmed or under construction represent opportunities for improving and/or expanding bicycle/pedestrian systems. Therefore, a consistent and systematic review process should be followed to ensure that bicycle/pedestrian issues are addressed and options developed in a timely fashion for network expansion, creation of well-defined system nodes and linkages, improved accessibility to other transit modes, and increased public safety.

Although establishing a permanent BPAC is not required by law, the BPAC provides a valuable source of community input for matters on bicycle and pedestrian facilities. It is with this in mind that a permanent BPAC was established to advise staff and to participate in bicycle/pedestrian planning, education, design and enforcement efforts. Following is a summary of the key elements used in creating the

BPAC:

- Committee Name: Bicycle and Pedestrian Advisory Committee
- Membership: Eleven (11) Member Committee
 Staff recommends that there be no age limit for the BPAC members and that at least one member represent each Council District. The selected members shall represent both bicyclist and pedestrian issues and be approved by the City Council. Committee should include the San Leandro representative to the Alameda County Transportation Commission BPAC.
- Responsibilities: In general, the BPAC will be charged with advising staff on matters relating to the status and condition of bicycle and pedestrian facilities within the City.
- Meetings: Meetings of the BPAC shall be held on an as-needed basis. It is anticipated that that BPAC will meet once or twice a year

In February 2011, at the same meeting adopting the draft Master Plan, the City Council also adopted a resolution approving the establishment of the permanent BPAC as well as approving the list of recommended appointees.

IMPLEMENTATION ACTIONS AND CONCLUSIONS

City staff called for the first permanent BPAC meeting on Tuesday, June 14, 2011 to follow up some ongoing bicycle and pedestrian projects in the City and in the countywide region. By following an established table of the High Priority Bicycle and Pedestrian Projects from the Master Plan (see Table 1), City staff has also tapped internal funds and external grants to implement as many high priority projects as possible from the list. This includes the installation of bicycle racks, accessible pedestrian signals and accessible pedestrian ramps; sponsoring the Bike-to-Work Day events, and featuring capital improvement projects like San Leandro Boulevard Bay Area Rapid Transit (BART) Pedestrian Interface Plan.

Updating the Bicycle and Pedestrian Master Plan every four to five years is crucial for the City of San Leandro. Through team work between City staff, concerned public members, the BPAC members, and consultants, a well documented Bicycle and Pedestrian Master Plan guides the City to make wise and efficient decisions on the bicycle and pedestrian related projects.

Table 1: High Priority Bicycle and Pedestrian Projects – 5-Year Expenditure Plan				
Committed Measure B Pass-Through and TDA Funding				
Type	Project #	Project	Limits/Location	Estimated Cost^a
Bike		Bike-to-Work Day	citywide program	\$25,000
Bike	CW-2	City Bike Rack Program	citywide program	\$50,000
Ped		Pedestrian accessible and safety equipment	citywide program	\$75,000
Ped		Accessible pedestrian ramps	citywide program	\$150,000
Ped	B-5.b	San Leandro Blvd BART Pedestrian Interface Plan (matching funds)	at Downtown San Leandro BART Station and surroundings	\$75,000
Ped	B-5.a	West Juana Ave redesign (matching funds)	at Downtown San Leandro BART Station and surroundings	\$50,000
Other Measure B Pass-Through Funding				
Both		Education programs	citywide program	\$100,000
Both	B-8	Hesperian Blvd Railroad Crossing improvements (matching funds)	Hesperian Blvd/Niles Subdivision railroad crossing	\$25,000
Bike	CW-1	Spot Improvements	citywide	\$50,000
Bike	34-1	Juana Avenue bike route	Grand Ave to San Leandro Blvd	\$9,360
Bike	60-1	Fairmont Dr-Halcyon Dr bike lanes	East 14th St to Washington Ave	\$53,600
Bike	60-2	Floresta -Farnsworth bike route	Fremont Ave to Vining Dr	\$36,200
Bike	58-1	Manor Blvd bike route	Norton St to Wicks Blvd	\$19,000
Ped	B-7.a	Dutton Ave/Bancroft Ave Intersection	Dutton Ave/Bancroft Ave Intersection	\$150,000
Ped	B-4.b	Manor Boulevard crosswalks	various locations	\$9,000
Ped	B-7.c	Bancroft Ave crosswalks	Dutton Ave to Callan Ave	\$3,000
Ped	C-1	Garfield Elem. School access	Marina Blvd	\$60,000
Ped	C-12	McKinley Elem. School access	East 14th St and Bancroft Ave	\$2,000
Ped	C-3	Cherry Grove Park access	Leonard Dr and Williams St	\$120,000
Ped	C-6	Bonaire Park access	Juniper St midblock crossing	\$20,000
Competitive Funds				
Both	5-2	Marina Park Trail	Fairway Dr to Estudillo Canal	\$337,500
Both	B-7.b/25-2	Bancroft Ave/136th Ave	Bancroft/136th Ave intersection	\$434,000
Bike	30-2	Davis St bike lanes	East 14th St to Alvarado St	\$34,400
Bike	33-1	East 14th Street Bike corridor feasibility study East 14th Street bike route	north to south city limits	\$150,000 \$103,200
Bike	70-1	Lewelling Blvd bike lanes/route	east city limits to Sedgeman St	\$30,600
Bike	30-1	Estudillo Ave bike route	east city limits to MacArthur Blvd	\$20,200
Ped	C-18	Jefferson Elem. School access	Bancroft Ave midblock crossing	\$100,000
Ped	C-9	Corvallis Elem. School access	Corvallis St intersections	\$100,000
Ped	B-10.a	Pedestrian access to Anthony Chabot Park	MacArthur Blvd to Anthony Chabot Park	\$200,000

China's Transportation Balancing Development Strategy Discussion

GENG Rui

Research Institute of Highway Ministry of Transport, No.8 Xi Tucheng Road, Beijing, China, 100088, E-mail: gr970207@163.com, Phone: 86-186111319033, Fax: 86-01-62079145-8199

ABSTRACT

This article analyzed the issue over two kinds of transportation development strategy in recent days. Illustrated the comprehensive background and faced challenges. Consequently, to come up with five overall development strategies, which are “Coordinated development of various modes of transport,” “Coordinated development of urban and rural regional transportation,” “Overall coordination of traditional freight forwarding and logistics development,” “Overall coordination of transportation and the development of resources and the environment,” and “Overall coordination of transportation construction and development services.” The key for transportation development could be conclude in five aspects, which are “Traffic structure Optimization and in service capabilities improvement,” “Modern passenger transport development and of service quality improvement,” “Traditional freight forwarding transformation and modern logistics development,” “Development mode Changing and of green traffic building,” and “Public administration Strengthen and services improvement.”

TRANSPORTATION DEVELOPMENT STRATEGIES

Based on our overall analysis of the situation at home and abroad, to sum up to take the two major transportation development strategic plans: one is the supply and demand balance model, the other is quality & benefit. In general, a country to realize the process of industrialization, transportation industry's main task is to meet the social economic development in the number needs to expand the transportation infrastructure scale and enhance the transport capacity as the key point, the connotation of the development strategy of the more embodied in the quantity and transportation capacity of the balance of supply and demand. As the social economy into a new stage of development, to transportation demand from mainly displays in quantitative surface quality of gradually more now, on the transportation industry requirements from growing improve transport capacity for change in the gradually improve the service level of the transportation is given priority to, in the development

and at the same time also more attention to traffic safety, resource-saving and environmentally-friendly , with the development of quality and efficiency, and toward to the intelligent transportation system development, at present, the developed countries of the transportation development strategy is clearly reflected on this characteristic.

CHINA'S TRANSPORTATION CHALLENGES

21st century is an important period to accomplish modernization, by the 2020s-2030s will complete the historical mission of industrialization, by the middle of the 21st century will reach the level of moderately developed countries at that time. The 12th Five-Year Plan, China is now in a new stage of building a well-off society, industrialization, informatization, urbanization, and speed up the process of market, the countries to speed up the transformation of the mode of economic development as the thread of the development, the economy continued to maintain growth, the economic structure speed up adjustment, escalating consumption structure, urban and rural area tends to coordinate, the market demand potential is tremendous, economic and social development to good long-term trends will no change.

The economic and social development for transportation demand from "go, transport" to "go well, and transport well" upgrade, not only requires the continuous improve transportation ability, but also demand more rapid ascent transportation service level, better service to economic and social development, China transportation go into a new stage of development.

On the other hand, the problems of land resources, energy and environment began to highlight, become a major factors restricting the development of transportation; Some of the traffic development profound question also gradually appear, traffic and economic and social development face as many new challenges. Mainly displays in: one is the transportation development need to take the land, land is more prominent contradiction. second is greatly increased traffic energy consumption, and increased energy nervous conditions. Third is a traffic pollution emission continued to increase, the environmental problems. Fourth is the highway transportation problem serious overloading overload, transport service quality is not high. Fifth is traffic development policy adjustment and reform of mechanism of system lags far behind, especially highway (including highway) management system, the highway maintenance system, urban and rural integration system and the toll road traffic system, the system of investment, administrative management system reform is in the crucial stage, and affects social harmony.

CHINA'S TRANSPORTATION DEVELOPMENT

Above all, as the transportation infrastructure and expansion of the size of the traffic and transport development need to pay more attention to the progress of science and technology and innovation, pay more attention to improving the efficiency of transportation, pay more attention to and resources environment harmonious, pay more attention to the quality and efficiency of ascension. In The 12th Five-Year Plan and for a time, China transportation development needs to take "adaptive development strategy" and "quality first development strategy," combining the strategy, which is "coordinated development" strategy, and reflect in the following five aspects:

Coordinated development of various modes of transport

Construction is distinct, layout, reasonable structure optimization and the function is perfect infrastructure network, constructing the rational division, complementary advantages, cooperation, the competition order integrated traffic system.

Coordinated development of urban and rural regional transportation

Establish fast passenger, main passenger, rural passenger transportation, tourist transportation and other components of the urban and rural areas to join each passenger the levels of passenger transport network system, provide large capacity, high efficiency, low cost, low pollution, good quality and safety public passenger service.

Overall coordination of traditional freight forwarding and logistics development

Transform and upgrade traditional freight industry, forming convenient to modern logistics service is the characteristic of freight transportation network, realize the traditional transportation outstanding "transport" to modern logistics of all-round service change.

Overall coordination of transportation and the development of resources and the environment

With resource conservation and environment friendly as the main line, through the optimization of industrial structure and improving the quality of development, the economical and intensive utilization of resources and achieve the development way of relies mainly on the extension of the material consumption to rely on scientific and technological progress, the extensive worker quality improve and promote conservation of resources environment friendly connotation intensive economy, realize the harmonious development of traffic and natural environment.

Overall coordination of transportation construction and development services

Set up the traffic intelligent comprehensive information service and operation management system, the realization of the electronic government affairs office automation system, constructing the benefit of the traffic public service system, and achieve a wider coverage, higher level service, easy to go.

KEY TASKS**Traffic structure Optimization and in service capabilities improvement**

As a whole infrastructure construction, maintenance and transport service coordinated development. Strengthen the weak links transportation infrastructure construction, improving infrastructure operation maintenance level, guide transportation service constantly optimize the structure, in developing realization structure adjustment, realize the effective utilization of resources, promote the coordinated development of the comprehensive transportation. [1]

Modern passenger transport development and of service quality improvement

Establish standard management, safety is convenient, service quality, due consideration to fairness and personalized needs passenger service system. Strengthen the mode of transportation of the close cohesion and cooperate, gradually realize "zero distance change". Guide traffic consumption idea, advocated bus priority, to provide a safe, efficient, high quality, the environmental protection public passenger service. Break passenger transportation in the urban and rural management system division, make tax concessions, financial subsidy policy, and standard passenger market, promote integrated passenger transportation in the urban and rural process.

Traditional freight forwarding transformation and modern logistics development

Transport is an important foundation of the development of modern logistics, the traditional freight industry should seize the opportunity to develop logistics service function, improve the transportation of specialization and socialization service level, to adapt to the needs of the development of modern service industry. Based on the market, with assets of the link, through the assets reorganization and corporations reforming way, cultivating and guide to build a few with strong competitiveness of large transportation company or group, guide transportation enterprise will purchase, manufacture, transportation, warehousing, agency, distribution, packing the processing, the sale, the information processing in the organic link in series with the positive development of the third party logistics services, consists of a single road transport carrier to modern logistics operator conversion[2]. Guide to small and

medium-sized transport enterprise "specialized, fine, special and new" direction, satisfy the transport demand.

Development mode Changing and of green traffic building

To save and intensive utilization of natural resources and protect the ecological environment as the main line, the energy conservation and environmental protection implement to traffic every level of development and each link, realize the transportation development and natural ecological harmony. Implementation of the country's most strictest arable land protection policy, realize the comprehensive utilization of land transportation, highway construction must give priority to choose to be able to maximize saving land, protect arable land scheme, and port construction should be of the economical and intensive utilization of resources, and improve the comprehensive use of coastal resources of efficiency. Deepening the circular economy development ideas, follow the "reduce, reuse and recycling" principle, and actively explore the transportation of circular economy effective way[3]. Positive promotion application traffic energy saving new technology, new techniques and new equipment, and gradually eliminate production facilities and equipment, promote transportation technology and equipment structure upgrade. Strictly carries out the ecological protection, soil and water conservation and Marine environmental protection laws and regulations, completes the planning and construction projects of environmental impact assessment, practically the environmental protection and supervision measures to implement the traffic planning, design, construction, operation of the entire process, strengthen the construction of the environmental protection and ecological restoration

Public administration Strengthen and services improvement

Transform the government functions, strengthen the public service and industry management, perfect transportation service standard, form a unified and open competition transport market, create the market environment of fair competition. Actively using expert consultation, social public, hearing and press release system, improve the transparency of the public participation and decision making, enhance the scientific decision, democratic decision-making, according to law, and the power of the decision-making level. To speed up the development of traffic electronic government affairs, the perfect traffic statistics system and statistical system and improve the efficiency of traffic administration. Make and improve the transport public emergencies emergency plan and emergency system, speeding up the traffic emergency platform construction, reinforce the traffic emergency team construction, and establishing a rapid and efficient emergency response system and improve the ability to cope with sudden public events. It can advance gradually realized, completes the various measures; Matter can control, timely response, rapid disposal; To settle up one's affairs in a sensible way, eliminate

future trouble and influence.

REFERENCES

- [1]YE Long, and WANG Yuee.(2007). “Analysis of Developing Trend of Hierarchy for Comprehensive Transportation in Our Country.” *J. Northern Communications*, Dec,88-89.
- [2]JIN Ling, and HE Ming, WU Cairui, et al. (2010). “A Model for Analyzing Interaction between Regional Comprehensive Transport System and Economic Development.” *J. Journal of Highway and Transportation Research and Development*, May.27,127-131.
- [3]SHI Baolin, OUYANG Bin, LI Zhongkui, et al. (2010). “Resource efficient and Environment-friendly Transport Development Policy in China.” *J. Journal of Highway and Transportation Research and Development*, Jun.27,154-158.

Comprehensive Evaluation Model for Programming Projects of Traffic Infrastructure Based on Rough Set

Jiang Shan¹, Liu Weiming², and Shi Ling¹

¹Highway Traffic Development Research Center, Research Institute of Highway Ministry of Transport, Beijing 100088, China; PH 010-62079745, 13521649368; Email: shan.jiang@rioh.cn

²School of Civil and Transportation Engineering, South China University of Technology, Guangzhou 510640, China; Email: mingweiliu@126.com

ABSTRACT

It's worthwhile to make an intensive study as to how to choose the programming project which can meet the requirements of traffic sustainable development, also can achieve harmonious development of social economy, resources and environment and traffic infrastructure construction. In this paper, the comprehensive evaluation model of traffic infrastructure planning is formed based on rough set. Firstly the indexes system regarding to attributes of technology, economy, environment and society is formed. Then reserving the classification ability, the attributes and their weights are determined by reduction and significance computation according to rough set theory, so the indexes system is reduced efficiently, the subjectivity in weight assignment is also eliminated and therefore the performance of programming projects is reflected more exactly and objectively. The result of the comprehensive evaluation of one logistics park site selection scheme shows this method is scientific, effective and feasible.

INTRODUCTION

It's essential to consider many factors such as technology, economy, environment and society ones to traffic infrastructure planning. Nowadays sustainable development is becoming the common understanding all over the world, so it's more and more important to evaluate the programming projects of traffic infrastructure subjectively and correctly so that reliable decision-making consultation can be given to government and investors.

There are four major comprehensive evaluation methods at present including evaluation by experts, evaluation by using operational research or other mathematical tools, evaluation by using new tools such as neural network or grey theory, and evaluation by hybrid method in which two or more tools above mentioned are used.

These methods have been employed to tackle many problems widely. For example, Wu (2002) has adopted grey theory to make decision on line schemes selection ; Zhang (2005) has used hybrid method of AHP and DEA in location of logistics distribution centre ; Ren (2010) has made use of Fuzzy knowledge in analysis of logistics distribution centre location ; Wu (2011) has employed fuzzy neural network on evaluation of complex product development decision.

To choose proper indexes, decide these indexes' weights and build an assessing mathematical model are the major steps of comprehensive evaluation, especially how to compute the indexes' weights is more difficulty. These traditional methods have some inherent defects in weight assignment so that evaluation and decision-making by them often is less objectively and exactly.

A recently developed mathematical method based on the rough set theory has been applied to decision support, mode identification, knowledge discovery and data mining from large data sets (Bazan, 2003). This method can deal with uncertain, incomplete and imprecise data. The advantage is that knowledge acquisition is driven completely by data and it does not have artificial hypotheses, compared with traditional methods. It is more scientific, more impersonal and easier to use (Herbert, 2009). In this paper the comprehensive evaluation model of traffic infrastructure planning is formed based on rough set. Firstly the indexes system including technology, economy, environment and society factors is established, then the indexes' weights are decided by using rough set. The weight assignment by doing so is more reasonable and reliable, and the method is easier and more applicable. The example of the decision evaluation of one logistics park site selection scheme in the end shows this method is feasible and effective.

COMPREHENSIVE EVALUATION METHOD BASED ON ROUGH SET

The theory of rough set was put forward by Z.Pawlak of Poland Scholar in 1982. It is a valid tool that deals with data of imprecise, uncertainty and incompleteness. Specifically, it is used to knowledge reduction on the premise of classification ability invariable of information system and reduces the decision-making and classification rules by the reduction of attributes.

The basic theory of rough set

Set Approximations.

Let a finite set of objects U and a binary relation $R \subseteq U \times U$ be given. The sets U , R are called the universe and an indiscernibility relation, respectively. A pair (U, R) is called an approximation space, where U is the universe and R is an equivalence relation on U . Let X be a subset of U , i.e. $X \subseteq U$.

The set of all objects which can be with certainty classified as members of X with respect to R is called the R -lower approximation of a set X with respect to R , and denoted by $\underline{R}(X)$, i.e. $\underline{R}(X) = \{x : R(x) \subseteq X\}$.

The set of all objects which can be only classified as possible members of X with respect to R is called the R -upper approximation of a set X with respect to R , and denoted by $\overline{R}(X)$, i.e. $\overline{R}(X) = \{x : R(x) \cap X \neq \emptyset\}$.

The set of all objects which can be decisively classified neither as possible members of X nor as members of $-X$ with respect to R is called the boundary region of a set X with respect to R , and denoted by $RN_R(X)$, i.e.

$$RN_R(X) = \overline{R}(X) - \underline{R}(X).$$

Then the definition of the rough set notion can be formulated as follows:

A set X is called crisp (exact) with respect to R if and only if the boundary region of X is empty.

A set X is called rough (inexact) with respect to R if and only if the

boundary region of X is nonempty.

Reduction of Attributes

Let $S = (U, A)$ be an information system, $B \subseteq A$, and let $a \in B$.

If $IND_S(B) = IND_S(B - \{a\})$, a is dispensable in B ; otherwise a is indispensable in B . A set B is called independent if all its attributes are indispensable.

Any subset B_1 of B is called a reduct of B if B_1 is independent and $IND_S(B_1) = IND_S(B)$.

Hence, a reduct is a set of attributes that preserves partition. It means that a reduct is the minimal subset of attributes that enables the same classification of elements of the universe as the whole set of attributes. In other words, attributes that do not belong to a reduct are superfluous with regard to classification of elements of the universe.

There are usually many reducts. The *Core* of B is the set of all indispensable attributes of B , i.e. $Core(B) = \bigcap Red(B)$, Where $Red(B)$ is the set of all reducts of B . Obviously the core is the intersection of all reducts, it is included in every reduct, i.e., each element of the core belongs to some reduct. Thus, the core is the most important subset of attributes, for none of its elements can be removed without affecting the classification power of attributes.

Significance of Attributes

The significance of an attribute can be evaluated by measuring the effects of removing this attribute from an information system.

In information system $S = (U, A)$, $A_1, A_2 \subseteq A$, let $a \in A_1$, then the significance of attribute a is defined by the following formula:

$$K_a = (|POS_{A_1}(A_2)| - |POS_{(A_1 - \{a\})}(A_2)|) / |U| \quad (1)$$

Where $POS_{A_1}(A_2)$ is a positive region of the partition U / A_2 with respect to A_1 .

Procedure of comprehensive evaluation based on rough set

Step 1 : Establishment of initial indexes system. Let $U = \{a_1, a_2, \dots, a_n\}$ is the set of the assessing subjects, and $R = \{R_1, R_2, \dots, R_n\}$ is the set of selected attributes. All indexes of attributes can be characterized qualitatively or quantitatively.

Step 2 : Discretization of attributes. The classic rough set theory can't deal with data containing continuous features, so discrete processing of continuous data is necessary to gain knowledge. There are many algorithm of discretization like K-means algorithm, interval method and greedy algorithm and so on.

Step 3 :Reduction of Attributes. After discrete processing of attributes, the set of attributes R can be processed according to reduction concept and a core can be found. Let the set of attributes after reduction be $Q = \{Q_1, Q_2, \dots, Q_t\}$.

Step 4 : Calculation of weights. According to the formulation of significance, the significance of attribute Q_s can be calculated and denoted as k_s , then W_s (weight of Q_s) can be calculated as follows:

$$W_s = \frac{k_s}{\sum_{i=1}^t k_i} \quad (2)$$

Step 5 : Comprehensive evaluation. At last, all assessing subjects in the set of U can be evaluated comprehensively by using the linear weighting method.

INDEXES SYSTEM OF TRAFFIC INFRASTRUTURE PLANNING EVALUATION

It's properly to evaluate traffic infrastructure planning according to the following principles: comprehensive, scientific, comparability, maneuverability, combining qualitative analysis and quantitative analysis. In this paper an indexes system regarding to technology, economy, environment and society is established to evaluate programming project of traffic infrastructure.

Indexes of technique evaluation. Technical indexes are the most direct form of performance of planning projects, and these indexes include line length or speed of highway, total length of urban rail transit network, and geographic conditions of logistics park and so on.

Indexes of economic evaluation. These indexes are so many, such as construction cost, land expropriation compensation prices, manpower cost, revenue financial net present value, internal rate of return and investment payback period, etc.

Indexes of environmental evaluation. Due to the construction and operation of traffic infrastructure, it will cause some unavoidable problems: environmental pollution, atmosphere deterioration and noise pollution and so on. For us to be sustainable development, mitigation methods should be proposed to solve or alleviate these problems.

Indexes of social evaluation. Most programming projects of traffic infrastructure have large investment, long instruction period, many questions involved, a wide range and long-term of impacts. For traffic infrastructure, analysis of social evaluation refers to the influence or benefit of planning projects to social economy, social development, natural resources utilization, social environment and natural eco-environment and so on. For instance, the social evaluation of programming expressway or logistics park is related to many aspects such as their impact on the regional economy development and land development, people's life and work, maintaining social stability and economic security, etc.

EXAMPLES

In this section the comprehensive evaluation of one logistics park site selection scheme is showed as to the establishment of the indexes system and the procedure of evaluation based on rough set.

Many factors should be taken into consideration about logistics park site selection. For example, logistics park is ideally located near source of goods like industrial park or warehouse district, or located as close to traffic trunk road as possible; site selection scheme of logistics park should not only meet the requirements of cargo flow, cargo owner and goods owner, but also should minimize the impact on city traffic, environment and people's life; also the park

should be fully furnished with facilities as water supply and drainage, power supply, traffic road, pollution discharge, etc. In short, logistics park site selection scheme can be evaluated in terms of technology, economy, environment and society factors. In its plan there are 6 sites among which one should be chosen as the most suitable for the logistics park after comprehensive evaluation. The major indexes are as follows:

Technical assessing indexes: R_1 -project conditions ; R_2 -existing infrastructures ; R_3 - regional position.

Economic assessing indexes: R_4 -cost of unit land area (Yuan/m²) ; R_5 -construction cost(Yuan/m²) ; R_6 - manpower cost (ten thousand Yuan /year-person).

Environmental assessing indexes: R_7 -pollution levels; R_8 -connection with freight access.

Social assessing indexes: R_9 -ability of economic radiation to local and hinterland area ; R_{10} -ability to promote employment and increase taxes; R_{11} -effect on land value increment ; R_{12} -influence on local traffic.

There are 12 indexes of attributes and 6 objects be assessed in sum, so the universe $U = \{A, B, C, D, E, F\}$ which contains the 6 locations selected, and attributes set $R = \{R_1, R_2, R_3, R_4, R_5, R_6, R_7, R_8, R_9, R_{10}, R_{11}, R_{12}\}$ which contains 12 attributes. Qualitative analysis and quantitative attributes are shown as table 1. It's obviously that only attributes of economic indexes are quantitative and the rest attributes are of qualitative.

After data discrete processing of economic indexes, table 2 shows the values of all attributes after discretization. The number 3, 2, 1 in this table mean low, moderate, high respectively as to economic attributes, and better, moderate, bad as to the rest attributes.

For data of line 1 and line 5 in table 2 are identical completely, and so do the data in line 10 and line 11, then line 5 and line 11 can be deleted from table 2. After table 2 is simplified, it can be reduced by rough set knowledge for the data in table 2. Since $U / IND(R) \neq U / IND(R - R_3) \neq U / IND(R - R_7) \neq U / IND(R - R_9)$, then the core of all attributes is $core(\{R\}) = \{R_3, R_7, R_9\}$. New indexes system is shown in table 3.

Let $C = \{R_3, R_7, R_9\}$, significance of the three attributes can be calculated.

For R_3 , since $U / IND(C) = \{\{A\}, \{B\}, \{C\}, \{D\}, \{E\}, \{F\}\}$,

$$U / IND(C - R_3) = \{\{A\}, \{B, D\}, \{C\}, \{E\}, \{F\}\},$$

Then $sig(R_3) = \frac{6-5}{6} = \frac{1}{6}$. In the similar way, $sig(R_7) = \frac{2}{6}$, $sig(R_9) = \frac{2}{6}$.

Thus the weights of the three attributes can be calculated:

$$weight(R_3) = \frac{1}{1+2+2} = 0.20, \quad weight(R_7) = weight(R_9) = \frac{2}{1+2+2} = 0.40.$$

At last the comprehensive evaluation of the six locations can be calculated by using linear weighting method. The result and ranking is shown in table 4.

According to the table 4, ranking of scheme F is the highest, so F is the best location of logistics park according to the comprehensive evaluation based on rough set.

Table 1. Qualitative or quantitative analysis of attributes.

1-level indexes	2-level 1	A	B	C	D	E	F
Technical indexes	R_1	moderat	better	moderat	better	moderat	moderat
	R_2	better	moderat	better	moderat	better	better
	R_3	bad	better	moderat	moderat	bad	moderat
Economic indexes	R_4	600	800	700	700	600	700
	R_5	800	600	700	600	800	750
	R_6	9.0	8.5	7.5	8.5	8.5	7.5
Environmental indexes	R_7	high	moderat	low	moderat	moderat	low
	R_8	moderat	moderat	better	moderat	moderat	better
Social indexes	R_9	better	moderat	bad	moderat	better	moderat
	R_{10}	better	moderat	moderat	moderat	better	moderat
	R_{11}	better	moderat	moderat	moderat	better	moderat
	R_{12}	moderat	moderat	bad	moderat	moderat	bad

Table 2. Result after data discrete processing.

1-level indexes	2-level indexes	A	B	C	D	E	F
Technical indexes	R_1	2	3	2	3	2	2
	R_2	3	2	3	2	3	3
	R_3	1	3	2	2	1	2
Economic indexes	R_4	3	2	2	2	3	2
	R_5	2	3	2	3	2	2
	R_6	1	1	2	1	1	2
Environmental indexes	R_7	1	2	3	2	2	3
	R_8	2	2	3	2	2	3
Social indexes	R_9	3	2	1	2	3	2
	R_{10}	3	2	2	2	3	2
	R_{11}	3	2	2	2	3	2
	R_{12}	2	2	1	2	2	1

Table 3. New indexes system after reduction

	R_3	R_7	R_9
A	1	1	3
B	3	2	2

Table 4. Result of evaluation

	Locations	Total grade	Ranking
A	A	1.80	4
B	B	2.20	2

C	2	3	1	C	2.00	3
D	2	2	2	D	2.00	3
E	1	2	3	E	2.20	2
F	2	3	2	F	2.40	1

CONCLUSIONS

In this paper the indexes system for comprehensive evaluation of traffic infrastructure planning is established regarding to technology, economy, environment and society, considering the requirements of traffic sustainable development, harmonious development of social economy, resources and environment and traffic infrastructure construction. The indexes system and their weights are determined by reducing the original selected indexes and computing the significance of every index according to rough set theory, so the indexes system is reduced efficiently. Then the comprehensive evaluation of the programming project can be calculated by using linear weighting method. An example of one logistics park location selection is illustrated to show how to evaluate comprehensively according to the indexes system and rough set theory. The result shows this method is effective to eliminate the subjectivity in weight assignment and so it is more simple, scientific and feasible.

REFERENCES

Bazan, J., Peters, J.F., Skowron, A., Nguyen, H.S., M., Szczuka, M. (2003).“Rough set approach to pattern extraction from classifiers.”*Electronic Notes in Theoretical Computer Science*, 82(4), 20-29.

Herbert, J.P. and Yao, J.T. (2009).“Criteria for choosing a rough set model.”*Computers and Mathematics with Applications*, 6, 908-918.

Pawlak Z. “Rough Sets.”*International Journal of Computer and Information Science*, 1982, (11): 341-356.

Ren Yongchang, Xing Tao, Zhao Guoqiang (2010). “Fuzzy decision analysis on logistics distribution centre location plan.”*Journal of Liaoning Technical University*, 29(3):517-520.

Wu Xiaoping, Chen Xiufang (2002). “A grey optimal selection model and its application in multiobjective decision making of line schemes.”*Theory and practice of systems engineering*, 22(7):101-105.

Wu Yanxun, Qin Xiansheng, Zhang Haifeng (2011).“Development decision evaluation method of complex product based on fuzzy neural network.”*Chinese Journal of Management*, 33(7):1575-1579.

Zhang Min, Yang Chao, Yang Jun (2005). “Location of logistics distribution centre based on AHP/DEA.”*Chinese Journal of Management*, 2(6):641-644.

Travel Characteristics of Different Social Groups in Large Scale Residential Areas in the Periphery of Shanghai: A Case Study of Jinhexincheng

Jinping GUAN

School of Transportation Engineering, Tongji University, Shanghai, China. Phone: (86)15216706980, Email: guanjinping.jenna@gmail.com

ABSTRACT

Shanghai is in the process of urban redevelopment. In order to reform old downtown and improve living conditions, poor houses are demolished and the government relocates the residents. Usually they are relocated in large scale residential areas in the periphery of Shanghai. Jinhexincheng is one of them. Data is collected through a random sampling survey. The study is conducted with two main social groups: workers (representing commuters) and the elderly (representing non-commuters). Results show that a large proportion of workers commute across districts while the elderly often travel inside the district. The logistic regression model is suggesting the most important factor that causes cross-district commuting is education. Mode choice and morning departure time are different between the workers and the aged. Compared to the world average commuting time (40 minutes), Jinhexincheng's commuting time is quite long. The results suggest that transportation planning must consider travel needs of different social groups.

INTRODUCTION

Over the past decade, Chinese cities have undergone enormous spatial restructuring due to the economic growth and urban development. Shanghai is an important one of them.

Nowadays, Shanghai is in the process of suburbanization. Urban residents rapidly migrate to the periphery area. Some movers have relocated willingly to modernized housing or for other lifestyle reasons (*1*). Some movers have chosen to live in the periphery because of the unacceptable high price of housing or rising urban rents in downtown. Others have to move outside the center as a result of the urban houses demolition and relocation.

Urban houses demolition and relocation is a part of urban redevelopment in Shanghai. In order to reform the old downtown area and improve the living conditions, old and poor houses are demolished and the government relocates the residents. Usually they are relocated in large scale residential areas in the periphery

of Shanghai. The case area in this paper named Jinhexincheng which is located in Jiading District of Shanghai is this kind of residential area in the periphery.

STUDY FOCUS AND SURVEY DATA

Study Focus

In this study, different social groups are decided according to the population pyramid, socioeconomic characteristics of the residents and travel characteristics in Jinhexincheng. Each social group's travel characteristics are studied in the following three aspects: travel purpose and destinations, travel mode choice and departure time and one-way-travel time. Travel characteristics of different social groups in large scale residential areas in the periphery of Shanghai (case in Jinhexincheng) are studied in this paper in order to support transit/transportation planning in this kind of area.

Survey Site: Jinhexincheng, Shanghai, China

Jinhexincheng is a residential community located to the northwest of downtown Shanghai (Figure 2). It is situated outside of the Outer Ring which is the border between Shanghai central city and suburbs. Jinhexincheng consists of ten housing projects. Eight of them are for central city relocated residents and the other two are commercial housing. Jinhexincheng has limited retail shopping and only a few small grocery stores at the time of the survey. The area has no metro service and conventional buses connect residents to the central city.

Sampling Approach and Survey Data

The survey was during November and December in 2010. Field survey (for on-site transport conditions), questionnaire survey and interviews with residential committees and residents were used. A random sampling approach was adopted for conducting this research. Above 16-year-old residents in Jinhexincheng were asked to complete a self-reported survey on travel behavior and personal attributes. 14008 invitations were posted, 613 persons replied and 324 effective samples were collected.

When samples are more than 269, probability of probable error within ± 0.05 is 90% (3)(4). Therefore more than 269 samples can support data analysis. 324 effective samples are enough for the analysis in this study.

SEPARATING PEOPLE INTO DIFFERENT GROUPS

After the invalid or incomplete records were deleted, the final sample included a total of 324 observations. According to age and gender, the population pyramid of Jinhexincheng is obtained (shown in Figure 1). It shows that 21-30-year-old people and 51-65-year-old people are the two main social groups.

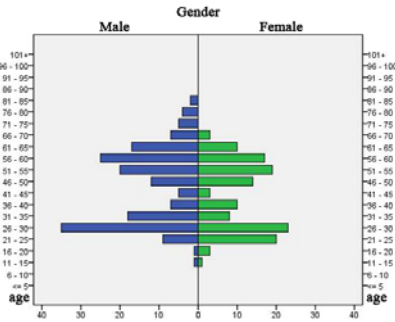


Figure 1. Population pyramid of Jinhexincheng.

Considering the population pyramid of Jinhexincheng, socioeconomic characteristics of residents (age, occupation, educational background, hukou (registered permanent residence or not) and home-ownership) and travel characteristics, two main social groups come out: the workers (representing commuters) and the elderly retired (representing non-commuters).

TRAVEL CHARACTERISTICS OF DIFFERENT SOCIAL GROUPS

Travel Characteristics of Workers

(1) Travel Destinations and Cross-district Commuting Factors

Workplace is obviously the destination of a worker. Result shows that workplaces which are located inside Jiading District take 27.4%, while outside of it take 72.6%. The destinations of workers are shown in Figure 2. Outside of Jiading District, the top three commuting destinations are Putuo, Changning and Jing’an District.



Figure 2. Desire Line Map of the Workers

Since 72.6% of commuters travel across district to work, logistic regression model is used to find out the most effective factor which causes cross-district commuting. We input gender, age, hukou, home-ownership, years of living here,

possession of a driver’s license, household structure and education as all factors. Among these factors, the most important one is education. Table 1 below shows that higher educated people tend to do cross-district commuting.

TABLE 1 Results of Logistic Regression Model

	B	S.E.	Wald	df	Sig.	Exp(B)
Hukou	1.010	0.458	4.862	1	0.027	2.744
Years of Living Here	-0.220	0.134	2.685	1	0.101	0.803
Education	0.684	0.219	9.783	1	0.002	1.982
Constant	-0.195	0.758	0.066	1	0.797	0.823

(2) Travel Mode Choice

In Jinhexincheng, there are 8 regular types of travel means (walking, bicycles, motorcycles or mopeds, company shuttle buses, buses, the metro, taxis and private cars) and 2 special travel means (illegal cars or motorcycles and supermarket shuttle buses). Workers’ commuting mode choices are shown in Figure 3.

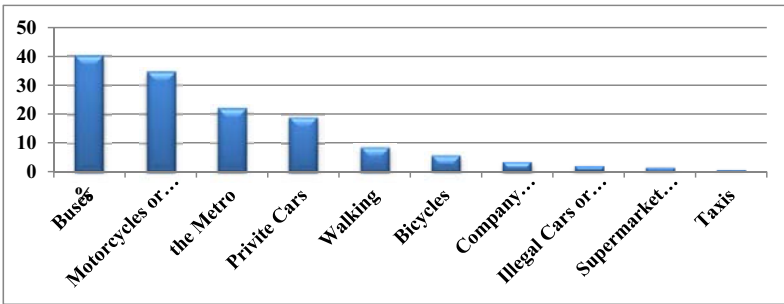


Figure 3. Workers’ Commuting Mode Choices

(3) Departure Time and One-Way-Travel Time

Workers’ departure time of morning in Jinhexincheng is earlier than morning peak in Shanghai city center.

To travel one way, 40% of workers need 30-60 minute while 33% of them need over an hour. Average commuting time is over an hour. The world average commuting time is 40 minutes. This is the average for people that work (7). People in Beijing spent 38 minutes on average to get to work under normal traffic conditions, the longest among 50 mainland cities, according to a report released by the Chinese Academy of Sciences (CAS) in 2011. Shanghai and Guangzhou ranked second, both with 36 minutes of commuting time on average. Typical commuting time in Beijing taking traffic congestion into account was 52 minutes. However, in Jinhexincheng, it is even longer. No wonder 44% of workers find the commuting time unsatisfied. The

commuting condition needs improvement.

Travel Characteristics of the Elderly

(1) Travel Purpose and Destinations

Shopping is the most-often travel purpose. Unlike commuters, 54% of the elderly often travel inside Jiading District while 46% often go to other districts. Among these districts, Putuo District gets the most visiting. This might because 52% of the elderly in Jinhexincheng used to live in Putuo District before they moved here.

(2) Travel Mode Choice

94% of the elderly have no driver's licenses. To workers, buses, motorcycles or mopeds, the metro and private cars are the popular mode choices. However, to the aged, buses, the metro, supermarket shuttle buses and walking are the popular choices. Detail percentage is shown in Figure 4.

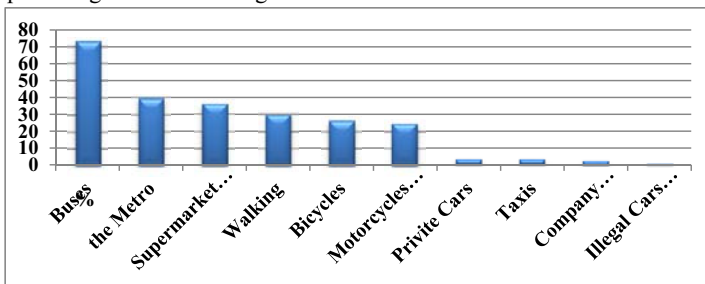


Figure 4. Travel Mode Choices of the Elderly

(3) Departure Time and One-Way-Travel Time

The morning departure time of the elderly is later than the workers'. And in the afternoon, there are aged people starting to travel as well, usually it is before 15:00. The departure time of workers and the elderly is shown in Figure 5.

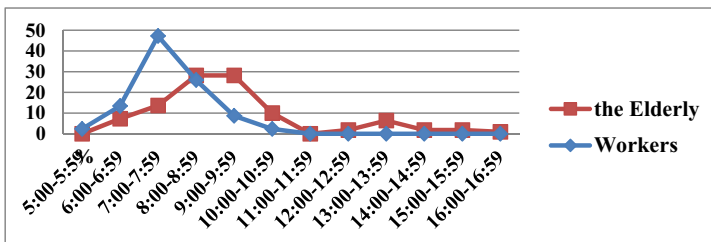


Figure 5. Departure Time of Workers and the Elderly in Jinhexincheng

Compared to workers, more elderly people travel less than 30 minutes to get to the destinations. And more elderly people travel more than two hours because of the long distance to hospitals. 15% of the aged find the travel time satisfied, 40% of

them think it is “so so” and 45% of them are unsatisfied with it.

CONCLUSION

Shanghai is in the process of urban redevelopment in which urban houses demolition and relocation play an important role. In order to reform the old downtown area and improve the living conditions, old and poor houses are demolished and the government relocates the residents. Usually they are relocated in large scale residential areas in the periphery of Shanghai. Jinhexincheng which is located in Jiading District of Shanghai is this kind of residential area in the periphery.

Considering the population pyramid, socioeconomic characteristics of residents (age, occupation, educational background, hukou (registered permanent residence or not) and home-ownership) and travel characteristics, two main social groups come out: the workers (representing commuters) and the elderly retired (representing non-commuters).

48% of residents are workers in Jinhexincheng. It is one of the main social groups here representing commuters. 45% of workers are relocated here from Shanghai central city because of urban houses demolition and relocation, 27% of them rent or buy apartment here because it is close to workplace and 24% of them live here due to the acceptable housing price.

35% of residents are the elderly and retired in Jinhexincheng. It is another main social group here representing non-commuters. Among the elderly and retired, 82% of them are relocated here from Shanghai central city because of urban houses demolition and relocation, the others rent or buy apartment here either due to the acceptable housing price or because it is close to their family's workplace.

The travel characteristics of the two social groups (the workers and the elderly retired) are studied. Results show that:

(1) Travel purpose and destination

The workers' most-often-happen trips are to work while most-often-happen travel purpose of the elderly is shopping.

72.6% of workers in Jinhexincheng commute across districts. Top three commuting destinations are Putuo, Changning and Jing'an District. The logistic regression model shows that the most important factor that causes cross-district commuting is education. Of those who cross districts to commute, 50% are workers who are relocated here from Shanghai central city but their workplaces are still in downtown (because of the urban houses demolition and relocation) and the other 50% live here because of the acceptable housing price.

Unlike commuters, 54% of the elderly often travel inside Jiading District while 46% often go to other districts. Among these districts, Putuo District gets the most visiting. This might because 52% of the elderly in Jinhexincheng used to live in Putuo district before they moved here.

(2) Driver's license and vehicle ownership

94% of the elderly and 58% of the workers don't have a driver's license. Low car ownership rate and low buy-car plan rate indicate that Jinhexincheng has a good basis of low car ownership and low carbon transport.

High bicycle-motorcycle-moped ownership rate and usage of the workers implies that since transit service is not good enough, residents (workers) here have to use private transport. Interesting thing is 58.2% of the workers own motorcycles or mopeds which is as high as the car ownership percentage in some developed countries. This is because to own a car in Shanghai needs to pay a high price of car and vehicle license, in the condition of low transit service level, instead of buying a car, people can only afford motorcycles or mopeds to travel long distance (also explains low car ownership and usage). If Jinhexincheng wants to remain low car ownership and develop low carbon transport, transit service has to be improved.

(3) Travel mode choice

To workers, buses, motorcycles or mopeds, the metro and private cars are the popular mode choices. However, to the aged, buses, the metro, supermarket shuttle buses and walking are the popular choices.

(4) Departure time and one-way-travel time

Workers' morning departure time in Jinhexincheng is earlier than morning peak in Shanghai city center. The morning departure time of the elderly is later than the workers'. In the afternoon, there are aged people starting to travel as well, usually it is before 15:00.

Furthermore, average commuting time in Jinhexincheng is over an hour. Compared to the world average commuting time (40 minutes), it is quite long. No wonder 44% of workers find the commuting time unsatisfied.

There are more elderly people traveling less than 30 minutes to get to the destinations than workers. Because of the long distance to hospitals, more elderly people travel more than two hours. Unlike workers, public transportation is the only choice for the older aged people since they are not capable of driving a car or motorcycle. So the elderly will find it more troubled if public transportation service level is low. And this is why fewer elderly people think the travel time is satisfied compared to workers.

In conclusion, a lot of differences exist in travel characteristics of the two social groups (the workers and the elderly) in Jinhexincheng. First, workers' most-often-happen trips are to work while most-often-happen travel purpose of the elderly is shopping. Second, a large proportion of workers commute across districts while a large proportion of the elderly often travel inside Jiading District. The logistic regression model shows that the most important factor that causes cross-district commuting is education. Third, to workers, buses, motorcycles or mopeds, the metro and private cars are the popular mode choices. However, to the aged, buses, the metro, supermarket shuttle buses and walking are the popular choices. Furthermore, the

morning departure time of the elderly is later than the workers'. The workers' morning departure time is earlier than morning peak in Shanghai city center. Last but not least, average commuting time in Jinhexincheng is over an hour, compared to the world average commuting time (40 minutes), it is quite long. Elderly people are more sensitive to public transportation service and fewer elderly people think the travel time is satisfied compared to workers.

Jinhexincheng has a good basis of low car ownership and low carbon transportation. However the transit service condition is not good enough. In order to satisfy the residents, including workers, the elderly and others, transit service needs improvement. During transit and transportation planning, different social groups' different travel characteristics should be considered. Solutions to different social groups are needed. Future research can use cluster analysis to divide people into different groups and how to satisfy different groups' demands needs to be studied.

REFERENCES

1. Day, J. and Cervero, R. Effects of Residential Relocation on Household and Commuting Expenditures in Shanghai, China. *International Journal of Urban and Regional Research*, Vol. 34, 2010, pp. 481–508.
2. Flannelly, K. J., McLeod Jr. M. S., Flannelly, L., and Behnke, R. W. Direct Comparison of Commuters' Interests in Using Different Modes of Transportation. In *Transportation Research Record: Journal of the Transportation Research Board*, No. 1321, Transportation Research Board of the National Academies, Washington, D.C., 1991, pp. 90–96.
3. Ke, H. and Shen, H. *Statistics in Survey Research*. Communication University of China Press, China, 2005.
4. Dillman, D. A. *Mail and Internet Surveys: the Tailored Design Method: 2007 Updated with New Internet, Visual and Mixed-Mode Guide, Second Edition*. John Wiley & Sons, Inc., Hoboken, New Jersey, 2007.
5. Lu, X., Tang, J. and Zhang, J. *Blue Book of Society Building: Annual Report on Analysis of Beijing Society Building*. Publication Beijing University of Technology and Chinese Social Science Academic Press, 2011.
6. The Economist Newspaper Limited. *Where Car Ownership is Highest*, Jan. 8, 2009. www.tfhr.gov/pubrds/july97/tam.htm. Accessed July.10, 2011.
7. The Worldmapper Project. *Commute Time*, 2005. www.worldmapper.org/display.php?selected=141. Accessed July.10, 2011.
8. Rosenbloom, S. The Mobility Needs of older Americans: Implications for transportation reauthorization. *Center on Urban and Metropolitan Policy*, 2003, pp. 227–254.
9. Cervero, R. Jobs-Housing Balancing and Regional Mobility. *Journal of American Planning Association*, 1989, pp.136–150.
10. Cervero, R. Job-housing Balance Revisited: Trends and Impacts in the

San Francisco Bay Area. *Journal of the American Planning Association*, Vol. 62, 1996, pp. 492–511.

11. Peng, Z. R. The Jobs-housing Balance and Urban Commuting. *Urban studies*, Vol. 34, 1997, pp. 1215–1235.

12. Shen, Q. Spatial and Social Dimensions of Commuting. *Journal of the American Planning Association*, Vol. 66, 2000, pp. 68–82.

13. Wang, F. Explaining Intra-urban Variations of Commuting by Job Accessibility and Worker Characteristics. *Environment and Planning B: Planning and Design*, Vol. 28, 2001, pp. 169–182.

14. Giuliano, G. Is Jobs-housing Balance a Transportation Issue? In *Transportation Research Record: Journal of the Transportation Research Board*, No. 1305, Transportation Research Board of the National Academies, Washington, D.C., 1991, pp. 305–312.

15. Zhang, Z., Mao B., Liu M., Chen J. and Guo J. Analysis of Travel Characteristics of Elders in Beijing. *Journal of Transportation Systems Engineering and Information Technology*, Vol. 7, 2007, pp. 11–20.

16. Smith, G. C. and Sylvestre, G. M. Determinants of the Travel Behavior of the Suburban Elderly. *Growth and Change*, Vol. 32, 2001, pp. 395–412.

17. Mercado, R. and Páez, A. Determinants of Distance Traveled with a Focus on the Elderly: a Multilevel Analysis in the Hamilton CMA, Canada. *Journal of Transport Geography*, Vol. 17, 2009, pp. 65–76.

18. Kim, S. and Ulfarsson, G. Travel mode choice of the elderly: Effects of personal, household, neighborhood and trip characteristics. In *Transportation Research Record: Journal of the Transportation Research Board*, No. 1894, Transportation Research Board of the National Academies, Washington, D.C., 2004, pp. 117–126.

The Research of the Eco-Port Group's Assessment System Based on ANP

LIU Cui-lian , LIU Jian-mei , YU Tiao-lan and GONG Bao-jun

Transportation Management College, Dalian Maritime University, Dalian 116026, China. E-mail: liu_cuilian@126.com

ABSTRACT

The concept of ecological civilization as a guide for building eco-ports is an inevitable trend in the development of port group, but there is still a lack of evaluation system for eco-port group. To determine the ecological level of development of the port group and found problems in the development, this paper established the of evaluation index system. Through the analytic network process (ANP), selecting Liaoning eco-port group as an example to establish evaluation system of Liaoning eco-port group of, studying systemic and comprehensive on evaluation of the Liaoning province eco-port group, and proposing some corresponding suggestion for the future development of the eco-port group based on the results of Liaoning province. The example shows that, the eco-port group's assessment system Based on ANP is feasible and effective, and this paper can provide reference for relevant departments to formulate standards of the evaluation system.

INTRODUCTION

At present, our country advocates low carbon economy. The competition between ports is not only dock resources、 service quality, but also carbon emissions. As a higher energy-consuming industry, the construction of eco-port becomes a strategic direction for ports' health and sustainable development.

Recent years, scholars at home and abroad make abundant researches in green port, green eco-port. WuPengHua expounds the intension of green eco-port on the perspective of requirements in the environmental development and greening, and points out the existing problems and the need of policy regulation、 incentive and related social support in domestic green eco-ports construction. KarimA.Abood applies green building assessment system to port area, and evaluates "green degree" of port with the combination of it characteristics. On "driving force-pressure-state-influence-response" model, ShaoChaoFeng studies eco-port index system. He takes Tianjin port's ecological construction as background to establish its ecological construction and evaluation index system.

The current study is all for green or eco-port respectively, while the research for the evaluation index system of eco-port group is very little. In this background, on the

base of the Analytic network process (ANP), we select Liaoning port group as an example to establish ecological assessment system. And the system comprehensively studies the assessment methods of its eco-port group, which has an important significance on the eco-port construction.

THE CONSTRUCTION OF ECO-PORT GROUP EVALUATION

According to the setting principles and screening principles of evaluation index system, we construct evaluation index system of eco-port group, which is shown as table 1.

Network AHP (Analytic Network Process) ANP is a new practical decision-making method, which is formed based on AHP. ANP divides the elements of system into two parts: the first part called control factors layer, including the target of problems and decision criterions. All the decision criterions are considered independent and only are distributed by target element. There can be no decision criterions in the control factors, but it must have one target at least. The second part is the network layer, which consists of the entire elements dominated by control layer, and the interior is network structure influencing each other. According to the ANP network structure built by above-mention index system and ANP principle for eco-port, see figure 1. In this model, the problem target of control layer is the comprehensive development level evaluation of eco-port group (A), and the sub-goal is the expert evaluation of eco-port group (B). There are five elements in the network layer, which respectively are C_1 、 C_2 、 C_3 、 C_4 、 C_5 .

EMPIRICAL ANALYSIS

This article takes Liaoning Province eco-port group as an example, and evaluates the development level of Liaoning Province port group using the ANP fuzzy comprehensive evaluation method.

Fuzzy comprehensive evaluation method of ANP for eco-port group

(1) Evaluation method and personnel confirmation

Refer to the index system built in table 1, we divide the evaluation questionnaire designed into five levels: worse (v_1), lower (v_2), and medium (v_3),

Table 1. Evaluation Index System of Eco-port Group

Target	Rule	Subrule layer	Index layer
Comprehensive development of eco-port group A	Expert evaluation of eco-port group B	C ₁ System ability of port group	C ₁₁ Years cargo throughput (ten thousand tons/year)
			C ₁₂ Scale of port group
			C ₁₃ Core competitiveness of port
			C ₁₄ Business profitability of port group (%)
			C ₁₅ Direct economic contribution to the third industry (%)
			C ₁₆ Employment (people)
			C ₁₇ Direct economic contribution to city (%)
		C ₂ System coordination of port group	C ₂₁ Competition degree in port group
			C ₂₂ Cooperation level between ports
		C ₃ Resources occupation	C ₃₁ Occupy basic farmland area's proportion (%)
			C ₃₂ Loss of Marine ecology and fishery resources (tons/year)
			C ₃ Occupy natural coastline's proportion (%)
			C ₃₄ Water consumption of ten thousand tons throughput(ton/ten thousand tons-years)
			C ₃₅ Energy consumption of ten thousand tons throughput(tons standard fuel/ten thousand tons-years)
		C ₄ Environment quality	C ₄₁ Exhaust water emission in port area and ships of ten thousand tons throughput(ton/ten thousand tons-years)
			C ₄₂ Major air pollutants emission of ten thousand tons throughput (ton/ten thousand tons-years)
			C ₄₃ Average value of port environmental noise (dB(A))
			C ₄₄ Solid waste emissions of ten thousand tons throughput (ton/ten thousand tons-years)
		C ₅ Environment management level	C ₅₁ Standardized rate of exhaust water (%)
			C ₅₂ Standardized rate of exhaust gas (%)
			C ₅₃ Standardized rate of vehicles, ships exhaust emission (%)
			C ₅₄ environmental noise coverage (%)
			C ₅₅ Comprehensive utilization rate of solid waste (%)

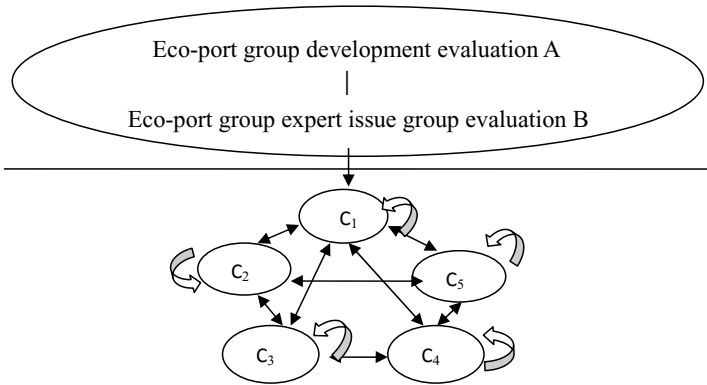


Figure 1. The network model of ANP for eco-port group

upper (v_4), good (v_5). The evaluation persons include experts of eco-port fields and researchers of eco-port group.

(2) Confirmation of single index evaluation matrix

① The quantitative of qualitative indicator

Assume the amount of subjective indicator is t , and there are h person to join in the survey. Meanwhile every surveyed person's evaluation results are recovered.

For each year's development condition of eco-port group " S_m ", assume that there

are $n_{ik}^{(S_m)}$ person whose evaluation level of C_i ($i=1, 2, \dots, t$) is v_k ($k=1, 2, \dots, 5$), we receive table 2:

Table 2. Statistics of the Evaluation Index System of Eco-port Group

	V ₁	V ₂	V ₃	V ₄	V ₅
C ₁	n ₁₁ ^(S_m)	n ₁₂ ^(S_m)	n ₁₃ ^(S_m)	n ₁₄ ^(S_m)	n ₁₅ ^(S_m)
C ₂	n ₂₁ ^(S_m)	n ₂₂ ^(S_m)	n ₂₃ ^(S_m)	n ₂₄ ^(S_m)	n ₂₅ ^(S_m)
⋮	⋮	⋮	⋮	⋮	⋮
C _t	n _{t1} ^(S_m)	n _{t2} ^(S_m)	n _{t3} ^(S_m)	n _{t4} ^(S_m)	n _{t5} ^(S_m)

The above element divided by h and we get the matrix below:

$$\left(\mu_{ik}^{(S_m)}\right)_{t5} = \begin{bmatrix} \mu_{11}^{(S_m)} & \mu_{12}^{(S_m)} & \dots & \mu_{15}^{(S_m)} \\ \mu_{21}^{(S_m)} & \mu_{22}^{(S_m)} & \dots & \mu_{25}^{(S_m)} \\ \dots & \dots & \dots & \dots \\ \mu_{t1}^{(S_m)} & \mu_{t2}^{(S_m)} & \dots & \mu_{t5}^{(S_m)} \end{bmatrix}$$

Among above formula, $\mu_{ik}^{(S_m)} = \frac{n_{ik}^{(S_m)}}{h}$, $i=1,2,\dots,t$; $k=1,2,3,4,5$;

$(\mu_{i1}^{(S_m)} \mu_{i2}^{(S_m)} \dots \mu_{i5}^{(S_m)})$ is the single-factor evaluation of C_i . $\mu_{ik}^{(S_m)}$ expresses the ratio that evaluated by h person as v_k level according to C_i . Generally we make

it normalized so that it meets” $\sum_{k=1}^5 \mu_{ik}^{(S_m)} = 1$ ”, $(\mu_{ik}^{(S_m)})_{t5}$ is the single-factor evaluating matrix of these t indicators for the development condition of the eco-port group S_m .

②Confirmation of objective indicator’s single-indicator evaluation matrix of the

The third-level indicator included in table 1 is objective indicator, We divide them into two types: one is positive indicator, which means the bigger the better, which includes C₁₁,C₂₂,C₁₅,C₁₄ etc.; the other is on the contrary, it includes C₃₁,C₃₂,C₄₁,C₄₄ etc. In order to be consistent with the qualitative indicator, we divide the qualitative indicators into five levels, that is: worse (v_1), lower (v_2), and medium (v_3), upper (v_4), good (v_5). The confirmation of the membership function is as follows (because the reverse indicator is similar with the positive indicator, so we just analysis the positive indicator):

According to practical experience, we take the lower limit value $r_1^{(i)}$ and the upper limit value $r_5^{(i)}$ of C_i as the boundary. Then we divide the interval $[r_1^{(i)}, r_5^{(i)}]$ into five levels. We define the membership degree of the point (the point of average

value) which can express the characteristic of some level appropriately as 1, while the membership degree of the intersection point is 0.5 for its unclear. Through comparing the indicator value X with the boundary point of each level, we receive five membership function of positive indicators C_i (1,2,...,t) as Table 3:

Table 3. Five Membership Function of Positive Indicators

Level	membership function
worse (v_1)	$v_{1,h}(x) = \begin{cases} 1, & x < r_1^{(i)} \\ \frac{r_2^{(i)} - x}{r_2^{(i)} - r_1^{(i)}}, & r_1^{(i)} \leq x < r_2^{(i)} \\ 0 & \text{o t h e r} \end{cases}$
lower (v_2)	$v_{2,h}(x) = \begin{cases} \frac{x - r_1^{(i)}}{r_2^{(i)} - r_1^{(i)}}, & x \in [r_1^{(i)}, r_2^{(i)}) \\ \frac{r_3^{(i)} - x}{r_3^{(i)} - r_2^{(i)}}, & x \in [r_2^{(i)}, r_3^{(i)}) \\ 0 & \text{o t h e r s} \end{cases}$
medium (v_3)	$v_{3,h}(x) = \begin{cases} \frac{x - r_2^{(i)}}{r_3^{(i)} - r_2^{(i)}}, & x \in [r_2^{(i)}, r_3^{(i)}) \\ \frac{r_4^{(i)} - x}{r_4^{(i)} - r_3^{(i)}}, & x \in [r_3^{(i)}, r_4^{(i)}) \\ 0 & \text{o t h e r} \end{cases}$
upper (v_4)	$v_{4,h}(x) = \begin{cases} \frac{x - r_3^{(i)}}{r_4^{(i)} - r_3^{(i)}}, & x \in [r_3^{(i)}, r_4^{(i)}) \\ \frac{r_5^{(i)} - x}{r_5^{(i)} - r_4^{(i)}}, & x \in [r_4^{(i)}, r_5^{(i)}) \\ 0 & \text{o t h e r} \end{cases}$
good (v_5)	$v_{5,h}(x) = \begin{cases} 1, & x \geq r_5^{(i)} \\ \frac{r_2^{(i)} - x}{r_2^{(i)} - r_1^{(i)}}, & x \in [r_4^{(i)}, r_5^{(i)}] \\ 0 & \text{o t h e r} \end{cases}$

Build the comparing matrix of ANP evaluation of Liaoning Province eco-port group development

According to the established evaluation indicator system and the network structure of eco-port group, we form the matrix group, and then take the average value as the final value of mutual advantage. Check its consistency, and then calculate the consistency ratio. In the formula of $C.R. = \frac{C.I.}{R.I.}$, $C.I. = \frac{\lambda_{max} - n}{n - 1}$ is the coincident indicator; n and λ_{max} respectively represent the order and the largest eigenvalue. R.I. is the average consistency index, and the value of R.I. is as table 4:

Table 4. Random Index RI

Dimension	1	2	3	4	5	6	7	8	9
RI	0	0	0.58	0.92	1.12	1.24	1.32	1.41	1.45

When the dimension of judgment matrix is less than or equal 2, the value of RI is 0, the judgment matrix has consistency. When the dimension of judgment matrix is bigger than 2, only in the case of “CR≤0.1”, we can consider that the result of single-level sorting column is satisfying. Otherwise we should adjust the value of element of judgment matrix until it meets the requirement of consistency check.

Build the single-factor evaluation matrix of Liaoning Province eco-port group development

Refer to the decision method of subjective and objective indicator evaluation matrix as introduced previously, we receive the evaluation value of Liaoning Province eco-port group’s development condition D_1, D_2, D_3, D_4 from year 2006 to year 2009 by calculating the function of membership degree. The resulted are listed in the table 5. The weight column is the weight of three-level indicator calculated by Super Decision1.6 Software.

Table 5. Evaluation Matrix for Liaoning Eco-Port Group Development

Index	Weight	D_1	D_2
C ₁₁	0.0275	(0.15,0.22,0.36,0.16,0.11)	(0.14,0.21,0.38,0.15,0.12)
C ₁₂	0.0236	(0,0,0.305,0.617,0.078,0)	(0,0,0.307,0.615,0.078,0)
C ₁₃	0.0272	(0.02,0.198,0.2,0.33,0.108)	(0.03,0.188,0.21,0.32,0.108)
C ₁₄	0.0265	(0.037,0.191,0.29,0.381,0.11)	(0.038,0.19,0.3,0.382,0.09)
C ₁₅	0.0198	(0.12,0.21,0.34,0.21,0.11)	(0.13,0.2,0.35,0.2,0.11)
C ₁₆	0.0184	(0,0,0.33,0.53,0.14)	(0,0,0.35,0.54,0.11)
C ₁₇	0.0195	(0,0.125,0.67,0.196,0)	(0,0.126,0.68,0.194,0)
C ₂₁	0.0208	(0,0,0.695,0.192,0.117)	(0,0,0.692,0.193,0.115)
C ₂₂	0.0236	(0,0.25,0.32,0.43,0)	(0,0.26,0.29,0.43,0)
C ₃₁	0.0375	(0,0.342,0.466,0.197,0)	(0,0.341,0.464,0.195,0)
C ₃₂	0.0238	(0,0,0.193,0.809,0)	(0,0,0.194,0.808,0)
C ₃₃	0.0396	(0,0,0.116,0.693,0.190)	(0,0,0.115,0.692,0.192)
C ₃₄	0.0473	(0.14,0.21,0.34,0.15,0.13)	(0.13,0.2,0.35,0.16,0.11)
C ₃₅	0.0456	(0,0,0.808,0.192)	(0,0,0.193,0.807,0)
C ₄₁	0.0732	(0.29,0.49,0.22,0.1,0)	(0.31,0.48,0.21,0.1,0)
C ₄₂	0.0658	(0,0.654,0.308,0.038,0)	(0,0.653,0.309,0.308,0)
C ₄₃	0.0543	(0,0.131,0.477,0.292,0.1)	(0,0.132,0.477,0.291,0.1)
C ₄₄	0.0776	(0,0.192,0.658,0.15,0)	(0,0.193,0.657,0.15,0)
C ₅₁	0.0718	(0,0.29,0.546,0.155,0)	(0,0.28,0.546,0.156,0)
C ₅₂	0.0697	(0,0.1,0.515,0.385,0)	(0,0.09,0.515,0.386,0)
C ₅₃	0.0539	(0,0.212,0.552,0.236,0)	(0,0.211,0.551,0.238,0)
C ₅₄	0.0636	(0,0.192,0.606,0.202,0)	(0,0.191,0.605,0.204,0)
C ₅₅	0.0694	(0,0,0.199,0.481,0.32)	(0,0,0.201,0.48,0.319)

Index	Weight	D ₃	D ₄
C ₁₁	0.0275	(0,0.09,0.296,0.538,0.076)	(0,0.11,0.286,0.525,0.077)
C ₁₂	0.0236	(0,0.1,0.208,0.654,0.038)	(0,0.11,0.198,0.652,0.04)
C ₁₃	0.0272	(0,0.153,0.501,0.346,0)	(0,0.152,0.5,0.348,0)
C ₁₄	0.0265	(0,0.14,0.244,0.578,0.038)	(0,0.139,0.243,0.58,0.038)
C ₁₅	0.0198	(0,0.199,0.236,0.565,0)	(0,0.201,0.235,0.564,0)
C ₁₆	0.0184	(0,0,0.202,0.644,0.154)	(0,0,0.201,0.643,0.156)
C ₁₇	0.0195	(0.15,0.22,0.36,0.16,0.11)	(0.14,0.21,0.38,0.15,0.12)
C ₂₁	0.0208	(0,0.192,0.658,0.15,0)	(0,0.193,0.657,0.15,0)
C ₂₂	0.0236	(0,0.29,0.546,0.155,0)	(0,0.28,0.546,0.156,0)
C ₃₁	0.0375	(0,0.1,0.515,0.385,0)	(0,0.09,0.515,0.386,0)
C ₃₂	0.0238	(0,0.212,0.552,0.236,0)	(0,0.211,0.551,0.238,0)
C ₃₃	0.0396	(0,0.192,0.606,0.202,0)	(0,0.191,0.605,0.204,0)
C ₃₄	0.0473	(0,0,0.162,0.211,0.672)	(0,0,0.161,0.212,0.672)
C ₃₅	0.0456	(0,0,0.199,0.481,0.32)	(0,0,0.201,0.48,0.319)
C ₄₁	0.0732	(0,0,0.695,0.192,0.117)	(0,0,0.692,0.193,0.115)
C ₄₂	0.0658	(0,0.25,0.32,0.43,0)	(0,0.26,0.29,0.43,0)
C ₄₃	0.0543	(0,0.342,0.466,0.197,0)	(0,0.341,0.464,0.195,0)
C ₄₄	0.0776	(0,0,0.193,0.809,0)	(0,0,0.194,0.808,0)
C ₅₁	0.0718	(0,0,0.115,0.365,0.52)	(0,0,0.114,0.364,0.522)
C ₅₂	0.0697	(0,0,0,0.692,0.308)	(0,0,0,0.69,0.31)
C ₅₃	0.0539	(0,0,0.023,0.731,0.246)	(0,0,0.022,0.73,0.248)
C ₅₄	0.0636	(0,0,0.115,0.365,0.52)	(0,0,0.114,0.366,0.52)
C ₅₅	0.0694	(0,0,0.153,0.482,0.365)	(0,0,0.512,0.481,0.367)

The comprehensive evaluation result and analysis of Liaoning Province eco-port group development

After weighting, we can receive the comprehensive evaluation result of Liaoning Province eco-port group development of four years. Then make normalization of it, we can get the results as follows:

The evaluation value of Liaoning Province eco-port group in 2006 is (0.1421 , 0.1121 , 0.4011 , 0.2491 , 0.0935), 2007 is (0.1203, 0.0803, 0.4131, 0.2641, 0.1221), 2008 is (0.0504, 0.0701, 0.3667, 0.3139, 0.1987), 2009 is (0.1016, 0.0822, 0.4213, 0.2655, 0.1295).

According to the maximum membership, Liaoning province's eco-port group is at the level of "medium", at the same time, it also proves the feasibility of evaluation index system.

CONCLUSION

Through study the relevant theory of eco-port, this paper establishes evaluation

index system of eco-port group, using the network analytic hierarchy process, we construct development evaluation system and model of eco-port group. Finally, Based on ANP_fuzzy comprehensive evaluation method, we calculate development level in eco-port of Liaoning province. The results show the feasibility of the index system, and provide a reliable reference for policymakers.

References:

- [1] Karim A.Abood. Sustainable and green ports: Application of sustainability principles to port development and operation[C]. *Ports 2007 Conference*, ASCE, 2007, 25-28.
- [2] LIU Cuilian. Study on construction and counter measures of Liaoning eco-port group[M].*China communications press*, 2009.
- [3] SHAO Chaofeng, JU Meiting, HE Ying, SUN Xin. Study on index system of eco-ports based on DPSIR model[J].*Marine environment science*, 2009,28(3): 333-337.
- [4] WU Penghua. Study on construction of green port[J]. *Marine environment science*, 2009,28(3):338-344.

Mechanism of Urban Spatial Structure Evolution under the Influence of Port Function Upgrading: A Case Study of Dalian

Liang, C. and Wang, N.

Transportation Management School, Dalian Maritime University, P.O.BOX 116026, Dalian; PH: (0086) 411-84726835; FAX: (0086) 411-84726835; email: liangchendl@126.com

ABSTRACT

The upgrading of port function produces a profound and lasting effect on the progress of a port city's spatial structure. To analyze the port city spatial structure evolution mechanism, this paper addresses the process of urban spatial structure evolution under the influence of port function upgrading. Dalian is the study object, and the study uses the technology of remote sensing analysis and geographic information systems to extract geographic information about urban land utilization, combined with the theory of fractal and spatial gravity center, and thus analyzes the law of port city spatial evolution. On the foundation of the law proposed, the port city spatial structure evolution mechanism model is established with overall consideration of both mechanism factors from industry and society implicated during the port function upgrading process. Results show that the mechanism study could reveal internal agents of port city spatial structure evolution and provide theoretical basis and decision-making support for the improvement of the port city spatial structure evolution's rationality, so as to achieve port cities' sustainable development.

INTRODUCTION

Port function upgrading and port industries aggregation is one of the most important trends of change with time-transgressive significance. Since the 1960s, the first-generation ports in developed countries, taking stevedoring as the principal operation work, have begun to progress to the second-generation, prioritizing port processing manufacturing, and to the third-generation, primarily focusing on commodity distribution and capital collocation. Along with the trend, port industry springs up, leading to the phenomenon of urban spatial reconstruction. Empirical observation indicates that port function upgrading and port industry aggregation have become the most relevant dynamic and direct powers driving urban spatial structure evolution, which in itself is considered an inevitable tendency for port cities. Therefore, it is of great practical importance to analyze urban spatial-temporal patterns in port cities and to study the mechanisms of port function upgrading to urban spatial structure, so as to enable improvement of the development of the port city in a harmonious and reasonable manner.

Urban spatial structure evolution has been discussed in many studies (Herold *et al.*, 2005; Long *et al.*, 2006; Taubenbok *et al.*, 2009). Within the studies, the theories

and methods for investigating urban shape are explored, but currently there is a lack of study of spatial structure with detailed discussion of related industry variation mechanism.

METHODOLOGY

Study area

Dalian is the southernmost city in the Liaotung peninsula. It includes administrative divisions such as Zhongshan, Xigang, Shahekou, Jinzhou, Wafangdian, Pulandian, and Zhuanghe, and it is geographically located at 39°01'–39°04' N and 121°44'–121°49' E with a population of 5.86 million as of the end of 2010.

Dalian started port construction in 1999. Within 10 years, the Dalian port became the biggest port in Northeast China. Before the Dayaowan harbor district opened its port, Dalian was developing near and overtaking the areas around the old port which was set up at the city center. As port function has been upgraded and the new harbor district expanded, Dalian has gradually come into being as a modern port city with multiple ports and multiple functions. Then Dalian central city is still developed around the old port area, and a new urban area is planned in the Jinzhou district relying on the new port area in Dayaowan. Aside from this, the Changxingdao district is 150 kilometers away from Dalian downtown and is of great competitive advantage due to its excellent port resources. Changxingdao has become the most significant port address after the Dayaowan port, and has made port operation and port industry into competitive industry. The study takes the spatial structure evolution in Dalian as a study objective and puts emphasis on how upgrading port function influences the spatial change in Dalian central city, the new urban area, and the Changxingdao industrial zone.

Data source & data preprocessing

The study is mainly based on satellite data of Dalian in 1995, 2000, 2005, 2010 derived by Landsat (TM / ETM) with 30m×30m spatial resolution. Geometric correlation is processed to the satellite data mentioned above, referring to a 1:100,000 scale relief map of the study area and employing the quadratic polynomial calibration model with error less than one image element. Then the satellite data is applied mosaic and mask according to 1:4,000,000 scale administrative maps, in order to create a complete image of the whole study area and is enhanced to facilitate the process of urban land classification. Thus 4 space-time urban land vectors are eventually obtained after sieving classes and classification to vector.

Spatial expansion rate model

In order to thoroughly discuss the sprawl scale of Dalian area since 1995, analytical indexes below are introduced. Urban land expansion rate (1) is the average annual increase of urban construction land sprawl in different stages within the study time range, indicating the urban construction growth scale and increase trend.

$$R = \frac{U_{fa} - U_{sa}}{U_{sa} \times \Delta t} \quad (1)$$

Urban land expansion intensity characterizes the ratio between urban construction land growth area and urban total area. The index (2) enables standardization of sprawl area to total area and essentially makes urban land increases in different time stages comparable.

$$I = \frac{U_{fa} - U_{sa}}{U_{ta} \times \Delta t} \quad (2)$$

Where R is urban land expansion rate and I is urban land expansion intensity, U_{sa} , U_{fa} , U_{ta} are urban construction area of the beginning, the end of the study period and the total urban area respectively, Δt is time span with a unit of year.

Fractal Dimension model

Fractal geometry studies irregular objects as research subjects and avoids the drawbacks of traditional geometry, which cannot be used to study non-integer dimension objects. It provides quantitative tools that can be used to describe and research complex and irregular study objects processed with the similarities present in both the local and global environment, and is based upon deep exploration of the regularity in irregularity. Thus the fractal model is feasible and suitable to studying the process of urban spatial structure evolution. The higher the fractal dimension, the more complicated the urban spatial shape, the more complex the city mosaic structure and the even higher level of the urban flat fill-up and the compactness of urban land use. In this study, the Box-counting dimension method is chosen and employed. Let A as non-empty subset of R^n space, for all $r > 0$, let $N(r)$ be the minimum amount of r edge length boxes covering the whole object, if there exists D , when $r \rightarrow 0$,

$$N(r) \propto 1/r^D \quad (3)$$

Then D is the Box-counting fractal dimension of A . The value range of D is from 1 to 2. The formula to calculate fractal dimension is listed as below.

$$N(r) \propto r^{-D} \quad (4)$$

Gravity center transfer model

The concept of gravity center from mechanics is introduced into urban study; this concept states that there exists one point, in the surrounding area, to achieve relative force equilibrium from every direction. Due to this characteristic, the gravity center could be conducted as one of the most indexes of urban evolution study. The transfer path of each year's urban gravity center could reveal the process of urban development and evolvement. To the area in spatial equilibrium, the gravity center of the city is exactly the geometric gravity center. The position of gravity center in disequilibrium could be calculated by mathematics model as below. Let there are n administrative regions in study area, i statistic unit's co-ordinate origin is (X_i, Y_i) ; P_i is one of the quantitative statistical indices of the administrative region.

$$\bar{X} = \frac{\sum_{i=1}^n P_i X_i}{\sum_{i=1}^n P_i} \quad \bar{Y} = \frac{\sum_{i=1}^n P_i Y_i}{\sum_{i=1}^n P_i} \quad (5)$$

While the center of gravity transferred with time, the transfer direction indicates the ‘high-clustering’ region in spatial phenomenon, and the distance to the geometric center of gravity represents the degree of disequilibrium. According to Equation 5, it is obvious that the position of the gravity center is decided by both geographic position and characteristic value of each statistic unit. Due to the fact that the geographic position of the study area remained unchanged, the variation of the gravity center reveals the transformation that occurred within the numerical range of the statistic unit.

RESULTS

Remote sensing information extraction

Comparing the interpreted data of each time phase, it is clear that since 1995 the urban land sprawl phenomenon in Dalian is significant. From the build-up area, it can be observed that the spatial structure in Dalian is evolved from sole-core structure in 1995 to dual-core between 2000 and 2005, then finally to joined-zone style in 2010 due to the dynamics of new urban sprawl and centralization.



Figure 1. The process of Dalian urban spatial structure evolution.

Spatial expansion rate calculation results

Table 1. 1995-2010 Dalian construction land sprawl rate and intensity.

Area	1995-2000		2000-2005		2005-2010	
	Sprawl rate	Sprawl intensity	Sprawl rate	Sprawl intensity	Sprawl rate	Sprawl intensity
Dalian	1.468%	0.133	1.197%	0.116	0.806%	0.083

During the study period, it is found that the total area of Dalian construction land continued to increase. From 1995 to 2010, construction land has expanded to 362.81km², summing up to 176.81km² within this 15 years, increased by 1.95 times compared to the beginning of the period, with an annual growth of 11.79km².

Calculated according to Equations 1 and 2, the sprawl rate and sprawl intensity of each year in Dalian is obtained (See Table 1). In phase I (1995-2000), the build-up area increased by 16 km², and the sprawl rate and intensity were 1.468% and 0.133 respectively. In phase II and phase III (2000-2010), although there was a descending trend of sprawl rate and intensity, relative positive growth was still maintained. The

land use structure also changed. The expansion of industry and warehousing land, which are highly related to port industry, is the most rapid, increasing by 1.7 and 2.3 times compared to 2000.

Fractal dimension results

According to the fractal dimension method, using software ArcGIS 9.3, a series of grids with various edge lengths are generated to cover the study region. Then, the amount of grids required is calculated. Double logarithmic figures of grid size r and non-empty $\ln N(r)$ are made, $\ln r$ as abscissa and $\ln N(r)$ as ordinate. The linear distribution among such figures are all significant, the negative power law between grid size and non-empty grid amount is obeyed and the coefficient of determination R^2 of linear fitting in figures are all above 0.99; therefore, it is reasonable to consider that urban land in the Dalian study area has fractal characteristics. Thus the fractal dimensions in Dalian city territory, central city, new urban and Changxingdao since 1995 to 2010 are illustrated in Table 2.

Table 2. Fractal dimension of city territory, central city, new urban and Changxingdao.

Year	Research area	Dimension	Mathematics model	R^2
1995	City territory	1.2977	$\ln N(r) = -1.2977 \ln r + 0.4690$	0.9999
	Central city	1.7246	$\ln N(r) = -1.7246 \ln r + 0.1415$	0.9992
	New urban	1.5289	$\ln N(r) = -1.5289 \ln r + 0.2809$	0.9999
	Changxingdao	1.2695	$\ln N(r) = -1.2695 \ln r + 0.6235$	0.9948
2000	City territory	1.5157	$\ln N(r) = -1.5157 \ln r + 0.5813$	0.9975
	Central city	1.7179	$\ln N(r) = -1.7179 \ln r + 0.2163$	0.9999
	New urban	1.4925	$\ln N(r) = -1.4925 \ln r + 0.5445$	0.9986
	Changxingdao	1.3341	$\ln N(r) = -1.3341 \ln r + 0.8683$	0.9886
2005	City territory	1.5873	$\ln N(r) = -1.5873 \ln r + 0.4755$	0.9990
	Central city	1.7240	$\ln N(r) = -1.724 \ln r + 0.2692$	0.9997
	New urban	1.6839	$\ln N(r) = -1.6839 \ln r + 0.2468$	0.9978
	Changxingdao	1.4919	$\ln N(r) = -1.4919 \ln r + 0.5069$	0.9984
2010	City territory	1.7037	$\ln N(r) = -1.7037 \ln r + 0.3361$	0.9994
	Central city	1.7285	$\ln N(r) = -1.7285 \ln r - 0.0088$	0.9992
	New urban	1.6935	$\ln N(r) = -1.6935 \ln r + 0.0275$	0.9988
	Changxingdao	1.5821	$\ln N(r) = -1.5821 \ln r + 0.2331$	0.9995

Compared with the fractal dimensions, the conclusions could be drawn as described below. Firstly, the fractal dimension in Dalian keeps increasing. In city territory, the fractal dimension increases from 1.2977 in 1995 to 2.5157 in 2000, then to 1.5873, finally to 1.7037 in 2010, presenting a steady ascending tendency. Secondly, the changes of different areas reveal different characteristics. The fractal dimension of central city does not show significant variation with the value approximately always as high as 1.7, illustrating that the urban structure of central city has fully developed, urban land layout is compact and homogenous, and urban structure is changed mainly due to reconstruction. In contrast, the situation in new

urban and Changxingdao is quite the opposite. The fractal dimension variation is clearly significant and amplitude is relatively large, demonstrating that sharp changes occurred in these areas, and that the structures develop from simplicity to complexity, mainly on expansion and fill-up with rapid transformation. Thirdly, it could be considered that the total change of Dalian is promoted by the rapid development in new urban areas and areas as Changxingdao, which greatly influence urban structure evolution in Dalian. Fourthly, according to Batty (1994), the fractal dimension would stabilize at 1.71 approximately, along with the port function upgrading and port transfer and rebuild, the aggregation level around the port is improved constantly; thus, the fractal dimension would fluctuate around 1.71; while the urban land is highly centralized near the port, the urban structure would no longer satisfy the requirement for port high-speed development. The scale enlarges, and then the port transfer and rebuild is driven and promoted.

Gravity center transfer results

The gravity center positions of Dalian in 4 time phases are derived based on the gravity center calculation method as Equation 5. From the gravity center transfer direction, it could be found that there is an obvious transfer phenomenon to the northeast, identical to the port transfer direction. The urban gravity center moves towards the new urban generally, which reveals the huge attraction of Dayaowan new port district to urban spatial structure.

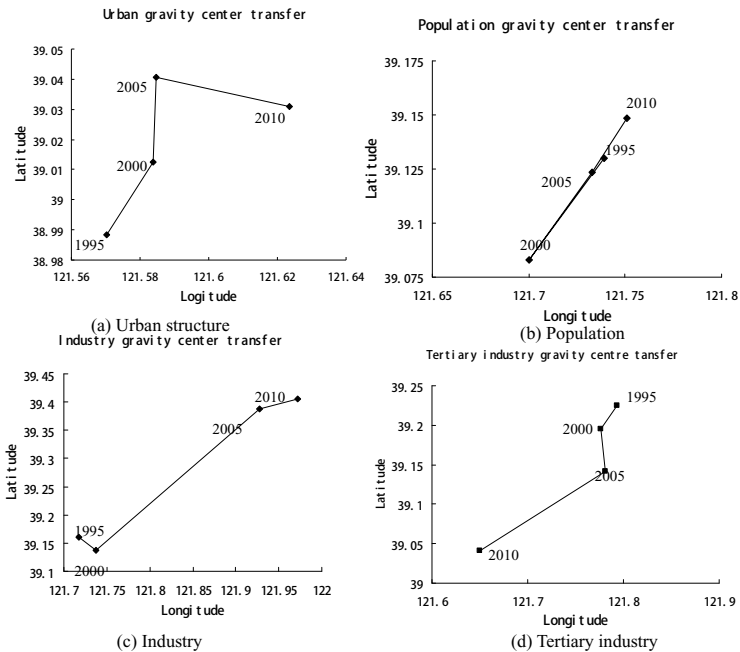


Figure 3. Dalian city gravity center transfer.

The gravity centers of city population, industry and tertiary industry in Dalian during these years are also obtained, with non-agriculture population amount, output value of industry and tertiary industry of each administrative region as weighted indicators. The urban population transfer trend is changed from centralization towards the city center to decentralization and shift to the new urban area, which is because new port and new port industrial zones create more and more employment chances and the supporting facilities in new urban are improved and perfected with the development of port and port industry, and while the central city becomes more and more crowded, so the new urban is another new and sensible choice to work and live in.

The circumstances of secondary and tertiary industry in the gravity center transfer are significantly opposed to one another. Secondary industry moved towards the northeast and then tertiary industry back to the southwest. The reasons are mainly the weakening of the old port, the strengthening of the new port, and new port industry among the port function upgrading. The old port gradually quits the stage and the throughput is basically held by the new port. The space of the old port in the central city decreases as the port transfers, and then city center land use changes to modern business, service business, and banking business. Also due to port function upgrading, the port city takes on more and more value-added activities and supply chain coordination operations related to port transportation, which are generally located in the central city. With the competitive advantages of the new port, port industry develops quickly in new urban areas, promoting secondary industry prosperity, so the secondary industry gravity center then clearly moves to the new urban area.

CONCLUSIONS

The development of a port, which acts as an important component of port city development, could have a significant effect on the evolution of urban spatial structure. Among with the port function upgrading, port city spatial structure variation is processed due to port position transfer and rebuild and port industry large-scale development. In Dalian, under the influence of port function upgrading, the urban area expands constantly with a steady growth rate, the land use structure is changed with more land occupied and employed for purposes related to port and port industry, urban spatial structure evolves from simplicity to complexity, the urban gravity center transfers from central city to new urban, urban population moves towards new urban, the industry gravity center transfers with port move, and third industry moves close to central city, all of which are generally driven by and related to port transfer and port industry development, making up the mechanism of urban spatial structure evolution. The mechanism study reveals the law of port city urban structure evolution, which could be of direct significance and reference value to port city urban planning and port development in achieving the objective of mutual prosperous and sustainable development.

REFERENCES

- Batty, M., Longley, P.A. (1994). "Fractal cities: a geometry of form and function." London: Academic Press, Marcount Brace & Company Publisher.
- Long, Y., Mao, Q.Z. & Dang, A.R. (2006). "Beijing urban development model: urban growth analysis and simulation." *Tsinghua Science and Technology*, (14)6:782-794.
- Herold, M., Couclelis, H. & Clarke, K. (2005). "The role of spatial metrics in the analysis and modeling of urban land use change." *Computers, Environment and Urban Systems*, (29):369-399.
- Taubenbok, H., Wegmannb, M., Roth, A., Mehl, H. & Dech, S. (2009). "Urbanization in India - Spatiotemporal analysis using remote sensing data." *Computers, Environment and Urban Systems*, (33):179-188.

Chongqing Urban Traffic Congestion Solution Method and Strategy

Xingzhong GAO

School of Traffic and Transportation, Chongqing Jiaotong University, Chongqing 400074, China

ABSTRACT

At present, the main business districts of Chongqing city are facing with the serious challenge of the problem of traffic congestion, to solve the problem of traffic congestion of Chongqing city has become the key of guarantee Chongqing's sustainable social and economic development, and of improve the quality of life . Chongqing is a mountain city and the traffic problem is a complicated system problem. To basically solve the problem of traffic congestion, we must use science of traffic planning method to establish the near future and the long-term strategy, these methods and strategies must according to certain procedures in Chongqing city integrated traffic planning framework on. First, author surveyed of Chongqing urban current traffic system, found out the cause of the traffic congestion, and made an analysis on the data. Secondly, in accordance with the above results, author used scientific methods, such as city road system optimization, traffic organization planning, traffic control, transportation structure optimization and the traffic system management to formulate the strategy to solve the problem. Finally, in accordance with the above strategy, author formulated a traffic planning system to solve the problem of traffic congestion in Chongqing urban area. According to the analysis, this traffic planning system can effectively solve the problem of traffic congestion of Chongqing, and it also laid a solid foundation of Chongqing's sustainable development of social, economy and transportation.

CHONGQING CITY TRAFFIC JAMS THE STATUS QUO

Along with the economic development of Chongqing city, the traffic situation increasingly nervous, especially the problem of traffic congestion is very serious, in some extent influence the further development of urban economy and the improvement of people's living standard (See Figure 1). To solve the problem of traffic congestion in Chongqing city is imminent.

After years of Chongqing road congestion condition investigation can be found, Chongqing urban congestion mainly appear in five big business circle center and around the trunk road, article a few over the Yangtze, the important trunk road and part of the Jialing river key nodes. Chongqing road congestion point to the great influences on the road network, cause of citizens of the

sensitivity of the high road congestion, enabled us to "jams" feeling is deep. Especially in recent years, Chongqing part of the bridge over the river, make urban congestion problem is becoming increasingly serious, and sometimes even on the flat peak time congestion more and more, conventional public traffic congestion caused people to buy their own cars, into a taxi rise, it caused more congestion, and pedestrians, bicycles, motorcycles a line disorderly wear, caused more congestion points.



Figure 1. Traffic congestion in Chongqing

THE CAUSE ANALYSIS OF THE TRAFFIC CONGESTION

Traffic is a very vast and complex system, urban congestion of the specific factors for, Chongqing urban congestion reason group to be in:

(1) The unreasonable resources disposition bus, rail transportation development is too slow. Big cities at home and abroad in the business center of the traffic development success experience tell us: Road traffic capacity limitation and traffic demand of the total amount of great sex decided the large-scale commercial center traffic through the ground primarily way is to allow the business centre traffic demand, commercial center must rely on many set in an integrated traffic system especially as the whole of traffic demand and track support, and at the same time in the construction and management of the active adoption of "bus priority" concept. At present, the Chongqing five business circle the ground is the main motor vehicle traffic transportation, cannot satisfy huge traffic demand.

(2) The car fast growing, roads extended always behind the rate of growth of vehicles, plus the network structure, the bus, the influence of factors such as the parking traffic capacity was the lack of roads are more difficult to fulfill its capacity, further intensifies the traffic demand and the contradiction between the supply of transportation. The network structure unreasonable make the traffic flow mainly concentrated in the major point where the traffic is not smooth, makes the connection segment traffic flow distribution ability.

(3) Transit site set is not reasonable. Bus lane and parking, into, out of lack of effective management of parking in Hong Kong, making the bus stops at the intertwined serious, very congested, with parking garage is also independent of each other, cannot connect into the whole induction system is not perfect, the driver in the region to find parking causing congestion to the area network burden.

(4) The impact of cross-border traffic of the larger district. High concentration of urban functions will inevitably lead to huge traffic demand, the five district of Chongqing City, a high concentration of urban functions, good traffic location, excellent business climate is bound to a huge shopping area traffic demand. According to statistics, the core area to attract business district peak-hour traffic flow total is 43000pcu/h, cross-border traffic is 24000pch/h, accounting for 55.8%, more than half.

(5) Large flow of people across the street, and walkways, pedestrian bridges, underpasses too, pedestrians crossing the road when the traffic impact would be, resulting in congestion.

(6) Since the special topography of Chongqing, the roadway is too narrow, too many one-way streets, traffic lights frequently, resulting in congestion of the special reasons.

RESPONSES TO SOLVE CONGESTION

To develop public transport

Traffic load from the perspective of public transport as an intensive way to travel, the per capita share of resources than the private road transportation is a significantly greater advantage. However, private transport to get around flexibility, comfort has advantages, but the transport system resource utilization is higher. Chongqing City's major shopping district a great background traffic, the existing transport infrastructure has been unable to meet the growing traffic demand, so it should be building to public traffic and transport system, to develop rail transport, full use of track capacity, the advantages of speed, to build the rail station-based hubs, making rail travel as an important transport business district one of the ways, Chongqing Rail Line 3 of the opening of Nanping district greatly slowed the traffic pressure, reducing traffic congestion as shown in Figure 2:



Figure 2. General view from the ground bus

Construction of large multi-functional parking lot

Flow distribution in the district where the construction of large-scale multi-functional large parking lot 5-10, in the formation of congestion will not increase the small parking lot where appropriate, multi-functional car park with parking, transfer station, car wash and other repair supporting function, the size of these car parks to be able to accommodate vehicles of all societies in Chongqing City.

Parking tickets can be implemented through these low fees and often stop the vehicle, pay the parking fee, the implementation of ticket system, no fixed parking, easy access to the owner.

Science and adjust the bus operation

Suggestions of a card for all day, passengers sit bus charge debits after a time, as long as the same person no matter all day on any bus, are only brush card, no longer debits, carry out through all day, trying not to pay the fare, passengers will choose the most efficient way to transfer to a bus. To appropriately increase the number of public buses and set to meet the social public transport vehicle large activities temporary personnel rally together.

Pedestrian system construction

Chongqing five business circle is the collection business, business, office, leisure, entertainment and so on many kinds of functional properties in an integrated urban central district, and in the business scope gradually to the extension, the area is more and more big, the walking street is also more and more long, these different nature of the passenger flow in commercial circle to shuttling

back and forth communication, the best transportation is on foot. Development business circle walking system, connected with the business in commercial circle outside walk channel, commercial circle of contact, the interval of different business circle and the surrounding bus stations track the station transport links and improve the whole business circle pleasant space environment is very necessary.

In five of the business situation on foot, need more pedestrian Bridges and underground passage, make the person flow separation, open up the pedestrian subway underground, through different business area connection to the business district underground area network.

CONCLUSION

This paper emphasis on the present situation of traffic problems of macro analysis, according to the trend of the development of future business circle, it put forward to enhance the business circle person, content distribution ability thoughts, the biggest phenomenon ease traffic congestion problem situation. This paper put forward the rail traffic, walking system, parking, both the improvement measures, improve the commercial environment, improve its competitiveness, this is the central business district of Chongqing city traffic congestion improve good countermeasures and methods.

TOD Mode and the Interface between the Urban Groups

Jin Nan

Chongqing Jiaotong University of Transportation, Chongqing, 400074, China.

Phone: 15923156427; E-mail: jinnan88421@163.com

ABSTRACT

Compared with traditional mono-central cities, clustered cities have more advantages in adapting to rapidly development of big cities , while they can effectively guide the healthy development of transport system. Therefore, this layout mode has more and more use to the urban planning. However, the interface between the groups is far from satisfactory. In order to achieve an effective interface between groups, to Chongqing, for example, now should analyze the spatial development trends in Chongqing and the situation of implementation of public transport-oriented development (TOD). For the current major traffic problems caused by the poor interface between the groups in Chongqing . Design to the planning process whose hub layout planning as the core. Described in the context of rapid urbanization in China the main content of a "public transport-led" TOD planning model, and survey content includes demand forecasting, program design, program evaluation and program implementation support system. Study result shows that based on TOD mode of public transport planning approach will be ideal planning model to support an effective interface between the city groups.

INTRODUCTION

Along with economic globalization and the accelerated process of urbanization in China, China's cities have been expanding, the level of motorization has been increasing, traffic problems have become increasingly prominent, and urban development will face a huge adjustment. Group layout as a rational distribution model to adapt to the expansion of cities and development of new towns, is conducive to a flexible combination of city, it is not easy to damage the ecological environment, and it can avoid the common problem of compact cities. However, if the tour cities can force the connection between construction sites, it will result in scattered cities, urban agglomeration performance degradation, or cause serious traffic congestion.

From the point of view of city to city traffic sustainable development, public transport is a high efficiency, low energy consumption, environmentally friendly mode of transport. From the overall regional coordination and long-term development interests, it is a sustainable development of the idea to introduce that the world has been the application of TOD strategy into the group city's public transport planning. ^[3] This article is based on the actual needs of urban

development groups, Chongqing City, for example, it starts from the interaction between land use and transportation systems, mutual feedback and the mechanism, to coordinate the interaction between the two for the purpose, to explore TOD model and the convergence of the relationship between the city tour, to establish for the transportation planning model of urban development groups, to propose the best way that a link between the city tour is based on to TOD mode of public transport as the main mode of urban transportation system planning.

TOD PATTERNS AND CHARACTERISTICS OF THE CITY TOUR

TOD Concept and Characteristics

TOD (Transit-oriented Development, or Transit-oriented Design, public transport-oriented development, referred to as TOD) concept is launched in the 1990s, the New Urbanism planning ideas in the United States, P. Calthorpe's. His "The Next American Metropolis" (1993), a book made a typical TOD design, shown in Figure 1.

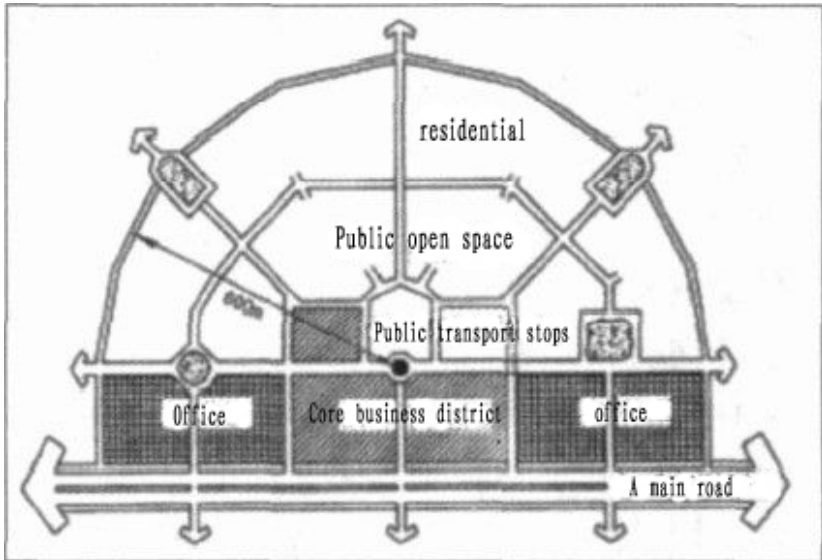


Figure 1 regional development model based on the TOD

Figure 1, the TOD is development and construction within the region of a bus station for the 2000 foot and a half arc. TOD is defined as the high-density residential, retail, office, public facilities and open space, mixed land use patterns. Calthorpe believes the number of commercial facilities for each TOD and mixed type depending on the commercial core of the TOD is to serve the nearby residents or service to the entire community. Taking into account more than 60% of U.S. non-work trip travel, this commercial core and transit site for the center of the mixed land-use form, is significant for reducing car use. ^[2]

TOD typically features include: Compact layout of urban development, support public transport; Shops, residences, parks, offices, public facilities construction located in the bus site services within walking distance; Pedestrian-friendly streets, and directly connected with the trip start and end point; Provide different types, different prices, different floor area ratio mixed residential; Protect the natural environment, the use of topography, building high-quality public space; Public space is the construction towards and public activity centers; Encourage to fill and reconstruct along the transit corridors in built-up area.^[1]

CHARACTERISTICS OF THE CITY TOUR

City Tour

Urban built-up area is composed of two or more relatively independent of the main clumps and several basic clumps, mostly due to large rivers or other terrain and other natural conditions, urban land is divided into several clumps of a certain size of partitions, they have their own centers and road system. Between the clumps have a certain distance, but there are convenient connections of the channel to make up a city entity. Figure 2, for a city tour diagram. The city has seven groups, the middle is the city's political, economic, business center, center tour of the city.^[8]

China's most typical, the largest city tour of Chongqing, shown in Figure 3, Chongqing is a very complex structure of the city tour. The larger group is the main city of Chongqing, outside the main city of Fuling, Wanzhou are two large groups over a million population. Within the main city of Chongqing, from the Jiangnan, Jiangbei, Yuzhong and other large groups and several large satellites which scales is comparable to large cities are composed of a megacity.

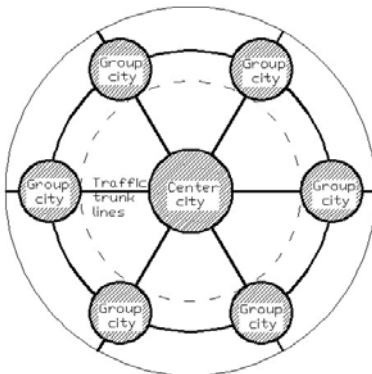


Figure 2 Schematic diagram of the city tour

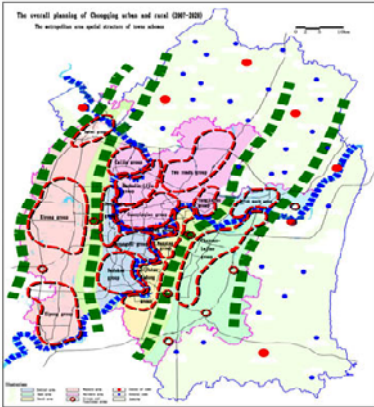


Figure 3 Schematic diagram of Chongqing Congress delegation

Transportation Characteristics of City Tour

Transportation system structure of the tour city layout is similar to the parallel processing distributed network in computer networks, such a structure makes concentrated in a central area of the traffic is separated into multiple groups, by their parallel processing. Therefore, this structure can effectively relieve urban traffic load imbalances, while traffic pressure from outside the cities to the center of the city during expansion of single-center urban spheres converts to transport links pressure between the various groups.

However, due to natural conditions, the key of group city's transport efficiency is to the various groups of traffic operation efficiency. Link road between the groups is the key to the entire road network and the bottleneck lies. Small-scale road network, poor road connectivity will make the transport node pressure too large, leading to poor transportation.

For Chongqing City, there are Jiangbei, Yuzhong, Nanan, Jiulongpo, Shapingba five major groups. According to the survey, in the links of the group range channel, commuter traffic is also a large share. In the morning and evening commuter peak there is a large passenger flow, the inter-city tour traffic dry road transport traffic load is too large. The difference between the traffic characteristics and general urban traffic characteristics are: 1) The distribution of residents travel distance showing two-peak phenomenon. That the proportion of long-distance travel is high than the average city; 2) Average vehicle travel distance is long, travel time is long, fewer daily trips; 3) group districts are more crossing vehicles, and more vehicles by entering from other groups; 4) trunk road is the closer group, the greater traffic, the speed also decreased significantly.

GROUPS OF URBAN PUBLIC TRANSPORT DEVELOPMENT NEEDS ANALYSIS

Level of Demand for Urban Development

From the tour city morphological analysis, dependence of the group urban development mobility is strong, the transportation system of group's city itself is very fragile, between the two there is a huge contradiction. Only use of large capacity, high efficiency, intensive public transport, to save the limited resources at the same time, and to meet the needs of people travel in the future, to guarantee the sustainable development of cities. TOD strategy of research and experience show that, public transport as the dominant mode of urban transport development can gradually lead urban land distribution to more intensive pattern of evolution of multi-center. This urban land use development model will help optimize the urban groups' limited space resources, and is suitable for multi-center, scattered groups pattern.

Level of Traffic Development Needs

The key of group layout city's transport efficiency is to the various groups traffic operating efficiency, and the commuter traffic which in time and space is very concentrated, the flow is clearly is the group city's most important transport, the double peaks of commuter traffic caused by traffic problems become a culprit. TOD strategy of research and experience show that, public transport as the dominant mode of urban transport development can gradually guide the flow of urban traffic, reduce car usage, relieve the serious problem of urban traffic.

Basic Method of Passenger Flow Forecast

The biggest difference between TOD mode of public transport passenger flow forecasting and general passenger traffic forecasts is the feedback within predicted and land development programs. From the perspective of transportation planning, land use patterns determine the incidence, attract of traffic and distribution patterns, and to some extent, determine the traffic structure; From the perspective of land use, Transport capacity and quality of service has changed urban structure and land use patterns. Specifically, under the guidance of the TOD concept, the hub overall function should be positioned as a guidance, considering the surrounding land development patterns of the hub and land features. And the surrounding road network distribution of the hub, transportation as well as other external traffic environment as a constraint, based on the four-phase method, to consider arising from induced increase passenger flow of the public transportation system improvements, as for public transport passenger demand forecasting.

CITY TOUR PLANNING BETWEEN THE TRANSIT HUB

The layout of the transit hub in the group city occupies a very important position, that hub layout is reasonable will play a multiplier effect for the interface

between the groups. For the hub site, should be set in the center groups of land use focus, of high traffic, join the sub trunk roads of functional areas, is mainly responsible for each region of urban to the urban centers passenger transport of distribution and transit transfer. For the group on the edge of travel demand, a higher concentration of traffic Area Center, you can also set the transit hub, it can give consideration to the group edge and center of the contact.^[4]

For the transit hub layout planning program, on the basis of forecasting hub passenger traffic, first predict long-term transit OD, combine with urban land use planning, look for major distribution point for passenger traffic, as an alternative set of hubs; Then make the public transport hubs set of alternative shape heart, divide into bus service partition, change planning period transit OD matrix to bus-based service partition, transit hubs alternative set of start and end points of the OD distribution matrix; Finally, on the new transformation transit OD distribution matrix, regard maximize the efficiency of transit transport systems to optimize the target, determine the hub layout, combined with the land nature of the hub and passenger distribution function and other factors, determine the specific location and scale of hubs.

Nanping, Chongqing City tour, for example, Nanping district traffic is relatively large, land use focus, existing transit hub station is located in Nanping district, origin and stop there are 22 bus lines, undertake in the group and other groups the transit traffic distribution and transfer. However, due to excessive traffic, excessive flow, causing traffic chaos in this region, and with the other group on linking place often appear serious traffic jam phenomenon. Now base on hub of passenger flow forecast, by OD bus forecast, base on the TOD mode, combine with nearby land use planning, propose to construct a large transit hub in the vicinity of Four kilometers. We believe the completion of this transit hub will effectively alleviate the traffic problems of the group, for the interface between the other groups will be much smoother.

PLANNING OF CHANNEL CONNECTION BETWEEN CITY TOURS

Inter-group Multi-channel, Three-dimensional Planning

On the road of contact the tour cities, trip purpose of the commute traffic flow is not easy evacuation and transfer of traffic flow, in order to solve a lot of commuter traffic congestion and other issues, TOD mode can rely on the one hand, try to a transport hub for the center, establish and improve the shopping, entertainment, leisure, work, living as one of the district, minimize residents across the group to travel. If you must travel across the group, a number of trunk roads can be laid to connect the groups, or the use of three-dimensional mode, the application rail travel to complete activities across the groups. In addition, on the highway bus lanes may be established, to ensure public traffic priority right. As a way to encourage residents to use public transport travel, this can relieve peak hour congestion between groups.

For example, traffic between Chongqing city tour mix, you can set up bus lanes to relieve traffic; Chongqing city tours' link more from the cross-river bridges, also can be three-dimensional transport model, a way to establish rail to transport passengers. Shown in Figure 4.

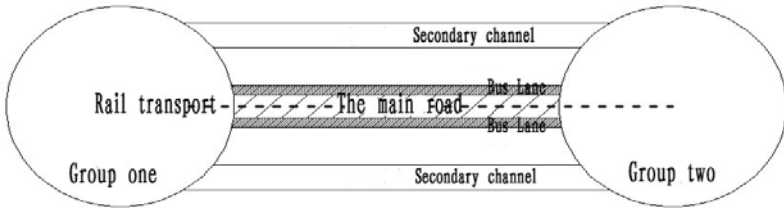


Figure 4 Inter-group multi-channel, three-dimensional arrangement

Interfaces of Channel Connection Between Group and Groups' Internal Road

Most group cities formation rely on trunk roads, there are many cross-border traffic, also the link between group node has produced lots of pressure, entry into the group's traffic and transit traffic through groups overlap, they will form a powerful range of dry road traffic flow. Therefore, the group must establish the independent channel and external transport systems (such as elevated road), make the cross-border traffic directly through the tour group.

For internal groups, should increase the density of road network, in the relatively high level group edge planning of the ring or tangential trunk road, distribution road through the tour edge, balanced and dispersed traffic flow which into groups, to provide a good foundation for the future increasing range of contact channels.

PROGRAM EVALUATION AND SUPPORT SYSTEM

Whether it is the hub planning between the groups or the interface channel planning between the groups, planning program evaluation must take into account users, operators and the public interests. Therefore, the evaluation should include the main content that public transport network technical evaluation, economic evaluation and social evaluation of environmental benefits.^[6]In the TOD concept and mode of guidance, the interface channel planning between the groups should be able to achieve better public transport in urban spatial structure optimization and adjustment, and a reasonable guide for land use, the level of coordination evaluation of land use as an indicator in evaluation system.

In order to protect the city tour mode to TOD development, thorough implementation of the transportation system planning under the concept of TOD, from a strategic positioning, design, management, and different levels to ensure the implementation of the legal system. But also from the humane, comfortable, convenient point of view, create a favorable condition for public transport, by the government to take the lead in encouraging residents to group internal travel, travel

by public transport.

CONCLUSION

In this paper, TOD concept as a guide, base on analysis of the group of urban public transport development needs, to introduce a hub-oriented planning thinking, and to develop the planning of channel connection between city tours, and to propose assessment and the security system. Analysis showed that, TOD model and the interface between urban groups are very close, base on the TOD model, the traffic problems between the city tour will be able to be alleviated.

REFERENCES

- [1] AnHao. "TOD Mode" and "Scattered Compact City Groups" [J]. Art and Design. 2007 (12).
- [2] JiangYulin,HanSunsheng. Public Transportation Guide Urban Development--TOD Idea and in China's Practice [M]. People Traffic Press. 2009 (09).
- [3] Lin Yan, Deng Wei, Ge Liang. The Study of Public Transit-oriented Development Model of Urban Land (TOD) [J]. Traffic and Transportation Engineering and Information Technology .2004,2 (4).
- [4] XiaShengguo, CaoGuohua. TOD Mode of City Public Transportation Hub Design Method [J].City Development Research. 2008 (S1)
- [5] Yu Ting, Lin Lian, Mountain Urban Rail Development and Land Use Reflections [J]. New West (second half) .2009 (01).
- [6] Yu Jie, Yang Xiaoguang, Yin Rui, Xia Shengguo. TOD Mode of Growth Urban Public Transport Planning [J]. Traffic and Transportation Engineering .2007,6 (7).
- [7] Yang Liya, Shao Chunfu, Nie Wei, Zhao Yi. TOD Mode of Urban Co-ordination between Transport and Land Use Assessment [J]. Beijing Jiaotong University, 2007 (03)
- [8] YePengyao, ChenXiaohong. The Study of Function Group City Road Network Structure Planning [J]. The Urban Traffic. 2006, (4).

The Social Cost of Traffic Congestion and Countermeasures in Beijing

Li-zeng MAO¹, Hong-ge ZHU¹, Li-ren DUAN²

¹ Beijing E-Hualu Information Technology Co., Ltd, Beijing, 100007, China

² Information Engineering College, Chang'an University, Xi'an, 710064, China

ABSTRACT

Based on the applying of congestion cost assessment methodologies, congestion cost calculation process was analyzed and construction of calculation models was deduced. According to the database of city traffic running status and Statistic Yearbook 2010 in Beijing, the social cost of Traffic Congestion was calculated. The result shows that Traffic Congestion costs about 58 billion Yuan RMB (4.22% of GDP) in Beijing in 2010, including time delay cost, extra oil combustion, traffic accident direct economic loss, vehicle loss cost, environment pollutants. The proportion of GDP is higher than the same scale cities, such as New York, London and St. Paul. The most congestion cost comes from trips by car and the time delay cost is the mainly and directly social cost. For saving of vehicle congestion, this paper suggests that government of Beijing should optimize city function construction around the urban railway station to scatter the function in central metropolitan area, and provide more hospital, school and job in nearby area of new railway station to reduce long distance trip demand.

INTRODUCTION

Traffic congestion is a concept which is difficult to quantify, people's awareness of traffic congestion is different in different cities. Common method to evaluate traffic congestion is average speed, road saturation, crowded rate or queue length, etc. United States, Japan and other developed countries have made a lot of researches about how to evaluate traffic congestion degree, for example, United States has established a relatively perfect congestion evaluation system that applies the expedite research report, traffic congestion evaluation system.

Traffic management evaluation system of city (2004) of the Ministry of public security of China, in which defines severe congestion as Green lights have displayed three times but none vehicle crossing the intersection within signal or length of queue that vehicle blocking at the outside lane of the intersection exceeding 400 meters at the intersections without signal. Beijing use the traffic congestion index to measure the level, congestion index is a conceptual value which is the comprehensive reflection of the state of road network or congestion, just as the digital equivalent of congestion (See table 1).

Table 1. Traffic Congestion Index Table of Beijing

Traffic index	Congestion level	Corresponding traffic	Travelling time
0~2	Fluent	Free traffic fluid	Running with the speed limit
2~4	Almost fluent	Congestion in some road	0.2~0.5 times longer
4~6	Light degree congestion	Congestion in part of the ring road or main road	0.5~0.8times longer
6~8	Middle degree congestion	Congestion in large part of ring road and main road	0.8~1.1times longer
8~10	Heavy degree congestion	Congestion in anywhere	1.1~ times longer

MODEL SPECIFICATION

Time Cost

The time cost includes time loss of drivers, passengers and pedestrian, and the economic loss as a result of the freight delay caused by congestion.

Time Cost of Travel

Traffic congestion causes slowdown of vehicle speed, resulting in the extension of travel time, according to the average speed, average delayed time of each travel can be deduced as following formula.

$$T_d = L \times \left(\frac{1}{V_c} - \frac{1}{V_0} \right)$$

Where T_d is average delayed time each travel; L is average travel distance each time per person; V_c is average speed when traffic is congestion; V_0 is average speed when traffic is free.

Value of unit time is calculated according to the average wage and working time.

$$R_h = \frac{I_a}{D_y \times 8}$$

Where R_h is value per unit time; I_a is average wage per year; D_y is the number of working days per year.

Considering the differences of the unit time value in different travel way, therefore, unite time value is calculated by travel mode and corresponding total travel, as following.

$$C_{pt} = \sum_{i=1}^n R_{i,h} \times T_d \times P_{i,c}$$

Where C_{pt} is time cost of passenger; i is the kind of transportation; $R_{i,h}$ is value of unit time of the i transportation; $P_{i,c}$ is total travel of the i transportation.

Freight Delay Cost

The total congestion cost C_t is calculated by transportation expenditure and the proportion of total congestion time in 24 hours every day.

$$C_t = C_{tr} \times \frac{T_d}{24} = C_{tr} \times \frac{L}{24} \times \left(\frac{1}{V_c} - \frac{1}{V_0} \right)$$

It's very difficult to separate the extra congestion cost C_{con} and total congestion cost, so percentage that extra congestion cost takes of total congestion cost as that P_t between extra congestion time and total congestion time was applied to evaluate the C_{con} .

$$P_t = \frac{T_d}{T_t} = \frac{L \times \left(\frac{1}{V_c} - \frac{1}{V_0} \right)}{\frac{L}{V_c}} = 1 - \frac{V_c}{V_0}$$

$$C_{con} = C_t \times P_t = C_t \times \left(1 - \frac{V_c}{V_0} \right)$$

Energy Cost

Under the condition of congestion, the vehicle run more fuel for longer driving time, at the same time, the vehicle keep braking, starting, whistling, the action as well as low level, low speed when the engine and vehicle matching is not in the ideal condition and other reasons, will increase fuel consumption. Figure 1 is a curve show the relationship between average speed and fuel consumption, It shows clearly that fuel consumption in low or idling speed (20km / h) is almost 1.5 times more than that in normal driving (city normal running speed is 40 ~ 60 km / h)

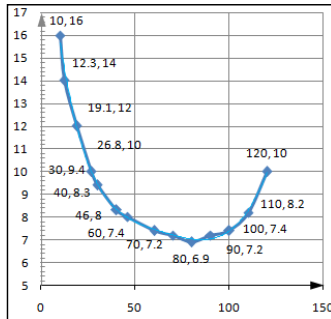


Figure 1. Relationship between average speed and fuel consumption

Fuel consumption in congestion minus the consumption in normal condition is the additional energy consumption, multiply by unit price of energy consumption, the formula shows as following.

$$C_{ex.g} = \sum_{i=1}^n \frac{L_{i,to}}{100} \times (V_{i,con.g} - V_{i,0.g}) \times Y_i$$

Where I is indicates different vehicle types ($i = 1, 2, \dots \dots n$); $L_{i,to}$ is total congestion distance corresponding to the vehicle type; $V_{i,con.g}$ is fuel consumption of different type of vehicle in a jam; $V_{i,0.g}$ is fuel consumption in 100 miles of different type of vehicle; Y_i is unit price of different fuel consumption.

Traffic Accident Cost

Traffic congestion increases more crashes such as scraping and tracing. The accident cost insurance company determines the total cost of traffic accident. Considering traffic congestion increase probability of accident and the insurance company can't claim all the accident loss, the factor ξ_a is multiplied to correct the final results, following is the formula.

$$C_{ac} = C_{to.a} \times P_t \times \xi_a = C_{to.a} \times \xi_a \times \left(1 - \frac{V_c}{V_0}\right)$$

Where $C_{to.a}$ is the accident cost caused by congestion, ξ_a is the accident cost insurance company claims, C_{ac} is the correction coefficient.

Vehicles Loss Cost

Driving in the congestion conditions will increase the fuel consumption, the vehicle use time, and accelerates the wearing of braking disc and tire, speed up the frequency of vehicle maintenance Congestion maintenance costs can be calculated by the proportion congestion time accounted for travel time. The additional loss cost due to congestion is expressed as:

$$C_d = C_0 \times A_t \times P_t = C_0 \times A_t \times \left(1 - \frac{V_c}{V_0}\right)$$

Where C_0 is vehicle average maintenance costs for congestion, the total number of vehicle is A_t .

Environmental Pollution Cost

Vehicle in congestion keep starting, braking and the condition that low level, low speed increases fuel consumption and exhaust emissions. At low speeds, the work situation of the engine do not reach economic region, leading to the fuel not burning adequately. Figure 2 is the graph of engine external characteristic; it shows that the optimal fuel economy is not in the low speed region, but at the n3 point.

Driving at low speed or idle pollutes more, when the speed is under 90 km/h, CO, HC of light vehicle increases as the speed increases, so pollution coefficient ξ_e is multiplied to modify the final results. Calculation formula is expressed as:

$$C_e = C_{envi} \times P_t \times \xi_e = C_{envi} \times \xi_e \times \left(1 - \frac{V_c}{V_0}\right)$$

Total Congestion Cost

$$C_{con} = C_{pt} + C_{con} + C_{ex.g} + C_{ac} + C_d + C_e$$

ESTIMATION METHODS AND PROCEDURES

Beijing city was applied to testify the calculation model, conducting the calculation of traffic congestion cost, the basic parameters (including average distance of Beijing citizens’ commuter, urban average speed in the morning and evening peak) involved in the calculation are in Table 2, value of unit time and travel times are shown in Table 3 and Table 4.

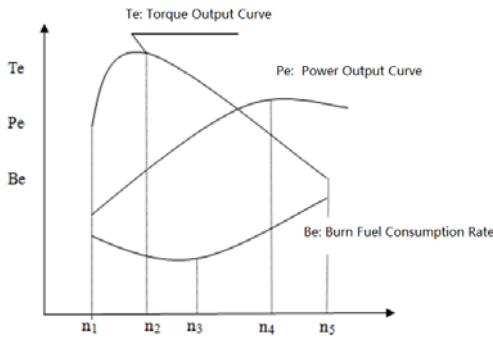


Figure 2. Fuel consumption rate under the different working condition

Table 2. Basic Parameters of Time Cost

Item	Parameter	Number	Unit
Average distance of Beijing citizens’ commuter	L	19.3	Km
Urban average speed in the morning and evening peak	V_c	23.85	Km/h
Urban average speed when traffic is free	V_0	40.0	Km/h
Average income per year	I_a	50415	Yuan
Number of working days per year.	D_y	243	Day

Table 3. Unit Time Value in Different Way of Travel

Item	Parameter	Number	Unit
By public traffic	$R_{1,h}$	26	Yuan/h
By taxi	$R_{2,h}$	31	Yuan/h
By car	$R_{3,h}$	39	Yuan/h

Table 4. Travel Times in Different Way of Travel

Item	Parameter	Number	Unit
By public traffic	$R_{1,c}$	756.2	Million
By taxi	$R_{2,c}$	138.0	Million
By car	$R_{3,c}$	660.9	Million

Calculation of Time Cost

Passenger's Time Cost

Substituting $R_{1,h}=26$, $R_{2,h}=31$, $R_{3,h}=39$, $T_d=0.911$, $P_{1,c}$ = RMB 756.216 million, $P_{2,c}$ = RMB 138.024 million, $P_{3,c}$ = RMB 660.960 million into formula, the passenger's time cost was calculated as following formula, and detail results are showed in Table 5.

$$C_{pt} = \sum_{i=1}^3 R_{i,h} \times T_d \times P_{i,c} = 452.93 \text{ billion}$$

Table 5. Congestion Cost Statistics in Different Way of Travel

	Bus	Taxi	Car	Total amount
Cost in different way of travel (billion)	179.1	38.9	234.8	452.9
Proportion (%)	39.5	8.6	51.8	100.0

Freight Delay Cost

GDP in Beijing in 2010 is 1.37779 trillion Yuan. Logistics cost takes 17.8% of GDP, transportation cost takes 53.1% of the logistics cost, therefore, freight delay cost was calculated as following.

$$C_{con} = C_t \times P_t = C_t \times \left(1 - \frac{V_c}{V_0}\right) = 20.0 \text{ billion Yuan}$$

Energy Cost

In 2009, energy consumption is 65.777 million tons standard coal in Beijing. According to the growth rate 3.96% in 2009 we can estimate that the total energy consumption in 2010 is 68.382 million tons of standard coal. So the transportation energy consumption will reach 13.6767 million tons. Table 6 shows the energy

consumption for traffic congestion differs with the Vehicle model.

Table 6. Consumption of different vehicle

Item	Parameter	Unit	Bus	Taxi	Car
Total traffic mileage	$L_{i.to}$	Million miles	502.3	151.3	33447.1
Congestion consumption	$V_{i.con.g}$	L/km	69.2	9.7	10.2
Fluent consumption	$V_{i.o.g}$	L/km	51.56	7.5	7.6
Price	Y_i	Yuan/Liter	7.15	7.3	7.3

$$C_{ex.g} = \sum_{i=1}^3 \frac{L_{i.to}}{100} \times (V_{i.con.g} - V_{i.o.g}) \times Y_i = 70.1 \text{ billion}$$

Traffic Accident Cost

In 2010 the insurance company claims for traffic accident compensation reaches about 1.8 billion Yuan. The factor ξ_a takes 1.05, so we can calculate the cost for traffic accident.

$$C_{ac} = C_{to.a} \times P_t \times \xi_a = 7.8 \text{ billion}$$

Vehicles Loss Cost

According to the data, average maintenance cost is 1402 Yuan per vehicle, 1/3 time is driving in the state of congestion, so the average congestion maintenance cost is estimated 467.3 Yuan. In Beijing, the total number of annual average vehicle is 4.5 million in 2010. The additional loss cost produced by the congestion was calculated as following.

$$C_d = C_0 \times A_t \times P_t = 8.5 \text{ billion}$$

Environmental Pollution Cost

Main proportion of the money spends on treatment of car emissions. According to the statistics of Beijing environment protection, approximately 73% HC (including volatile organic compounds VOC), 50% NOx and 63% CO come from vehicle exhaust emissions, so it is 40% atmospheric pollution in Beijing. According to estimation of private cars in Beijing, congestion attributes to CO2 emissions increasing by 2.08 million tons all year.

The statistics show that environmental management cost was 33 billion Yuan in 2010 in Beijing. Based on 40% of the traffic pollution, traffic environmental cost will be 13.2 billion Yuan in 2010. At the condition that 1/3 time is driving in the state of congestion, total pollution cost is 4.4 billion Yuan. The factor ξ_a takes 1.15; extra environment cost for congestion was calculated as following.

$$C_E = C_{envi} \times P_t \times \xi_e = 20.4 \text{ billion}$$

RESULTS

According to the calculated data we can get the comparison table with all kinds of traffic cost (see Table 7).

Table 7. Comparison Table of Congestion Cost in Beijing

Congestion cost	Direct costs					Indirect costs	Total
	Time cost		Energy cost	Accident cost	Vehicle loss cost	Environmental pollution cost	
	Passenger	Freight					
Number(billion Yuan)	452.9	20.0	70.1	7.8	8.5	20.4	579.8
Proportion of GDP(%)	3.29	0.15	0.51	0.06	0.06	0.15	4.22

CONCLUSION

The calculation model specification of economic congestion costs was presented, and calculated the congestion cost of Beijing city in 2010, from which we can get the following enlightenment:

(1) According to the calculation model that presented in this paper the traffic congestion cost is 57.98 billion Yuan, which is slightly lower than (FENG Xiaoshan et al., 2011), which congestion cost is 72.5 billion Yuan, higher than the 14.6 billion Yuan in the literature. Considering the congestion getting heavier from 2004 to 2010, the higher congestion cost than that literature 7 is reasonable, and (FENG Xiaoshan et al., 2011) takes per capita congestion time while this paper adopts average speed at flat peak to calculate. On contrast, average speed at flat peak can be investigated and accessed more easily through the testing equipment has been installed.

(2) Compared with similar city around the world, the proportion traffic congestion cost accounts for the GDP, the proportion in Beijing (4.22%) is far higher than other similar cities, New York is 0.49%, St. Paulo is 0.62%. It means the traffic congestion in Beijing is rather serious.

(3) From table 6, the car congestion cost accounts for 51.8%, higher than the 35% that the percentage people who use car, indicates that car congestion cost is much higher than the average level of various transportation, unit time value of driving private car is 50% higher than the public traffic affects the results and calculation process. Compare to the people by public transportation, the numbers of travellers who have relatively high income increase in Beijing, traffic congestion cost ratio of car users will gradually decline.

(4) Seen from table 7, time cost is the main cost of traffic congestion, it accounts for about 82% of total traffic cost, therefore, the time cost is the most

important and intuitive among the traffic congestion. At the same time, it is worth noting that in addition to traffic congestion economic cost, environmental pollution caused by traffic congestion (especially atmospheric pollution) and the resulting anxiety cost are the same high with other corresponding social cost.

REFERENCES

- CHEN Lairong. Study on Key Problem of Urban Congestion Charge [D]; Doctor Dissertation Beijing University of Technology, 2005
- FENG Xiangshao ,ZHOU Ji, GUO Guangming. Estimation on the External Cost Caused by Urban Transport Congestion [J]. Environment and sustainable development, Issue 34(3), 2009.
- Ian W . H . Parry, Antonio Bento . Estimating the Welfare Effect of Congestion Taxes: The Critical Importance of Other Distortions within the Transport System [J]. November 2000, 50-51
- LUO Qingyu, JUAN Zhicai, SUN Baofeng, JIA Hongfei. Method Research on Measuring the External Costs of Urban Traffic Congestion [J]. Systems Engineering and Information Technology, 2007, 7(5), 9-12.
- “Traffic Congestion in Beijing Ranks One” [WEB/OL], <http://www.bjjtgl.gov.cn/publish/portal0/tab 120 /info16233.htm>
- WU Qibing, CHEN Feng, HUANG Yao, HU Yingyue. Calculation and Analysis of Traffic Congestion Cost in Beijing [J]. Journal of Transportation Systems Engineering and Information Technology, 2011, 1(11):1009-6744.
- XIA Kaixuan, HE Mingsheng, ZHANG Hua. The Economic and Ecological Efficiency of Car Sharing Service and the Feasibility to Implement the Service in Beijing [J], China Soft Science, 2006, (12)

An Analysis of Airport Runway Designs to Maximize New Airport Throughput to meet China's Long-Term Air Travel Demand

William F. Yim

Santa Barbara County Association of Governments (Retired)
260 N. San Antonio Rd., Suite B, Santa Barbara, CA 93110
wym@sbcbglobal.net (805) 815-9595

INTRODUCTION

For the last decade, China's civil aviation sector has undergone rapid transformation and unprecedented growth. Between 2005 and 2010, the average annual growth of air passengers was more than 13 percent per year. In 2010, total air passengers almost doubled that of 2005, reaching 609 million¹ (CAAC, 2007 and 2011). The number of airports has increased from 142 to 190 for the same period. The country has a commercial airline fleet of 2,600 aircraft and is expected to order more than 2,000 aircraft over the next five years, resulting in a fleet of more than 4,500 aircraft by the end of 2015 (CAPA, 2011). According to Chinese aviation officials, 56 new airports are expected to be built in the next five years (Perrett, 2011). China's goal is to build 240 airports to attain 1.5 hour drive range to an airport for more than 80 percent of the national county-level administrative units and to provide an efficient access to air services for more than 82 percent of the China's population (CCAR, 2009).

However, China's airport industry still faces tremendous challenges in fulfilling its modernization program. These challenges range from imbalanced airport development between large hub airports and underdeveloped regional airports, fierce competition from other modes of transportation such as high-speed rail and new freeways (Liu, 2009), and how to maximize airport infrastructure throughput for individual new airports to meet China's long-term air travel demand.

This paper examines the issues of China's latest air traffic growth and the massive ongoing new airport building program. The focus is to analyze how China could maximize its new airport throughput capacity with respect to new runway configuration designs in order to pursue a modernized and well-balanced airport expansion system nationwide toward its strategic and long-term aviation growth.

CURRENT AND FUTURE AIRPORT DEVELOPMENT TRENDS IN CHINA

For the last decade, traffic growth for China's top 11 airports (including Hong Kong International) was phenomenal. Between 2000 and 2010, the annual growth

¹ Total 2010 air passengers were 608.7 million including 50.1 million from Hong Kong International Airport.

percentage of air passengers was in double digits (10% to 22%) (Figure 1). Similarly, the annual growth of aircraft operations (takeoffs and landings) was between 8% and 19% (Figure 2). Furthermore, between 2008 and 2010, the rate of growth was accelerating. With the exception of Hong Kong International, the total growth of air passengers for the top 11 busiest airports was experiencing growth between 22% and 51% (Table 1).

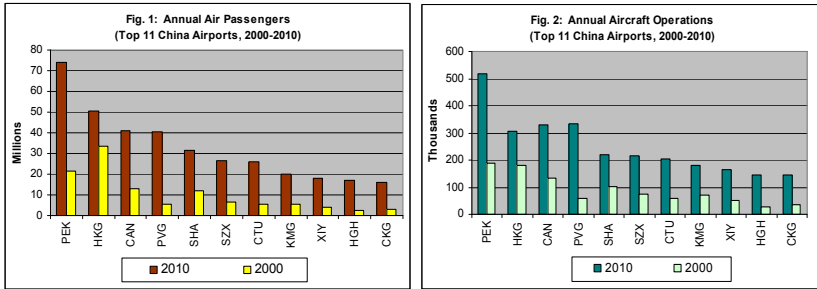


Figure 1. Percentage changes from 2000 to 2010 (Source: CAAC 2003 and 2011)

Table 1. Total Passengers for China’s Top 11 Airports, 2008 to 2010

China's Top 11 Airports	Airport Code	Total Passengers (m)		% Incr. (2008-10)
		2008	2010	
Beijing (Capital/Nanyuan International)	PEK	55.9	73.9	32.2%
Hong Kong Intern'l (ChekLapKok)	HKG	47.9	50.3	5.0%
Guangzhou (Baiyun International)	CAN	33.5	41.0	22.4%
Shanghai (Pudong International)	PVG	28.3	40.6	43.5%
Shanghai (Hongqiao International)	SHA	22.8	31.3	37.3%
Shenzhen (Baoan International)	SZX	21.4	26.7	24.8%
Chengdu (Shuangliu International)	CTU	17.2	25.8	50.0%
Kunming (Wujiaba International)	KMG	15.8	20.2	27.8%
Hangzhou (Xiaoshan International)	HGH	12.7	17.1	34.6%
Xian (Xianyang International)	XIY	11.9	18.0	51.3%
Chongqing (Jiangbei International)	CKG	11.1	15.8	42.3%

Source: CAAC 2009 and 2011

Comparison of Airport Development between China and the U.S.

While the land sizes of China and the U.S. are relatively similar, China’s population is 4.3 times the U.S.’s (1.3 billion vs. 313 million). However, in terms of airport distribution and development, China and the U.S. present very different pictures. Currently in the U.S., as many as 24 airports have total annual passengers over 20 million. In China, only eight out of 100 airports have over 20 million annual passengers.

In the U.S., air-carrier airports are evenly spread across the country. Almost every major city in the U.S. has an air-carrier airport. China’s airport development has been focusing on major international gateway cities such as Beijing, Shanghai, Guangzhou, Shenzhen, and Hong Kong. Over 45% of air passengers and 74% of air cargo are

concentrated at these hubs (**Table 2**). Existing regional airports are either largely undeveloped or inefficiently operated primarily due to the lack of infrastructure and capability to market and operate them.

Table 2: Traffic Growth for Top Six China Airport, 2010

Airports	Code	2010					
		Passengers	%	Operations	%	Air Cargo	%
Beijing Capital International Airport	PEK	73.9	12.6%	517.6	10.5%	1.6	10.2%
Hong Kong International Airport	HKG	50.3	8.6%	306.5	6.2%	4.1	26.9%
Guangzhou Baiyun International Airport	CAN	41.0	7.0%	329.2	6.7%	1.1	7.5%
Shanghai Pudong International Airport	PVG	40.6	6.9%	332.1	6.7%	3.2	21.1%
Shanghai Hongqiao International Airport	SHA	31.3	5.3%	219.0	4.4%	0.5	3.1%
Shenzhen Bao'an International Airport	SZX	26.6	4.5%	216.7	4.4%	0.9	5.3%
Total		263.7	44.9%	1,921.1	39.0%	11.4	74.2%
Rest of top 50 Airports		297.8	55.1%	2,804.9	61.0%	3.2	25.8%

Source: CAAC 2011

China's Aviation Expansion Plans

According to China's 2011-15 five-year airport construction program, China is building 56 new airports in order to meet the rapid growth of air travel demand. The questions are:

- How would each of these new airports be best designed to process a rapidly increasing demand in air travel?
- How would these airports be built in the most efficient and cost-effective manner while at the same time providing a long-term balanced airport system nationwide?

The following section analyzes the various runway configuration designs to maximize airport throughput to meet China's long-term air travel demand.

ANALYZING VARIOUS RUNWAY DESIGNS TO MAXIMIZE NEW AIRPORT THROUGHPUT TO MEET CHINA'S DEMAND

Factors Affecting Airport Capacity

One way to define airport throughput is the hourly capacity of the runway system. Hourly capacity of a runway system is its ability to process the number of aircraft operations (takeoffs and landings) within each hour. The hourly capacity is influenced by four groups of factors: 1) Air Traffic Control, 2) Characteristics of Demand, 3) Environmental Conditions (Visual Flight Rules or VFR and Instrument Flight Rules or IFR), and 4) The layout and design of the runway system. This paper focuses on addressing the last group of factors – runway layout and design of the runway system as it applies to new airport development.

In 1976, the U.S. Federal Aviation Administration (FAA) published a comprehensive handbook that provided procedures for determining the ultimate airfield capacities (and delays) based on a 4-year study. The study examined the following variables that affect the hourly capacity of an airport:

- Fleet Mix (aircraft mix)
- Runways available for serving both arrivals and departures
- Variety of runway configurations and uses
- Tough and go operations
- Taxiway exit configuration
- Environmental conditions (VFR, IFR)
- Wind coverage

Among these variables, fleet mix is particularly crucial. Fleet mix refers to the percentage of Class C (large aircraft as defined by more than 12,500 lbs to 300,000 lb) and Class D (heavy aircraft for more than 300,000 lb) when calculating airport capacity. The “Mix Fleet Index” is based upon the percentage of Class C aircraft plus three times the percentage of Class D aircraft. In general, the higher the fleet mix index, the lower the estimated hourly capacity for a given runway system (**Table 3**).

Table 3: Effects of Fleet Mix on Airport Hourly Capacity

Runway Configuration	Configuration Diagram	Fleet Mix Index	Hourly Capacity	
			VFR	IFR
Single Runway		21 - 50	74	57
		51 - 120	63	53
Independent IFR Parallels		21 - 50	149	114
		51 - 120	126	105
Parallels + One Intersecting Crosswind		21 - 50	149	63
		51 - 120	126	70

Source: Ashford, N. 1984

When a unidirectional runway system (either E-W or N-S direction) is able to capture 95% or more of the wind coverage, the most efficient runway configuration that offers the highest hourly capacity is a pair of parallel runways with separation of 4,300 feet or more. This configuration is able to provide the highest hourly capacity under IFR, which is critical under inclement weather conditions, and at the same time, allow an independent and simultaneous operation on each of the parallel runways. With recent technological advances in air traffic control (ATC) and operational procedures, independent simultaneous runway operation can be achieved with a much-reduced runway separation, e.g., down to 3,000 feet of separation or even lower.

If a runway system were unable to provide 95% wind coverage, a *crosswind* runway will be required. However, adding a *crosswind* runway to a runway system may not necessarily increase the hourly capacity due to the potential runway conflicts present innate to crosswind runways. Thus, a 3-runway system with a crosswind may not necessarily display higher hourly capacity.


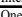
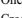

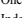
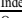
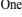

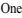

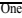

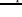


Runway Configuration Design vs. Airport Hourly Capacity

Calculating airport capacity on any runway system can be a complex task. Ongoing research has indicated that capacity limitations at many major hub airports are essentially the restrictions placed on the ability for air carriers to add flights to

accommodate increased demand. Thus, the increased demand can only be handled by either upgrading existing airports, the use of larger seating capacity aircraft, or building new airports.

The airport systems in the U.S. probably are the most complex. The diversification of runway configurations allows airport hourly capacity to be calculated under many different scenarios. In addition, the ongoing research on technological advances in aviation makes airport planning in the U.S. cutting edge. Still, U.S. is largely hammered by the high cost of airport expansion, significant environmental concerns, and operational and political constraints. Adding to the challenge is the ongoing encroachments of land use developments around airports, which severely restrict large-scale capacity improvements for existing airports. Thus, viable options for airport capacity improvements in the U.S. are largely dependent on a “bandage approach”, i.e., applying short-term fixes to incrementally improve and/or expand existing systems. **Table 4** examines the hourly capacity of various runway configurations for major U.S. airports.

Table 4: Runway Configuration vs. Hourly Capacity²

Airport	Runway Configuration	Hourly Capacity				(% IFR Capacity Increase)	Remarks
		Current		with New Rwy			
		Optimum	IFR	Optimum	IFR		
SAN	 Single Runway	56-58	48-50	--	--		
LGA	 Intersecting Runways	78-85	69-74	--	--		
EWR	 One Pair of Closed Parallel & One Crosswind	84-92	61-66	--	--		
FLL	 One Crosswind Intersects a Pair of Independent of Parallels	60-62	52-56	--	--		
CLE	 One Pair of Closed Parallel & Two Crosswinds	80	64	115	88	44%	3 Closed-In Parallels & 2 Crosswinds
CVG	 One Pair of Independent Parallel & One Crosswind	120-125	102-120	176	141	35%	Triple Independent Parallels & One Crosswind
JFK	 One Pair Independent & One Pair Dependent Crosswind	75-87	64-67	--	--		
SFO	 Two Pairs of Closed Parallels	105-110	68-72	--	--		
LAX	 Two Pairs of Independent Parallels	137-148	117-124	--	--		
ATL	 Currently Operates as Triple Independent Parallels	180-188	158-162	243	221	32%	Triple Simultaneous Independent Parallels, 2013
DCA	 Triple Intersecting Runways	72-87	48-70	--	--		
DEN	 Three Pairs of Independent Parallels	210-219	159-162	281	236	22%	3 Pairs of Independent Parallels
ORD	 Three Sets of Parallels and One Crosswind	190-200	136-144	--	--		
DFW	 Four Pairs of Independent Parallels	270-279	186-193	303	205	22%	Quadruple Simultaneous IFR Operations
ATL	 Two Pairs of Parallels and/or Triple Independent Parallels	180-188	158-162	243	221	32%	Can operate under Triple Simultaneous Independent Parallels, 2013

The following observations are apparent:

² Analysis based on “Airport Capacity Benchmark Report, 2004.” U.S. Department of Transportation, Federal Aviation Administration and Mitre Corporation.

Note: Red line denotes new runway built or under construction.

- An airport with one single runway has limited capability to increase capacity unless land is available for adding new runways to the system.
- Increasing IFR capacity for an airport is paramount because weather (wind, cloud ceiling, visibility, etc.) is one crucial element that significantly affects airport capacity.
- Significant capacity improvements can be achieved if additional parallel runway(s) are added allowing for independent simultaneous operation.

Mega metropolitan airports in the US, such as, Los Angeles International, Atlanta Hartsfield, Denver International, and Dallas Fort-Worth International, etc. have and/or are developing multiple independent parallel runway systems in order to substantially increase their airport throughput to meet the ever-increasing demand.

Best Runway Configuration Options for New Airport Development in China

Unlike the U.S. system, China is building new airports not only to increase individual airport capacity to meet its unprecedented growth but also to increase airport capacity nationwide in the short term. In this case, the “bandage” approach would not work. Building 56 airports in five years require considerable coordination efforts among various entities and jurisdictions. New airports will need to be built to capture its maximum throughput potential in the most cost-effective manner with flexibility for future expansion. **Table 5** summarizes the real-life hourly capacities for various parallel runway configurations in the U.S.

Table 5: Optimum Airport Hourly Capacity for Parallel Runway Systems³









US Airport Example	Runway Config. Diagram	Runway Configuration	Runway Length (ft)	Hourly Capacity				% IFR Capacity Increase
				Optimum		New R/W Added		
				Optimum	IFR	Optimum	IFR	
SAN		Single Runway	9,401	56-58	48-50	NA	NA	NA
ONT		A Pair of Dependent Parallel	10,200, 12,197	63-74	56-57	NA	NA	14%
AUS		A Pair of Independent Parallel	12,248, 9,000	112-116	96-100	NA	NA	100%
PHX 1/		Triple Parallels including a Dependent	11,289, 10,300, 7,800	128-150	108-118	NA	NA	14%
LAX		Two Pairs of Independent Parallels	8,925, 10,284, 12,091, 11,096	137-148	117-124	NA	NA	24%
ATL		Triple Independent Parallels	9,000 x 3, 11,890, 10,000	180-188	158-162	243	221	32%
DEN		Three Pairs of Independent Parallels	12,000 x 5, 16,000	210-219	159-162	281	236	22%
DFW		Quadruple Independent Parallels	13,400 x 4, 9,300, 9,001, 8,500, One NA	270-279	186-193	303	205	22%

³ Analysis based on Horonjeff, R., *Planning and Design of Airports*. 1994 and “Airport Capacity Benchmark Report, 2004.” U.S. Department of Transportation, FAA, and Mitre Corporation. Note: Dotted red line denotes new runway built or under construction.

Evidently, a simple parallel runway system with runway length of 10,000 feet or more coupled with independent simultaneous operational capability offers the best choice for maximizing capacity for new airport construction, particularly with new super-jumbos like the A380. Such configuration is the only one that can offer 100% increase in IFR capacity for aircraft operation under inclement weather conditions.

Table 6 evaluates the pros and cons of various parallel runway systems. Given land availability, the independent parallel runway design appears to offer the best configuration for China's plan to build a large number of airports in the short-term. It also offers flexibility for large-scale capacity increases in the future. If sufficient land is protected for new airports, additional capacity can easily be achieved by simply adding more parallel independent and/or dependent runways, as appropriate. The triple parallel runway system such as Atlanta Hartsfield and the quadruple parallel system such as Dallas Fort-Worth International are classic examples. A parallel runway system with independent and simultaneous operation is essentially the foundation for world-class airports like London Heathrow, Amsterdam Schiphol, and Moscow Sheremetyevo International, and incidentally, China's Beijing Capital and the Nanyuan International Airports, etc.

Table 6: Evaluation of Parallel Runway Configurations

Runway Diagram	Runway Configuration	% Cap Inc. for One Add'l Rwy		Evaluation of Runway System Configuration*
		Opt.	IFR	
	Single Runway	NA	NA	Limited capacity available
	A Pair of Dep. Parallel	28%	14%	IFR capacity is constrained
	A Pair of Indep. Parallel	100%	100%	1st Choice for new airport development in a short term (5-years).
	Triple Parallels w/ one Dep.	29%	18%	Preferred choice for incremental airport expansion.
	Two Pairs of Indep. Parallels	28%	24%	Preferred choice for major airport hub development
	Triple Indep. Parallels	64%	32%	Best alternative choice for long-term hub design
	3 Pairs of Indep. Parallels	16%	22%	Alternative choice for long-term hub design
	Quadruple Indep. Parallels	8%	22%	Alternative choice for long-term hub design

* 95% wind coverage and sufficient land availability is assumed.

CONCLUSION

China's increasing demand in aviation calls for not only modernization of existing airports but also building new airports to alleviate congestion. China is building 56 new airports in the next five years. An ideal way to start each new airport is to build a parallel runway system that offers independent and simultaneous operation with runway lengths of 10, 000 feet or more. This configuration offers maximum airport

capacity throughput initially and flexibility for expansion to meet short-, medium-, and long-term objectives.

REFERENCES

- CAAC (2003). "2001 年全国机场吞吐量排名". Civil Aviation Administration of China. March 2003.
- CAAC (2007). "2006 年全国机场吞吐量排名". Civil Aviation Administration of China. March 2007.
- CAAC (2009). "2008 年全国机场吞吐量排名". Civil Aviation Administration of China. March 2009.
- CCAR (2009). "2009 China/US Aviation Symposium." *China Civil Aviation Report*. 7:2. (2009).
- CAAC (2011). "2010 年全国机场吞吐量排名". Civil Aviation Administration of China. March 2011.
- Airport Capacity Benchmark Report, 2004. U.S. Department of Transportation, Federal Aviation Administration, Mitre Corporation.
- Ashford, N. and Paul W. (1984). *Airport Engineering*. 2nd Ed. New York: John Wiley & Sons, Inc., 158-159.
- China Airports, (2011). Photograph. Maps of World. Web. 9 Sept 2011. <<http://www.mapsofworld.com/international-airports/asia/china.html>>.
- CCAR (2009). "China Civil Aviation Development Forum 2009." *China Civil Aviation Report*. 11:3.
- CAPA (2011). "China's airlines to order more than 2000 aircraft over the next five years." Centre for Asian Pacific Aviation (CAPA). March 2011. <<http://www.centreforaviation.com/analysis/chinas-airlines-to-order-over-2000-aircraft-over-next-five-years-47747>>
- Horonjeff, R. (1994). *Planning and Design of Airports*. 4th Ed. New York: McGraw-Hill Inc, 348-349.
- Liu, W. and Luk, M. (2009). "Reform and opening up: Way to the sustainable and harmonious development of air transport in China." *Transport Policy*. 215-233.
- Mohler, G. (2008). "Airport Capacity Planning and NextGen." Federal Aviation Administration (FAA).
- Perrett, Bradley (2011). "Cluster Effect, China will add at least 56 airports in its 2011-15 five-year plan." *Aviation Week & Space Technology*.
- Yang, X. and Yu, H. (2010). "China's Airports: Recent Development and Future Challenges." East Asian Institute.

Comparison of Software Packages for Life Cycle Cost and Benefit Analysis of Highway Projects

Yi Jiang¹, Guangyuan Zhao², and Shuo Li³

¹ Ph.D., P.E., Professor, Department of Building Construction Management, Purdue University, West Lafayette, Indiana 47907. Tel.: (765) 494-5602; E-mail: jiang2@purdue.edu

² Graduate Student, Department of Building Construction Management, Purdue University, West Lafayette, Indiana 47907. E-mail: zhao179@purdue.edu

³ Ph.D., P.E., Research Engineer, Indiana Department of Transportation, Office of Research and Development, 1205 Montgomery Street, West Lafayette, Indiana 47906. Tel.: (765) 463-1521. E-mail: sli@indot.in.gov

ABSTRACT

As part of the effort to develop an economic analysis methodology for evaluating highway projects, the commonly utilized software packages for highway life cycle cost analysis (LCCA) were examined and evaluated. The software packages include MicroBENCOST, California Life-Cycle Benefit/Cost Analysis Model (Cal-B/C), and the Redbook Wizard. Through this study, the methodologies applied by these packages were examined. The similarities and differences among the methodologies were identified and compared. Cost and benefit data from real highway projects were applied using the software packages to evaluate and compare the economic analysis results. It was found that even though the general frameworks of economic analyses are similar in these packages, there exist many differences in the specific processes and parameter values. This paper presents the results of the comparisons and evaluations. The evaluation procedures are illustrated. The similarities and differences of the methods are outlined. The impact of the differences on the results of highway economic analysis is discussed. It is believed that the results of this study will be helpful for highway engineers and planners to understand the capacities and limitations of the software packages.

INTRODUCTION

Economic analysis is a critical component of a comprehensive project or program evaluation methodology that considers all key quantitative and qualitative impacts of highway investments. It allows highway agencies to identify, quantify, and value the economic benefits and costs of highway projects and programs over a multiyear timeframe. With this information, highway agencies are better able to

target scarce resources to their best uses in terms of maximizing benefits to the public and to account for their decisions. It is important in the transportation development process that each transportation alternative is properly evaluated for its costs and benefits during its entire life-cycle. Highway agencies make use of measures such as the net present value of costs and benefits, benefit-cost ratio, or the internal rate of return to compare different competing alternatives. The alternative that gives the highest net present value, benefit-cost ratio or return on investment is selected and is placed to be funded, programmed, and eventually implemented. Cost items in the economic analysis include capital, operating, maintenance and preservation costs while the considered benefits are travel time savings, reduction in vehicle operating costs, and safety benefits. Other benefits such as economic development, improvement in air quality, reduction in energy use, and improvement of the quality of life are not included in the economic analysis framework because these items are considered external and they are difficult to be monetized.

As part of the effort to develop an economic analysis methodology for the Indiana Department of Transportation (INDOT) to evaluate highway projects, the commonly utilized software packages for highway life cycle cost analysis (LCCA) were examined and evaluated. The software packages include MicroBENCOST (McFarland et al., 1993, Meemott et al., 1999), California Life-Cycle Benefit/Cost Analysis Model (Cal-B/C) (Caltrans, 2009), and the Redbook Wizard (AASHTO, 2010). Through this study, the methodologies applied by these packages were examined. The similarities and differences among the methodologies were identified and compared. Cost and benefit data from real highway projects were applied using the software packages to evaluate and compare the economic analysis results. This paper presents the results of the comparisons and evaluations.

THE SOFTWARE PACKAGES EXAMINED

MicroBENCOST was developed in the early 1990's by the Texas Transportation Institute through the National Cooperative Highway Research Program for doing highway user benefit-cost analysis. It is designed to analyze different types of highway improvement projects. With MicroBENCOST, seven types of highway projects can be evaluated: (1) capacity enhancement, (2) bypass construction, (3) intersection or interchange improvement, (4) pavement rehabilitation, (5) bridge improvement, (6) highway safety improvement, and (7) railroad grade crossing improvement. Highways may contain several different types of HOV facility configurations. The benefits considered in MicroBENCOST include user travel times, vehicle operating costs, and accidents. The costs include total initial cost, salvage (residual) value at the end of the evaluation period, and rehabilitation and maintenance costs during the analysis period. The program lets the user specify the year when each construction cost component is incurred, and when future year benefits begin to flow. The analysis period, including the time needed for construction prior to the start of benefits, may last up to 40 years. The economic performance measures provided for the proposed project are:

- Net present worth;
- Gross B/C ratio (User Benefits/Construction + Maintenance Cost - Salvage Value);
- Net B/C ratio (User Benefits + Salvage Value + Maintenance Cost Saving/Construction Cost);
- Internal rate of return.

It should be pointed that even though MicroBENCOST is a powerful computer program, it is a DOS based program and thus it is not as user friendly as a Windows based one.

Cal-B/C was developed for the California Department of Transportation (Caltrans) as a tool for benefit-cost analysis of highway and transit projects. It is an Excel (spreadsheet) application structured to analyze several types of transportation improvement projects in a corridor where there already exists a highway facility or a transit service (the base case). Highway projects may include general improvements, high-occupancy vehicle (HOV) lanes and passing lanes, interchange improvements, and constructing a bypass highway. Benefits in Cal-B/C include user benefits (time savings), reduced vehicle operating costs (for highway users), and accident reductions. Costs include total life cycle investment and annual operating and rehabilitation costs. The economic performance measures provided for the proposed project are:

- Net present worth;
- Benefit-cost ratio;
- Internal rate of return;
- Payback period.

The “User and Non-User Benefit Analysis for Highways”, also known as the Red Book (AASHTO, 2010), was published by the American Association of State Highway and Transportation Officials (AASHTO) in 2010. This AASHTO publication helps state and local transportation planning authorities evaluate the economic benefits of highway improvements. The Red Book contains a computer program “Wizard” for conducting and presenting benefit–cost analyses of highway improvements. This interactive Microsoft Excel wizard takes the user through a series of dialogs where information about a project is collected and then calculates and presents the results of a benefit–cost analysis in a printable format. A series of Microsoft Excel spreadsheets also are included to help the user organize data and make calculations to carry out benefit–cost analyses. These spreadsheets are electronic versions of the calculation worksheets in the manual. The user can choose to examine just user benefits, non-user benefits or both.

COMPARISON OF THE ECONOMIC ANALYSIS PACKAGES

In order to compare the three software packages for economic analysis, the types of the highway projects that can be analyzed, input requirements, and outputs

were examined. Benefit and cost calculations were conducted using the software packages to compare the outcomes from the same input data.

Types of Highway Projects

Highway improvement projects are the common types that the three software packages are designed to analyze their economic impacts. In addition to highway improvements, MicroBENCOST can also analyze bridge projects, safety projects, railroad crossing projects, and high occupancy vehicle (HOV) lanes projects. It also provides options for estimate the impacts of work zones, incidents, and vehicle emissions.

Cal B/C can handle such projects as rail or transit projects, highway operational improvement projects, and transportation management systems. The specific projects under these categories include passenger rail, light rail, auxiliary lane, freeway connector, ramp metering, and incident management.

The Redbook Wizard has the ability to analyze the following types of projects: additional lanes, traffic control, signal control systems, intelligent transportation systems (ITS), roadside lighting, and pavement preservation or maintenance.

The complete lists of project types that the three packages can be used for are shown in Table 1. As can be seen in the table, the Redbook Wizard deals with only highway related projects, while MicroBENCOST is able to analyze bridge as well as highway projects and Cal B/C handles highway, rail and transit projects.

Input and Output

The input requirements depend on the functions and objectives of each software package. To fully utilize a selected software package, it is necessary to have all the required information on the project to be evaluated. For each project, the basic information, such as type of highway, type of improvement, and traffic volume, is common for all three software packages. The details of other required information vary among the three packages.

Table 2 lists the input data required by MicroBENCOST. The input data include the following types: the basic input common for all projects, minor route cross street data, HOV project data, intersection or interchange data, bridge project data, work zone data, incident data, and railroad grade cross data.

The input items for Cal B/C are presented in Tables 3 and 4. The inputs for Cal B/C are under three categories: the project feature data, the project cost data, and

the highway design and traffic data. The types of projects are also under three categories: highway capacity expansions, highway operational improvements, and transportation management systems.

The input requirements for the Redbook Wizard are shown in Table 5. The input data include nine groups, such as cost, user class, benefit on improved segment and unimproved segment, and traffic.

As shown in Tables 2 through 5, the input requirements for the three analysis packages are different in the specific items as well as in categories. However, many of the general requirements are common or similar. In order to effectively utilize any of the analysis packages, it is important for a user to obtain the required information. A database should be created for the economic analysis so that the input data are readily available for the selected software package.

The output items from the software packages are shown in Table 6. All three of the packages produce the expected costs and benefits from the proposed project. However, the individual items of costs and benefits differ in many aspects among the three packages.

CASE STUDIES

To further examine the differences among the software packages, three case studies were conducted. The three highway projects in the case studies were 1) adding traffic lanes to existing highways; 2) pavement overlay; and 3) widening pavement shoulders. For each of the projects, the three packages were used to generate expected costs and benefits. The software packages involve many default values, including oil and fuel costs, value of time, and incident costs. To make the comparison meaningful, attempts were made, whenever possible, to change these default values so that these values were equal in all three packages.

Table 1. Types of Projects Analyzed by Software Packages

CAL B/C		MICROBENCOST	Redbook-Wizard
1. Highway Capacity Expansion	3. Transportation Management System	1. Bypass Projects	1. Additional Lanes
General highway	Ramp metering	2. Added Capacity Projects	2. Traffic Control
HOV lane addition	Ramp metering signal coordination	3. Intersection/Interchange Projects	3. Signal Control Systems
HOT lane addition	Incident management	Upgrading existed to higher design standards	4. ITS
Passing lane	Traveler information	4. Highway Reha./Pavement Improv. Projects	5. Geometric Improvement
Intersection	Arterial signal management	Improved horizontal and vertical alignment	6. Intersection Improvement
Bypass	Transit vehicle location (AVL)	Increase lane widths	7. Roadside or lighting
Queuing	Transit vehicle signal priority	Add paved shoulders	8. Preservation or Maintenance
Pavement	Bus Rapid Transit (BRT)	Pavement rehabilitation/overlay	
2. Highway Operational Improvement	4. Rail or Transit Capacity Expansion	5. Bridge Projects	
Auxiliary lane	Passenger rail	Functional or structural characteristics improved	
Freeway connector	Light rail (LRT)	Build a new bridge	
HOV connector	Bus	Major bridge rehabilitation	
HOV drop ramp	Highway-rail grade crossing	6. Safety Projects	
Off-ramp widening		7. Highway Railroad Crossing Projects	
On-ramp widening		Railroad grade crossings	
HOV-2 to HOV-3 conversion		Warning device upgrad	
HOV lane conversion		8. HOV Projects	
		9. Emission Option	
		10. Workzone Option	
		11. Incident Option	

Table 2. Input Data of MicroBENCOST

The Basic Inputs needed in every project		Minor Route Cross Street Data	HOV Project Data	Intersection/Interchange Project Data
Area type	Type of intersection /interchange/structure	AADT, base year	Type of HOV facility	Percent major route volume with interrupted flow
Project category	Number of intersection /interchange/structure	Access control	HOV beginning hour, inbd. and outbd. direction	Percent minor route volume with interrupted flow
Alternate route switch	Number of lanes, inbound direction	Number of lanes, inbound/outbound direction	HOV ending hour, inbd. and outbd. direction	Ramp type
Total construction costs	Number of lanes, outbound direction	Median width	HOV operation data	Interrupted flow, end of ramp
Functional class	Median width	Arterial class-design category		
Types of traffic distribution	Degree curvature	Segment length to next intersection		
Initial AADT, base year	Percent no passing zones			
Average Annual Traffic Growth Rate	Additional local AADT, base year			
Access control	Number of work zones			
Segment length	Number of Incidents			
Bridge Project Data		Work Zone Data	Incident Data	Railroad Grade Crossing Project Data
Type of bridge structure		Year of work zone closure	Number of incidents per 100 million vehicle-miles	Type of warning device
Diversion of traffic around bridge		Number of days work zone in place	Number of lanes closed	Number of trains per day
Bridge deck width, inbound/outbound		Number of lanes closed	Average duration of incident	Percent reduction in speed crossing tracks
Approach width greater than bridge width		Beginning hour of work zone closure		Time to lower and raised gates
Bridge length		Ending hour of work zone closure		Average train speed
Diversion distance				Train length

Table 3. Cal B/C Cost Data Required

Type of Projects		Project Cost Data Item				
		Right-of-way acquisition costs	Construction costs	Maint. and operating costs	Rehabilitation costs	Mitigation
Highway Capacity Expansion	General Highway	X	X	X	X	X
	HOV Lane Addition	X	X	X	X	X
	HOT Lane Addition	X	X	X	X	X
	Passing Lane	X	X	X	X	X
	Intersection	X	X	X	X	X
	Bypass	X	X	X	X	X
	Queuing	X	X	X	X	X
	Pavement	X	X	X	X	X
Highway Operation Improv.	Auxiliary Lane	X	X	X	X	X
	Freeway Connector	X	X	X	X	X
	HOV Connector	X	X	X	X	X
	HOV Drop Ramp	X	X	X	X	X
	Off-Ramp Widening	X	X	X	X	X
	On-Ramp Widening	X	X	X	X	X
	HOV-2 to HOV-3 Conver.	X	X	X	X	X
	HOT lane Concersion	X	X	X	X	X
Trnsp. Mgmt. Systems (TMS)	Ramp Metering	X	X	X	X	X
	Ramp Metering Signal Coord.	X	X	X	X	X
	Incident Management	X	X	X	X	X
	Traveler Information	X	X	X	X	X
	Arterial Signal Mgmt.	X	X	X	X	X

Table 4. Cal B/C Design and Traffic Data Required

Type of Projects		Highway Design and Traffic Data Item					
		Hov Restriction	Highway Free-Flow Speed	Ramp Design Speed	Highway Segment Length	ADT	Actual 3-Year Accident Data
Highway Capacity Expansion	General Highway		X		X	X	X
	HOV Lane Addition	X	X		X	X	X
	HOT Lane Addition		X		X	X	X
	Passing Lane		X		X	X	X
	Intersection		X		X	X	X
	Bypass		X		X	X	X
	Queuing		X		X	X	X
	Pavement		X		X	X	X
Highway Operation Improv.	Auxiliary Lane		X	X	X	X	X
	Freeway Connector		X		X	X	X
	HOV Connector	X	X		X	X	X
	HOV Drop Ramp	X	X		X	X	X
	Off-Ramp Widening		X		X	X	X
	On-Ramp Widening		X		X	X	X
	HOV-2 to HOV-3 Conver.	X	X		X	X	X
	HOT lane Concerision		X		X	X	X
Transportation Mgmt. Systems (TMS)	Ramp Metering		X		X	X	X
	Ramp Metering Signal Coord.		X		X	X	X
	Incident Management		X		X	X	X
	Traveler Information		X		X	X	X
	Arterial Signal Mgmt.		X	X			

Table 5. Redbook Wizard Input Requirements

Segment Data	Analysis Period	User Classes	Economic and Other Parameters	Construction Management Alternatives
Number of segments	Year construction begins	User class names	Real discount rate	Management alternative names
Name of each segment	Year operation begins	Vehicle types	Inflation rate	Project
Functional classifications	First year of analysis period	Vehicle occupancy	Financing rate	Number of accidents
Improvement types	Last year of analysis period	Value of time	Financing term	Total travel delay during construction
Segment length	Base year	Fuel cost	Insurance cost	Total added VMT on detour route
		Fuel cost as % of operating cost	Traffic growth rate	Vehicle speed on detour route
			Growth of value of time	
			Accident costs	
Unimproved Segment User Benefit Data	Improved Segment User Benefit Data			Traffic Conversion Factors
Delay calculation methods	Peak hour, peak direction traffic	Earlier model year		K factor
Daily two-directional traffic	Peak direction capacity	Without-improvement travel time in the later model year		D factor
Peak direction capacity	Free-flow speed	With-improvement travel time in the later model year		Weekday-to-week factor
Peak hour traffic	Additional peak hour change in delay	Later model year		Week-to-month expansion factor
Peak direction capacity	Highest exponent on volume	Without-improvement travel time in the model year		Seasonality factor
Free-flow speed	% of traffic of each user class	With-improvement travel time in the model year		
Daily two-directional traffic	Opening year accidents	Model year		
Peak direction capacity	Annual agency operating costs	Growth rate for delay		
Free-flow speed	Without-improvement travel time in the earlier model year	Terminal value		
Annual number of accidents	With-improvement travel time in the earlier model year			
Annual agency operating costs				

Table 6. Outputs from the Packages

CAL B/C	MICROBENCOST	Redbook-Wizard
Life-Cycle Costs	Discounted Construction Cost	Capital Costs
Life-Cycle Benefits	Total Discounted User Benefits	User Benefits from Operation
Net Present Value	Net Present Value	User Benefits from Construction
Benefit/Cost Ratio	Gross Benefit-Cost Ratio	Total User Benefits
Rate of Return on Investment	Netted Benefit-cost Ratio	Net Benefits
Payback Period	Internal Rate of Return	Benefit-Cost Ratio
Additional CO₂ Emissions	Discounted Salvage Value	Total Operation Delay
Additional CO₂ Emissions	Discounted Increase in Maintenance and Rehabilitation	Total Construction Delay
Itemized Benefits:	Fuel Consumption Savings	Total Construction VMT Benefits
<ul style="list-style-type: none"> • Travel Time Savings • Vehicle Operation Cost Savings • Accident Cost Savings • Emission Cost Savings • Person-Hours of Time Saved 	Fuel Savings, Adj. for Induced Traffic	Itemized Benefits: <ul style="list-style-type: none"> • User Value of Time Benefits • User Operating Cost Benefits • User Accident Reduction Benefits • Agency Operating Benefits
	Carbon Monoxide Emission Reduction	
	Carbon Monoxide Reduction, Adj. for Induced Traffic	
	Itemized Benefits:	
	<ul style="list-style-type: none"> • Delay Savings • Reduction of Vehicle Operating Costs • Reduction of Accident Costs 	

Case Study 1: Adding Lanes to Existing Highways

This case study involved a proposed project to construct two additional lanes on a 2.2-mile segment of an interstate highway. The project information is shown in Table 7.

Table 7. General Project Information

Route Number	Project Type	District	Project Location	Highway Length	Length of Const.	# of Lanes	Free Flow Speed
I 64	Added Travel Lanes	Seymour	I-265 to SR111	2.2 miles	2 years	from 4 to 6	70 mi/hr
Annual Growth Rate	ADT (2009)	ADT (2030)	Road Type	Construction Costs	PE Costs (2009/2010)	Maint./Op. Costs	Analysis period
1.50%	62156	84971	Rural Interstate	\$8,440,000	\$20,000 /\$100,000	\$50,000 per year	20 years

Using the data in Table 7, the three software packages were run for the economic analysis of this highway project. As the software packages contained different default values, such as unit fuel costs, truck unit operation costs, and accident costs, the default values of Cal B/C and Redbook Wizard were changed to the default values of MicroBENCOST to make the outputs comparable. The results from the three software packages are presented in Table 8. The values in the table indicate that the outputs from the software packages differ significantly.

Table 8. Life Cycle Analysis Results of Adding Lanes (in \$10⁶)

	MicroBENCOST	Cal-B/C	Redbook
Net Present Value	2.047	-0.5	-2.849596
Life-Cycle Costs	8.556	5	3.85
Life-Cycle Benefits	10.603	4.5	1.000404
B/C Ratio	1.581	0.5	0.048
Travel Time Savings	9.51576	1.8	-0.1635
Vehicle Operation Cost Savings	0.57019	-0.9	-9.6E-05
Accident Cost Savings	0.51662	3.8	1.164

For easy comparison, the values in Table 8 are plotted in Figure 1. The figure clearly exhibits that there are major differences in costs and benefits from the three methods. MicroBENCOST yielded the greatest cost and benefit values, while the Redbook Wizard produced the smallest values. The most significant differences are in the travel time savings. In MicroBENCOST results, the life-cycle benefit is greater than the life-cycle cost, resulting in a positive net present value and a B/C ratio greater than 1.0. However, the net present values are negative and the B/C ratios are

less than 1.0 from both Cal B/C and Redbook methods. As decision-making tools, the results from these methods would provide conflicting conclusions on whether the highway agency should carry out the project.

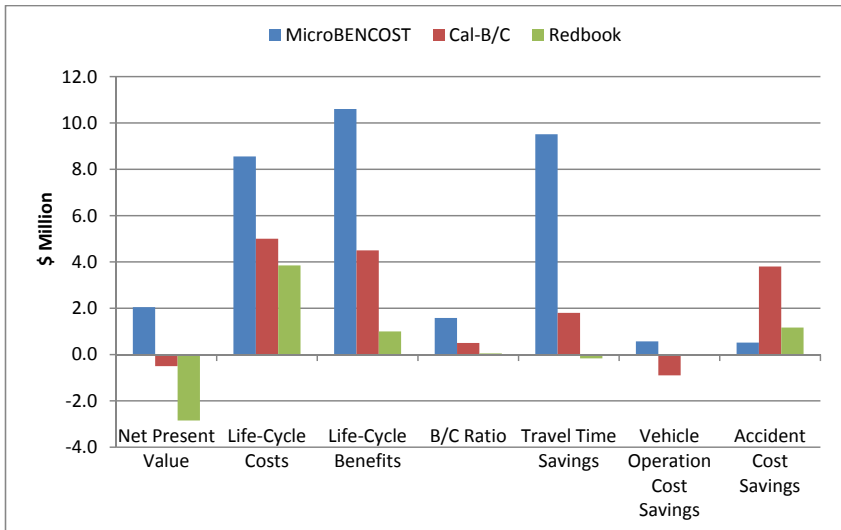


Figure 1. Cost and Benefit Values for the Pavement Widening Project

Case Study 2: Pavement Overlay

This project was a 10.5-mile section of a rural two-lane highway with shoulders. The pavement was deteriorated and was to be overlaid. The ADT on the highway was 4,000 with an estimated annual growth rate of 2.6%. The default values were changed to those of MicroBENCOST whenever possible when entering the project data into Cal B/C and Redbook Wizard. The analysis results are shown and illustrated in Table 9 and Figure 2.

Table 9. Life Cycle Analysis Results of Pavement Overlay (in \$10⁶)

	MicroBENCOST	Cal-B/C	Redbook
Net Present Value	8.98497	-1.9	-3.010036
Life-Cycle Costs	3.619	3.7	1.89
Life-Cycle Benefits	12.60397	1.8	-1.12004
B/C Ratio	4.264	0.6	-0.123
Travel Time Savings	3.501	0.5	-2.32
Vehicle Operation Cost Savings	9.101	1.3	-3.6E-05
Accident Cost Savings	0.00197	0	1.2

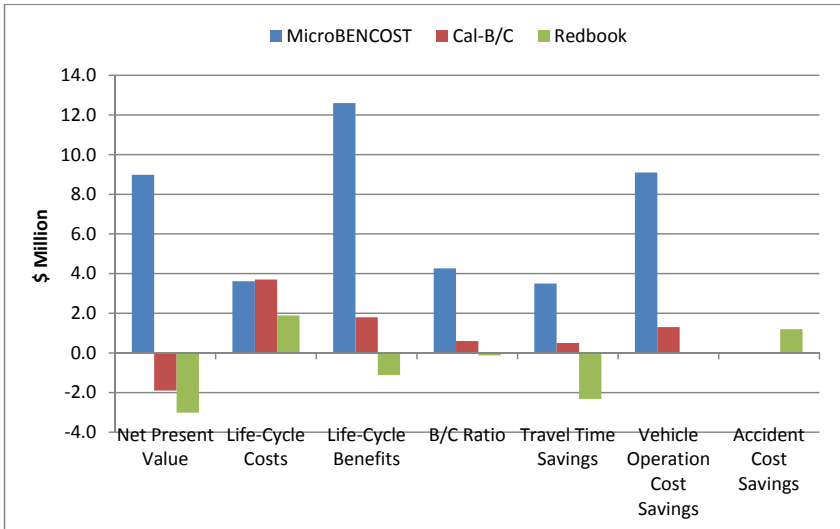


Figure 2. Cost and Benefit Values for the Pavement Overlay Project

MicroBENCOST yielded a significantly greater benefit value than the other two methods. The Redbook Wizard produced a negative life-cycle benefit and a negative net present value. The most significant differences are in the vehicle operation cost savings. Similar to Case Study 1, in MicroBENCOST results, the life-cycle benefit is greater than the life-cycle cost, resulting in a positive net present value and a B/C ratio greater than 1.0. The net present values are negative and the B/C ratios are less than 1.0 from both Cal B/C and Redbook methods.

Case Study 3: Shoulder Widening

This case study was to analyze a shoulder widening project in order to reduce accidents on a section of a 2-lane principal arterial roadway. The width of the existing shoulder was 10 feet and it was proposed to widen it to 14 feet. As in the above two case studies, the default values of Cal B/C and the Redbook Wizard were also changed to the same values in MicroBENCOST. The analysis results from the three packages are given in Table 10 and are graphed in Figure 3.

The life-cycle benefits of all three methods are relatively greater than their respective life-cycle costs. Consequently, the B/C ratios are much greater compared to the previous two cases. As can be seen in the table and in the figure, the B/C ratios are 61.67, 46.5, and 13.56, from MicroBENCOST, Cal B/C, and the Redbook Wizard, respectively. The net present values from all three methods are positive.

Table 10. Life Cycle Analysis Results of Shoulder Widening (in $\$10^6$)

	MicroBENCOST	Cal-B/C	Redbook
Net Present Value	7.342	9.1	2.136
Life-Cycle Costs	0.197	0.2	0.164
Life-Cycle Benefits	7.463	9.3	2.224
B/C Ratio	61.675	46.5	13.561
Travel Time Savings	0	0.5	-0.345
Vehicle Operation Cost Savings	-0.000004	1.3	-0.00006
Accident Cost Savings	7.462	7.5	2.569

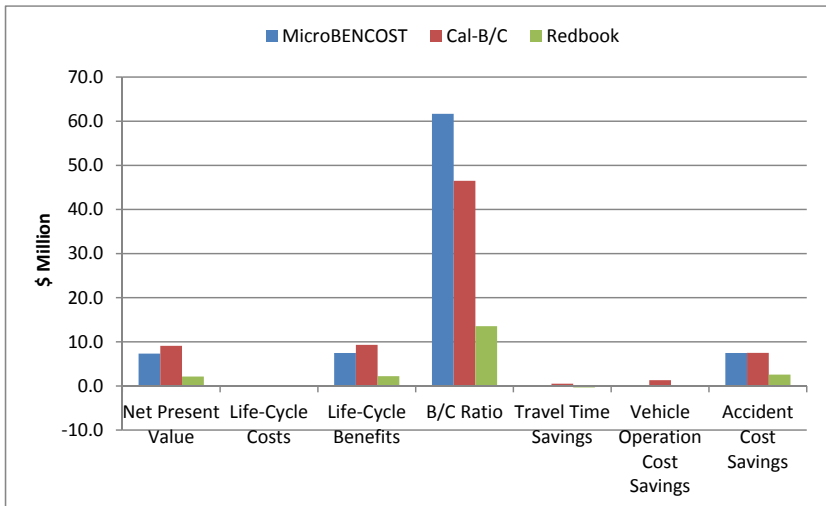


Figure 3. Cost and Benefit Values for the Shoulder Widening Project

CONCLUSIONS

This study examined and compared the three economic analysis software packages for highway projects, MicroBENCOST, Cal B/C, and the Redbook Wizard. It was found that even though the principles of the economic analyses are generally same, the specifics in the software packages are different significantly. The differences are reflected in the input requirements of the three analysis software packages. The capacities of the three software packages also differ. MicroBENCOST can analyze highway improvement projects, bridge projects, safety projects, railroad crossing projects, and high occupancy vehicle (HOV) lanes projects. Cal B/C can be used to study transit projects, highway operational improvement projects, and transportation management systems. The Redbook Wizard has the ability to analyze such projects as additional lanes, traffic control, signal control

systems, intelligent transportation systems (ITS), roadside lighting, and pavement preservation or maintenance.

Through three case studies, it was illustrated that the analysis results from the three methods were not consistent. It is important for the highway planners and engineers to understand that the three packages may provide totally different conclusions. Therefore, a thorough study should be performed before adopting a specific software package so that the package is suitable for the conditions of the particular agency.

REFERENCES

AASHTO. (2010). *User and Non-User Benefit Analysis for Highways*, American Association of State Highway and Transportation Officials. Washington, D.C.

Caltrans. (2009). *California Life-Cycle Benefit/Cost Analysis Model (Cal-B/C) User's Guide (version 4.0)*. System Metrics Group, Inc. In association with Cambridge Systematics, Inc.

McFarland, W. F., J. Memmott, M. Chui, M. Richter, and A. Castano-Pardo. (1993). *MicroBENCOST User's Manual*. Texas Transportation Institute, Texas A&M University. College Station, Texas.

Meemmott, J.L., Richter, M., Castano-Pardo, A. & Wildenthal, M. (1999). *MicroBENCOST Version 2.0 User's Manual, prepared for National Cooperative Highway Research Program*. Project 7-12(2). Texas Transportation Institute, the Texas A&M University System College Station, Texas.

Coordination between Comprehensive Transportation and Social Development at the Regional Level in China

Jing SHI¹, Nian ZHOU², and Zhaozhang WU²

¹ Corresponding Author, Institute of Transportation Engineering, Room 311, Dept. of Civil Engineering, Tsinghua University, Beijing 100084, P. R. China. Tel & Fax: 86-10-62772300; E-mail: jingshi@tsinghua.edu.cn

² Graduate Student, Institute of Transportation Engineering, Department of Civil Engineering, Tsinghua University, Beijing 100084, P. R. China.

ABSTRACT

This study aims at analyzing the coordination between comprehensive transportation and social development at the regional level in China. Firstly the country (Hongkong, Macao, Taiwan are not included) is zoned into 9 regions according to its administrative partitions. Then the main indexes (operational index & infrastructure development index) for evaluating comprehensive transportation were selected and analyzed using factor analysis and principal component analysis methods. Regional comprehensive transportation systems were evaluated by using these indexes, and obvious disparities among different regional systems were found. The coordination of the comprehensive transport systems and social development of each region was analyzed, using the results of evaluation and HDI (Human Development Index). The results showed that the vulnerable relationship exists between the two. Furthermore, the paper proposed some advices for future development.

INTRODUCTION

Transportation has a huge impetus to regional economic and social development. With the continuous development of large-scale social production and division of labor among regions, inter-regional economic cooperation and social contacts keep increasing, which makes transportation significant to the provincial economy. Being both a manufacturing industry and a service industry, transportation and regional economic development are closely related (Jing SHI, etc, 2003; Jing SHI, 2010): a well-functioning transport system has an enormous stimulus to social development. Therefore, a region's transportation development is usually considered to be positively correlated to social level of development. Research on this will help us to figure out whether the transportation is getting proper investment and improvement, which are significant in resource allocation among different projects.

In recent years, China's comprehensive transportation system has been developing rapidly, and gradually becomes an integrated one which consists of railway transportation, road traffic, aviation transportation, inland shipping system, pipeline system (Editorial board of Geographic Science, 2004; Yuanfeng HAN, 2000; Ji ZHAO, Chuankang CHEN, 1999). However, there are still huge diversities in social and transportation developments among different regions.

Provincial-level administrative units were divided into distinct regions on certain criteria of classification. To understand the overall development of China's comprehensive transportation development and their regional characteristics, quantitative analysis of the regions' comprehensive transportation system is implemented. Further analysis of the causes of the status quo was done, and development advices were proposed.

REGION DIVISIONS

Region divisions would change as the social developing forwards or defers because of the research purposes (CHEN Ruying, 2011; ZHOU Da, 2003), e.g. the widely used four regions division (i.e., western, North-east, central and eastern areas) was put forward in *Recommendations of the Eleventh China National Economy and Social Development Five-Year Plan*.

Transportation economic region, which was lately proposed under the notion of a distinct economic region, is determined by the geographic character distribution of the transportation industry. In this research, the main concern of the division is the provincial-units and both the spatial and economic connections. The provincial economic development overall China was analyzed according to consumption expenditure, consumer spending per capita, GDP per capita and GDP. The whole country was divided into nine regions with each one has a provincial-level economic center, which are Beijing, Liaoning, Shanghai, Shandong, Fujian, Guangdong, Sichuan, Shaanxi, and Xinjiang. The components of each region are listed as follows.

Table 1. Division of the Region

No.	Region composition
1	Beijing, Tianjin, Hebei, Inner Mongolia
2	Liaoning, Jilin, Heilongjiang
3	Shandong, Henan, Anhui
4	Shanghai, Jiangsu, Zhejiang
5	Fujian, Jiangxi, Hunan
6	Guangdong, Guangxi, Hainan
7	Sichuan, Yunnan, Chongqing, Guizhou, Tibet
8	Xinjiang, Gansu, Qinghai
9	Shaanxi, Hubei, Shanxi, Ningxia

These nine regions have different spatial patterns. The relationships between economic center and geographical center in different regions are diverse: economic center is also the geographical center in some regions, while in others the two are far apart. Considering the emergence of regional economic growth poles are not only caused by the topographical conditions, the resource-intensive and many other constraints, such diversity is reasonable.

EVALUATION OF COMPREHENSIVE TRANSPORTATION SYSTEM

Transportation system has a huge influence on multiple social classes and social groups, which is hard to be quantitatively evaluated. The usual way to implement a quantitative evaluation is to build a multi-objective evaluation system. The process of such a system is started by setting multiple objects for evaluation, then scores each subentry and calculates the result by summing the weighed scores. In this study, Factor Analysis and Principal Component Analysis were used to calculate the main index used in the evaluation system. The quantitative scores of comprehensive transportation system and the ranking list could be derived from this evaluation system.

To build the evaluation system, we firstly selected quantitative indicators which could represent the features of a transportation system. Then Date Reduction Method was used to get the main indexes which were the key elements of the evaluation system.

Railway transportation, road traffic, aviation transportation, inland shipping system, pipeline system are the main five modes of comprehensive transportation in China. As for the regional transportation system, aviation transportation is mainly for long-distance passenger transport and the development of the inland shipping system as well as the pipeline system largely depends on the natural constraints, which means the three transportation modes do not exist around the whole country. Taking into account the availability of statistical data and the characters of a comprehensive transportation system in China, the eight indicators from railway transportation and road traffic were selected. Indicators and the correspondent considerations are as follows.

X_1 : density of railway in service ($\text{km}/10,000\text{m}^2$). Railway transportation is the main regional transportation mode for its large volume and low cost, so the density of railway in service which represents the development of railway infrastructure construction is selected.

X_2 : density of highways in service ($\text{km}/10,000\text{m}^2$). Road traffic plays a role no less important than the railway transportation does in regional transportation in China. Comparing to railway transportation, road traffic is more convenient and faster though the cost is higher. Road traffic is important in transportation economy and that's why this indicator was selected.

X_3, X_4 : passenger volume and passenger person-kilometers. The units are thousand

million persons and thousand million person-kilometers. The two indicators could reflect the development of passenger traffic inside a region. Together with X_1 and X_2 , the passenger efficiency of the transportation system could be evaluated.

X_5 , X_6 : freight volume and rotation volume of freight transport. The units are thousand million tons and thousand million ton-kilometers. Together with X_1 and X_2 , the cargo efficiency of the transportation system could be evaluated.

X_7 : investment in transportation industry (0.1 billion Yuan). This indicator reflects another important aspect of transportation development.

X_8 : regional GDP (0.1 billion Yuan). This one is used to indicate the demand for regional comprehensive transportation system.

SPSS is used to process the data from *China Statistical Yearbook of 2009*. Through data reduction, the correlation matrix of indicators was calculated as presented in Table 2.

Table 2. Correlation Matrix

	X_1	X_2	X_3	X_4	X_5	X_6	X_7	X_8
X_1	1.000	0.813	0.370	0.749	0.782	0.690	0.317	0.673
X_2	0.813	1.000	0.569	0.839	0.849	0.766	0.342	0.786
X_3	0.370	0.569	1.000	0.752	0.583	0.394	0.524	0.725
X_4	0.749	0.839	0.752	1.000	0.934	0.624	0.356	0.762
X_5	0.782	0.849	0.583	0.934	1.000	0.759	0.435	0.788
X_6	0.690	0.766	0.394	0.624	0.759	1.000	0.595	0.905
X_7	0.317	0.342	0.524	0.356	0.435	0.595	1.000	0.736

Huge development of a comprehensive transportation system is usually hard to observe in a few years, for the improvement of infrastructure and level of service both need time to take effect. So the data of the year 2009 is thought to be a well representative for the contemporary state of regional comprehensive transportation system.

Analysis using the KMO method of data in Table 2 is 0.691 and the analysis using Bartlett's method shows the matrix is identity. Factor Analysis is proper according to those analyses. The main components are selected using the principal component analysis method. Among these components, two have a latent root larger than 1 while accumulated loading over variables is more than 80%. Therefore the two components are selected as main indexes. The relationship between components and

indicators is as follows.

Table 3. Rotated Factor Loading Matrix

Indicator	Component		Indicator	Component		Indicator	Component	
	1	2		1	2		1	2
X_2	0.903	0.282	X_4	0.869	0.338	X_8	0.630	0.749
X_1	0.888	0.153	X_6	0.664	0.550	X_3	0.420	0.659
X_5	0.880	0.355	X_7	0.092	0.943			

Table 4. Principal Components Score Matrix

Indicator	Component		Indicator	Component		Indicator	Component	
	1	2		1	2		1	2
X_1	0.336	-0.231	X_4	0.256	-0.089	X_7	-0.323	0.654
X_2	0.293	-0.143	X_5	0.254	-0.081	X_8	-0.009	0.304
X_3	-0.068	0.319	X_6	0.083	0.146			

According to Table 3 and Table 4, the main components represented as V_1 and V_2 are as follow.

$$V_1 = 0.336X_1 + 0.293X_2 - 0.068X_3 + 0.256X_4 + 0.254X_5 + 0.083X_6 - 0.323X_7 - 0.009X_8 \quad (1)$$

$$V_2 = -0.231X_1 - 0.143X_2 + 0.319X_3 - 0.089X_4 - 0.081X_5 + 0.146X_6 + 0.654X_7 + 0.304X_8 \quad (2)$$

From the formula (1) and (2) it is easy to find X_1 (density of railway in service) and X_2 (density of roads in service) have greater positive effect on component V_1 while X_7 (investment in the transportation industry) and X_8 (regional GDP) have greater positive effect on component V_2 . Hence we take V_1 and V_2 as an operational index and infrastructure development index.

ANALYSIS OF REGIONAL COMPREHENSIVE TRANSPORTATION SYSTEM

To score each region's comprehensive transportation system according to the main indexes, normalization process was implemented first by using formula (3).

$$X_{11}' = \frac{X_{11}}{\sqrt{X_{11}^2 + X_{11}^2 + \dots + X_{81}^2}} \tag{3}$$

Then the quantitative results according to the formula (1) and (2) are calculated. The positive score means the development of the corresponding regional transportation system is above the average level of China, and vice versa. The value of the score largely depends on how developed the system is. The scores can be marked on the coordination system with V_1 and V_2 as the two dimensions.

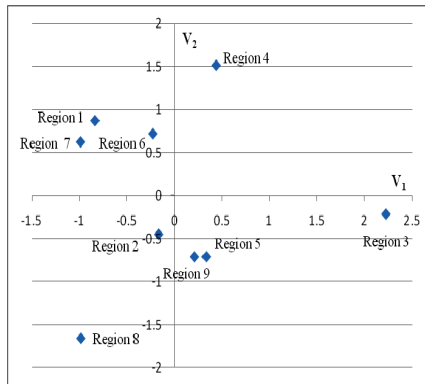


Figure 1. Coordinates representation of public factor scores

Regions close to each other shows similar characteristics and could be figure out easily from Figure 1. Region 1(Beijing, Tianjin, Hebei, Inner Mongolia), 6(Guangdong, Guangxi, Hainan), 7(Sichuan, Yunnan, Chongqing, Guizhou, Tibet) can be analyzed as a group as well as region 2(Liaoning, Jilin, Heilongjiang), 5(Fujian, Jiangxi, Hunan) and 9(Shaanxi, Hubei, Shanxi, Ningxia). The other 3 regions will be analyzed separately.

COORDINATION RESEARCH ON THE COMPREHENSIVE TRANSPORT SYSTEMS AND SOCIAL DEVELOPMENT

Quantitative indicator for social development

GDP is a widely used indicator of economic development and is usually seen as a representative of social development. However, social development is more than economic development with many other important factors involved, like average lifespan and the development of education. To ensure a healthy and sustainable development of society, we cannot focus on the development of the economy only (Liping GUO, 2001).

The human Development Index (HDI) is brought out by United Nations Development Programme (UNDP) in the *Human Development Report 1990* to make up the drawbacks of GDP. The HDI is a comparative measure of life expectancy, literacy, education and standards of living for countries worldwide. It is a standard means of measuring well-being, especially child welfare. There are also HDI for cities or provinces nowadays. In this research, HDI is used as the quantitative indicator for social development. The newest HDI data of China are available in *China Human Development Report 2010*, which is accomplished under the lead of UNDP China.

Coordination research on comprehensive transportation system and HDI

The provincial HDI is available in *China Human Development Report 2010*. The weighted average of provincial HDI is taken as regional HDI with the population of each province taken as the weight.

Table 5. Regional HDI

Region No.	HDI	Region No.	HDI	Region No.	HDI
1	0.826	4	0.847	7	0.738
2	0.820	5	0.781	8	0.734
3	0.793	6	0.839	9	0.785

The relationship between comprehensive transportation development and social development can be found by using the results of Cluster Analysis and the regional HDI.

Region 2, 5 and 9 were clustered into one group and they gained similar regional HDI. Region 4, which has the highest scores in both V_1 and V_2 , has the highest regional HDI. Meanwhile region 8 has the poorest HDI while getting low scores in a comprehensive transportation system evaluation. The comparison of these regions reveals a positive correlation might exist between comprehensive transportation systems and social development.

However, the development of a comprehensive transportation system does not always coordinate with the social development. In Cluster Analysis, region 7 is grouped with region 1 and region 6. But region 7 has a much lower HDI than region 1 and region 6. Region 1, 6, 7 gets similar score and their distances are no more than 0.767. They all have negative V_1 and positive V_2 , which means that their transportation infrastructure is better than the average level of the whole country while the transportation economy is not. The reason region 1 and 7 get negative V_1 might be that vast land there has a low population density where a few transportation

infrastructures are invested. And province Hainan and Guangxi where few railway was constructed because of the natural constrains could explain why the region 6 gets negative V_1 . Beijing, Tianjin in region 1 and Guangdong in region 6 are among the most developed places of China, where the population is large and HDI is high. Therefore it is not hard to understand the disparity of HDI among region 1, 6 and 7.

One important fact can be found that the development of a comprehensive transportation does not always bring about the social development. This fact would be effective deeper thought on how investment in a comprehensive transportation system could better serve the social development and how the system could function more effectively.

With all the analysis above, advice for better development of comprehensive development can be proposed. There should be huge enhancement in transportation infrastructure in the region 7 to promote the social development. And the development of comprehensive transportation in region 3 should concentrate on the improvement of both infrastructure and operational aspects.

CONCLUSION

The coordinated development of a comprehensive transport system is necessary for sustainable social development. A comprehensive transportation system is influential to many aspects of the society. This study firstly zoned the country (Hongkong, Macao, Taiwan are not included) into 9 regions according to its administrative partitions and then analyzed these regions with the operational index and the infrastructure development index, using factor analysis and principal component analysis methods. Obvious disparities among different regional systems were found in the research. Then coordination research on comprehensive transport systems and social development of each region was done, using the results of evaluation and HDI as representatives for each development. The result of coordination research showed that the vulnerable relationship exists between the two and possible explanation was given. The research is innovative in two aspects. The first is that an evaluation method for a comprehensive transportation system is proposed considering possible available impact factors. The second is that a coordination research between the development of comprehensive transportation and social development was implemented. However, further study is needed to make the evaluation models more practical and reliable.

REFERENCE

- CHEN Ruying, LUO Hongxiang. (2011). *Analysis of the compartmentalization of the standard economic area in China*. Economic Research Guide 8: 279-281.
- Editorial board of Geographic Science. (2004). *Geographic Science*, Science Press, Beijing, 59-86.

- Yuanfeng HAN. (2000). *Regional Geography of China (In Chinese)* . Guangdong High Education Press, Guangzhou, 366-398.
- Ji ZHAO, Chuankang CHEN. (1999). *Geography of China*, High Education Press, Beijing, 67-94.
- Jing SHI, Dan ZHANG , Zhaozhang WU. (2009). *Study of the Interactive Relationship between Regional Coordinated Development and Transport System*. Journal of Railway Engineering Society 11: 104-108.
- Jing SHI, Qian HUANG, Zhaozhang WU. (2010). *Interactive Relationship Between Transportation and Economic Development in China* . JOURNAL OF WUHAN UNIVERSITY OF TECHNOLOGY (TRANSPORTATION SCIENCE & ENGINEERING) 6:1077-1080.
- Liping GUO, Yuanping FANG. (2001). *Provincial Human Development Index Comparison and Analysis of China (In Chinese)* . Academic Research 5: 172-174.
- ZHONG Cheng, WU Zhenhua. (2008). *An empirical study of overall urban-rural development level in eight major regions of China*. Journal of Chongqing Technology and Business University (West Forum) 1:13-17.
- ZHOU Da, LIU Rui. (2003). *Research on the Division of Controlling Region for China s Macro-controlling*. China Industrial Economics 4: 42-50.

Service Excellence: Road Tunnel Safety

William Cheung

Traffic Manager, Western Harbour Tunnel Company Limited, The Administration Building, Western Harbour Crossing, Yaumateai, Hong Kong, Tel: (852) 23025766; Fax (852) 27811729; email: cheungwf_william@yahoo.com.hk

ABSTRACT

Tunnel road crashes continue to cause significant human trauma and unacceptable economy cost. To ensure providing safe and quality services to the public, a key component reclines in a well tunnel road safety plans. This paper will outline the past data of traffic accident in the tunnel area as well as analyses their main causes. In view of the factors that contributed to the high accident rate, it will discuss several implemented remedial measures so as to generate and sustain road safety awareness within the tunnel area, both now and into the future. Finally, this paper will examine whether these measures are success or not, and make suggestion to enhance tunnel road safety improvement.

BACKGROUND

On 30 April 1997, transport in Hong Kong entered a new era with the opening of Western Harbour Tunnel (WHT) – a major infrastructure achievement that provides a safe, smooth and efficient cross-harbour road link, along with a number of other public benefits. In May 2000, its engineering achievements were recognized when it received the “First China Civil Engineering – Zhan Tian Grand Award”.

WHT is the first and the largest dual three-lane harbour tunnel to have been built in Hong Kong, and in South East Asia. It links Sai Ying Pun on Hong Kong Island and West Kowloon, and is acknowledged as the quickest of cross-harbour routes for road traffic.

INTRODUCTION

WHT is committed to being the leading tunnel operator providing safe and quality services to the public and to the satisfaction of the stakeholders i.e. WHT’s missions.

Traffic accidents in WHT tunnel area as well as public road will definitely cause significant human trauma and unacceptable economy cost. Safety of our motorists, the public and employees is an absolute pre-requisite. WHT is committed to maintaining a climate of safety awareness and employing safety management system that will lead to continuous improvement in safety performance so as to provide safe services to the public.

SAFETY MANAGEMENT SYSTEM

Safety Management System (Figure 1) has been employed in Operations Department since in July 2008 so as to improve safety performance continuously in WHT tunnel area resulting in provision of safe services to the public.

In this regard, a Safety Review Working Group has been set up in Operations Department comprising of management team of Operations Department led by Head of Operations Department to review the public safety including traffic accidents as well as staff safety periodically.

The Safety Review Working Group will implement control measures including feedforward control, concurrent control and feedback control according to the findings and root causes in the investigation and keep on monitoring the safety performance in WHT tunnel area.

ROAD SAFETY PERFORMANCE IN WHT

The safety performance of WHT in terms of occurrence rate of traffic accident per million vehicles is 1.44 in 2011. The performance is excellent in comparison with the performance of other cross harbour tunnels in Hong Kong i.e. the occurrence rate of traffic accident per million vehicles is 5 – 14 on average.

According to the record, the occurrence rate of traffic accident per million vehicles is reduced from 5.38 to 1.44 (Figure 2) after the implementation of Safety Management System in Operations Department since July 2008. Besides, zero accident on the roads in WHT tunnel area was recorded in February 2009 and April 2011.

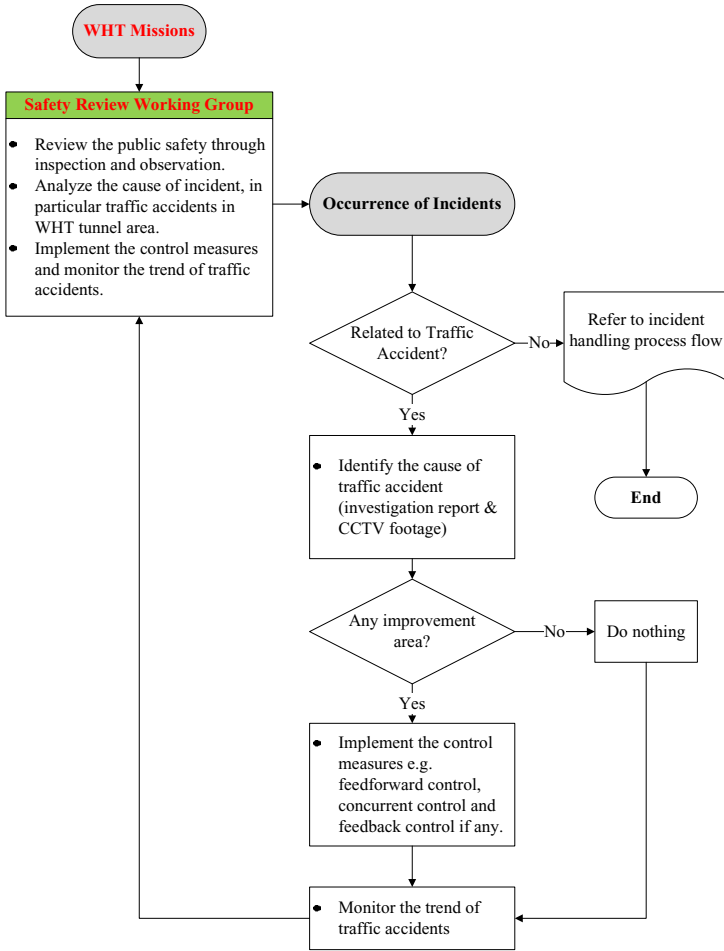


Figure 1. Safety Management System

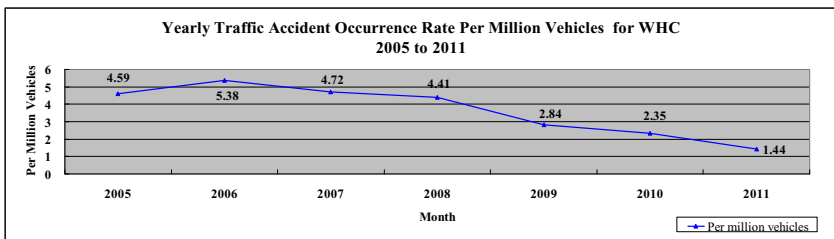


Figure 2. Occurrence rate of traffic accident per million vehicles

CONTROL MEASURES

Control measures play a key role in the Safety Management System to reduce traffic accidents in WHT tunnel area. There are three types of control measures being adopted in WHT viz. Feedforward Control Measures, Concurrent Control Measures and Feedback Control Measures.

According to the findings from our investigation and observation, we implement the control measures in an innovative way since July 2008. Nevertheless, the guidelines and standard of traffic management devices issued by Highways Department are strictly followed.

1. Feedforward Control Measures

- a) Traffic cones with “Slow” sign placing along the sharp bends to remind motorists to watch out for the sharp bends and adjust the speed accordingly (Figure 3).

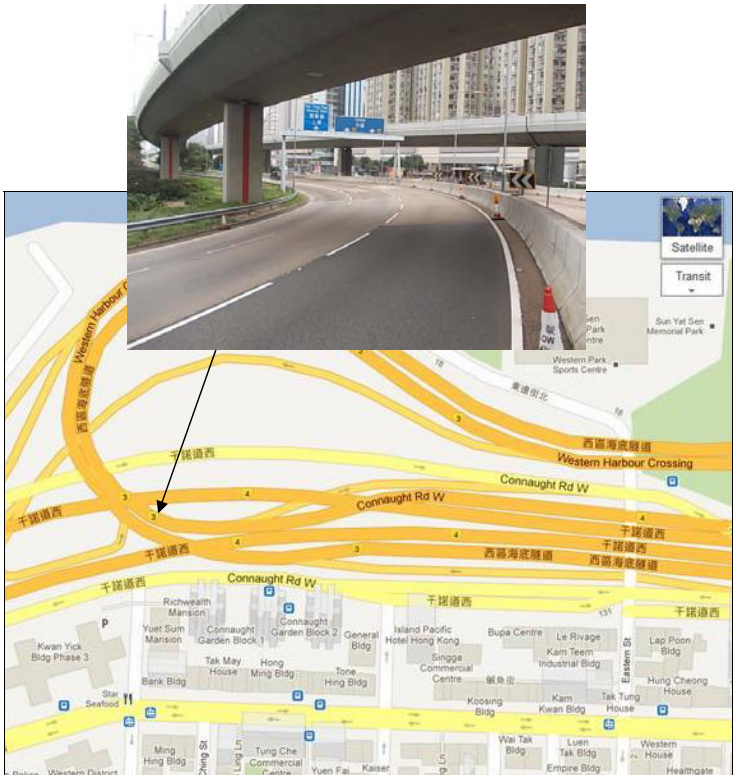


Figure 3. Traffic cones with “Slow” sign placing along the sharp bends

- b) Traffic cones of 1000 mm placing at the Autotoll Lanes with a curve near toll booth to remind motorists (Figure 4), in particular the drivers of heavy goods vehicle and coach to watch out for the bend and adjust the speed accordingly when passing these Autotoll Lanes.



Figure 4. Traffic cones of 1000mm placing at the Autotoll Lanes

- c) Speed Enforcement at Ingress and Toll Plaza Area – According to the cause analysis of traffic accident, speeding is one of the major causes of traffic accident. To tackle this problem, speed enforcement is implemented not only at tunnel tube but also at the areas of ingress and toll plaza.
- Using speed radar set at the toll plaza area (Figure 5) and tunnel tube



Figure 5. Using speed radar set at the toll plaza area

- Placing mock speed radar set at various locations
- Joint operation with Police to carry out speed enforcement operation at tunnel areas (speed enforcement laser and video camera) (Figure 6)



Figure 6. Joint operation with Police to carry out speed enforcement operation at tunnel area

- d) Reroute the traffic flow – To reduce the number of traffic accidents at the merging points (Figure 7) traffic flow should be re-routed so as to reduce traffic merging points as far as possible. For example, when manual toll booth N1A is in operation, traffic will be diverted to other road after passing manual toll booth N1A to reduce the merging point with the traffic coming from Loop Road of Administration Building.



Figure 7. Reroute the traffic flow – to reduce the number of traffic accidents at the merging points

- e) Erection of temporary traffic signs (Figure 8) – In addition to the permanent traffic signs approved by Transport Department, temporary traffic signs are erected at the locations where traffic accidents may occur to remind motorists to pay special attention to the traffic there, for example, temporary traffic merges from left / right signs.



Figure 8. Erection of temporary traffic signs

2. Concurrent Control Measures

- a) Enhancement of traffic control management at toll area and tunnel entrance (Figure 9) – Traffic congestion occurs at Western Harbour Tunnel because of whatever reasons e.g. traffic accident within / outside WHT tunnel area. Traffic control management will be implemented at the tunnel entrance so as to regulate the traffic approaching the manual toll & Autotoll lanes and tunnel entrance.
- All the traffic will be stopped at the manual toll & Autotoll lanes for the traffic regulation during traffic congestion in the tunnel.
 - Staff will be posted at the tunnel entrance to regulate traffic approaching the tunnel entrance during serious traffic congestion in the tunnel.

By enhancing the above-mentioned traffic control management, traffic accidents at the tunnel entrance were zero.



Figure 9. Enhancement of traffic control management at toll plaza and tunnel entrance

- b) Flashing lanterns at the sharp bends (Figure 10) – As mentioned in item 1a, traffic cones with “Slow” sign are placed along the sharp bends. Flashing

lanterns (high intensity battery operated beacons) which are hung on the traffic cones will be switched on during drizzly weather.

After the implementation of such control measures, no traffic accidents at this sharp bend have been recorded so far.



Figure 10. Flashing lanterns at the sharp bends

3. Feedback Control Measures

As continuous improvement in safety service performance, feedback control is a key step to identify the cause of traffic accidents in tunnel area. As I have mentioned before, the Safety Review Working Group will analyze the cause(s) of traffic accidents by means of viewing the relevant CCTV footage and investigation reports. In addition, the Safety Review Working Group will closely monitor whether the control measures are effective and will revise the control measures if required.

BENEFITS

By adopting Safety Management System in Operations Department, safety service performance in WHT has greatly improved. In other words, WHT could provide safe and quality services to the public and to the satisfaction of the stakeholders hence satisfying customer needs.

According to traffic control management in item 5.2, guided traffic entering the tunnel will have higher cruising speed, this translates into higher flow, hence smooth traffic flow in the tunnel tube. The control measures could definitely alleviate traffic congestion at the bottle neck of tunnel entrance. The orderly flow of traffic will result in less collision, hence reducing traffic accidents at the tunnel entrance. This will bring about many benefits to all.

In the meantime, the traffic flow is smooth with reduced pollution especially from slow moving heavy goods vehicles and buses. This will have immediate benefit on the air quality and congestion to neighbouring areas and all roads feeding the tunnel. The saving in fuel and time for everyone is substantial.

As for operational effectiveness, WHT spends less resource on handling traffic accidents after the implementation of Safety Management System, e.g. handling of the traffic accidents (Operations Department); repairing of the damaged

equipment (Engineering Department) and handling of the insurance issues (Finance Department). For example, the number of traffic accidents to be handled in 2007 is 84, whereas the number of traffic accidents in 2011 is 30 i.e. reducing 64 percent.

CONCLUSIONS

According to the record, the safety service performance has greatly improved. This proves that the Safety Management System and control measures are workable and effective. By adopting the methodology / theory of quality management system, WHT has made a breakthrough in the improvement of safety service performance in WHT tunnel area continuously.

City Development and Public Transportation Planning A Case Study of the Taichung City

Chao-Fu YEH¹ Ying-Chih LU²

¹ Senior Specialist, Bureau of Transportation, Taichung City Government, No.101, Minquan Rd., West Dist., Taichung City 40341, Taiwan; Tel:(886)4-2228-9111; Fax:(886)4-2225-8839; email: yeh@taichung.gov.tw

² Associate Professor, Department of Traffic and Transportation, Fujian University of Technology, Fuzhou City, 350108, China; email: ethan424@gmail.com

ABSTRACT

This study aims to discuss the relation between city development and transportation system. A case study of Taichung City will describe the development progress and future plan, and then analyze the traffic demand of user. To consider sustainable development of Taichung city, this study will draft the public transportation planning of intercity and urban area to provide high quality public transportation service in new development stage.

INTRODUCTION

Urban development is closely related with public transportation. Transit Oriented Development (TOD) is planned with low-cost, high quality and community-based public transportation. By various transportation systems and transfer modes combination, it will create a system of urban development and transport coordination. Public transportation needs to plan with urban type, urban development, urban history, landscape maintenance and other characteristics of urban culture in harmony, and combined with other non-motorized vehicles and pedestrian modes to construct the new face of urban sustainable development.

Taichung City is the important economy area in the central area of Taiwan. Since it reformed in the end of 2010, the city includes the harbor and airport, local and high speed rail, urban transport and highway transit to connect different

development intensity area¹. Therefore transit planning not only must consider the city center, high-capacity and fast transport network, but also need to take into account the remote areas people basic trip demand, and the recreational travel demand of tourist areas, to ensure passenger and goods transport smooth and construct one hour living area.

The paper is divided in three sections. The first section presents the background of the urban and transportation related problems, and the potential solutions. The second part presents the characteristics and Taichung City. The paper concludes by providing recommendations about master plan of high quality public transportation service for Taichung city.

CHARACTERISTICS OF URBANIZATION AND TOD

Over the years, car and highway-oriented development and land use zoning in North America result in urban sprawl and discrete suburban development. Since 1980, long-distance commuter trips and reversed commuter trips increased rapidly. The downtown area recessed, air and noise pollution, energy waste, traffic accident and low usage of public transportation, ecological destruction, excessive consumption of land resources, environmental and social issues, especially the traffic accidents and air pollution and noise hazard on public health.

In twenty years, South America and Asia faced rapid urbanization and motorization development. Many cities used American urban development model departure from sustainable development, such as Mexico City, Delhi, Manila and Bangkok. In China, with rapid development economic reforms in 1978 caused the rapid spread of urbanization. Xie (2008) pointed out that the city number between 1978 to 2007 jumped from 193 to 656, and urban population also grew from 79 million to 590 million. When population growth and urbanization level exceed than expected economic development and rapid growth of private motorized transport, the government often use short-sighted way, more construction of the highway and the ring road are respited traffic congestion problems. This way results the city more expansion of the distribution, and form the "Chinese Version of Urban Sprawl" (Lu, 2007). There are two major characteristics of this development: First, it caused agricultural land and urban land unreasonable fluctuation. From 1990 to 2007 urban population increased 17.8%, and urban area increased from 11,608 to 32,521 square

¹ Since 25th December 2010, new Taichung city has merged old Taichung city and Taichung county.

kilometers (Nu, 2008). Another characteristic is the large-scale development of suburban areas, especially are the development of hi-tech park, software park and other low-growing district located far away from the city center. In addition, because of lack of integration planning of land use development public transportation systems, building and related development management mechanism is not perfect, so the city residential community and commercial activities are generally along the roadside development, and gradually repeat car-oriented urban development in the past.

In Taiwan, although land development density in urban areas is high and with most compact urban development in west cities, but the transportation planning only solved urban traffic congestion issues in the past, neglect to consider the effective land use planning to guide the rational development of spatial structure, so it results in excessive urbanization and urban expansion even with some jumping suburbanization. Without regional integrated organization to coordinate transportation planning and development, it is not specific to implement TOD policy, results in most urban area incompatible land use mix and mutual interference. In addition, after 1980 the city over depends on rail-technology-based of public transportation system construction policies, lack of financial resources and neglected bus system, public transportation has long been unable to suitable the demand of people mobility. Thus format the emphasis "Personal Mobility" unlimited growth, and affect urban environmental quality. Although Taipei City has constructed the world-class MRT (mass rapid transit) system, but it took twenty years and over \$ 16 billion, only formed nearly 90 km road network, only responsible for the daily 13 million (1/10) of Taipei trip. To discuss the reason, in addition to the MRT system construction process due to engineering-based thinking without land use, urban renewal, urban design and other methods to implement TOD policy, another reason is no taxes and fees management systems for private motor vehicles, and without integration of public transportation services are all critical issues.

Transit-Oriented Development (TOD) is an integration process with public transportation system and urban development planning. By the transportation system and the overall planning of land development and management, combined with appropriate pedestrian space design (Walkable Environment), construct an integrated public transportation system with walking and green public transport to increase usage and to guide the station area land development effectively, ensure the win-win strategy of land use and public transportation.

Cervero and Kockelman (1997) proposed the 3D elements of TOD: (1) to enhance land use "Density" of the station's surrounding area and increase the public

transportation system utilization; (2) compatible "Diversity" in land use, to increase activity convenience and reduce the use of private transport; (3) to create walkable space "Design", and to improve transfer and feeder convenience between transportation. In recent years, Zhang (2007) extension of 3D elements, especially for Hong Kong, Taipei and Chinese cities TOD development model, summarize the "5D":

- Differentiated Density: the strength development is higher near public transportation station in surrounding area.
- Dockized District: to consider walking service levels, define the maximum distance people are willing to walk, and integrate business and services to reduce the cost of walking in the area.
- Delicate Design: TOD provides the desired characteristics, such as livable neighborhoods, local and regional accessibility, and the channel and regional marketing window.
- Diverse Destination: residents can reach the demand of feeder transportation services and satisfy basic living functions in residential areas.
- Distributed Dividends: station development can help the public transportation system for financial sustainability.

By the concept of TOD planning, people can reduce the use of cars and other private motor transport to increase the use in walking, cycling, buses and other green transportation mode. People can finish school, community, employment and other economic and social activities within walking distance or by public transportation system with right of way. In this study, the concept integrated national scholars planning and Zhang and Du (2001) study about the development in Taipei metropolitan area, create the following ideas of how to transfer car-based environment development model to TOD:

- High population density enhances the development of public transportation, and encourages people to use public transportation. However, the land use and urban planning with high population density need better integration and more detailed design, in order to create the human environment.
- Residential areas, work areas and retail shops must be spread along the public transportation system routes to form a life, functional improvement, comprehensive community services.
- Make it possible to include variety of urban activities, working and shopping functions in walking area.
- Unlike the concept of car-oriented roads for the road system in the past, public transportation station is not only a node on the network, but also is the economic,

social, cultural and other activities of living space; for the old downtown, TOD station can reshape a new look by urban design and integration planning of transportation systems.

- Urban design with TOD concept must compatible with the good urban landscape and pedestrian-oriented pedestrian system and seamless transfer and feeder facilities with green transportation mode to encourage people to use public transportation.

DEVELOPMENT STATUS OF TAICHUNG CITY

Taichung City is located in central Taiwan. Before 2010, the city is divided to two parts: Taichung City (old) and Taichung County. Since it reformed in the end of 2010, the new Taichung City includes the harbor and airport, local and high speed rail, urban transport and highway transit to connect different development intensity area. In the past, population of Taichung County is about 1.5million in 1999 and 1.56 million in 2009, from 2000 to 2009 the average annual growth rate of about 0.49%; population of old Taichung City is about 0.97 million, from 2000 to 2009 it increased to 1.07 million, average annual growth rate of about 1.18%. Total population of Taichung city (new) was 2.65 million in 2009, about 11.5% of total in Taiwan. Due to the degree of urbanization and industry changes make the slow increase in population trends.

In land use planning, the Taichung County area is about 2,051 square kilometers , the old Taichung City area is about 163 square kilometers and total new Taichung City area is 6.15% of Taiwan total area, and 21.08% of central region area the second largest administrative region. In the urban planning land use planning, the urban planning area in Taichung County is total 334 square kilometers, accounting for 16.28% of Taichung County. The highest proportion of agricultural areas for 32.22%, and the second is public facilities for 17.93%; old Taichung urban planning area is 159 square kilometers is about 97.29% of total area, including public facilities, the highest proportion about 31.43%, the second is residential areas about 25.45%. In non-urban planning land use, net of plan area not includes urban planning area and specific areas in Taichung County is about 1,718 square kilometers, accounting for the total area of Taichung County 83.72%, which is compiled by the regional planning land use areas is 652 square kilometers, accounting for non-urban land area of 37.11%. non-urban planning land use includes specific agricultural land area, generally agricultural areas, rural areas, industrial areas, forest areas, hillside conservation areas,

national park area, a particular precinct, the highest proportion is hillside conservation areas (56.95%), the second is specific agricultural area (30.99%). non-urban planning land use in old Taichung City is only 4.4 square kilometers, accounting for 2.71% of the total area of old Taichung City, and are all the partitions are not delineated.

In transportation systems, after Taichung County and City merged in 2010, the new city includes airport, harbor, high-speed rail, regional rail and three freeways. In the shipping and air transportation, because the harbor and airport are not non-urban area, Taichung Harbor and Taichung Airport do not result in serious competition for space resources situation in the outside the road construction. Harbor and airports surround with good road network system support. Close to Taichung Airport, is Freeway #3, and Taichung Harbor, there are Expressway #61, and #17 convergence to West Coast Expressway and Freeway #4.

Although the road system is fairly complete, but the harbor and airport in this area the most criticism is the lack of public transportation system, personnel trips must depend on private transportation mode. The airport public transport system is very weak, with less frequency and quality, and always faced with the old problem of less utilization.

As for the road public transportation in Taichung city, it includes high speed rail, local rail, freeway bus, highway bus, urban bus and taxi now in which bus system shares about 60% of total public transportation ridership, see Fig. 1. Although the ridership of urban bus grows quickly since decade, the use rate of public transportation is still weak.

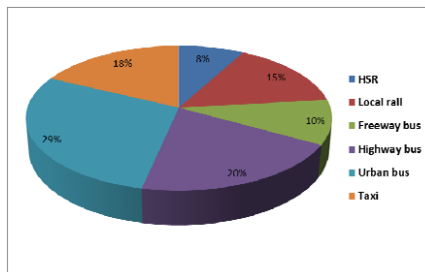


Figure 1: modal split of road public transportation in Taichung city in 2010

In tourism, the central region in Taiwan contains six counties and cities, with much and diverse tourism resources. In 2009, visitors in main tourist recreation area are 2,957 million, and Taichung City is the tourism hub excellent location in central

region. Since the high speed rail operated, Taichung City became the major transportation node, most tourists make Taichung area for entrance door, as the first visit to the central region of the station or terminal. Therefore, the planning must take advantage of its access gateway features, master tourism and recreation resources, to strengthen the relevant recreation industries.

According to the above, the main traffic critical issues in Taichung City are as follows:

- Traffic in downtown is heavy without rapid transit mode and major roads in downtown lack of enough alternative road network.
- Taichung Harbor / Taichung International Airport lack of good public transportation system.
- Rail transportation network integrated insufficiently.
- Since Taichung City and County merged, the bus route is too long or too short, and the fare is not convenient to passengers.

To solve the above problems, planners make the public transportation planning by TOD model.

Taichung City public transport plan

The public transportation development objectives in Taichung City should be summarized as follows: construction based on human, environmental protection, high-quality public transportation system. Based on the above objectives, the current transportation development in Taichung City should be directed to develop public transportation first and then private transport. The TOD concept should be taken into the future urban development to create more competitive, integrated public transportation service system, use more energy-efficient vehicles to reduce carbon emissions to improve the quality of public life. Thereby to integrate public transportation is a core task, bus routes, road network, charges, transfer and feeder of integration of operations planning is a priority focus needed to be promoted. Based on this, the program may develop as follow:

1. To train demand of public transportation in all corridors, and promote the Taichung MRT in different phases.
2. To strength efficient integration of the LRT, rail and (express) bus system.
3. To implement functional classification structure to adjust the bus network
4. To expand the coverage and door-to-door accessibility.
5. To improve the convenience and comfort of transfer and feeder.

6. To enhance the transfer mechanism between highway and local bus.

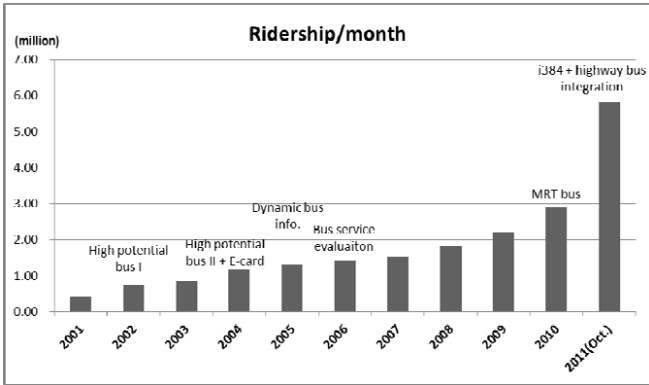


Figure 2: increasing tendency of bus ridership in Taichung from 2001

According to the above features, Taichung City bus implement the “High-Potential Bus” in 2001 and promote peak hour free MRT bus² in 2009, because the results are obvious, in 2010 continue to launch the "2010 Taichung City MRT Bus Plan". As for 2011, new project “i384” is proposed in order to follow the MRT bus policy³, the urban bus ridership are from 40 million per month in 2001 to now take the volume growth of nearly 580 million people per month in October 2011, nearly 14 times the growth, see Fig. 2. The strategy for improving bus in Taichung gets a great response, but the use rate of public transportation in Taichung city is only 7.8% in 2010. Therefore, the following describes the development direction in the short and long term for public transportation network in Taichung city in which it could be divided by three episodes.

● **First stage : bus reform**

Since 2001, the Taichung city government proposes a series of bus improvement in order to increase bus ridership in which the high-potential bus, MRT bus and related subsidies plan etc. In this stage, there are two major directions: first, it must create new bus line for virgin corridors (saving missing link), and second, it has to

² MRT bus : using high frequency and free bus in the planning corridor of MRT in order to cultivate basic MRT ridership.

³ i384 means under bus number 300 in Taichung city which integrates all E-card for public transportation and free ticket for initial 8 km in the trip.

improve the service quality of bus, especially for main road in city (high frequency, low floor bus, accuracy of timetable and bus information system).

Furthermore, in Taichung city, there is a transfer triangle project (see Fig. 3) which could separate bus network according to bus service form, as inter-cities, intra-city or tourist bus. Based on the bus reform plan, Taichung city government aims at solving two important problems, traffic congestion and operation efficiency.

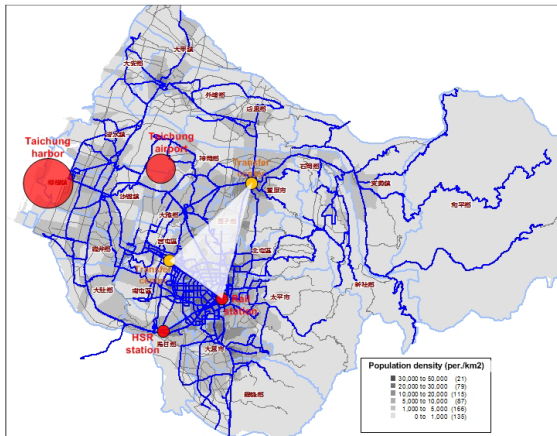


Figure 3: bus network based on the population density in Taichung city

● Second stage : BRT network

Regarding the major corridor in city, first task of public transportation aims at ameliorating the service capacity in order to increase the competitive power and attract more addition users. Thus, the project of bus rapid transit (BRT) has been approved for cultivating more ridership of public transportation before mass rapid transit (MRT) plan. The short-term BRT plan up to 3 years (2011-2014) focus on three BRT in the core corridors; the long-term plan aims at constructing BRT network which includes 6 BRT lines through 29 administrative zones in Taichung city. The long-term rapid transit network involves 6 BRT lines, 1 MRT line and 1 advanced local train line, see Fig. 4.



Figure 4: rapid transit network in the long-term in Taichung city

● **Third stage : complete public transportation network**

In the long-term plan of public transportation development, it aims at creating a complete public transportation network which is composed by local rail, MRT, BRT, bus. Based on long-term objective of public transportation, it could have 4 crucial development elements:

- ✓ Applying the classification concept in the public transportation, like trunk line (rail, MRT, BRT), feeder line (bus), circle line (express bus) and rural line (mini bus & DRTS⁴).
- ✓ Creating the seamless use environment based on 4 evaluation factors, as time, space, information and service.
- ✓ Adjusting the existing bus network in order to reinforce the crosswise and terminal feeder capacity of rapid transit system (providing the door-to-door service by public transportation).
- ✓ Developing the intermodal transport combines non-motorized vehicles, public transportation and motorized vehicles in which it could employ monetary skill, information platform and public policy.

REFERENCE

Cervero, R. and Kockelman, K. (1997), Travel demand and the 3Ds: Density, diversity, and design, *Transportation Research Part D*, 2 (3): 199-219.

⁴ Demand responsive transportation system (DRTS)

- Chang, S. K., Chen, S. T. and Du, Y. L.(2000), Transit-Oriented Development of urban development strategy, *MRT Technology*, 22, 1-16.
- Hsieh, R. H. (2008), Urbanization reached 44.9% in China in 2007, *Economic Research, Reference*, 2164, 37-38.
- Lu, D. D. (2007), Urbanization process and the spatial expansion in China, *Journal of Urban Planning*, 170:47-52.
- Nu, F. R.(2008), *Urban development report in China* , Social Sciences Academic Press, Beijing.
- Taichung City Government (2011), *Integration planning of Taichung Metropolis bus system*.
- Taichung City Government (2010), *Integration planning of Taichung Metropolis transportation system*.
- Taichung City Government (2011), *Taichung City important statistical index reference*.
- Taichung City Government (2010), *White Paper on transportation policy of Taichung City*.

Car Parking in China - Issues and Solutions

Vincent Au¹

¹ Chairman, the Parking Association of Hong Kong, Director (Business Consultancy), MetroSolutions Limited, Suite 1202, Pacific Plaza, 410 Des Voeux Road West, Hong Kong, E-mail: vincent_au@metrosolutions.com.hk

ABSTRACT

Car-parking has always been an unresolved issue in most municipal cities in China. Despite efforts by officials of the relevant government departments to put forth new policies and launch various solution proposals from time to time; followed by aggressive actions in the implementation of improvement action plans, their work seldom yield tangible/visible outcome, and the problem remains. This paper aims to examine what has gone wrong in the government policies and actions, and to make suggestions to resolve the long-standing entangled issues of car-parking in municipal cities in China.

BACKGROUND

Since the opening up of China three decades ago, the country has steadily grown into a strong economy as commonly recognized in the global arena. A direct consequence is the improvement in the overall earning of the general public, and owning a private car is no longer an unreachable dream. Since China became a member of the WTO in 2006, there was tremendous reduction in import tax on imported cars. Coupled with the improvement in quality and reduction in price of local-made cars, the increase of private cars in the coming years will continue.

A recent report issued by China's Traffic Police Department states that up to end of September 2011, there are 199 million motor vehicles, equivalent to one motor vehicle per seven persons, of which, over 85 million are private cars. The industry foresees China shall overtake USA as the largest auto-market in 2015. According to government's forecast, the annual production of motor vehicles in China by then shall reach 8.6 million cars and forecast local sales 8.3 million cars.

From late 1990 till the present, the shortage of car parking spaces has been huge. "Difficult to Park (停车难)", or "Parking Headache", a common saying throughout China, has long been a hot topic among car-owners which caused frustration to people living in municipal cities. Take Guangzhou as an example, every day there are over 200 new car registrations. The "Parking Headache" issue is worsening day after day, becoming the nightmare for everyone living in Guangzhou.

Although the government is determined to find solutions to rectify the problem and has formulated policies and actions such as building multi-storey public car parks, introducing meter on-street parking wherever possible, increasing patrol frequency and fines, etc., tangible outcome is rarely seen.

CURRENT SITUATION

The increase in earnings and hence vehicle ownership results in increased traffic. In the old days when the number of vehicles was much less, parking at shop-fronts was a common practice and tolerated. With the rapid growth of the economy, the development of infrastructure, parking facilities fail to meet the growing demand. “Parking Headache” is a hot issue for the Transportation Committee, which prompted a series of actions to increase the provision of car parking spaces. However, the actions taken so far fail to solve the problem. “Parking Headache” remains an unresolved issue in nearly all municipal cities in China (see Figure 1).



Figure 1. Traffic congestions everywhere, day and night

CAUSES OF PARKING DIFFICULTY

Town Planning

The lack of sufficient parking spaces occurs not only in the old neighborhood, towns and commercial areas, but also the newly constructed commercial and residential developments. This is partly due to myopic view and lack of foresight of town planners and real estate developers, and partly due to commercial reasons of the poor return on investment on parking facilities. Hotels, restaurants, hospitals, etc - places that call for high demand of parking spaces - are disastrous areas. It is a common sight that cars are illegally parked on road-sides regardless of whether there is properly provided meter-on-street parking. To make matters worse, property owners convert parking spaces in existing buildings to shops such as renting out basement car parks to supermarkets or storage godown. This adds salt to the wound of the already scarce supply of car parks. Similarly, some of the on-street meter parking spaces are illegally occupied by hawkers and/or occupants in the vicinity. In a nutshell, this difficulty may be due to a number of reasons. However, poor town planning is considered one of the major causes (see Figure 2).



Figure 2. Huge parking demand

The Role of Property Developers/ Investors

Apart from the government having to bear the major responsibility for the current situation of “Parking Headache”, another guilty party are property developers and real estate investors. Despite making huge profits, they do not feel obliged to helping the government or the society at large. The Price Bureau (物价局) plays a role in most commercial activities in price setting and price standardization. The car parking tariff must follow a pre-approved fee-table that provides clearly defined guidelines, or rather, instructions, on parking levies applicable to different types of buildings, hotels, residential area, on-street and temporary car parking sites, etc. In other words, car park owners do not have the freedom of setting the parking charge according to supply and demand and the property land value. This is one vital factor that deters developers from investing in providing car parks for their own buildings, not to mention investing in building parking facilities for the public. The direct consequence is that the government must shoulder the provision of car parking spaces on its own. Without the support of the commercial sector, the parking space shortage shall always remain an unsolvable issue (see Figure 3).



Figure 3. Illegal parking all over the place, day and night

The Local Government and Law-enforcers

Different government departments possess the authority to interfere with car parking-related matters. For instance, the Commission of Transport (交委), Traffic Police (交警), Traffic Management Bureau (交管局), Urban Management Bureau, or Cheng-guan (城管局), Municipal Bureau (市政局), Street Office (街道办), Industrial and Commerce Bureau (工商局), and Price Bureau (物价局) each possesses some authority to put a hand in matters relating to car-parking. This creates a major obstruction for the effective formulation of car-park planning, control policy, law-enforcement, etc. It also results in the already scarce resource of spaces not effectively utilized. These departments jointly render multi-point governance or indeed no governance.

Selfish Behavior of Drivers and Shop Owners

The selfish habit of some drivers and sometimes, the general public could be part of the reason for “Parking Headache”. It is a common sight that cars are parked illegally on road sides or even on pavements in narrow streets of the neighborhood community even though proper car parking facilities are available in the vicinity. Many drivers park their cars illegally to avoid paying parking fees. This will affect the income of car park owners and investors. Also, the non-drivers may contribute to the “Parking Headache” by illegally occupying the parking spaces for private use in front of their shops (see Figures 4 and 5).



Figure 4. Abused use of parking spaces



Figure 5. Illegal occupying of parking spaces

CHALLENGES AND OPPORTUNITIES

Town Planners

China is undergoing a huge transformation to modernization. The economy is growing so rapidly that town planners must have a good foresight in order to meet the demand. To provide sufficient parking facilities in their planning is also a good opportunity for planners to implement new concepts and give a new look to municipal cities in China, as well as yielding stable income for property owners.

Policy Makers and Law Enforcers

The policy makers are charged with the responsibility for making suitable policies in coping with the parking problems. Without a suitable policy, any action in enforcing control or professionally manage the matter is bound to fail. To effectively solve this long lasting problem, it is important to improve the quality of law enforcers such as traffic police and the Chang-guan and Street Office personnel through training and stringent control and monitoring of the forces' performance.

Property Investors and Car Park Operators

The stringent price control is a major deterrent for the investor in commercial consideration. Also the common perception of most people that car park operators are held fully liable for damages and losses to parked vehicles adds huge operating costs and open-ended risks in running a public car park. The up side, on the other hand, is that sooner or later the government must face reality and revise its price control policy. Coupled with the ever-rising demand, investing in car park infrastructures shall provide good potential for growth and development.

RECOMMENDATIONS

(1) What the government can do:

Adopt new concepts

Since ex-Premier Zhou-en-lai declared the "Four Modernization" national policy in 1975 to basically achieve modernization in 20 years, the current day China is no longer the same as most people perceive in terms of economy, politics and the people's livelihood. Accordingly, decision makers in car parking policy must be open-minded in adopting new concepts to cope with the new challenges such as abandoning price control and allowing investors operate car parks on commercial principles.

Town planning

Ensure good foresight and new concepts in the provision of car parking facilities with long term consideration on the rising need. Learn from advance countries the valuable experience that they have gathered. Encompass car parking as an integral part of the overall plan in the long term growth of economy. Encourage park-and-ride by providing parking facilities near to mass transit systems such as terminal train stations thus encouraging drivers to forsake driving into the CBD area.

Participation of the business sector

It would be too much burden for the government to provide all the facilities for public parking on its own. Government should encourage participation of private sector investment by providing favorable policy such as providing cheap land, introducing flexible and favorable tax plans, lifting price control on parking fee setting, etc. Traditionally the government, with good intent, exercises control on private businesses in various forms to ensuring things does not go off the track. The business operators indeed wish the authorities assist more and interfere less.

Law and ordinance

The multi-point governance by different departments inhibits rather than assists. Government should unify the control and confine this to a couple of relevant departments such as Commission of Transport and Traffic Police of the Gong-An Department. The law enforcers should ensure the team of public servants is provided with good training and professional knowledge. Government should provide support to the law enforcement departments by taking stringent legal actions against illegal parking. Simplify the fine and penalty procedure by using “fixed penalty ticket” against offenders of the relevant law (see Figure 6).



Figure 6. A well-trained disciplined staff force is important

Educate the general public

Through the media launch educational programs to educate drivers the importance of courtesy and consideration in driving and car parking, and to inform the general public how they can contribute as well.

(2) What investors and operators can do:

Build infrastructures

Property developers should ensure ample parking space is provided for commercial buildings and residential developments instead of maximizing the use of space for shops and other rental-attractive tenants. Investors should also consider building parking facilities exclusively for car parks. The return is attractive as proven by successful stories in Hong Kong where their valuable experiences can be shared in China (see Figure 7).



Figure 7. Privately owned car park buildings

Employ professionals and talents

Seek international and professional advice from the car parking field. Consider using car parking professionals with recognized qualification in the relevant industry such as the CAPP (Certified Administrator of Public Parking) of USA. Employ their talents to work out policies and implementation plans including doing effective and sustainable town planning.

Adopt modern management

Extensively utilize the proven management and hardware such as using suitable PARCS (parking access and revenue control system), mechanical stack parking machines and facilities, etc. Avoid providing reserved space service but all spaces are used flexibly for floating parking. Provide convenience-store type service in car parks to increase income such that the operator has more financial support to doing a better job. These are effective tools to improve the overall parking discipline thus maximizing the functionalities of the scarce resource (see Figure 8).



Figure 8. Mechanical parking facilities

CONCLUSION

China is not the only country facing “Parking Headache”. It is common in all advanced countries due to the rapid rise of vehicle numbers. As mentioned earlier, just Guangzhou alone, there are 200 new cars being put on the road every day. The rising need of car parking is an unstoppable trend. To overcome the difficulty, it is crucial that the government has the determination to solve the problem. Among all the recommendations, the writer opines that the most effective measure is to be able to call for the proactive participation of the business sector in building car parks. The key to successfully attracting their investment is the uplifting of price control on car parking tariff. The government has no more room to allow the matter to worsen. Immediate action is a must.

Evaluation of Construction Equipment Fleets through Fuel Use and Emissions Inventories

Phil Lewis, PhD, PE¹ and Apif Hajji²

¹Assistant Professor, School of Civil and Environmental Engineering, Oklahoma State University, 207 Engineering South, Stillwater, OK 74078, PH 405-744-5207, email: phil.lewis@okstate.edu

²Ph.D. Candidate, School of Civil and Environmental Engineering, Oklahoma State University, 207 Engineering South, Stillwater, OK 74078, PH 405-744-5207, email: apif.hajji@okstate.edu

ABSTRACT

All types of construction vehicle fleets can benefit from fuel use and emissions inventory evaluation, including publicly-owned fleets that are used for infrastructure construction and maintenance. Fleet managers can use these types of inventories for minimizing the equipment's contribution to air pollution and climate change. The purpose of this paper is to evaluate the current status of the nonroad diesel construction equipment fleet for the City of Stillwater, Oklahoma by developing and analyzing a fuel use and emissions inventory. This inventory evaluates equipment attributes such as equipment type, engine size, engine age, and pollutant regulations; equipment usage in terms of total hours of operation and average annual use; fuel use in terms of total fuel consumed over the life of the equipment and average annual fuel use; and carbon dioxide (CO₂) emissions in terms of total CO₂ emitted over the life of the equipment and average annual emissions. Results indicate that backhoes have the greatest energy and environmental footprint of any equipment type in the fleet. Furthermore, approximately 20% of the fleet is over 20 years old and almost 75% of the fleet is either unregulated or meets only the minimum standard of nonroad diesel engine emissions standards. It is anticipated that this paper can serve as a case study that can be used by managers of publicly-owned fleets to address their specific concerns related to energy consumption and emissions.

INTRODUCTION

The United States Environmental Protection Agency (EPA) considers emissions from diesel engines one of the most important health concerns facing the country (EPA 2005a) and they are also substantial contributors to greenhouse gas emissions, including carbon dioxide (CO₂). One prominent source of these emissions is the two million items of construction equipment that contribute significantly to local air pollution (EPA 2005b). In order to accurately assess the environmental impact of construction equipment, it is necessary to inventory the fuel used and pollutants emitted from construction equipment fleets, including those owned by local governments and municipalities.

The City of Stillwater (Oklahoma) provides services to a population of approximately 46,000 people, including infrastructure operations such as utility

installation, road maintenance, and landscaping. To effectively provide these services, the City of Stillwater must maintain a fleet of nonroad diesel equipment including backhoes, bulldozers, excavators, motor graders, skid-steer loaders, tractors, and wheel loaders. This equipment consumes diesel fuel and consequently emits mass quantities of CO₂. In order to manage fuel use and emissions effectively, they must first be measured, hence the need for a fuel use and emissions inventory.

Equipment fleet managers can benefit from fuel use and emissions inventory evaluation. For example, identifying and correcting sources of excessive fuel use not only saves money for the fleet owner but also reduces the quantities of harmful pollutants and greenhouse gases that are emitted into the atmosphere. Whereas the former is related to the overall profitability of an organization, the latter is particularly important with regard to current and impending federal regulations related to air quality (EPA 2009). The purpose of this study is to evaluate the current status of the equipment fleet for the City of Stillwater by developing a fuel use and CO₂ emissions inventory which can be used as a decision support tool to maximize the environmental benefits of equipment objectives.

METHODOLOGY

The data needed to compile the fuel use and emissions inventory was obtained from the City of Stillwater's fleet management database. This database contains records for each item of equipment in the fleet and includes information such as the equipment type, purchase date, model year, and engine size. Based on model year and engine size, the EPA Engine Tier was determined (EPA 2004). EPA Engine Tier regulations are requirements that are placed on nonroad diesel engine manufacturers that mandate them to meet increasingly stringent emission standards for nitrogen oxides (NO_x), hydrocarbons (HC), carbon monoxide (CO), and particulate matter (PM). These regulations began to be phased-in during the 1990s and many larger diesel engines are just now being required to meet Tier 4 standards. Tier 0 indicates that the engine is unregulated whereas Tier 4 is the strictest standard. CO₂ emissions are not regulated under the EPA Engine Tier standards.

The database also includes fuel use records that indicate the date when the equipment was fueled and the hour meter reading at the time; however, this data was incomplete or inaccurate for many items of equipment. When invalid or missing data were found, field measurements were used to supplement the database. For example, oftentimes the hour meter reading was not recorded when the equipment was fueled, or an invalid number was recorded, such as 999, which obviously did not correspond with the other hour meter readings for the equipment. In this case, the item of equipment was located in the field and a current hour meter reading was obtained.

The total fuel use and CO₂ emissions over the life of the fleet was estimated based on the total hours of operation for each item of equipment. Since the fuel use records in the database were incomplete, the total fuel use for each item of equipment was computed using a diesel fuel use factor of 0.04 gallons per horsepower-hour (Peurifoy and Oberlender 2002). The total CO₂ emissions were estimated by using a diesel emission factor of 10.15 kilograms per gallon of fuel consumed (EPA 2005c) and then converted to tons based on 454 grams per pound and 2,000 pounds per ton.

For example, Backhoe 1 (98 hp, 3,811 hr) was estimated to have consumed 14,939 gallons of diesel fuel and emitted 167 tons of CO₂ over its current life.

Fuel use and emissions estimates are typically adjusted for average engine load because nonroad diesel construction equipment usually does not operate for long periods at maximum or near maximum load. These load factors are expressed as a percentage of maximum engine loads, such as 75%. The fuel use and emissions estimates presented here have not been adjusted for engine load because, at the time of the study, the estimated engine load for each item of equipment was not known. Therefore, the fuel use and emissions estimates represent the maximum total based on an unadjusted 100% engine load for each item of equipment. Although these results are likely higher than the actual results, they do represent the probable worst case scenario based on the given information.

The estimated age of the equipment was determined by the difference in the date of the most recent hour meter reading and the purchase date. This age was used as the basis for estimating the average annual fuel use and average annual CO₂ emissions for each item of equipment. The average annual fuel use and emissions were calculated by dividing the total fuel use and emissions by the estimated age at the most recent hour meter reading from the equipment. Although only a rough indicator that does not show the true year-to-year values, these annual averages provide a reasonable estimate of the fuel use requirements and corresponding CO₂ emissions for each item of equipment over its current life.

RESULTS

The City of Stillwater's nonroad fleet consists of 47 items of equipment including 17 backhoes, three bulldozers, two excavators, two motor graders, seven skidsteer loaders, 14 tractors, and two wheel loaders. The most represented items of equipment are backhoes, skidsteer loaders, and tractors, which comprise over 80% of the fleet. It is estimated that the current fleet, over its life, has totaled over 118,000 hours of operation, consumed nearly 375,000 gallons of diesel fuel, and emitted approximately 4,200 tons of CO₂. On an average annual basis, the fleet is used over 12,000 hours per year and consumes about 39,000 gallons of fuel per year while emitting about 435 tons of CO₂ per year.

According to equipment type, backhoes accumulated the most hours of operation (6,410 hours per year) and also consumed the most fuel (20,474 gallons per year) and emitted the most CO₂ (229 tons per year). This is not unusual given that they are the most represented equipment type in the fleet with 17 units. However, backhoes also have the second highest average annual use per unit (377 hours per year) behind the two excavators (488 hours per year). Based on the total number of units and the average annual use per unit, backhoes have the largest energy and environmental footprint of any equipment type in the fleet.

The average age of the equipment in the fleet is 12.5 years. There are 15 items (32% of the total) that are over 15 years old, including 10 items (21%) that are over 20 years old; the oldest items of equipment in the fleet, Bulldozer 1 and Wheel Loader 2, are 35 and 39 years old, respectively. Furthermore, there are 19 items (40%) that were manufactured with no EPA emissions standards (Tier 0) and another 15 items (32%) that meet only the minimum emissions standards (Tier 1); thus,

nearly three-quarters of the entire fleet are not within EPA Tier 2 or higher emissions standards. Although fuel use and CO₂ emissions are not regulated by EPA Engine Tier standards, other diesel pollutants such as NO_x, HC, CO, and PM are.

On an annual basis, each item in the fleet operates an average of 256 hours per year, consumes approximately 830 gallons of fuel per year, and emits over nine tons of CO₂ per year. Backhoe 15 is the most frequently used machine in the fleet with an average of 1,118 hours of operation each year. Likewise, this item of equipment consumes an average of 2,907 gallons of fuel per year and emits an average of 32 tons of CO₂ per year, both maximums for the fleet. The least used machine in the fleet is Wheel Loader 2, which has an average of 42 hours of operation per year; this item of equipment is also the oldest in the fleet at 39 years old. However, Backhoe 4 consumes the least amount of fuel each year (82 gallons) and emits the least amount of CO₂ per year (0.9 tons) even though it is used almost twice as much annually as Wheel Loader 2. This is because Wheel Loader 2 has an engine size nearly six times greater than Backhoe 4 (170 hp compared to 28 hp), thus consuming more fuel and emitting more CO₂. In addition to the hours of use, the engine size based on rated horsepower is an important factor in estimating fuel use and emissions. For example, Excavator 1 and Backhoe 11 have approximately the same average annual use, 343 hours and 369 hours respectively, but Excavator 1 has an engine that is about 2.5 times larger than Backhoe 11 (190 hp versus 75 hp); hence, Excavator 1 consumes over twice as much fuel and emits over twice as much CO₂ on an annual basis.

In general, backhoes, bulldozers, skidsteer loaders, and tractors have similar sized engines with an average of about 68 hp and excavators, motor graders, and wheel loaders have larger engines with an average of approximately 146 hp. Furthermore, the equipment with the larger average engine size have a slightly higher average annual usage of 290 hours per year compared to the equipment with the lower average engine size with an average annual usage of 251 hours per year. It should be noted, however, that there are many more items of equipment with the lower average engine size (n=41) than there are with the higher average engine size (n=6). Even though excavators, motor graders, and wheel loaders constitute only 13% of the total fleet composition, they are still responsible for approximately 25% of the fleet's total average annual fuel use and emissions.

With regard to the relationship between equipment age and annual usage, it appears that the equipment is used less on an average annual basis as it gets older. For example, the 10 items of equipment that are more than 20 years old have an average annual usage of 144 hours per year whereas the other 37 items of equipment that are less than 20 years old have an average annual usage of 291 hours per year. Moreover, the two oldest machines in the fleet, Bulldozer 1 (35 years old) and Wheel Loader 2 (39 years old) are used only 46 and 42 hours per year, respectively.

Although the methodology used here for estimating the average annual usage (total hours divided by age) does not track the actual hours of use on an annual basis, it does indicate a pattern of decreased usage as the equipment ages. The most likely explanation for this phenomenon is that fleet managers and equipment operators seem to prefer using newer equipment when given a choice and older equipment tends to be placed on stand-by for emergency use only. This is, however, an assumption and was not documented by the study or in discussions with the fleet managers.

Table 1. Fuel Use and Emissions Inventory for City of Stillwater Fleet

Equipment Type	ENGINE ATTRIBUTES				ENGINE USAGE		FUEL USAGE		CO ₂ EMISSIONS	
	EPA Tier	Engine (hp)	Model Year	Age (yr)	Total (hr)	Annual (hr/yr)	Total (gal)	Annual (gal/yr)	Total (ton)	Annual (ton/yr)
Backhoe 1	1	98	2002	8.9	3,811	429	14,939	1,682	167	19
Backhoe 2	0	58	1993	17	4,305	254	9,988	588	112	6.6
Backhoe 3	0	58	1992	19	3,549	186	8,234	432	92	4.8
Backhoe 4	0	28	1982	28	2,078	73	2,327	82	26	0.9
Backhoe 5	0	75	1995	15	4,655	305	13,965	916	156	10
Backhoe 6	2	95	2005	5.7	2,379	417	9,040	1,586	101	18
Backhoe 7	0	75	1997	14	4,136	298	12,408	895	139	10
Backhoe 8	3	79	2008	2.9	1,418	481	4,481	1,520	50	17
Backhoe 9	2	95	2007	3.8	2,402	627	9,128	2,383	102	27
Backhoe 10	1	75	1999	11	5,654	495	16,962	1,486	190	17
Backhoe 11	1	75	2000	11	3,925	369	11,775	1,108	132	12
Backhoe 12	1	75	2000	11	2,597	241	7,791	723	87	8.1
Backhoe 13	2	95	2007	4.0	1,103	277	4,191	1,051	47	12
Backhoe 14	1	98	2001	9.3	3,290	354	12,897	1,389	144	16
Backhoe 15	0	65	1991	3.6	4,013	1,118	10,434	2,907	117	32
Backhoe 16	1	95	2002	4.0	1,378	342	5,236	1,300	59	15
Backhoe 17	0	75	1997	14	1,915	141	5,745	424	64	4.7
Bulldozer 1	0	78	1975	35	1,593	46	4,970	142	56	1.6
Bulldozer 2	1	87	2002	8.4	2,171	258	7,555	898	84	10
Bulldozer 3	2	70	2006	5.4	959	177	2,685	495	30	5.5
Excavator 1	2	190	2003	7.2	2,464	343	18,726	2,610	209	29
Excavator 2	1	114	1999	12	7,284	633	33,215	2,885	371	32
Motor Grader 1	0	150	1982	25	1,681	67	10,086	402	113	4.5
Motor Grader 2	1	140	2002	8.6	2,401	279	13,446	1,561	150	17

Table 1. continued

Equipment Type	ENGINE ATTRIBUTES				ENGINE USAGE		FUEL USAGE		CO ₂ EMISSIONS	
	EPA Tier	Engine (hp)	Model Year	Age (yr)	Total (hr)	Annual (hr/yr)	Total (gal)	Annual (gal/yr)	Total (ton)	Annual (ton/yr)
Skidsteer 1	2	82	2007	4.1	294	72	964	237	11	2.7
Skidsteer 2	3	82	2008	3.0	164	54	538	177	6	2.0
Skidsteer 3	4	46	2009	2.1	501	234	922	431	10	4.8
Skidsteer 4	2	90	2006	5.1	515	101	1,854	364	21	4.1
Skidsteer 5	1	61	1998	12	1,869	152	4,560	370	51	4.1
Skidsteer 6	1	61	2001	9.5	1,019	107	2,486	262	28	2.9
Skidsteer 7	2	63	2005	4.9	345	70	869	176	10	2.0
Tractor 1	0	43	1998	3.6	585	162	1,006	279	11	3.1
Tractor 2	1	81	2001	10	944	92	3,059	299	34	3.3
Tractor 3	2	35	2007	4.2	380	91	532	127	6	1.4
Tractor 4	1	36	2001	6.8	3,948	581	5,685	836	64	9.3
Tractor 5	0	37	1974	24	2,040	86	3,019	127	34	1.4
Tractor 6	1	30	2001	9.5	785	83	942	99	11	1.1
Tractor 7	0	38	1978	22	3,207	147	4,875	224	54	2.5
Tractor 8	0	33	1979	24	2,569	106	3,391	140	38	1.6
Tractor 9	0	70	1989	23	4,477	194	12,536	544	140	6.1
Tractor 10	0	40	1996	15	3,931	265	6,290	425	70	4.7
Tractor 11	1	80	2001	9.7	5,102	528	16,326	1,690	183	19
Tractor 12	0	85	1995	15	766	51	2,604	174	29	1.9
Tractor 13	2	114	2003	8.8	776	88	3,539	402	40	4.5
Tractor 14	0	18	1985	26	3,124	119	2,249	86	25	1.0
Wheel Loader 1	0	110	1990	21	7,935	379	34,914	1,667	390	19
Wheel Loader 2	0	170	1972	39	1,643	42	11,172	286	125	3.2
Total					118,080	12,018	374,558	38,889	4,187	435

CONCLUSIONS AND RECOMMENDATIONS

The City of Stillwater has a substantial fleet of nonroad diesel construction equipment with respect to the number of machines, hours of operation, fuel consumption, and greenhouse gas (CO₂) emissions. They have attempted to record much of the information that is necessary to compile a fuel use and emissions inventory in their equipment database, however, some of this data is either missing or inaccurate. It is recommended that the City of Stillwater update this information frequently and completely in order to correctly assess the energy and environmental footprint of their nonroad fleet.

The fleet is old with regard to age and pollution regulations. Even though nonroad diesel equipment may last around 30 years, approximately 20% of the fleet is over 20 years old and two items of equipment are approaching 40 years old. Furthermore, about 75% of the engines in the fleet either meet none of the EPA pollution standards (Tier 0) or the minimal level of pollution standards (Tier 1). Although these standards do not regulate requirements for fuel use and CO₂ emissions, they do regulate emissions of NO_x, HC, CO, and PM. Thus, this fleet may well be a significant source of these harmful pollutants. In addition to expanding the fuel use and emissions inventory to include these pollutants, it is recommended that the City of Stillwater develop an equipment strategy that focuses on replacing these older items of equipment with modernized, less polluting equipment that meets current EPA engine standards for nonroad diesel equipment.

Engine age is a factor that must be considered for fuel use and emissions estimates. Although difficult to quantify, engines typically become less efficient as they age and therefore they use more fuel and emit more pollutants and greenhouse gases. It is recommended that additional studies be conducted to evaluate the deterioration rates of nonroad diesel engines to determine the true nature of fuel use and emissions over the life of the fleet. Likewise, older engines typically are unregulated or have less stringent standards with regard to air pollutants compared to more recently manufactured engines. It is recommended that fleet managers and equipment operators select engines with the highest available EPA engine tier to complete activities when there is a choice to do so.

Other factors to consider when estimating total fuel use and emissions include time of use (hours of operation) and engine size (rated horsepower). As either or both of these factors increase, the total fuel use and emissions increase. Although not included in this analysis, engine load factor should be considered as well. It is recommended that further studies be conducted on the fleet to determine the average engine load factor for each type of equipment in order to more accurately assess its fuel use and emissions. Also, as a practical step towards reducing fuel use and emissions for the fleet, it is recommended to use equipment with a smaller engine size when there is a choice to do so.

The fuel use and emissions inventory presented here provides a base level of knowledge for a particular municipal construction equipment fleet. The methodologies used may be refined and duplicated by other fleet managers to develop inventories for their fleets or to augment existing inventories. The results may be used as benchmark data to compare outcomes of various equipment management strategies aimed at reducing fuel use and emissions.

ACKNOWLEDGEMENT

The authors wish to express gratitude to Mr. David Higgins and Mr. John Maehs with the City of Stillwater for their cooperation in providing information from their equipment database and providing access to the equipment in order to complete this study.

REFERENCES

- EPA. *Exhaust and Crankcase Emission Factors for Nonroad Engine Modeling - Compression-Ignition*. EPA-420-P-04-009, NR-009c, U.S. Environmental Protection Agency, Ann Arbor, MI, 2004.
- EPA. *National Clean Diesel Campaign Fact Sheet*. EPA-420-F-05-012. Available at <http://epa.gov/cleandiesel/documents/420f05012.pdf>. U.S. Environmental Protection Agency, Ann Arbor, MI., 2005a.
- EPA. *Clean Construction USA*. EPA-420-F-05-032. Available at <http://epa.gov/cleandiesel/documents/420f05032.pdf>. U.S. Environmental Protection Agency, Ann Arbor, MI., 2005b.
- EPA. *Emission Facts: Average Carbon Dioxide Emissions Resulting from Gasoline and Diesel Fuel*. EPA420-F-05-001, U.S. Environmental Protection Agency, Office of Transportation and Air Quality, Ann Arbor, MI, 2005c.
- EPA. *Report to Congress: Highlights of the Diesel Emissions Reduction Program*. EPA-420-R-09-006. U.S. Environmental Protection Agency, Washington, D.C., 2009.
- Peurifoy, R. and Oberlender, G. *Estimating Construction Costs, Fifth Edition*. McGraw-Hill, New York, NY, 2002.

Developing a Sustainable Freight Transportation Framework with the Consideration of Improving Safety and Minimizing Carbon Emissions

Rita Neff¹ and Yong Bai²

¹Undergraduate Research Assistant, Department of Civil, Environmental, and Architectural Engineering, The University of Kansas, 1503 W. 15th Street, 2160 Learned Hall, Lawrence, KS 66045, U.S.A. Phone: (785) 218-4903; Email: neff.mf@gmail.com

²Associate Professor, Department of Civil, Environmental, and Architectural Engineering, The University of Kansas, 1503 W 15th Street, 2150 Learned Hall, Lawrence, KS 66045, U.S.A. Phone: (785) 864-5631; Email: ybai@ku.edu

ABSTRACT

Not only does freight transportation use a large percentage of America's resources but also contributes significantly to its share of carbon emissions and affects the safety of the transportation system and all its users. These problems are expected to increase as the volume of freight transportation is already reaching the limits of the transportation infrastructure's capacity while demand continues to increase. The primary objective of this research was to compile a list of technologies and practices that should be included in the sustainable freight transportation frameworks of government agencies and commercial fleets to reduce their carbon footprint and increase their safety by providing recommendations on promising legislation, research, technology, and practices. Data was gathered through a literature review of available materials and a survey of the state Departments of Transportation. The success of this research project provides the needed knowledge for the development of a sustainable freight transportation framework.

INTRODUCTION

AASHTO estimated that if economic growth averages 3 percent per year, domestic freight tonnage will increase by 57 percent by 2020. This would add another 6,600 million tons of freight transported over highways, a 62 percent increase, and another 888 million tons of freight transported by rail, a 44 percent increase (2011). America's freight transportation network is already close to or above its maximum capacity, causing congestion. The larger number of vehicles increase both greenhouse gas emissions and the likelihood of an accident. Infrastructure expansion can be expensive and some locations do not have space available for expansion even if they do have the funding.

LITTERATURE REVIEW

Lane Restriction

Lane restriction is the practice of designating one lane of a multiple lane highway for only trucks to drive on, illegal for civilian vehicles to use. The goal is to reduce accidents by separating cars and trucks. Lane restriction requires a large

capital investment and extended time periods to design and instal.

The South Carolina DOT (SCDOT) conducted a pilot study on the effect of lane restriction on a major north-south route with a high concentration of heavy trucks (AASHTO 2004). The study found a 78 percent reduction in truck related crashes; however, since the actual implementation of the restrictions, truck crash frequency has increased slightly although fatalities involving heavy trucks have decreased. The Texas Transportation Institute (TTI) conducted traffic studies both before and after lane restrictions were implemented on the I-10E in Houston (AASHTO 2004). The TTI study estimated that of the factors affecting crash rates, lane restrictions had likely helped to reduce vehicle crashes by 68 percent. The North Carolina DOT (NCDOT) implemented lane restrictions along 123 miles of three lane interstate highway and identified a number of safety benefits due to the separation of trucks and cars (AASHTO 2004). NCDOT excluded lane restrictions from highway sections with left-side exits and merging areas and between closely spaced interchanges for safety concerns.

Speed Limits

Lower speed limits have been promoted as a means to reduce fuel use. According to the American Trucking Association (ATA), the efficiency of truck engines rapidly decline the faster the vehicle travels above 60 mph. For example, a truck traveling at 75 mph consumes 27 percent more fuel than one traveling at 65 mph (2011). The ATA predicted that reducing speed limits for trucks to 65 mph would save 2.8 billion gallons of diesel fuel in 10 years and reduce CO₂ emissions by 31.5 million tons. One study predicted that limiting trucks to 68 mph in Canada would result in fuel savings of \$8,000 per year for the typical tractor trailer (Carey 2006). On the other side of this issue, fleets argue that reduced speeds would make trucking slower, not only delaying deliveries but also potentially inflating the driver shortage as many drivers are paid by miles logged. Proponents believe the lower speed limits would not have much impact (Carey 2006).

Large trucks also require greater distances for stopping and turning than smaller vehicles, so some attention has been given to separate speed limits for highways, mandating a lower speed limit for trucks than for lighter vehicles. So far, studies have not shown a reduction in crashes on highway segments employing different speed limits for trucks. Neeley and Richardson analyzed state crash data from 1991 through 2005 and found that higher speed limits for both cars and trucks increased fatalities but separate speed limits for cars and trucks did not have a significant impact unless there was a large difference between the speed limits in which case there was a significant increase in fatal accidents (2009).

Alternative Fuels

Over the years a number of alternative fuels have been developed to limit the environmental impact of the vehicles using them. They have varying benefits at reducing emissions and effectiveness as fuel sources. The greatest barrier to the use of alternate fuels in the trucking industry is the scope of the necessary infrastructure alterations. Trucks must be able to cover long distances along a wide variety of routes without risking being stranded in an area without the fuel their engine requires.

Therefore, fuels which can be used in a modified diesel engine present the only viable alternate fuels for the trucking industry. These are typically more expensive than diesel. Rail already has a limited number of centralized fuel stations and is in a better position to introduce alternative fuels.

Electricity

Electricity production, in centralized facilities, can be better regulated and provide cleaner energy than numerous engines of various makes and models. Unfortunately there are a number of problems with its widespread use. Electric engines cannot also run on petroleum when electric fuel stations are unavailable, making them infeasible for long-haul trucking. They have all the associated costs of new vehicles, or possibly retrofitting, and can be more expensive to purchase and maintain than a traditional diesel engine, to say nothing of the increased refueling time. Although these flaws make electric vehicles unsuitable for most trucking, they should be examined as an option for support vehicles short-haul deliveries. In Europe, electric vehicles have mostly seen use for similar short-range services such as milk and post office delivery (De Neufville et al. 1996). Short-haul vehicles parked in a garage overnight are the best candidates as the garage can be retrofitted as a recharging station.

So far, hybrid trucks are uncommon and prohibitively expensive costing approximately \$40,000 more than traditional diesel trucks (Katz 2008).

Logistics

Freight is not always shipped by the most efficient route and mode. Route and mode should be investigated to see if simple switches might be beneficial, usually transporting freight by rail as opposed to truck. A study by the Federal Railroad Administration found that railroads average four times the efficiency of trucks, reducing greenhouse gas emissions by 75 percent when goods are shipped by rail instead of truck (AAR 2010). In cases where the closest rail station is too far from either the point of origin or deliver moving freight from trucks onto rail would not be beneficial for either net emissions or cost reductions. An analysis by Lawyer also found transporting some smaller and lighter shipments by rail can actually use more resources to transport than if they had traveled by truck (1986).

As congestion increases throughout the United States, freight travel times increase and more fuel is wasted during stop-and-go traffic. Due to the greater amounts of road space taken up by trucks, a reduction in the number of trucks on the roads could have a greater percentage impact on congestion than changes to the numbers of cars (Bryan et al 2006). Fuel wasted by congestion can also be battled with anti-idling technology: engine augmentations which shut the engine off while it is not being used, such as when the vehicle is waiting at a stop light. It is a relatively cheap way to significantly reduce fuel consumption and can be added on to existing engines. The ATA estimates that if congestion were completely eliminated in all 437 main urban congestion areas it would reduce truck CO₂ emissions by 45.2 million tons over 10 years.

Vehicle Weight Limits

Truck weight limits are a very controversial issue. Proponents argue that increasing truck maximum weight limits would decrease the number of vehicles on the roads; thereby using less fuel, reducing both CO₂ emissions and expenditures, and increasing road safety. Opponents worry that the increases in truck weight would increase the number and severity of accidents, resulting in more fatal crashes. There is also concern that the cost benefits would be offset by the higher expenses of maintaining roads and updating bridges to support these heavier trucks.

In 2009, Wisconsin published a comparative cost-benefit study of six types of heavy truck: the six-axle 90,000 lb tractor-semi-trailer, the seven-axle 97,000 lb tractor-semi-trailer, the seven-axle 80,000 lb single unit truck, the eight-axle 108,000 lb double, the six-axle 98,000 lb tractor-semi-trailer, and the six-axle 98,000 lb straight truck trailer. Researchers found that when bridge costs were included only three of these configurations resulted in net benefits to the state. The most beneficial configuration was the six-axle 98,000 lb semi-trailer, which exceeds the current Federal Bridge Formula weight limits. The second most beneficial truck was the seven-axle 97,000 lb semi-trailer, followed by the marginally successful six-axle 90,000 lb semi-trailer (Cambridge Systematics et al. 2009).

McKinnon conducted a before and after study of the effects of increased weight limits in Britain when maximum truck weight was raised from 41 metric tons to 44, approximately 90,400 lbs to 97,000 lbs (2005). Unfortunately, neither analysis considered the costs and emissions associated with strengthening bridges to support the increased weight as Britain had already made the updates. Nor were the safety impacts of the change studied. The before study predicted, as its mid-range estimate, a yearly reduction of truck traffic of 100 million vehicle kilometers (more than 62 million miles) driven, an annual cost savings of about £60–80 million (in 2000 prices), and an annual reduction in CO₂ emissions of 80–100 thousand metric tons (88–110 thousand short tons). In 2001, the first year after the changes were implemented, there was a reduction of 53 million vehicle kilometers (more than 32 million miles) driven, the actual cost savings to vehicle operating costs were £44 million, and there was a reduction of about 53 thousand metric tons of CO₂ emissions. In both 2002 and 2003 all of these figures continued to increase.

Horvath and Facanha's life-cycle emissions study estimated that increasing truck capacity while also requiring an additional axle or more could cut pollutants of all kinds by 4 to 16 percent even including emissions generated from the increased maintenance, assuming that wear and tear on the road was proportional to weight per axle (2007).

OBJECTIVE AND SCOPE

The primary objective of this research was to compile a list of technologies and practices that should be included in the sustainable freight transportation frameworks used by government agencies and commercial fleets to reduce their carbon footprint and increase their safety by providing recommendations on promising legislation, research, technology, and practices.

A comprehensive literature review was conducted to gain an understanding of technologies currently in use to improve safety and reduce carbon emissions in the

freight transportation industry. It also included information on laws and corporate practices related to these areas and investigated some technologies currently being developed. This review contained information from journals, periodicals, government documents, conference proceedings, and other sources.

To get a better understanding of freight transportation's current legal environment and a more accurate picture of how that environment may be expected to change in the near future, a survey was sent out to the state DOTs. The survey response was very limited, with only two surveys returned. In an effort to increase the understanding of current policies the authors reviewed documents put forth by state agencies, most notably: long-term transportation plans, highway safety plans, commercial drivers manuals, and air quality conformity reports.

DATA ANALYSIS AND SURVEY

Enforcement is the the first step toward policy effectiveness. All state plans and reports contain sections on funding and both the surveys we received listed the ability to enforce policies as important. To ensure success, legislation must include or be attached to some sort of action plan as to how it will be implemented and how its success will be measured.

Safety

Interstate speed limits are within about 10 mph of each other. 7 states have separate speed limits for cars and trucks on rural interstates. Of these, 4 have differences of 10 mph, 2 have a difference of 5 mph, and 1 has a difference of more than 10 mph. Only 1 state has separate speed limits on urban interstates, a 10 mph difference. 25 states have rural interstate speed limits over 65 mph and 12 states have urban interstate speed limits over 65 mph.

32 states have primary seat belt laws, 17 have secondary seat belt laws, and New Hampshire does not have a primary or secondary seat belt law. The rail safety act of 1970 (Public Law 91-458) authorized states to work with the Federal Railroad Administration to enforce federal railroad safety regulations. These enforce standards for track and freight car safety, locomotive and signal inspection, hours of service, hazardous material inspection, and grade crossing safety. So far 29 states and the District of Columbia have chosen to adopt the rail safety participation program.

Emissions

There seems to be a dearth of environmental regulation over freight transportation. It is believed, due to survey responses and state air quality reports, that many states work to have overall emissions policies but have yet to make specific policies as regards transportation. Vehicle inspections are the main method of ensuring that vehicles meet emission standards. Most states use only the federally mandated EPA emissions regulations. 15 states have adopted the harsher California emissions standards. 21 states, and the District of Columbia, currently have statewide anti-idling policies, some of these states have idling policies for specific cities and counties within them and 6 states without statewide idling policies have policies within specific locations.

20 states and Washington DC have idling restrictions are for periods of 5 minutes in any 60 minute period. Of these, 11 are for 5 minutes, 5 are for periods less than 5 minutes, 3 are for 10 minute periods, and 2 are for 15 minutes. Utah did not specifically define a time limit. There are 21 different idling policies for specific cities or counties within states. Of these: 8 are for 5 minutes, 7 are for less than 5 minutes, there were 5 policies with 15 minute limits and only 1 with a 10 minute limit. Some policies vary by temperature, becoming stricter as the temperature increases.

CONCLUSIONS AND RECOMENDATIONS

A number of technologies and strategies examined within this report stand out as being more or less effective for use in the creation and planning of sustainable freight transportation frameworks of government agencies and commercial fleets attempting to reduce their carbon footprints and increase their safety. These have been included below with brief recommendations as to their most effective uses.

Existing Strategies for Sustainable Freight Transportation

Any fleet trying to reduce its carbon footprint should perform a logistics audit to determine whether transferring some or all of its freight to alternate modes of transportation would be environmentally or economically beneficial, particularly if the goods shipped are not time sensitive and there is a nearby station or port for the alternate mode being considered. Audits should examine both modes and routes, taking into account projected economic and emissions savings and the safety of all parties involved.

The most widely used fleet improvements increase fuel efficiency and have low initial costs. Anti-idling technologies are becoming more and more popular as a relatively inexpensive way to get more out of an engine without compromising the vehicle's ability to find fueling stations on a variety of routes. They save fuel and money, reduce the fleet's carbon footprint, and are becoming legally required as more and more states adopt anti-idling policies.

Speed limits of below 65 mph have been shown to accrue significant safety and emissions reductions benefits. Also, the possible reduction to congestion and logistics efficiency caused by increasing truck weight limits has great potential. Both reduced speed and increased weight limits should be introduced nationwide, preferably together. Introducing them together will help to address the fears of commercial fleets that reduced speed limits will cut into their profits and reassure groups opposed to increased weight limits due to safety concerns. It may be beneficial to make the change gradual over a number of years to allow states time to upgrade their bridges to support the higher weights. It is possible that this would divert freight from rail on to trucks, moving it to a less efficient transportation mode. Another problem is that for these policies to truly be effective they would have to be adopted by the nation at a whole. If only individual states changed their policies the effects would be highly limited and potentially a source of great confusion to fleet managers transporting goods through multiple states, making the policies more difficult to legislate and less beneficial. If such a trial run in only a few states is deemed necessary it would be most appropriate to choose states near an international border, preferably a group of states sharing borders between themselves.

Opportunities exist to utilize petroleum blend fuels, which allow trucks to continue to use standard, or modified, engines capable of using petroleum fuels when alternates are not available. Incentives and requirements should be implemented to encourage use of these fuels.

The unavailability of electric vehicles refueling stations makes them unsuitable at present for long-haul trucking. However, they should be considered for use as support vehicles in ports and for short-haul deliveries. A small fleet operating in a limited area, particularly if parked in a centralized garage overnight which could be retrofitted to recharge them during this time, could make effective use of electricity.

Strategies which Hinder Sustainable Freight Transportation

A few strategies have been shown to be ineffectual and potentially harmful to sustainable freight transportation. They use resources which could be allocated elsewhere and may have other drawbacks. These strategies should be avoided.

At this time, research suggests that having separate speeds for commercial and commuter vehicles has either little impact on safety or may actually increase traffic fatalities when there are large gaps between the limits. Therefore, separate speeds should not be used.

The trucking industry depends upon widespread fueling stations throughout the US and it is unrealistic to expect that the necessary changes to infrastructure and equipment could be made quickly and economically enough for alternate fuels requiring engines which cannot also run on diesel, at times when alternates are unavailable, to be a viable option.

ACKNOWLEDGEMENTS

This research project was funded by a grant from the US Department of Transportation, University Transportation Centers Program to the Mid-America Transportation Center at the University of Nebraska-Lincoln. Further thanks to the states which responded to our survey and to Leo Penne of the American Association of State Highway Officials (AASHTO) for distributing the surveys.

REFERENCE

- American Association of State Highway Transportation Officials (AASHTO) (2004). *Strategic Highway Safety Plan*. <http://safety.transportation.org/htmlguides/> .
- American Association of State Highway Transportation Officials (AASHTO). Standing Committee on Rail Transportation. *Freight-Rail Bottom Line Report*. <http://rail.transportation.org/Documents/FreightRailReport.pdf>. Read 2011.
- Association of American Railroads (AAR) (2007). *Freight Railroads and Greenhouse Gas Emissions*. <http://www.aar.org/incongress/energyandenvironment/~media/aar/backgroundpapers/freightrar>.
- American Trucking Association (ATA) (2009). *A Sensible Approach to Biodiesel for the United States*. <http://www.truckline.com/AdvIssues/Energy/RENEWABLE%20DIESEL%20%20BIODIESEL/White%20Paper%20%E2%80%93%20A%20Sensible>

- [%20Approach%20to%20Biodiesel%20%28January%202009%29.pdf](#).
American Transportation Research Institute (ATRI) (Last Updated September 2010).
Idling Regulations Compendium. http://www.atri-online.org/index.php?option=com_content&view=article&id=164&Itemid=70
- Bryan J., Weisbrod G., and Martland C. D. (2006). *Rail Freight as a Means of Reducing Roadway Congestion: Feasibility Considerations for Transportation Planning*. http://ctr.ra.utk.edu/LRRFT/cmte_activities/papers/TRBAM%2007-Bryan-Weisbrod-Martland.pdf.
- Cambridge Systematics Inc., National Center for Freight and Infrastructure Research and Education at the University of Madison-Wisconsin, Cohen, Harry, Woodrooffe Dynamics, LLC, Statenfeld Associates, LLC, Earth Tech/AECOM, Prime Focus, LLC, TranSmart Technologies, Inc. (2009). *Wisconsin Truck Size and Weight Study*. Wisconsin Department of Transportation.
- Carey, B. (2006). "Slow Speed Ahead". *Traffic World* 270 no11 26-7. March 13.
- Katz, J. (2008). "Paccar's Hybrids: Building a Heavy-Duty Supply Chain: Special Reprt: Anatomy of a Product". *Industry Week*. December 1.
- Horvath, Arpad, and Facanha, Cristiano (2007). "Evaluation of Life-cycle Air Emissions Factors of Freight Transportation". *Environmental Science & Technology*. Volume 41, issue 20. October.
- Lawyer, D. S. (1986). *Ideas For Freight Railroad Modernization*.
http://www.lafn.org/~dave/trans/rail/rail_modernize.html#s3.
- McKinnon, A. C. (2005). "The Economic and Environmental Benefits of Increasing Maximum Truck Weight: The British Experience". *Transportation Research*. Part D, Transport and environment, Volume 10, Issue 1. January.
- National Cooperative Highway Research Program (NCHRP), American Association of State Transportation and Highway Officials (AASHTO) (2004). *Strategic Highway Safety Plan*. <http://safety.transportation.org/htmlguides/default.asp>.
- National Cooperative Highway Research Program (NCHRP). Knipling, R. R., Waller, P., Peck, R. C., Pfefer, R., Neuman, T. R., Slack, K. L., and Hardy, K. K. (2004). *Guidance for Implementation of the AASHTO Strategic Highway Safety Plan*. DC, Washington: Transportation Research Board.
- Neeley, G. W., and Richardson, L. E. "The Effect of State Regulations on Truck-Crash Fatalities". *American Journal of Public Health* 99 no3 408-15. March 2009.

Application of the Theory of Minimum Rate of Energy Dissipation to River Regulation

Jun-hong Zhang ^{1,2}, Guo-xiang Gong ², Jia-an Luo ², and Yang-fei Ou ²

¹State Key Laboratory of Water Resources and Hydropower Engineering Science, Wuhan University, Wuhan, 430072, China;PH(086)18971676115;
e-mail:zjh411891611@163.com

²Communications Planning and Design Institute of Hubei Province,Wuhan 430051,China

ABSTRACT

To elucidate the mechanism of river bed's self-adjustment under given boundary and amount of water and sediment, the principle and formula of minimum rate of available energy dissipation were put forward in the river regulation projects according to the theory of entropy and energy dissipation about dynamic equilibrium stability of irreversible process in fluvial river. The formula is applied to the river regulation of Han River in the middle of China for predicting its regulated parameters. The comparisons between the computed and measured navigable depths and width show that the formula is effective. The result of the present work implied that the theory used in the regulation projects can provide engineers the needed theoretical basis for river morphology and river engineering studies.

INTRODUCTION

A certain pattern of river is the product of its self-adjustment product of its self-adjustment under given boundary, discharge and sediment conditions. By adjusting its roughness, channel geometry, length, slope, manmade conditions and so on, a river goes into the stable situation gradually. So far, there have been many extreme hypotheses proposed and used to explain the self-adjustment of alluvial river .

Lacey (1929) earliest attempted to describe the quasi-equilibrium geometry of rivers by the empirical approaches. Later, theoretical approaches based on the dynamics of flow and sediment transport were developed by Florey and Glover (1951).

Leopold and Langbein (1962) first applied the concept of entropy to the evolution process of stream system. Yang (1971, 1976) further developed the concept and proposed the theory of minimum rate of energy dissipation and unit stream power. For the open channel, Yang (1990) derived the optimum geometry based on the theory of minimum rate of energy dissipation in conjunction with Yang's sediment transport equation and Manning's equation for water discharge. Xu (1996) proposed an optimum method for canal design, based on the principle of equilibrium of eroded and silting by combining the optimal techniques with the

theory of minimum rate of energy dissipation. Zhang et al. (2001) showed that there exists a good empirical relationship between the energy dissipation rate and channel morphology. According to their relationship and the theory of minimum rate of energy dissipation, the authors explained the metamorphosis of the model channel with the development of the braided river. Chen (2004) considered river as an open system with structure of thermodynamic energy dissipation by turbulence and viscosity. The author put forward the theory of hydraulic entropy in open channel and fluvial river based on the theory of entropy and energy dissipation about dynamic equilibrium stability of irreversible process in open system dissipation structure.

The theory of minimum energy dissipation rate is applied to the river regulation in this paper to determine the optimum channel size for a given set of water discharge and sediment transport rate.

METHODOLOGY

The theory of minimum energy and energy dissipation rate in the dissipative system was directly applied by Song and Yang (1982). On the other hand, a river is an open system with extensive energy partition and exchange. Accordingly, Chang(1979) introduced the derivation of formula for minimum rate of available energy dissipation from the theory of fluvial entropy is considered to completely express the basic principle of automatic regulation about riverbed evolution of fluvial river. The minimum energy dissipation rate due to water and sediment transport per length of the channel is

$$\Phi = (\gamma Q + \gamma_s Q_s) J \quad (1)$$

where γ, γ_s are the specific weight of water and sediment, Q, Q_s are the discharge and the sediment transport rate, and J is the bed slope.

If the sediment transport rate in an open river system is small, and the energy dissipation rate due to sediment transport is negligible, the total energy dissipation rate of the system is

$$\Phi = \gamma Q J \quad (2)$$

Seen from the above equation, the value of Φ is associated with Q and J . If the sediment transport rate cannot be neglected, it also affects the variation of cross-section and the final evolution results of Φ in the river regime.

APPLICATION

In the river regulation projects, the channel top width can have a fixed value either naturally or by manmade structures. In this case, the minimization of Φ is achieved by the adjustment of channel size and bed slope.

Continuity equation of water flow in the open channel as follows:

$$Q = AV \quad (3)$$

where Q is the discharge, A is the channel area, V is the mean velocity.

The open channel flows equation can be figured out with simultaneous equations of the Maning and the flow continuum as follows:

$$Q = CA\sqrt{RJ} = \frac{1}{n} AR^{2/3} J^{1/2} \quad (4)$$

When the channel shaped like or nearly like a rectangle and with the

width-to-depth ratio as β , the objective function is set up as follows:

$$\frac{nQ}{J^{1/2}} = h^{8/3} \frac{\beta^{5/3}}{(2+\beta)^{2/3}} \quad (5)$$

In the above equations, n is the coefficient of roughness, h is the average water depth of cross-section.

In the erosion and deposition balance reaches, sediment exchange happens at the riverbed constantly. The constraint condition of the river regime in the states of balance is the sediment transport equation. Many of sediment transport equations are the results of theoretical derivation and experimental methods, among the equations, Engelund-Hansen formula is a relatively accurate one:

$$f \frac{g_s}{\rho_s g \sqrt{\frac{\rho_s - \rho}{\rho} g d^3}} = 0.4 \left[\frac{\tau}{(\rho_s - \rho) g d} \right]^{2.5} \quad (6)$$

where g_s is sediment transport rate of unit width, ρ_s is the sediment density, f and τ are the resistance coefficient and the bed shear stress, the definitions are as follows:

$$f = \frac{8gRJ}{V^2} \quad (7)$$

$$\tau = \rho g RJ \quad (8)$$

By using Eqs (4),(6),(7)and(8),the sediment discharge can be expressed as

$$Q_s = g_s b = K J^{2.5} h^{23/6} \frac{\beta^{23/6}}{(2+\beta)^{17/6}} \quad (9)$$

From the above equation (9), h can be obtained as the following expression

$$h = \frac{1}{K^{6/23}} \frac{Q_s^{6/23}}{J^{15/23}} \cdot \frac{(2+\beta)^{17/23}}{\beta} \quad (10)$$

where

$$K = \frac{0.05 \rho_s g}{n^2 d \sqrt{g} \left(\frac{\rho_s - \rho}{\rho} \right)^2}$$

Similarly, from the Eqs (5) and (10), the objective function can be expressed as

$$Z = \frac{K^{16/23} Q J^{57/46}}{Q_s^{16/23}} = \frac{(2+\beta)^{30/23}}{\beta} \quad (11)$$

Obviously, the extreme value of the objective function is as follows

$$\frac{dZ}{d\beta} = \frac{(2+\beta)^{7/23}}{\beta^2} \left(\frac{7\beta}{23} - 2 \right) = 0 \quad (12)$$

Namely, when the width-to-depth ratio $\beta=46/7$, Z achieved the extreme value.

Meanwhile,

$$\left. \frac{d^2 Z}{d^2 \beta} \right|_{\beta=46/7} = 0.01355 > 0 \quad (13)$$

From the above mathematical derivation, the objective function arrives at the minimum value when the width-to-depth ratio is $\beta=46/7$. There are three physical quantities in the objective function, Q , Q_s and J . The alluvial river reaches regime state by adjusting its geometry parameters and geometrical forms of the river bed.

Before river regulation projects, a river can be considered on the states of relatively steady through a long time adjustments. Unit stream power has reached the minimum value. When some river regulation projects such as transverse dike and bank revetment were set up, the primary stabilization of river hydraulic geometry was undermined and the value of unit stream power would also increased during a period of time. Subsequently, with the adjustments of the regulated reaches, the value of unit stream power decreased gradually and the reaches come back the steady state. However, the new value of unit stream power was not the same as the primary one.

Based on the theory of minimum rate of energy dissipation of natural stream system, the regulated depth and the stable depth of the river regulation engineering of Hanjiang River in the central China were predicted.

The Hanjiang River is the source of water for the middle route of the well-known South-to-North Water Diversion Project (SNWDP) in China, as shown in Figure 1. The researched reaches are from Nianpanshan to Shizikou. Regulated width was calculated by the water sediment equilibrium method as follows

$$B_2 = B_1 \left(\frac{h_1}{h_2} \right)^{4/3} \quad (14)$$

where, h_1 is the average depth before regulation engineering, h_2 is the regulated depth, B_1 is the depth of river before regulation engineering, B_2 is the regulated width. According to the international standards of Class-III waterways, the minimum navigable depth is not less 2.4m, that is to say, h_2 should be greater than 2.4.

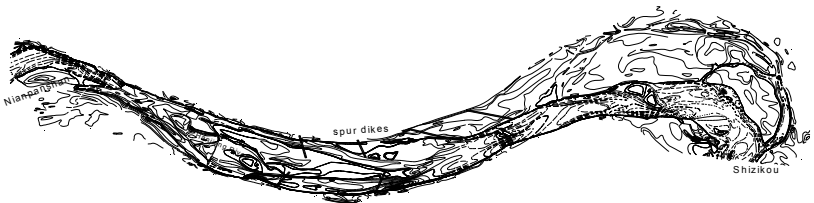


Figure 1. The sketch of researched reaches in Hanjiang River

The regulated reach is located in the middle and lower reaches of Hanjiang River, the length is 50.9km. There are four shoals along the regulated reach; the total length is 6.7km. In order to improve the navigation condition of the regulated reach, a series of spur dikes were set up in 2005. Before the waterway regulation works, the river hydraulic geometry is shown in Table 1. 20 river cross-sections were selected for calculating along the reach. The calculated results of the river section from Nianpanshan to Shizikou are also shown in the Table 1. It is seen that from Table 1 the calculating depth were slightly larger than the measured value. This may be due to the not long enough time from the completion of works to the

engineering survey. The river channel was not up to stabilization condition. Despite all this, the results can be also considered as reasonable and credible ones.

Table 1 Result of the calculating of the river section from Nianpanshan to Shizikou (m)

No	Interval s (km)	2005		Regulate d width B ₂	2011		Absolut e error	Relativ e error (%)
		h ₁	B ₁		Measure h ₂	Calculate h ₂		
1	3.0	3.7	505.4	90.5	12.3	13.6	1.3	9.5
2	3.0	6.7	473.3	121.9	16.9	18.6	1.7	9.2
3	2.0	5.8	654.3	129.4	18.2	19.7	1.5	7.6
4	2.0	5.4	350.5	94.8	13.1	14.4	1.3	9.0
5	1.3	5.0	754.5	126.3	18.1	19.2	1.1	5.7
6	2.2	3.7	908.1	114.2	15.6	17.4	1.8	10.4
7	3.4	4.0	615.0	102.1	14.1	15.5	1.4	9.0
8	3.0	4.6	514.8	101.4	14.5	15.4	0.9	5.8
9	1.6	10. 6	685.7	185.7	26.1	28.3	2.2	7.8
10	2.4	4.0	541.8	96.0	13.4	14.6	1.2	8.2
11	2.0	8.8	641.6	162.0	23.5	24.7	1.2	4.9
12	2.0	4.3	870.4	123.1	17.8	18.7	0.9	4.8
13	2.7	11. 9	1059. 1	239.1	33.2	36.4	3.2	8.8
14	1.9	6.6	845.7	154.5	21.4	23.5	2.1	9.1
15	4.1	5.0	635.1	116.8	16.5	17.8	1.3	7.3
16	3.4	4.5	501.1	98.9	14.9	15.1	0.2	1.3
17	3.0	6.6	463.3	120.0	17.3	18.3	1.0	5.5
18	4.0	6.4	671.4	137.5	19.2	20.9	1.7	8.1
19	1.9	4.1	666.6	106.4	15.7	16.2	0.5	3.1
20	2.0	4.9	566.8	109.6	16.0	16.7	0.7	4.2

CONCLUTIONS

This paper showed the theory of the energy dissipation rate in the channel development process and gave an application in the navigation channel regulation projects. The formations of the finally stable channel patterns are the results of the flow to carry necessary sediment load with minimizing rate of energy dissipation and the given boundary conditions of the regulated reaches of the river.

The application results also confirm the theory of minimum energy dissipation rate that there exists a minimizing tendency of energy dissipation rate in the evolution of the alluvial channel. These application results of the theory of the energy dissipation rate in the channel are also in agreement with the theory analysis. From the above analysis, the theory used in the regulation projects can provide engineers the needed theoretical basis for river morphology and river engineering studies.

ACKNOWLEDGEMENTS

This study is sponsored by Western Traffic Science and Technology Research Program of Ministry of Communications of China (Grant No. 20113280001520).

REFERENCES

- Chang, H.H. (1979), *Geometry of Rivers in Regime*, ASCE, Vol.105, No.HY6.
- Chen, X. (2004). Research on the Theory of Minimum Rate of Available Energy Dissipation and Static Entropy in Rivers. *Journal of Sediment Research*, No.6.
- Chih, T. and Charles, C.S. Song (1990). Optimum Channel Geometry and Minimum Energy Dissipation Rate. *International Journal of sediment research*, Vol.5, No.1.
- Glover, R.E., and Florey, Q.C. (1951). *Stable Channel Profiles*, U.S. Bureau of Reclamation, Denver, Colorado.
- Lacey,G.(1929). *Stable Channels in Alluvium Proceedings of Institute of Civil Engineering*, London, 229.
- Leopold, L.B., and Langbein, W.B. (1962). *The Concept of Entropy in Landscape Evolution*, U.S. Geological Survey Professional Paper 500-A.
- Song,C.C.,and Yang, C.T. (1982). Minimum Energy and Energy Dissipation Rate, ASCE, Vol.108, No. HY5.
- Xu, G. (1996). An Optimum Design Method for Stable Canals, *Journal of Hydraulic Engineering*, Vol.8, No.11.
- Yang, C.T. (1971). Potential Energy and River Morphology, *Water Resources Research*, Vol.7, No.2.
- Yang, C.T. (1976). Minimum Unit Stream Power and Fluvial Hydraulics, ASCE, Vol.102, No. HY7.
- Zhang. et al. (2001). Relationship between Energy Dissipation Rate and Channel Morphology in the Development of the Model Braided Channel. *Journal of Geographical Sciences*, Vol.11, No.3

Low Carbon Management Concept in TOD Planning

Chia-Nung Li

Assistant Professor, Department of Natural Resources, Chinese Culture University, Taiwan.
E-mail: ljn@ulive.pccu.edu.tw

ABSTRACT

Low carbon management is an important issue to cities around the world today. Various research sects discuss about the way to reduce urban heat island effect and reduce greenhouse gas emissions, such as carbon dioxide and others. In transportation and land use, transit-oriented development (TOD) that increase the ratio of taking public transports and the benefits of increased city tightness are considered capable to improve the greenhouse effect and the establish low-carbon development urban structure. Whereby, the impact to urban cities by transportation and land use when facing climate changes is adopt in this research to propose the positive and negative benefits to the impacted objects by applying 5D models of land-use planning (Density, Diversity, Distance, Destination and Design). The relations between positive and negative benefits due to climate changes and 5D planning methods are further discussed. Finally, the paper focused on the part of negative effect and proposed some possible adjustments and ways to deal with climate change for a future reference for the city government's policy formulation establishing in transportation integration development strategy.

INTRODUCTION

In the recent two past decades, cities around the world move towards urban type development of "automobile-oriented development, referred to as AOD" with the urban model of integration of low-density land use and private vehicles, resulting in many issues of urban development, such as urban sprawl, environmental pollution, dire financial straits, resource consumptions, economic recession, insurance costs, traffic congestion, transportation costs, personal safety, physical health and interpersonal alienation whose negative impacts are much higher than positive benefits. In the background of limited land resources in the city and the rapid growth of cars, every nation's transport policies were mainly focus on highway construction s of low-cost and high building efficient, thus contributed to the urban sprawl, resulting in disordered live and industry ratio and the serious natural environmental pollutions prior to 1990s. The urban model oriented by road system and demands contributed to the continued rise of greenhouse gas temperature, in addition to seriously effect of land and resources efficient use. Accordingly, mitigation of greenhouse gases is the main topic of current research. In 2007, Urban Land Institute (ULI) in United States, Smart Growth America, Center for Clean Air Policy (CCAP) and National Center for

Smart Growth co-sponsored the concept of "Growing Cooler," which is to discuss the way to construct a new type of urban development and transportation system for promoting Growing Cooler. Transit-oriented development (TOD) in within is the core concept of development strategy of reducing greenhouse gases in cities.

Greenhouse gas emission in Taiwan has continued to rise in recent years. Over the past decade, the average carbon dioxide emissions per person per year increased substantially from 5.6 tons to 11.6 tons which has raised for about 2 times. From the statistics by International Energy Agency (IEA), Carbon dioxide emission in Taiwan ranked the 22nd in the world. Also, Taiwan's greenhouse gas emission in 2025 would be 4 times more than it was in 1990 according to National Energy Conference. The growth of greenhouse gases caused environmental pollution and urban heat island effect, impeding urban health growth. From energy consumption point of view, transportation energy consumption in the country's total is 15.3% in 2010 which is also the 2nd largest proportion of Taiwan's energy-consuming sector that grew up to 112.8% in the past 10 years. In within, the energy consumption amount of highway system is up to 93.5% of the transport sector while mass rail transport system took less than 2%.

In spite of the many TOD development strategies and ideas proposed by Taiwan's government at all levels, there is still lack of verification that whether TOD will bring the Taiwan cities a positive effect and the mitigation of greenhouse gases. Thus, this study sort relevant literatures about TOD to analyze factors of climate changes from the two aspects of land use and transportation to include the 5D (Density, Diversity, Distance, Destination and Design) concept in TOD planning model and sum up the 5D and the positive benefits and negative effects of climate changes from the literatures. The place with high density of population, grid transport system (Destination) and pedestrian-oriented urban design (Design) would produce positive and negative effects to climate changes. Finally, this study would propose the modified TOD planning model to meet the target of urban growth cool down and slow down the speed of climate change by the basis of TOD-related researches.

TRANSPORTATION & LAND USE IMPACT FROM CLIMATE CHANGE

The relationship between transportation and land use is like business cycle phenomenon of economics. Assuming that the more developed transport infrastructure is, the higher travel mobility and the more diverse the urban activity function will be to promote the recovery of urban land use as well as the more prosperous phenomenon. On the other hand, the less developed transportation is, the less travel mobility and less diverse the urban activity function will be, followed by urban land use promotion recession and even depression. Therefore, the relationship of transportation and land use that caused significant impact on urban overall development has been an important issue since the 1960s, such as the shape the mobilized city, as well as the public transport city with green transport as the backbone (Cervero and Landis, 1992; Newman and Kenworthy, 1999; Porter, 1997).

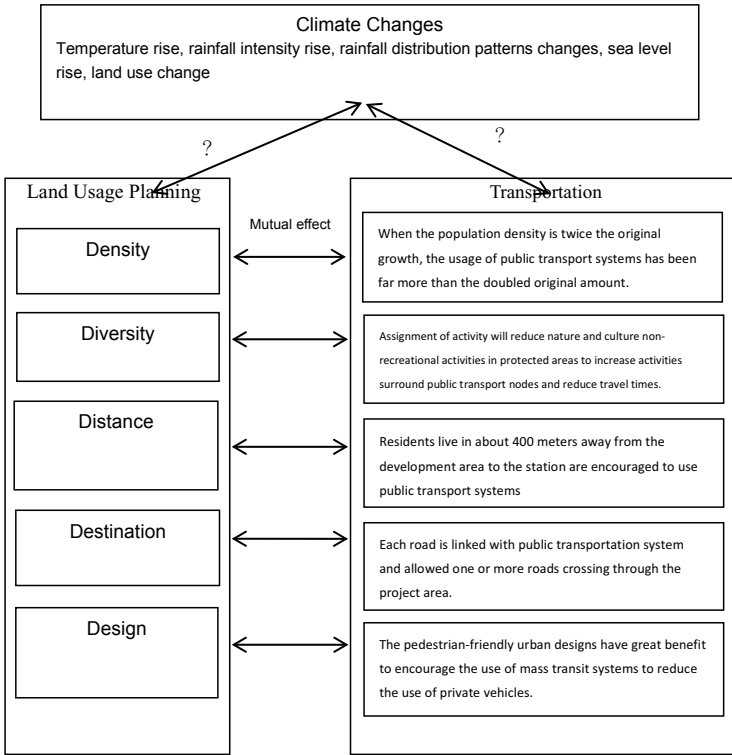


Figure 1: Effect relation of climate changes to transportation and land use

A consensus was formed from various researches that land-use patterns will affect travel operation behavior and feedback to changes of land-use with constant circulation and interaction. However, with the threat of climate change, the impact of urban spatial structure was directly associated to illustrate the concept of climate change on land use and transportation impacts with TOD land-use planning model (5D: Density, Diversity, Distance, Destination and Design). As shown in Figure 1, climate change causes global geography changes that led to impacts of land use and transportation. And human land-use planning model and transportation system will also affect to climate changes. In which, there is interactional affecting factors occur between land use and transportation and form "triangular relationship" to be verified. Literature reviews and analyses would be adopted in this research to have discussion of the effect brought by this triangular relationship to TOD planning model to understand the positive benefits and negative effects as the reference for correction of TOD planning model.

THE IMPACT OF 5D TO CLIMATE CHANGES

As shown in Table 1, the study collected empirical researches and found the 5D concept in TOD planning model has a positive benefits to climate changes. The more dense population as Density, the higher strength of use will be. After the integration of public transportation planning, it will be able to increase the usage of public transport to reduce private vehicle usage and reduce carbon dioxide emissions. However, it may also cause another negative side effect that if there is over population development concentrate in a single district, their living environment will be affected to increase carbon dioxide emissions of the single region, lead to severe climate changes from the view of land carrying capacity. In Diversity, there are positive benefits but not negative effects. There should be spread residential areas, work areas and retail shops along the line around the mass transit system. The close compacted and mix-using community development is able to strengthen the use of public transport and reduce private vehicles, thereby reducing carbon dioxide emissions. In Distance, there are positive benefits but not negative effect. Public transportation nodes within walking distance can increase the willingness of walking and achieve the effect of reducing energy and carbon reduction. In Destination, there is a positive benefit as well as negative effects. The checkerboard network structure can reduce the length of trip in order to achieve the goal of lower carbon emissions.

Table 1: The Impact of 5D to climate changes

5 D		Positive	Negative
1	Density	The more density the population is, higher strength of the use will be. Combined with public transportation to increase the utilization rate and reduce the use of private vehicles to reduce carbon dioxide emissions.	From the point of land carrying capacity, population over-development will affect the environment and it's conducive to climate change.
2	Diversity	Residential areas, work areas and retail stores should be distributed along the mass transit system. Compact with the mixed- use concise community development to strengthen public transport use, reduce use of private vehicles and carbon dioxide emissions.	Mixed land use influences quality of the living environment, e.g. noise, pollution and discordant housing type. (Li and Lai, 2009)
3	Distance	The public transportation node within walking distance will increase the willingness in walking and reduce the use of transportation modes to achieve the effect of reducing energy and carbon reduction.	When establishing public transport network, high conservation of public transport operation will deepen the damage to conservation area that breach the sustainable development concepts if the land development area is located in remote areas.

4	Destination	To construct the public transport network for reducing the transportation modes usage to achieve the goal of lower carbon emissions.	The intersection traffic signals would delay travel time, increase air waste emissions, resulting in carbon dioxide concentration increase and causing greenhouse effect and climate changes.
5	Design	Good urban design helps in relevant entities of the building or base configuration of walking, biking and public transportation taking and others along with the more people-centered public transportation network system tightly tie up the community and public transport stations to reduce the use of private vehicles and strengthen public transport. (Li and Lo, 2011)	The absence of ecological elements in urban design did not considerate the impacts of climate change and global warming. (Li and Lo, 2011)

However, the excessive intersections and traffic signals not only delay the travel time but increase the emissions of air waste. In Design, there is a positive benefit as well as negative effects. The public transportation network system with people-oriented center is able to reduce the use of private vehicles and strengthen public transport use. But the lack of conservation elements in urban design will not cool the urban island.

LOW CARBON MANAGEMENT CONCEPT IN TOD PLANNING

As the above analysis, this paper integrates low carbon management concept with the TOD planning model to response in issues and measures of climate change process, which was divided into two aspects of land use and transportation for in-depth analysis as shown in table 2.

Table 2: Low carbon management in The TOD planning to respond climate changes

	5D	Land use strategy	Transportation strategy
1	Density	✓ From the land carrying capacity point of view, over-development population will affect the environment and is not conducive to climate change. Based on the perspective of carrying capacity and growth management, to establish the mechanism of volume control, maintain and control the reasonability of growth in urban areas.	✓ The higher population density and use intensity, the higher public transport usage that can reduce use of private vehicles and lower carbon dioxide emissions.

2	Diversity	<ul style="list-style-type: none"> ✓ Reduce travel times in order to avoid unnecessary or excessive land use (as parking space is concerned). 	<ul style="list-style-type: none"> ✓ Residential areas, work areas and retail stores should be distributed along the mass transit system. Compact with the mixed-use concise community development to strengthen public transport use, reduce use of private vehicles and carbon dioxide emissions
3	Distance	<ul style="list-style-type: none"> ✓ The population density around the stations strengthens its strength to development of the city, inhibit the spread and damage to agricultural land or ecologically sensitive land and maintain the environment for climate changes. 	<ul style="list-style-type: none"> ✓ The public transportation node within walking distance will increase the willingness in walking and reduce the use of transportation modes to achieve the effect of reducing energy and carbon reduction.
4	Destination	<ul style="list-style-type: none"> ✓ Under the establishment of checkerboard transportation system with mass transportation net work, when establishing public transport network, high conservation of public transport operation will deepen the damage to conservation area that breach the sustainable development concepts if the land development area is located in remote areas. Limit the MRT traveling times to the volume range. 	<ul style="list-style-type: none"> ✓ To construct the public transport network for reducing the transportation modes usage and the number of transfer times of the passengers to achieve the goal of lower carbon emissions and transportation performance. ✓ There are more intersections than it was in traditionally planned road in the establishment of checkerboard transportation system. The intersection traffic signals would delay travel time, increase air waste emissions, resulting in carbon dioxide concentration increase and causing greenhouse effect and climate changes.
5	Design	<ul style="list-style-type: none"> ✓ The surrounding of the stations adopts pedestrian space design to create a pedestrian environment that can reach the commercial, residential, office, open space destinations concentrated. It emphasized on transportation and land mixed use as well as pedestrian accessibility and integrate as the strategy to improve urban environment. ✓ Human scale, smaller buildings 	<ul style="list-style-type: none"> ✓ Positive benefit: Good urban design helps in relevant entities of the building or base configuration of walking, biking and public transportation taking and others along with the more people-centered public transportation network system to tightly link with community and public transport stations to reduce the use of private vehicles, and strengthen public transport.

		<p>and streets, applicable roads, urban design compact with considerations of pedestrian point of view.</p> <ul style="list-style-type: none"> ✓ Current urban design is lack of relative ecological considerations. To allow more sustainable TOD development, ecological design that is lack in traditional TOD is reinforced from ecological and environmental aspects. ✓ Develop the concept of "Green-TOD" to reinforce the ecological design that is lack in traditional TOD from the ecological and environmental aspects by means of urban design, such as green building, eco-basement facilities, and appropriate district settlement creation to construct ecological public transport-oriented development. 	<ul style="list-style-type: none"> ✓ Designed the "transportation transferred from walking, biking or public bus riding," rather than "car ride transferring" system . ✓ Conduct transportation policies of a variety of transportation modes to promote walking, biking and public transportation usage to reduce use of private vehicles. ✓ Make streets mixture sites with multiple purposes, rather than specifically for automotive use and promote pedestrian and bicycle system to a comfortable, fun, high quality and safe place to be linked with the system.
--	--	---	--

CONCLUSIONS

The close mutual effect relationship of transportation and land use formed the urban development model that integrated transportation and land-use. The urban model constructed by transportation and land use can be divided into two kinds, namely, automobile- oriented development and transit-oriented development, referred to as TOD. There was a number of urban planning around the world towards TOD urban model since 1990s. In the past, the concept of TOD planning model is to solve the automobile- oriented urban problems, including urban sprawl, suburbanization, traffic congestion, energy consumption and a variety of pollutions to construct 5D models Density, Diversity, Distance, Destination and Design) of land use planning. Under the global climate change, how 5D model be adapted to meet the elements of sustainable development. This study has obtained the following conclusions through the link of low carbon management concept.

TOD planning model is mainly for the integration of land use and transportation, while this article focuses on the mutual relationship in climate changes and land use and makes a correction for the pattern. The follow-up research can investigate the relationship between transportation and climate changes, and further construct a set of land use and transportation modes in response to climate changes to achieve the goal of urban model sustainable development. However, 5D model of land-use planning is certainly beneficial to climate change in the literature review, but there is lack of

evidence of proof currently. The further researches can certainly confirm the pattern by empirical examples.

REFERENCES

- Chia-Nung Li and Tsung-Yu Lai (2011). "An empirical analysis on connections of Transport and land-use." Proceedings of the Institution of Civil Engineers-Transport. accepted.
- Chia-Nung Li and Chien-Wen Lo (2011). "Does Pedestrian-Oriented Design Influence Public Transit Rideships in Chinese City." Taipei, IEEE- Journal of ICETCE, Vol. 2, pp. 1182- 1185.
- Chia-Nung Li and Tsung-Yu Lai (2009). "Why should cities change from DOT to TOD?," Proceedings of the Institution of Civil Engineers- Transport. Vol.162, No.2, pp.71-78.
- Jen-Jia Lin and Chia-Nung Li (2008). "A grey programming model for regional transit-oriented development planning." Papers in Regional Science. Vol. 87, No. 1, pp.119-139.
- Cervero, R. and Landis, J. (1992). "Suburbanization of jobs and the journey to work: a submarket analysis of commuting in the San Francisco Bay Area." Journal of Advanced Transportation, 23(3),275-297.
- Freilich, Robert H., (1998). "The Land-Use Implication of Transit-Oriented Development: Controlling the Demand Side of Transportation Congestion and Urban Sprawl." The Urban Lawyer, 30(3),547-572.
- Newman, P. and Kenworthy, J. (1999). "Sustainability and Cities: Overcoming Automobile Dependence. Washington. "D.C.: Island Press.
- Quade, Parsons Brinkerhoff and INC. Douglas.(1996). Transit and Urban Form.Report 16, Transit Cooperative Research Program.Transportation Research Board. National Research Council, National Academy Press, Washington: D. C.
- White, Attorney, Freilich, Leitner and Carlisle. (1999). "The Zoning and Real Estate Implications of Transit-Oriented Development." Transit Cooperative Research Program. Transportation Research Board. National Research Council. National Academy Press, Washington: D. C.
- Porter, D. (2002). "Making Smart Growth Work." Washington. D.C.: Urban Land Institute.
- Sinn, H. (2007). "Public Policies Against Global Warming." Cesifo Working Paper No. 2087(2007) See CESifo website: www.CESifo-group.org/wp.
- Stern, N. (2008). "The Economics of Climate Change." American Economic Review, 98, 1-37.
- Luca Bertolini & Frank le Clercq.(2003). "Urban development without more mobility by car? Lessons from Amsterdam, a multimodal urban region." Environment and Planning A, 35,579-589.

Characteristics of Fuel Consumption and Vehicular Operations of Buses in Taipei's Exclusive Bus Lanes

Y. C. Hu, Ph.D., PE¹, W. T. Lin², G. P. Chen³ and Y. W. Yang⁴

^{1,2,3} THI Consultants, Inc., 5Fl., No. 130, Sungshan Road, Taipei, Taiwan, PH (886-2)-27488822; FAX (886-2)-27486600; Email: ¹amyhu@thi.com.tw;

²grace@thi.com.tw; ³william@thi.com.tw

⁴Institution of Transportation, No. 240, Tun-hua North Road, Taipei, Taiwan; PH (886-2)-23496789; FAX (886-2)27176381; Email: yyw@iot.gov.tw

ABSTRACT

The objectives of this research are to (1) investigate the fuel consumption characteristics of bus operations in bus lanes and on regular city streets; (2) identify probable causes of inefficiency, and (3) identify probable improvements. Fuel consumption data were collected by using an On-board Emissions Measurement System (OEM) on a bus while the bus is in service. Study results show that a bus in an exclusive bus lane (1) is more energy-efficient when operating in mid-blocks due to reduced friction from other road traffic; and (2) has high percent of idling time due to station and intersection delay. Improvements for enhancing both energy and operational efficiency may include redesign of traffic signaling, renovation of bus station design/operations, and eco-driving training for bus drivers. Policies for promoting use of energy-efficient bus fleet, especially at idling and acceleration/deceleration, would also be helpful in fuel savings in city street operations.

INTRODUCTION

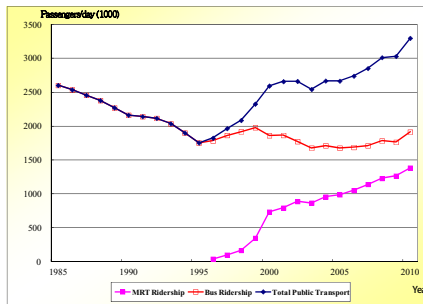
Prior to 1996, buses were the primary mode of public transport in Taipei, Taiwan. Private automobiles ownership increased at a fast rate, and bus patronage continued declining, as shown in Figure 1. In 1996, Taipei City Government implemented 41-kilometer of exclusive-bus-lane network on major arterials in Taipei. The bus-lane network was composed of 3 lines in the north-south direction, and 4 lines in the east-west direction. The bus-lane network upgraded bus services in terms of line speeds, safety and convenience in making transfers. It attracted passengers back to the bus system, and subsequently provided convenient feeder services for the transit network, which was put in revenue service line by line, starting in 1997. Taipei's patronage for public transport system has drastically increased since then. Total public transport ridership almost doubled from that in 1995, with steady bus patronage, without losing riders to the rapid transit system.

The bus-lane network is characterized by the following features:

- ✓ All bus lanes are in single-lane operations with variations in placement in the roadway to fit in traffic conditions and adjacent developments along the

- ✓ arterials;
- ✓ Buses wait for green lights as other road traffic;
- ✓ Traffic signaling is designed for all traffic, without special considerations and priorities for buses;
- ✓ Buses wait in line at stations, without a by-pass lane; and
- ✓ Stations located at the near-side of intersections, instead of mid-blocks, to facilitate transfers;

The bus-lane network was welcomed by city residents, and another 4 lines with a total length of 16 kilometers of bus lanes were added to the network in the following few years. Discount fare for transfers was also implemented as the ticketing system was automated. Currently about 60 percent of the bus patronage benefit from the use of a part or all of their daily trips in bus lanes. Bus operators consider those lines primarily in bus lanes as “gold lines”, and are always interested in acquiring the right-of-ways for bus operations in the bus lanes.



Data Source: Department of Transportation, Taipei City Government

Figure 1. Historical Public Transport Ridership in Taipei Metropolitan Area

With all the benefits from the system, many questions are still raised today to inquire whether the system is being operated to its utmost efficiency and how it may contribute to the current issues on the reduction of energy consumption and greenhouse gas emissions. The objectives of this research, therefore, are to (1) investigate the bus operations and fuel consumption characteristics of buses in bus lanes relative to those on regular urban arterials; (2) identify probable causes of inefficiency, and (3) identify probable actions for further improvements.

DATA COLLECTION

The data used in this research came out of a project sponsored by the Institute of Transportation (IOT), Ministry of Transportation and Communications, to build a fuel and greenhouse gas (GHG) emissions model... The model is described in detail in a paper entitled “Developing a Time-Based Model for Buses for Integration with Planning Model for Greenhouse Gas Analyses “to be presented at the same forum. The data collection for this research is summarized below.

Test Route and Test Bus

Route 226 of Taipei City was selected for the experiment. The route extends from Sanchong City in Taipei County, enters Taipei City from Taipei Bridge, runs through 4 major bus lanes and some city streets in Taipei, and terminates at Wuxing Street south of the New City Center. The total round-trip route length is 34 kilometers, with 33% of its length in exclusive bus lanes. Taipei City has a speed limit of 40km/hr for all buses, and therefore the data collected rarely exceed 40km/hr.

The test bus is a 2009 Daewoo BS120CN model, with an engine displacement of 7640 c.c. The tare weight is about 12,000 kilograms, and it satisfies EU4 emission standard. The driver has a clean driving record, and has a mild driving pattern.

On-board Emissions Measurement (OEM) System

The Horiba OBS-2200 system was used for collecting fuel consumption and emission data on roads. This system has been certified for Code of Federal Regulations (CFR) Part 1065 subpart J testing by the U.S. Environmental Protection Agency (EPA). It is also equipped with a Global Positioning System (GPS), which may be used to record vehicle positions over time, so that instantaneous speeds and acceleration rates may be recorded and related to emissions and fuel consumption. It is capable of measuring emissions of CO, CO₂, THC and NO_x. The fuel consumption is estimated by using a carbon balance methodology.

Sampling

The survey period of the IOT project extends from 6/17 to 6/24 in the year of 2011. For this analysis, the day of 6/21 (Tuesday) was selected. The first and last trips of the day were excluded, because they may not represent a typical run in a day. A total of about 32,397 seconds of samples were collected, which covers a travel distance of about 137.41 kilometers, or 4 full round-trips of the test bus throughout the weekday, as shown in the bottom part of Table 1. The data are segregated into four combinations of

- ✓ peak period (7:00~9:00 and 17:00~19:00) and off peak period; and
- ✓ bus-lane and regular city streets.

Table 1 Total Sampled Time and Travelled Distances

	Bus lane, Peak	Bus lane, Off-peak	Regular Streets, Peak	Regular Streets, Off-peak	Total
Time in Samples (sec)	3,627	8,049	7,186	13,535	32,397
Travelled Distance (km)	14.06	34.41	29.86	59.08	137.41

CHARACTERISTICS OF VEHICLE OPERATIONS

Travel Time in Speed Intervals

Table 2 shows the percent of time spent in various speed intervals. The distributions are typical of buses, with high percent of time spent in idling, as well as the speed close to the speed limit. The following observations are made:

- ✓ The percents of idling times are notably higher in bus-lanes or about 40% as compared with the 34% in the regular street portion. This is probably because (1)

bus lanes are located on major arterials in the city center, where traffic congestion is more pronounced; (2) passengers volumes are much higher in bus lanes, requiring longer time for boarding and alighting; and (3) the large volumes of buses in a bus lane without a bypass may also add to stop time when waiting to get into bus stations.

- ✓ The test bus spent similar percent of time idling during both peak and off-peak periods. Since the numbers of bus passengers are considerably less during off-peak periods, the long idling time in off-peak periods may be caused by signal design that is not responsive to the current bus flows.
- ✓ The combination of bus lanes in off-peak periods shows a considerably different distribution of time over speeds than the other three. The percent of time spent in speed above 35 km/hr amounts to 20.4%, while the other three only spend about 15~17% of time in the same speed interval. Moreover, the bus lanes in off peak period show about 4~5% of time in each of the 5 km interval below 25km/hr, as compared with the 5~8% of time spent in the same speed interval in the other three. This indicates bus lanes may operate more efficiently than the city-street portion when reasonable volumes of buses are in operations.

Table 2 Travel Time by Speed Interval

Speed Interval (km/hr)	Bus lane, Peak	Bus lane, Off-peak	Regular Streets, Peak	Regular Streets, Off-peak
0	41.0%	40.4%	34.1%	34.3%
0-5	5.4%	4.7%	5.6%	5.1%
5-10	5.1%	4.8%	7.2%	5.6%
10-15	5.9%	5.0%	8.1%	6.8%
15-20	7.3%	5.1%	8.6%	7.9%
20-25	5.9%	4.5%	6.8%	6.9%
25-30	5.6%	6.3%	6.1%	7.9%
30-35	8.5%	8.9%	7.8%	8.2%
>35	15.3%	20.4%	15.7%	17.2%
Total	100.0%	100.0%	100.0%	100.0%

Average Acceleration Rates

Fuel consumption rates are very much relevant to vehicular acceleration rates, but not so much to deceleration rates. Figure 2 shows the average acceleration rates, with deceleration excluded, of the test bus at various speed intervals. We can observe that:

- ✓ The test bus consistently applied much higher acceleration rates in bus lanes during off-peak period than the other three, indicating there may be (1) pressure from the buses behind to speed up; and/or (2) less disturbances from other road traffic in mid-blocks. The differences are most distinctive in the speed intervals between 10 and 25km/hr;
- ✓ For all four combinations of bus-lane/regular-street and peak/off-peak periods, the average acceleration rates are highest when the test bus is operated below 5km/hr, and generally decrease as the bus approaches the speed limit; and
- ✓ Off-peak operations show generally higher acceleration rates than those of peak operations, showing the preferred maneuvers of a good driver.

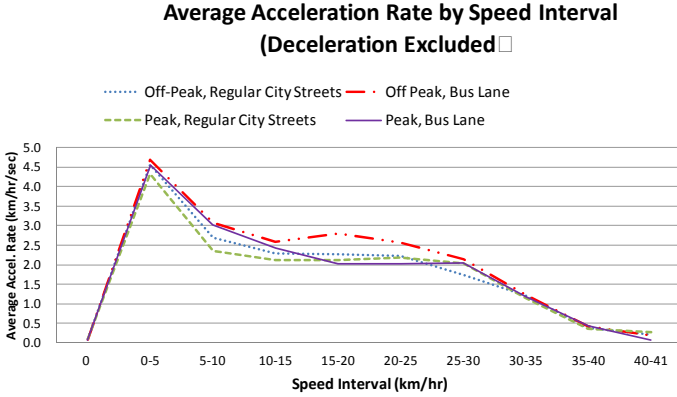


Figure 2 Average Acceleration Rates by Speed Interval

Travelled Distance by Speed Interval

Table 3 shows the travelled distances in various speed intervals. It shows that

- ✓ During off-peak hours, the test bus can travel close to 70% of the distance at speeds above 30 km/hr in bus lanes, which is considerably longer than the 57~61% in the other three.
- ✓ Below 10% of the distance was travelled by speeds between 10 and 20 km/hr in bus lanes during off-peak periods, as compared with the 14~17% in the other three. This is consistent with the observations for acceleration rates in Table 2. They show buses in bus lanes tend to be able to accelerate to speeds close to the speed limit, while they may be kept at much lower speeds for longer period of time on regular city streets and/or during peak periods.
- ✓ As expected, off-peak periods show higher percent of distances travelled at high speed than peak periods.
- ✓ Generally, bus lanes demonstrate higher operating speeds of 23 and 25 km/hr on line segments in peak and off-peak periods, respectively, as compared with the 22 and 23 km/hr on regular streets. This shows that the bus lane is functioning well in terms of reduction of disturbances from other roadway traffic in mid-blocks.

Table 3 Speed Distribution of Travelled Distance

Speed Interval (km/hr)	Bus lane, Peak	Bus lane, Off-peak	Regular Streets, Peak	Regular Streets, Off-peak
0-10	3.6%	3.0%	4.3%	3.3%
10-20	14.6%	9.9%	17.0%	14.4%
20-30	20.6%	17.9%	21.5%	23.9%
>30	61.2%	69.2%	57.2%	58.4%
Total	100.0%	100.0%	100.0%	100.0%
Average Operating Speed, Excluding Idling (km/hr)	23.00	25.14	22.10	23.31

CHARACTERISTICS OF FUEL CONSUMPTION

In making comparisons between bus lanes and regular city streets, it should be noted that the average fuel rates of the two portions of the bus route can only be compared with discretion, because they represent completely different traffic operating conditions and passenger demands. The bus-lane portion of the route is in city center, with generally much higher levels of traffic congestion and bus passenger demand than the city-street portion, while the latter is partially in the suburb, or on secondary arterials. The traffic conditions along the arterials with bus-lane operations tend to be highly congested, and may be even less energy efficient if no bus lane was provided.

Fuel Consumption Rates by Speed Interval

By accumulating the second-by-second fuel consumption and distance travelled in the same speed group, the fuel consumption per unit distance may be calculated, as shown in Table 4. Table 4 also shows the average fuel rates of the bus-lane vs. city-street portions at the bottom.

The following observations can be made:

- ✓ Off-peak idling fuel rates are 0.87 and 0.90 grams/sec, and peak idling fuel rates are 0.81 and 0.84 grams/sec, for bus-lane and regular streets, respectively. This indicates off-peak periods have higher idling fuel rates than those of peak periods by about 7~8%. This may be due to the variations of energy demand for air-conditioning. Since most off-peak hours are higher in temperature than peak hours, more energy for air conditioning is required in Taiwan's weather in June. .
- ✓ The fuel rates are the highest when speeds are below 5 km/hr, and generally decrease with respect to the increase of speed. As speeds extend into the intervals of 35~40 km/hr, for example, the fuel rates only amount to about 15~18% of those in the interval of 5~10 km/hr. This implies reduction of congestion would raise average operating speeds, and may cause notable positive effects on energy efficiency of buses.
- ✓ If fuel consumed for idling is excluded, the average fuel rates amount to 0.35~0.40 l/km. This fuel rate is close to the fuel rates at about 30 km/hr, as shown in the table. This implies a city bus needs to travel at a speed at about 30 km/hr or above to operate at a below-average fuel rate.
- ✓ The longer the distance a bus may travel at fuel-saving speeds, the higher the overall fuel efficiency. Thus, bus lanes provide favorable operating conditions for buses to accelerate to speeds of low fuel-consumption. This is supported by the lower fuel rates of 0.35~0.36 l/km for bus-lane, than the 0.38~0.40 l/km for the regular- street portion, as shown in the table. .
- ✓ When idling is included, the bus-lane portion still has lower fuel rates of 0.57~0.59 l/km, but to a narrower margin. This indicates that the high idling time in the bus-lane portion reduces somewhat the energy efficiency of the bus-lane.

Table 4 Fuel Rates by Speed Intervals

unit : l/km

Speed Interval (km/hr)	Bus lane, Peak	Bus lane, Off-peak	Regular Streets, Peak	Regular Streets, Off-peak
Idling, grams/sec	0.81	0.87	0.84	0.90
0-5	4.68	5.11	4.61	4.84
5-10	1.46	1.54	1.35	1.48
10-15	0.99	1.09	1.00	1.05
15-20	0.64	0.83	0.74	0.78
20-25	0.61	0.72	0.58	0.65
25-30	0.44	0.47	0.43	0.40
30-35	0.37	0.37	0.38	0.41
35-40	0.23	0.23	0.24	0.23
>40	0.10	0.15	0.15	0.16
Fuel Rate, Idling Excluded (l/km)	0.36	0.35	0.40	0.38
Fuel Rate, Idling Included (l/km)	0.59	0.57	0.60	0.57

Fuel Consumption vs. Travelled Distance

By comparing the percent of fuel consumed and of travelled distance in each speed interval, the energy efficiency of operating speeds may be described in further details.

- ✓ As shown in Table 5, the test bus uses 28~34% of fuel in idling and at speed below 10 km/hr. The total travelled distances in the two speed categories only amount to 3~4% of the distance. At the other end, about 27~29% of the fuel is used at a speed above 30 km/hr, to travel 58~69% of the distances. This compares well with the observations of energy consumption rates in Table 4.
- ✓ About 15~21% of fuel is used in idling, with the bus lane portion taking the high end due to high percent of time idled. Reducing idling time for buses would considerably lower the overall fuel rates and would improve the energy performances of not only Route 226 buses, but all bus routes in the bus-lane network. The way for improvement may include traffic signaling with priorities or pre-emption for buses for buses. Station design on platform lengths and the provision of bypass lane would also be helpful.

Table 5 Fuel Consumed vs. Distance Travelled by Speed Interval

Speed Interval (km/hr)	Bus lane, Peak		Bus lane, Off-peak		Regular Streets, Peak		Regular Streets, Off-peak	
	Dist.	Fuel	Dist.	Fuel	Dist.	Fuel	Dist.	Fuel
0	0%	20.9%	0%	18.8%	0%	16.8%	0%	15.6%
0-10	3.6%	13.1%	3.0%	12.0%	4.3%	13.8%	3.3%	12.4%
10-20	14.6%	19.2%	9.9%	17.0%	17.0%	24.1%	14.4%	22.0%
20-30	20.6%	18.3%	17.9%	18.5%	21.5%	18.1%	23.9%	21.1%
>30	61.2%	28.6%	69.2%	32.7%	57.2%	27.2%	58.4%	28.9%
Total	100.0%	100.0%	100.0%	100.0%	100.0%	100.0%	100.0%	100.0%

CONCLUSIONS AND RECOMMENDATIONS

The study reaches the following conclusions and recommendations:

- ✓ Taipei's exclusive bus lane system has been very successful and effective in improving bus efficiencies and attracting bus passengers in past decades. It is

effective in sheltering buses from disturbances caused by other road traffic, and it enables buses to reach speeds of low fuel rates more easily than regular city streets.

- ✓ The percents of idling time appear too high for the bus-lane operations in both peak and off-peak periods, which reduce the efficiency both in bus operations and in fuel consumption. For reducing idling time in the bus lanes, it is necessary to (1) upgrade traffic signaling systems by, e.g., bus-pre-empt or bus-priority signaling; and (2) stations may be re-designed to better accommodate the current passenger demands. More detailed analyses are required to finalize the design details.
- ✓ Fuel consumption rates are considerably higher in the low-speed zone than the high-speed zone. Therefore, any kind of congestion management strategies for improving vehicular efficiencies would also help improving energy performances of buses, especially when priority treatments are provided for buses.
- ✓ City bus operations require frequent stops, acceleration and deceleration. The buses with regenerative brake systems, hybrid technologies, or other efficient stop/go features may stand out in energy performances.
- ✓ Since bus operators favor operations in the bus lanes because of their high patronage and high operating efficiencies, a policy for prioritizing right-of-way assignment to those operators providing “Green Buses” and “eco-drivers” to operate on the bus lane system may help the overall energy performances of the entire bus-lane system.

ACKNOWLEDGMENT

The Institution of Transportation, Ministry of Transportation and Communications, is acknowledged for providing funding for the research, with a project entitled “*A Study on the Relations Analyses between Energy Consumption, Emissions and Transportation Planning.*” Taipei’s Capital Bus Co. is also acknowledged for their support in providing the test bus for conducting the bus experiment while in operations.

REFERENCES

- THI Consultants, Inc., (2012). *Characteristics of Fuel Consumption and Greenhouse Gas Emissions as Measured by On-Board Emissions Measurement System- A Study for Buses*, Report for the Institution of Transportation. (in Chinese)
- Wen, P.C., Hu, Y.C., Chen, S.Y., Chen, H.H. and Chang, C.W., (2012), “**Developing a Time-Based Model for Buses for Integration with Planning Model for Greenhouse Gas Analyses**” paper accepted to be presented at the Annual Conference of International Chinese Transportation Professionals Association in Chongqing.
- Wen, P. C., Hu, Y. C., Chung, A. H., and Lin, K. H., (2010), “**Time-based Model for Estimating Fuel Consumption by Linking Field and Lab Measurements**”, presented at the *2010 TRB annual meeting*.

Developing a Time-Based Model for Buses for Integration with Planning Model for Greenhouse Gas Analyses

P. C. Wen¹, Y. C. Hu², S. Y. Chen³, H. H. Chen⁴ and C. W. Chang⁵

² Corresponding author; THI Consultants, Inc., 5Fl., No. 130, Sungshan Road, Taipei, Taiwan; PH: (886-2)-27488822; FAX: (886-2)-27486600; E-mail: amyhu@thi.com.tw

^{1,3,4} Chung-hua Institution for Economic Research, No. 75, Chang-hsing Street, Taipei, Taiwan; PH: (886-2)-27356006; FAX: (886-2)-27390610; E-mail: ¹pam@cier.edu.tw; ³shinyi@cier.edu.tw; ⁴hsuehng@cier.edu.tw

⁵ Institution of Transportation, No. 240, Tun-hua North Road, Taipei, Taiwan; PH: (886-2)-23496789; FAX: (886-2)27176381; E-mail: changcwn@iot.gov.tw

ABSTRACT

This research came out of a 5-year research project for enhancing the capabilities of the planning model in environmental analysis. A Time-Based Model (TBM) is developed to project fuel consumption and greenhouse gas (GHG) emissions under various traffic conditions for various highway classes. It is based on real-world measurements by using a certified on-board emissions measurement (OEM) system, and a global positioning system (GPS) for deriving vehicular operations characteristics, such as speed, acceleration, deceleration, etc.

The first three years of the research was focused on building a model for passenger cars, and the following two years dedicated to intercity and city buses. This paper describes the research findings on buses, including the experiment design, model-building and validation. With the bus module and passenger-car module integrated into the planning model, the energy and GHG effects of transportation demand management policies, such as the provision of high speed rail, bus lanes, and preferential tolling operations, etc. may be easily investigated.

INTRODUCTION

In 2007, the Institution of Transportation (IOT), Ministry of Transportation and Communications launched a 5-year research project to enhance the capabilities of the planning model in environmental analysis. With concerns for climate change and energy security, and a need for developing action plans, the Ministry needs an effective planning tool for evaluating environmental effects of transportation policies to meet the requirements for reducing energy consumption and CO₂ emissions from the transportation sector. For easy integration with the planning model, a Time-Based Model (TBM) is developed to project fuel consumption and CO₂ emissions under various traffic conditions and for various highway classes. It is based on second-by-second fuel consumption and CO₂ emissions data collected by using a certified on-board emissions measurement (OEM) system for making real-world measurements.

The first three years (2007-2009) of the research was focused on building a model for passenger cars, and the following two years (2010~2011) were dedicated to buses, including intercity buses and city buses. This paper describes the research findings on buses, including the experiment design, TBM model-building and validation, and how it may be integrated with the planning model.

TIME-BASED MODEL (TBM)

The Time Based Model (TBM) developed in this research has three distinctive features, as follows:

- ✓ It is built on second-by-second measurements, and would project per-second fuel consumption and emissions, rather than per unit distance;
- ✓ Instead of directly building a model on fuel rate, the TBM model is developed by building mathematical models on adjustment factors relative to fuel consumption statistics pertaining to the vehicle. The statistics represent vehicular variation, while the operational variations would be reflected in the adjustment factors;
- ✓ The final results of the TBM model is a series of adjustment factors in the format of look-up tables for easy integration with the planning model.

For passenger cars, a series of adjustment factors are developed by using data collected in the laboratory by following the Federal Testing Procedures (FTP), as well as by normal driving on road. The published fuel economy at car sales is the variable representing vehicular features. For buses, however, currently no vehicle tests can be conducted in the lab for heavy-duty vehicles. Therefore, monthly fuel consumption statistics from the bus operators are used as the variable accounting for vehicular characteristics.

As a time-based model, total fuel consumption by a specific vehicle on a highway section would be the sum of fuel consumption over time. That is

$$F = \sum_t N_t \quad (1)$$

where

F = Total fuel in grams (g) consumed by a vehicle traveling on a highway link over a period of time;

N_t = fuel consumption at time t in grams/sec.

To account for the effects of highway classes and vehicular speeds, a set of adjustment factors, $R_{Field,class}(v)$, is introduced:

$$N_{Field,class}(v) = N_{Field,T} \times R_{Field,class}(v) \quad (2)$$

or

$$R_{Field,Class}(v) = \frac{N_{Field,class}(v)}{N_{Field,T}} \quad (3)$$

where

$N_{Field,class}(v)$ = Field measurements of fuel consumption in grams/sec on various classes of highways, and expressed as functions of vehicular speeds;

$R_{Field,class}(v)$ = Adjustment factors for normal driving on highways relative to the monthly fuel consumption statistics from the bus operator, and expressed by highway classes as functions of instantaneous speeds;

$N_{Field,T}$ = Average fuel economy statistics from operators (km/l), converted to (grams/sec) by applying the average speed of the same period.

EXPERIMENT DESIGN

1. On-board Emissions Measurement (OEM) System

The Horiba OBS-2200 system was used for collecting fuel consumption and emission data on roads. This system has been certified for Code of Federal Regulations (CFR) Part 1065 subpart J testing by the U.S. Environmental Protection Agency (EPA). It is also equipped with a Global Positioning System (GPS), which may be used to record vehicle positions over time, so that instantaneous speeds may be recorded and related to emissions and fuel consumption. It is capable of measuring emissions of CO, CO₂, THC and NO_x. The fuel consumption is estimated by using a carbon balance methodology.

2. Test Routes

The intercity test route extends from Taipei City to Luodong in Yilan County. After passengers' boarding in Taipei, the buses travels through city streets, and then along Freeway 5, which traverses through mountainous terrain and long tunnels. In Yilan County, the Freeway extends on a viaduct in a flat terrain. The route then passes through small towns on primary and secondary highways before it reaches its terminal in Luodong. The total route length is 66 kilometers. The route passes through the following highway classes:

- Freeways (speed limit: 110 km/hr)
- Freeways (speed limit: 90 km/hr)
- Freeways (long tunnel)
- Urban expressways (long tunnel)
- Secondary highways: Urban, 2 lanes
- Primary highways: Urban, 4 lanes or more
- Urban arterials or city streets.

As for city bus, Route 226 of Taipei City was selected. It extends from Sanchong City in Taipei County, enters Taipei City from Taipei Bridge, runs through 4 major bus lanes and some city streets in Taipei, and terminates at Wuxing Street south of the New City Center. The total round-trip route length is 34 kilometer, with 33% of its length on exclusive bus lanes.

A total of 550,000 seconds of valid samples were collected, including 350,000 seconds of samples for intercity bus, and 200,000 seconds for city bus. The large sample size is necessary to ensure a minimum of 10,000 seconds of valid samples for each highway class.

3. Test Buses

The test buses are selected from the bus fleet servicing the respective bus routes, as shown in Table 1. The two test buses show considerable differences in their engine displacements and weights.

Table 1. Characteristics of Test Buses

Items	Intercity Bus	City Bus
Model year	2009	2009
Manufacturer	SCANIA	DAEWOO
Model	K380	BS120CN
Engine	I6 DC1213	I6 DL08S
Weights (kg)*	13,500 (17,000)	11,920(16,090)
Displacement	11,705 c.c.	7,640 c.c.
Emission Standards	Euro 4	Euro 4

Note: *Tare weight (Gross weight).

RESULTS

A step-wise regression analysis was used for fitting polynomial equations for each highway class, using instantaneous speed as the independent variable. The equations can be expressed in the following form:

$$R^{Field,class}(v) = a + bv + cv^2 + dv^3 + ev^4 \quad (4)$$

$$C^{Field,class}(v) = R_{CEM} \times R^{Field,class}(v) \quad (5)$$

where

$R^{Field,class}(v)$ = Estimated adjustment factors as a function of instantaneous speeds for road driving, as in Equation (3);

v = Instantaneous speed when emissions measurements are taken (km/hr);

a, b, c, d, e = coefficients of Equation (4)

$C^{Field,class}(v)$ = Estimated CO₂-emission adjustment factors for road driving;

R_{CEM} = Adjustment factor for carbon balance calculations.

Table 2 shows the fitted coefficients, R^2 , and their T-test values of $R^{Field,class}(V)$. The fitted adjustment factors $C^{Field,class}(v)$ are shown in Figure 1.

Table 2. Coefficients of Equations $R^{Field,class}(v)$ by Highway Classes.

Bus Type	Highway Class	Coefficients of ($R^{Field,class}(v) = a + bv + cv^2 + dv^3 + ev^4$)					adj- R ²	F Value
		a	b	c	d	e		
Inter-city Bus	Freeways (110)	0.36411486		0.00150188	-0.00003321	0.00000020	0.55	36.78
	t value	5.60***		6.77***	-5.64***	4.91***		***
	Freeways (90)	0.24159450	0.02890651	-0.00041961	0.00000253		0.82	137.81
	t value	4.91***	6.07***	-3.40***	2.81***			***
	Freeways (tunnel)	0.22042210	0.02870037	-0.00043310	0.00000210		0.59	43.27
	t value	3.96***	5.38***	-3.14***	2.09**			***
	Urban expressways	0.40783203	0.01193866				0.35	43.50
	t value	4.83***	6.60***					***
	Secondary	0.31817413	0.02580748	-0.00032552			0.63	55.30
	t value	8.25***	9.12***	-7.49***				***
City Bus	Primary	0.36148960	0.02167745	-0.00026710		0.59	48.92	
	t value	10.34***	8.85***	-7.44***			***	
	Urban Arterials	0.26054946	0.02370913	-0.00025459		0.73	79.12	
t value	6.83***	7.94***	-5.20***				***	
City Bus	Urban Arterials	1.33760167	-0.07819389	0.01113436	-0.00041931	0.00000454	0.67	22.18
	t value	12.68***	-2.14**	3.02***	-3.08***	2.76***		***

Note: * p<0.05, ** p<0.01, *** p<0.001.

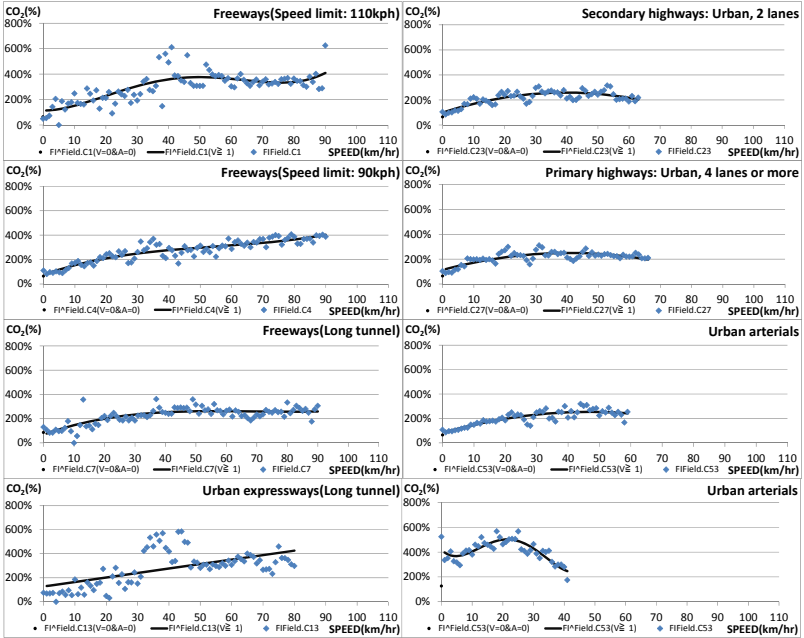


Figure 1. CO₂-emissions adjustment factors by highway classes

For projecting,

$$N^{Field.class}(v) = R^{Field.class}(v) \times N_{Field.T} \tag{6}$$

$$\begin{aligned} E^{Field.class}(v) &= R_{CEM} \times N^{Field.class}(v) \\ &= R_{CEM} \times R^{Field.class}(v) \times N_{Field.T} \\ &= C^{Field.class}(v) \times N_{Field.T} \end{aligned} \tag{7}$$

where

$N^{Field.class}(v)$ = Projected fuel consumption rates in grams/sec, as functions of vehicular speed by highway class;

$E^{Field.class}(v)$ = Projected CO₂ emission rates in grams/sec by highway classes.

The projected CO₂ emissions rates in grams/sec by highway classes are shown in Figure 2. Figure 3 shows the CO₂ emissions rates in l/km for selected highway classes, for demonstrating the equivalent curves for a distance-based model. The curves demonstrate considerable differences between the fuel consumption features of intercity and city buses. With more frequent stops, and acceleration/deceleration operations, the curve for city buses shows much higher emission rates at the low speed end, as compared with the urban-arterial curve for intercity buses. It also demonstrates that the city bus is more energy-efficient in the speed range of about 30~50 km/hr, probably due to its smaller engine size, and smaller weight.

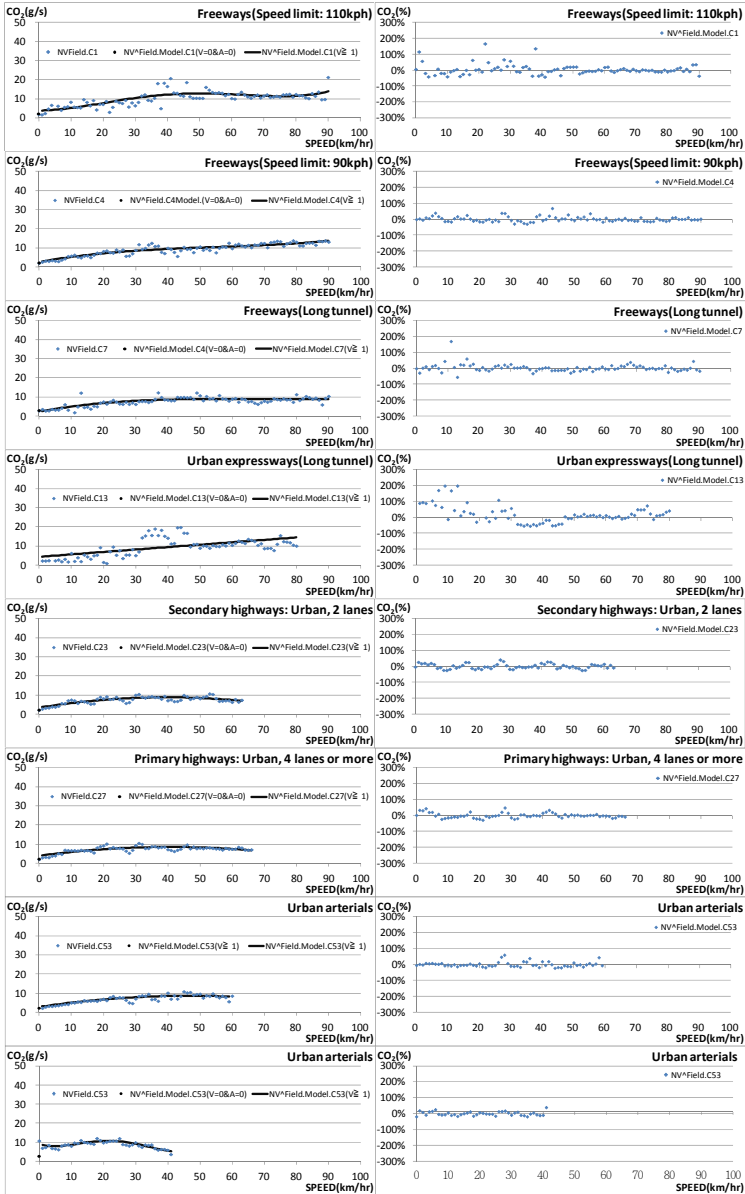


Figure 2. Projected CO₂ emissions rates (grams/sec)

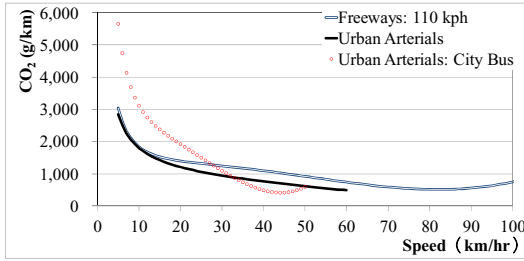


Figure 3. Projected CO₂ emission rates

VALIDATION

Table 3 shows the projected fuel economy of various buses by using the TBM model. Records from digital speed recorders for a number of buses were obtained from bus operators. These records were segregated by weekday and weekends. These profiles are input into the TBM for estimating their fuel consumption by day, and the results aggregated by month for comparison with the monthly fuel consumption statistics from the operators. For the buses compared,

- ✓ #270 demonstrates errors resulting from route variation;
- ✓ #222 demonstrates errors resulting from buses of different emission standards;
- ✓ #285 demonstrates errors resulting from buses both of different emission standards and operated by an aggressive driver;
- ✓ #53 & #75 in Taichung show the errors resulting differences in operations regions, considerably smaller engines, as well as the operating conditions without bus lanes.

Table 3. Model Validation: City Bus.

Area	Route	Vehicle (year)	Driving Behavior	Monthly Fuel Economy (km/l)	Average Day Speed (km/hr)	TBM Projected Fuel Economy			
						Daily (km/l)	Error	Monthly (km/l)	Error
Taipei	#226, Bus lane 33.3%*	Daewoo, EU4, 7640c.c. (2009)*	moderate	1.63	WD 14.50 WN 15.25	-	-	-	-
	#270, Bus lane 27.5%	Daewoo, EU4, 7640c.c. (2010)	moderate	2.48	WD 14.28 WN 16.04	2.53 2.73	1.9% 9.9%	2.58	4.0%
	#222, Bus lane 20.6%	Isuzu, EU3, 7790c.c. (2006)	moderate	2.29	WD 14.67 WN 16.69	2.27 2.56	-0.9% 11.6%	2.34	2.3%
	285, Bus lane 20.00%	Isuzu, EU3, 7790c.c. (2005)	Aggressive	1.88	WD 14.37 WN 15.69	1.99 2.16	6.1% 14.7%	2.03	8.1%
Tai-chung	#53, No bus lane	King Long, EU4, 6692c.c. (2009)	moderate	2.94	WD 14.45 WN 13.96	3.04 2.94	3.4% 0.4%	3.02	2.6%
	#75, No bus lane	King Long, EU4, 6692c.c. (2010)	moderate	2.62	WD 14.44 WN 14.71	2.48 2.59	-5.3% -1.1%	2.51	-4.3%

Note: * The Test bus and the test route; shaded area highlights differences with the test bus; WD: Weekday; WN: Weekend.

The following observations can be made from the comparison:

- ✓ Errors generally stay within 10% of the fuel consumption statistics, which shows high transferability of the TBM model, if applied to different route, bus type,

- driver behavior and even different regions in Taiwan;
- ✓ The largest error of 8.1% is recorded from the #285 bus, which meets a lower EU3 emissions standards, and was driven by an aggressive driver, as compared with the test bus.

CONCLUSIONS

Based on data collected from the test buses in service, the estimated emissions would represent real-life fuel consumption and emissions performances of buses in use, rather than measurements in a lab. With vehicular and operational characteristics accounted for separately in model building, the TBM model shows high transferability, regarding differences among vehicles, routes, driver behaviors and regions,. The model is easily integrated with the current planning model, by building a set of internal look-up tables. With the modules for buses successfully integrated to the planning model, which has already been equipped with similar passenger-car module from research of the first three years, the IOT would have the capacity for investigating the energy and GHG effects of transportation demand management policies, such as the provision of high speed rail, bus lanes, and tolling operations, etc.

ACKNOWLEDGMENT

The Institution of Transportation, Ministry of Transportation and Communications, is acknowledged for providing funding for the research, with a project entitled “*A Study on the Relations Analyses between Energy Consumption, Emissions and Transportation Planning.*” Taipei’s Capital Bus Co. is also acknowledged for their support in providing the test buses for the experiments.

REFERENCES

- Chung-hua Institution for Economic Research (2009). *A Study on the Relation Analysis between Energy Consumption, Emissions and Transportation Planning*, Report for the Institution of Transportation. (in Chinese)
- THI Consultants, Inc. (2010). *Integration the Applications of Sustainable Transportation Planning Model and Models for Projecting Energy Consumption and Air Pollutants Emissions*, Report for the Institution of Transportation. (in Chinese)
- THI Consultants, Inc. (2012). *Characteristics of Fuel Consumption and Greenhouse Gas Emissions as Measured by On-Board Emissions Measurement System-A Study for Buses*, Report for the Institution of Transportation. (in Chinese)
- U.S. Environmental Protection Agency (1993). *Federal Test Procedure Review Project: Preliminary Technical Report*.
- Wen, P. C., Hu, Y .C., Chung, A. H., Lin, K. H. (2010). “**Time-based Model for Estimating Fuel Consumption by Linking Field and Lab Measurements**”, presented at the *2010 TRB annual meeting*.

A Sustainable Multi-User Multi-Criteria Transportation Network Equilibrium Model

Hu Wenjun¹ and Zhou Xizhao²

¹School of Transportation, Shanghai Maritime University, Shanghai, China; PH: (021)58855200; email: huwenjun0@yahoo.com.cn

²School of Management, Shanghai Maritime University, Shanghai, China; PH: (021)58855200; email: xizhaozhou@163.com

ABSTRACT

A Sustainable multi-user multi-criteria transportation network equilibrium model considering emission effects is proposed, under the hypothesis that there are many different types of users in the network and each type of users has their own emission preferences. The model explicitly introduces three criteria in the generalized costs rather than one single criterion to describe users' travel behavior in the transportation network, thus forming a multi-criteria model. These three criteria are travel time, travel cost and emission. A finite-dimensional variational inequality problem is used to describe the sustainable multi-user multi-criteria transportation network equilibrium model. Then a modified projection method is used as an effective algorithm to solve the variational inequality problem. At last a simple illustration network is used to prove the correctness and feasibility of the model.

INTRODUCTION

Traffic congestion and environmental pollution, two evils which are accompanied by vehicles in our modern urban society, have attracted a great deal of attention both at home and abroad for a long time. Transportation network equilibrium models have long been used by researchers to study transportation phenomena and alleviate the traffic congestion and environmental pollution problems. Since 1952, the famous expert Wardrop proposed the first and second Wardrop principle of equilibrium assignment, a lot of transportation network equilibrium models have been proposed since then. However, many of them did not include the effects of traffic emission. Among the few who consider it [1][2][3][4][5], some suppose that there is only one type of user in the network, or all of the users are homogenous; some suppose that travelers' decisions are all based on one criterion: the minimization of environment pollution, ignore users' selfishness. In fact, this is not the case in practice. On the

one hand, the heterogeneity of the users should be considered. Different users have different properties; they act differently in the network, they could also have different emission preferences and emission functions. If they are not differentiated, traffic demand model will bear great errors. On the other hand, users' travel behaviors are complex and a single criterion usually can not reflect the richness of users' choices and preferences in real life.

To complement these disadvantages, we establish a sustainable multi-user multi-criteria transportation network equilibrium model to examine the vehicle emission effects on urban transportation system, especially on traffic assignment and travel behavior. In the model there are many types of uses and each type has their own weight of emission, corresponding to the emission function which is included in the generalized costs of users. Users' paths choices are based on three criteria: travel time, travel cost and emission. A finite-dimensional variational inequality problem (VIP) is used to describe the sustainable multi-user multi-criteria model. Then use a modified projection method as an algorithm to solve the variational inequality problem. At last, a test network is used to verify the feasibility and practicability of the model.

A SUSTAINABLE MULTI-USER MULTI-CRITERIA NETWORK EQUILIBRIUM MODEL

Use an empowering digraph $G(N, A)$ to represent a transportation network, where N is the set of all the nodes in the network, A is the set of all the links in the network. Users in the network can be divided into M types, M is the number of a typical user type m ($m=1,2,\dots,M$) with their own sense of environmental protection, reflected in their weight on pollution emission. Variable \mathbf{rs} means an OD pair and \mathbf{RS} is the set of OD pair which satisfies $\mathbf{rs} \in \mathbf{RS}$, \mathbf{p} is a path between OD pair \mathbf{rs} . $\mathbf{P}_{\mathbf{rs}}$ is the set of all the simple paths connecting OD pairs $\mathbf{rs} \in \mathbf{RS}$ and \mathbf{P} is the set of all the simple paths in the network, $\mathbf{p} \in \mathbf{P}$.

In the network containing m types of users, use $\mathbf{f}_p^{m,rs}$ to represent flow on path \mathbf{p} between OD pair \mathbf{rs} of user type m , \mathbf{f}_p^{rs} to represent flow on path \mathbf{p} between OD pair \mathbf{rs} of all users, \mathbf{x}_a^m to represent flow on the link a of user type m , \mathbf{x}_a to represent flow on the link a of all users.

Then we have a relationship between \mathbf{x}_a and \mathbf{x}_a^m :

$$\mathbf{x}_a = \sum_{m \in M} \mathbf{x}_a^m \quad (1)$$

The relationship between \mathbf{f}_p^{rs} and $\mathbf{f}_p^{m,rs}$ is:

$$f_p^{rs} = \sum_{m \in M} f_p^{m,rs} \quad (2)$$

And the relationship between f_{pw}^m and x_a^m is:

$$x_a^m = \sum_{rs \in RS} \sum_{p \in P_{rs}} f_p^{m,rs} \delta_{ap}^m \quad a \in A, m \in M \quad (3)$$

In equation (3), δ_{ap}^m is 0-1 variables. If for user type m , link a is on path p between OD pair rs , then it equals 1, else equals 0. Besides, all variables above should satisfy nonnegative constrains.

Suppose d_{rs}^m is the demand between OD pair $rs \in RS$ of user type m , d_{rs} is the demand between OD pair $rs \in RS$ of all users, then we have the relationships (4) and (5):

$$d_{rs} = \sum_{m \in M} d_{rs}^m \quad (4)$$

$$d_{rs}^m = \sum_{p \in P} f_p^{m,rs} \quad (5)$$

Next we will define users' generalized cost functions. Suppose users in the network choose their paths according to three criteria: travel time, travel cost and pollution emission rather than one single criterion. Then for a typical user type m , his or her generalized cost function can be written as an additive function of the three criteria. The generalized cost function of user m on link a has the form:

$$h_a = w_{1a}^m t_a + w_{2a}^m c_a + w_{3a}^m e_a, \forall m \in M, a \in A \quad (6)$$

In equation (6), t_a^m is the travel time function of user type m , where travel time is a separable function of link flow, that is, $t_a^m = t(x_a^m)$. c_a^m is the travel cost function of user type m , where travel cost is a separable function of link flow, that is, $c_a^m = c(x_a^m)$. e_a^m is the pollution emission function of user type m , where emission is a separable function of link flow, that is, $e_a^m = e(x_a^m)$. So u_a^m is also a separable function of link flow, that is, $u_a^m = u(x_a^m)$. w_{1a}^m, w_{2a}^m and w_{3a}^m are nonnegative weights corresponding to travel time, travel cost and emission, represent user m 's tradeoff among travel time, travel cost and emission.

When $w_{2a}^m = 0, w_{3a}^m = 0$, then the sustainable multi-user multi-criteria transportation network equilibrium model degenerates into a traditional travel time based transportation network equilibrium model. When $w_{1a}^m = 0, w_{3a}^m = 0$, then

the model degenerates to a traditional travel cost based transportation network equilibrium model. When $w_{1a}^m = 0, w_{2a}^m = 0$, then the model degenerates into a model which regards suitable environment as its optimum objective, such as [8]. When $w_{3a}^m = 0$, the generalized cost of a user is based on travel time and travel cost and it degenerates into a bi-criteria model in [7].

Use v_p^m to represent the generalized cost function of user m on path p .Then the generalized cost function of user m on path p can be written as:

$$v_p^m = \sum_{a \in A} q_a^m \delta_{ap}^m, \forall m \in M, p \in P \quad (7)$$

Now we have the following transportation network equilibrium conditions, they are multi-user multi-criteria transportation network equilibrium conditions which take into account the effect of pollution emission, so they can be called sustainable multi-user multi-criteria transportation network equilibrium conditions:

For each user type m, all the OD pairs $rs \in RS$, all the paths $p \in P$, a flow pattern f^* is in equilibrium if the following condition is satisfied:

$$v_p^m(x^*) \begin{cases} = \pi_{rs}^m & \text{若 } f_p^{m,rs*} > 0 \\ \geq \pi_{rs}^m & \text{若 } f_p^{m,rs*} = 0 \end{cases} \quad (8)$$

π_{rs}^m is the minimum generalized cost between OD pair rs of user type m. In other words, for each type of users, all used paths have the minimum and same generalized cost, and generalized cost of unused paths is the same or greater than the used paths.

Define feasible

$$\text{region } K \equiv \left\{ \hat{x} \mid \hat{f} \geq 0, \text{ s.t. } x_a^m = \sum_{rs \in RS} \sum_{p \in P_s} f_p^{m,rs} \delta_{ap}^m, x_a = \sum_{m \in M} x_a^m, d_{rs}^m = \sum_{p \in P} f_p^{m,rs} \right\}, \text{ and we can}$$

write the finite-dimensional variational inequality form of equilibrium conditions. The VIP of sustainable multi-user multi-criteria transportation network equilibrium model satisfying equilibrium condition (8) is:

$$x \langle u(x^*)^T, x - x^* \rangle \geq 0 \quad (9)$$

Or equivalently in a standard form of VIP:

$$\langle F(x^*)^T, x - x^* \rangle \geq 0 \quad (10)$$

In (9) and (10), $\langle \cdot, \cdot \rangle$ represent inner product in \mathbf{R}^n . The existence, uniqueness, monotonicity, Lipschitz continuity and other details of VIP can be seen in reference [2].

ALGORITHM

Projection method [6] is a commonly used algorithm for the solution of VIP. It usually divides VIP to a series of sub problems, of which every sub problem is equivalent to a solution of nonlinear quadratic programming problem. The algorithms of quadratic programming problems are rather mature and different software can be used to solve them, thus solve the VIP easily. When strict monotonicity is not satisfied, we can use modified projection method to solve any kind of standard VIP, that is, exist $\mathbf{x}^* \in \mathbf{N}$ satisfy $\langle \mathbf{R} \mathbf{x}^* \rangle^T, \mathbf{x} - \mathbf{x}^* \geq 0, \forall \mathbf{x} \in \mathbf{M}$. As long as function $F(\mathbf{x})$ is monotonic and Lipschitz continuous, the convergence of the modified projection method can be guaranteed. The procedures of the algorithm can be written as:

Step 0: Initialize. Start from $\mathbf{x}^{(0)} \in \mathbf{N}$, select parameter ρ which satisfy $0 \leq \rho \leq \frac{1}{L}$,

L is a Lipschitz constant. Set counter $n=1$.

Step 1: Compute. Compute $\bar{\mathbf{x}}^{(n)}$ from the following VIP:

$$\sum_{m=1}^M \sum_{a \in A} \{ \bar{\mathbf{x}}_a^{m(n)} + \rho [\mathbf{u}_a^m(\mathbf{x}^{(n)}) - \mathbf{x}_a^{m(n-1)}] \} (\mathbf{x}_a^m - \bar{\mathbf{x}}_a^{m(n)}) \geq 0, \forall \mathbf{x} \in \mathbf{N}$$

Step 2: Modification. Compute $\mathbf{x}^{(n)}$ from the following VIP:

$$\sum_{m=1}^M \sum_{a \in A} \{ \mathbf{x}_a^{m(n)} + \rho [\mathbf{u}_a^m(\bar{\mathbf{x}}^{(n)}) - \mathbf{x}_a^{m(n-1)}] \} (\mathbf{x}_a^m - \mathbf{x}_a^{m(n)}) \geq 0, \forall \mathbf{x} \in \mathbf{N}$$

Step 3: Convergence check. If $|\mathbf{x}_a^m - \mathbf{x}_a^{m(n)}| \leq \varepsilon, m=1,2,\dots, M, a \in A, \varepsilon > 0$, then stop.

Or else let $n=n+1$ and return to Step 1.

The procedures of the algorithm can be described by figure 1 below.

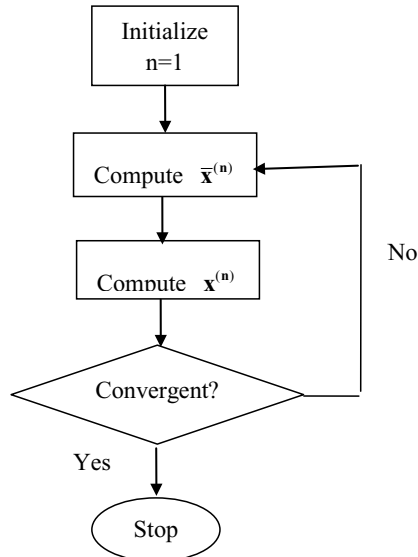


Figure 1 the procedures of the algorithm

A NUMERICAL EXAMPLE

To testify the model, we use a numerical network which contains five nodes and six links. It has two origins a and b and two destinations d and e, c is an intermediate node. There are two paths can be chosen from origin a to destination d: path 1 (link 1) and path 2 (link 2-3). There is only path from origin a to destination e: path 3 (link 2-5). There is one path from origin b to destination d: path 4 (link 4-3) and two paths from origin b to destination e: path 5 (link 4-5) and path 6 (link 6). See figure 2.

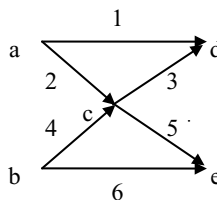


Figure 2 a simple network

Suppose the demands of two OD pairs are respectively: $\mathbf{d}_{ad} = 30$, $\mathbf{d}_{ae} = 50$, $\mathbf{d}_{bd} = 40$, $\mathbf{d}_{be} = 60$. For each type of users, all traffic demands between OD pair are distributed evenly to every path under initial status. There are two types of users in the network, of which the first type is more environment oriented, they have more sense of environmental protection, so their put more weight on emission parameter than the second type. The weights of two types of users are respectively:

$$\begin{aligned} \mathbf{w}_{1,1}^1 &= 0.25, \mathbf{w}_{1,2}^1 = 0.25, \mathbf{w}_{1,3}^1 = 0.4, \mathbf{w}_{1,4}^1 = 0.5, \mathbf{w}_{1,5}^1 = 0.4, \mathbf{w}_{1,6}^1 = 0.3, \mathbf{w}_{2,1}^1 = 0.25, \mathbf{w}_{2,2}^1 = 0.25, \\ \mathbf{w}_{2,3}^1 &= 0.4, \mathbf{w}_{2,4}^1 = 0.5, \mathbf{w}_{2,5}^1 = 0.5, \mathbf{w}_{2,6}^1 = 0.3, \mathbf{w}_{3,1}^1 = 0.8, \mathbf{w}_{3,2}^1 = 1.0, \mathbf{w}_{3,3}^1 = 0.8, \mathbf{w}_{3,4}^1 = 0.9, \\ \mathbf{w}_{3,5}^1 &= 1.0, \mathbf{w}_{3,6}^1 = 0.8, \mathbf{w}_{1,1}^2 = 0.5, \mathbf{w}_{1,2}^2 = 0.5, \mathbf{w}_{1,3}^2 = 0.4, \mathbf{w}_{1,4}^2 = 0.3, \mathbf{w}_{1,5}^2 = 0.5, \mathbf{w}_{1,6}^2 = 0.7, \\ \mathbf{w}_{2,1}^2 &= 0.5, \mathbf{w}_{2,2}^2 = 0.4, \mathbf{w}_{2,3}^2 = 0.3, \mathbf{w}_{2,4}^2 = 0.2, \mathbf{w}_{2,5}^2 = 0.4, \mathbf{w}_{2,6}^2 = 0.6, \mathbf{w}_{3,1}^2 = 0.5, \mathbf{w}_{3,2}^2 = 0.4, \\ \mathbf{w}_{3,3}^2 &= 0.6, \mathbf{w}_{3,4}^2 = 0.3, \mathbf{w}_{3,5}^2 = 0.5, \mathbf{w}_{3,6}^2 = 0.7 \end{aligned}$$

As is explained before, $\mathbf{w}_{2,3}^1$ means the weight of the second criterion on link 3 of user type 1, of which the second criterion is travel cost, the first is travel time and the third is emission. The travel time functions, travel cost functions and emissions functions on different links of two types of users are respectively:

$$\begin{aligned} {}_1\mathbf{t}(\mathbf{x}) &= 4x_1 + 2x_2 + 2x_3, {}_2\mathbf{t}(\mathbf{x}) = 2x_2 + x_3 + 1, {}_3\mathbf{t}(\mathbf{x}) = x_3 + 0.5x_2 + 3, {}_4\mathbf{t}(\mathbf{x}) = 7x_4 + 3x_1 + 1, \\ {}_5\mathbf{t}(\mathbf{x}) &= x_3 + 5x_2 + 5, {}_6\mathbf{t}(\mathbf{x}) = 3x_3 + 0.5, {}_1\mathbf{c}(\mathbf{x}) = 5x_1 + 1, {}_2\mathbf{c}(\mathbf{x}) = 4x_2 + 2x_3 + 2, \\ {}_3\mathbf{c}(\mathbf{x}) &= 3x_2 + x_3 + 1, {}_4\mathbf{c}(\mathbf{x}) = 6x_2 + 2x_3 + 4, {}_5\mathbf{c}(\mathbf{x}) = 4x_3 + 8, {}_6\mathbf{c}(\mathbf{x}) = 7x_3 + 2x_2 + 6, \\ {}_1\mathbf{e}(\mathbf{x}) &= 2x_1 + 4, {}_2\mathbf{e}(\mathbf{x}) = 3x_2 + 2, {}_3\mathbf{e}(\mathbf{x}) = 0.5x_3 + 4, {}_4\mathbf{e}(\mathbf{x}) = 0.5x_4 + 2, \\ {}_5\mathbf{e}(\mathbf{x}) &= 2x_5 + 1, {}_6\mathbf{e}(\mathbf{x}) = x_6 + 2 \end{aligned}$$

Suppose other parameters in the modified projection algorithm are: $\mathbf{r} = 0.01$, $\varepsilon = 0.001$.

Use the modified projection algorithm to solve the VI and the optimum flows on the six links of two types of users in equilibrium are:

$$\mathbf{x}_1 = 46.4352, \mathbf{x}_2 = 33.5648, \mathbf{x}_3 = 23.5648, \mathbf{x}_4 = 23.9059, \mathbf{x}_5 = 33.9059, \mathbf{x}_6 = 76.0941.$$

The optimum and minimum generalized cost on the six paths of two types of users are respectively:

For user type 1:

$$\mathbf{f}_1^1 = 195.3079, \mathbf{f}_2^1 = 195.3077, \mathbf{f}_3^1 = 76.0166, \mathbf{f}_4^1 = 316.1929, \mathbf{f}_5^1 = 223.3156, \mathbf{f}_6^1 = 223.315$$

For user type 2:

$$\mathbf{f}_1^2 = 282.4584, \mathbf{f}_2^2 = 282.4585, \mathbf{f}_3^2 = 62.2472, \mathbf{f}_4^2 = 156.4047, \mathbf{f}_5^2 = 195.2203, \mathbf{f}_6^2 = 195.2205$$

From the above results we can see that for each type of users, all used paths have the minimum and same generalized cost, and generalized cost of unused

paths is the same or greater than the used paths, which is in accordance with Wardrop principles.

CONCLUSION

A sustainable multi-user multi-criteria transportation network equilibrium model considering emission effects is proposed, under the hypothesis that there are many different types of users in the network and each type of users has their own emission preference, which is reflected in users' weight of emission functions. Users choose their paths based on a generalized cost which contains three criteria: travel time, travel cost and emission, each corresponds to a weight. A variational inequality problem is used to describe the sustainable multi-user multi-criteria model. Then use a modified projection method as an algorithm to solve the variational inequality problem. At last, a test network is used to verify the feasibility and practicability of the model. The model can reflect the sense of environmental protection of different types of users and their effect on the assignment of traffic flows, thus showing the importance of classification of users and criteria. However, there are still several issues haven't been solved and they need further research :(1) The demands of all types of users are fixed in the model, elastic demand or stochastic demand is more realistic, they should be considered in further researches; (2) In order to apply the model to practical, dynamic models are needed, so time-varying flows between OD pairs should be introduced.

REFERENCES

- [1] Rilett L. R., Benedek C. M. (1994) .”Traffic assignment under environment and equity of objectives.” *Transportation research record*, 1443: 92-99.
- [2] Nagurney A., Dong J., Mokhtarian P.L. (2002) . ”Traffic network equilibrium and the environment: a multicriteria decision-making perspective.” *Economics and Finance*, 501-523.
- [3] Zhang Haozhi, Gao Ziyou, Zhang Bei.(2006).”Model and algorithm of transportation network design for emission reduction.”*China Civil Engineering Journal*, 39(11):114-119.
- [4] Xiong Wei, Yan Xinping. (2008).”A modified projection method for solving a multiclass assignment equilibrium model considering emission traffic effects. “*Journal of Wuhan University of Technology (Transportation Science and Engineering)*, 32(5):786-789.
- [5] Xiong Wei, Yan Xinping. (2009).”Research on Traffic Assignment Model and Solution Algorithm Considering Emissions Effect under Different Engine Operating Modes.” *Journal of Highway and Transportation Research and Development*, 26(9):112-115.
- [6] Nagurney A. (1999). “*Network economics: a variational inequality approach (Revised Second Edition)*.” Boston, Dordrecht, London: Kluwer Academic Publishers.

- [7] Nagurney A., Dong J., Mokhtarian P.L. (2000b). "Teleshopping versus shopping: a multicriteria network equilibrium framework." *Mathematical and computer modeling*, 34.
- [8] Ji Abing, Ding Yizhong, Zhou Xizhao. (2002). "Transportation Network flow assignment model based on environment." *Environmental Protection in Transportation*, 23(1):7-9.

Transfer Mode Selection of High-speed Rail Passengers Based on Travel Time Variability

Ling JIANG¹, Shijun YU², and Yandong ZHU³

¹ School of Automation, Nanjing University of Science and Technology, Nanjing, 210094, China. E-mail: jianglingzxc@163.com

² School of Automation, Nanjing University of Science and Technology, Nanjing, 210094, China. Phone: (025)84315833; E-mail: fishte@163.com

³ School of Architecture, Southeast University, Nanjing, 210096, China. Phone: (025)83795284; E-mail: 39050992@qq.com

ABSTRACT

With the increasing concerns on timely arrival, travel time variability, which leads to the uncertainty of arrival time, becomes more important for high-speed rail passengers. This paper mainly focuses on how travel time variability impacts on the transfer mode selection of high-speed rail passengers. The variables that have significant effects on the transfer mode selection were determined, and the transfer mode selection model was presented based on the travel time variability. A stated preference experiment was conducted to collect the high-speed rail passengers' personal properties, transfer time, transfer cost, and their expected transfer modes. Then the model was calibrated with the data collected and the impacts of travel time variability on transfer mode selection were discussed. The results showed that the travel time variability of taxi has the greatest impact on high-speed rail passengers' transfer mode selection. The model proposed can be used for the transfer mode sharing forecasting and provide theoretical basis for the optimization of traffic transfer system.

INTRODUCTION

As an important external traffic node, High-speed rail station gathers various transport modes in the city. Besides achieving external transport services, high-speed rail station meet the transport organization of the city's passenger traffic transfer in cooperation with the urban transport. Generally, travel modes include subway, bus, taxi and community vehicles. In the past, travel characteristics and the level of transport properties were taken into account in the analysis of travel mode selection. Yao Liya et al.(2006) analyzed the factors affecting the residents' transfer mode choices between rail transportation and ground transportation. The result showed that travel time, costs, gender, age, occupation, income and trip purpose were all important influencing factors. In order to get the impaction of travel time and cost on all kinds of travelers, Zhao Shuzhi et al.(2009) proposed MNL model of residents' travel mode selection according to the Changchun city residents travel data. Liu Ruien(2008) used five commonly transportation modes as travel mode choice limbs, such as buses, taxis and private cars. In particular, the traveler's personal characteristic factors were taken into the MNL model to improve

prediction accuracy and usefulness of the model. We find that traveler characteristics, trip characteristics and the service level of transport facilities are all factors that influence passengers' transfer mode selection.

As the time of high-speed rail hub service line is determined, high-speed rail passengers must arrive before the trains departure. Transfer modes have variable characters because of random changes in traffic demand and different road conditions. As for the high-speed rail passengers, especially the commuters who have the ability to take high-speed rail, are more sensitive with the travel time variability. Therefore, in the analysis of high-speed rail passengers' transfer mode selection behavior, it is necessary to take travel time variability into account. In this paper, passengers' transfer mode selection model was built based on travel time variability. Theoretical analysis and verification results of the model showed that it was effective and reliable to consider travel time variability in transfer mode selection behavior analysis, with high precision and practicality.

TRAVEL TIME VARIABILITY

As an important feature of transport systems, Travel time variability adds additional costs and uncertainty to travelers, that may impact travel choices ,such as time, route and mode. Taking this factor into account can improve the existing travel behavior analysis theory. Travel time variability was classified into three categories in transport study:(1) inter-day variability;(2) inter-period variability;(3) inter-vehicle variability(Bates et al.,1987). Inter-day variability caused by seasonal and day-to-day variations, such as demand fluctuations, accidents, road construction and weather changes. Inter-period variability which reflects the impact of differences in departure times and the caused changes in congestion. And inter-vehicle variability mainly due to individual driving styles and traffic signals.

Gaver(1968) presented one of the earliest studies to investigate the relationship between individuals' behavioral and travel time variability within a framework based on utility maximization. Since 1970's, travel time variability as a variable can be seen in a large number of behavioral models(see e.g.,[Guttman,1979], [Senna,1994] and [Small et al.,1999]). These models show that it is necessary to consider the impact of travel time variability when residents choose transport modes. Many of the earlier travel time variability studies assumed that variability was the source of disutility, similar to the mean travel time, and that time variability can be represented by the variance or standard deviation of travel time(Jackson and Jucker, 1982). In order to simplify the investigation and calculation, travel time variability is measured by travel time deviation in this paper, which is equal to the absolute subtraction value between the travel time and the expected travel time.

$$B_i = |T_i - \bar{T}| \quad (1)$$

In (1), B_i ; T_i and \bar{T} denote travel time variability; measured travel time and mean travel time respectively.

Measured travel time is actual travel time of observation from the beginning to the end. Mean travel time is calculated by the arithmetic mean value of the test statistic t_1, t_2, \dots, t_n , formula is as follow:

$$\bar{T} = \frac{1}{n}(t_1 + t_2 + \dots + t_n) \quad (2)$$

Theoretical Frameworks

This paper assumed that traveler's selection behavior obeyed the principle of utility maximization. Assuming that factor which affected the transfer mode choice had an influence on the overall effectiveness of passengers, passengers always chose the most effective transfer modes.

According to random utility theory, traveler n choose transfer mode i , the utility function U_{in} can be expressed as follows:

$$U_{in} = V_{in} + \varepsilon_{in} \quad (3)$$

Where V_{in} is the observable fixed item of the utility function; ε_{in} is unobservable random fluctuation item. When there is a linear relationship between V_{in} and contained description variables, the utility function is expressed as:

$$V_{in} = \theta \bullet X_{in} = \sum_{k=1}^K \theta_k X_{ink} \quad (4)$$

Where X_{ink} is k th characteristic variable that n th traveler choose i th transfer mode; K is the number of characteristic variables; θ_k is parameter values that solve the model, reflecting the utility value sensitivity of corresponding changes.

According to MNL model, n th passenger choose i th transfer mode, probability expression as follows:

$$P_{in} = \frac{\exp(V_{in})}{\sum_{j \in A_n} \exp(V_{jn})} \quad (5)$$

Where P_{in} is the probability that n th passenger choose i th connected mode; V_{in} is fixed item of the utility function that n -th passenger choose i th connected mode; A_n is the sets of transfer modes for travelers.

The parameters can be obtained by using maximum likelihood estimation and Newton—Raphson method (see e.g., [Yao Yali,2008] and [Guan Hongzhi,2004]).

TRANSFER MODE SELECTION MODEL

Factors Analysis

High-speed rail passengers are most concerned about how to reach the high-speed rail station quickly using less costs (refer to generalized cost), whose travel behavior are dominated by transport needs. Passengers consider a variety of travel modes available between origins and destinations before departure, the most satisfactory mode will be chosen after judgment.

Mode selection model should be able to imitate judging progress of travelers appropriately, so main factors that affect the modes selection would be taken into account. Four aspects of travel mode selection factors in this paper are traveler characteristics, travel characteristics, the service level of transport facilities and travel time variability. Traveler characteristics include personal or family basic properties, such as private car ownerships, age, occupation and family income. As travel characteristics, travel time and trip distance may also have impact on travel mode selection. For example, travelers may be opt to take subway if the starting time is in the morning peak period. The service level of traffic facilities includes costs, time-consuming, comfort and reliability. Walking time to the station, waiting time are both important factors. With the increasing concerns on timely arrival for high-speed railway passengers, travel time variability is an important factor which has an impact on travel mode choice.

Mode Selection Model

According to survey data of passengers' travel characteristics in Nanjing South Station in 2011, three main transfer modes were bus, subway and taxis. In order to simulate high-speed rail passengers' mode selection process as accurately as possible, we selected gender, transfer time, costs and travel time variability as characteristic variables. 56% male, 44% female were in transferring high-speed railway station. Settings of model variables are shown in Table 1.

The utility function expressions for three kinds of connecting modes:

$$\text{Bus 1: } V_{1n} = \theta_1 X_{1n1} + \theta_3 X_{1n3} + \theta_5 X_{1n5} + \theta_6 X_{1n6} + \theta_7 X_{1n7} \quad (6)$$

$$\text{Subway 2: } V_{2n} = \theta_2 X_{2n2} + \theta_4 X_{2n4} + \theta_5 X_{2n5} + \theta_6 X_{2n6} + \theta_7 X_{2n7} \quad (7)$$

$$\text{Taxi 3: } V_{3n} = \theta_5 X_{3n5} + \theta_6 X_{3n6} + \theta_7 X_{3n7} \quad (8)$$

After estimating the parameters that affect the results, transfer modes selection model based on travel time variables will be achieved.

Table 1. Settings of Model Variables

Options	Options constant		Options features				
	Dum-my1	Dum-my2	Gender		Transfer time (min)	Travel cost (RMB)	Travel time variable (min)
Variables	X_{in1}	X_{in2}	X_{in3}	X_{in4}	X_{in5}	X_{in6}	X_{in7}
Bus	1	0	Male:1 female:0	0	Actual value	Actual value	Actual value
choice Sub-limbs way	0	1	0	Male:1 Female:0	Actual value	Actual value	Actual value
Taxi	0	0	0	0	Actual value	Actual value	Actual value
Parameter	θ_1	θ_2	θ_3	θ_4	θ_5	θ_6	θ_7

Calibration

In the model, transfer time is travel time from origin to high-speed railway station; cost is total cost of this trip; travel time variability is calculated by formula 1 and formula 2. According to the survey results, we input characteristic variable values and calibrate the utility function coefficients using biogeme software. Related statistics results are shown in Table 2:

Table 2. Coefficient Calibration and Test Values

Variable Number	Description	Coeff. estimate	Robust Asympt. Std.error	t-stat
1	θ_1	2.79	0.890	3.13
2	θ_2	0.34	0.681	0.50
3	θ_3	-0.605	0.688	-0.88
4	θ_4	0.534	0.522	0.97
5	θ_5	-0.0573	0.0174	-3.30
6	θ_6	-0.0366	0.0234	-1.56
7	θ_7	-0.242	0.0948	-2.55

From the model's accuracy analysis, $\rho^2=0.248$, generally it is acceptable when the value is from 0.2 to 0.4. So the model can be used to describe the passengers' selection behavior, and the chosen factors may affect the selection results of high-speed rail passengers. But t-stat of gender is relatively small,

indicating that it has less affection. Therefore, we re-calibrate after removing this gender property, the results are shown in Table 3:

Table 3. Coefficient Calibration and Test Values

Variable Number	Description	Coeff. estimate	Robust Asympt. Std.error	t-stat
1	θ_1	1.85	0.622	2.98
2	θ_2	-0.0128	0.135	-0.09
5	θ_5	-0.0483	0.0144	-3.35
6	θ_6	-0.0467	0.0192	-2.43
7	θ_7	-0.260	0.0809	-3.21

$\rho^2=0.248$, which meets the accuracy requirements. The symbols of calibration coefficients are negative, indicating that the effectiveness of the transfer modes is reducing with transfer time, travel cost and travel time variability increasing. $|t|$ is the statistical parameters of total transfer time, travel cost and travel time variability, and $|t| > 1.96$ indicates that the three variables have significant influence on the selection behavior under a confidence level of 95%. Modeling results show that there is a more stable relationship between the passengers' transfer mode selection and transfer time, travel costs, travel time variability.

The value of $|\theta_7|$ is maximum, so travel time variability has the most affection on passengers' transfer mode selection when travel time, cost, travel time variability and other factors all affect the passengers' transfer mode selection. For the high-speed rail passengers, the importance of travel time variability is greater than travel time and travel cost. From calibration results, $|\theta_7|/|\theta_5|=5.38$, $|\theta_7|/|\theta_6|=5.57$. In other words, the utility of 1 minutes travel time variability reducing is equal to 5.38 minutes total travel time reducing, or ¥ 5.57 reducing of total travel cost. Assuming travel time variability is very small, probability of the mode being selected is large even if transfer time is long and travel cost is high.

According to the coefficient of obtained utility function, the utility function expression is determined. We can predict variety transfer modes proportions of different high-speed rail passengers. For example, according to passengers' survey data and history data, the proportion of bus transferring to high-speed rail may be predicted, from that we can reduce travel time variability by optimizing bus departure schedules, bus lines, etc, which will improve the efficiency of bus operations, so it is more comfortable and convenient for travelers' transferring. Travel time variability as an important factor is taken into account in the model, it is a more comprehensive way to analyze passengers' transfer modes selection

behavior, and it will play an important role on travelers' behavior analysis in the future.

CONCLUSION

Characteristics and representations of travel time variability were discussed after analyzing previous studies. Transfer mode selection model was constructed based on travel time variability, which was used to analysis transfer mode selection behavior of high-speed rail passengers in Nanjing. The model was high consistent with actual situation, and it had more comprehensive consideration of various factors.

The main findings can be summarized as follows:

- (1) Unlike previous studies, we introduced travel time variability to analyze transfer mode selection behavior. It can improve transfer mode selection model's prediction accuracy and usefulness.
- (2) Model parameters calibration results showed that travel time variability had a great influence on mode selection. The larger travel time variability was, the smaller probability of being chosen was. The influence of travel time variability is five times more than transfer time and travel cost.
- (3) In order to meet the needs of current passenger transit transferring and long-term development of urban transport, it is necessary to analyze passengers' transfer mode selection behavior of high-speed station. Therefore, we set the passengers' transfer prediction of Nanjing high-speed rail South Station as an example, but the overall ideas and methods can be applied to passengers' transfer options prediction of other types of transportation. This method is also the main basis for determining size of transfer station facilities, operating organization and convergence transfer program.

ACKNOWLEDGEMENTS

The research team would like to give thanks to the Natural Science Foundation of Jiangsu Province for providing foundation-the project "Traffic and Land Space coupling Mechanism of High-speed Railway Station Area in China". (No. BK2009258).

REFERENCES

- Bates, J., Dix, M., May, T. (1987) "Travel time variability and its effect on time of day choice for the journey to work." [C]: Transportation Planning Methods, Proceedings of Seminar C held at the PTRC Summer Annual Meeting, vol. P290, pp. 293-311.
- Gaver, D.P. (1968), "Headstart strategies for combating congestion." *Transportation Science* 2, pp. 172-181.
- Guan Hongzhi. (2004), "Disaggregate Model-A Tool of Traffic Behavior Analysis." [M]: People's Communications Press.
- Guttman J.M. (1979), "Uncertainty, the value of time, and transport policy,"

- Journal of Transport Economics and Policy 13 (2), pp. 225–229.
- Jackson W.B. and Jucker J.V. (1982), “An empirical study of travel time variability and travel choice behavior.” *Transportation Science* 16 (6), pp. 460–475. View Record in Scopus | Cited By in Scopus (26).
- Liu Ruien, Juan Zhicai, Li Yanling. (2008) “Development of a Multinomial Logit Model for Travel Mode Choice of Residents.” [J]: *JOURNAL OF HIGHWAY AND TRANSPORTATION RESEARCH AND DEVELOPMENT*, 25(5):116-120.
- Senna L.A.D.S. (1994), “The influence of travel time variability on the value of time.” *Transportation* 21, pp. 203–228. Full Text via CrossRef | View Record in Scopus | Cited By in Scopus (13).
- Small, K.A., Noland, R.B., Chu, X., Lewis, D. (1999). “Valuation of travel-time savings and predictability in congested conditions for highway user-cost estimation.” NCHRP Report 431, Transportation Research Board, National Research Council.
- Yao Liya, Guan Hongzhi, Sun Lishan, Chen Shuhong (2006). “Public transport travel mode choice influencing factors analysis.” [C]: Proceedings of the 6th International Conference of Transportation Professionals (Vol.1).
- Yao Yali. (2008), “Study on rail traffic volume demand forecasting methods based on Disaggregated Model.” [D]: Beijing Industrial University, Beijing Key Laboratory of Traffic Engineering.
- Zhao Shuzhi, Zhao Bei, Zhu Yonggang. (2009) “Choice model of trip mode and policy of public transport priority based on SP survey.” [J]: *Journal of Jilin University (Engineering and Technology Edition)*, 39(2):187–190.

Miami Intermodal Center: Airport Connection for the Future

L. David Shen¹

¹Lehman Center for Transportation Research (LCTR), Florida International University, *Miami's public research university*, Miami, Florida, 33174; PH (305) 348-3814; FAX (305) 348-2802; e-mail: ShenL@fiu.edu

ABSTRACT

The \$2 billion Miami Intermodal Center (MIC) project is the most advanced and forward-looking “all-in-one” airport intermodal center in the U.S. It has four major components: 1) the Rental Car Center (RCC) opened for business on July 13, 2010; 2) the Miami International Airport (MIA) Mover opened to the public on September 9, 2011; 3) the Metrorail Airport Link is scheduled to open in April 2012; and 4) the Miami Central Station (MCS) is scheduled to be completed by September 2013. The Tri-Rail connection at MCS allows MIA to serve as the convenient international get-away airport of choice for the entire South Florida, from Palm Beach to the north to the Ft. Lauderdale in the middle, thus enlarge the service radius of MIA from 30 miles to 70 miles. The MIC enables MIA to continue grow without worrying about the ever-worsening ground access problems other airports have to face and deal with.

INTRODUCTION

In the late 1980s, with the Miami-Dade County's population growing and moving westward, serious traffic congestion problems become part of daily life in South Florida. Local officials foresaw the need to create transportation connectivity; this will not only encourage the use of public transit, but also alleviate ever-worsening traffic problems [Shen, 2002]. At the same time, the area's vital aviation industry forecast the need to decongest roadways in and around Miami International Airport (MIA), one of the largest international airports in the country and Miami-Dade County's most important economic generator.

Since the creation of a major connection hub near MIA will involve the participation of various federal, state, and local agencies; Florida Department of Transportation (FDOT) was asked to be in charge of this ambitious task, at the time, the most ambitious intermodal transportation project in the country. The goal is to link the community's disparate transportation services and to find a way to relieve MIA of the burdensome traffic that was clogging its access roadways and terminal ramps [FDOT, 2008].

In 1995, FDOT's Major Investment Study (MIS)/Draft Environmental Impact Statement (DEIS) for the MIC was approved by the Federal Highway Administration, and in 1998 a Record of Decision by the US Department of Transportation (USDOT) was granted giving location and design concept approval. There were numerous meetings between FDOT and various federal, state, and local agencies in finding the optimum solution to meet all stake-holders' interests. FDOT plays a key role in

leading the design and construction of the MIC Program in partnership with USDOT, Miami-Dade County, and Miami-Dade Expressway Authority and the South Florida Regional Transportation Authority. To facilitate the process, a consultant management group assists FDOT in the planning, design and implementation of the program. Highway and access roads have been completed. Construction on the Rental Car Center began in August 2007 and opened for business on July 13, 2010.

The MIC is the first fully integrated (all-in-one) airport intermodal centers in the U.S. The MIA-MIC automated people mover (MIA Mover) opened to the public on September 9, 2011 allows quick and easy connection between MIA and MIC. The Miami Central Station, which includes Airport Link (Miami’s Metrorail extension to MIC), Tri-County (Miami-Dade, Broward, and Palm Beach Counties) Commuter Rail (Tri-Rail), Amtrak, and bus services is currently under construction and scheduled to be completed by September 2013 [2011-7]. When completed in 2013, the MIC will become the country leading airport intermodal center with driverless MIA people mover provide fast and convenient connection to the largest international airport in the southeast. In addition, it will also provide commuters and travelers in South Florida to go to and from airport with Metrorail and Tri-Rail, further reducing traffic congestion. It also has one of the largest consolidated rental car facilities in the country, allowing travelers smooth airplane to car transition. The MIC is gradually becoming a reality after nearly 20 years of planning and design [Shen, 2002]. The MIC site map is shown in Figure 1.

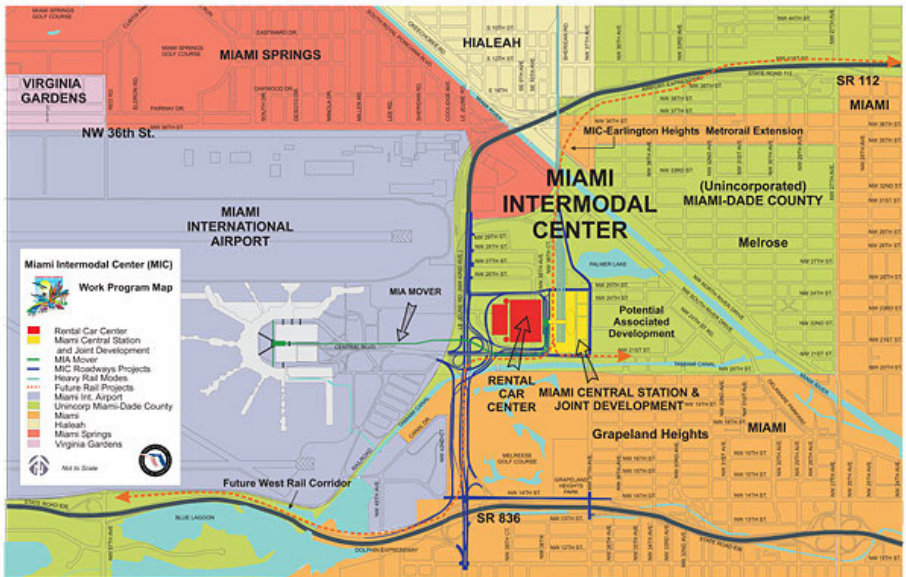


Figure 1. The Miami Intermodal Center (MIC) site map [FDOT, 2011-7].

OVERVIEW

The \$2 billion plus MIC project has six components and they are [FDOT, 2011-7]:

- 1) Right of way and environmental - \$339 M,
- 2) Roadway improvements - \$187 M,
- 3) Rental Car Center (RCC) - \$395 M,
- 4) MIA Mover - \$270 M,
- 5) Miami Central Station (include Airport Link) - \$739 M, and
- 6) Program contingency and other costs - \$113M.

Before the MIC Program could be built, FDOT needed to acquire the land that they were building the facilities on. Early on, FDOT allocated \$350 million for Right-of-Way (ROW) acquisition, laying the groundwork for the entire MIC Program (see Figure 2). Had all the land not been assembled at one time, skyrocketing costs would have made the program prohibitively expensive. FDOT initiated a speedy ROW acquisition plan in order to secure rights over the needed land, due west of MIC [FDOT, 2008].

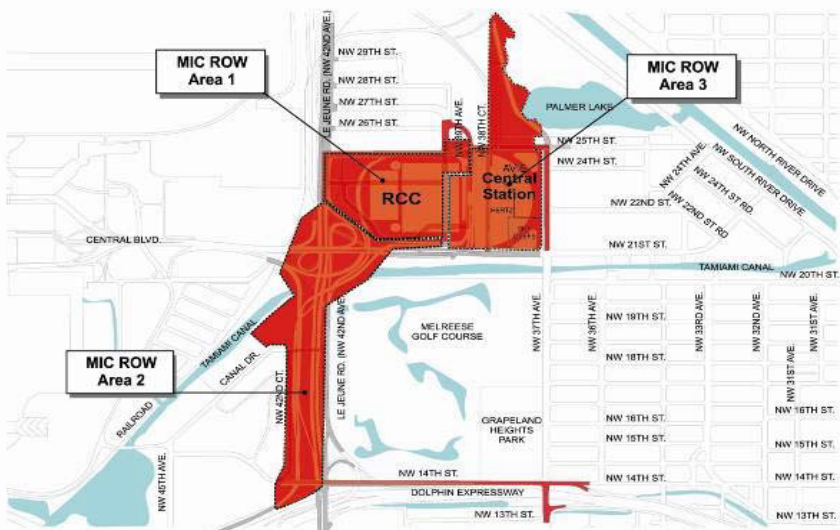


Figure 2. Right of way acquisition plan for the MIC [FDOT, 2008].

The 3.4 million square feet, 6500 car-capacity Rental Car Center (RCC) is designed to minimize the hassle of renting a car and in the process, make it safe and reduce traffic congestion at airport that was created by the endless moves of rental car company courtesy vans. It was first opened on July 13, 2010. The cost of the RCC is estimated to be over \$348 million. It decongests the MIA curbside traffic by 30%, and further reduces air pollution in the terminal area [FDOT, 2011-3]. All rental car

companies operating inside MIA and many located near the airport have relocated into the RCC's four level building. This leads to significant reduction in traffic congestion in the arrival/departure terminals and airport roadways.

The first three floors of RCC are dedicated to storage and maintenance operations and the fourth level accommodates a spacious customer service lobby where vehicle renters enter and choose their best option among rental car company offers - a virtual rental car shopping mall [FDOT, 2011-3]. The interior look of the 4th floor of RCC is shown in Figure 3. Permits and other safety precautions needed to be made because each floor will house a fuel distribution center where gasoline may be pumped into the rental cars. The Miami RCC will be the first building in the United States to have elevated fuel distribution capability.

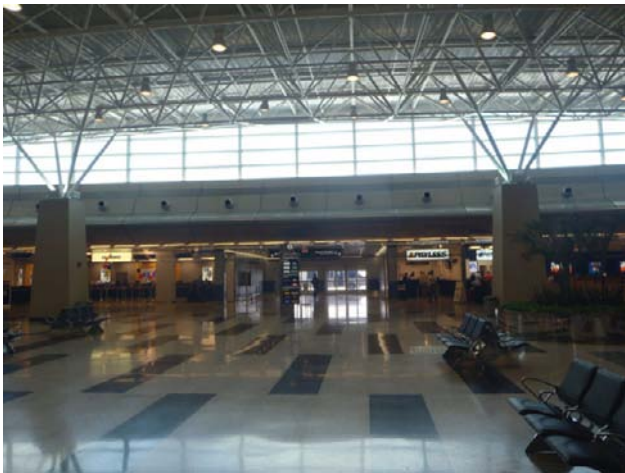


Figure 3. Spacious interior of the Rental Car Center (RCC).

The MIA Mover is a driverless transit (automated people mover) that travels between the MIA, the RCC, and the Miami Central Station. The Miami-Dade Aviation Department began construction on it on March 2, 2009 and was operational in September 2011. It was designed to have two stations; one located in the MIA on the third level in between the Flamingo and Dolphin garages (see Figure 4) and the other on the fourth level of the RCC, right next to the Miami Central Station where passengers can board the Metrorail and Tri-Rail starting in April 2012 and September 2013 [FDOT, 2011-12].

The MIA Mover is an important component of the MIC Program because it is an intermodal connector. It is a driverless transit line (reduce labor costs and could operate 24-7) that will link the airport to Amtrak, Tri-Rail and Metrorail, upon completion of the Airport Link. This brings travelers a host of transportation options and further encourages the use of public transportation. It will serve the growing number of air passengers using MIA, which totaled 35.7 million in 2010, who rent vehicles or choose to use public transportation to reach their destination. It will also

allow airport employees and greeters/well-wishers to travel to airport by public transit.

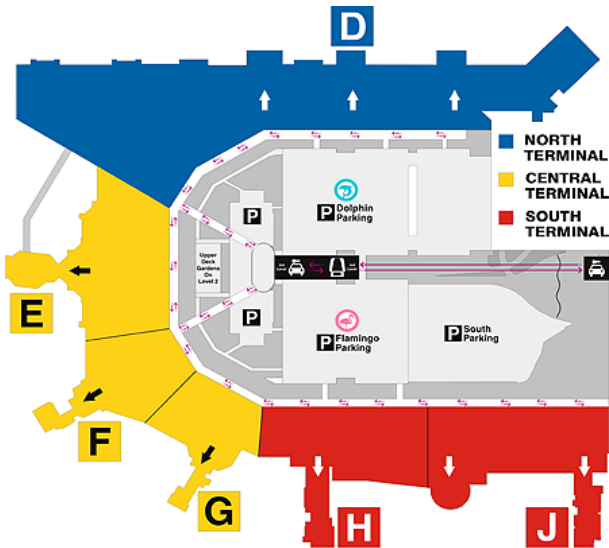


Figure 4. MIA Mover station at Miami International Airport [FDOT, 2011-12].

The MIA Mover will also decongest the traffic on the roads around the airport because the rental car shuttles that used to crowd the terminals will be removed. It is estimated that once the MIA Mover is operational, the need for more than a half-million shuttle bus trips to off-site rental car companies each year will be eliminated, a significant traffic reduction and an air pollution improvement [FDOT, 2011-12].

The MIC program schedule is shown in Table 1. The Airport Link: Metrorail (Rail Rapid Transit) extension from existing Metrorail Earlington Heights Station is currently underway as most civil engineering construction is finished and the link is scheduled to open in April 2012. The rendering of Miami Intermodal Center is shown in Figure 5 [2011-12].

Table 1. Miami Intermodal Center Program Schedule.

Component	Phase	Date
Roadway Improvements - ROW acquisition - Roadway improvements	Completed Completed	December 2003 November 2009
Rental Car Center	Operational	July 2010
MIA Mover	Operational	September 2011
Miami Central Station (Airport Rail: 2.4 mile extension of Metrorail)	Construction Construction	September 2013 April 2012

The Miami Central Station (MCS) is anticipated to be the largest public transportation hub in Florida. The goal of the MCS is to offer connectivity through a variety of transportation modes. The comparison of MIA MIC and other airports is shown in Table 2. Developed around the existing Tri-Rail tracks at its Airport Station, the MCS (center of Figure 5) will feature grade level tracks for Tri-Rail, Metrorail (upon completion of the Airport Link), Amtrak, and future High-Speed Rail (HSR) service. Even though the Florida HSR has been an on and off topic of discussion over the last 25 years, its future development could not be ruled out and thus was factored in the planning and design of MIC. On the ground level of MIC, arrangements were made so bus depots will be located for Greyhound, Miami-Dade Metrobus, intercity buses, courtesy buses and passenger shuttles currently serving MIA, and taxis.



Figure 5. The rendering of Miami Intermodal Center [FDOT, 2011-12].

Table 2. Comparison of MIA-MIC and other Major Airports in the U.S.

U.S. Rank	Airport	2010 Passengers In Millions	Direct Rail Connection		APM to Airport Connection		
			Rail Rapid Transit	Commuter Rail	Rail Rapid Transit	Commuter Rail	Rental Car Center
1	Atlanta	89.3 M	X				X
2	Chicago	66.8 M	X				
3	Los Angeles	59.1 M					
4	Dallas - Ft. Worth	56.9 M		X			
6	New York JFK	46.5 M			X	X	X
9	San Francisco	39.3 M	X				X
12	Miami	35.7 M			X	X	X

As indicated in the center of Figure 5, an elevated pedestrian walkway will also span across the rail tracks from the public walkway into the MIA Mover's MIC Station, which is located right next to the RCC (upper left of Figure 5). The MIA Mover MIC Station is located west of the MCS at the fourth level next to the RCC Customer Service Lobby. The MIA Mover, which opened for service in September 2011, is designed to take passengers to and from MIA into the MIC. Upon their arrival they may choose to go into the RCC so they could rent cars; or continue into the MCS through the elevated pedestrian walkway to take either Metrorail, Tri-Rail, or Amtrak trains; or they could proceed to the east side of the MCS to board local, express, or long-distance buses. The MCS is expected to be a main transfer point between rail and bus systems and is currently under construction. The Metrorail Airport Link is scheduled to open for service in April 2012. The MCS construction will be completed in September 2013. The estimated cost of the MCS, not including the Airport Link (\$540 M) or the MIA Mover station (\$52M), is \$147 million [FDOT, 2011-7].

SUMMARY AND CONCLUSIONS

The major findings of this study can be summarized as the follows:

- 1) The MIC is the most advanced (all-in-one) and forward-looking airport intermodal center in the U.S. with consolidated rental car center, MIA Mover, rail rapid transit, commuter rail, Amtrak, and bus services all integrated into one convenient multi-modal transportation center.
- 2) Consolidated RCC allows passengers seamless transition between air transportation and highway transportation.
- 3) Due to land availability issue, the MIC is located about one mile east of the airport, however, with MIA Mover driverless transit, the integration and connection is seamless.
- 4) By removing rental car company courtesy vans and other shuttles away from MIA, MIC greatly facilitates the passenger traffic flows at MIA.
- 5) By integrating various public transportation modes, the MIC has the positive impact of alleviating parking shortages at MIA.
- 6) The RCC at MIC allows significant reduction of previous commercial van circling traffic at MIA and further improves the air quality at the arrival curbside (lower level roadway).
- 7) The Tri-Rail connection at MIC allows MIA to serve as the convenient international get-away airport of choice for the entire South Florida, from Palm Beach to the north to the Ft. Lauderdale to the middle, thus enlarge the service radius of MIA from 30 miles to 70 miles.
- 8) The MIC enables MIA to continue grow without worrying about the ever-worsening ground access problems other airports have to face and deal with.

REFERENCES

Florida Department of Transportation (FDOT), Miami Intermodal Center (MIC) Website, December 12, 2011, Miami, Florida.
<<http://www.micdot.com/index.html>>.

- Florida Department of Transportation (FDOT), Miami Intermodal Center: Project Overview, July 27, 2011, Miami, Florida.
- Florida Department of Transportation (FDOT), the Miami Intermodal Center, Transportation Infrastructure Finance and Innovation Act (TIFIA) presentation, July 26, 2011, Miami, Florida.
- Florida Department of Transportation (FDOT) and Miami-Dade Department of Aviation, Quick Response Vehicle Safeguards Public at Miami Rental Car Center, March 8, 2011, Miami, Florida.
- Florida Department of Transportation (FDOT), Miami Intermodal Center, presentation to the Regional Transportation Committee, March 7, 2011, Miami, Florida.
- Florida Department of Transportation (FDOT), Miami Intermodal Center Brochure, Fall 2008, Miami, Florida.
- Shen, L.D., Planning and Design of Intermodal Center, Lehman Center for Transportation Research (LCTR), Florida International University, Miami, Florida, 2002.

Driverless Medium-Capacity Transit as an Airport Connector: Taipei's Experience

Jiun-Jia Hsu¹ and L. David Shen²

¹Dept. of Transportation Technology and Management, Kainan University, No.1 Kainan Road, Luzhu Shiang, Taoyuan 33857, Taiwan; PH(886)3-341-2500; FAX(886)3-270-5695; e-mail: jjhsul@gmail.com.

²Lehman Center for Transportation Research, Florida International University, *Miami's public research university*, 10555 W. Flagler Street, Miami, Florida 33174; PH(305)348-3814; FAX(305)348-2802; e-mail: ShenL@fiu.edu

ABSTRACT

The one-runway Taipei Songshan Airport is located near the center of Taipei city and was the only international airport in Taiwan prior to February 26, 1979. The airport lost most of the traffic when international flights moved to the new Taoyuan International Airport after 1979. Regular cross-strait charter flights to mainland China started on July 4, 2008, with Songshan receiving the majority of flights. On July 4, 2009, a driverless medium-capacity transit (MCT) linking Taipei Songshan Airport with Taipei rapid transit system network (total system daily ridership of 1.56 million) was opened. The improved accessibility makes the airport more attractive to passengers. The smaller size of the MCT vehicles makes it difficult for airport passengers with luggage to get in and out during the rush hours when the system is already at capacity. The seating arrangement of the MCT vehicles further complicates the situation and improvements in new vehicle design should be considered to alleviate this problem.

INTRODUCTION

Taipei Songshan Airport (TSA) is located in the heart of Taipei City. The airport was constructed in 1936 and was mainly used for military purposes at that time. As air transportation takes off after World War II, civilian flights increase significantly at the airport. TSA is the only international airport in Taiwan prior to February 26, 1979 and one of the oldest airports in Taiwan. The airport lost most of the traffic when international flights moved to the new Taoyuan International Airport after 1979, about 22 miles southwest of Taipei. The airport slowly built up traffic (mainly north to south inter-island domestic flights) and reached its peak in 1996. When Taiwan High Speed Rail began service on the same route in 2007, the passenger load at the airport dropped sharply from 6.7 million in 2006 to 4.4 million in 2007. Regular cross-strait charter flights to mainland China started on July 4, 2008, with Songshan receiving the majority of flights. This new development injects new life to this old airport. Starting in October, 2010, EVA Air, China Airlines, Japan

Airlines, and ANA will each operate two flights a day from Taipei-Songshan to Tokyo-Haneda airports, an attractive, direct downtown-to-downtown airport flight service.

Airport ground access is one of the most important factors in airport planning and design. Public transportation with exclusive right of way is an attractive option for airport passengers, greeters, and airport employees to by-pass the congested roadway to get to and from the airport. Most major airports around the world have fixed guideway transit connection to the center of the cities they serve. Guideway transit serving the airports ranges from the most popular Rail Rapid Transit (RRT), to Light Rail Transit (LRT), to Commuter Rail (CR), and Driverless Medium-Capacity Transit (MCT). Some airports also have High-Speed Rail (HSR) connection, thus enlarge their service radius from 30 miles to more than 200 miles as is the case of Charles de Gaulle International airport in Paris (CDG). On July 4, 2009, a driverless medium-capacity transit (MCT) linking Taipei Songshan Airport with Taipei rapid transit system network (total system daily ridership of 1.56 million) was opened (see Figure 1). The underground driverless MCT station is located just south of Terminal 1 and has convenient direct underpass connecting the airport Terminal 1. This greatly increases the popularity of the airport for business travelers who routinely commute from Taipei to major cities in China such as Beijing, Shanghai, and Guangzhou.

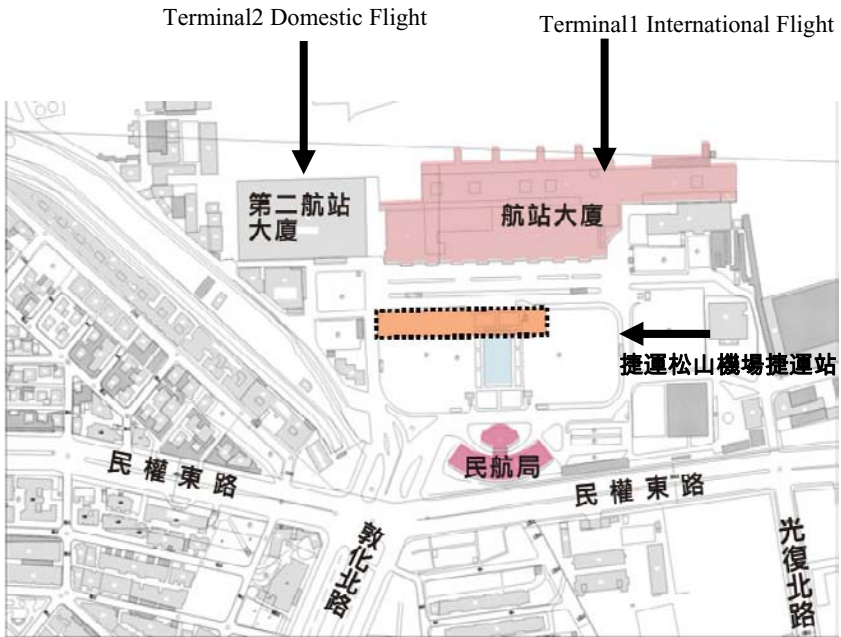


Figure 1. The layout of Taipei Songshan Airport (TSA). (1)

In early 2000, planning for additional business and leisure travelers from China and Japan to visit TSA, the government initiated a USD\$2 billion project to connect TSA to the Taipei Rapid Transit Network. This is basically an extension of the original driverless MCT (Brown Line) which stops just a mile south of the airport, at Zhongshan Junior High School north to TSA and continues to Neihu and Nankang in the northeast (see Figure 2). This extension was opened on July 4, 2009.

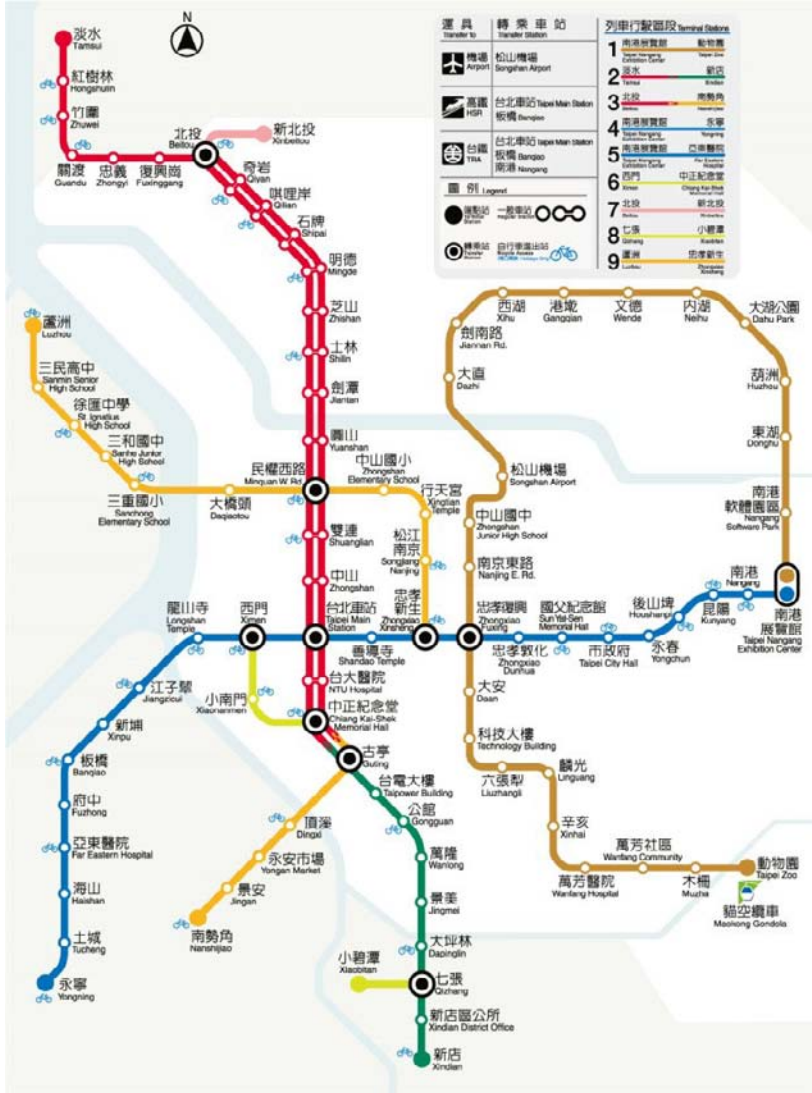


Figure 2. Taipei Rapid Transit System Route Map. [TRTC, 2011]

OVERVIEW

The airport connector at TSA is an extension of the driverless MCT Muzha Line (Brown Line) in a mostly high-capacity Rail Rapid Transit (RRT) network. Taipei rapid transit system network has a total system daily ridership of 1.56 million at the end of 2011 [TRTC, 2011]. The 16-mile (25.7 kilometers) Brown Line driverless MCT accounts for more than 181,800 daily passengers in 2011, about 9,000 passengers a day were getting on and off at the Songshan Airport Station. The Brown Line, after extension opened in July 2009, connects Muzha Taipei Zoo Station in the southeast corner of Taipei to Taipei Nangang Exhibition Center in the northeast. The daily passenger rate of 11,362 per route mile is more than Washington, D.C. Metrorail and most U.S. RRT systems. This is a clear indication of the Brown Line driverless MCT's success.

Many passengers of direct flights to mainland China and Japan use this new rapid transit service. The average saving time in using TSA rather than the further away Taoyuan International Airport is more than an hour each trip – a major travel time reduction and game changer. The popularity of the airport grows substantially as the location of the airport (right in the center of the city) and its convenient rapid transit access becomes a strong selling point of the airport. However, what separated Taipei from other cities who have similar driverless MCT service: it is the only one that is located in the middle of a 16-mile (25.7-km) north to south trunk line service of a large metro area of 6.9 million people (see Figure 3).



Figure 3. Brown Line: a driverless MCT system in Taipei, Taiwan.

The original Brown Line (Muzha Line) 4-car train used VAL 256 cars built by Matra (now part of Siemens Transportation Systems) in 1993. The Muzha Line began service on March 28, 1996. The Brown Line extension to the airport (TSA) and beyond (Neihu Line) opened on July 4, 2009. The extension 4-car train is built by Bombardier in 2006. Due to problems encountered in integrating two different proprietary automated people mover technologies, many problems and systems shut-downs were experienced in the summer of 2009. This is highly unusual for a driverless MCT system to have two completely different technologies integrated into one system. In hindsight, many of the people involved in this would hope that this problem could have been avoided in the beginning. The comparison of Matra (Muzha Line) and Bombardier (Neihu Line) driverless MCT cars is shown in Table 1. Even though the new Bombardier car is only 0.02 meters narrower than the Matra car, many passengers complain about the new car is too narrow (see Figure 4).

Table 1. Comparison of Matra and Bombardier Vehicle Design

Builder	Year Built	Car Length In meters	Car Width In meters	Seating Capacity Per Car	Total Capacity Per Car	Maximum Speed In km/hr	Total # of Cars Purchased
Matra	1993	13.78	2.56	24	114	80	102
Bombardier	2006	13.78	2.54	20	142	80	202



Figure 4. Interior of the new Bombardier car (MCT Neihu Line).

The problem facing airport passengers is that since the airport station is not the end-of-line station but in the middle of the system; during rush hours when the MCT trains are packed with passengers, it would be a real challenge for passengers with luggage the squeeze through the doors to get in or out. Subsequently, many complaints from the passengers were received about this “lack of room” problem. It

is noted by the authors that the seating arrangement and vehicle interior design may also contribute to this problem. The blue bench seats may be wider than desired and further reduce the middle “isle” width (see Figure 4). If passengers facing each other extend their legs when seated, there won’t be any room for standing passengers, let alone an airport passenger with luggage. The monthly ridership total for the MCT Songshan Airport station in 2010 is shown in Figure 5. As can be seen from Figure 5, traffic at TSA station continues to grow in 2010 and at the end, December 2010, an average of more than 8,000 passengers ($2 \times (120,000 / 30) = 8,000$) each day entering and exiting the airport station.

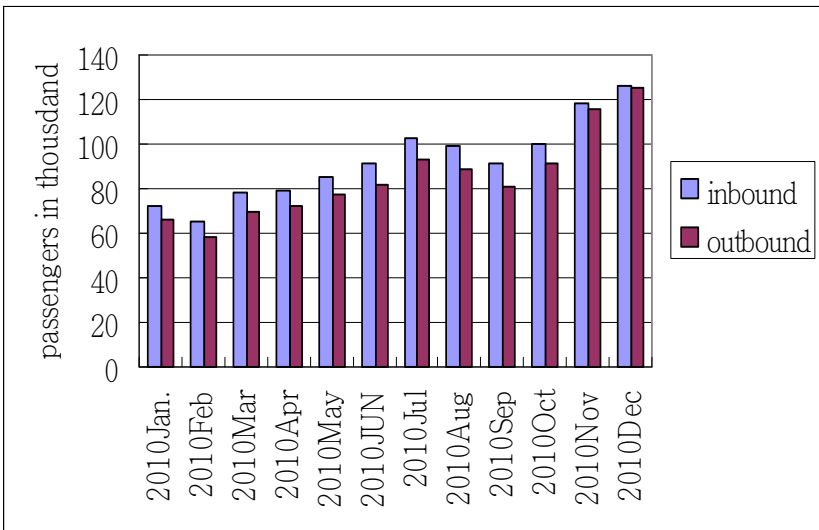


Figure 5. Monthly passengers total at MCT Songshan Airport Station in 2010.

Taipei is a much larger metropolitan area than Lille or Vancouver. Unlike Lille or Vancouver, it also has a predominantly heavy rail (Metro) system with the driverless transit system accounts for only 12 percent of the total rapid transit system. The phase I of Brown Line is the 10.9 km and 12-stations Muzha Line (now Wenshan Line after October 8, 2009) in Taipei was built at a cost of approximately USD\$84 million/km (USD\$135 million per mile) in the early 1990s. It is a fully automated, driverless; rubber tire on concrete track system that is based on the Siemens VAL system design (entire VAL system has been removed and now operated by Bombardier CITYFLO 650 system), with maximum capacity of 30,000 passengers per hour per direction.

The Neihu Line (Phase II of Brown Line) is the extension of phase I; it opened for business on July 4th 2009. The Neihu Line continues as a mostly elevated

and partially underground driverless transit system. The system starts from the northern end of the Muzha Line (now Wenshan Line) – Zhongshan Junior High School Station and heading north to the Taipei Songshan Airport, continues eastward toward Neihu and Nangang (see Figure 2). Its total length is approximately 14.8 km (9.2 miles) with 12 stations and one maintenance depot. The construction budget is approximately USD \$2.02 billion (USD \$136.5 million per km or USD \$218.4 million per mile). The route has been lengthened by 1.9 km over the original plan because of the addition of Songshan Airport (old Taipei Airport) Station (2). This airport is the first airport connected with metro system in northern Taiwan. Comparison of various driverless MCT systems around the world is shown in Table 2.

Table 2. Comparison of Various Driverless MCT Systems around the World

City	City/Metro Population in Millions	Daily MCT Ridership	MCT System Length in Miles	Daily Passengers Per Route Mile	Connection To Airport
Taipei, Taiwan	2.62/6.90	181,800	16.0	11,362	YES
Lille, France (VAL)	0.23/1.16	262,465	28.4	9,242	NO
Vancouver (SkyTrain)	0.59/2.12	406,300	42.8	9,493	YES
London (Dockland LR)	7.83/13.95	192,000	21.0	9,143	YES

Taipei MCT system is similar to Lille (France) vehicles in sizes and both are much smaller than Vancouver's SkyTrain or London's Dockland Light Railway. Both Vancouver and London's MCT systems use steel wheel on steel track technology, versus Taipei/Lille's rubber tire on concrete track technology. London and Vancouver MCT trains are much wider and longer than Taipei and Lille, thus higher in capacity potential. It is clear from the table that Taipei's MCT has the highest daily passengers per route mile – an interesting fact reflecting Taipei's higher population density over the other three cities. In Vancouver, the airport station is located at the end of Canada Line (opened in 2009). The Dockland Light Railway's London City Airport Station is near the end of the line (southeastern corner of London).

SUMMARY AND CONCLUSIONS

The findings from this study can be summarized as the follows:

- 1) Taipei Songshan Airport driverless MCT connection gives passengers more choice is consistent with international airport development trend.

- 2) Airport passengers have a difficult time getting in and out of the driverless MCT trains during the rush hours as those trains are already close to capacity and made any maneuver with luggage an impossible task.
- 3) The design of the TSA station, right in the middle of the transit network further complicates the problem as most other airport stations such as Vancouver and London are located at the end of driverless MCT line.
- 4) The driverless MCT vehicle design is another problem facing Taipei in attempting to lure airport passengers due to the compact size of the MCT vehicles (only 2.54 meters wide).
- 5) Taipei Songshan Airport driverless MCT has the highest daily passengers per route mile when comparing with the other three more established systems: Lille, Vancouver, and London.
- 6) Larger driverless MCT vehicles are recommended for other cities who are attempting to connect their airports with such system.
- 7) Vehicle design changes (lesser and narrower seats – wider aisle) are recommended for Taipei for future MCT vehicle purchase, the current design is proven unable to meet the peak demand.

REFERENCES

1. 張澤雄 (2005). ”松山機場聯外捷運計畫(Taipei Airport MRT Link Project)”, 機場聯外運輸系統研討會, 交通部運輸研究所, Taipei, Taiwan.
2. East District Project Office (EDPO). (2005). (<http://english.taipei.gov.tw/edpo/index.jsp>), Taipei, Taiwan.
3. Taipei Rapid Transit Corporation (TRTC) (2007). “*TRTC Annual Report*”, Taipei, Taiwan.
4. Taipei Rapid Transit Corporation (TRTC) (2010), “*TRTC Annual Report*”, Taipei, Taiwan.
5. Taipei Rapid Transit Corporation (TRTC) (2011), <http://english.trtc.com.tw>, (Dec. 20, 2011).
6. 陳淵楠(2004), 中正國際機場聯外捷運系統最適營運機構之研究, Institute of Traffic and Transportation, National Chiao Tung University, Taiwan.
7. 徐瑞彬(2007), 以社會經濟與土地使用因素探討臺北都會區總體旅運型態, Institute of Traffic and Transportation, National Chiao Tung University, Taiwan.
8. 張育豪(2006), 日常旅運之交通工具使用依賴度研究—以台北都會區民眾為例, Institute of Traffic and Transportation, National Chiao Tung University, Taiwan.

Research on Urban Bus Stop Parking Capacity Reliability

CHEN Chenghui¹, CONG Cong², and XU Yongneng³

¹ T.Y.Lin International Engineering Consulting(China) Co., Ltd, Furong Road #6, Chongqing, 401121, China; Email: chenchenghui@tylin.com.cn

² T.Y.Lin International Engineering Consulting(China) Co., Ltd, Furong Road #6, Chongqing, 401121, China; Email: congcong@tylin.com.cn

³ Department of Transportation Engineering, Nanjing University of Scie&Tech, Xiaolingwei Street 200, Nanjing, 210094, China; Email: x780906yn@163.com

ABSTRACT

Bus stops represent a key bottleneck that supply loading area for buses to service the passengers, this paper focus on the relationship between bus stop accumulative capacity and parking demand, and provides analytical methodology to measure the probability that bus stop accumulative capacity meet parking demand, which is defined as parking capacity reliability in this paper. Bus arrivals and departs at a multi-routes bus stop is considered as the birth and death process, In view of co-ordination of supply and demand, we establish the parking capacity reliability model for multi-routes bus stop with multi-parking spaces, and based on the sensitivity analysis of parameters, this paper further discuss how the available parking space, average parking time as well as amount of bus lines impact on bus stop parking capacity reliability, aiming at providing essential reference for bus stop design and optimization. Finally, the model is applied to evaluate the operational situation of an actual bus stop in Chongqing, China, and methods for improvement are put forward based on the analysis.

INTRODUCTION

The strategy of giving priority to public transportation has been set as the goal of urban transportation development in many Chinese cities. In order to complete this task, more emphasis were laid on enlarging bus route network, increasing bus coverage rate, and putting more vehicles in use. While the service of individual bus stops, was ignored. The imbalance of macro and micro development has led to consequences like the overload of a bus stop, the accumulation of arriving buses and the jam of road traffic.

This problem can be explained by supply-demand theory: On one hand, most of the bus stops serve more than one route in major Chinese cities. Even 10 or 20 routes may share the same stop in some transition nodes, which brings huge demand of bus

arrival in peak hours. On the other hand, the requirement of parking spaces in one bus stop has not been clearly regulated, and the lack of research on bus stop capacity has led to poor design of stop size and insufficient supply of parking spaces.

At this background, article [1] proposes multiplying the capacity of a single bus stop by the effective number of loading areas. The formula given in this article is good for reflecting the amount of bus flow but not for the relationship of number of bus routes and parking space requirement; On the basis of article [1], article [2] made further research on the relationship between bus stop capacity and route demand, however, the simple M/M/S queuing system is not enough to simulate the operation of a bus stop; article[3] focuses on the capacity gain of a tandem bus stop in the case where there are buses waiting in line. The impacts of dwell time to the capacity of a double-berth bus stop was analyzed in this model, but the other factors such as bus route parameters and the situation of multi-berth stops were not yet taken into account. Generally speaking, in the previous research, the impact of random arrival and variation of dwell time to the capability of a bus stop was not well analyzed, and level of service of a bus stop was not well defined.

In this article, the operation of a bus stop will be depicted as a birth and death process, the capacity of a multi-route bus stop will be analyzed with supply-demand theory, and sensitivity analysis will be used to discuss how the available parking space, average parking time as well as amount of bus lines will impact on bus stop parking capacity. The results will serve as reference for the design and optimization of bus stops.

PARKING CAPACITY RELIABILITY METHODOLOGIES

Bus stop operation analysis

In major cities, bus stop usually serves more than 3 bus lines with at least one parking space, in this paper, N, M respectively denote for the number of bus routes and parking spaces. Figure 1 depicts a topical bus stop with two parking spaces.

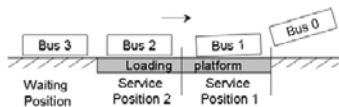


Figure 1. Layout of a topical bus stop

To analysis bus stop operation process, we first separate the operation of a bus at the stop into 4 stages: waiting outside the stop, arriving at the platform, loading and unloading the passengers, and departing from the stop. Present research mostly assume that buses came in and out of the bus stop one by one, no overtaking allowed, but actually, latter buses may find space to overtake when it finished its service before former bus. Take the above bus stop as an example, As Figure 1 shows, bus 1 is ready to leave service position 1, and for bus 2 and bus 3, there are serious possible

scenarios, represented in Figure 2.

As the left part of Figure 2 shows, Bus 2 has 3 possible scenarios: ① finished its service before bus 1 and find space to overtake; ② finished its service before bus 1 and have to wait until bus 1 leave; ③ finished later than bus 1; D D' D'' respectively denotes dwell time for 3 scenario at parking space.

Right part of figure 2 shows that for bus 3, there are 2 possible scenarios, ① no parking space available and have to wait at waiting position until service position 1 free and it can find room to overtake bus 2; ② wait until former bus leave; here, W W' means waiting time, P is the time bus move from waiting position to service position.

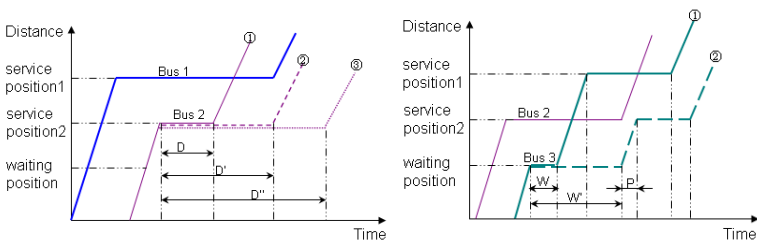


Figure 2. Trajectories of bus parking process when overtaking allowed

In light of the probability of overtaking, the operation of bus stop can be hardly depicted by $M/M/N$ queuing system. Instead, the birth and death process, is introduced here to depict the state transition of a typical bus stop, as Figure 3 shows:

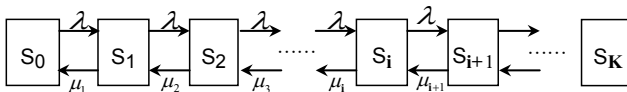


Figure 3. State Transition of a Bus Stop

In figure 3, S_i denotes the state when i buses are at the stop, $i \in [0, K], K$ denotes the maximum capacity of the bus stop, also the capacity limit of this birth-death system. λ denotes the arriving rate of the platform, which is the input rate of this system. Assuming N bus routes stop at a certain station and the frequency of route j obeys Poisson Distribution, then $\lambda = \sum_{j=1}^N \lambda_j, j=1, 2, \dots, N$. μ is the departure rate of the platform. As showed in figure 2, the total time of the process $T=W+D+P$, this is a random variable and its mathematical expectation can be expressed according to Equation 1,

$$E(T)=E(W)+E(D)+E(P) \tag{1}$$

This value is the average cycle time needed to deal with one bus, and μ_1 is the reciprocal value of $E(T)$, which is the given by Equation 2.

$$\mu_1= 1/E(T) \tag{2}$$

When more than 2 buses are at the stop, the latter bus may overtake the former one. Assuming the proportion of overtaking is α , then μ_1 can be depicted as:

$$\mu_1 = \begin{cases} \mu_1 + (\mathbf{i} - 1) \cdot \alpha \cdot \mu_1 & \mathbf{i} \leq \mathbf{M} \\ \mu_1 + (\mathbf{M} - 1) \cdot \alpha \cdot \mu_1 & \mathbf{i} > \mathbf{M} \end{cases} \quad (3)$$

Here, \mathbf{M} denotes the parking spaces. When the expectation of λ equals the expectation of μ , the birth and death process approaches equilibrium. Denoting $\mathbf{P}(\mathbf{i})$ as the possibility of state S_i , or the possibility of i buses stopping at the platform, the following equation will be satisfied in the equilibrium state:

$$\begin{aligned} \lambda_{i-1} \mathbf{P}(\mathbf{i}-1) + \mu_{i+1} \mathbf{P}(\mathbf{i}+1) &= (\lambda_i + \mu_i) \cdot \mathbf{P}(\mathbf{i}) \quad (1 \leq \mathbf{i} < \mathbf{K}) \\ \mu_1 \mathbf{P}(1) &= \lambda_1 \mathbf{P}(0) \\ \mu_K \mathbf{P}(K) &= \lambda_{K-1} \mathbf{P}(K-1) \end{aligned} \quad (4)$$

Given that $\sum P(\mathbf{i})=1$, if we input data of arriving rates and dwell time into equation(4), the probability of each state in the birth-death process can be gained.

Parking Capacity Reliability Definition and Modal

Being important node in urban transportation, bus stops should supply loading area for buses to service the passengers. Subjectively known to us, when the capacity is settled, the less the arriving bus, the lower the utilization of the platform; on the contrary, the more the arriving bus, the more possibility of waiting, the worse service it can provide. Similarly, when the amount of arriving bus is settled, the less the parking space the stop can offer, the more possibility of waiting. The waiting bus outside the stop may result in long queue to upper stream intersections and cause problems to roadway traffic operation. Therefore, the accumulative ability of a bus stop not only affects the bus service efficiency and quality, but also influences the traffic capacity of the roadway near the bus stop.,

In the co-ordination of supply and demand point of view, if the supply cannot meet the demand, the system is not reliable. To bus stops, the reliability depends on whether the maximum capacity of parking space is enough to meet the peak-hour parking need. So, the parking capacity reliability is defined as follows:

Definition: Parking capacity reliability of multi-route bus stop is the probability of the ratio of maximum parking capability and peak-hour parking demand less than a certain value. This index is to evaluate how the parking space can meet the need of bus parking.

Based on the above definition, PCR model is built with calculated formula as follow:

$$\mathbf{PCR} = \mathbf{P}_r \left\{ \frac{\mathbf{x}}{\mathbf{M}} < \delta \right\} = \sum_{\mathbf{i}=0} \mathbf{P}(\mathbf{i} | \mathbf{i} < \delta \cdot \mathbf{M}) \quad (5)$$

Here, R is Parking Capacity Reliability for a bus stop; x is the number of buses

parking at the bus stop, δ is the maximum value of demand-supply ratio. Other parameters refer to previous definition.

DISCUSSIONS

Supposing the average interval of a bus stop with N routes is 5.0min, the arriving rate of each route is $\lambda_0=0.2$ bus/min, then the total arriving rate λ for the bus stop is $\lambda=N*\lambda_0$. Supposing the possibility of overtaking $\alpha=0.3$, the maximum value of demand- supply ratio $\delta=1.2$, then the birth-death system can be set up and parking capacity reliability can be calculated. With the above-mentioned formulas, this article shows in figure 4 how the results of parking capacity reliability changes with different number of parking space, bus routes, and average parking time:

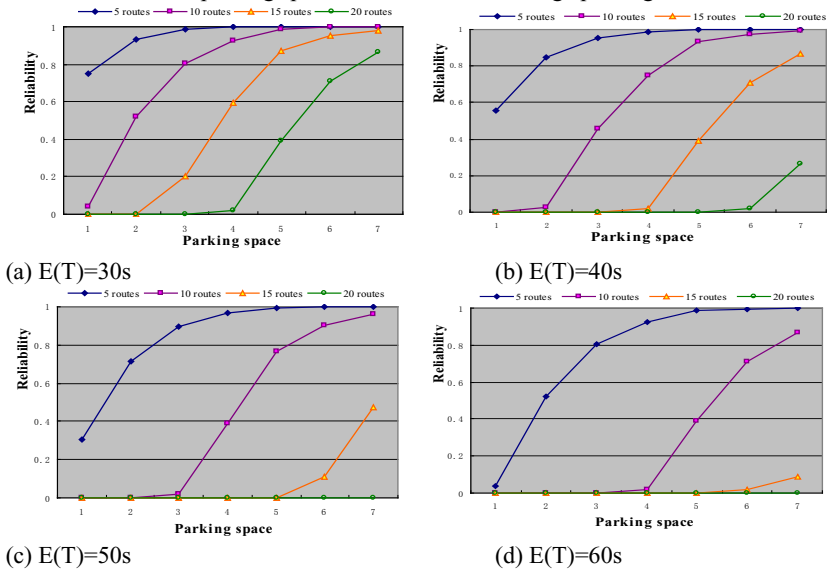


Figure 4. Parking capacity reliability analysis with different bus routes and average parking time

As shown in figure 4, the more bus routes (or demand) the stop serves, the more average parking time each stop takes and the lower reliability it shows. However, the more parking space (or capacity) the stop holds, the higher reliability it shows. So demand-supply can be reflected here by the index of parking capacity reliability.

When the number of parking spaces bus routes changes, further discussion can be made on its impact on PCR. As figure 5 shows, when average parking time is 35s and the number of parking space remains unchanged, PCR declines with the rising of routes. So the birth-death system of a bus stop is unstable and it fails when demand exceeds its capacity.

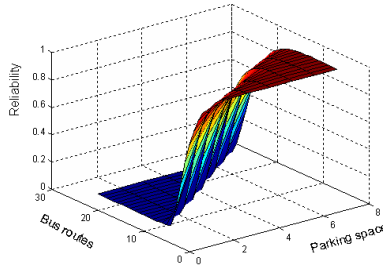


Figure 5. Parking capacity reliability analysis with different bus routes and parking space

The change of parking space may cause the similar result. When average parking time is 35s, same as figure5, and the number of bus routes remains unchanged, assuming ΔR_{3-4} and ΔR_{4-5} separately denote the increase of bus routes when the number of parking spaces changes from 3 to 4 and from 4 to 5, the change of ΔR_{3-4} and ΔR_{4-5} is shown in figure 6.

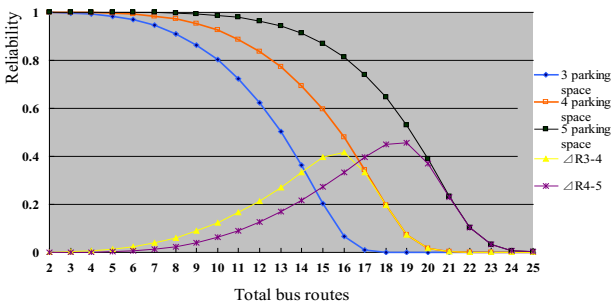


Figure 6. Parking capacity reliability analysis with the change of parking space

As we can see, ΔR_{3-4} ΔR_{4-5} changes approximated well by a parabola curve. So increasing parking spaces is not always effective to the improvement of reliability both when the number of bus routes is too small and too large. When the number of bus routes is limited, the extra parking berth will be wasted; if the number of bus routes is more than 20, emphasis should be put on the control of demand instead of the increase of capability, and method should be taken to extend intervals, combine or reduce redundant bus routes.

Table 1 shows the relationship between the number of bus routes and parking spaces, when the reliability is separately above 0.5 and 0.8.

Table1. Relationship between Number of Bus Route and Parking Spaces

Parking space	Average Dwell time																							
	25s			30s			35s			40s			45s			50s			55s			60s		
	R≥0.8	R>0.5	R>0.8	R>0.5	R>0.8	R>0.5	R>0.8	R>0.5	R>0.8	R>0.5	R>0.8	R>0.5	R>0.8	R>0.5	R>0.8	R>0.5	R>0.8	R>0.5	R>0.8	R>0.5				
1	6	9	5	7	4	6	3	5	3	4	3	4	3	4	2	3	2	3	2	3				
2	9	12	8	10	6	8	5	7	5	6	4	6	4	6	4	5	3	5	3	5				
3	12	16	10	13	9	11	8	10	7	8	6	7	5	7	5	7	5	6	5	6				
4	15	19	12	16	10	13	9	12	8	10	7	9	6	8	6	8	6	7	6	7				
5	20	23	16	19	14	16	12	14	11	13	10	11	9	10	8	9	8	9	8	9				
6	23	26	19	22	16	19	14	16	12	14	11	13	10	12	9	11	10	12	9	11				
7	26	29	21	24	18	21	16	19	14	16	12	15	11	13	10	12	9	10	12	9				

When R≥0.8, the capacity of a bus stop is satisfying; When R<0.5, the capacity is not acceptable as more than 50% buses will have to wait in a queue to enter the stop. So we take the number of routes under R>0.5 as the upper limit, when the number of parking spaces is unchanged.

NUMERICAL ANALYSIS

In this section, the proposed model is applied to an actual bus stop at Chongqing China to demonstrate the bus stop parking capacity reliability. It is a bay stop located in one of the largest commercial area of Chongqing serving 20 routes with the total length of 80m and 5 parking spaces. Records were made in spot investigation including the number of arriving bus, the number of overtaking bus and the arriving time and departing time of each bus in peak hour 7:30am-9:30am. 482 vehicles were recorded with 168 overtaking ones. Datas are as follows.

Table 2. Statistics of a Bus Stop in Chongqing

Bus Route Number	Average Dwell time	Average arrival headway	Bus Route	Average Dwell time	Average arrival headway
112	28.87 s	4.38 min	601	34.9 s	3.58 min
115	39.8 s	6.79 min	603	24.1 s	5.92 min
125	28.7 s	4.75 min	606	37.7 s	6.02 min
127	42.9 s	6.29 min	608	28.4 s	11.7 min
128	55.6 s	7.77 min	611	37.3 s	6.53 min
132	27.3 s	5.66 min	630	21.4 s	20.0 min
181	28.3 s	5.12 min	818	27.6 s	5.86 min
183	35.3 s	3.81 min	863	27.8 s	3.20 min
426	42.9 s	2.50 min	872	45.2 s	6.92 min
465	35.4 s	3.35 min	879	37.3 s	4.55 min

As the arriving rate λ equals the reciprocal of arrival headway, we can get λ=∑λ_j=3.958, while j=1,2,……N,N=20. Through the comparison between the arrival frequency and Poisson distribution (λ=3.958) in figure 7, the arrival of buses in am peak hour well obeys Poisson distribution.

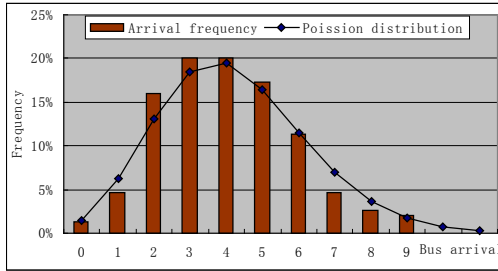


Figure 7. Comparison between the arrival frequency and Poisson distribution

With the overtaking rate $\alpha=0.348$, and the average parking time $E(T)=34.3s$, then $\mu_1=1.75$ according to equation(2). Assuming that the maximum value of demand-supply ratio is $\delta=1.2$, then $PCR=0.652$ according to equation(5). So the parking needs can be satisfied at this stop, but the reliability is relatively low as buses may arrive in a batch.

As above mentioned, parking reliability of this bus stop can be raised either by increasing parking spaces and reducing parking demands.

The increase of parking spaces from 5 to 6 will just cause a slight rise of PCR from 0.652 to 0.702. The rise of PCR to 0.8 requires more than 7 parking spaces, which will increase the total length of platform to more than 100m. Long platform is not encouraged as it causes trouble for passengers to find and get on the bus, and is usually restricted in civil development.

Parking demand can be reduced by extending average arrival headway, cutting down the number of bus routes and average parking time. Take the data in figure 1 as an example, bus routes with tight schedules such as 426, 465, 601 and 863 should be readjusted in arrival intervals. If the headway is extended to about 4.5min, PCR will be improved to 0.784, which is a significantly better result compared to increasing parking spaces. What’s more, redundant and repeated bus routes should be analyzed and rearranged. For example, PCR can be improved to 0.804 by cutting down repeated bus routes such as 125, 132 and 608. If both the two methods are taken to this stop, PCR will rise to 0.898, and batch arrival will be greatly reduced.

CONCLUSIONS

This paper depicts the arrival and departure of buses at a bus stop as a birth and death process, In view of co-ordination of supply and demand, we defines the bus stop parking capacity reliability in order to measure the probability that bus stop accumulative capacity meet parking demand, put forward the parking capacity reliability model for multi-routes bus stop with multi-parking spaces. Based on sensitivity analysis of the parameters, analyses how the available parking space, average parking time as well as amount of bus lines impact on bus stop parking

capacity reliability. The result can be served as essential reference for bus stop design and optimization as well as the regulating of bus operation.

REFERENCES

- Kittelson & Associates Inc.(2003) **Transit capacity and quality service manual** 2nd ed. WashingtonDC, 4-1-4-109.
- BaiHaijian, LiWenquan. (2007) Calculation process research of routine bus-stop routes capacity. **Journal of southeast university(Natural Science Edition)**,Vol-37 No-6 :1077-1080.
- M. Estrada, J. Ortigosa, F. Robusté. (2011) Tandem Bus Stop Capacity. **TRB Annual Meeting** Washington D C.
- National Research Council. (2000)Highway Capacity Manual. Washington DC.

The Planning Strategy of Combination Mode of Slow Traffic Ways in Central City of Chongqing

CHEN Xia¹, LIU Wei¹, HUANG Dan², and GAO Jianjie²

¹School of Traffic and Transportation, Chongqing Jiaotong University, Xuefu Rd.66,Nanan District, 400074,Chongqing, China, Tel:15922528684,
Email:ilcheryl@163.com.

¹School of Traffic and Transportation, Chongqing Jiaotong University, Xuefu Rd.66, Nanan District, 400074, Chongqing, China, Tel:008602362647131
Email:neway119@qq.com.

ABSTRACT

By analyzing some slow traffic ways in some domestic and international cities, this paper proposes a combination mode of slow traffic ways which is suitable for Chongqing, a typical mountain city. The combination mode is composed of personal rapid transit system, Crossing-river cableway, pedestrian access and overhead pedestrian trails, which are corresponding to the pedestrian corridor, pedestrian street and pedestrian unit, with the consideration of interface between them. This model can solve the problem which bicycles are inappropriate for Chongqing people fundamentally, and make a high efficiency, low power consumption slow traffic patterns.

INTRODUCTION

With over 32 million residents Chongqing is one of the fastest growing urban areas in the world. The core city is situated in mountainous terrain between the Jialing River and Yangtze River which create many challenges for pedestrians, when climbing some of the hundreds of steps and stairs in the city. According to a study by Gehl Architects, it found large numbers of pedestrians walking in the city, but very poor quality in the urban environment. Unlike many western cities in China, nowadays, Chongqing has many elderly citizens, children and large numbers of vendors to support a very vibrant urban street cuisine in traditional areas of the city.

Based on study of public space and public life, Gehl Architects has developed strategies for creating a pedestrian network and recommendations for public space quality. These included the creation of a continuous riverfront park, an extensive pedestrian network throughout the core city designed with particular emphasis on the topography rise and connections to public transportation. Adopting which slow traffic way or a combination mode composed of variety slow traffic ways at certain places is the key problem of Chongqing that this article solve.

TRAFFIC PLANNING IN CHONGQING

In 2006, a research for 《Pedestrian System Planning》 was conducted by Chongqing Institute of Transportation Planning. Combining the main characteristics of “mountain city” and “river city”, this study has formed an unique pedestrian space where people can have a wonderful journey, enjoy the beautiful scenery and do some leisure and fitness exercise. The pedestrian space is found on the important pedestrian areas, ecological parks and tourist attractions within the city.

In this study, the pedestrian space was divided into 3 levels, they are pedestrian corridor, pedestrian street and pedestrian unit.

Pedestrian corridor: it refers to a long and strong continuity distance in a certain area. As the main transportation travel channel, the surrounding area residents usually walk through it to do some leisure and fitness exercise. To ensure the safety and comfortable, pedestrian corridor should be strong structural and functional, and the time of walking through the whole gallery is not less than an hour.

Pedestrian street: it is a certain area where there are a large number of commercial facilities, attracting many concentrated flows of people. Normally, pedestrian street is an area of about 3 to 8 square kilometers, which refers to the business district in the center of downtown and has a strong pedestrian demand. Overall, pedestrian street is a concentrated, intensive and diversified system.

Pedestrian unit: it is a certain area with a strong peak-hour traffic where a variety of traffic modes are gathered. At these places, there are many transportation hubs, such as bus stations, rail stations, and airports. Generally speaking, a pedestrian unit area is 1 square kilometers and also treated as the center of transport facilities.

According to the pedestrian traffic systematic survey, planners have proposed a planning composed of 18 pedestrian corridors, 8 pedestrian streets, and 18 pedestrian units (see Figure 1).

FOUR KINDS OF SLOW TRAFFIC

Personal rapid transit (PRT)

Personal rapid transit (PRT), also called podcar, is a public transportation mode featuring small automated vehicles operating on a network of specially built guide ways (see Figure 2). PRT is a type of Automated Guideway Transit (AGT), a class of system which also includes larger vehicles all the way to small subway systems. In PRT designs, vehicles are sized for individual or small group travel, typically carrying no more than 3 to 6 passengers per vehicle. Guide ways are arranged in a network topology, with all stations located on sidings, and with frequent merge/diverge points. This approach allows for nonstop, point-to-point travel, bypassing all intermediate stations. The point-to-point service has been compared to a taxi or a horizontal lift.



Figure 1. Pedestrian system planning in central city of Chongqing illustration



Figure 2. Personal rapid transit illustration

Table 1. Key Indicators of PRT

Line capacity(vehicle/h)	5000-7200
Site service capabilities(per vehicle)	1500
Speed(km/h)	32-97
Energy consumption(J/km)	90(when speed is 40km/h)
Maximum gradient(/%)	15(i=H/L)
Minimum turning radius(/m)	11
Adaption of climate	Normal operation in the conditions of rain, snow, ice and less than 120 km / h wind speed
Waiting time	Non-peak hours, no waiting time; peak hours, 80% of passengers waiting less than 30s, 99% of passengers waiting less than 2min

Because of the traffic management of single cycle, large numbers of pedestrians have many challenges when they are walking through business districts in Chongqing. But the PRT track can pass through these pedestrian traffic bottlenecks, so that pedestrians can travel through these places smoothly by PRT.

Crossing-river cableway

Because of the mountainous terrain in core city, people had to rely on the ships to cross the river. In 1970's, the traffic way between the core cities mainly relied on 36 ferries. What's worse, this traffic way was depend on weather to a large extend.

At the beginning of the 1982, Chongqing has built a cableway across the Jialing river, which was the first passenger cableway in China (see Figure 3). From then on, the average passengers were more than 12,000 person-day until 1990's, and the most was up to 25400 person-day. In 1987, the second ropeway, named “Yangtze River passenger ropeway” was completed and put into operation (see Figure 4). The cableway starts at Changan temple in Yuzhong District, goes across the Yangtze River and stops at the Shangxin street in Nanan district. The total length is 1166 meters. Carrying 10500 passengers daily, the cableway is called “the first air corridor in the magnificent Yangtze river”. At that time, the ropeway became an indispensable traffic way, greatly decreasing the traffic pressure between each district.

With the passage of time, many roads in Jiangbei District and the Huanghuayuan Bridge have been built and put into operation. Traffic pressure has been greatly alleviated, the Jialing river ropeway was not popular as before. In fact, it would be removed by the government.



Figure 3. Jialing river ropeway



Figure 4. Yangtze river ropeway

Pedestrian access

In some older streets, especially streets in Yuzhong district, pedestrian traffic is very inconvenient, such as the narrow and crowded pedestrian road, full of obstacles, vehicular road, exhaust pollution of motor vehicle, lacking of crossing facilities, road signs and sunlight and rain shading facilities. What is worse, the elderly and the disabled feel very inconvenient when they use.

Pedestrian road is the basic element of pedestrian network. In general, the pedestrian road should have sufficient width to meet the requirements for pedestrian. Pedestrian routes must be provided with a recognizable landmark, and should not place any obstacles. To enhance the connectivity of pedestrian passage and solve the problems of difference, automotive facilities should be provided for pedestrians, such as escalators, lifts and automatic sidewalks (see Figure 5).



Figure 5. Comfortable pedestrian access illustration

Overhead pedestrian trails

Despite of setting the road crossing facilities, Overhead pedestrian trails (see Figure 6) could also be built in crowded places for pedestrians crossing a busy street conveniently, such as Jiefangbei, Sanxia Square. Long distance elevated walkway can also be used as a solid pedestrian network, connecting important interval hub. Elevated walkway has a number of advantages, including: vehicle separation, directly providing, continuous and all-weather pedestrian network, safety and convenience, and the efficiency of connecting the main commercial buildings, sports facilities, residential area and traffic hub, which reduce part of travel demands.

The elevated walkway system has been built in high density commercial district (Yangjiaping commercial center) and achieved good effects. Connecting a plurality of housing developments, the elevated walkway system should also be developed at some interchanges of commercial buildings and public transportations in other business districts.



Figure 6. Overhead pedestrian trails in construction in Chongqing

The transfer and connecting between slow traffic ways and public transportation

Pedestrian corridors, pedestrian streets, pedestrian units were seen as three sub-systems of pedestrian system. Their distribution pattern generally is that the walking corridors cross through the walking streets and connect with walking units, and walking units are randomly distributed in the walking streets. The pedestrian traffic system throughout the urban city of Chongqing is such a distribution pattern, as is shown in Figure 1. In the previous section, we introduce 4 slow traffic ways and illustrate their service area. So only do we combine the slow traffic ways and take the conversion into consideration can solve the traffic problems in a pedestrian area.

To illustrate the combination of slow traffic ways and conversion patterns, we simulate a commercial center (see Figure 7), which is treated as a virtual walking transportation system. In this system, the roads crossing the region are treated as pedestrian corridors, the central business district is treated as the pedestrian street, groups of buildings are treated as pedestrian units.

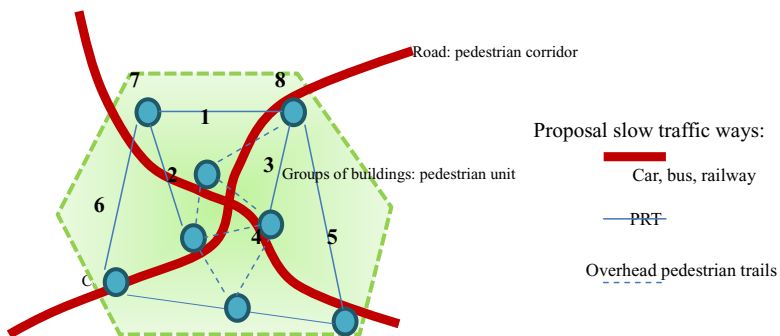


Figure 7. A virtual walking transportation system illustration

As is shown in the above picture, the road treated as pedestrian corridor is usually supplied for motor vehicles and public transport (represented by the heavy

solid line), such as private cars, buses and rail transit. The pedestrian corridors links up the communication lines between the buildings aside by the roads. We can see two lines of 6-2-8 and 7-1-3-5 in the picture. You can also set personal rapid transit system along the gallery, but there will be a contradiction between the rail line. In view of the completion of rail transportation system planning in the core city of Chongqing, the personal rapid transit system should be specially planning and design.

Due to the long distance, residents can't easily pass through the walking units where there is lack of slip roads to connect, such as between 6 and 7, and between 8 and 5 in Figure7. PRT (represented by the thin solid line) can be used as a certain mode of transport to make up for the shortcomings of the various traffic ways and exert their strengths. For example, we can establish the PRT system network around a major subway station, so the multi-level transportation system is formed by short-range using PRT, long-distance using subway. What's more, using PRT system can reduce road traffic during the peak period and give full play to the capillaries system effect because of the public transport and taxies' over-reliance on road traffic, and also reduce the buses and taxies operation density in branches, take full advantage of resources into bus rapid transit and mainline transport, improve the operating speed of the vehicle and enhance transport efficiency.

The distance between the walking units in the core area is usually short, but due to the blocking of roads, pedestrian access is not very convenient, such as between 1 and 3, and between 2 and 4 in Figure7. You can build elevated walkways (represented by the dotted line) to connect the buildings. Thus, not only effectively dredge the flow of people, but also make the crowd directly walk into floor without crossing busy city streets. Overhead walkway can connect with the two layers of space between commercial buildings. It not only strengthens the commercial building links, but also forms a new street corridor in the ground outside the space. Corridor width should be 5-10 meters. Aside the corridor, people can properly set some plants or a small amount of recreation spaces.

The convergence between pedestrian channel and traffic facilities should be considered as a whole. Such as, walking system should be well integrated with bus stops, rail stations, the entrances of pedestrian bridges and underground channels should connect with bus stations and railway stations.

CONCLUSION

Slow traffic is directly related to people's livelihood, which is the focus of government's concerning. To solve the pedestrian traffic problem, it requires a lot of efforts from every department. For example, the construction of facilities demands enough fund protection, it should make some verification scientifically before making any decisions. Depending on the existing slow traffic planning, it should implement each measure as soon as possible, and make a high efficiency, low power consumption slow traffic patterns.

REFERENCES

- Gehl Architects. (2010) Public Space Public Life Survey
http://www.gehlarchitects.dk/files/projects/110524_China_Chongqing_OG_EN_G.pdf
- Chongqing Institute of Transportation Planning. (2006) “Pedestrian System Planning”. Chongqing.
- Personal rapid transit. From Wikipedia.
http://en.wikipedia.org/wiki/Personal_rapid_transit
- HE Shan, ZH U Yan, YUAN J ia. (2011) “Application of Persona lRapid Transport System in Low Carbon Urban Transportation System. Zhejiang Construction. ” Vo.128, No.1.
- TAN Bao-yao. (2011)“The Slow-Traffi c System and Pedestrian Environment Planning in Hong Kong. ” 1673-1530(2011)01-0078-04.
- GAO Jianjie ,WU Xiaokang. (2011)“Pedestrian Traffic System Planning in Central City of Chongqing”. Traffic Information and Safety. Vo.29, No.1.

Comparison of BRT Systems in Four Chinese Cities: Beijing, Changzhou, Xiamen and Jinan

Ying-Chih LU¹, S. K. Jason CHANG² and Ming YU³

¹ Associate Professor, Department of Traffic and Transportation, Fujian University of Technology, Fuzhou City, 350108, China. E-mail: ethan424@gmail.com

² Professor, Department of Civil Engineering, National Taiwan University, Taipei City 10617, Taiwan. Tel: (886)2-23625920-302; FAX: (886)2-23639990; E-mail: skchang@ntu.edu.tw

³ Professor, Department of Architecture and Planning, Fujian University of Technology, Fuzhou City, 350108, China. Tel: (86) 0591-22863125; E-mail: yuming@fjut.edu.cn

ABSTRACT

This paper provides a comparison of planning, implementation, and operation on bus rapid transit (BRT) in four Chinese cities with significantly different populations and city scales, namely Beijing, Changzhou, Xiamen and Jinan. In Beijing, the Nanzhongzhou Line is the first operational BRT system with full functions in China since late 2006. In early year of 2008, BRT systems in Changzhou, Xiamen and Jinan start their commercial operation. This paper conducts an overview on planning and design process, service performance and capital investments of each system. Nevertheless, many features have been applied and implemented differently in these four BRT systems, such as bus lane allocation, station design, ticketing and pricing schemes, financial and institutional arrangement and integration to other transportation systems. The paper concludes by providing recommendations for planners, engineers and decision makers in implementation of BRT systems in various city environments.

INTRODUCTION

In the past 20 years, developing countries or transition economies have dramatic urbanization and motorization. In China, after the economic reform since

1978, major metropolitan areas have also faced big challenges in traffic congestion, noise and air pollution, energy consumption, and traffic safety mainly contributed by the car or highway oriented development approach. Economic loss and public health threat due to traffic congestion and pollution have been significantly affect living quality in major Chinese cities.

These critical challenges have been recognized in central and local governments while various policies related to sustainable urban development and green transportation have been proposed. National policy on promotion of public transportation systems and non-motorized transportation had also been officially announced by the Ministry of Construction. After the institutional reform, the new Ministry of Transportation, now in charge of urban transportation, has also announced its public transportation policy in which transit-oriented development policy is included. And, in addition to continuously developing urban rail systems, bus rapid transit has also been considered as one of the crucial systems in the national plan.

With the advantages of short construction period and comparatively low capital investment, bus rapid transit has been considered as an alternative for rail rapid transit and light rail transit systems. Following the successful operation of the first BRT line in Beijing, which replaced the light rail transit line in Nanzhongzhou Road, more than 30 cities are under planning or construction of BRT since 2003.

BRT combines with dedicated right of way, efficient fare collection, comfort platform, real time passenger information, advanced vehicle technologies, land use planning and transportation policy, has created a high quality public transportation service. With an affordable cost, BRT can quickly form a network and therefore helps of achieving the service objectives of reliability, convenience, comfort, energy saving and low emissions. By integrating the information and communications technologies, BRT can enhance the efficiency and reliability of the transportation system. By these reasons, BRT become one of the best solutions to promote public transportation and alleviate the urban traffic congestion, especially in developing cities.

This paper conducts a comparison of BRT in four Chinese cities, namely Beijing, Changzhou, Xiamen and Jinan. BRT systems have been developed in various approaches in these four cities with significantly different population densities and city scales. The Nanzhongzhou Line of Beijing BRT has been opened in late 2006 and it is the first operational BRT system with full functions in China. Since January 2008, BRT systems in Changzhou, Xiamen and Jinan BRT have also started for operation. More and more BRT systems begin to operate in Chinese cities in recent years. In viewing of diversity in BRT systems, it is worth summarizing various

experience of BRT development so that guidelines for planning, design, and operation of BRT might be able to obtain.

The paper is divided in three sections. The first section presents the background of these cities, the urban and transportation related problems, and the potential solutions. The second part presents the characteristics and differences of these BRT Systems. The paper concludes by providing recommendations for planners, engineers and decision makers in implementation of BRT systems in various city environments.

CITY BACKGROUND

In Beijing, the Nanzhongzhou Line is the first operational BRT system with full functions in China. It was planned as an urban light rail corridor, which had originally been scheduled for operation after 2012. Because of the Olympic Games coming in 2008, the city government was thinking about an alternative public transportation system with considering the urgent needs in the corridor. Therefore, a strategy meeting was hold by Beijing Transportation Commission of the City Government in March 2003. International and domestic experts are invited to have a series discussion for the decision on BRT system. Detailed design and operational strategies were proposed in late October 2003. The first stage of 4 km BRT opened for operation in the end of 2004 while total 16 km Nanzhongzhou BRT Line completed by the end of 2005. The total construction cost of this first BRT system is equivalent to the two year interest of capital investment for an urban rail with same scale [4].

This BRT line has been included in the overall public transit network in Beijing while total length of 360 km urban rail and 100 km BRT system are planned. Until the end of late 2010, it has completed three BRT lines in total of 54 km.

Changzhou is a medium-sized city located between Nanjing and Shanghai. Its daily bus trips are about 750,000 people. In 2004, the Changzhou government finished an urban rail planning in which it was suggested that Changzhou needs a light rail system from 2018. It is also suggested that Changzhou needs to upgrade the bus transit services to meet the need of general public in the sustainable transportation plan. After a technical tour led by Mayor in January 2007, it is decided to implement BRT system and a network to form the main public transportation system. The first BRT line of 15km took only 11 months from planning to commercial operation. This has been recognized as the shortest time for construction of BRT in the world. The route connects new development area and old town, uses open system with good arrangement on bus routes and free transfer in all BRT stations. Now, three BRT lines with total 52 km have completed for operation.

With the Xiamen harbor city development and rapid growth of private cars, the bus network structure is irrational. The city proposed to develop "urban public transportation priority system", integrated bus network with different levels of transportation services and convergence. Based on the existing road and traffic conditions in Xiamen, the city government decided to respect the principle of minimum interference with traffic and proposed the idea of an elevated BRT system. According to international BRT technical standards, the city government planned to construe Xiamen BRT system on January 19, 2007. On September 1 2008, the system began opening for commercial operation. From the plan to operation, it took only 11 months, which is the another shortest construction BRT system as the international project. Comparing other BRT system, Xiamen has higher capital investment mainly because its original planning that the civil engineering works use standards of light rail system in order to have a flexibility to change from BRT to LRT in the future. However, due to a remarkable success on BRT system, it has decided not to change the system to LRT.

Jinan is famous for her spring and garden in almost everywhere in the city. Although there is urban rail system project for many years, it is not decided due to huge capital investment and a uncertainty on the influence of the construction on spring water. Therefore, city government decided to implement BRT system when faced a pressure of providing high quality of public transportation for the national sport gymkhana in 2009. In November 2004, Jinan City Government started BRT planning, design and construction work. The first line was open on April 2007 while the island station is used in the dedicated bus lane area. To keep the flexible operation of bus vehicles outside the bus lane area, Jinan bus transit group proposed doors opened in two sides of the bus. GPS and ITS technologies have been applied to ensure that the doors on the two sides of the bus will open safely and appropriately.

In 2009, six BRT routes started commercial operation. Jinan BRT station costs an average cost of 2 million with the advanced ITS technologies while the length of platform is 36 to 40 meters for two vehicles. The headway in peak hour is 2 minutes while it is 5 to 10 minutes in the off-peak period. Now, the BRT systems of 6 lines have a total of 500,000 daily ridership. System riders roughly save about 50% travel time and 20% of energy saving. Jinan BRT has been recognized as the first BRT network in China.

SYNTHESIS OF BRT FEATURES

Design Elements

Comparison of basic design elements in these cities is showed in Table 1. In Fact, BRT in the four cities are with many different characteristics in terms of the flexibility and specific city environments, such as traffic flow, urban land use, passenger flow, and public transportation availability.

Table 1 Design Elements [1]

Elements	Beijing	Changzhou	Jinan	Xiamen
Population	13.3 million	3.8 million	6 million	3.5 million
Total length of existing trunk corridors (km)	54 (Line 1, 2 and 3)	44.9 (Line 1 & Line 2)	34.4 (Line 1~6)	51 (Line 1 & Line 2)
Location of bus lanes	Center	Center	Center	Elevated busway
Type of platform	Island(Line 1)	Side	Side	Side
Number of stations	60	51	46	40
Stop spacing (m)	940	900	760	1,300
Number of stations with passing lanes	7	0	2	2
Special stations and terminals to facilitate transfers	Partial	Free in the same platform	Free in the same platform	Free in the same platform
Passenger access	Flyover or underpass	Crossing	Crossing	Flyover & Crossing
Segregation with other traffic	Metal Fencing	Marking	Metal Fencing	Elevated busway
Trunk vehicle type	Low Floor Articulated Bus	Low Floor Articulated Bus	Low Floor Articulated Bus	Conventional Bus (before 2010) Low Floor Articulated Bus (from 2010)
ITS technologies	Dynamic Information on the bus and station, Signal Priority, Control Center, Electronic Payment System	Dynamic Information on the bus and station, Signal Priority, Control Center, Electronic Payment System, Enforcement System	Dynamic Information on the bus and station, Control Center, Electronic Payment System	Dynamic Information on the bus and station, Control Center, Electronic Payment System
Average operating speed (km/hr)	21	18	15-17	27
Number of total system passenger-trips per day	150,000	250,000	220,000	200,000
Construction cost (RMB/km)	40 million	30 million	8.8 million	45 million

Infrastructural Design

Location of busway lanes must be considered with other traffic flow. In general, the busway lane is preferred to design in the center of the road since it can avoid the conflict of the bus and turning vehicles. Figure 1 shows the location of busway in Beijing and Changzhou.



Figure 1. Location of busway in Beijing and Changzhou BRT

In the Figure 1, the type of platform also is showed. Island platform of Beijing make the passengers more be convenient to transfer to the reverse line, but it also make passengers confused to take the right bus. Island platform can save more construction cost and land use. In Beijing BRT Line #1, since the use of the central island platform, so the bus must be with left side doors, it is very inconvenient to dispatch other regular bus with right side door in rush hours. As the Figure 2, on the platform, BRT often design the automatic platform door to protect the passenger safety. In Changzhou, all of the stations have automatic platform doors, but in Beijing only few stations have automatic platform doors.



Figure 2. Automatic platform doors in Beijing and Changzhou BRT

In Xiamen, BRT build in elevated type, with the Light Rail Rapid Transit (LRRT) infrastructure, but use bus without any railroad. BRT line 1 has 21 stations, which

with 18 elevated and three ground stations. The Stop spacing is about 600 m in CBD and 1 km in suburban. Elevated station is the third layer (see Figure 3); ground floor is for road and bus station to provide convenient transfer.



Figure 3. Xiamen BRT Station

Jinan BRT combines different forms of busway and bus lanes. For higher passenger demand area, central busway is applied while bus lane on curb side is applied for lower passenger demand area. The BRT system in Jinan is considered as an open operational model, in which the construction and operating costs are comparatively low and it is also comparatively flexible to expand service coverage based on passenger demand.



Figure 4. Jinan BRT station

One of the characteristics of BRT is to provide passengers a convenient and safe access to the station. In Beijing and Xiamen, the underground passages or flyovers are designed for passengers as shown in Figures 5 and 6. The daily ridership is about 150,000 persons and 220,000 persons in rush days, so safety of passenger across the road in Beijing is very important. In Changzhou BRT, the traffic is not too crowded; only use markings to guide passengers to access the station, show in Figure 7. In 2010, the Changzhou Line #2 also began use underground passages in some crowded stations.



Figure 5. Passenger Access of Beijing BRT



Figure 6. Passenger Access of Xiamen BRT



Figure 7. Passenger Access of Changzhou BRT

When Beijing BRT opened to operation in 2004, the fleet size is only 60 buses for operation. It is not enough to carry so much ridership, especially in peak hour and Golden Week of National Holiday. The bus company must dispatch the regular buses to support the BRT system. The BRT bus door is on the left side, but the regular bus is only with the right side door. Passengers must walk to the other side to take on the bus, and it is very dangerous, show in Figure 8. When Xiamen BRT opened in 2008, it only used 12 feet standard bus and soon reached the capacity. Now, all main BRT system in China use 18-feet low floor articulated bus, show in Figure 9.



Figure 8. Passengers of Beijing BRT in rush hours



Figure 9. Bus of Beijing, Changzhou, Xiamen and Jinan BRT

ITS Technologies

By integration of traffic control measures and exclusive bus lane, BRT can increase travel speed and reliability of bus operation. To achieving the goals of BRT, US Federal Transit Administration suggests a set of guidelines as follows [2, 5, 10]:

- Shorten travel time by fewer stations, faster travel and less traffic jam.
- Shorten waiting time by more intensive service and headway of bus.
- More reliable service- Exclusive bus lane enables driving the bus more steadily and makes the bus on time.
- More convenient to use- Simple fare collection method and obvious route guide.

- More accessibility- Handicap or elder's use.
- Comfortable terms- The comfortable bus for taking and environment for waiting.
- Combine the service- Convenience to park or transfer.
- Characteristic service- Prevail and obvious vehicle and design of station.
- Protection for environment- Bus with low noise and low pollution and are designed.
- Increase the industry to develop- Because of demand the new technologies, greatly improvement of relevant demand of industry will develop.

ITS technologies application in all BRT are the same, but the control center in Changzhou is more comprehensive than the other systems, as shown in Fig 10.



Figure 10. Control center of Changzhou, Beijing and Xiamen BRT

Another important ITS technologies application are information system and smart card ticketing system. Passengers know the arrival time of the next bus, and use the smart card to take on the bus shall be able to reduce their waiting time. Another important issue is that pre-payment can help the BRT operation more efficiency. Figure 11 and 12 shows the information system and pre-pay smart card in Changzhou and Xiamen, respectively.



Figure 11. Smart card pre-payment in Beijing and information system in Changzhou



Figure 12. Smart card pre-payment and information system in Xiamen

BRT Performance

After the Beijing BRT opened, the bus operational speed increased from 16 km/hr to 21 km/hr, and the ridership is 4 times of conventional bus route. The average daily trip is 150,000 persons and in rush hour are almost 220,000 persons [4, 9]. The Beijing BRT has reached the planning goal and successfully replaced the original light rail plan. Other three BRT routes in Beijing have also open for commercial operation.

In Changzhou, the bus operational speed increased from 15 km/hr to 22 km/hr, and provided an accessibility for the city center and old town. Changzhou BRT also attracts more than 10% other private mode users to take BRT [7]. The average daily trip is 70,000 persons and is almost 94,449 persons in snow storm in 2008[4]. And, when the Line 2 opened in 2010, the daily ridership reached 250,000 persons and it is four times of the situation with the only Line 1. Therefore, it verified that the network effectiveness is obvious. It is also the same in Jinan, in which the BRT network of 6 lines have daily trips of more than 320,000 persons.

Finance

It is also worth discussing the advantage of construction cost on BRT systems. The capital investment in Beijing BRT is about RMB 657million, includes public sector invested 415million in main infrastructures plus bus company invests 242million in stations, ITS, and vehicles. In Changzhou, the capital investment is about RMB 350 million. In Xiamen, the capital investment is about RMB 3000 million for 115km BRT network which is only 1/5 of light rail system.

The average cost of BRT system is as follows: Beijing BRT is RMB 40 million/km, Changzhou is 30 million/km. The vehicle cost is RMB 2.2 million per vehicle in Beijing and 2.1 million per vehicle in Changzhou. Another important issue is the operation subsidy in Beijing: the average revenue is RMB 0.39

dollars/passenger while the average cost of one passenger is 1.86 dollars [8] .

These cost analysis has shown that BRT with the cost advantage compared to rail transit systems. The capital investment of BRT is about \$1~7 million/km, but the LRT and MRT construction cost is between \$3 million/km and \$200 million/km. However, it has been verified that the operation performance of BRT is not less than MRT or LRT. The flexibility advantages in operations and services of BRT have also been recognized as the unique features.

KEY FACTORS FOR SUCCESS

BRT must integrate the urban and user characteristics, and BRT can design with its high flexibility. Therefore, almost all new BRT systems shall be able to adjust its design, operation and management with local environments. Besides the design and operation elements, some key decision factors must be considered in the planning process. Based on the development experience of BRT systems in China, it could summarize some key factors as follows [4]:

- Strong support from mayors and senior leaders.
- Strong support from city council.
- Coordination of all departments related to public transportation and traffic management.
- Teamwork of various departments and bureaus, including planning, design, construction, operation, enforcement, etc.
- Comprehensive planning and design works.
- Applying operation-oriented approach rather than manufacturer oriented decision making process.
- Contribution of international experts and teams.

CONCLUSIONS AND RECOMMENDATIONS

BRT becomes a new approach to improve the urban public transportation system. In this paper, BRT systems in Beijing, Changzhou, Xiamen and Jinan are four successful BRT plans with variety of city scales, urban environments, population density, and public transport systems. It has been recognized from the function, design and operation that BRT can be various with its flexibility. But some elements are more important, such as pre-payment scheme, application of ITS technologies, and dedicated right of way, etc. Besides these elements, some decision factors must be considered in the planning process.

It is worth noting that Beijing and Jinan proposed BRT network by grasping the opportunity of providing high quality of public transportation service for mega-event in the city. With strong support and mission-oriented decision, these two cities come out a world class BRT system. This development model has also been observed in other country such as South Africa and Korea.

From 2009 to 2011, many new BRT systems have been developed and successfully opened for operation in cities around the world, including Guangzhou and Yan Cheng in China, Bangkok in Thailand, Delhi and Ahmedabad in India, and Johannesburg in South Africa, etc. It is believed that this comparative analysis of these new systems will be beneficial for all other systems under planning and construction. In addition to comparison study, further researches are also worth noting: (1) optimization of BRT station spacing, (2) design integration with other transit modes, (3) integration of ticketing system and pricing schemes, (4) design guideline for station and transfer facilities, (5) guideline for determination of open or closed systems, and (6) integration of land use and BRT system (BRTOD).

REFERENCES

1. Beijing Changdatong Transit Ltd. (2006), *Constructions and Development of Beijing BRT*. Published by Yu-han Sustainable Transportation Research Center, Beijing.
2. Beijing Changdatong Transit Ltd. (2006), *Invitation of Public Bidding for Design of ITS System for ChaoYang BRT*. Beijing.
3. Bureau of High Speed Rail. (2008), *BRT System of Chiayi High Speed Railway Station*, Technical Report, Taiwan.
4. Chang, S.K. (2008), *Rationale of Bus Rapid Transit Oriented Development*, Training Workshop on Mass Transportation System, organized by GTZ, SUMA, and the Energy Foundation, Jinan, China.
5. Chang, S.K., Lu, Y.C., and Lin, C.H. (2007), "Evaluation of ITS Technologies for Bus Rapid Transit Systems". *Proceedings of ITS World Congress Conference*, Beijing.
6. Hidalgo, D. and Graftieaux, P. (2008), "BRT Systems in Latin America and Asia: Results and Difficulties in 11 Cities." *Transportation Research Board 87th Annual Meeting*, Washington, D.C.
7. Tsai, C.C and Hsu, K.M. (2008), "*Changzhou BRT System*." BRT China, <<http://www.brchina.org>> (Sept 20, 2008)
8. Wang, H.Y. (2007). "BRT Construction in Chinese Cities." *Journal of City*

Transportation, 2007(4), 55-69, China.

9. Wu, C.C and Lin, C. (2007), "Performance of Beijing Nanzhongzhou BRT." *Journal of City Transportation*, 2007(4), 76-80, China.
10. Wright, L and Hook, W. (2007), *Bus Rapid Transit Planning Guide*, published by the Institute for Transportation Development and Policy.

Research on Travel Behaviors of the High Speed Train's Passengers Based on Frequency and Distance of the Trip

Zou Xin¹, Wang Ji Feng¹, and Zhao Hongbin¹

¹ China Academy of Urban Planning and Design, No.9 San Li He Road, Hai Dian District, Beijing, China 100037. E-mail: zouxin_caupd@yahoo.com.cn

ABSTRACT

With the rapid progress of our country's urbanization and the construction of transportation, the problem of trip becomes the key to the transportation planning. We step into a period which emphasizes the structural adjustment of transportation. The focus of transportation's construction transfers from highway to railway. In view of this, this paper organized a large-scale investigation in order to explore the passengers' travel behaviors. The investigations were held in Beijing, Tianjin, Nanjing, Hefei and Kunshan cities which successfully ran the high speed trains. The paper indicates that travel behaviors including the purpose of trip, the source of charge for trip, etc. are related to the frequency and distance of trip. Furthermore according to these behaviors, this paper will summarize some trends which is helpful to the construction of railway especially the stations of high speed railway.

SIGNIFICANCE AND BACKGROUND OF THE RESEARCH

China is undergoing a massive construction of the high-speed rail, therefore there will be a large number of passengers who take the slow-speed train and airplane transfer to high-speed rail, while the construction of the high-speed rail system will also foster many more new passengers.

The travel characteristics of the passengers must be emphasized through the high-speed developing construction of the railway system. And the design of the system should relay on the travel characteristics of the railway passengers. Therefore, based on this background the article organized a survey of the characteristics of the high-speed rail passengers and carried out a preliminary analysis.

RESEARCH METHODS AND DATA SOURCES

Research Methods

Questionnaire Survey

Questionnaire survey is one of the most widely used methods in social survey, which is a way to collect data through the unified-design questionnaire to ask the respondent for information and opinions. The investigator distributed and recycled the questionnaires.

Mathematical Statistics

In this paper the data from the questionnaire is classified and ordered by using the contingency table, and visually display the distribution of the option which the respondents choose from the questionnaire. Contingency table is a statistical technique which uses tabular form to reflect the joint distribution of the two variables who only have limited class. Contingency table analysis is an important way to reveal the links of the options.

Through the contingency table analysis of the options, the chi-square test of the options and different classification travel, reveal the relationship between them. The chi-square test in statistical analysis, namely the χ^2 test in interaction analysis, which applied in the goodness of fit test and the variables independent (related or not) test, in the situation that given the significance level and known the degree of the freedom, we can judge the degree of association by the corresponded threshold limit value. If the statistic is greater than the critical value, that the variables are related; on the contrary, they are not related.

Research Object

Based on the construction process of our country's high-speed rail, this survey picks Beijing South Railway Station, Tianjin East Railway Station, Hefei Station and Kunshan South Station as the survey sites. In the waiting rooms of these sites we distributed the questionnaire to the passengers.

Questionnaire Design

The data is based on the survey. Therefore, the design of the questionnaire should accord with the study direction and the highlight of the paper. The questionnaire interpose the question about orientation and destination of the passenger's travel, in order to reveal the distribution in space, moreover the questionnaire interpose the question about the travel frequency. Such as, the number of your train is _____, you will get off at the _____ station, you have been here _____ times by railway in the past 3 months.

Data Acquisition

In Beijing South Railway Station, the planed sample number for 3000, recycle number for 2911, recovery rate for 99.7%. In Tianjin East Railway Station, the planed sample for 3000, recycle number 2992, recovery rate for 99.7%. In Hefei Station, the planed sample number for 3000, recycle number for 2862, recovery number for 95.4%. In Kunshan South Station, the planed sample number for 3000, recycle number for 3000, recovery rate for 100%.

TRAVEL CLASSIFICATION OF THE HIGH-SPEED RAIL

Travel Classification Based on the Space Elements

China's railway system is divided into three different levels system, the organization, operation and planning of each three transportation systems are entirely

different in policies and technical methods. The policies and technique are based on travel study, so accord to transportation system's space frame, the study on travel need to be divided into: inter-regional travel, inside-regional travel and city travel.

□ Inter-regional travel: in space inter-regional travel is the travel whose orientation and destination locate in two populated areas or two metropolitan areas, generally, the travel distance is long;

□ Inside-regional travel: in space inside-regional travel is the travel whose orientation and destination locate in the inner of the populated area;

□ City travel: in space city travel is the travel whose orientation and destination locate in the inner of the city, generally, the travel distance is not so long.

Urban development and the difference of planning, operation and management in transportation system, which will guide the difference increasing of the traveler's travel characteristics.

Travel Classification Based on the Travel Frequency

For the travel in the multi-level transportation network, its demand characteristics are totally different. Travel frequency is the best way to measure the need and capability from the individual view point.

This paper divides the travel accord to the travel frequency:

□ Routine travel: whose travel frequency per unit time is the highest, the influence factors are fixed;

□ Frequent travel: whose travel frequency per unit time is high;

□ Non-recurring travel: also known as occasional travel, whose travel frequency is the lowest, and the impact factor when travelling is hard to confirm, moreover, the travel purpose are unexpected.

Travel frequency can indirectly reflect the traveler's characteristics and their travel demands, also it is a manifestation of the travel purpose's other aspect. The demand of the travel in different frequency for the transportation is entirely different. For example, in city the core demand of the work and school in high-frequency for the transportation system is fast and on time, but the requirement of the business and shopping in low-frequency is comfortable and convenient. In addition, the division in travel frequency is relatively simple, easy in data acquisition and high in data reliability.

Travel Split Based on Space an Frequency of the Railway Passenger

Combined the travel time with travel distance, this paper make the travel whose time is 2 hours and distance is 250 kilometers as a demarcation line: the inside-regional travel sample is the travel whose time is within 2 hour and distance is within 250 kilometers; inter-regional travel sample is the travel whose time is longer than 2 hours and distance is longer than 250 kilometers too.

By statistics, the characteristics of the travel frequency are different between inside-regional and inter-regional. For the inter-regional passenger's travel, the distribution of the frequency is concentrated, but the discrete is larger; for the inside-regional passenger's travel, the distribution of the frequency is discrete. The

frequency of the inter-regional passenger’s travel concentrated in low frequency (0~2times/quarter), but the frequency of the inside-regional passenger’s travel is relatively discrete, the frequency is distributed in each band as shown in Figure 1.

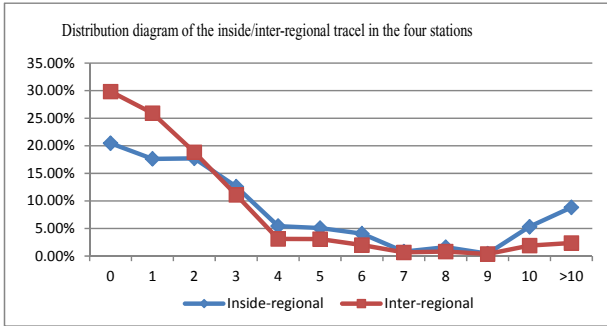


Figure 1. Distribution of inside and inter-regional travel in the four stations

Judging from the trend, passenger’s travel distance and frequency are relevant more or less, the higher the frequency the closer their travel, the lower frequency the further their travel as shown in Figure 2.

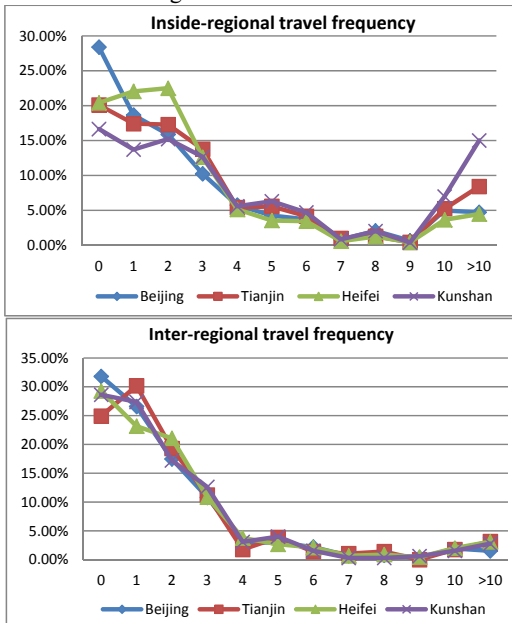


Figure 2. Inside and inter-regional travel frequency

The frequencies of the inter-regional long travel are consistent in the four stations, a lot of the travel concentrated in 4 times/quarter; however, for the four stations’ inside-regional short travel frequencies, there is some differentiation: the

distribution of the passenger’s travel frequency is the most average in Kunshan South Station which operate the inter-city trains between Shanghai and Nanjing, but, the travel frequency is low in Beijing Station and Hefei Station which operate the long-distance passenger special line.

The distribution curves between inside-regional an inter-regional travel intersect in the 2 times/quarter, however, there is a sharp decrease in 2~3 times/quarter in the distribution of the inter-regional travel frequency. Based on this phenomenon, this paper make the critical value between the frequent and non-recurring railway travel 2 times/quarter—if the travel times in a quarter below 2 times, that the travel was defined as non-recurring travel; if the travel times in a quarter more than 2 times, that the travel was defined as frequent travel (see Table 1). Be noted that, 2 times/quarter is not a precise and unique division standard, based on the passenger survey in stations this paper ascertain the standard.

Table 1. Rail Passenger Travel Division based on Travel Frequency and Travel Space

Frequency Space	Frequent travel	Non- recurring
Inside-regional travel	Inside-regional frequent travel	Inside-regional non- recurring travel
Inter-regional travel	Inter-regional frequent travel	Inter-regional non- recurring travel

To sum up, based on travel space and frequency, this paper divide the rail passenger travel into inside-regional frequent travel, inside-regional non- recurring travel, inter-regional frequent travel, inter-regional non- recurring travel.

TRAVEL CHARACTERISTIC ANALYSIS OF DIFFERENT CLASSIFICATION

Research Hypothesis

Income Level

The income level of passenger can determine the travel cost and travel mode. Economic income stands for one’s personal purchase ability, and the purchase capacity and willingness depend on the purchase ability. Traveler’s income level will determine their sensitivity degree to the travel cost.

Travel Purpose

It is very important to analysis and study the traveler based on travel purpose in transportation planning. Only after knowing the traveler i.e. the transportation facility user’s information clearly, can we serve the traveler, who has different need and behavior, with different and hierarchical transportation service.

Waiting Time

The waiting time can reflect the arrangement of passenger's travel better, different waiting time will decide the number of the passenger in the waiting room, thus affecting the design standard of the passenger capacity.

Hypothesis Testing and Correlation Analysis

Making Hypothesis

According to the aim of this study, propose the following hypotheses:

H₀₁: Travels in different types are significantly related to the passengers' income level, and there is a prominent difference in passengers' income level in different travel types.

H₀₂: Travels in different types are significantly related to the passengers' travel purpose, and there is a prominent difference in passengers' travel purpose in different travel types.

H₀₃: Travels in different types are significantly related to the passengers' waiting time, and there is a prominent difference in passengers' waiting time in different travel types.

Income Level Hypothesis Testing and Correlation Analysis

After analyzing traveler's income level in different travel type, we can find all the travelers' income level concentrate on the level between 2000~4000yuan/month, frequent traveler's income level is higher than non- recurring travelers' (see Figure 3).

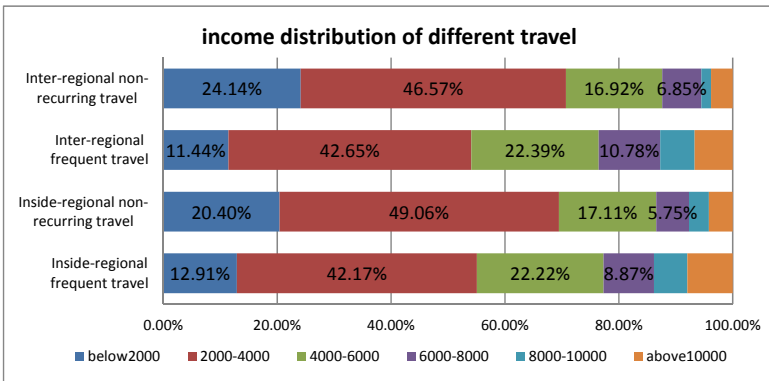


Figure 3. Income distribution for different travel

For the χ^2 test, $Q_p=135.39$, degree of freedom: $df=(r-1)(c-1)=(4-1)(6-1)=15$. Take the significance level: $P = 0.05$. Then the corresponding critical value of 25.00. $Q_p > 25.00$, so, the reliability is 95% to deny the hypothesis that there is no relationship between passenger's income and travel's frequency and distance, it can be thought there is no significant correlation between passenger's income and travel's frequency and distance.

From the survey’s results, traveler who always travels has a higher income than who travel not so often, and traveler who travels inside the region has a little higher income level than who travels inter the region. Distribution of the inter-regional frequent passenger is the most in high income level.

Travel Purpose Hypothesis Testing and Correlation Analysis

After analyzing traveler’s travel purpose in different travel type, we can find the travel purpose of the frequent traveler concentrates on the business travel, the non-recurring traveler’s travel purpose concentrates on visiting friends and relatives (see Figure 4).

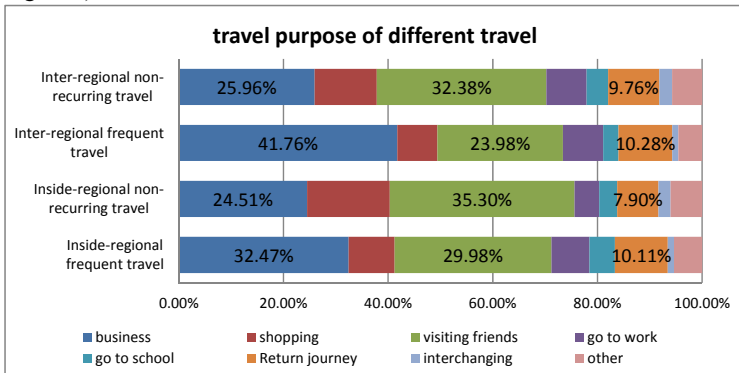


Figure 4. Travel purpose of different travel

For the χ^2 test, $Q_p=158.86$, degree of freedom: $df=(r-1)(c-1)=(4-1)(8-1)=21$. Take the significance level: $P = 0.05$. Then the corresponding critical value is 32.67. $Q_p>32.67$, so, the reliability is 95% to deny the hypothesis that there is no relationship between passenger’s travel purpose and travel’s frequency and distance, it can be thought there is no significant correlation between passenger’s travel purpose and travel’s frequency and distance.

From the survey’s results, at this stage in China, the high-speed rail passenger’s travel purpose mainly in business travel and visiting friends and relatives, the business travel has the highest frequency, at the same time, distribution of the business travel in long-distance regional is more.

Waiting Time Hypothesis Testing and Correlation Analysis

After analyzing traveler’s travel waiting time in different travel type, we can find the waiting time of the frequent traveler is shorter than the non-recurring traveler’s, the inside-regional passenger’s waiting time is shorter than the inter-regional passenger’s.

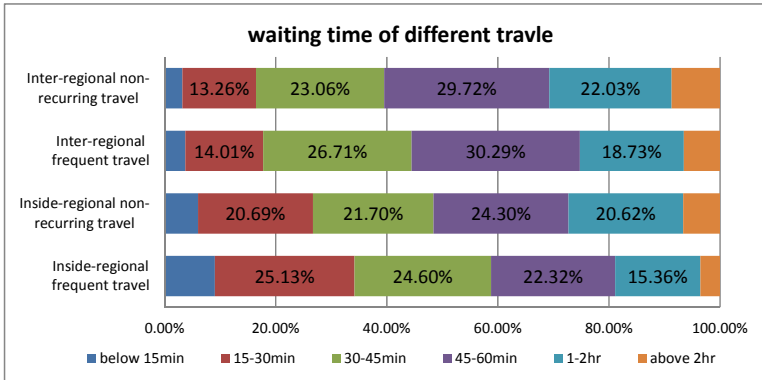


Figure 5. Waiting time of different travel

For the χ^2 test, $Q_p=212.31$, degree of freedom: $df=(r-1)(c-1)=(4-1)(6-1)=15$. Take the significance level: $P = 0.05$. Then the corresponding critical value is 25.00. $Q_p > 25.00$, so, the reliability is 95% to deny the hypothesis that there is no relationship between passenger's waiting time and travel's frequency and distance, it can be thought there is no significant correlation between passenger's waiting time and travel's frequency and distance.

From the survey's results, passenger's waiting time is somewhat related to travel distance, waiting time of the passenger who travel a long distance is longer than who travel a short distance, it somewhat related to passenger's scheduling, the shorter the travel distance, the less waiting time of the passenger. Therefore, for the station that operates the inter-city train, there is no need to make the scale of the waiting room in station too large.

CONCLUSION

This paper classifies the high-speed passengers with method that using travel distance and frequent, it can reflect the characteristics of the high-speed rail passenger better. Then, through this classification method to analyze three travel characteristics, which is income level, travel purpose and waiting time, of the passengers in different travel types, and we find these characteristics have a significant correlation with the different travel type, what's more, the correlation can be better to provide a reference for the high-speed rail system.

REFERENCES

- [1]Martina G. Gallarza. Value dimensions, perceived value, satisfaction and loyalty: an investigation of university students' travel behavior, *Journal of Tourism Management*, 2006: 437~452.
- [2] Stephane Hess, John W. Polak, Andrew Daly, Geoffrey Hyma. Flexible substitution patterns in models of mode and time of day choice: new evidence from the UK and the Netherlands, *Journal of Transportation*, 2007: 213~238.

- [3] Saratchai Ongprasert. Passenger Behavior on Revenue Management Systems of Inter-city Transportation, Japan: Kochi University of Technology, 2006
- [4] Stefan Schönfelder, Some notes on space, location and travel behaviour. Proceedings of the 1st Swiss Transport Research Conference, Monte Verità/Ascona, 2001
- [5] Francisco.J.Tapiador. Characterizing European high speed train stations using intermodal time and entropymetric, Journal of Transportation Research, Part A, 2009: 197~208

Fleet Size Metamodel for Dial-a-Ride Services with Time Constraints

Ying Luo¹ and Paul Schonfeld²

¹ Key Laboratory of New Technology for Construction of Cities in Mountain Area (Chongqing University), Ministry of Education, Chongqing, 400030, China

² Department of Civil and Environmental Engineering, University of Maryland, College Park, USA

ABSTRACT

Explicit performance models of a transit system are often very useful for system design, optimization, alternative comparison, and gaining insights into relevant system relations. In this paper, a performance metamodel has been developed for many-to-many dial-a-ride service, in which flexible routes and schedules are provided and service quality is guaranteed by time constraints. The model predicts minimum vehicle fleet size requirements. A simulation-based response surface methodology is used to model the functional relation between performance and contributing factors through experiments and statistical analysis. A detailed vehicle routing and scheduling algorithm and passenger time constraints, which are oversimplified or omitted in most other analytical approaches, are incorporated in the simulation experiments from whose results our model is statistically estimated. A face-centered central composite design is used to determine the experiment design points. The metamodel is validated using an additional set of randomly generated data. The resulting model is relatively simple in structure, inexpensive to use and fairly robust.

INTRODUCTION

At the planning or design stage of transportation systems, explicit performance models of a proposed system are often very useful in optimizing the controllable variables of the system, comparing and selecting of alternatives, or gaining insights into the system relations. This article develops an explicit performance model for demand responsive many-to-many dial-a-ride (DAR) services, which predict fleet size requirements. Such DAR services are intended to provide the general public intermediate services in terms of cost and service quality between conventional fixed-route buses and flexible taxi services.

In a DAR system, passengers specify transportation requests with their origins, destinations, and desired pickup or delivery times. A set of flexible routes and schedules must be determined to best accommodate the demand under time constraints. Traditional DAR services have met financial problems due to low vehicle productivity and high operating cost. With the introduction of intelligent transport systems and more efficient routing and scheduling algorithms which reduce operating cost, demand-responsive transport has been increasingly applied in recent years to a

niche market that replaces or feeds (usually via small low floor buses or taxis) conventional transport where demand is low and possibly widely dispersed.

Performance models are useful tools helping in better planning and designing a system. Since the performance models are intended for use at the high-level system planning stage, they should be easy to acquire and use (e.g. in explicit form other than running simulations to obtain the performance results), and not require excessive data which might not yet be available at the planning stage. Model prediction should be reasonably accurate and sensitive to relevant policy alternatives (e.g. maximum waiting time and vehicle operating speed). The form of the models should be relatively simple to use.

The prediction of performance measures for DAR services is more complex than for conventional fixed-route bus systems. For the latter the relations between operating cost and service quality are relatively straightforward and can be formulated with relatively simple equations in analytic models. The average route spacing and headway for each route can determine the number of vehicles required. For DAR services, passenger requests arrive in real-time, the DAR routes and schedules are flexible and change daily, operations require solving the DAR problem considering special passenger precedence and travel time constraints, only near-optimal solutions are likely to be found, and the performance measures are closely related with vehicle operating speed, time constraints and service coverage. Manual dispatching is relatively simple for very small systems, but is much less efficient than computerized dispatching with sophisticated algorithms, and seems obsolete given the present availability of powerful and inexpensive computers.

The literature review in the next section indicates that existing performance models developed through theoretical analysis (e.g. based on geometric probability or queuing theory) generally suffer from the limitations of using manual or very simple vehicle routing algorithms and neglecting passenger time constraints. Meanwhile, empirical data from real world DAR operations are scarce and the operations differ considerably in factors such as area covered, form of DAR implemented and routing algorithm used. Besides, most of those systems are designed for handicapped passengers. (The handicapped DAR services differ from the general DAR services in that the former usually have lower demand, allow longer time deviations and require 24-hour advance reservations.) Simulation is still a promising method to replicate the complex DAR operation since it can represent the vehicle routing algorithm and take into account other constraints and randomness in the system. Simulation data are an alternative when real data are scarce or unavailable. However, simulation models are not directly suitable for high-level decision making due to their extensive data inputs and computation burdens. Available explicit performance models based on statistical methods and simulation data are limited. Most models are based on a MIT simulation model (Wilson et al. 1971) without time constraints in which the passengers are assumed to be picked up as soon as possible (in practice, passengers may want to be picked up or delivered close to their desired times).

The remainder of the paper is organized as follows. We first review the literature on the existing performance models in the field of demand responsive services. Then, we briefly describe the operation scenario of the DAR system

analyzed in our study. The performance model is developed through a simulation-based metamodeling approach and then validated. Concluding remarks then follow.

LITERATURE REVIEW

Performance models for DAR systems can be categorized as simulation models, analytical models (i.e. based on notions from geometric probability or queuing theory), and empirical models statistically estimated from either real or simulated data. Computer simulation is the first and the most generally accepted approach for predicting the system performance of demand responsive systems. Simulation models are capable of generating individual service requests from specified time and space distributions, employing the specified routing and scheduling algorithm and obtaining disaggregate measures, which are summarized statistically to specify the system performance. Thus, simulation models are able to replicate the complex nature of a DAR operating system and reliably estimate performance measures.

Simulation models for DAR systems have been developed and utilized extensively by many researchers, including. Those models are generally used to evaluate the efficiency of routing and scheduling algorithms, to predict performance measures of specific systems, and/or to predict system response to specific parameter changes. However, simulation models tend to be difficult to acquire and their successful use typically requires fairly sophisticated planners with no pressing time constraints. They are also time-consuming to develop for specific cases. Simulation models are not quite suitable at the planning level since they provide no explicit relations between system outputs and inputs. Despite that, simulation plays an important role in generating simulated data and in the calibration of analytical performance models, as will be seen in the following review.

Lerman and Wilson (Lerman et al. 1977) modeled the many-to-many service as an M/M/1 system, in which the mean of the exponentially distributed service time is based on a linear function of trip length and productivity. The linear function is calibrated using simulation results. The predictions are considered valid only in relatively uncongested systems, and an assumption that service times vary linearly with interstop distance and productivity should limit the model's applicability to narrow range.

Most recently Diana et al. (Diana et al. 2006) provide a probabilistic model to forecast the number of vehicles needed to operate a demand responsive transit service under time window constraints. Certain assumptions have to be made for the probability density function of the time intervals between two successive pickup times and the distance between two successive points in a route. As the authors point out, their approximation of the distribution of the leg length can alter the results when the time windows are wide and further investigation is needed.

Wilson et al. developed the first empirical model for many-to-many DAR service using an intuitive model form, calibrated with data from simulation experiments with many-to- several and many-to-many demands. The results are based on simulation experiments with limited variations in operating conditions. The

requests are assumed to be served as soon as possible. Furthermore, variations in vehicle speed and time constraints are not considered. Arillaga and Medville (1974) have developed demand, supply and cost models by fitting a simple linear form to observed operating data, based on results from thirteen existing systems with various operating types (i.e. many-to-many, many-to-few and many-to-one). The thirteen sets of data used for estimation are very limited. Furthermore, the models fail to capture the critically important non-linear character of the performance relations (Wilson and Hendrickson 1980). Recently, Fu (2003) developed an analytical model which predicts the minimum fleet size requirement for many-to-many static DAR service by calibrating the proposed model form with simulation data. A sequential insertion heuristic is used and the objective is to minimize the fleet size while satisfying all the demand and service quality constraints (time window and ride time constraints).

OPERATION OF THE DIAL A RIDE SERVICE

The dial-a-ride service operation considered in our study can be described as follows:

1. Both advance requests and same-day requests are allowed in the reservation systems. Since this system serves the general public, same-day service is deemed more reasonable for attracting more patronage from the general population.
2. Each passenger requests a trip by specifying trip origin and destination, and either a desired pick-up time DPT at origin or a desired delivery time DDT at destination.
3. A passenger with a desired pick-up time will be picked up during time window $[DPT, DPT + TW]$ and a passenger with a desired delivery time will be delivered during time window $[DDT - TW, DDT]$. TW is the pre-specified maximum deviation from desired time.
4. A passenger's actual ride (in-vehicle) time will not exceed a given maximum ride time MRT , which is usually a function of the passenger's direct (shortest path) ride time DRT as $MRT = a + b \cdot DRT$. a and b are constants.
5. A vehicle is not allowed to wait idly while carrying passengers.
6. Vehicle capacity should not be exceeded. In the DAR context, due to the low vehicle productivity, the vehicle capacity is usually not a relevant constraint.

The level of service is guaranteed by the constraint on deviation from desired pickup or delivery time and by the maximum ride time constraint, which limit the worst case bounds for the service quality. The fifth constraint assures that the passengers do not sit in an idle vehicle during their trips just waiting for other passengers (except to board or exit), which would deteriorate the DAR service quality.

DEVELOPMENT OF THE PERFORMANCE METAMODEL

In this study, a simulation-based response surface methodology is used to develop the performance model. Response surface methodology is a very popular metamodeling technique used to approximate complex functional relations, and has been used effectively in various areas (Box and Draper 1987). The most extensive

applications of responsive surface methodology are in situations where several input variables potentially influence some performance measure of quality characteristic of the product or process. This performance measure or quality characteristic is called the response. The input variables are sometimes called independent variables. The resulting functions (or models) are usually called metamodels in that they provide a “model of the model” (Kleijnen 1987). The approximation formula or equations could be used to predict the performance resulting from various combinations of input parameters.

Response surface methodology is a set of statistical and mathematical techniques that encompasses: (a) Setting up a series of experiments that will yield adequate and reliable measurements of the response of interest; (b) Determining a mathematical model that best fits the data collected from the design; (c) Determining the optimal settings of the experimental factors that produce the optimal value of the response. The first two techniques are employed in this research to develop the performance metamodels.

The approximate empirical functions or models are usually built using statistical regression methods. The most common models used in response surface methodology are the polynomial first-order and second-order response surface models. Note that response surface methods are additional techniques employed before, while, and after a regression analysis is performed on the data. The experiment must be designed, that is, the input parameters must be selected and their value during experimentation must be designated before the regression analysis. After the regression analysis is performed, certain model testing procedures are applied.

The technique used for developing the performance model is summarized as follows:

- Design simulation experiments, which include the determination of input factors, their ranges of interest and selection of design points
- Execute experiments (apply heuristic to solve simulated scenarios)
- Collect data from experiments
- Develop relations among performance and input factors through statistical estimation
- Validate the metamodel

Experimental Design

In experimental-design terminology, the input parameters and structural assumptions composing a model are called factors, and the output performance measures are called responses. The main tasks in the experimental design include:

- Selecting the input factors (parameters) which most affect the response
- Setting the range of interest for the factors
- Determining the number and values of the experimental points (one point corresponds to one combination of the factors)
- If the experiment includes simulation, setting the simulation parameters (i.e. simulation length, number of replications)

Input Factors

Six factors have been identified as the main contributors to the vehicle resource requirements, as shown in Table 1.

TABLE 1. Lower and Upper Values of the Factors

i	Factor	Lower value	Upper value
1	Service area (sq. mi.)	9	81
2	Demand density (trips/hr/sq. mi.)	1	10
3	Maximum time deviation (min)	10	30
4	Maximum ride time ratio	1.5	2.5
5	Vehicle operating speed (mph)	10	40
6	Boarding or alighting time (min)	0.5	1.5

Other input parameters are considered as fixed aspects of the models and are described as follows:

- Demand spatial pattern differs considerably in each practical scenario and is difficult to fully describe quantitatively. A uniform distribution of all origins and destinations is used to represent the general case.

- For the temporal demand distribution, the time interval between successive passenger requests is assumed to have a negative exponential distribution.

- The service area is assumed to be square. Simulation results by Eilon et al. (1971) suggest that minor variations in the shapes of zones (e.g. square, circle and equilateral triangle) with uniform internal demand do not greatly affect the length of traveling salesman tours within them.

- It is assumed that half of the total requests are advance (previous day) requests and the lead time for the remaining real-time requests is uniformly distributed as $U \sim [0,120]$ minutes. The lead time is the measure indicating how far in advance the requests are made and is defined as the time elapsed between the passenger's request (calling) time and the earliest pickup time (Luo 2006). A system serving requests with certain lead times is believed to be more cost-effective than one serving immediate requests in that better routing and scheduling may be achieved by exploiting the available advance information.

- The rolling horizon rejected-reinsertion heuristic with periodical improvement, which is efficient in solving the large-scale dynamic DARP, is used for routing and scheduling.

- The probability that a passenger specifies a desired pick up or delivery time follows a binary distribution with a probability of 0.5.

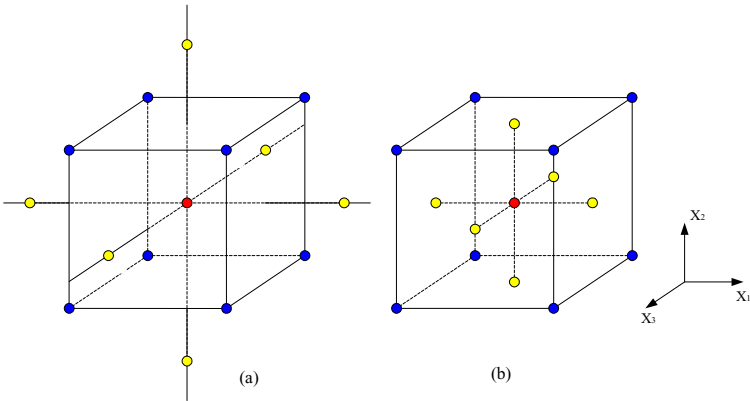
- A 1.15 road circuitry factor (ratio of the actual distance to the direct distance) is used. Note that the road circuitry affects the vehicle travel time. However, the effect of increasing road circuitry on the vehicle travel time is equivalent to the effect of decreasing vehicle operating speed on the vehicle travel time; therefore its effect can be incorporated in the vehicle operating speed.

Region of Interest

Table 1 shows the lower and upper values of the six factors considered. They are considered to sufficiently cover the general region of interest for a DAR service.

Factorial Design and Face-Centered Central Composite Design

Factorial designs are widely used in experiments involving several factors where it is necessary to study the joint effect of the factors on a response (Montgomery 2001). Assuming that the input variable is coded to take the value -1 at its low level and +1 at its high, a 2^k factorial design is such a design that requires $2 \times 2 \times \dots \times 2 = 2^k$ observations with each factor chosen at the -1 and +1 levels. The 2^k factorial design is an economic strategy for measuring factor interactions and screening out unimportant factors. Since only two levels are measured for each factor, the 2^k factorial design is one of the first-order designs that are used to estimate first-order models. Similarly, a 3^k factorial design requires $3 \times 3 \times \dots \times 3 = 3^k$ observations with each factor chosen at the -1, 0 and +1 levels. The 3^k factorial design is one of the second-order designs that are used to estimate second-order models. 3^k factorial design requires a large number of design points even for moderate values of k . For example, for $k = 6$ as in this study, a 3^k factorial design requires $3^6 = 729$ design points. If each design point needs 5 replications in a simulation experiment context, the total number of simulation runs would be 3,645, which is computationally expensive. The class of central composite designs introduced by Box and Wilson (1951) is an alternative class of designs to the 3^k factorial design. A central composite design consists of a 2^k factorial design points augmented with $2k$ axial points at $(\pm\alpha, 0, 0, \dots, 0)$, $(0, \pm\alpha, 0, \dots, 0)$, \dots , $(0, 0, 0, \dots, \pm\alpha)$ and n_c ($n_c \geq 1$) center points $(0, 0, 0, \dots, 0)$. In Figure 1a for $k = 3$, a central composite design consists of a $2^3 = 8$ factorial design points augmented with $2 \cdot 3 = 6$ axial points and n_c center points. If the region of interest is cuboidal, a useful variation of the central composite design is the face-centered composite design with $\alpha = 1$ (Figure 1b), which is chosen in this study. Since the number of factors considered is 6, the design consists of $2^6 = 64$ factorial design points and $2 \cdot 6 = 12$ axial points. The number of center points is set at 6.



**FIGURE 1. Central composite design (CCD) for $k = 3$
 [(a) General CCD, (b) Face-centered CCD]**

Generation of Demand Scenarios

Monte Carlo simulation is used to generate specific demand attributes such as the origin, destination and calling time of each request. Here Monte Carlo simulation means a scheme employing random numbers to generate scenarios of demand configurations. It is assumed that origins and destinations of requests are uniformly distributed over the service area. The inter-arrival times of calls have a negative exponential distribution. Requests are generated for a three-hour service period, which represents a typical peak hour period. In each demand scenario, the aforementioned online heuristic is used to route the vehicle fleet and schedule the pickup and delivery times of requested trips, and the minimum fleet size required to accommodate all requests are collected from each of the simulation run. To deal with the randomness of the demand, each experiment (each of the factor combination) is repeated five times. Average performance over those five replications represents one design point.

Regression Analysis for Vehicle Fleet Requirement Model

The notation used for the performance model is defined as follows:

Response N : Minimum number of operating vehicles which satisfy all demand for given time constraints. Factors A : Service area size (sq. mi.), b : Total boarding and alighting time per person (min), D : Demand density (trips/sq. mi./hr), R : Maximum ride time ratio, V : Vehicle operating speed (mph), W : Maximum time deviation (min).

In the first step, a first-order linear model is fitted to the response, which is the vehicle fleet size N . However, residual analysis suggests a transformation of the response N may result in better fit. A multiplicative form is hypothesized for the vehicle requirement model as follows:

$$N = \alpha_0 \frac{A^{\alpha_1} D^{\alpha_2} b^{\alpha_6}}{W^{\alpha_3} R^{\alpha_4} V^{\alpha_5}} \quad (1)$$

Equation (1) can be transformed into the following linear form:

$$\log_{10} N = \log_{10} \alpha_0 + \alpha_1 \log_{10} A + \alpha_2 \log_{10} D - \alpha_3 \log_{10} W - \alpha_4 \log_{10} R - \alpha_5 \log_{10} V + \alpha_6 \log_{10} b \quad (2)$$

Polynomial first-order and second-order models with transformed response $\log_{10} N$ are also analyzed and their regression results along with the multiplicative model are compared. No interaction terms are considered in the second-order model.

All three models are estimated using linear regression with SPSS software (version 11.0). The estimated parameters with standard errors, the corresponding adjusted R^2 values, F values, the normal probability plots and the plots of residual against the predicted value are reported and analyzed for each of the three models. The results indicate that the multiplicative model and the second-order model predict better than the first-order model. The multiplicative model is preferred to the second-order model due to its relatively simple form. The multiplicative model, whose adjusted $R^2 = 0.989$ is:

$$N = 4.79 \frac{A^{1.07} \cdot D^{0.72} \cdot b^{0.21}}{W^{0.29} \cdot R^{0.37} \cdot V^{0.68}} \quad (3)$$

To incorporate the effect of road circuitry f_c on the vehicle requirements (a 1.15 circuitry factor is used in all experiments for metamodel development), the model can be rewritten as:

$$N = 4.79 \frac{A^{1.07} \cdot D^{0.72} \cdot b^{0.21}}{W^{0.29} \cdot R^{0.37} \cdot (1.15V / f_c)^{0.68}} \quad (4)$$

Vehicle productivity can be estimated from the above model by dividing the hourly demand by the number of vehicles.

METAMODEL VALIDATION

Regression analysis, used to develop the general linear metamodel, is very much a data-based technique. It finds the model with the best possible fit to the data. Models thus estimated might not perform well on new data. In this study, the metamodel is validated against 30 new design points other than those used to build the metamodel. The new design points are randomly generated within the region of interest. More specifically, values for each factor are generated from uniform distributions bounded by their respective lower and upper values. In the face-centered composite design, most design points used to develop the metamodels are located in the “corner” or “boundary” of the design space. The metamodel validation, in some sense, tests how well the models fit the points that are more internally distributed in the design space.

Table 2 shows the observed values from the simulation and the estimated values from the performance models for the fleet size model. The validation experiments span a wide range of input parameters and the required number of vehicles resulting from simulation range from about 3 to 120. The gaps between the estimated values from the fleet size model and the observed values from the simulations range from 0.6% to 17.6%, but most are within 10%. Those models can provide fair estimates to be used at the system planning stage.

TABLE 2. Observed vs Estimated Values for the 30 Validation Experiments

Experiment	Number of vehicles		Experiment	Number of vehicles	
	Estimate	Difference		Estimate	Difference
1	19.3	14.8%	16	2.4 (2.8)	-14.8%
2	22.6	8.7%	17	107	6.0%
3	50.3	-0.6%	18	19.6	14.0%
4	94.2	-2.1%	19	46.4	8.9%
5	31.7	15.6%	20	22.5	-6.9%
6	15.1	10.8%	21	15.7	12.0%
7	43.7	5.5%	22	53.6	-3.3%
8	46.7	6.6%	23	36.6	11.1%
9	25.6	10.1%	24	40.8	9.7%
10	3.5 (3.6)	-2.2%	25	98.5	5.5%
11	65.1	-9.1%	26	7.2 (6.8)	6.0%
12	11.8	11.8%	27	48.0	7.7%
13	68.4	-3.6%	28	35.2	5.9%
14	9.9 (8.4)	17.6%	29	63.9	5.8%
15	118 (120)	-1.7%	30	24.1	7.5%

CONCLUSIONS

In this paper, a performance metamodel has been developed using the simulation-based response surface metamodeling approach for dynamic many-to-many DAR services. The model predicts the minimum vehicle fleet requirement for the system. The functional relations are modeled through well designed simulation experiments and subsequent statistical analysis on data collected from experiments. Polynomial first-order, second-order and multiplicative models are estimated and their statistical results are analyzed and compared. The best model in terms of both statistical properties and simplicity of form is identified. The metamodel is validated using an additional set of randomly generated data.

The resulting model is relatively simple in structure and inexpensive to use. Further sensitivity analysis also indicates that the performance metamodel is fairly robust, in that deviation from the assumptions of square service area, uniform demand distribution and percentage of passengers specifying desired pickup time in the practical range would not affect much the accuracy of the predictions. They are

approximate in nature, and mostly suited for use at the high-level planning stage of a system.

The developed performance model can be directly applied in predicting vehicle requirements for a given demand and operating scenario. Hence they can be used to evaluate the system operator and user costs, for comparisons with other system alternatives such as fixed-route bus services. Other applications include the optimization of the service in terms of the policy variables such as the maximum time deviation. The developed performance model might be applied to optimize an integrated system including both flexible and fixed route transit services.

Field operating data from similar systems should be collected, if they become available, in order to further compare and evaluate the developed model.

REFERENCES

- Arrillaga, B., and D. M. Medville. Demand, supply, and cost modeling framework for demand-responsive transportation systems. In *Demand-Responsive Transportation Special Report 147*, 1974), pp. 32-48.
- Box, G. E. P., and N. R. Draper. *Empirical Model-Building and Response Surfaces*, Wiley, New York, 1987.
- Box, G. E. P., and K. B. Wilson. On the experimental attainment of optimum conditions. *Journal of the Royal Statistical Society*, Vol. 13, 1951, pp. 1-38.
- Diana, M., M. M. Dessouky, and N. Xia. A model for the fleet sizing of demand responsive transportation services with time windows. *Transportation Research*, Part B, Vol. 40, No. 8, 2006, pp. 651-666.
- Eilon, S., C. D. T. Watson-Gandy, and N. Christofides. *Distribution Management: Mathematical Modelling and Practical Analysis*, Hafner, New York, 1971.
- Fu, L. Analytical model for paratransit capacity and quality-of-service analysis. In *Transportation Research Record: Journal of the Transportation Research Board*, No. 1841, Transportation Research Board of the National Academies, Washington, D.C., 2003, pp. 81-89.
- Lerman, S., M. Flusberg, W. Pecknold, and N. H. M. Wilson. *A Method for Estimating Patronage of Demand Responsive Transportation Systems*. U. S. Department of Transportation Report DOT-TSC-977, 1977.
- Luo, Y. *Heuristics and Performance Metamodels for the Dynamic Dial-a-Ride Problem*. Ph.D. Dissertation, Department of Civil and Environmental Engineering, University of Maryland, College Park, 2006.
- Montgomery, D. C. *Design and Analysis Experiments*, 5th edition, Wiley, New York, 2001.
- Wilson, N. H. M., J. M. Sussman, H. Wong, and B. T. Higonnet. *Scheduling Algorithms for Dial-a-Ride Systems*. Technical Report USL TR-70-13, Massachusetts Institute of Technology, Cambridge, MA, 1971.
- Wilson, N. H. M., and C. Hendrickson. Performance models of flexibly routed transportation services. *Transportation Research*, Part B, Vol. 14, 1980, pp. 67-78.

Development of Intercity Through Train Services Between Mainland China and Hong Kong

Carmen Li¹

¹ MTR Corporation, General Manager-Intercity, 2/F Fo Tan Railway House, 9 Lok King Street, Fo Tan, Hong Kong, PH (852) 26881337; FAX (852) 26880420; Email: cli@mtr.com.hk

Abstract

This paper outlines the past, current and future development of intercity train service between major cities in Mainland China (including Beijing, Shanghai and Guangzhou) and Hong Kong. It also describes the role of intercity train service in fostering the social and economic development of Hong Kong and Mainland China, particularly Guangdong province. The cross-boundary passenger markets and profiles are analyzed, followed by an elaboration of major business initiatives to address the identified market and passenger needs. Finally, in view of the rapid development of high speed rail network in Mainland China, it looks into the challenges and opportunities to the existing intercity train service.

Introduction

Intercity train services between Mainland China and Hong Kong go back over a hundred years to October 1910 when the single-track British Section of the Kowloon-Canton Railway from Tsim Sha Tsui to Lo Wu was opened. The Chinese Section of the railway, covering just over 22 miles from Lo Wu to Canton (known as Guangzhou now), became operational the next year and commenced Intercity through train services between Hong Kong and Canton. For the following century, this rail line served as Hong Kong's principal lifeline to Mainland China.

Train services were suspended during wartime, and all through traffic ceased in 1949. After a recess of 30 years, services were resumed in 1979 - the beginning of Mainland China's economic reform and opening up. Since then the Intercity through train has played a key role in linking up Hong Kong with Guangdong, the window of southern China. The Intercity through train soon became the preferred choice of people returning home during the Chinese New Year as well as business people attending the Canton Trade Fair held in Guangzhou twice every year or doing everyday business and trade.

As patronage grew steadily, Intercity through train services to Guangzhou were enhanced from one round trip in 1979 to four. With the implementation of the Closer Economic Partnership Arrangement (CEPA) and Individual Visitor Scheme (IVS) in 2003, through train services were increased to eight, then 10 round trips per day. Starting from 2004, the number of trains running between Guangzhou and Hong Kong increased to 12 round trips per day, with stopovers at Dongguan.

To mark the handover of Hong Kong to Mainland China in 1997, the Intercity through train services to Beijing and Shanghai were launched in the same year. The

three existing through train routes are shown in Fig. 1.



Figure 1. Intercity through train routes

Sustainable Development of Intercity Through Train Services

The three Intercity through train routes are jointly operated by MTR Corporation and various railway authorities under the Ministry of Railways of China. The Intercity through train running between Guangzhou and Hong Kong, known as the Guangzhou-Kowloon Through Train (GZTT), is currently the most popular mode of direct transport because of its safety, comfort and customer service standards. It accounted for 19% of the cross-boundary travel market in 2010. The total number of passengers carried between Guangzhou and Hong Kong over the past 30 years was more than 50 million. The average number of passengers travelling by the Intercity through train (inclusive of Guangdong, Beijing and Shanghai lines) reached 8,888 per day in 2010 (see Fig. 2) and stood at around 10,200 per day at the end of 2011.

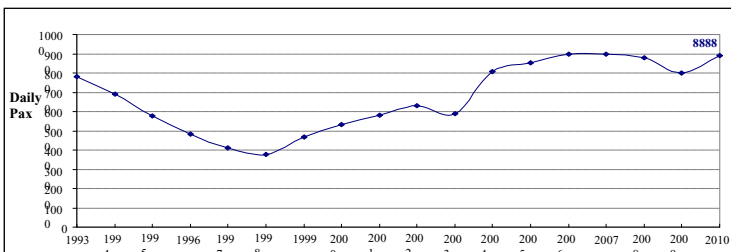


Figure 2. Average Daily Patronage of Intercity Through Trains (1993-2010)

Over the past decade, Intercity train services have encountered several major challenges. These challenges were overcome through focused strategic initiatives implemented at opportune moments, paving the way for sustainable development.

Up until 1998, Intercity train sets were provided solely by the Chinese railways, and daily patronage of GZTT reached its lowest ebb at 3,782 in 1998 owing to keen competition from buses running on the Guangzhou-Shenzhen Highway which opened in 1997. In August 1998, a double-deck electrified train, Ktt, managed by the then Kowloon-Canton Railway Corporation and now by MTR Corporation (see Fig. 3), was introduced between Guangzhou and Hong Kong. This initiative transformed the

Intercity through train services. The two electric locomotives were produced in Switzerland, while the coaches were imported from Japan, bringing in a brand new travel experience. Train crews onboard Ktt were all recruited from Hong Kong and onboard facilities were benchmarked to the service standards of airlines.



Figure 3. Ktt - the double-deck electrified train managed by MTR Corporation

Ktt soon became the preferred choice of many businessmen who travelled frequently between Guangzhou and Hong Kong. GZTT service was enhanced from four to seven round trips a day in 1999, with three round trips operated by Ktt, and patronage surged by 25% when compared to 1998.

The Intercity service experienced another downturn in 2003 due to the SARS pandemic earlier that year. Average patronage dropped to less than 5,900 per day but reached a turning point in June 2003 when CEPA, the first free trade agreement ever concluded by Mainland China and Hong Kong, was signed. CEPA opened up huge markets for Hong Kong goods and services, greatly enhancing the already close economic cooperation and integration between Mainland China and Hong Kong, and stimulated passenger traffic by rail. One month later, the Individual Visitors Scheme (IVS) was launched in four Guangdong cities, allowing residents of these cities to visit Hong Kong in an individual capacity. The Scheme then expanded gradually to cover 49 other Mainland cities, including Beijing, Shanghai and the entire Guangdong province. This policy provided impetus for the expansion of Intercity through train services. GZTT was increased to eight round trips a day, then 10, and eventually to 12 in April 2004. Patronage jumped by 38% in 2004 and grew at an average of about 8% annually from 2003 to 2008.

Train services to Beijing and Shanghai also expanded considerably since their commissioning in 1997. These trains, which operate on alternate days, benefited from the nation-wide speed acceleration in 2000, 2007 and 2009. Total journey times had been shortened from over 30 hours to 23.5 and 18.5 hours respectively. These services have successfully captured leisure travellers, especially group tours.

A significant move to facilitate sustainable development of these long-haul trains, provided and managed by the Chinese railways, was the rolling stock upgrade. New trains featuring better on-board facilities and electric-powered locomotives came into service in January 2008. All these initiatives have helped boost a double-digit growth of average daily patronage year on year.

GZTT also replaced its diesel locomotives with environmental-friendly electric-powered locomotives in phases between 2009 and 2010. Air pollution due to

diesel smoke was reduced to make the station environment greener. Another improvement to the Mainland rolling stock of GZTT was made in 2011 where conventional toilets (which must be closed on the Hong Kong section due to environmental requirements) were replaced with vacuum toilets. All these transformations have helped enhance the sustainable development of Intercity through train services.

Analysis of Passenger Segmentation

In the 1970-80s, through train passengers travelling between Guangzhou and Hong Kong were mainly foreigners, overseas Chinese and residents of Hong Kong and Macau. Since the 1990s, especially after the launch of Ktt, business travellers have formed the main market segment of GZTT. The proportion of leisure travellers from Mainland China, however, has increased noticeably in recent years (see Tables 1 and 2).

Table 1. Segmentation analysis of through train passengers by trip purpose

	Guangdong through trains			Beijing/Shanghai through trains	
	Business	Leisure		Business	Leisure
Year 2010	56%	44%	Year 2010	12%	88%
Year 2006	60%	40%	Year 2006	15%	85%
Variance	-4%	+4%	Variance	-3%	+3%

Table 2. Segmentation analysis of through train passengers by nationality

All through trains	HK residents	Mainland Chinese	Overseas travellers
Year 2010	45%	35%	20%
Year 2006	56%	23%	21%
Variance	-11%	+12%	-1%

The above statistics clearly showed that the rising trend of Mainland Chinese business visitors coming to Hong Kong would continue, and that more Mainland Chinese would travel to Hong Kong for leisure.

To grasp the opportunities arising from this growth, Intercity through train services have focused more efforts on capturing the market segment of Mainland Chinese leisure travellers.

Major Business Initiatives to Achieve Sustainable Development

To address the needs of the expanding leisure traveller segment, since 2008, Ktt has been selling tourist products onboard for the convenience of passengers from Guangzhou. These products included admission tickets to popular scenic spots in Hong Kong, such as Ocean Park, Disneyland and Ngong Ping 360. MTR Corporation also partnered with shopping malls and hotels in both Guangzhou and Hong Kong to offer other exclusive offers for Intercity through train passengers.

Another strategic move was the launch of the Weekend Through Train Travel Package in May 2009. To capture the growing number of leisure travellers, round-trip tickets on specific GZTT during the weekend were bundled with tours to scenic spots or hotels in Guangzhou and sold through appointed travel agents. Based on the

Weekend Package, themed tours such as cuisine and festival tours to Guangzhou and the neighbouring areas were organized in cooperation with travel agents. These tours have successfully attracted incremental passengers who have never travelled on through trains before.

Brand building was another key objective for the sustainable development of Intercity through train services in recent years. The 2010 Asian Games held in Guangzhou provided an opportune occasion to promote Ktt as an ideal means of direct transport to Guangzhou. In cooperation with the Asian Games Organizing Committee, Ktt was appointed the Guangzhou 2010 Asian Games Through Train. The exterior car body of Ktt was decorated in the theme of Guangzhou Asian Games from April until the end of the year. This proved to be a huge success by matching up travel by Ktt with a sports extravaganza.

As the rising trend of Mainland Chinese visitors coming to Hong Kong continued in 2011, the Intercity through train has introduced a series of service improvement initiatives during the year. To enhance customer experience, some popular Hong Kong style snacks and beverages, such as egg tarts and milk tea, were launched on Ktt and in the Through Train Departure Hall at Hung Hom Station. To broaden the ticket sales network and enhance customer convenience, GZTT tickets were available for sale at e-Instant Bonus terminals at 42 MTR stations. A Free Internet Zone was set up in the through train departure hall, providing five computers for free use by through train passengers. Wi-Fi service was provided on Ktt throughout the journey from Hong Kong to Guangzhou to allow passengers to stay connected. The through train departure hall was improved with new seats; and the installation of large screen displays for broadcasting infotainment also provided a valued service to passengers.

These measures have undoubtedly produced the desired outcome of increasing the number of passengers using the service. Intercity through train patronage rebounded from the average daily of 8,002 after the global financial crisis in 2009 to 8,888 in 2010. A single day record high of 14,481 was registered in April 2011 and the average daily patronage for 2011 was around 10,200.

Future Challenges and Opportunities

The biggest challenges to Intercity through train services in the near future would come from rail itself. There has been cannibalization by the CRH train which has made a one-hour journey possible between Guangzhou and Shenzhen since 2007. GZTT, being a direct mode of transport between Guangzhou and Hong Kong, still has advantages over its main competitors in terms of convenience and customer service.

Results from market surveys indicated that there is passenger demand for the extension of GZTT operating hours in the early morning and late evening in both directions, and additional train services from 12 to 15 round trips a day. This is consistent with the travelling pattern of the growing number of passengers from Mainland China. Statistics from the Hong Kong Tourism Board showed that among the 20.9 million visitors from Mainland China in the first three quarters of 2011, 10.4 million returned on the same day. The possible extension of the multiple-entry IVS to the entire Guangdong province will further stimulate the growth of the Mainland Chinese leisure traveller segment. Therefore, GZTT frequency enhancement and extension of operating hours will become a key operating strategy for Intercity through train services in the short term.

The opening of the Express Rail Link (XRL) in 2015 will be another challenge to the existing Intercity through train services. The XRL will be the second direct rail link between Hong Kong and Guangzhou via Shenzhen. The patronage of GZTT is expected to drop by a big margin in the first year following the opening of XRL, but will pick up in 2017 and thereafter. The main reason is that these two lines have different alignments (see Fig. 5 below) and catchment areas. The existing GZTT terminal at Guangzhou East is located in Tian He District – the CBD of Guangzhou; the future XRL will terminate at Guangzhou South which is in Panyu - a developing district that will provide an interchange for the national high-speed rail network.



Figure 5 – Rail links to Guangzhou

The Way Forward

To sustain the sustainable development of Intercity through train services, further improvements will be made by launching more customer-focused initiatives. These will include replacement of the conventional cardboard type GZTT ticket with soft ticket, introduction of more ticketing channels like mobile phone apps and use of Octopus card for payment in Hong Kong. The Intercity through train will continue to strive to be the preferred mode of transport to the city centre of Guangzhou; it will also play a complementary role to the XRL and the Pearl River Delta intercity rail network, thereby serving a population of more than 50 million within the prosperous regions of China.

References

- Peter Moss (2007), "A Century of Commitment", Prelude: A World too New and too Brave
http://www.hopewellhighway.com/WebSite_chn/ir/doc/HHI_Economic_Backdrop_Chi.pdf (Retrieved in March 2011)

Chongqing Intelligent Transport System Plan

Fu Yan

Chongqing Transport Planning Institute, Yang He Er Cun, No.18, Jiangbei District, Chongqing, P. R. China; PH: (86)13637958790 ; FAX: (8623)67862200, Email: 13637958790@126.com.

ABSTRACT

With the increasing urbanization and additional traffic it brought, the urban congestion, together with traffic accident and air pollution problems it created, has seriously confronted the society as a whole. Applying intelligent transportation system (ITS) tools to solve these problems in Chongqing are presented in this paper. The ITS is also perceived as the sustainable development tool to address this ever worsening urban traffic problems. The proposed Chongqing ITS Development Plan, which covers 11 domains and 52 subsystem constructions, are discussed in this paper.

OVERVIEW

ITS can provide traveler information service, provide fast and efficient emergency service, improve traffic safety, reduce traffic congestion, improve road efficiency, reduce travel costs, etc. Properly used, it can also improve the overall quality and efficiency of the system, while preserving the environment. Through continuous development, ITS has grown from the original phase of intelligent management of people, vehicles, and roads, to broader areas, including the level of government decision-making on the management of various departments and enterprises. The goal is to effectively improve transportation decision-making efficiency and effectiveness of system operation. In China, ITS has grown into a huge new industry.

Japan, the United States and Europe are the world's leaders in ITS development. Their experience is worthy of learning and reference. In general, their development models are divided into top-down and bottom-up.

America's ITS research is the top-down model, including the following characteristics: (1) the organization of research done by government agencies (such as the Department of Transportation); (2) research projects are generally established by the government; (3) the research project is conducted by the research institutions involved, with the collaboration of other institutions.

Europe and Japan by contrast, adopt the bottom-up model of ITS, with the following characteristics: (1) basic research of the organization is an independent research entity, without government or a higher level of direct supervision; (2) research projects are generally determined by the research institutions themselves, and to raise funds, research results generally apply only to its internal; (3) research program and direction determined by independent research institutions, research institutes lack of unity of purpose, with loose contact .

Both top-down and bottom-up models, have its corresponding advantages and disadvantages. Europe and the United States are gradually moving closer to a combination of both modes.

Table 1 Comparison advantages and disadvantages of the two modes

	Advantages	Disadvantages
Top-down mode	Has a strong unity and coordination	Because of incomplete information and the relative stability of the implementation of the scheme, making this guide does not meet the needs of reality, and easy to give the government a great deal of financial pressure
Bottom-up mode	Research and development work carried out by an independent organization, the information at their disposal a more comprehensive, timely decision making, flexibility, relatively large, easy to solve financial problems	Coordination between subsystems is very difficult

Beijing, Shanghai, Guangzhou, and Shenzhen are at the forefront of ITS development in China. By using public transport information platform as the core, they began to construct a series of ITS related projects. Shenzhen in 2006 carried out the construction of the ITS Master Plan. The construction of Shenzhen ITS provides comprehensive guidance to carry out and to promote the Shenzhen City ITS effectiveness and efficiency.

At present, Chongqing has no comprehensive plan for the ITS, several independent projects are conducted by various agencies such as road monitoring, intersection channelization, Jiefangbei CBD parking guidance system, and public transportation and other travel information platform. These separate systems in their respective areas play a role, but belong to different departments. Resources and

information cannot be shared. It is difficult to achieve a high level of coordination.

CHONGQING TODAY

Municipal People's Government General Office of Government sponsored public platform, including government information, services, work, interactive communication, the mayor-mail and other functions, the main provider of policy issued, work service, the public questions and other services, while providing various government departments, county government links, etc., the information platform focuses on policy, information dissemination and related convenience services, major decisions for the public understanding of the government, a very good platform to answer questions, convenient services in the government played a good role.

Municipal government under the transport-related sectors, including the Planning Bureau, Construction Committee, Traffic Management Bureau, Exchange Commission, transportation Authority and other departments, these departments have their own information platform, especially the Traffic Management Bureau, established a set of traffic monitoring, traffic management is one of the information platform, mainly for traffic management and the establishment of internal management platform; traffic management is open to the public information network (<http://www.cqjg.gov.cn>), the leading provider of network illegal queries, dynamic traffic management, laws and regulations and other information inquiries, did not provide real-time traffic, road traffic and other relevant health information query, but the long-term and traffic Radio traffic Management Bureau, provide real-time operational status of the broadcast road, convenient for public travel by car.

Research institutions, including municipal traffic departments under the Institute of Transportation, are units of information disclosure outside the window. Most closely with the public travel for bus and rail, the two companies have their own information site, providing a route query, map navigation, the relevant policy inquiries, complaints and other services, provides a more convenient convenience services.

Yuzhong district government established a parking guidance system in Jiefangbei CBD area, which began in May 2005, the system covers the CBD area 25 indoor parking garage, opened the current network, mobile telephone parking information, while traffic broadcasting regularly broadcast parking information, major roads and intersections in the Jiefangbei set the parking guide cards, dynamic broadcast the exact location of the parking lot and parking spaces remaining cases, the convenience of motorists looking for parking spaces, to avoid looking for parking bypass the traffic congestion .

Overall, the department has the appropriate office platform and service platform convenience, not one by one in this example, the current information platform for all departments showing the following characteristics: First, have their own

independence; second, limit function to agency-based needs; third, the information is difficult to distribute.

Chongqing traffic problems. In an effort to solve the urban traffic problems in Chongqing, too much manpower and resources were invested without proper coordination and planning, resulted in waste, resource depletion, and even environmental degradation. To address this problem, we should look at solving the problems from a systems approach and using technology to fully tap the potential of existing resources to better serve the community. Based on intelligent traffic information, information technology is the core foundation of openness and sharing of data. However, a lack of information sharing and system integration, plus the barriers in sharing data resources is still the bottleneck of ITS development here.

The general public is requesting the government to be more responsive in data sharing. This would not only reduce duplication of investment by various traffic-related departments, but also through resource sharing and system integration to achieve win-win situation.

In Chongqing, we should first consider a system which guarantees the sharing of resources and a unified standard, but more resources should be available to public so they can travel with ease. We start from the following aspects to address these issues:

- (1) Agency coordination and resource sharing: the sharing of resources to avoid duplication of work.
- (2) Public service: provide public with advanced traveler information.
- (3) Traffic Safety: to provide prompt emergency services.
- (4) Freight movement: to improve freight movement efficiency and safety.
- (5) Regional development: to improve urban traffic management and level of traffic throughout the region.

ITS goals in Chongqing. The goals of ITS construction in Chongqing are to build safe, efficient, and effective transport systems that serve the public interests in the city, including the following:

- (1) To expand and cover the entire metropolitan area cities such as the regional center Aikawa, Jiangjin, Yongchuan, longevity, Fuling, Wanzhou, Qianjiang multi-way traffic information collection system.
- (2) Integrate the city traffic information platform with the western region of

Chongqing traffic information center.

(3) Build central management platform to improve government decision-making process.

(4) Encourage research institutions to improve the level of scientific research and better decision tools.

(5) Built business management platform to improve enterprise management level.

(6) Establish advanced traveler information to reduce travel time

CHONGQING ITS PLAN

The users of Chongqing ITS are divided into five categories: government, administration, research institutions, transport companies, traveler.

Table 2 Classification refine the user table

User class	User
Government	Government, mainly for government decision-making
Management	Planning department, highway management, municipal management, traffic management, transportation management, public safety, customs, environmental protection agencies, disaster relief departments, fire departments, etc.
Research institutions	Institute of Transportation
Transport enterprises	Freight sector, passenger transport sector, bus companies, taxi companies, etc.
Traveler	Drivers, bus passengers, cyclists, pedestrians, disabled, etc.

Under the Chongqing ITS, We plan to establish 11 systems, namely traffic information collection, traffic information processing, government decision-making, transportation information management, traffic management, emergency management, charge management, public transport management, passenger management, freight management, and traffic information service system.

(1) Traffic information collection. By covering all urban traffic detection equipment, the operation of state metropolitan area distributors to detect traffic flow conditions;

With the trunk road traffic flow collection system, by increasing the incident detection devices, traffic incident detection; Cargo flow through the positioning technology to obtain location information.

(2) Traffic information processing platform. According to the agreed rules of the exchange and sharing of data, the field of intelligent transportation applications for the standardization of data organization and information integration, information resources on the ITS encoding rules defined for the field of intelligent transportation applications of information processing, system architecture to meet the access to new equipment or services.

(3) Government decision-making. Application of ITS technology for roads, communications, electrical and mechanical systems can pay infrastructure maintenance and management, statistics collection and maintenance of transportation infrastructure management data generated on this basis and implementation of appropriate management and maintenance plan. in the relevant transport planning and traffic demand for the exchange of information, collaborate to produce the best overall planning strategy, provide the calculation of transport planning, simulation tools, resulting in current and future traffic conditions based on the needs of transportation and planning, and evaluate major construction project to provide traffic analysis tools, support for project feasibility studies, project construction and post-evaluation.

(4) Traffic information management. Buses for real-time information collected for processing, combined with the bus lines into bus traffic, average speed, operating conditions and other data. Acquisition of vehicles for real-time information, event information processing reflecting the real-time traffic conditions, such as road congestion, etc. Easy to access and extract data would provide historical data for the transportation decision-making support.

(5) Traffic Management. Using a variety of detection methods to achieve the detection of traffic management-related information and data processing to detect. To transport test data based on-line through the understanding and knowledge of road traffic operating conditions, under the guidance of the correct decision, the use of traffic signals, traffic signs, traffic markings and other facilities, limited by the ban, constraints, organizing and directing other means, to the movement of vehicles in the guidelines, induction and transfer control to make it safe and smooth operation. Application of advanced monitoring techniques, to collect timely and accurate

information in violation of traffic laws event, without affecting the normal operation of traffic under the premise of automatically or manually execute the appropriate measures to deal with. Application of advanced detection means, the conversion at the transfer points were detected, the purpose to facilitate passengers.

(6) Emergency Management. Before the incident occurred, for a variety of possible development of contingency plans, including incident type and classification, relief response strategy to rescue the implementation of strategies. Implementation of emergency relief, including relief program development, to send rescue resources, emergency vehicles priority access, scene of the incident management.

(7) Management fees. Implementation of "City Card", will be public transportation, parking, subway, telephone, fuel filling, water, electric and other fees in one payment.

(8) Public transport management. According to information such as bus travel demand, rational planning public transportation network and station, and to assist in the development of public transportation business plan, the actual operation of the circuit for performance analysis, the public transportation system efficient, safe and efficient manner to meet the travel needs of users. Of public transport facilities and vehicles, surveillance, monitoring, control, provide security for public transport services to participants.

(9) Passenger Management. Includes management of road passenger transport practitioners, management practitioners driver, passenger station management, passenger lines management, passenger inspection management, passenger transport management.

(10) Freight Management. Practitioners include the management of freight transport, freight transport management, the management of freight transport practitioners, intermodal freight transportation management, intermodal freight transfer station management, freight management employees, the management of road transport services, practitioners, employees in road transport services management, vehicle maintenance business qualification management, vehicle maintenance, business operations management, vehicle inspection station qualification management, vehicle inspection station management behavior management, freight audit and management.

(11) Traffic information service. To a variable, multi-level information dissemination screen as a carrier to travel to provide parking lots (garages) the specific location of parking spaces in real-time data and other information current, reasonable drivers parking guide, and data processing.

Building a successful ITS is a complex process, it requires long-term cooperation of many departments, plus adequate funding and policy support to ensure the implementation of ITS. The most important step is the collaboration of various departments, thus setting up a coordination unit for the horizontal coordination of resources for a unified management, responsible for the advancement of the project is necessary. The departments include Planning Bureau, Construction Committee, Traffic Management Bureau, the City Political Commissar, Transportation Authority, Environmental Protection Agency, and Information Industry Bureau.

CONCLUSION

Intelligent Transportation Systems (ITS) is a large system that can be expanded into a variety of user services, including public convenience services, for internal management services, scientific research institutions of the historical data for analysis, decision-making system for government we propose the framework of the ITS system is a huge part in the ITS system is based on the current problems facing the reality of Chongqing's, on this basis, can also be expanded to service the system for more objects in the city face increasingly sharp contradiction between the premise of traffic, ITS will be the development of hot spots and traffic areas of focus, we hope such a framework and implementation plan, and protective measures under the guidance of the ITS construction in Chongqing will be gradually carried out, the optimal allocation of limited traffic resources would allow our transportation infrastructure moves toward sustainable development and healthy growth.

REFERENCES

- Wan Xiaojing, etc, (2006). China Intelligent Transportation System Development Strategy, People's Communications Press.
- Yang Dongyuan, Lin Qun, (2007). Intelligent Transportation Systems, Shenzhen Construction Review, Urban transport.
- National Standardization Technical Committee of Intelligent Transport Systems, (2005).
- National Intelligent Transportation Systems 2004 Annual Report for Standardization.

A Practical Intelligent Method to Quickly Screen Pedestrian Related Potential Conflicts with Motor Vehicles

F. Qiao¹, P.-H. Kuo² and L. Yu³

¹President of ICTPA Texas Chapter and Associate Professor in Department of Transportation Studies, Texas Southern University, 3100 Cleburne Avenue, Houston, TX 77004, PH (713) 313-1915, FAX (713) 313-1856, Email: qiao_fg@tsu.edu

²Department of Transportation Studies, Texas Southern University, 3100 Cleburne Avenue, Houston, TX 77004, PH (713) 313-1915, FAX (713) 313-1856, Email: ckin44@gmail.com

³Dean, College of Science and Technology and Professor in Department of Transportation Studies, Texas Southern University, 3100 Cleburne Avenue, Houston, TX 77004, PH (713) 313-7282, FAX (713) 313-1856, Email: yu_lx@tsu.edu

ABSTRACT

While pedestrian related incidents at intersections are not so popular in developed countries, there are always potential conflicts between pedestrians and right-turn motor vehicles. Other potential conflicts include those between right-turn vehicles and stopped through movement vehicles encroaching crosswalks. All these are potential threats to pedestrians, and affect their comfort and safety. The relationships between potential conflicts and the causing factors are very complicated and nonlinear, which can hardly be depicted by simply models. In this paper, the intelligent fuzzy table look-up scheme is employed to model such relationships. The constructed fuzzy system is based on the rule base from observed data, which is intelligent and very helpful for field engineers to quickly screen pedestrian related potential conflicts. A case study in Houston, TX, USA illustrates the modeling procedure, and shows the model validations. With more surveillance data collected, the rule base and fuzzy system could be even better improved.

INTRODUCTION

Intersection safety is always a considerable issue in urban traffic operations. In 2009, 33,808 fatalities occurred on nation's roadways in USA. Of these, 20.8% percent of all traffic fatalities with about 7,043 were intersection related (FHWA, 2011). Among all modes of road users at intersections, pedestrians often have difficulties mixing with on-street motorized traffic because travel behaviors pedestrians are quite different from motorists. In 2008, 1,050 pedestrians were killed at intersections in USA (NHTSA, 2011a; NHTSA, 2011b).

Several studies have shown that Right-Turn-On-Red policy that were adopted in USA in late 1970s, increased the frequency of right-turning crashes at signalized

intersections, especially crashes involving pedestrians (Zador, 1984). The conflict between pedestrian and right turn mobile have long been a significant issue.

The current design manuals and standards such as the “Guide for the Development of Bicycle Facilities” by American Association of State Highway and Transportation Officials (AASHTO, 1999), and the “Manual on Uniform Traffic Control Devices” (MUTCD) by Federal Highway Administration (FHWA, 2009) provide limited guidance on pedestrian crossings at freeways interchanges. There is also no detailed description on how to reduce such conflicts.

The endangerment of pedestrian by right-turn and stopped through vehicles that are encroaching crosswalks is a serious concern of safety. The right turn on red policy, which allows drivers to turn right when the traffic light is on red (normally vehicles need completed stop before the crosswalk), though is widely accepted in many cities, affects the smooth proceeding and even safety of pedestrian actually.

In the past decades, extensive research was conducted to protect the vulnerable pedestrians and bicycles at intersections via right-turn vehicles, including the determination of right-turn lanes (Kikuchi and Kronprasert, 2008), the safety analyses of right-turn truck (Niewoehner and Berg, 2005), and stop line design for various types of right-turn vehicles (Qiao, et al., 2010b). However, there is no solution on how to model and predict the potential conflicts between pedestrians and vehicles at intersections.

RESEARCH OBJECTIVE

The objective of this research is to develop an explicit technical method to model and estimate the potential conflicts between pedestrian and motor vehicles at intersections nearby freeway interchanges. The identified method should be helpful for field engineers to quickly synthesize suitable treatments to reduce such potential conflicts.

PROBLEM STATEMENT

Potential Crossing Conflicts. At a four-way intersection there are 32 possible conflict points between vehicles to vehicles. For pedestrian to vehicle, the total possible potential conflicts are 24 at crosswalk and six for each side (CGSC, 2011). Pedestrians who have to face six possible conflicts cross at intersection.

Potential Crossing Conflicts with Through and Right Turn Vehicles. In this research, right turn and through vehicles are considered to be two essential issues. First, vehicle right turn on red is seriously to threaten the pedestrian crossing. The drivers would focus on the through vehicle, which is form left side and not pay enough attention to the pedestrian crossing. During the field observations of vehicle stopping positions, research team found that, when necessary, both right turn and through vehicles are used to encroach the pedestrian lane. When the crosswalk is encroached by those mobiles, pedestrian may bypass and walk on the driveway. This behavior may cause a serious accident and affect the coordination of intersection. In

Figure 1, the red circles show the examples of the potential conflicts for right turn vehicles and through vehicles.

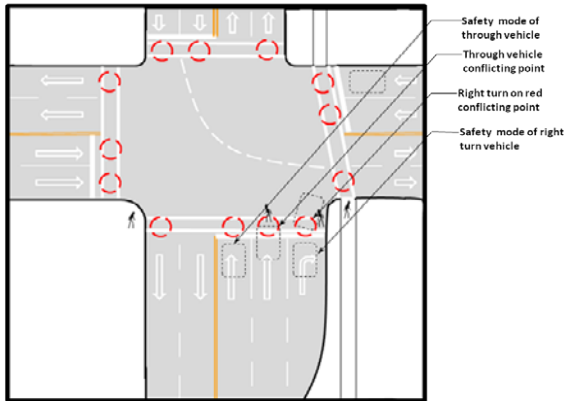


Figure 1. Examples of potential conflicts with right turn and through vehicles.

Level of Treatments. As is described by Qiao, et al. (2010a), there could be three levels of treatments applied at intersections based on how serious the potential conflicts are. Level 1: Proper placement of traffic signs such as yield sign, color pavement marking, and speed limited warning...etc. to warn drivers for pedestrian crossing safety. Level 2: Placement of advanced sensors to detect/sense pedestrians' requests and provide suitable traffic control strategies at the intersection. Level 3: To construct interchanges or retrofit the intersection.

FUZZY TABLE LOOK-UP SCHEME FORMULATION

Methodology Description. Pedestrians could be conflicted when crossing an intersection with (a) right-turn vehicles; and/or (b) stopped through movement vehicles encroaching crosswalks. The variables that may affect the potential conflicts at least include: right-turn vehicle speed, right-turn volume, through traffic volume, lane width, and crossing depth. Obviously, the relationship between these influencing variables and the resulted potential conflicts are very complicated and nonlinear. Fuzzy logic theory is capable of dealing with systems where the input-output relationships are too complex and where the human knowledge is reachable to be combined into the system (Zadeh, 1965). The fuzzy table look-up scheme is proven to be an effective way for nonlinear modeling (Wang, 1997; Qiao, 2009), and so is adopted.

Fuzzy Table Look-up Scheme. The fuzzy table look-up scheme depends on the collected input-output data pairs (Zadeh, 1965; Qiao, et al., 2010b). Suppose that the input-output pairs are represented as $(x_1^p, x_2^p, \dots, x_n^p) \in U$, where $U = [\alpha_1, \beta_1] \times [\alpha_2, \beta_2] \times [\alpha_3, \beta_3] \times \dots \times [\alpha_n, \beta_n]$ are considered input variables to the conflict determined model. $p = 1, 2, \dots, N$ represents each data pair and N is the total number of data pairs. The input variables could be right-turn vehicle speed, right-turn volume, through

traffic volume, lane width, and crossing depth, etc. The output y_0^p is the potential conflict in domain $y_0^p \in V = [v_y, \omega_y]$. The proposed fuzzy system should be based on the rule base constructed from these N input-output pairs.

Define the Fuzzy Sets to Cover the Input and Output. For each $[\alpha_i, \beta_i]$, $i = 1, 2, \dots, n$, define N_i fuzzy sets A_i^j ($j=1, 2, \dots, N_i$), which should be complete in $[\alpha_i, \beta_i]$. This means that, for any $x_i \in [\alpha_i, \beta_i]$, there exists A_i^j such that its membership $\mu_{A_i^j}(x_i) \neq 0$. The class of pseudo-trapezoid membership functions are such candidates. Generate One Rule from One Input-Output Pair. First, for each input and output pair $(x_1^p, x_2^p, \dots, x_n^p; y^p)$, determine the membership values of x_i^p ($i = 1, 2, \dots, N_i$) in fuzzy set A_i^j ($j=1, 2, \dots, N_i$), determine the membership values of output y^p in fuzzy set B^l ($l = 1, 2, \dots, N_y$). Then, for each input variable x_i , determine the fuzzy set $A_i^{j^*}$ in which x_i^p has the maximum membership value. Similarly, the fuzzy set B^{l^*} for output can also be determined. The IF-THEN Rule **1** obtained is: "If x_1 is $A_1^{j^*}$ and x_2 is $A_2^{l^*}$ and $\dots x_n$ is $A_n^{l^*}$, then y is B^{l^*} ", and the degree of rule **1** generated from data pair $(x^p; y^p)$ is calculated as: $D(\text{Rule}) = \prod_{i=1}^n \mu_{A_i^{j^*}}(x_i^p) \mu_{B^{l^*}}(y^p)$.

Create the Fuzzy Rule Base and Construct the Fuzzy System. By accumulating the rules generated from all data pairs, a desired rule base is created to form a look-up table. Base on such rule base, a workable fuzzy system can be constructed with suitable inference engine, fuzzifier, and defuzzifier.

Procedure of Fuzzy Based Modeling of Potential Conflicts. This fuzzy system constructed will yield out the desired potential conflicts if all input variables prepared. The procedure contains: (1) Field Surveillance. Field traffic and roadway information should be collected through suitable traffic surveillance procedure such as video recording and lab data processing. The information collection should cover all typical types of intersections and different level of traffic volume. (2) Data Preparation. The required input and output data pairs should be prepared such as the right-turn vehicle speed, right-turn volume, through traffic volume, lane width, crossing depth, and the rate of potential conflict. These will be used to create the rule base for modeling. (3) Define Membership Functions. Membership functions for each input and output variable should be well defined. The triangle one is a suitable one for this algorithm (Wang, 1997). (4) Create Fuzzy Rule Base. Based on all available input and output paired, the fuzzy rule base will be created. The degree of each rule can also be calculated. (5) Construct Fuzzy Table. Base on the rule base from step 4, a fuzzy look-up table can be constructed. (6) Check the Modeling Error. Using a different set of input-output data pair to check the modeling error. The possible adjustments include the modifications of membership functions, double checking the coverage of input-out pairs used for modeling, and even the inference engine, fuzzifier and defuzzifier, etc. (7) Suggest Level of Treatments. The level of treatments should be based on the level of potential conflicts.

CASE STUDY

A case study with thirteen intersections in Houston, TX, USA was conducted to model the potential conflicts using fuzzy table look-up scheme.

Site Selection. After several rounds of pilot site visits and close discussions with local transportation engineers, thirteen freeway interchanges in Houston that can reflect the typical traffic and roadway features in Texas, USA are selected. Each interchange contains at least a pair of intersections with pedestrians. The 12 interchanges are: North Post Oak at I-10; Southmore Rd. at SH-288; Antoine at US-290; Richmond Ave. at I-610; Bellaire Rd. at Beltway-8; Westpark Rd. at US-59; Kirby Rd. at US-59; Beltway 8 at US-290; SH 242 at IH-45; Wesleyan Rd. at US-59; Buffalo Rd. at US-59; and University Dr. @ TX Highway 6.

Data Collection and Preparation. For each field, two groups of people were assigned with two surveyors within each group. The equipments used for data collection include a Mobile-Van equipped with two Autoscope Solo Pro cameras that are mounted on a 42' telescoping mast, two additional cam-recorders supported by tripods, and other necessary field testing instruments. Geometric designs were measured directly on the sites. The surveillance on vehicle, bicycle and pedestrian movements were conducted on regular weekdays 7am - 5pm. The Mobile Van was used to record two right-turn movements at each intersection, and two cam-recorders (A and B) were placed on both sides of the intersection to cover blind areas (Figure 2).

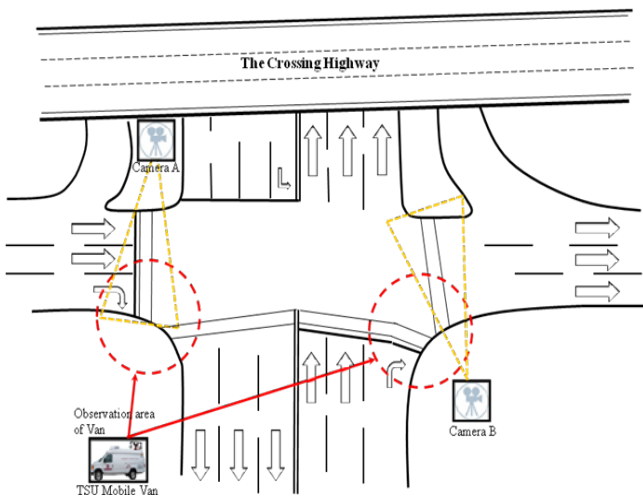


Figure 2. Field surveillance using mobile van cameras and cam-recorders A & B.

Analysis and Determination of Crossing Potential Conflict. According to the videos which collected from the cam recorders and Mo-bile Van cameras, stopping position of the through and right turn vehicles contained their individual behavior.

Observation 1. Through vehicles can be easily defined to two types. First type is vehicle stop before pedestrian crosswalk. It is a perfect position for pedestrian crossing intersection because people can easily cross without any inconvenience or dangerous situation. Another one is vehicle encroach pedestrian cross-walk. This position will define an inconvenience and dangerous behavior because pedestrian may cross and do not walk on the pedestrian crosswalk. For encroaching crosswalk, the red arrow line shows the range which will cause pedestrian into inconvenience or dangerous positions (Figure 3).

Observation 2. Right-turn vehicles tended to stop at various positions. For the clearly and convenience of analysis potential conflicts, the stopping positions at a right-turn channel were divided into 3 types (Figure 3). In Figure 3, the stopping type 1 is related to an “ideal” case where the right-turn vehicle stopped fully in front of the pedestrian lane with no intruding to the lane. For stopping types 2, the rear or front, or the main body of the right-turn vehicle was encroaching on the pedestrian lane. Type 3 is right turn vehicle do not slow down and passes the pedestrian lane without yield pedestrian. Figure 3 shows the conflict classification of the through and right turn vehicles.

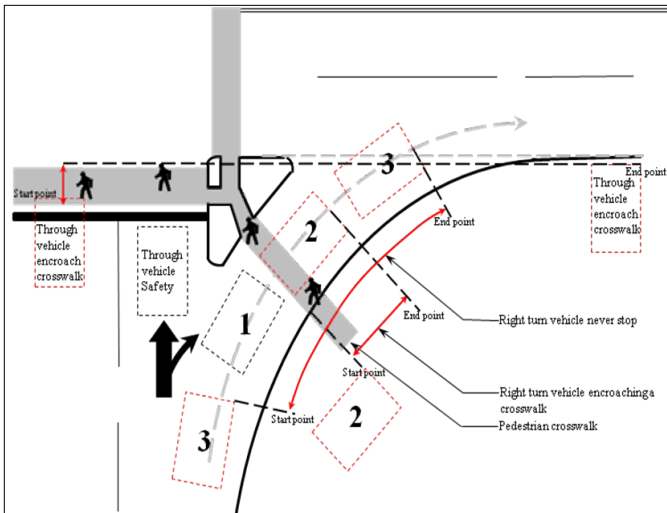


Figure 3. Conflict classifications of right turn and through vehicles.

Preparing Input-output Data Pairs and Membership Function. All input variables can be direct obtained from the measured and surveyed data, while the output potential conflict rates (i.e. average potential conflicts per traffic signal cycle) were observed from the video tapes. The membership functions were selected as the typical pseudo-trapezoid membership functions with each variable classified into three fuzzy sets: Small (S), Medium (M) and Large (L).

Fuzzy Rule Base. Among the 24 input-output data pairs from the field surveillance in 12 intersections, 11 pairs were used to identify the relationship between the five input variables (IF part) and the output (THEN part). The rest 13 pairs were reserved for validation purpose. The proposed fuzzy look-up table based method was implemented in a MS Excel program. Simple operations were conducted within MS EXCEL spreadsheets. Even though these rules were based on the input-output data pairs from twelve typical intersections in Houston, the created rule base covers all possible situations in the region since these intersections were carefully selected.

Model Validation. In order to validate the model, the 13 groups of input data (the IF part) from all reserved intersections are applied with the constructed rule base in Table 2. Results show that 12 out of the total 13 conflict levels (the THEN part) were correctly predicted. In this case, the model can be said basically validated.

Level of Treatments for Each Tested Site. The validated model (the rule base) can be used to predict the level of potential conflicts (S, M, L), and therefore the level of treatments (S, M, L) for the target intersection. The name of each level of treatment is listed in section 3.3 and several examples of typical treatments are in reference (Qiao, et al., 2010b).

CONCLUSION

In this paper, the intelligent Fuzzy table look-up scheme was used to model pedestrian related potential conflicts at intersections within freeway interchange areas. The case study in field sites around twelve typical intersections in Houston, Texas, USA was conducted to illustrate the executive procedure. The model validation results show that the constructed model can basically identify levels of conflicts. Normally it could be very expensive, or sometimes almost impossible for field engineers to conduct detailed observations for all types of potential conflicts at all intersections under their jurisdictions. The input data of the proposed model is however very easy to obtain. Obviously, the proposed fuzzy model can assist field engineers to easily screen all intersections, and quickly assign limited manpower and budget to further diagnose more specific safety threats around the intersections that are alarmed by the proposed method. Since the constructed fuzzy model in this particular case study was based on observations at very limited intersections in Houston, further similar studies are necessary to build up an even larger rule base for more accurate model estimations.

ACKNOWLEDGEMENT

The authors acknowledge that this research is supported in part by Texas Department of Transportation project 0-6173, the Southwest Region University Transportation Center project 161043, the National Science Foundation (NSF) under grant #1137732, and the Tire 1 National University Transportation Center (UTC) TransLIVE, USA. The opinions, findings, and conclusions or recommendations in this material are those of the author(s) and do not necessarily reflect the views of the funding agencies.

REFERENCES

- American Association of State Highway and Transportation Officials (AASHTO). (1999). **Guide for the Development of Bicycle Facilities**AASHTO.
- City of Greenville South Carolina (CGSC). (2011). **Driving A Modern Roundabout, South Carolina** <http://www.greenvillesc.gov/publicworks/Roundabouts.aspx>. Accessed July 24, 2011.
- Federal Highway Administration (FHWA) (2011). **Intersection Safety** <http://safety.fhwa.dot.gov/intersection/>, Accessed Date: July 24, 2011.
- Federal Highway Administration (FHWA). (2009). **Manual on Uniform Traffic Control Devices (MUTCD)**.
- Kikuchi S., and Kronprasert N. (2008). "Determining Length of Right-Turn Lane at a Signalized Intersection." **Transportation Research Record: Journal of Transportation Research Board** Issue 2060, ISSN-0361-1981.
- National Highway Traffic Safety Administration (NHTSA). (2011a). **2008 Pedestrians Traffic Safety Fact Sheet** Publication Number: DOT HS 811163. <http://www-nrd.nhtsa.dot.gov/Pubs/811163.pdf>, Accessed Date: July 24, 2011.
- National Highway Traffic Safety Administration (NHTSA). (2011b). **2008 Bicyclists and other cyclists Traffic Safety Fact Sheet** DOT HS 811156. <http://www-nrd.nhtsa.dot.gov/Pubs/811156.pdf>, Accessed Date: July 24, 2011.
- Niewoehner, W. and Berg, F.A. (2005). "Endangerment of bike/ped at intersections by right-turn trucks. National Highway Traffic Safety Administration." **Proceedings of 19th International Technical Conference on the Enhanced Safety of Vehicles** June 2005, Washington DC. <http://www-nrd.nhtsa.dot.gov/pdf/nrd-01/esv/esv19/05-0344-O.pdf>. Accessed July 24, 2011
- Qiao, F.X., Gampala, R., and Yu, L. (2010a). "Advanced Traffic Devices in Bicycle and Pedestrian Crossings at Freeway Interchanges." **Proceedings of the 2010 ITS World Congress** Bu-san, Korea 2010.
- Qiao, F.X., Liu, X., and Yu, L. (2009). "Arrow Exit Sign Placement on Highway Using Fuzzy Table Look-up Scheme." **Applications of Soft Computing** ISC 52, Eds: Avineri E, Koppen M, Dahal K, Sunityoso Y, Roy R. Springer Publishing. ISBN: 978-3-540-88078-3, pp. 260-269.
- Qiao, F.X., Zhu, Q., Kuo, P.-H., Li, Y., and Yu, L. (2010b). "Fuzzy C-Means Based Stop Line and Crosswalk Placement at Right Turn Vehicle Exclusive Lane." **Soft Computing in Industrial Applications** ISC 75, Eds: Guo X-Z, Gaspar-Cunha A, Koppen M, Schaefer G, Wang J. Springer Publishing. ISBN: 978-3-642-11281-2, pp. 271-279.
- Wang, L.-X. (1997). **A Course in Fuzzy Systems and Control** Upper Saddle River, NJ : Prentice Hall PTR, c1997
- Zadeh, L.A. (1965). "Fuzzy Sets." **Information and Control**:338-353
- Zador, P. L. (1984). "Right-Turn-on-Red Laws and Motor Vehicle Crashes: A Review of the Literature." **Accident Analysis and Prevention** Vol. 16, No. 4, 1984, pp. 241-245.

Spatial Approaches for Conflating GIS Roadway Datasets

Yingfeng Li¹ and Chunxiao Liu²

¹Ph.D., Texas Transportation Institute, 1100 NW Loop 410 Suite 400, San Antonio, TX 78213; PH (210) 979-9411; FAX (210) 979-9694; email: y-li@tamu.edu

²Department of Civil, Environmental, and Architectural Engineering, University of Kansas, 24619 Long Arrow, San Antonio, TX 78258; PH (210) 979-1651; email: springlxs@yahoo.com

ABSTRACT

Transportation communities have been developing a variety of Geographic Information System (GIS) roadway datasets. Although many of those datasets are relatively comprehensive and flexible, complex and novel transportation problems with data needs beyond any single existing dataset continue to emerge. In many cases, extracting necessary data elements from multiple datasets and accurately integrating them into a single roadway network becomes a cost-effective solution. This research developed two approaches that can be used for the conflation of data from multiple roadway datasets. One of the approaches was further demonstrated in a case study where it was used to match the Highway Performance Monitoring System (HPMS) data and a private-sector roadway dataset for the contiguous United States.

BACKGROUND

For various purposes, transportation communities have been developing a variety of geographic information systems (GIS) roadway datasets, frequently overlapping in spatial and/or attribute coverage. Those roadway datasets vary in various aspects such as spatial resolution, positional accuracy, feature representation (e.g., single lines versus double lines), roadway segmentation, attribution, and completeness. As a result, different datasets with the same geographic coverage frequently can not be integrated accurately and efficiently. Therefore, it becomes important to provide effective data conflation and integration protocols to reduce data collection redundancy yet meet additional data needs.

This paper presents two procedures that enable relatively accurate GIS roadway data conflation and integration with reasonable time and computing demands. The first procedure is based on linear referencing and the second conflates data primarily based on spatial relationships. The rest of this paper first reviews the major GIS roadway datasets available at the national and state level, and then describes the data conflation procedures. The paper also includes a case study where the second spatial conflation approach was used to match roadway and traffic data of a private-sector GIS dataset to the Highway Performance Monitoring System (HPMS)

database to enable better urban mobility estimation for the Texas Transportation Institute (TTI) Urban Mobility Report (UMR) (TTI 2011).

MAJOR GIS ROADWAY DATASETS

HPMS. As part of the national HPMS program, Federal Highway Administration (FHWA) requires state highway agencies (SHAs) to collect, assemble, and report information about National Highway System (NHS) and other major on-system (i.e., state maintained) highways to support informed highway planning, policy development, and decision-making at the Federal and State levels (FHWA 2010). Different data practices at states result in inconsistent data format and quality throughout the HPMS database. For instance, states use different spatial resolutions and roadway segmentation standards/methods. Some states use dual lines representing both traffic directions while others use centerlines with aggregated traffic information for both directions. In addition, different states vary significantly in coding standards for certain key data elements, causing difficulties for multi-state analyses.

State roadway inventories. Each SHA maintains an inventory of statewide on-system roadways with yearly traffic information to support their operations and to meet federal data requirements. **Texas Department of Transportation (TxDOT) uses Texas Reference Marker System (TRM) as a central roadway data repository (TxDOT 2005).** TRM uses the statewide reference marker network as a georeferencing tool, where the location of features on the ground is defined in terms of mileage displacement from the nearest marker. Reference markers are physically installed along statewide on-system highways and can be mapped based on their coordinates. The system enables the calculation of cumulative distances (i.e., distances from origin [DFOs]) by using the relative location of the markers along the highway network. Using DFOs as a linear referencing mechanism, TRM data records are georeferenced to a roadway centerline layer by locating the corresponding roadway segments along routes.

Similar to the roadway data systems in many other states, the structure and characteristics of TRM have shortcomings that limit its usability. For example, TRM is centerline based; indicating the positional accuracy of any feature does not exceed that of the underlying centerline network. The lateral positional accuracy of the official TxDOT centerline map varies by location, from a few feet in most cases to much larger values in certain areas. TRM is also cumulative-distance dependent, which means the positional accuracy of a feature cannot be better than the longitudinal positional accuracy of **both** reference markers and the underlying centerline map. The physical locations of the markers can change over time due to damages or unintended movements. Therefore, the statewide reference marker network needs to be calibrated periodically. However, performing a statewide calibration is extremely time-consuming and labor-intensive and therefore is frequently not done timely.

Proprietary roadway datasets. The private sector has been developing geospatial roadway databases for many purposes such as navigation, routing, traffic information, and mapping. Examples of major roadway and traffic data providers at the private sector include TomTom® - formerly known as Tele Atlas®, NAVTEQ®, and INRIX®. In addition, Google® has been developing their roadway and traffic database in the North America region (Schutzberg 2011).

Several issues limit the application of private roadway and traffic data in transportation research and studies. For example, private data are mostly collected for vehicle navigation and related purposes. In addition to traffic data, private data include very limited information on roadway characteristics and physical properties. For routing purposes, private roadway networks typically document roadways to the greatest level of detail possible, e.g., by including minor road features such as ramps and turnaround lanes. Although data producers typically provide mechanisms to filter out individual types of roadways, their roadway classification standards can be different from those at SHAs and the overwhelmingly detailed networks result in unnecessary complications for macroscopic planning, operations, and corridor studies. In addition, the lack of integration protocols between public and private roadway data is also a major obstacle hindering private data application at SHAs.

Other roadway networks. Various public and private agencies maintain roadway networks for purposes such as cartography or traffic demand modeling. Those roadway networks typically do not contain detailed attribute data and vary in positional accuracy and level of detail. Many of the networks can be traced back to the same origins as those of the aforementioned roadway databases. Examples at the national level include TIGER/Line® Shapefiles (Census 2011) and Bureau of Transportation Statistics National Transportation Atlas Database (BTS 2011); examples at Texas include StratMap at Texas Natural Resources Information System (TNRIS 2011) and TDM models at TxDOT and Metropolitan Planning Organizations.

Challenges for data integration. Because individual roadway databases are developed for different purposes, it is frequently necessary to extract data elements from multiple sources to solve complex transportation problems. Due to inconsistent data resolution, spatial representation, and feature identification, conflating data based on the spatial relationship of the same features in different datasets becomes the only option for data integration in many cases.

GIS-BASED DATA CONFLATION PROCEDURES

Due to the aforementioned and many other potential issues, conflating or integrating GIS roadway data from different data sources becomes a major challenge. This section describes two GIS procedures that enable the integration of data from different GIS roadway datasets. The first procedure (Figure 1a) is based on linear referencing and can be effectively used for different datasets of which the positional accuracy through the entire layers is generally consistent with each other. The second procedure (Figure 1b), which this paper focuses on, conflates GIS roadway datasets

based on cartographic relationship between the datasets and is suitable for datasets from different sources with relatively major positional accuracy.

Data conflation Based on linear referencing. Figure 1a is the flowchart for the linear referencing conflation approach. The flowchart assumes that data from R2 (i.e., join dataset) are to be joined to R1 (i.e., target dataset). Before conflation, it is critical to project both layers onto the same projected coordinate system, which ensures that the GIS correctly understands the relative spatial relationship between the same roadway features of the two datasets and therefore to avoid potential errors during the subsequent steps. The two critical steps in the linear referencing approach are linear referencing and data conflation.

Linear referencing. The purpose of this step is to georeference both datasets onto the same route layer (i.e., the route layer generated based on the target dataset) to enable conflation. This step requires that the two roadway networks to be conflated have consistent positional data accuracy relative to each other such that the selected spatial tolerance when using “Locate Features Along Routes” can sufficiently enclose and linearly reference most, if not all, roadway segments of the join layer. Notice that the tolerance value needs to be sufficiently small to minimize the number of segments being incorrectly enclosed.

Data conflation. This step conflates the two linearly referenced datasets through table operations. The step involves the following key tasks that can be executed with common database management systems such as Oracle® or Microsoft® Access®:

- Create a linking table. The two datasets resulted from the linear referencing step contain common route IDs and from- and to- DFOs (F-DFOs and T-DFOs) based on the same route origins. The DFOs of each roadway segment in the attribute tables of the two datasets are used to create a linking table enabling data conflation. For each route, the linking table should contain sequential pairs of DFOs from all segments along the same route on both layers.
- Join the two attribute tables to the linking table. Since the linking table contains all common segments of both datasets, the two attribute tables can be joined to the linking table through an unequal join. The result table will include all data elements from both datasets for all common roadway segments. This is the conflated dataset in tabular format, which is sufficient for many analyses that do not involve GIS mapping.

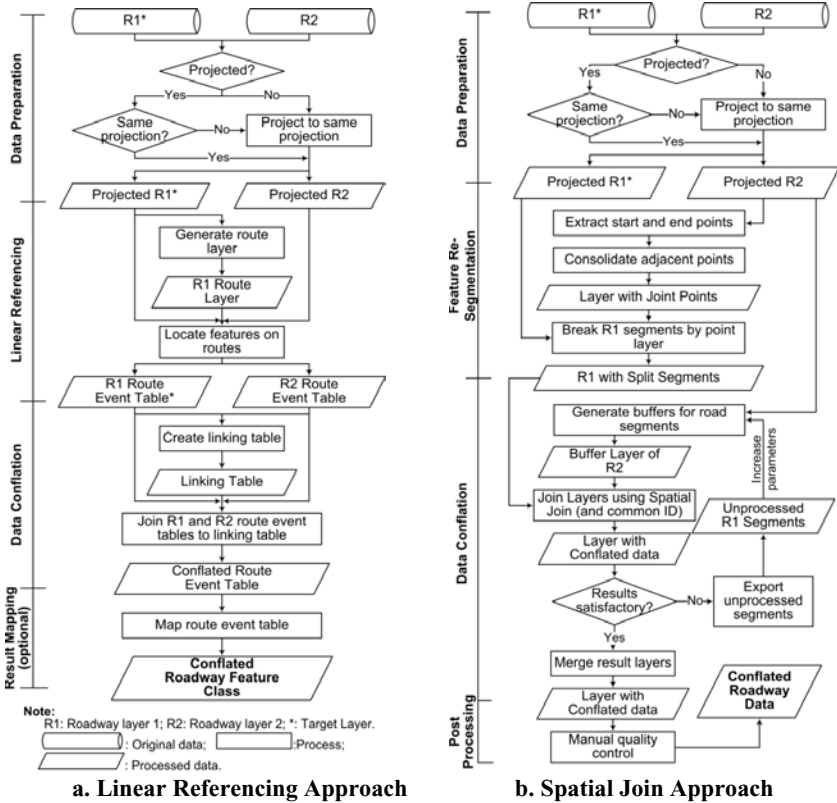


Figure 1. Data conflation procedures

Cartographic conflation of spatial roadway data. The previous procedure provides a method suitable for conflating datasets of which roadway networks closely resemble each other. In reality, data integration is frequently required between roadway datasets originated from very different sources. What further complicates the problem is the fact that some datasets are resulted from assembling data from sub-datasets and therefore contain inconsistent spatial data quality within the same layer. Such an example is the nationwide HPMS dataset produced by assembling data submittals from each individual state.

An alternative for roadway data conflation is to purely rely on the positional relationship of the same roadways in the different layers as they appear when overlaid in a GIS (Figure 1b). The approach conflates roadway data using spatial joins completed in iterations with adjusted parameters. Because the entire conflation process is executed on a mapping program, it is relatively easy to visually identify problematic segments during the process and adjust parameters accordingly during

subsequent iterations or correct them during the final quality control. The following are the major steps involved in this approach.

Data preparation. Similar to the previous approach, both the join layer and the target layer need to be projected on the same projection system to ensure accuracy during subsequent processing steps.

Feature re-segmentation. Because the roadways in the conflating datasets are divided into segments based on different criteria, roadway segments in the two datasets generally do not start or end at the same locations. Therefore, it is necessary to re-segment the roadway features in the target dataset so that each segment of the join dataset can find the correct segments in the join layer to which the attribute information is joined. In the linear referencing approach, this is done during the data conflation when creating the linking table in a database management system.

Data conflation. During this step, a buffer layer is first generated from the join layer and each buffer contains the necessary attribute information of the corresponding roadway feature. The attributes of each buffer are then joined onto the roadway segments of the target layer that the buffer completely encloses. In reality, this step is completed in several iterations as needed. The spatial join starts with a relatively small buffer radius so that most roadways are conflated while minimizing the likelihood of enclosing incorrect segments. The unprocessed features in the target layer are then exported and conflated during another iteration using a large buffer radius. This ensures that a sufficient number of roadway features are conflated yet accuracy is not significantly compromised.

During each spatial join, common roadway identification attributes (e.g., roadway name or classification) can be utilized so that a buffer is only joined to the roadway segments that share the same identification attributes in the target layer, given that such common attributes exist. This mechanism will help filter out the segments that are incorrectly enclosed in a buffer and therefore improve conflation accuracy.

Post processing. During the previous step, each iteration results in a separate layer containing the joined attributes of the processed features during the iteration. At the post processing step, those layers are first merged into one roadway layer, on which a thorough quality control is applied to correct the problematic segments identified by visually comparing the two roadway layers and the buffers used during the conflation. Symbology and labeling techniques can be used to facilitate the visual identification of problematic segments and attribute editing. Depending on the quality of original data and the sizes of the conflation datasets, the quality control can be time-consuming.

CASE STUDY

TTI publishes a UMR annually that assesses the traffic mobility in major U.S. urban areas and recommends strategies to address congestion. The report draws traffic and roadway data from multiple sources including the HPMS database and a private roadway dataset (referred to as TMC [Traffic Message Channel] dataset hereafter) (Lomax et al. 2011). Because the two datasets were developed for different

purposes and by different data producers, it was necessary to conflate or match the two datasets for mobility-related analyses.

The researchers received the HPMS data in different regions for the contiguous United States. In addition to the general observations as discussed during the HPMS data review, the dataset had the following challenges that the data conflation task team had to confront:

- Unnecessarily short segments. The roadway dataset for some states contained a large number of records including many tiny roadway segments that were divided unnecessarily possibly due to linear referencing issues. The existence of many short roadway segments resulted in increased processing time and challenges for final quality control.
- Multipart features. Certain states in the HPMS datasets contained a large number of multipart features where a single data record is associated with multiple roadway segments at different locations possibly resulted from a problematic linear referencing system. The multipart features had to be converted into single-part features first in order to be correctly processed.
- Null-geometry feature. Some states contained a number of records in the attribute table that were not linked to any features in the roadway network. Those records needed to be deleted before conflation to avoid potential errors.
- Densely located roadways. Many major cities included areas with very densely spaced roadways and needed extensive quality control after conflation.

In addition to those issues associated with the HPMS dataset, the TMC data included many detailed roadway features such as frontage roads, express lanes, ramps, and turnaround lanes. Those features further clustered the picture and had to be deleted before conflation or manually checked during final quality control.

Because of the inconsistent positional accuracies of the two datasets and the many other challenges discussed previously, the research team used the spatial join-based approach to conflate the two datasets. Although this approach demanded more computing resources and processing time, it provided more flexibility for the researchers to control each step and allowed for easier (not necessarily faster) final quality control. During the conflation process, the research team divided the TMC dataset into multiple regions according to those used by the HPMS dataset. The research team used ArcGIS Desktop software throughout the processing, supplemented with tools developed using Visual Basic for Application (VBA) and plug-in applications. An extensive quality control was performed for each of the regions after conflation to improve accuracy particularly for major urban areas. At the end of the conflation, the researchers randomly drew a sample of 500 roadway segments and checked their accuracy. Overall, the conflation method enabled an accuracy rate of over 85 percent in terms of number of segments or over 95 (95.4) percent in terms of roadway miles.

CONCLUSION AND RECOMMENDATIONS

This research developed two approaches that can be used for the conflation of data from multiple roadway datasets. The first approach lays its basis on linear referencing and utilizes both a GIS and database management software for data

conflation. This procedure requires relatively less processing time and is particularly suitable for GIS datasets derived from the same sources. The second approach was developed surrounding the Spatial Join function available in common GIS software and performs the data conflation in iterations. It is more flexible, allows better quality control, and is used when the datasets for conflation are not consistent in positional accuracy both within and between the datasets. This approach was further demonstrated in a case study where it was used to match the HPMS data and a private-sector roadway dataset for the contiguous United States. Through the case study, the approach showed its flexibility and robustness for accommodating a variety of data issues and challenges.

Based on this research, the researchers recommend several improvements pertaining to GIS roadway data quality and practices for federal, state, and private stakeholders. Federal and state transportation agencies should:

- develop and use a standardized route identification and route naming convention in their official GIS roadway datasets for consistency and to simplify data processing efforts for transportation studies and processes that use multi-state roadway data;
- centralize official GIS roadway data production and reduce/eliminate data inconsistencies across jurisdictional boundaries within the same state;
- verify and calibrate their linear referencing systems routinely to maintain and improve roadway data quality; and
- consider the use of private roadway data to support some functions and processes at state transportation agencies.

In addition, private-sector data producers should:

- incorporate roadway naming and identification (e.g., functional classification) information used at SHAs into their roadway datasets for increased compatibility with public datasets and data needs; and
- separate roadway auxiliary features such as ramps, express lanes, and turnaround lanes from main lanes on their GIS roadway networks and incorporate mechanisms to enable easy filtering of those features.

REFERENCES

- Texas Transportation Institute (TTI). (2011). *Annual Urban Mobility Report*, College Station, Texas, <<http://mobility.tamu.edu/ums>>(Jul. 25, 2011).
- Federal Highway Administration (FHWA). (2010). *Highway Performance Monitoring System Field Manual*. Washington, D.C.
- Texas Department of Transportation (TxDOT). (2005). *Texas Reference Marker System User's Manual*, Austin, Texas.
- Schutzberg, A. (2011). "Google Resets Its Data Providers." *Directions Magazine*, <<http://apb.directionsmag.com/entry/google-resets-its-data-providers/161380>>(Apr. 4, 2011).
- U.S. Census Bureau (Census). (2011). *2010 Census TIGER/Line Shapefiles*. Washington, D.C.<<http://www.census.gov/geo/www/tiger/tgrshp2010/tgrshp2010.html>>(May 3, 2011).

- Bureau of Transportation Statistics (BTS). (2011). *National Transportation Atlas Database*, Washington D.C., <http://www.bts.gov/publications/national_transportation_atlas_database/2010/> (May 3, 2011).
- Texas Natural Resources Information System (TNRIS). (2011). *Data Catalog*, TNRIS, Texas Water Development Board, <<http://www.tnris.state.tx.us/DataCatalog/DataDictionary.aspx#26>>(May 3, 2011).
- Lomax, T., Wang, B., Schrank, D., Eisele, W., Turner, S., Ellis, D., Li, Y., Konecz, N., and Geng, L. (2011). *Improving Mobility Information with Better Data and Estimation Procedures: Final Report*. Publication UTCM 09-17-09, Texas Transportation Institute, College Station, Texas.

Bus and Metro Integration Improvements in Beijing

Sun Mingzheng¹, Song Lijing², Chen Feng³ and Xian Kai⁴

Beijing Transportation Research Center, No.9 Liu Li Qiao South Road, Fengtai District, Beijing, China 100073. Phone: 8610-57079796; Fax: 8610-57079800; E-mail: ¹sunmz@bjtrc.org.cn, ²songlj@bjtrc.org.cn, ³chenf@bjtrc.org.cn, ⁴xiank@bjtrc.org.cn

ABSTRACT

This research focuses on developing a scientific methodology to evaluate integrated service planning for bus and metro services in Beijing. One of the five newly built metro lines opened in Beijing in 2010, the Daxing Line, was selected as a demonstration metro corridor for this methodology. A detailed public transport passenger trip matrix is developed using data from the Beijing public transport IC card data. Building on this data, different bus service patterns were evaluated using a pivot point demand model and PT model. In the final section of the paper, the schemes are evaluated using a set of 6 weighted indicators to decide on an optimal outcome. The bulk of the recommended service planning adjustments recommended by the study are currently being implemented in the corridor. The study concludes that the proposed approach is practical and can provide meaningful input to service planning in multi modal corridors in Chinese cities. Given the rapidly expanding metro networks in many Chinese cities, there is a large potential for replication of the approach described in the paper.

INTRODUCTION

Beijing's rapidly growing population and economic development as well as a rapid increase in motorization have made congestion. In response, Beijing has adopted a multi-dimensional strategy to give priority to all modes of public transport. Specific actions reflecting this strategy include accelerating the expansion of the metro network. And metro services should be integrated with the more extensive surface transportation system, so that more direct and convenient trips can be provided and thus more riders will be attracted.

The objective of this study was to develop and apply a scientific approach for improving the integration of Beijing's metro and surface public transport systems so that together, they can provide an efficient and attractive transport option for the

maximum number of transit users. This scientific approach will reflect the functions of:

- the metro: primary “backbone” for public transport; directly serving highest volume/trip length corridors and largest activity centers
- bus system: Basic coverage on all arterials; complimentary services in metro corridors parallel and intersecting; extending metro access beyond terminals; providing trunk services in other, lower volume (e.g., outer circumferential) corridors.

SELECTION OF A SINGLE DEMONSTRATION CORRIDOR

In 2010, five new metro lines were opened in Beijing, comprising a total of 130 Km. There were: Changping Line, Metro 15, Yizhuang Line, Fangshan Line and Daxing Line (see figure 1).

The first step for the study was to choose a single corridor for demonstration purposes. This was necessary to avoid the need to develop and analyze a large number of combinations and permutations of integration schemes in multiple corridors.

Each corridor was different in terms of its position in the topology of the metro and bus networks and roadway system, as well as its demand and performance. This study utilized a small number of factors that indicated how successful a demonstration was likely to be in the respective corridor. The factors used here were:

- Rail line construction timing and phasing (open to its extremity before the end of 2010 most highly ranked)
- Major corridor roadway congestion, especially as it effects ground public transport (the greater the better)
- Degree of physical separation between major roads and the respective rail line (the closer the higher ranked)
- Degree of duplication between current bus PT services and the rail line (the greater, the better)

If a corridor was highly ranked in all the factors relative to the others, it would be selected for analysis. If not, the corridor which did the best in the largest number of factors and ranked in the top half in all the rest would be selected, etc(see table1).

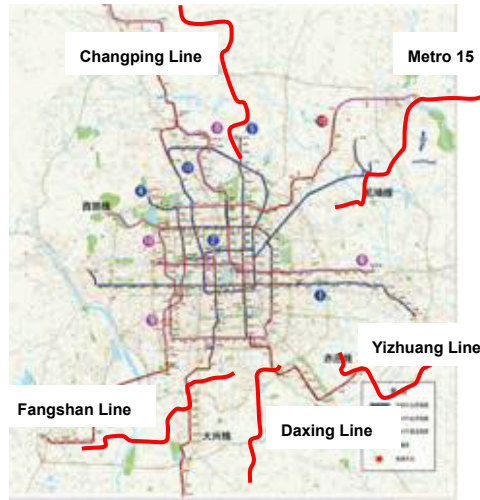


Figure1. Metro in 2020

Table1. Factor Result

Line Name	Construction time	Congestion index	Road/Rail Coincidence (KM)	duplication along the rail line (route)		
				Parallel	Intersect	total
Changping line	2012	3.3	2.11	17	9	26
M 15	2012	6.2	0.22	34	36	70
Yizhuang line	2010	6.5	3.56	24	14	38
Daxing line	2010	8.1	1.12	41	7	48
Fangshan line	2010	4.4	3.24	22	6	28

Of the five, the Daxing corridor, shown in the exhibit above was selected for analysis.

DEVELOPMENT OF ANALYSIS METHODOLOGIES

One of the biggest challenges of this research was the development of the pivot point demand model and the PT model. From them, the mode share, total ridership and every line's ridership could be derived.

At one level, the PT model was extremely disaggregate, with each bus stop serving as a zone, while the demand model was calibrated and applied at two levels, stop and zone. A base trip table was derived from IC card data at the stop level, itself a very

complex task, which was then aggregated to a zonal level. A pivot point demand model using parameters derived from Beijing’s regional conventional four step model was then applied to generate zonal level trip tables corresponding to each of the integration schemes to be tested. These trip tables were then disaggregated back down to a stop level for assignment (see Figure2).

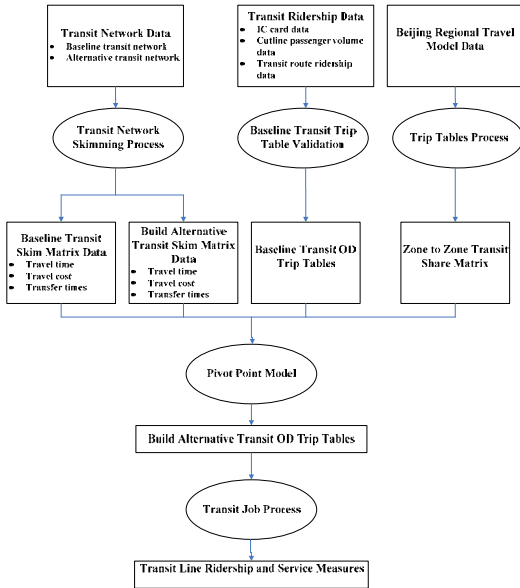


Figure2. Analysis flowchart

Immediately after the opening of the metro, the total forecasted morning peak period(7:00 A.M. to 9:00 A.M.)passenger trips by public transport number 183,000, an increase of 1,500 passengers compared to the situation before the metro line opened to traffic. After metro line opening, bus passenger ridership reached 161,000, which is 23,000 trips lower than that before rail is opened, while the passenger traffic on the new subway line is predicted to be 24,000 trips.

According to the calculation of the PT model, after Daxing Line is opened, the ridership of the impacted Daxing municipal bus lines will be reduced. In particular, those lines with less passenger traffic and high route overlap will have larger passenger transfer ratio, for example, 32% of Line 841 will transfer to the subway, 43% of Line 844. And Daxing local bus connecting to Daxing Line will have ridership increase to a certain extent, such as the passenger traffic increased 22% at

Daxing New Town Line 1 and 41% at Daxing New Town Line 2.

DEVELOPMENT OF ALTERNATIVE BUS/METRO INTEGRATIVE SCHEMES

There are almost an infinite number of ways that bus networks can be adjusted or integrated with a new metro line. The task here was to develop schemes representing a reasonable envelope within which all would lie, and then to identify a one to proceed with. After analysis of the current situation in the selected Daxing corridor, simple rules were applied to each bus route to produce comprehensive schemes forming the integrated envelope extremes. The least aggressive scheme involved eliminating or turning back only those bus routes that were completely duplicated by the Daxing line. There were few of these bus routes whose alignments were significantly changed to “feed” the metro. This scheme also included establishing several new “feeder” route connecting areas at the outer edge of the corridor to the nearest metro Daxing Line station.

The other, more aggressive side of the envelope consisted of a scheme which either eliminated or turned back as many bus routes as possible. Significant diversions of many bus routes were made to “feed” various stations on the metro line. A third scheme, developed after analysis of the other two, was somewhere in between.

Based on the current line spatial distribution, combined with demand distribution, and focusing on passenger demand, the number of feeder bus routes was also increased at the road segments with favorable roadway condition but no bus service to facilitate residents of the region transferring to rail.

To determine which routes to modify, an initial run of the model was conducted with the metro network in place but with no modification of the bus network.

Routes that saw a significant number of their former passengers transfer to rail were considered for modification or elimination if that capacity is no longer required. This was done for all routes in the project corridor.

Based on the methodology motioned above, we analyzed the current status and demand forecast of 41 bus routes along the Daxing corridor one by one.

ANALYSIS OF ALTERNATIVE BUS/METRO INTEGRATION SCHEMES

The biggest challenge here was to select a small number of evaluation criteria capable of differentiating among the integration schemes, and then use models to produce the criteria. The evaluating system includes six indicators chosen from three

basic public transport attributes, public transport level of service, network structure and costs.

The six indicators were: Travel Time, Transfer times, Peak period Load Factor, Degree of Bus/Metro Overlap, Proportion of area within walking distance of a bus stop and Bus revenue kilometers.

Based on the model calculation, all the bus service patterns are graded(see table 2). The evaluation criteria for the “do- nothing” scenario and the recommended by the study was as follows:

Table2. Evaluation Results

Indicator Category	Evaluation Indicator	Status	do minimum	After Adjustment
service standard	Travel Time (minutes Average all zones within 5km of rail line/key zone)	41.78/60.11	40.1/55.2	40.7/54.44
	Transfer Times (5km/key zone)	0.83/1.53	0.82/1.60	0.81/1.63
	Peak period Load Factor	38%	43%	51%
network structure	Degree of Bus/Metro Overlap	4.84	4.84	4.67
	Bus stations 500 meters coverage	62%	72%	74%
operating costs	Bus revenue kilometers (vehicle km / day)	15059	13756	12684

The fuzzy model is used here to evaluate different scenarios. The model used is described as below:

$$B = (b_1, b_2, \dots, b_m) = A \cdot R = (a_1, a_2, \dots, a_n) \cdot \begin{bmatrix} r_{11} & r_{12} & \dots & r_{1m} \\ r_{21} & r_{22} & \dots & r_{2m} \\ \dots & \dots & \dots & \dots \\ r_{n1} & r_{n2} & \dots & r_{nm} \end{bmatrix} \quad (1)$$

$$W = B \cdot V^T \quad (2)$$

V- Evaluation vector. Evaluation results are divided into” very good”, “good”, “fair”, “poor”, “very poor”, presence as vector: V=(2.1.0.-1.-2)

A- weighted scores

r_{ij} - each indicator is measured in five grades, r_{ij} indicates the percentage of

indicator i being graded as j among all the experts.

R- Membership matrix, formed by r_{ij}

Through this grading system, each indicator is weighted as 0.3, 0.2, 0.2, 0.05, 0.05, and 0.2 respectively. The Evaluation Vector is demonstrated in Table 3.

Table 3. Membership Matrix

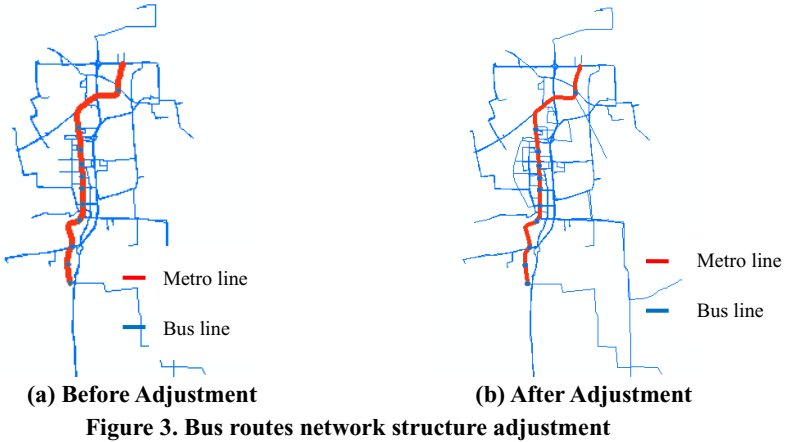
		very good	good	fair	poor	very poor
do nothing	Travel Time	0.3	0.2	0.3	0.1	0.1
	Transfer Times	0.4	0.1	0.1	0.2	0.2
	Peak period Load Factor	0.1	0.2	0.4	0.1	0.2
	Degree of Bus/Metro Overlap	0.2	0.1	0.2	0.3	0.2
	Bus stations 500 meters coverage	0.3	0.1	0.2	0.2	0.2
	Bus revenue kilometers	0.1	0.1	0.2	0.2	0.4
	do minimum	Travel Time	0.4	0.2	0.3	0.1
Transfer Times		0.3	0.3	0.3	0.1	0
Peak period Load Factor		0.5	0.5	0	0	0
Degree of Bus/Metro Overlap		0.3	0.2	0.2	0.2	0.1
Bus stations 500 meters coverage		0.5	0.5	0	0	0
Bus revenue kilometers		0.3	0.3	0.4	0	0
after adjustment		Travel Time	0.5	0.3	0.2	0
	Transfer Times	0.2	0.3	0.2	0.1	0.2
	Peak period Load Factor	0.5	0.5	0	0	0
	Degree of Bus/Metro Overlap	0.5	0.4	0.1	0	0
	Bus stations 500 meters coverage	0.4	0.3	0.2	0.1	0
	Bus revenue kilometers	0.4	0.4	0.2	0	0

Based on fuzzy comprehensive evaluation method, the status score is 0.045, the “do minimum” scheme is graded as 1.005 , while the score for the recommended adjustment program score is 1.09, indicating that after adjustment, service customer

performance, and operating costs are all improved.

IDENTIFICATION OF RECOMMENDED SCHEME

Based on the analytical results, the recommended scheme is as follows: add four new Feeder Lines; eliminate one overlapping bus route; and truncate five bus routes for the redundant parts (see figure 3).



CONCLUSIONS

This research studied the status and future demand of bus routes along the Daxing Metro line, and proposed a ‘scientific approach’ to identifying the best plan for adjusting bus service in the corridor. The proposed scenario has been approved by the Beijing Municipal Commission of Transport, and was partially implemented in the year 2010.

This project is innovative for developing a method for evaluating service changes in a multi modal transport corridor that weigh competing objectives against one another including service side characteristics such as bus level of service, bus route structure, operational cost as well as demand side variables of total travel time and total number of transfers. By including a mix of variables, the methodology provides a way to quantify the interest of government, public transport riders and the bus company order to achieve the best optimization.

The study concludes that the proposed approach is practical and can provide meaningful input to service planning in multi modal corridors in Chinese cities. Given the rapidly expanding metro networks in many Chinese cities, there is a large potential for replication of the approach described in the paper.

REFERENCES

- Fan Haiyan.(2005). “*Bus Line Networks Adjustment on Rail Transit Basis.*” Urban Mass Transportation Research,2005(4):36-38.
- Zhang Fa Cai.(2006). “*Research on Adjustment Method of Integration of Public Transit and Metro.*” China Urban Transportation Planning Annual Meeting.

An Iterative Procedure for the Estimation of Dynamic Toll Demand, Toll and Level-of-Service on Toll Facilities

Jinghua Xu, Ph.D, P.E.¹ and Steven Ruegg, P.E.²

¹Parsons Brinckerhoff, Inc. 505 S. Main Street, Suite 900, Orange CA 92868; PH (714) 564-2776; FAX (714) 973-0358; email: xuji@pbworld.com

²Parsons Brinckerhoff, Inc. 501 E. Tennessee Street, Suite A, Tallahassee FL 32308; PH (612) 840-5530; FAX (612) 371-4410; email: ruegg@pbworld.com

ABSTRACT

Increasing congestion in the urban highway system, combined with limited funds for new construction has lead to new managed lane strategies designed to provide improved level of service at a lower cost. One of the most popular strategies for managed lanes is dynamic tolling of single-occupant vehicles combined with preferential treatment of high-occupancy vehicles, known as High-Occupancy Toll (HOT) lanes. In order to evaluate these types of strategies, dynamic toll modeling is used to model the relationship of toll demand and toll pricing within different time periods, or more specifically, at different levels of congestion.

In this paper, an assignment-based toll choice routine is designed to estimate toll demand within the context of a traditional 4-step travel demand model. This approach uses a dynamic toll demand estimation embedded within an equilibrium highway assignment, assuming the toll choice is a path choice rather than a mode choice. In application, an iterative procedure was employed, involving a modification of the assignment routines for each hour. In each iteration, the toll is adjusted according to the level of service, while the likelihood of a traveler choosing a toll path and ultimately the toll demand is estimated based on the marginal cost saving between toll path and non-toll path. The results of this routine are toll and non-toll trip tables, with associated toll values. A case study is shown to explain how this routine is applied to a toll study where toll and toll demand vary by level of service on toll segments.

INTRODUCTION

Highway travel demand in the United States keeps growing in the past decades, particularly in metropolitan areas. Although the construction to expand highway capacity hasn't been stopped, it still cannot keep pace with the demand due to constraints on both funding and engineering feasibility. It is estimated that in 2010, congestion in 439 metropolitan areas caused urban Americans to travel 4.8 billion hours more and to purchase an extra 1.9 billion gallons of fuel for a congestion cost of \$101 billion. [Texas Transportation Institution 2011]

With ever-increasing congestion level on the urban highway system, a number of high-priority efforts to help alleviate congestion are recommended by Federal

highway Administration (FHWA). The toll road is one of these efforts to be able to effectively reduce congestion by charging fees or tolls for road use. [FHWA 2011]

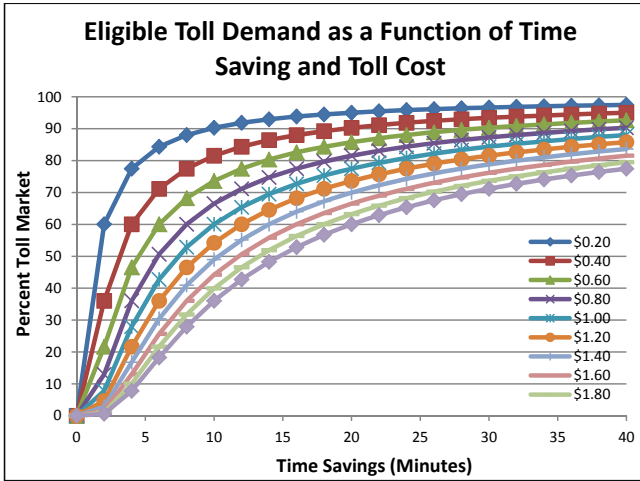
The implementation of a modern toll facility in the highway system requires the development and implementation of a dynamic toll scheme that determines the toll during different time periods that maintains an attractive level of service (LOS) while maximizing use of the toll facility. This requirement raises the need for an effective planning tool to model the new behavior between the toll and the demand for toll facilities. In the next section, a methodology to formulate the relationship between the toll and the demand is established. The results from an example implementation of this methodology are presented in section of Case Study.

METHODOLOGY

The decision to use a toll facility can be thought of as either a mode choice or a path choice. In a metropolitan area with heavy congestion and a well-developed transit system such as Los Angeles or Washington D.C., the existence of toll facility has significant influence on people when planning their trip on daily basis. Many users regularly plan on using a toll facility, and think of this choice along with the choice of using transit or a non-toll auto mode. Under these conditions therefore, the toll mode is differentiated from the non-toll highway mode in the mode choice scheme and can be evaluated separately within the mode choice model. However, in a relatively less-congested metropolitan area where the use of highway is dominant, e.g., Kansas City metro, especially where transit is used by a more captive group of people, the choice of a toll is more of a path choice. In this context, the user is seen as a generic auto user, who may choose a toll facility to minimize their travel time and cost. In actuality, travelers within any metropolitan area are a mixture of these choice models, based on their demographic characteristics, and available mode choices. The methodology described in this paper is based on the assumption that toll is a path choice, where the path type is chosen to minimize overall cost. Drivers are willing to trade off time savings for toll cost based on their value of time (VOT), and have full knowledge of alternative paths. No mode shift from transit is considered with addition of the toll facility.

The goal of this approach is to develop a dynamic procedure that generates the toll based on the current road congestion condition, varying by hour to adjust the toll demand and thus maintain superior LOS. One of the requirements for this dynamic procedure is to recognize the distribution of Willingness to Pay (WTP), which the model uses to automatically balance toll with demand and LOS on a regional scale. Figure 1 below illustrates an example toll diversion curves, the results from a stated preference toll study conducted for the Minnesota Department of Transportation (MnDOT) as a part of an evaluation of the MnPASS tolling system in the Twin Cities metropolitan area. [University of Minnesota 2006] These curves show the model's assumed relationship between travel time savings (over non-tolled paths), the toll assessed, and the likelihood of a traveler choosing a toll option. This data was collected through a series of panel surveys, in which participants were asked their travel preferences given varying toll levels and time savings. Respondents included those currently using the I-394 toll facility in Minneapolis. Note that since this relationship is applied to all drivers, it assumes a single average income and

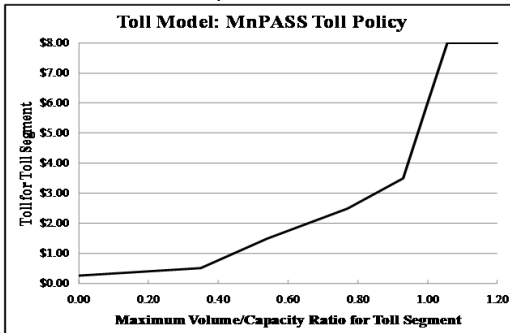
average value of time. In actuality, of course, value of time varies by trip purpose and socioeconomic level, so this is an approximation of that average for the entire population. However, it is possible to supply multiple WTP curves in this model application. Using this flexibility, it would be possible to supply a set of stratified WTP curves based on income groups, if the assignment classes were similarly stratified.



Source: Minneapolis UPA Model

Figure 1. Toll Diversion Curves

Figure 2 is an example toll policy curve depicting the MnDOT toll policy, as employed in the “UPA” model which was used to estimate toll demand on the I-35W managed lane toll facility in Minneapolis. It relates the estimated toll to the maximum segment volume to capacity (V/C) ratio of the toll lane as estimated by the model. The segments are defined as those links which share a common toll. This toll policy curve can be varied to represent different tolling policies by the operating agency. A flat curve can be used to represent a fixed toll.



Source: Minneapolis UPA Model

Figure 2. Toll Policy Curve

An assignment-based toll choice routine is designed to estimate toll demand for the toll alternatives. Following the WTP and toll policy curves, this approach uses a dynamic toll demand estimation embedded within an equilibrium highway assignment, assuming the toll choice is a path choice among auto users rather than a mode choice. In application, an iterative procedure was employed to updated toll and toll demand dynamically, involving a modification of the assignment routines for each hour. In each iteration, the toll value and toll demand are adjusted, and the resulting LOS (in terms of V/C on toll segments) is examined until an acceptable LOS would be obtained, insuring the maintenance of a relatively free-flowing toll facility. The results of this procedure are hourly toll and non-toll trip tables, with associated toll values. The procedure is illustrated in Figure 3 for the implementation of this routine using a TransCAD software platform.

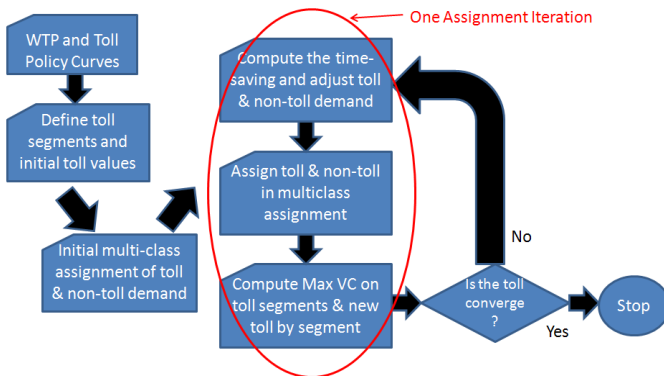


Figure 3. Dynamic Toll Procedure Flow Chart

As shown in Figure 3, the WTP and toll policy curves are developed for the application of the dynamic procedure. After initial multi-class assignment, the likelihood of a traveler choosing a toll path and ultimately the toll demand can be estimated based on the marginal time savings per toll cost between toll path and non-toll path. A multi-class assignment will follow using the adjusted toll demand, and the LOS for toll segments can be calculated. Based on the LOS, the toll cost is adjusted following the toll policy curve. If the difference of the toll before and after the adjustment is larger than the threshold, the process will repeat until the toll converges.

CASE STUDY

The dynamic toll procedure has been applied to the Kansas 5-County Regional Model, newly built upon the TransCAD software platform to develop the travel demand forecasts of the Kansas City metropolitan area. Anchored by Kansas City, the Kansas City metropolitan area is bisected by the border between the states of Kansas and Missouri, encompassing the entire Kansas City metro area. The model

covers the 5 core counties of the region in the state of Kansas, i.e., Counties of Douglas, Johnson, Leavenworth, Miami and Wyandotte, as well as a “buffer zone” made up of areas surrounding the 5-County region, including the counties at the side of the state of Missouri, as shown in Figure 4. A total of 1799 zones are included. The highway network in the region includes freeway, expressway, arterial, collector, and toll road. As shown in Figure 5, the I-70 is the major east-west toll facility through the 5-County area [Kansas Department of Transportation 2009] which currently uses a static, distance-based toll/ticket scheme. With the ever-increasing congestion level over the year, the toll road will attract more demand which may compromise its performance. The model is applied to evaluate an alternative which would establish an effective toll scheme to control the toll demand and therefore to maintain reasonable LOS. The dynamic toll procedure is applied to the model to study how the change of toll impacts on the toll demand and the use of toll road.

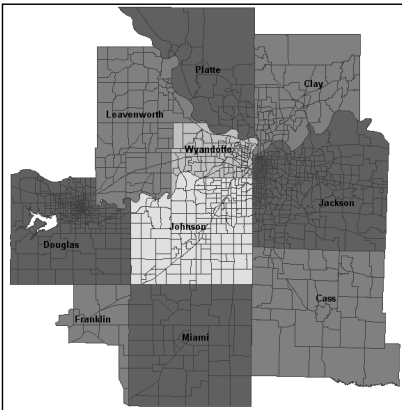


Figure 4. Counties in the 5-County Model Region



Figure 5. Facility Type in the 2010 Highway Network

Figure 6 shows the assigned volume of a representative segment on I-70 over the consecutive 24-hour periods in the base year 2010, the pattern that the other segments on I-70 are similar to. As shown in the figure, the use of the toll road peaks at three time periods, i.e., AM (8-9am), midday (12-13pm) and PM (15-18pm) periods, although AM peak is much lower than the other two. The incur of the midday peak is mostly due to the fact that the use of I-70 in the Kansas city region is not for the home-work purpose alone, but is also significantly used by non-home other purposes which occur mostly in the off-peak period.

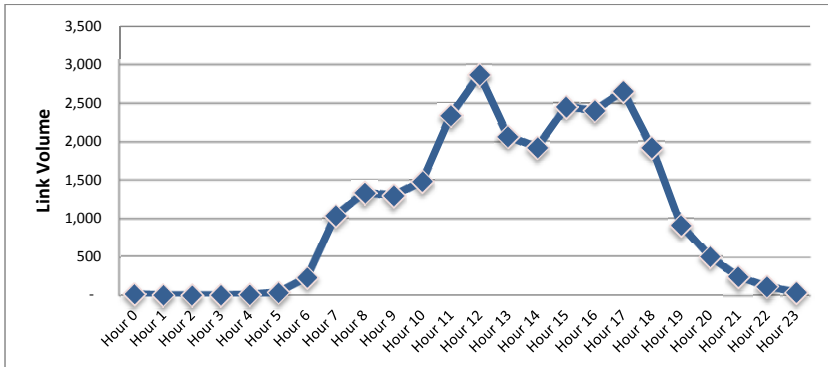


Figure 6. Assigned Toll Segment Volume over 24-Hour Period before Applying Dynamic Toll Procedure

After the dynamic toll procedure is applied, the new model-estimated tolls on this segment of I-70 over the 24-hour period are shown in Figure 7. The pattern of the tolls over time is similar to the volume on the toll road, starting at 25 cents, the toll increases to the point as high 45 cents between 8-9am, decreases a bit and increases quickly to 75 cents between 12-13pm, then decreases and peaks again between 15-18pm at 70 cents. The toll pattern is consistent with the link volumes on the toll road indicated in Figure 6. With the toll adjusted based upon the congestion level, the toll demand is affected as well as the assigned volume on the toll facility, as shown in Figure 8.

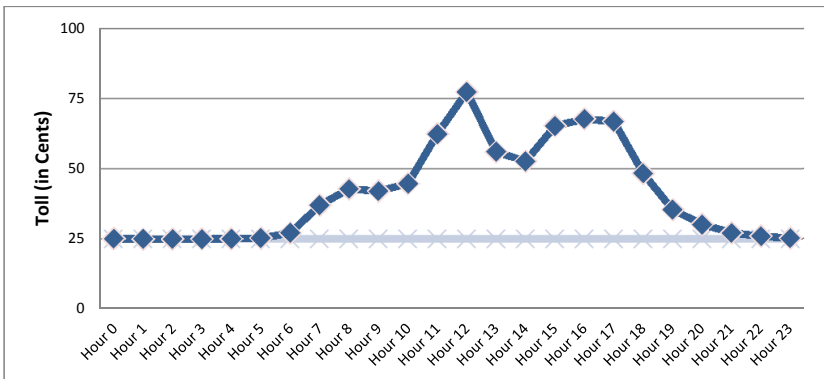


Figure 7. Tolls Evolution over 24-Hour Period after Applying Dynamic Toll Procedure

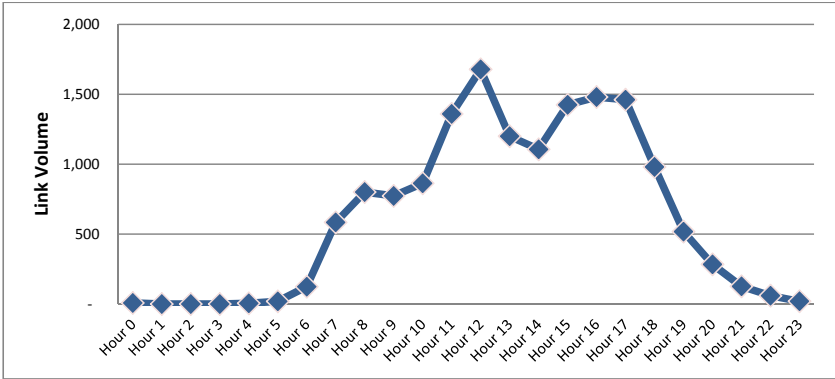


Figure 8. Assigned Toll Segment Volume over 24-Hour Period after Applying Dynamic Toll Procedure

The volume difference on the same example toll segment before and after the dynamic toll procedure is shown in Figure 9. As shown in this figure, the volumes in those three peak periods are affected the most, resulting from the higher tolls and ultimately from the higher congested levels in those periods. The change of V/C ratios before and after the procedure is applied are illustrated in Figure 10. With the adjusted toll and toll demand, the congestion on the toll facility has been effectively alleviated, especially during the peak periods.

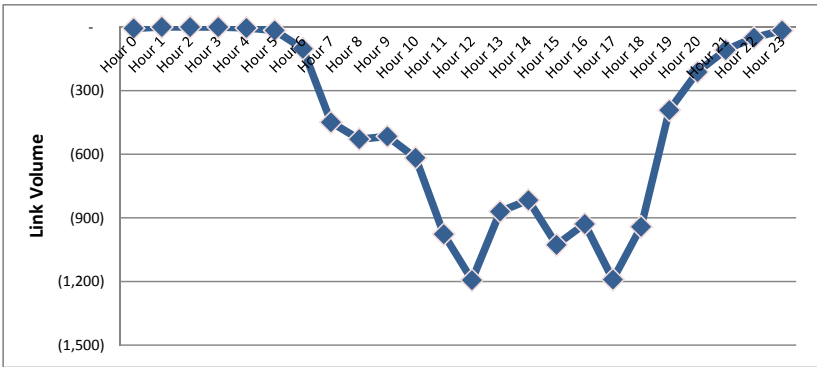


Figure 9. Toll Segment Volume Difference over 24-Hour Period before and after Applying Dynamic Toll Procedure

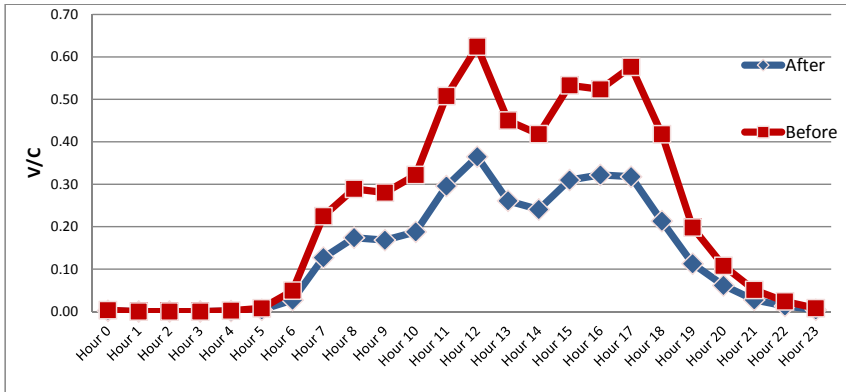


Figure 10. V/C Comparison over 24-Hour Period before and after Applying Dynamic Toll Procedure

CONCLUSION

This dynamic toll procedure can be used to study a wide range of toll policies due to its flexibility to incorporate observed WTP curves on a variety of toll facilities such as urban HOT lanes, urban Tolloed freeways, or even rural turnpike. It also allows studying multiple toll policies or for multiple markets, e.g., income- or purpose-stratified market. This procedure does not require an a priori assumption of toll, and can ensure no congestion on toll facility to maximize revenue.

This procedure is established based on the assumption that the toll is a path choice rather than a mode choice, hence no mode shift is assumed from transit.

REFERENCES

- Federal Highway Administration (2011). <http://www.fhwa.dot.gov/congestion/>. December 28, 2011
- Kansas Department of Transportation (2009). "5-County Regional Transportation Study Phase 1 Final Report." http://www.5countystudy.org/get_more_info/reports.aspx. December, 2010
- Texas Transportation Institution (2011). "2011 Urban Mobility Report." <http://tti.tamu.edu/documents/mobility-report-2011.pdf>. September, 2011.
- University of Minnesota (2006). "MnPASS Evaluation: Attitudinal Panel Survey Wave 3 Final Report." <http://www.mnpass.org/pdfs/MnPassFinalReport%2027NOV06.pdf> NuStats and Humphrey Institute of Public Affairs. Completed under contract to Minnesota Department of Transportation, August 2006.

Experience of Radio Taxis in Algeria

H.Bencherif¹ and F. Boubakour²

¹ Transport-Logistics-Management Laboratory, Institute for Health and Safety University of Batna, Chahid Boukhouf street, 05000, Algeria; PH: (213) 772703253; FAX: (213) 033864367; Email: bencherifhouria@yahoo.fr

² Transport-Logistics-Management Laboratory, Faculty of sciences of Management University of Batna, Chahid Boukhouf street, 05000, Algeria; PH: (213) 0550512008; FAX: (213) 033864367; Email: fares_boubakour@yahoo.fr

ABSTRACT

The objective of this study was to evaluate the current position of radio taxis in the urban transport sector in Algeria, its operation, its relevance and its limitations. The methodology adopted is mainly based on questionnaires to know the viewpoints of drivers and users of radio taxis as regards this new form of urban transportation in the city of Batna. The work was conducted from May to July 2011. The results obtained showed that the service offered by taxis is confused with the one of the radio taxi because of their mode of operation which is based on the free spins rather than the use the phone. In this context, strengthening the role of radio taxis requires the launching of sensibilizing campaigns to raise awareness and information to promote the benefits of radio taxis on the one hand and the improvement of conditions in which they activate on the other hand.

INTRODUCTION

The urban transport sector in Algeria was marked mainly by significant changes in the configuration of the organizational scheme of the most major Algerian cities which are characterized by high urbanization, a profound socio-economic change and a strong demand for displacement (Boubakour, 2009). To meet the growing demand for the mobility of the population and by increased awareness of the congestion and environmental problems related to the increase in urban traffic, improvement of urban transport became essential and urgent (Salhi, 2010). It is in this context that the law 01/13 on the management and organization of the activity of land transport has come to supply the government with the necessary and essential means to improve the quality of the service, the comfort and the security in urban transport (Law No. 01-13, 2001) (Executive Decree No. 2-448, 2002). This strategy of improving the urban transport was enhanced from 2003 through the integration of a new form of urban transportation: **radio taxis**. This is a clean, efficient and practical transport which allows meeting some of the needs of the urban transport in certain jurisdictions or for particular categories of users. The objective of this study is to evaluate the current position of radio taxis in the urban transport sector in Algeria, how it works, its interest and its limitations. The methodology is

mainly based on questionnaires to know the views of drivers and passengers of taxis radio on this new form of urban transport in the city of Batna¹. To meet this goal, we distributed 126 questionnaires: 46 for drivers (this number corresponds to the total radio taxi drivers in the city) and 80 for the users of radio taxis. The questions approached two aspects, the exploitation of radio taxis and their usage. For the first aspect we discussed the profiles of drivers, the organization of work and the real mode of the functioning of radio taxis. Concerning the second aspect related to the use of these taxis, we discussed the modes of transport the most used by the users and the quality of service offered by the public transport, by the taxi and then by the taxi radio. This work took place from May 10 to July 17, 2011. It is the first research on radio taxis in Algeria.

GENESIS OF RADIO TAXIS

The first company of radio taxis in Algeria was put into service on February 1st 2005 in Algiers under the name "Taxi-Minute" with a car fleet consisting of 60 vehicles and 120 drivers. These taxis run all the weekdays 24H/24H, including weekends and the days off (Mokrani, 2005). The tariffs are calculated according to the number of kilometres - **the Executive Decree No. 02-448 of 17 December 2002**. After the creation of this company, the Ministry of Transport has received twenty-five (25) applications in eight (08) days for the creation of new companies in the country. In the town of Batna there are currently three radio taxi companies with a total of forty (40) cars and forty six (46) drivers. The presentation of the radio taxis in the city of Batna is made according to the date of creation, the identification number, the number of vehicles and drivers, the working hours and the rates (see Table 1).

Table 1. Presentation of the radio taxi companies in the city of Batna.

Naming	Chabab Aurès	Gharbi Samir	El Bark
Characteristics			
Creation date	March 12 th 2005	July 4 th 2010	July 1 st 2011
Number	1*...	2 ≠...	3*...
Number of drivers	17	17	12
Number of vehicles	15	15	10
Types of vehicles	Chevrolet Aveo	Chevrolet Spar	Hundai Atos
Hours of work	7 am – 6 pm	7am- 8 pm	8 am- 6 pm
Night work	yes (2 vehicles)	yes (2 vehicles)	None
Rates	Flat	Flat	Flat

The table shows that the first two companies of radio taxis in the city of Batna have the same number of vehicles and drivers and apply the same work organization which is working day and night. Concerning El Bark Company, its activities are

¹ Batna is a north-eastern city in Algeria. Its area is about 13 000 km² with a population estimated at 1,175,643 inhabitants in 2011

limited to the day working. This may be due to its recent creation date and size of its fleet. It also appears that the three companies have opted for fixed rates, what is contrary to the current regulations. It would be important to know that the real exploitation of taxis from their operation by drivers to their use by different users.

EXPLOITATION OF THE RADIO TAXIS

The description of this first aspect related to the operation of radio taxis, is based on the results of the questionnaires distributed to the radio taxi drivers in the city of Batna and their profiles, including age, gender and experience. It also includes the real mode of operating of the taxis and the difficulties encountered by the drivers in the field. The main results are presented later in this work.

Young experienced drivers. The Radio taxi drivers are almost young men with ages between 20-35 years and 35-40 years and a total percentage of 84.77%, which allows them to practice best their profession day and night (see Figure 1).

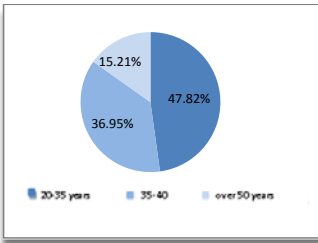


Figure 1. Drivers' ages.

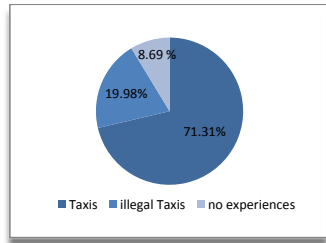


Figure 2. Drivers' experiences.

Moreover, the majority of these drivers were already in the public transport of people which certify the qualification of these drivers for the job (see Figure 2).

Two types of operation for radio taxis. The real mode of operation of the radio taxis is much more based on the free spins than on phone usage as shown in Figure 3. This is due to the lack of information on the functioning of these taxis and therefore confusion with other taxi service.

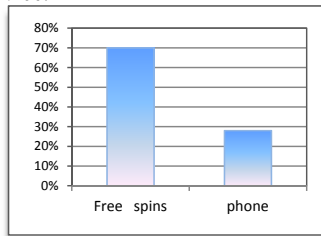


Figure 3. Operating mode of radio taxis.

Variable offer depending on the time and place. The Periods when the demand for radio taxis is important correspond to the peak at the beginning of the day (6:30 am to 8 am) and the end of the day (5 pm-6:30 pm) as shown in Figure 4.

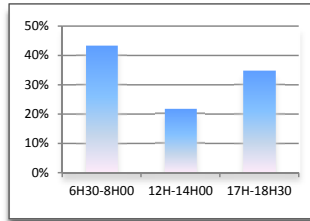


Figure 4. Periods of displacement.

These periods of demand can last till (10 pm) especially in summer. The results also show that it is on Friday which is a weekend that the demands are more important and where the service taxi is limited. Furthermore, among the requested destinations we find the hospitals, clinics, universities and the bus station. Actually the drivers reported that they have encountered a number of difficulties which are related to the lack of information on this form of urban transportation which made them adopt the free spins mode. They also mentioned the absence of the role of the department of transport in the management, the organization and regulation of transport in urban areas.

USE OF RADIO TAXIS

For the second aspect related to the use of the radio taxis, and after presenting the profiles of the users: age, sex, education level and occupation, we tried to know the modes of transport used to get around the city, the quality of service offered by the urban transport to approach finally the use of radio taxis and the quality of service offered by this form of transportation in the city.

Variety of users. The study sample consists of two main age groups: 20-40 years and 40-60 years as shown in Figure 5, less than 20 years and over age 60 years are less important. It is clear therefore that the sample consists of different age groups which allows for diverse results. Figure 6 shows that the sample consists mostly of men.

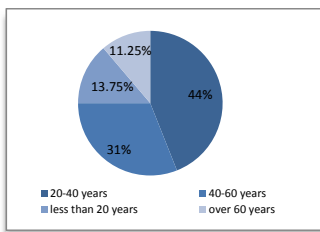


Figure 5. The sample by age

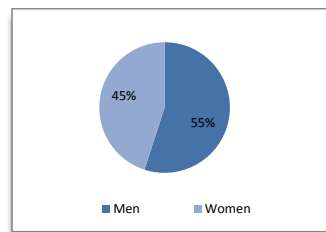


Figure 6. The sample by sex

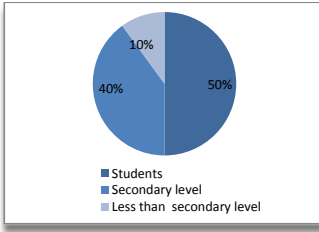


Figure 7. The sample by the educational level

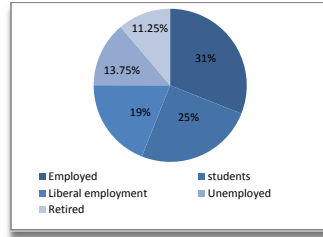


Figure 8. The sample by profession

Concerning the educational level, the results presented in Figure 7 show that the sample consists generally of academics, university students and those with secondary level. This made it easy for us to use the questionnaire and its exploitation. Concerning the jobs, they are allocated, in decreasing order, to officials, students, professionals, unemployed and retired persons (see Figure 8). This variety of jobs allows us to collect various points view expressed by different people with different status.

Reluctance to use the taxi service. Figure 9 shows that the mode of transport the most used is the bus followed by the private cars, the walking, the informal taxis and then the taxi service.

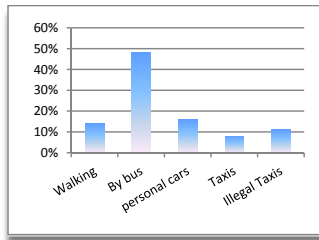


Figure 9. Transport used mode.

It is important to note at this level the place deserved to the taxi service in the city of Batna in comparing to other modes of transport used and particularly the urban informal taxis as an integral part of urban transport in the city (Boubakour, 2007). Moreover, the reluctance on the use of taxis service may affect the use of radio taxis if they adopt the same mode as the taxis service which is based on the free spins.

Not satisfied users by the urban transport services. The degree of users' satisfaction by the quality of service offered by public transport has been assessed according to the following indicators: the lack of comfort, non-compliance with directions, travel time, the lack of security and the low capacity of the transport. The results, presented in Figure 10, show that the lack of comfort was discussed first followed by the non-compliance with directions, the travel time and finally the lack

of security and the low capacity of the transport. These frustrations are related to the characteristics of the buses of some private operators who, in the absence of the technical control by the concerned instances, continue to operate using buses in poor condition, particularly in certain areas of the urban network which does not allow them to ensure a quality service (Report, 2008).

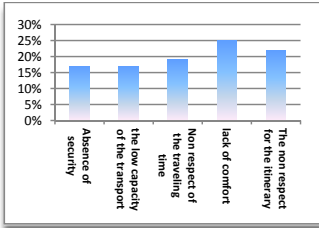


Figure 10. Indicators for quality of service

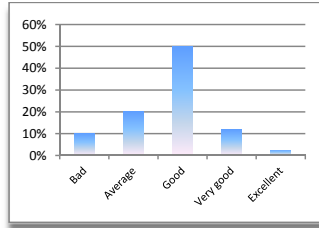


Figure 11. Evaluation of the quality of service

We asked then the users to evaluate the quality of service offered by public transport (bus and taxi service) in the town of Batna according to a scale of five (5) levels: Poor, Average, Good, Very Good and Excellent. The results showed that the quality of service was estimated good by the half of the surveyed. It was considered average by 20% of cases. The assessment is considered by the rest of the surveyed as, very good by 12.5%, poor by 10% and excellent by 2.5% (see Figure 11). This variety of responses is perhaps due to the existence of differences between the characteristics of the existing urban transport in the city of Batna. These features are of quality especially for the bus owned by the Company of Urban Transport in the city of Batna (ETUB) and taxi service but no longer meet the standards of conformity and safety for the buses of some private operators (Report, 2008).

Limited use of radio taxis. Regarding the use of radio taxis, the results obtained showed that the majority of users ignore the existence of these taxis as shown in Figure 12. This is due to the lack of information about this mode of urban transportation and how it works which led to confusion with the taxi service.

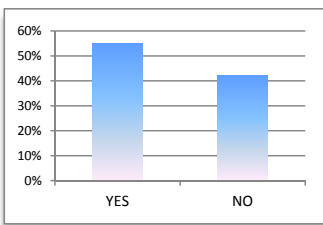


Figure 12. Availability of radio taxis

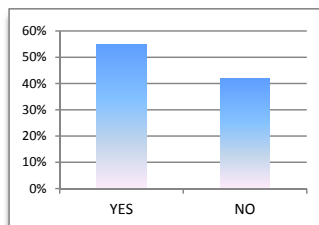


Figure 13. Use of taxi radio

The answers to the question "have you ever used the radio taxis", the responses presented in Figure 13 showed that the majority of users have already used these taxis without knowing that these are taxis radio.

The quality of the service offered by taxis radio. To gather information on the quality of service offered by the taxis radio, we have adopted the same evaluation method already used to evaluate the quality of service provided by the public transport (see section 4.3) which is based on the scale of five (5) levels.



Figure 14. Radio taxi services quality.

The results presented in Figure 14 show that the quality of service was estimated good in most cases. This may be due to the characteristics of the relatively new vehicles belonging to the taxi radio companies and the experienced drivers. Finally, to improve the quality of the radio taxi service, the users questioned proposed to increase in the number of cars and to launch campaigns of information on the functioning of this form of urban transportation and its benefits in terms of comfort, safety and quality.

CONCLUSION

The radio taxis is a form of urban transport that contributes to satisfy the needs of the motorized mobility of a proportion not neglected of the population, although poorly known and used in its normal operating mode (phone usage). Their use is limited due either to the lack of information about their advantages or by the lack of information about their mode of functioning, which create confusion with the taxi service. These observations enable us to propose a set of actions to strengthen the role of radio taxis by improving the operating conditions and the use of taxis (reinforcement of the systems of information and of the sensitization) and by the establishment of an organizing / regulating urban transport authority that coordinates the efforts of all stakeholders (users, drivers, operators, companies and the state) in order to improve the quality of service offered by the urban transport. These observations also push us to reconsider the urban transport policy for the medium and for the long term. They require necessarily a reflection and a debate on the future of cities for the integration of new modes and forms of urban transport.

REFERENCES

- Boubakour, F. (2009). "Urban transport in Algeria facing the challenges of sustainable development: the problems and proposed solutions." <http://www.codatu.org> (May 2011).
- Boubakour, F. (2007). "The illegal taxi or the offering tailor-made: a unique experience. Case of Batna (Algeria), The taxi, a solution for the future urban mobility.", Conference in Lisbon on September 20th and 21st 2007.
- Executive Decree N° 02-448 (2002). Tariff ceilings passenger transport by taxi car, <http://www.radp.dz>.
- Mokrani, K. (2005). "The radio-taxi company operating: beginning today in Algiers.", Tribune (Algerian daily) of February 2nd 2005. <http://www.Latribune.dz>
- Law N°. 01-13. (2001). The orientation and organization of land transport; <http://www.radp.dz>.
- Report. (2008). "Feasibility study of the tramway Batna: Diagnosis.", Engineering Transurb-Technirail, Wilaya Department of Transport, Batna, Algeria.
- Salhi, S. (2010). "The Urban Transport in Algeria: Current Situation and Prospects.", Ministry of Transport, Algeria. [http://e-civis.org/24_presentation Algerie.pdf](http://e-civis.org/24_presentation_Algerie.pdf).

Vehicle Speed Determination based on Front Windshield Glass Rupture Area

Chuanjiao SUN, Jie ZHANG, and Xiaojing BAN

Department of Traffic Engineering, Research institute of highway ministry of transport, 100088, City, Beijing, China PH (010)8201-9588-9554; FAX (010) 8201-9556; Email: sunchuanjiao@163.com

ABSTRACT

In this paper, through designing object such as a ball, coconut and bricks, and the vehicle front windshield glass collision experiment, data of front windshield glass rupture area and the collision object quality, speed is collected. The regression function of rupture area and speed, quality relations is given. The actual traffic accident case is used to validate the function reliability. The paper will provide a new method for vehicle speed determination in traffic accident, which has very important reference significance.

INTRODUCTION

The collision usually happened in very short time, about 2 to 3 second. So it is important to reconstruct the vehicle speed in the crash. The current method always based on the marked on the ground, the trace of the tires. However, some time there is no sign left on the traffic scene only the broken vehicle front windshield. In the paper, the experiment is designed to find the relationship between the vehicle speed and the collision objectives. A good method is provided for calculate the speed without other sign but broken vehicle front windshield.

EXPERIMENT PROCESS AND RESULTS

The experiment includes three parts: the steel ball collision with windshield, the windshield image processing and the experiment analysis. The experiment windshield is Jetta car windshield. The collision objectives include steel ball, coconut, grapefruit and bricks.

In order to study the windshield fracture morphology in the traffic collision, the experiments of different objectives collision to the windshield are held in August of 2010 and January of 2011 in the experimental field of RIOH as shown in Figure 1.



Fig. 1 Windshield rupture morphology experiment

Total 23 experiments were hold. In the experiments process the collision objectives are determined, the quality of the objectives are measured, then let the objectives go at free ball on the height of 3.5m, 4.5m, 5.3m, 8m and 9m, collision with the windshield on the ground.

The experiment information is shown in table 1 with the collision objectives, the quality and the falling height.

Table 1 Experiment Information

NO.	Objectives	Quality (kg)	Height (m)	NO.	Objectives	Quality (kg)	Height (m)
01	Brick vertex	1.46	8.2	11	Steel ball	0.18	3.5
02	Brick plane	1.48	9	12	Steel ball	0.18	4.5
03	Brick edg	1.48	9	13	Concrete block	0.36	9
04	Brick vertex	1.48	5.3	14	Concrete block	0.36	9
05	Brick plane	1.48	3.5	15	Concrete block	0.36	5.3
06	Coconut	2.2	8.2	16	Grapefruit	1.5	8
07	Steel ball	0.18	8.2	17	Grapefruit	2.5	8
08	Steel ball	0.18	9	18	Grapefruit	2.5	5.3
09	Steel ball	0.045	9	19	Grapefruit	2.5	3.5
10	Steel ball	0.18	5.3				

WINDSHIELD RUPTURE MORPHOLOGY BASED ON THE IMAGE PROCESSING

In order to figure out the relationship between the area of windshield rupture and the collision, the image should be processing. The image processing steps include: gray-scale image processing, edge extraction, trimming and noise filtering.

- (1) **Gray-scale image processing.** The weighted average method for processing is used in the paper. Based on the importance of the basis color, different

weight is given to R , G and B. $\omega_r=0.299$ 、 $\omega_g=0.587$ 、 $\omega_b=0.114$, that is:

$$R=G=B=(0.299R+0.587G+0.114B)$$

- (2) **Edge extraction.** The overall value of the two algorithm Otsu algorithm is used. The global value of two is actually choosing a threshold of the pixels in the image into two classes. Otsu algorithm is to find the tow class of the within class variance minimum (i.e, the maximum between -class variance) of the threshold, as shown below.

$$\sigma_B^2(k^*) = \max_{1 \leq k < L} \sigma_B^2(k)$$

That, k^* is the optimal threshold , $\sigma_B^2(k^*)$ is maximum between-cluster variance. B is the gray scale class and $\sigma_B^2(k)$ is between-cluster variance.

- (3) **Trimming after the edge extraction.** In order to improve the contrast between the foreground and the background image, the two processing threshold should be increased for trimming.
- (4) **Noise filtering.** The median filtering method is used to remove the image noise. Integrated image size and other factors, the filter operator $W=[5,5]$.

The image after processing is shown in Figure 2.



Fig. 2 The glass rupture image after processing

RELATIONSHIP BETWEEN THE RUPTURE AREA AND THE COLLISION OBJECTIVES

Image of 50*50 is selected to have grid processing. The result is shown in Figure 3.

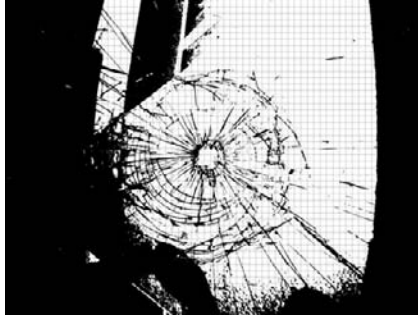


Fig. 3 The glass rupture image after grid processing

By the analysis of Fig.3, the character center of the rupture image is in the image space distance of $L_{img} = 620$ pixel. So the actual distance in the real space is $L_{real} = 8.3$ cm. So the relationship between the image space and the actual space $L_{img} \sim L_{real}$.

The broken arc center distance of the top marks in the image space distance $L_{img_1} = 675$ pixel, the actual distance $L_{real_1} = L_{real} / L_{img} \times L_{img_1} = 9.04$ cm; the broken actuate trace center distance to the right in the image space distance is $L_{img_2} = 800$ Pixel, the actual distance is $L_{img_2} = 8.3/620 \times 800 = 10.71$ cm. The broken glass morphology is approximately elliptical trace, trace area of the calculated results for the broken:

$$\pi \times L_{real_1} \times L_{real_2} = 304.01 \text{cm}^2$$

After the processing of the experiment image, the result is shown in Table 2.

Table 2. Relationship between the Rupture Area and the Collision Objectives

NO.	Quality (kg)	Height (m)	Speed (m/s)	rupture Area (cm ²)	rupture Area (m ²)
1	1.46	8.2	12.68	264.33	0.03
2	1.48	9	13.28	2551.76	0.26
03	1.48	9	13.28	1995.25	0.20
04	1.48	5.3	10.19	289.53	0.03
05	1.48	3.5	8.28	706.86	0.07
06	2.2	8.2	12.68	4536.46	0.45
07	0.18	8.2	12.68	201.06	0.02
08	0.18	9	13.28	304.01	0.03
09	0.045	9	13.28	3.8	0.00
10	0.18	5.3	10.19	3.14	0.00
11	0.18	3.5	8.28	0	0.00
12	0.18	4.5	9.39	2.54	0.00
13	0.36	9	13.28	1983.16	0.20
14	0.36	9	13.28	1809.55	0.18
15	0.36	5.3	10.19	615.75	0.06
16	1.5	8	12.52	921.56	0.09
17	2.5	8	12.52	1350.49	0.14
18	2.5	5.3	10.19	706.86	0.07
19	2.5	3.5	8.28	481.5	0.05

RELATIONSHIP AMONG RUPTURE AREA, QUALITY AND SPEED

The fitting relationship among the automobile windshield rupture area, the collision objective’s quality and speed is established by using MATLAB data fitting. The linear equation of two unknowns fitting results as shown in Figure 4.

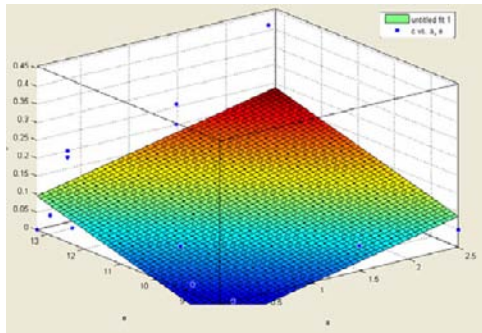


Figure 4. The linear equation of two unknowns fitting results

The fitting equation is: $S = -0.30885 + 0.05801 * m + 0.03005 * v$. S is the rupture area of the windshield, m is the collision objective mass, v is the collision speed.
The quadratic equation of two unknowns fitting result is shown in Fig.5.

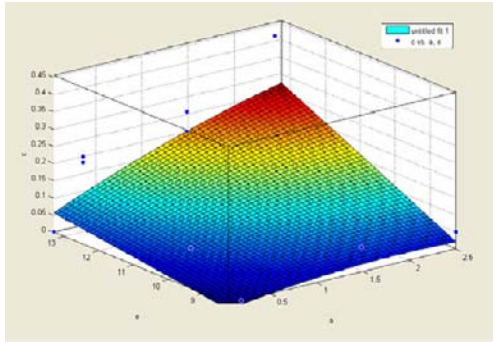


Figure 5. The quadratic equation of two unknowns fitting results

The fitting equation is:
 $S = -0.1318 - 0.07906 * m + 0.01372 * v - 0.01105 m^2 * v + 0.01472 m * v$. S is the rupture area of the windshield, m is the collision objective mass, v is the collision speed.
The cubic equation of two unknowns fitting result is shown in Fig.6.

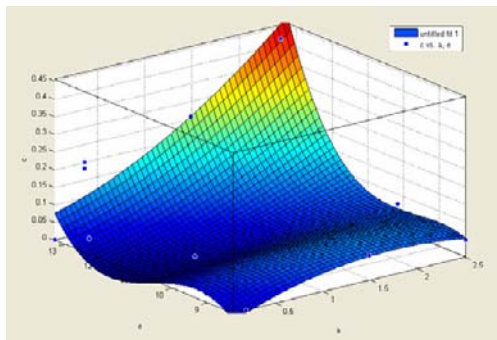


Figure 6. The cubic equation of two unknowns fitting results

The fitting equation is:
 $S = -10.65 + 1.284 * m + 3.11 * v - 0.1431 m^2 - 0.2252 * m * v - 0.229 v^2 + 0.01348 m^2 * v + 0.01008 * m * v^2 + 0.009456 * v^3$
S is the rupture area of the windshield, m is the collision objective mass, v is the

collision speed.

The quartic equation of two unknowns fitting result is shown in Fig. 7.

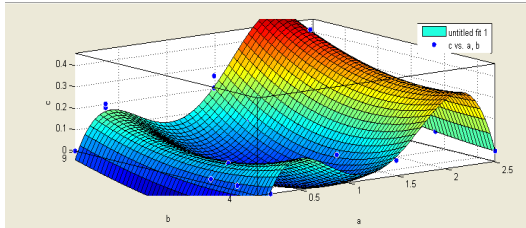


Figure 7. The quartic equation of two unknowns fitting results

The fitting equation is:

$$S = -0.2285 + 6.91 * m - 0.02911 * v - 6.052 * m^2 - 0.8656 * m * v + 0.002866 * v^2 + 2.475m^3 + 0.4038m^2 * v + 0.03524m * v^2 - 0.4509m^4 - 0.02507m^3 * v - 0.01392m^2 * v^2$$

S is the rupture area of the windshield, m is the collision objective mass, v is the collision speed.

Table 3. Fitting Results Comparison

Data	Fit type	SSE	R-square	DFE	Adj R-sq	RMSE
S vs. m, v	Poly 11	0.1441	0.4091	16	0.3352	0.0949
S vs. m, v	Poly 21	0.1304	0.465	14	0.3127	0.0965
S vs. m, v	Poly 23	0.1024	0.5800	10	0.2441	0.1012
S vs. m, v	Poly 42	0.0222	0.9091	7	0.7661	0.0563

Note: Sum of squares SSE - closer to 0 the better; Correlation coefficient R-square - closer to 1 the better; The corrected correlation coefficient Adjusted R-square - closer to 1 the better; Root mean square error RMSE - closer to 0 the better.

It can be seen from Table 4, linear equations and quadratic equation almost has the same effect. The best effect is Poly 42, the quartic equation of two unknowns fitting result.

CONCLUSIONS

The factors affecting the maximum radius of the collision on the vehicle front windshield include: the collision speed, the glass structure and material, the location of the collision center.

1) The instantaneous vehicle speed in the collision. Based on the traffic accident case studies, the higher the collision speed is, the greater the impact energy is to make

the maximum radius of the glass cracks.

2) The quality of collision objectives. The vehicle rupture area has direct relationship with the quality and speed of the collision objectives.

3) The structure and materials of front windshield. Different structure and materials of windshield has different collision morphology.

4) According to the experimental results of broken vehicle windshield, the relationships among the rupture area and the collision speed, quality can be expressed as follows:

$$S = -0.2285 + 6.91 * m - 0.02911 * v - 6.052 * m^2 - 0.8656 * m * v + 0.002866 * v^2 \\ + 2.475 m^3 + 0.4038 m^2 * v + 0.03524 m * v^2 - 0.4509 m^4 - 0.02507 m^3 * v - 0.01392 m^2 * v^2$$

S is the rupture area of the windshield, m is the collision objective mass, v is the collision speed.

All of the experiments are low-speed collisions which cannot reach the actual traffic conditions in the high-speed collision. So the applicability of the formula are at less than 40km/h and less than 2.5kg.

REFERENCES

- Xu Hongguo (1995). *Glass fragments thrown from the theoretical model used to calculate the speed of car crash*. Automotive Engineering. (4):246- 251.
- Ling Yang (2011). *Practical car accident forensic science*. Beijing: People's Communications Press.
- Strobl, H. (1996). "Betrachtung zum Thema Steinschlag" [J], Verkehrsunfall und Fahrzeugtechnik, 1996 (9).
- Hong-guo Xu (1992). "Theoretische und Empirische Modelle von Glassplitter Wurfweiten"[C], Vortrag bei IFT TU Berlin, 1992.
- Wang Lifang (2002). *Study on headlight glass fragments distribution pattern in Car crashes*. Ji Lin University, master's degree thesis, 2002.
- Du Xuejing, Xu Hongguo, and Chang Sheng (2008). *The effect of Material properties on the car crash fallout movement characteristics*. Journal of System Simulation. 20 (21): 5999~6001.
- Zhang Liang (2007). *Traffic simulation model of fallout*. Ji Lin University, master's degree thesis.
- Zhao Guangyao, Fan Xinhua, and Di Jianwei (2008). *Vehicle collision analysis and evaluation of computer simulation*. Journal of Northeastern University, 7(29):1020-1024.

The Timing to Retime and Maintain Traffic Signal Systems

Pei-Sung Lin¹, Ph.D., P.E., PTOE, Aldo Fabregas², and Hongyun Chen³, Ph.D.

¹Program Director, ITS, Traffic Operations and Safety Program, Center for Urban Transportation Research (CUTR), University of South Florida, 4202 E. Fowler Ave., CUT 100, Tampa, FL 33620; PH: (813) 974-4910; FAX: (813) 974-5168; Email: lin@cutr.usf.edu

²Research Associate, ITS, Traffic Operations and Safety Program, Center for Urban Transportation Research (CUTR), University of South Florida, 4202 E. Fowler Ave., CUT 100, Tampa, FL 33620; PH: (813) 974-3296; FAX: (813) 974-5168; Email: fabregas@cutr.usf.edu

³ Postdoctoral Research Associate, ITS, Traffic Operations and Safety Program, Center for Urban Transportation Research (CUTR), University of South Florida, 4202 E. Fowler Ave., CUT 100, Tampa, FL 33620; PH: (813) 974-3120; FAX: (813) 974-5168; Email: hchen@cutr.usf.edu

ABSTRACT: Currently, most agencies in the United States retime their traffic signal systems either every 2-4 years or based on complaints received. With limited budget and resources, it becomes essential for agencies to retime and maintain their traffic signal systems cost-effectively to maximize the benefits. To achieve this goal, this paper reviewed traffic signal retiming practices, and investigated the impact of signal timing degradation on traffic signal system performance. The impacts of signal timing degradations on the system performance for various growth rates were intensively simulated at three selected corridors. It was found that the elements of average traffic volume per hour per lane and the growth rate of traffic volume on a main corridor can be used to effectively estimate the signal timing degradation. This paper offers a simple and practical guideline to determine when to retime and maintain a traffic signal system.

BACKGROUND

Substantial capital investments have been made by transportation agencies to modernize their traffic signal systems. The benefits achieved by these investments are affected by the signal timing degradation due to traffic growth. With various rates of growth, the original coordinated signal timing plans may become outdated at different paces. It is important to update the signal timing plans consistent with traffic patterns, thus to ensure the benefits in an effective way. While under current poor economic situation, it is even essential for agencies to retime and maintain their traffic signal systems cost-effectively to maximize the benefits with limited budget and resources.

The objective of this is to investigate the impact of signal timing degradation on traffic signal system performance by focusing on traffic growth, and determine the timing to retime and maintain traffic signal systems. It is organized as follows: first,

traffic signal retiming practices were reviewed and a traffic signal system performance measure based on the signal timing degradation was established; the impacts of signal timing degradations on the system performance for various growth rates were intensively simulated at three selected corridors; then, the simulation results and measurements of degradation were analyzed and followed by the results conclusions, and recommendations on the timing of traffic signal system retiming.

SIGNAL RETIMING PRACTICE

To understand the impact of signal timing degradation, it is necessary to gain the insight regarding current practice of signal maintenance for the traffic agencies. Currently, most traffic agencies in the United States retime their traffic signal systems either every 2-4 years or based on complaints received. However, signal timing is more complicated than the freeway operation. The degradation of traffic signal timing may change the ongoing operations of the entire traffic signal system if the timing is not comparable to the ongoing traffic characteristics (FHWA 2008). The research team conducted an agency survey in 2008 among 57 transportation agencies in Florida, with responses from 34 agencies that maintain approximately 12,000 signals. The survey collected information on the general practices for traffic signal system maintenance mainly focusing on three components, communication, detection, and signal timing. The agencies were asked to rank their system components from 1 (worst) to 5 (best) for each question. The survey results are summarized in Figure 1.

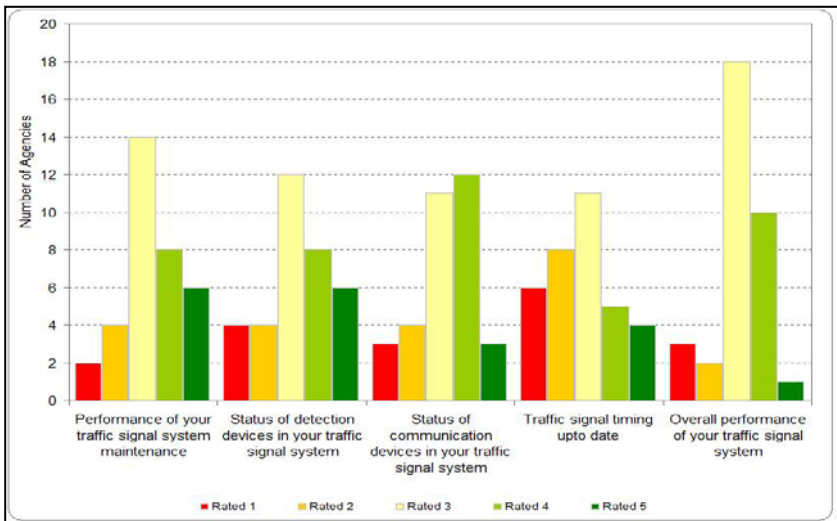


Figure 1 Ratings of status of traffic signal system components

The number of agencies rating signal timing at 1 or 2 is relatively large. The performance of communication and detection components was rated higher than timing. In addition, 48 percent of the agencies stated that they retime their signals

every 1 to 3 years and another 15 percent every 3 to 5 years. However, the degradation of a traffic signal system's performance comes not only from the degradation of the physical system but also from traffic signal timing. The survey results indicate that communication and detection systems were better maintained with fewer complaints, while signal retiming required more resources and attention.

PERFORMANCE MEASUREMENT

In the current practice, only the numerical values of the observed performance measures of a traffic signal system under a specific prevailing traffic condition are reported. However, the numerical values of the observed performance measures cannot reflect traffic signal system performance itself because the same observed performance can result from numerous combinations of physical system status, existing timing, and traffic conditions. To effectively evaluate traffic signal systems, a traffic signal system performance measure based on the signal system degradation needs to be established.

When both the status of the physical system and the signal timing are ideal, the traffic signal system can achieve its ideal performance which can generally represent the best performance the system can achieve under a specific prevailing condition. Ideal performance generally cannot be easily observed in the field except for the most recent retimed signal systems with a fully-functional physical system or a fully-functional adaptive traffic signal system. However, ideal performance under specific prevailing traffic conditions can be obtained through carefully calibrated traffic simulations. Any departure from ideal conditions due to degradation of the physical system or signal timing plans will cause a gap in any performance measure between the full potential of the system and the current conditions.

Travel time is one of the most commonly-used performance measures for corridors. To adequately evaluate the performance of a traffic signal system itself, this paper defines a Degradation Index (*DI*) of a traffic signal system as the percent of increased travel time due to system degradation relative to its observed travel time. The Performance Index (*PI*) is defined as the percent of ideal travel time relative to the observed travel time. The "ideal travel time" is the travel time the system can achieve under fully-functional detection and communication systems and ideal signal timing usually through signal retiming. The *DI* can be expressed in the Equation 1 and the relationships among observed travel time, ideal travel time, and increased travel time are shown in the Equation 2:

$$DI = \frac{TT_{increased}}{TT_{Observed}} \quad (1)$$

$$PI = \frac{TT_{ideal}}{TT_{Observed}} = 1 - DI \quad (2)$$

Where *DI* is Degradation Index and *PI* is the Performance Index, in decimal format or percent (%) by multiplying the decimal value by 100; $TT_{increased}$ is the travel time increased due to system degradation; $TT_{observed}$ represents the observed travel time

under existing conditions; and TT_{ideal} is the travel time under fully functional detection and communication systems and ideal signal timing plan.

As illustrated in Figure 2, three different signal conditions exist: current condition, degraded condition, and ideal condition. The current condition, at $t=1$, is the optimized signal timing for the prevailing volume conditions when the timing was implemented. The degraded condition, at $t=2$, represents the growth traffic demand with the original signal timing at $t=1$. Due to the increasing volume, the signal timing at $t=1$ did not meet the traffic demand at $t=2$. Therefore, the traffic signal timing is outdated, presenting a certain level of degradation. The ideal condition, at $t=3$, is the optimized signal timing after the volume increases. The degradation performance index is used to measure how the gap between the degraded and ideal conditions.

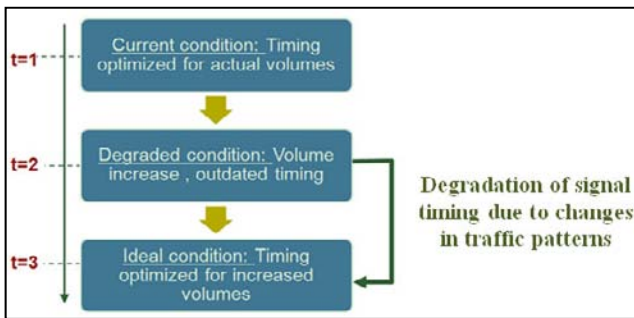


Figure 2 Degradation due to changes in traffic patterns

For the signal timing, a Weighted Degradation Index (WDI) was calculated as a measure of the overall degradation. The weights are based on vehicles per hour per lane (vphpl) for each direction. The objective of this Weighted Degradation Index is to give more importance to the direction of major volume and to have a single measure of degradation for the control section. Also, this performance measure is to compensate for the interaction of the coordinated directions. It is common to encounter cases in which the improvement in one direction leads to major delays in the other. The WDI is calculated using the following equation:

$$WDI = \frac{WTT_D - WTT_I}{WTT_D} \quad (3)$$

Where WDI is the weighted Degradation Index; WTT_D is the weighted travel time in degraded conditions; and WTT_I is the weighted travel time in ideal conditions. The Weighted Travel Time (WTT) is calculated using the following expression:

$$WTT = \frac{V_1 * TT_1 + V_2 * TT_2}{V_1 + V_2} \quad (4)$$

Where WTT is the weighted travel time; V_1 is the average vphpl for direction 1 (EB, NB); V_2 is the average vphpl for direction 2 (WB, SB); TT_1 is the travel time for direction 1 (EB, NB); and TT_2 is the travel time for direction 2 (WB, SB).

STUDY CORRIDOR

The generic control sections were used to analyze the degradation performance of traffic signal timing. The impacts of signal timing degradations on the system performance for various growth rates were intensively simulated at three selected control corridors upon the original signal timing data availability. The first control section comprises 10 intersections on US 41 in Sarasota, Florida, as presented in Figure 3. It is a six-lane divided highway with a speed limit of 45 mph. The selected road segment was retimed during 2008. The second control section is located in the jurisdiction of City of Sarasota in Florida. Figure 4 illustrates the selected roadway segment. All the intersections in the corridor are actuated-coordinated, and the speed limit for the section is 35 mph. The traffic volume and turning movements are available and were counted in 2008. The third control section comprises eight intersections on W. Broward Boulevard in Fort Lauderdale, Florida, as presented in Figure 5. The speed limit for the section is 35 mph. SimTraffic simulation tool was used to simulate the three control corridors and measure the system performance.



Figure 3 Selected control section on US 41



Figure 4 Selected control section on Fruitville Road

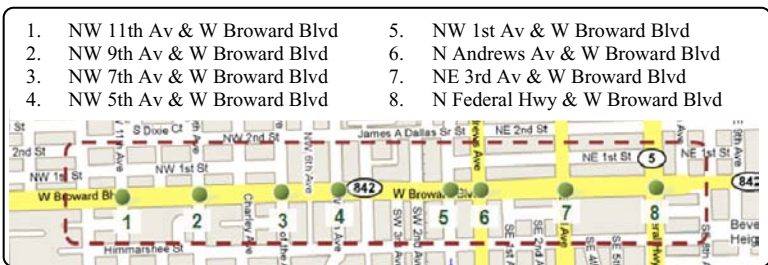


Figure 5 Selected control section on W Broward Boulevard

DATA ANALYSIS

Degradation Due to Change in Traffic Patterns

The Weighted Degradation Index for the studied traffic signal systems was calculated for traffic growth values ranging from 2.5 to 25 percent to represent system degradation due to traffic growth. The results are presented in Figure 6. It shows the Weighted Degradation Index due to changes in traffic growth for different traffic conditions in the test models (AO: AM off-peak; PM: PM peak hour; EH: evening hour; MD: midday hour). It can be observed that the magnitude of the increase in the Weighted Degradation Index varies between sites. It is necessary to include additional variables to characterize each test case. The variable found to be most significant and useful to explain between-sites variations was the average volume per hour per lane (vphpl) used in the last signal system retiming along the coordinated corridor. The Weighted Degradation Index can be computed using the average corridor volume and its growth rate since the last signal system retiming. From this study the maximum Weighted Degradation Index was about 16 percent.

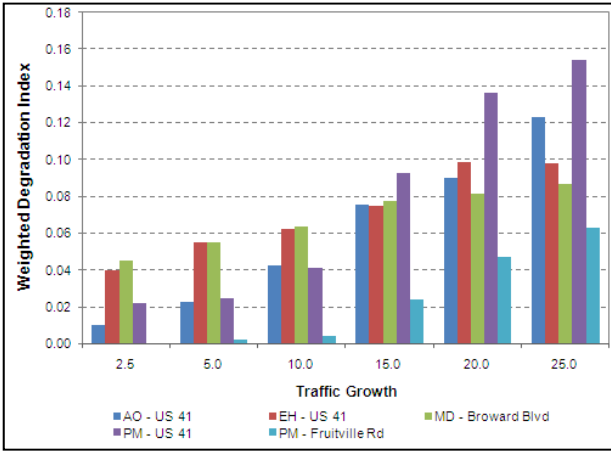


Figure 6 Weighted degradation index of studied corridors due to growth

Degradation can occur from signal timing itself as traffic volumes increase through time. Several scenarios of volume increase were tested to construct a performance model as a function of average traffic volume of the corridor in vphpl from the last retiming and its growth rate since then. The increase in travel time due to a growth of traffic volumes was predicted by a linear model, and the resulting predicted value was used estimate the Degradation Index. Table 1 lists the result of the performance model in terms of travel time increase for signal timing degradation.

Table 1 Model for Predicting Change in Travel Time Based on Traffic Growth

Variables	Coefficient	Std. Err.	p-value
Intercept	-74.50	11.37	<0.001
Traffic Growth Rate (G)	2.34	0.28	<0.001
Volume per Hour per Lane (VPHPL)	0.14	0.02	<0.001

The coefficient of determination, R^2 for the model was 0.81, and the model represents the seconds of increase in travel time due to signal timing degradation. It can be observed that the travel time increases with respect to the average volume per hour per lane and the traffic growth rate for the control section, as shown in Figure 7.

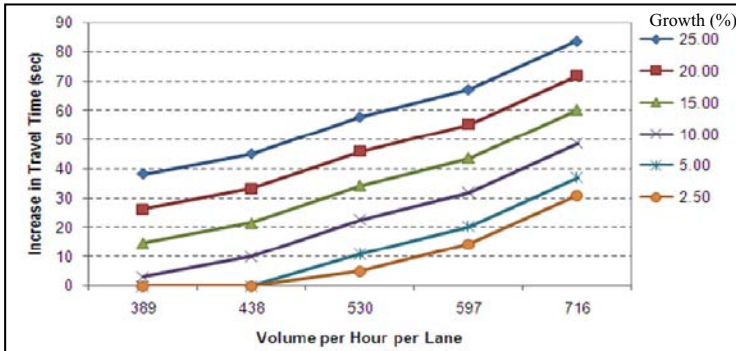


Figure 7 Increase in travel time with respect to traffic volumes on major street

The estimated increase in travel time was used to derive a prediction of the Degradation Index as a function of the average volume and its traffic growth. Figure 8 shows the predicted Degradation Index with respect to average volumes used in the last signal system retiming and its growth rates since then. At congested volumes (vphpl>700), the degradation due to growth tends to slow down for 15 to 25 percent growth rate. When volume is light (e.g., 300 to 400 through vphpl on a main street), the opportunity to improve the system is also limited because the existing timing may handle the traffic increase reasonably well. There is a range of critical volumes where there can be significant improvements by traffic signal system retiming. For the growth rate of 15% or higher, the Degradation Index reaches its maximum for volumes between 400 and 500 vphpl; therefore, corridors with this characteristic should be monitored regularly to seek opportunities for improvement.

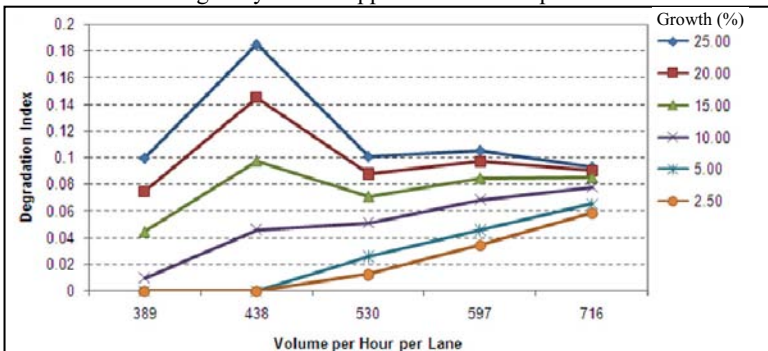


Figure 8 Predicted DI with respect to traffic volume on major street

CONCLUSION

A practical traffic signal performance should measure the performance of a traffic signal system itself and include the impact on system degradation. Outdated signal timing plans can adversely affect the performance of a traffic signal system. A signal

system Degradation Index and Performance Index developed in this study provide a simple way to measure the performance of a traffic signal system itself.

There are many potential causes for outdated traffic signal timing plans. This study found that the benefit of traffic signal retiming can reduce the average travel time on a typical corridor from 10 to 18 percent for a 25 percent growth of traffic volume since the last traffic signal system retiming. The benefits can increase more than the above stated percentages if the coordination signal timing was not properly retimed in the past. It is most beneficial to retime traffic signal systems when significant growth between 20% and 25% occurs on a control section with medium traffic volume because there is a significant room for improvement. When traffic volume is light, the benefit of signal retiming is less than that of medium volume. When traffic volume is heavy, there is also less room for a significant improvement.

This paper provides practitioners with a simple and practical guidance on how to effectively estimate the impact of signal timing degradation of a generic traffic signal system, and determine the timing to retime and maintain the system.

REFERENCES

- Kittelson & Associates, Inc. (2008). Signal Timing Manual, Publication Number: FHWA-HOP-08-024, U.S. Department of Transportation, Federal Highway Administration (FHWA).
- Lin, P, Fabregas, A. Chen, H., and Rai S. (2009). "Impact of Communication/Detection Degradation on Advanced Traffic Management Systems Operations", The Florida Department of Transportation.

Assessment of a Flashing Yellow Arrow Signal Implementation using Gap Acceptance Measures

Pei-Sung Lin¹, Ph.D., P.E., PTOE, Aldo Fabregas², and Enrique Gonzalez-Velez³, Ph.D.

¹Program Director, ITS, Traffic Operations and Safety Program, Center for Urban Transportation Research (CUTR), University of South Florida, 4202 E. Fowler Ave., CUT 100, Tampa, FL 33620; PH: (813) 974-4910; FAX: (813) 974-5168; Email: lin@cutr.usf.edu

²Research Associate, ITS, Traffic Operations and Safety Program, Center for Urban Transportation Research (CUTR), University of South Florida, 4202 E. Fowler Ave., CUT 100, Tampa, FL 33620; PH: (813) 974-3296; FAX: (813) 974-5168; Email: fabregas@cutr.usf.edu

³Research Assistant, ITS, Traffic Operations and Safety Program, Center for Urban Transportation Research (CUTR), University of South Florida, 4202 E. Fowler Ave., CUT 100, Tampa, FL 33620; PH: (813) 974-9795; FAX: (813) 974-5168; Email: egonzal@cutr.usf.edu

ABSTRACT: The use of flashing yellow arrow (FYA) displays for protected-permitted left turn (PPTL) operations has been increasing in recent years. With its inclusion in the MUTCD, more traffic agencies will likely adopt FYA for PPTL operations in the future. The intent of FYA is to replace traditional green ball displays to make drivers more cautious when making permissive left turns. In this case study, a before-and-after study of an FYA deployment was performed. The study used gap acceptance as a short-term safety measure to evaluate the FYA deployment under different traffic conditions. It was found that under similar low to moderate traffic conditions, by implementing FYA, most drivers accepted longer gaps to make their permissive left turns, hence improving the safety. No noticeable benefits from FYA were found under heavy opposing traffic conditions when available gaps were short. Opposing traffic volumes also have a significant impact on gap acceptance behaviors.

INTRODUCTION

The use of flashing yellow arrow (FYA) displays for protected-permitted left turn operation (PPLT) has emerged in recent years as an alternative signal display for preventing the yellow trap, increasing movement capacity, and providing flexibility for signal phasing configuration (Noyce et.al., 2007). The 2009 *Manual on Uniform Traffic Devices* (MUTCD) included formal guidance for the optional implementation of FYA for PPLT operations. With such guidance in place, it is anticipated that more traffic agencies will adopt FYA for PPTL operations in the near future. In some states, such as Oregon, FYA operation has been adopted as the state standard for PPLT operations. In Florida, FYA operation has been adopted as an optional signal configuration by the state. Local agencies have started implementing FYA at selected

locations first, with plans to gradually expand to larger deployments. In this case study, a before-and-after study of an FYA deployment was performed at a location in the Tampa Bay area in Florida. The major objective for this before-and-after study was to assess the effectiveness and benefits of the FYA on improving safety and operations of permissive left turns at the study intersections.

PERFORMANCE MEASURES

Crash data are generally used as the main performance measures for traffic safety evaluation. Ideally, crash data three years prior to and three years after the implementation of the FYA display should be used to produce a reliable assessment of its effects. Due to the timeframe of the study only short-term performance measures of the possible safety and operational benefits of FYA were considered. These measures were aimed at finding an indication of driving behavior changes following the implementation of the FYA operation for PPLT.

Traffic conflicts were also included as short-term performance measure for safety. The definitions of traffic conflicts were adapted from Parker and Zegeer (1989). The conflicts related to permissive left turns were defined based on the work of Brehmer et al. (2003). Conflict counts were performed at the study intersections. However, no major conflicts were detected in either the before or after studies.

Because of very limited crash data and conflicts for this short-term study, critical gap and crossing tolerance were used in this study as approximate short-term performance measures to assess capacity and safety for the FYA implementation, respectively. Both short-term performance measures of critical gap and crossing tolerance are described in detail in the following paragraphs.

According to the *Highway Capacity Manual* (HCM 2000), gap is the time, in seconds, for the front bumper of the second vehicle, of two successive vehicles, to reach the starting point of the front bumper of the first vehicle. Similarly, gap acceptance is defined as the process by which a minor stream vehicle accepts an available gap to maneuver. Typically, gap acceptance is observed during permissive left turn signaling when the driver of the turning vehicle has to judge the available gaps and decide which one to accept (i.e., when to cross). The critical gap according to HCM 2000 is the minimum time in seconds between successive major stream vehicles in which a minor-stream vehicle can make a maneuver. The critical gap is determined by a graphical procedure in which the rejected/accepted gap curves are plotted against the gap duration. For shorter gaps, the rejected gap curve is above the accepted gap curve. The point at which gaps become accepted (i.e., the accepted gap curve intersects the rejected gaps curve) can be assumed as the critical gap.

The crossing tolerance is a measure of the safety involved in the process of gap acceptance. For instance, a driver can accept a long gap, but if he/she decides to cross at the last minute, then the maneuver could end in a harmful event. The crossing tolerance is the time between the moment the turning vehicle clears the gap reference

point and the moment the front bumper of the opposing vehicle touches such reference point. This concept is illustrated in Figure 1. The crossing tolerance was analyzed for gaps less than or equal to a global critical gap.

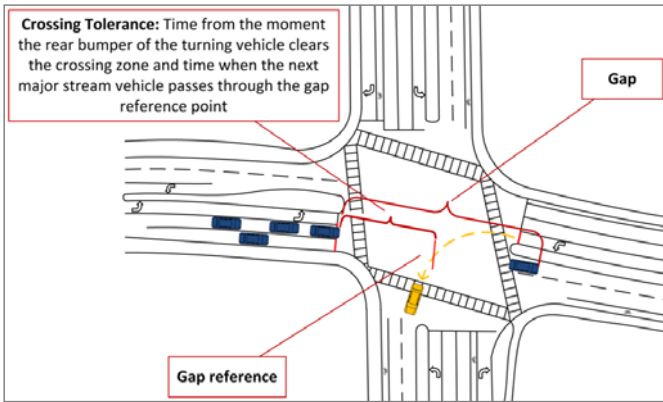


Figure 1. Crossing tolerance

STUDY SITE AND DATA COLLECTION

An aerial view of the studied intersection at the Belcher Road and Nebraska Avenue in Pinellas County, Florida is presented in Figure 2. The main direction covers the north and south approaches, and the minor direction corresponds to the east and west approaches. Both approaches in the main direction have exclusive left turn lanes, two through lanes and one exclusive right turn lane. The side street approaches have an exclusive left turn lane, one exclusive through lane, and one shared lane for through and right turn movements. Both approaches have bicycle lanes.



Figure 2. Aerial view of test site

The FYA operation was implemented on all of the approaches. Data were collected one month before the implementation of the FYA operation and two months after the implementation. Turning movement counts, time-stamped events (conflicts) and gap acceptance data were collected as part of the study. Gap acceptance data were collected through a customized video processing application. Videos from the before-and-after data collection were analyzed frame-by-frame with a precision of 1/10 of a second. The intersection was divided into zones, as presented in Figure 3. The video processing tool was used to time-stamp different events such as open gap, closed gap, arrival to stop line, enter decision zone, start crossing, and finish crossing. The information was input to a database for processing. Over 5,000 gaps were registered in the database for the before and after studies.

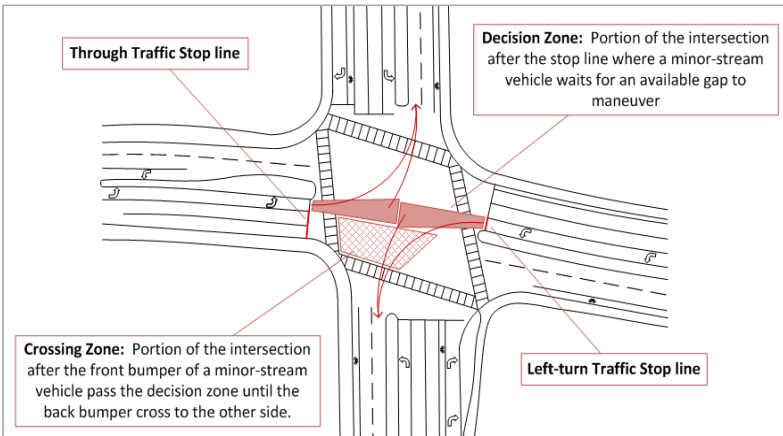


Figure 3. Zones for gap acceptance data collection

RESULTS

The performance measure chosen to carry out the evaluation on capacity by the deployment of FYA was the critical gap, which can be determined by the intersection of the gap rejection and gap acceptance curves. Critical gaps were determined for before and after the implementation of the FYA operation. The critical gaps were organized by time of day and approach for permitted left turn movements. Figure 4 presents an example of a critical gap graphic calculation procedure. The blue (dark) lines represent gap acceptance behavior before the implementation of the FYA operation. The yellow (light) lines represent the gap acceptance behavior after the implementation of the FYA. The critical gap is the intersection of the rejected gaps and accepted gaps. Gaps of duration greater or equal to the critical gap are very likely to be accepted.

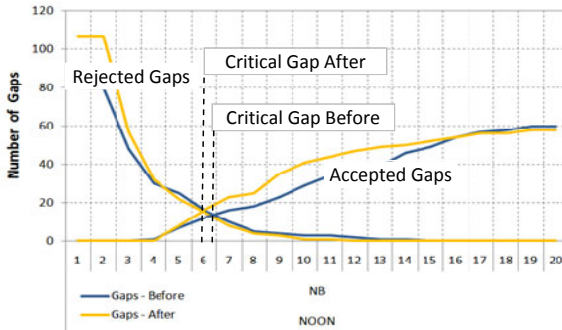


Figure 4. Critical gap example

The critical gap (tc) results by time of day and approach before and after the implementation of the FYA operation are presented in Table 1. It can be observed that the critical gap is either unmodified or reduced with the implementation of the FYA operations. It was also observed that the greatest reductions were observed for longer gaps whereas for shorter gaps the before and after values remained similar.

Table 1. Critical Gap Results

	Time Of Day	tc1(s) Before	tc(S) After	Average Opposing Volumes	Capacity Ratio
Northbound	AM	5.80	5.80	672	1
	NOON	6.45	5.95	360	1.0512
	PM	6.00	5.50	380	1.0541
Southbound	AM	6.45	5.45	364	1.1063
	NOON	5.85	5.80	374	1.005
	PM	5.10	5.10	902	1

With the implementation of the FYA the longest critical gaps seem to be reduced. It can be stated that for this particular implementation of the FYA the critical gaps were normalized to a minimum value inherent to the physical characteristics of each approach. The FYA allows vehicles to continue to make left turns without any intermediate red signal indication. This allowed more vehicles to enter the intersection, enabling drivers to judge and accept more gaps of shorter durations than without the FYA. Therefore, the representation of accepted shorter gaps was increased in the collected data. This can be observed in Figure 4 by a steeper accepted gap curve after the implementation of FYA. This reduction in critical gap can be translated into a capacity improvement based on the potential capacity formula for minor traffic stream suggested by the HCM 2000.

$$C_{p,x} = V_{c,x} \frac{e^{-\frac{V_{c,x}t_{c,x}}{3600}}}{1 - e^{-\frac{V_{c,x}t_{t,x}}{3600}}}$$

Where $C_{p,x}$ is the potential capacity for minor movement x (veh/h), $V_{c,x}$ is the opposing traffic volume x (veh/h), $t_{c,x}$ is the critical gap, and $t_{t,x}$ is the follow-up time for queued vehicles in the minor stream. When all the conditions remain unmodified, the capacity ratio due to a reduction in the critical gap is given by the expression:

$$\frac{C_2}{C_1} = e^{\frac{V}{3600}(t_{c1}-t_{c2})}$$

The response surface for the NB-NOON scenario for the before and after scenarios is presented in Figure 5. The average opposing volume was 360 veh/h. The response surface reflects a conservative variation of the opposing volumes and critical gap. With a critical gap reduction of 0.5 seconds the potential increase in capacity varies from 4 to 6 percent but depending on the volume it may reach up to 12 percent.

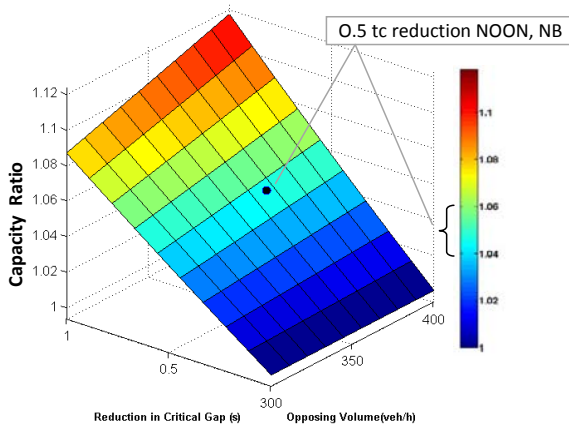


Figure 5. Response surface for capacity ratios due to critical gap reduction

The performance measure chosen to carry out the evaluation on safety was the crossing tolerance. This performance measure is related to the gap acceptance behavior and was assumed as a field indicator of the risk taken by the driver when performing a permissive left turn. If the crossing tolerance decreases for the after condition, it is deemed that the risk for the after condition increases. This could imply that drivers are making the left turn when the opposing vehicle is too close. On the other hand, if the crossing tolerance increases, then it is an indirect field indication that drivers are making safer left turns with respect to a base condition which in this case is the before scenario.

In this study a global critical gap was set at 7 seconds based on the critical gap analysis as shown in Table 1 . Figure 6 shows the comparison of crossing tolerances between the before and after scenarios for permissive left turn maneuvers below the

global critical gap of 7 seconds. It can be observed that for the northbound left turns during AM peak (NBL-AM), northbound left turns during noon time (NBL-NOON), and southbound left turns during noon time (SBL-NOON) cases, there was an improvement in the crossing tolerance. This could be an indication that drivers are crossing the intersection (i.e. permissive left turns) more safely for the after conditions.

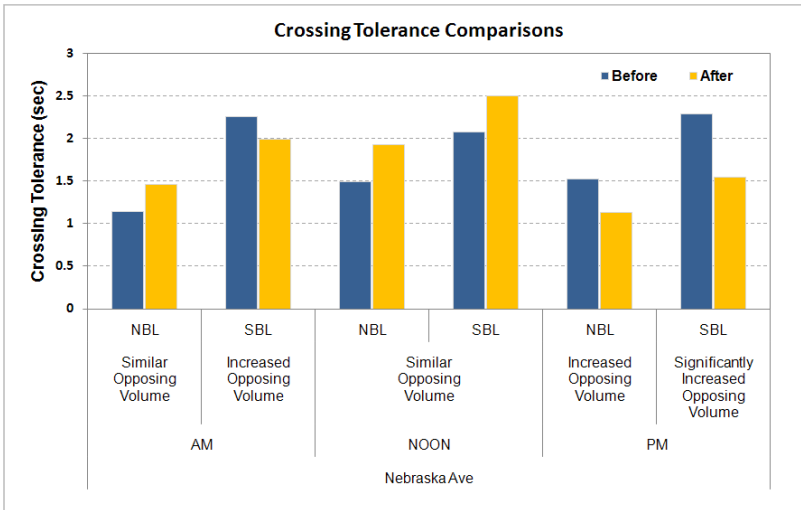


Figure 6 Crossing tolerance for the intersection of Belcher Rd & Nebraska Ave

The cases in which no improvement in the crossing tolerance was observed had significantly increased opposing volumes for the after conditions. These cases include southbound left turns during AM peak (SBL-AM), northbound left turns during PM peak (NBL-PM), and southbound left turns during PM peak (SBL-PM). When opposing through and right turns increase, the number of available gaps and the lengths of available gaps will be likely to decrease. The crossing tolerance will also be likely to decrease.

CONCLUSIONS

In this study, a before and after evaluation of potential safety and operational impacts of the implementation of the FYA operation for PPLT was performed on an intersection in the Tampa Bay area. The evaluation of the FYA display was based on gap acceptance-related variables as an indication of short-term behavioral changes of drivers making permissive left turns.

The implementation of FYA has the potential to increase the capacity of the left turn movement during the permissive phase. This was determined by calculating the critical gap for before and after the implementation of the FYA operation. Capacity is

increased by allowing more vehicles to turn during the permissive phase. In this case study, potential improvements in capacity for up to 10 percent can be achieved under moderate opposing traffic volumes. For high opposing traffic volumes the FYA did not show a capacity improvement due to shorter gaps in the traffic stream.

For this short-term evaluation, the implementation of FYA at the test site shows a potential to consistently, and slightly, reduce the risk of permissive left turns if traffic conditions remain similar after the implementation of FYA. Under the same traffic conditions, the FYA display seemed to help warn drivers to be more cautious when making permissive left turns. The study shows that the opposing through volume has a strong impact on permissive left turn operation. Opposing right turns also have the potential impact. When the opposing traffic increases, the left turn vehicles are generally forced to accept shorter gaps. In the situations of heavy opposing traffic, the potential risk reduction induced by a signal display of FYA may not be noticeable.

REFERENCES

- Noyce, D. A., Bregh, C. R., & Chapman, J. R. (2007). *NCHRP web-only document 123: Evaluation of the Flashing Yellow Arrow Permissive-Only Left-Turn Indication Field Implementation*. Washington, D.C., TRB, National Research Council.
- Brehmer, C. L., Kacir, K. C., Noyce, D. A., & Manser, M. P. (2003). *NCRP report 493: Evaluation of Traffic Signal Displays for Protected/Permissive Left-Turn Control*. Washington, D.C.: TRB, National Research Council.
- Highway Capacity Manual (2000). Washington, D.C., TRB, National Research Council.
- Parker, M. R., & Zegeer, C. V. (1989). *Traffic Conflict Techniques for Safety and Operations Observer's Manual*. Publication FHWA-RD-01-113. FHWA, U.S. Department of Transportation.

Traffic Signal Control of Fuzzy Neural Network Based on Line Length of Cars in Waiting

Xue LI, Bai-chuan LU, and Yi LI

School of Traffic and Transportation, Chongqing Jiaotong University, Chongqing, 400074, China. PH: 13708342676; E-mail: pengyouxinqing@163.com

ABSTRACT

With the advances and development in technology, transportation becomes one of the centers of life, and urban area control is one of its important parts. However, the increase of vehicles inevitable creates the phenomenon of road congestion, especially at the intersection. Intersection signal time optimization can effectively reduce traffic delays, improve the intersection's traffic capacity and is an important measure to improve the traffic condition. This paper proposes a fuzzy neural network traffic signal control method based on line length of cars in waiting. First, the method initial coordinates the intersection signal time according to the traffic status information. Then, with fuzzy control and artificial neural network, the traffic signal is adjusted to achieve the optimization of the whole system. Simulation results show that, compared with the general time-set control, this method can get superior results.

INTRODUCTION

Traffic is very important to city life. However, with the increasing of cars, it inevitably causes congestion. The effective of ordinary method about road and bridge construction decreases. So how to develop the road capacity and play the validity of traffic control plenary under the existent road situation is the focal point of solving the road congestion. In recent years, more and more people focus their attention on intelligent traffic system (ITS), which combined electronic information, auto-control and some other advanced technology. ITS is the effective method to solve road congestion.

Intersection is the key to determine the capacity of road network. Optimization the traffic signal timing in intersection can effectively reduce cars' parking delays and the number of cars' stops, and it can also develop road capacity and so on. The traditional signal control adopts time-set control. This control method is prone to fewer vehicles on the green light phase, while much more waiting vehicles on red light phase, causing road congestion easily. Therefore, it is an effective way to solve this problem in accordance with the number of cars to determine the extent of the green signal ratio to adjust the signal cycle. In view of this situation, author proposes a traffic signal control method about fuzzy neural network based on line length of cars in waiting.

First, this method initially set the traffic signal of the intersection under real-time traffic status information about the intersection, setting the green signal ratio. Then regarding the vehicle queue length of the intersection and the next intersection as a parameter, adjust the length of green light for traffic signal combined the fuzzy

control and artificial neural networks together, to alleviate intersection congestion and achieve the overall best.

SET SIGNAL CYCLE

Intersection Phase Model

As vehicles on the right direction will not conflict with cars on the other phases, this article don't consider these cars separately. These vehicles can directly access the intersection. Set a four-phase intersection, shown in Figure 1.

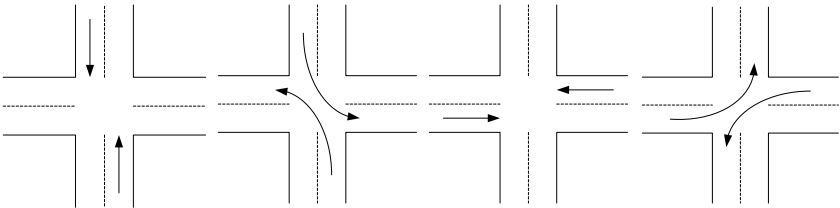


Figure 1. Intersection model

Determine the Cycle Length

Congestion is vehicles averagely stop two times or more in a intersection. Set the signal cycle reasonably can slow down the congestion in the intersection. Thus, according to the actual situation, determine traffic signal cycle length by the size of traffic flow. Generally speaking, when the traffic flow is small, the signal cycle can be set shorter, but it should be noted that the signal period should be set not less than the minimum cycle time, to avoid the vehicles in waiting can't cross through the intersection; when traffic flow is large, periodic time should be made larger, but it must take into account the traffic on other phases and the drivers' feeling[3]. Therefore, it must set a maximum cycle and all the cycle should be less than it.

Cycle Losing Time

Cycle losing time is general consisted of two parts: First, when the green light brights, time loses because of pedestrian crossing interference, the drivers reflects delay and so on; second part is the second half of yellow time .It shows in Figure 2.

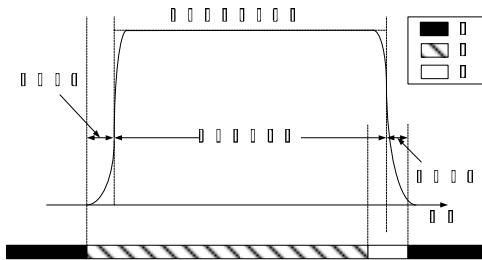


Figure 2. Cycle losing time

In reality, there is losing time in every cycle time, and regardless of the length of cycle time, the losing time is basically the same. So the shorter cycle time will lead more losing time as a whole and the lower utilization of the intersection. Therefore, the cycle length can not be set too

short, so as not to reduce the utilization of the intersection.

Vehicles Waiting Time

Vehicles' total waiting time is the sum of the time after each vehicle's reached the intersection. Suppose if vehicles continuously reach the intersection as the reach ratio is f , when the red light bright, the cars began to wait after stop line. After the green light bright, cars leave the intersection in maximum traffic capacity M of the intersection. After t_p seconds all the waiting cars aggregated in red light evacuate completely. the evacuation time t_p [4] as follows:

$$t_p = \frac{f(1-g)T}{M-f}$$

In the formula, g is the green signal ratio, then the red light time is $R = (1-g) T$.

The total vehicles' waiting time includes two parts:

(1)The waiting time that vehicles prohibit to cross the intersection during red light.

Vehicle's arrival rate is f , so the number of vehicles reaching the intersection is $f * dt$ during dt seconds. If this part of vehicles arrive the cross after red light has brighten for t seconds, the vehicles' waiting time in red light is $(R-t) * f * dt$, so during red light the reaching vehicles' total waiting time t_{w1} is:

$$t_{w1} = \int_0^R f * (R-t) * dt = \frac{1}{2} fR^2 = \frac{1}{2} f(1-g)^2 T^2$$

(2)After green light bright, the behind vehicles required to wait until the vehicles in front it leaving the intersection.

After green light bright, waiting vehicles leave the intersection as the largest traffic capacity M . The number of vehicles is $M * dt$ during dt seconds after green light brighten for t seconds. So after green light bright, the total number of this part of vehicles is $M * dt * t$. During the time that green light brighten to all the waiting vehicles left the intersection, the total waiting time t_{w2} of all vehicles is:

$$t_{w2} = \int_0^{t_p} M * t dt = \frac{1}{2} M t_p^2 = \frac{1}{2} M * \frac{f^2(1-g)^2 T^2}{(M-f)^2}$$

Then during a week the total waiting time t_w is:

$$t_w = t_{w1} + t_{w2} = \frac{1}{2} \left[f + \frac{Mf^2}{(M-f)^2} \right] (1-g)^2 T^2$$

In the formula above, if the traffic arrival rate and maximum traffic capacity of intersections are certain, f , M is a constant. It can be concluded that the total waiting time is inversely proportional with the green light ratio g , and the cycle length T is proportional with it. In reality, the total waiting time must as small as possible. Therefore, in the premise of good traffic situation, minimize the cycle length and maximize the green light rate. From the above analysis about cycle losing time, the minimum cycle length should be greater than the cycle losing time.

FUZZY NEURAL NETWORK

Fuzzy Control

Blur the detected vehicles' queue length as queue length is a parameter. On the current driveway the line length of vehicles in waiting is L_1 . The values are S_s (short), M_s (middle) and L_s (long). The queue length of vehicles between current intersection and downstream intersection is L_2 , and values are S_n (short), M_n (middle), L_n (long). On the other driveway that vehicles wait to turn direction the vehicles' queue length is L_3 . The values are S_l (short), M_l (middle), L_l (long). The fuzzy partition shows in Figure 3. The fuzzy control rules have been shown in Table 1 below.

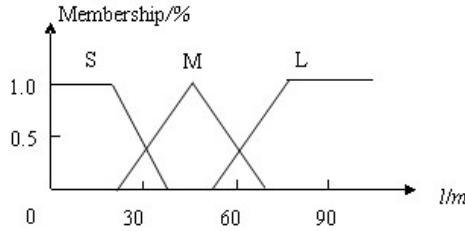


Figure 3. Fuzzy Partition Model

Table 1. Fuzzy Control Rules

L_n		S_n	M_n	L_n
L_s	L_t			
S_s	S_t	*	**	***
	M_t	&	*	**
	L_t	#	&	*
M_s	S_t	**	*	&
	M_t	*	&	#
	L_t	&	#	##
L_s	S_t	#	&	*
	M_t	##	#	&
	L_t	###	##	#

In the table above, "#" represents the extension of green time, "*" means to reducing the green time and "&" prefer to not change the green time. The number of "#,*" stands for the length of green time and each of it is on behalf of 5 seconds. Meanwhile, set maximum green time T_{max} in order to avoid one phase taking too long. Set minimum green time T_{min} to prevent that cars can't pass the intersection. In the whole control process the green time T_s should satisfies the condition: $T_s \geq T_{min}$, $T_s + \Delta T \leq T_{max}$.

Fuzzy Neural Network Control

Neural network has learning capabilities. Introduced fuzzy algorithm or fuzzy weights in neural network, it constitutes a new type of neural network. Fuzzy control adapts to nonlinear, time-varying and hysteresis control system. This fuzzy neural network can take advantages of fuzzy control about its robustness and advantages of neural network about its self-learning. The fuzzy neural network control model has shown in Figure 4.

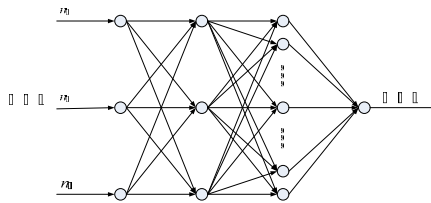


Figure 4. Fuzzy neural network control model

In this model, layer (1) is input layer, to receive traffic state information of both this junction and the downstream junction. Layer (2) and (3) mainly correspond to fuzzy control. Among it, layer (2) is fuzzy layer, to blur the input data. While layer (3) is a fuzzy rule layer, each neuron

corresponds to a fuzzy rule. Layer (4) is output layer.

FUZZY NEURAL NETWORK CONTROL ALGORITHM BASED ON LINE LENGTH OF CARS IN WAITING

As the traffic conditions of adjacent cycle are similar, set the detectors in front of the stop line at the intersection, using the detected traffic situation for the next cycle's signal timing. This paper controls the traffic lights according to the relevant information of this junction and the downstream junction. Then deliver the information of this intersection to the upstream intersection, in order to achieve the coordination of the entire road. Thus the vehicle in the intersection can get the shortest total waiting time.

Algorithm steps are:

Step1: Set initial values. Set the initial green light rate is g_0 and initial cycle time T_0 .

Step2: When $t = 0$, the cycle starts. The vehicle counter is initialized to $n = 0$.

Step3: Detectors detect the number of vehicles. Each vehicle is assumed to be detected only once, and the detection frequency of the detector is Δt . When $t = t + \Delta t$, the number of vehicles corresponding to the detected frequency is:

$$\Delta n = \begin{cases} 0, & \text{There is no cars druing } \Delta t \text{ seconds.} \\ 1, & \text{There is one car during } \Delta t \text{ seconds.} \end{cases}$$

Step4: If $t < T$, repeat step3; if $t \geq T$, turn to step5.

Step5: Determine the signal cycle length.

From the reference [4], the first car needs 2.5s to leave the stop line, while the second car to the fifth one through the stop line requires 3.1s, 2.8s, 2.4s and 2.2s. Then the average time other vehicle required is 2.1s. If assumed that ignore the different required time of the vehicles through the stop line, each vehicle through the stop line needs 2.1s. Make judgement on the number of detected vehicle n , setting minimum number of vehicles n_{min} and maximum number of vehicles n_{max} . If $n < n_{min}$, cycle length is $T^* = T_0 - (n_{min} - n) * 1.9$. If $n \geq n_{max}$, the cycle length is $T^* = T_0 + (n - n_{max}) * 1.9$. Otherwise, the cycle length is $T^* = T_0$. But it must be noted that T^* meets the above analysis about cycle losing time and waiting time. Meanwhile, if T^* is less than the minimum period, the signal period is set to the minimum period; if T^* is greater than the maximum period, signal period should be set to maximum cycle.

Step6: Fuzzy process the number of detected vehicles. The number of vehicles on current lane is n_s ; the number of waiting vehicles between this junction and downstream junction is n_n ; the number of vehicles on the other driveway that wait to turn direction is n_r . The corresponding datas of vehicles' queue length after fuzzy processing are l_s , l_n and l_r . Then determine that whether to change the green time according to the line length of cars in waiting.

Step7: Calculate the best green signal ratio. Step5 has determined the cycle length, then based on equation (4) and the green time determined by step6, calculate the best green signal ratio.

Step8: Set signal time with the new cycle length and green signal time. Start a new cycle. Repeat step2 - step7, can optimize signal time.

Algorithm flow chart shows in Figure 5.

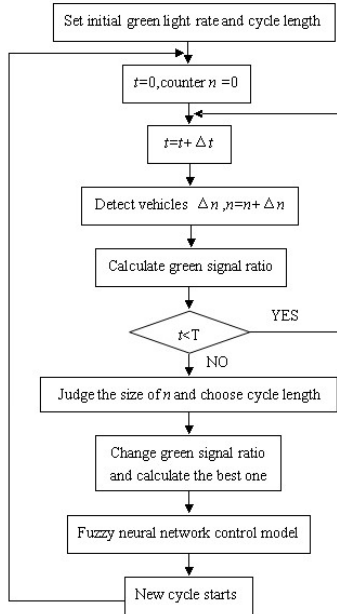


Figure 5. Algorithm flow chart

SIMULATION EXPERIMENT

Intersection signal control is a complex system. In order to save time and experimentation expenses, simulate this program in simulation software and compare with other programs.

Make the four-phase model in figure 1 as example, to simulate the traffic flow, and compared the control method with the traditional time-set control. The phase of two methods is the same settings. Road length is set to 300m, and vehicle speed is 40m / s. Cycle length of time-set control method is set to 60s, 80s, 100s, 120s, vehicles' arrival rate in all directions is $f = 0.35$ units / s, the maximum traffic capacity of intersections is $M = 0.6$ units / s, the green signal ratio is 0.5. The initial cycle length of fuzzy neural network traffic signal control based on queue length is set $T_0 = 60s$; to determine the signal cycle, set the minimum number of vehicles $n_{min} = 10$ units, the maximum number of vehicles $n_{max} = 30$ units, and the average car length is 5m; set a minimum cycle time $T_{min} = 30s$, the maximum cycle time $T_{max} = 120s$. The simulation results of vehicles' queue length control method shows in Figure 6.

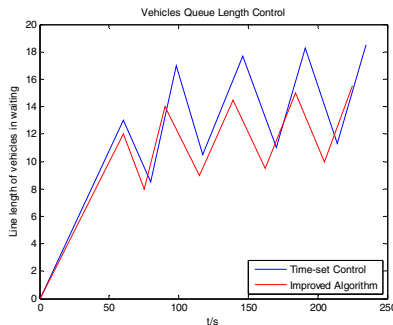


Figure 6. Vehicles' queue length control method simulation
Comparison the waiting time of two control strategies shows in Table 2 below.

Table 2. Waiting Time of Two Control Strategies

	Time-set control cycle length/s	60	80	100	120
Waiting time /s	Time-set control method	33	28	39	43
	New control method	29	24	33	38
Proportion of reducing waiting time/%		12%	14%	15%	12%

CONCLUSION

This paper analyzed the intersection signal control. Intersection signal cycle length should consider cycle losing time and total waiting time of vehicles. Taking into account of the sparse traffic level, this paper has set different cycle length. After determining the cycle length, optimize green time settings based on fuzzy neural network control. Then calculate the best green signal ratio of the intersection for signal timing. Simulation results show that the control program can effectively reduce vehicles' waiting time and improve road access rate, improving overall traffic conditions.

REFERENCES

- Ren Hui, Wang Weizhi, *Multi-Path Cross Traffic Signal Control Method Based on Line Length of Cars in Waiting* [J], Electrical & Electronics, 2010 (1) :29-31
- Yu Wanxia, Du Taihang, *Fuzzy Neural Network Model for Controlling Traffic Based on Particle Swarm Optimization* [J], Computer Information, 2008 (24) :18-19, 179
- Zheng Jin. *Smart city optimized traffic signal simulation system* [J]. Fujian Computer, 2010 (5) 139,151
- Xu Ji Wan, *Xudong Ling, etc. Computer urban traffic control and management* [M], Beijing: Surveying and Mapping Press, 1988.
- Qiu Weikang, Wang Weizhi, etc. *Traffic Signal Control Based on Fuzzy Neural Networks*[J], Jiangsu Electric, 2008 (4) :22-26, 53
- He Zhaocheng, Yang Wenchen, etc, *Intelligent Transport System Research Center*[J], *Computer Engineering and Applications*, 2010, 46(33):239-243
- Huang Meiling, Lu Baichuan, *Optimization of Multiphase Traffic Signal Timing at Intersection Based on Species Niching Particle Swarm Optimization Algorithm*[J], Information and Control, 2011, 40(1):115-118, 123
- Tian Feng, Bian Tingting, *Traffic Signal Timing Optimization Based on Adaptive Genetic Algorithm*[J], Computer Simulation, 2010, 27(6):305-308.

Study of Carpool User Behaviors and Route Characteristics in Taiwan

C. L. Chung¹, J. Y. Jeng², Z. Y. Lee², and June-Shian Lee²

¹ Chih-Lin Chung, corresponding author, Ph.D., 3904 University Ave. #101, Grand Forks, ND, 58203, USA; PH: 1-701-777-9400; email: cchung@uci.edu

² Jeng-Yuan Jeng, Zong-Yi Lee, THI Consultants Inc., 5F 130 Sung-Shan Road, Taipei, 110, Taiwan; PH: 886-2-2748-8822; email: niw921@thi.com.tw, ian_lee@thi.com.tw

ABSTRACT

This paper conducts a thorough study on the carpool characteristics in Taiwan. The subjects were 9,924 registered members and 4,176 posted routes retrieved from the nation's largest carpool website. A majority of the members were 25- to 45 year-old males in northern Taiwan. The regular routes were primarily short working trips within 60 minutes and 30 kilometers. The one-time routes presented dual characteristics of short business trips on weekdays and long homecoming trips on Friday and Saturday. Nearly three quarters of the members were not route posters but searchers. Over 73% of the carpool members and route posters were private mode users, indicating that one carpool match would most likely combine two car/motorcycle trips instead of reducing transit rides. Carpool can effectively lessen on-road traffic and is concluded not to compete with but complement public transit. The carpool movement requires sustainable momentum and an integrated program with full policy support.

INTRODUCTION

Carpool or ridesharing by car is known as a transportation demand management (TDM) strategy commonly seen in the urban areas. Carpool was initiated in Taiwan during early 1990s, but not until mid 2000s did carpool receive public awareness. The largest carpool platform in existence is a government-administered website launched in August 2008. It was the moment when the international crude oil reached a record high at \$145 per barrel, and the Internet had become a daily necessity. Founded by the Environmental Protection Department of New Taipei City (formerly Taipei County) Government, the carpool website was named "GREEN carpool" that not only literally responded to its eco-friendliness but recognized the five keys to promoting carpool, i.e., Guaranteed ride home programs, Rapid high-occupancy vehicle (HOV) lanes, Easy online matching, Economical commute, and Nearby park-and-ride lots (Chung 2007). As of December 2011, the website had over 12,000 registered members and 4,200 posted routes.

The research objective is to verify the carpool user and route characteristics for policy making. Especially, there has been an argument whether the carpoolers primarily consist of transit riders or car users. Such an argument is one of the reasons why the transportation authorities in Taiwan hesitate to support carpool (Chung 2008; Chung and Yeh 2011a). Unlike typical carpool investigations that rely on various (phone/questionnaire/interview) survey techniques to collect data, the website offers first-hand information about the registered members and posted routes. Those with noticeably missing data were filtered out, resulting in the valid subjects of 9,924 members and 4,176 routes.

CARPOOL CHARACTERISTICS

As an emerging mode in the local transportation environment, security is a major concern for the potential carpoolers who are probably strangers to one another. In response to the concern, the GREEN carpool took an innovative action (along with the online security handbook and FAQ) that the carpool membership is granted under a thorough check via the national household registration system and police criminal database, a cooperative mechanism among the government departments. Applications will be denied should the applicants provide incorrect data or with a security issue; although they are still able to browse the carpool routes, they cannot access the contact information to make the trip.

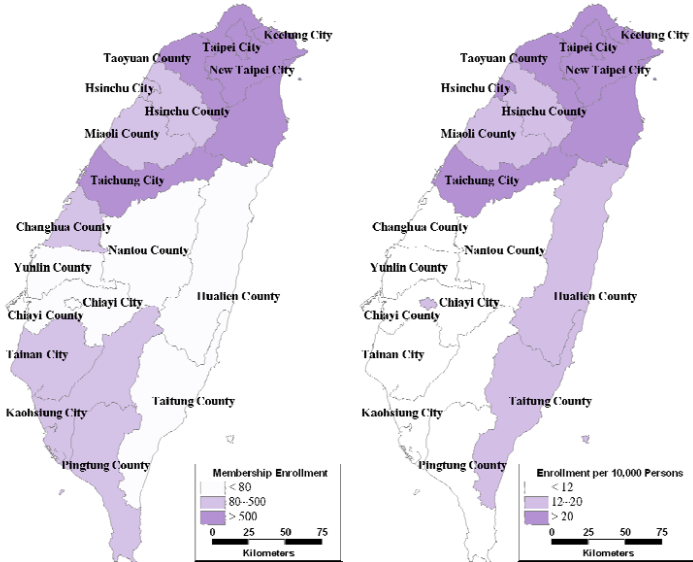
Growth Trend

The GREEN carpool originally targeted five city/county jurisdictions in northern Taiwan. Owing to the intensive advertisement, high gas price, and government-based carpool, the website made a remarkable record that there were 4,980 members and 1,340 routes in the first three months of operations. Such success soon encouraged the participation of another six jurisdictions, expanding the coverage officially to central Taiwan and substantially the whole country. Like a commercial product, the website has experienced the introduction stage in 2008, the growth stage from 2009 through mid 2010, and afterward the mature stage till now. The current (2011) monthly enrollment is 98 members on average. A significant drop of the monthly posts from 89 routes in 2010 to 59 in 2011 may be a warning of the website toward a decline stage.

Carpooler Characteristics

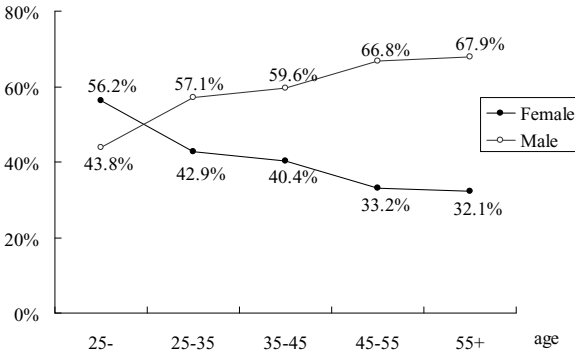
The five northern jurisdictions - New Taipei City, Taipei City, Keelung City, Yilan County, and Taoyuan County - had larger numbers of enrollment than others, as shown in Figure 1(a) and 1(b). Males were more than females (59.3% vs. 40.7%). A majority (80.3%) of the carpoolers were from 25 to 45 years old. Those under 25 were the only age level with more females than males. Male participation appeared to increase with age, as shown in Figure 1(c). The main transport modes were cars and

motorcycles (73.6%) while public transit accounted for 26.4%. The 26.4% is greater than the national public transit ridership (about 17%) because the members were mostly populated in the region with better transit service. The weight of the private modes was 86.8% for males and 52.1% for females. Service, technology, and manufacturing industries were the top three vocations; it is consistent with the facts that 1) the northern region is highly commercialized and 2) the website specified major technology/industrial parks as the carpool hotspots. Most enrollment occurred on Thursday (30.2%), followed by other weekdays (12.7%~16.1%) and weekend (5.7%~6.3%). These characteristics are summarized in Table 1.



(a) Membership Enrollment

(b) Enrollment per 10,000 Persons



(c) Age Distribution by Gender

Figure 1. Carpooler Demographics

Table 1. Carpooler Characteristics

Item	Category	Weight	Item	Category	Weight
Enrollment day	Monday	14.0%	Transport mode	Car	62.6%
	Tuesday	16.1%		Motorcycle	11.0%
	Wednesday	15.1%		City bus	8.0%
	Thursday	30.2%		Highway bus	7.6%
	Friday	12.7%		Urban rail	7.3%
	Saturday	5.7%		Regional rail	3.3%
	Sunday	6.3%		High speed rail	0.3%
Gender	Female	40.7%	Vocation	Service	18.7%
	Male	59.3%		Technology	18.1%
Age	25-	7.5%		Manufacturing	14.5%
	25~35	50.3%		Gov't employee	8.2%
	35~45	30.0%		Student	8.1%
	45~55	9.6%		Unemployed	2.8%
	55+	2.7%		Other 9 vocations	29.6%

Route Characteristics

Carpool consisted of regular routes (73.9%) and one-time routes (26.1%) with distinct characteristics. Trip purposes were not inquired but assessable through the attributes of the routes and posters. The regular routes were overall work trips as the students and unemployed accounted for only 4.6% of the posters, and the route demand was nearly uniform during weekdays (87.1%~89.1%). By relating the route data to the travel time and distance from the demand model (IOT, 2008), it was found that the regular routes were primarily short trips within 60 minutes and 30 kilometers (about 18.75 miles). The one-time routes occurred on each day of the week but with higher percentage on Wednesday through Saturday, especially Friday. Travel time was primarily less than one hour or greater than three hours, indicating the dual characteristics of short (business) trips on weekdays and long (homecoming) trips on Friday and Saturday, a local tradition that young people work/school in the urban area and visit their parents on weekend.

Compared to the one-time routes, the regular routes had less drivers looking for riders (64.6% vs. 77.9%), less male carpoolers (62.5% vs. 72.8%), less private mode users (81.0% vs. 93.1%), and major distinctions in certain vocations (like technology, government employees, etc.) and age levels (over 35). People over 55 years old in general showed little carpool potential except for the one-time routes. Given the above differences, the two route types also share some things in common: more drivers looked for riders to utilize the car capacity, males posted more routes than females, and more posters were private mode users instead of public transit riders. These characteristics are summarized in Table 2.

The top 20 routes are depicted by city/county and by town/district. Figure 2(a) shows strong demand among the northern jurisdictions and from Taipei to Taichung and Kaohsiung. When the 4,176 routes were split to the town/district level, only the top two routes had over 55 posts while others were fewer than 40. It reveals the difficulty of carpool match under the seemingly large but actually limited amount, needless to say if the time window is accounted. All routes were in the northern region except the two in Taichung, as shown in Figure 2(b).

Table 2. Carpool Route-based Characteristics

Item	Category	Regular route	One-time route	Item	Category	Regular route	One-time route
Day-of-week demand	Monday	88.7%	10.9%	Gender	Female	37.5%	27.2%
	Tuesday	87.3%	10.8%		Male	62.5%	72.8%
	Wednesday	88.0%	15.7%	Age	<25	3.3%	4.3%
	Thursday	87.1%	15.2%		25-35	46.2%	44.5%
	Friday	89.1%	20.1%		35-45	36.8%	23.7%
	Saturday	6.7%	14.6%		45-55	12.6%	17.2%
	Sunday	5.2%	10.2%		>=55	1.1%	10.3%
Travel time (minute)	<30	16.2%	19.3%	Transport mode	Car	76.4%	84.7%
	30-60	58.4%	19.6%		Motorcycle	4.6%	8.4%
	60-90	13.2%	11.8%		City bus	4.8%	1.6%
	90-120	2.0%	6.9%		Highway bus	7.7%	2.3%
	120-150	3.3%	7.8%		Urban rail	3.9%	2.3%
	150-180	5.0%	9.7%		Regional rail	2.4%	0.6%
	>= 180	1.9%	25.0%		High speed rail	0.2%	0.1%
Travel distance (kilometer)	<10	7.1%	14.8%	Vocation	Technology	21.1%	8.3%
	10-20	26.8%	9.6%		Service	19.4%	16.2%
	20-30	24.9%	9.9%		Manufacturing	16.7%	10.7%
	30-40	18.3%	7.4%		Gov't employee	8.0%	28.2%
	40-70	11.4%	7.3%		Business	6.5%	4.3%
	70-100	7.9%	13.2%		Construction	3.7%	2.4%
	100+	3.6%	37.7%		Student	3.2%	5.5%
Carpooler	Driver	64.6%	77.9%	Unemployed	1.4%	3.2%	
	Rider	35.4%	22.1%	Other 7 vacations	30.1%	27.8%	

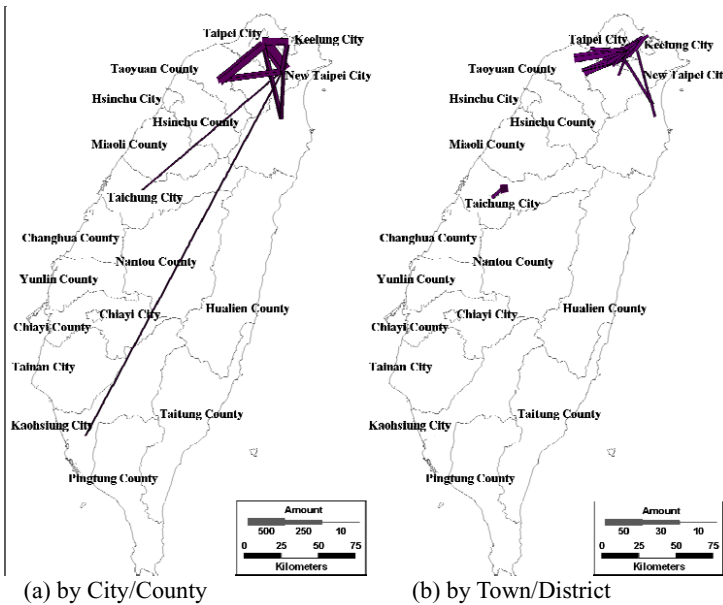


Figure 2. Top 20 Routes

DISCUSSION

The GREEN carpool has adopted two successful strategies. First, the security protection offered by the government was the first of its kind. It relies on a strong household registration system as well as inter-departmental cooperation. Second, the website targeted four types of hotspots: 1) working-oriented industrial parks and government buildings, 2) housing-oriented large communities, 3) education-oriented schools, and 4) traffic-oriented terminals and interchanges. These four types cover major trip generation ends and the carpoolers can quickly browse the posted routes related to the hotspots. None of the hotspots are related to a shopping destination; it supports the above inference that most routes were home-work-based trips. 47 out of the total 77 hotspots are in Taichung City with a majority related to government buildings and schools. The number is greater than the sum of all other jurisdictions, making the carpool demand within Fengyuan - the fifth largest district in Taichung and one of the City's administration centers - the top one route. Clearly, support from the local government would boost carpool demand.

The central and southern regions overall had less participation. Further efforts should be made to realize carpool. Although there are mechanisms among certain local jurisdictions to jointly address cross-city/county issues, the frameworks are informal and less effective in comparison with the official metropolitan planning organizations (MPOs) or regional governments in the U.S. In fact, carpool demand could be in a much larger scope beyond the existing cross-city/county mechanisms, and carpool matching depends deeply on the "economies of scale." Meanwhile, carpool will not be possible without firm support from the individual cities/counties. Given the two-sided conditions, it is suggested that each local jurisdiction may have a separate or joint carpool portal website to cope with area disparity, e.g. political considerations, financial constraints, social-economic and/or geographical differences, etc. However, the carpool demand should be integrated into one database that shares all the city/county-, region-, and nation-wide carpool information. This is similar to the operation of search engines like Google and Yahoo with area-specific portal websites but an integrated database.

It appears that the 25- to 45-year-old were most interested in carpool. Typically, people in these ages can afford driving to work, and embrace the Internet that offers an alternative of green and economical transport. While enforcing the participation from this age range, it is worth expanding carpool to those under 25 who had the highest percentage (25.8% vs. 11.0% on average) of using motorcycle, and to those of 45- to 55-year-old who may have similar status as the 35- to 45-year-old. The number of the female carpoolers decreased with age. It is probably because their self-defense senses (against carpool) and transport independency increase with age. In such a case, company/organization/agency-based carpool with colleagues, friends, or female partners could provide additional security. In prompt of the U.S. ridesharing program, the companies may assign a coordinator for carpooling their employees; however, legal requirements and incentives are essential to make such arrangement possible (Chung 2007; Chung and Yeh 2011a).

The 4,176 routes were posted by 2,667 "active" members, just about a quarter of

the 9,924 members analyzed. Most members chose to search the routes instead of posting their needs. Triggering willingness-to-post will be the key to enlarging the route database since one active member on average contributed 1.6 routes. Contrasting Table 1 with Table 2 shows that the active members had even higher percentage of using private mode (81.0%~93.1%) than the registered members on average (73.6%). Compared to females, males were more willing to post routes. Were those without posting routes primarily transit riders who tried to become carpoolers? The answer is "NO". 70.6% used private modes, and quite a few were motorcyclists. The huge amount of motorcycle has been a big headache for major cities in Taiwan, and it is infeasible to prohibit the use of motorcycle. Encouraging the motorcyclists to post their needs will most likely reduce motorcycle usage, providing a solution to the dilemma.

One of the reasons why the carpool plan in early 1990s was called off is that most participants did not own a car but relied on public transit; it potentially shifted public transit riders to cars. But the current situation has substantially changed. For both genders, the carpool majorities were private mode users (86.8% for males and 52.1% for females), and males accounted for 59.3% of the members. A successful carpool match most likely combines two car/motorcycle trips instead of reducing one transit rider. While the departments of transportation (DOTs) in Taiwan are devoted to build a better public transit environment, such efforts could reinforce the existing ridership, and possibly turn those open to both public and private modes into transit. For those rigid private mode users, carpool provides an alternative to reduce on-road cars/motorcycles. The central DOT of Taiwan just disclosed a national market share of 30% as the long term vision for public transit. A complementary and missing part of the vision is: the vehicle occupancy should be doubled through carpool, making on-road private traffic half the number. It will effectively mitigate vehicle-related issues, such as parking, energy/gas consumption, air emissions, noise, infrastructure renovation, and so on.

The carpool movement requires continuous attention. Being away from the news spotlight and the extraordinarily high gas price, carpool is losing its momentum to sustain steady growth on the membership enrollment and route posts. The opening of Taiwan's first HOV lane in late 2012 is expected to be a carpool stimulus. The HOV lane will be configured in the northern section of the National No. 1 Highway to serve the high carpool demand passing or ending in New Taipei City and Taoyuan County. Meanwhile, it is essential to initiate a comprehensive carpool plan that integrates the individual programs (Chung and Yeh 2011b, Chung 2007; TTI 1994). Obviously, the carpool movement will not be possible without strong policy support from the central and local DOTs under joint cooperation with the environmental production and energy departments. (Chung and Yeh 2011a)

CONCLUSIONS

The carpool movement launched by New Taipei City Government has received extensive public awareness. More than 12,000 members and 4,200 routes make the GREEN carpool website the largest ridesharing information platform in Taiwan. Two

highlights of the website are the enhanced carpool security and major trip-generation hotspots. A majority of the members were 25- to 45 year-old males in northern Taiwan with a preference for private modes. The regular routes were primarily short urban working trips within 60 minutes and 30 kilometers; on the other hand, the one-time routes presented possible dual characteristics of short business trips on weekdays and long homecoming trips on Friday and Saturday. It is suggested that each local jurisdiction may have a separate or joint carpool portal website to cope with area disparity, but the carpool information should be integrated. Triggering willingness-to-post is the key to enlarging the route database as nearly three quarters of the members were not route posters but simply searchers. A successful carpool match will most likely combine two car/motorcycle trips, and thus reduce on-road traffic. Most importantly, the carpool movement, not a competitor but a complement to public transit, requires continuous attention and an integrated carpool program with full support from the DOTs.

ACKNOWLEDGEMENT

The authors greatly appreciate the Environmental Protection Department of New Taipei City Government, which provided the raw carpool data. The contents of this paper reflect the views of the authors, who are solely responsible for the opinions, findings, and conclusions presented herein. These views do not represent any policies of New Taipei City Government.

REFERENCES

- Chung, C.L. (2007). "Perspectives of Rideshare in Taiwan via California's Experiences." *Urban Traffic*, Taipei Society for Traffic Safety, 22(1), 50-63. (in Chinese)
- Chung, C.L. (2008). "Key Topics of High-occupancy-vehicle Lane Implementation in Taiwan." *Urban Traffic*, Taipei Society for Traffic Safety, 23(1), 15-33. (in Chinese)
- Chung, C.L., Yeh, C.C. (2011a). "Cooperative Relationships between Environmental, Energy, and Transportation Departments on Promoting Ridesharing in Taiwan." *International Chinese Transportation Professional Association 24th Annual Conference*, Los Angeles, California.
- Chung, C.L., Yeh, C.C. (2011b). "What Can Taiwan's Carpool Moment Learn from U.S. Ridesharing Programs?" *International Chinese Transportation Professional Association 24th Annual Conference*, Los Angeles, California.
- Institute of Transportation (IOT). (2008). *Taiwan Intercity Transportation Demand Model V.2008*, Taipei, Taiwan.
- Texas Transportation Institute (TTI). (1993). *National Review of Statewide Rideshare Programs and Survey of Texas Rideshare Programs*, Texas.

Characteristics of Truck-Related Crashes in Highway Work Zones

Yue Li¹, Feifei Cheng², and Yong Bai³

¹Graduate Research Assistant, Department of Civil, Environmental and Architectural Engineering, The University of Kansas, 1530 W. 15th Street, 2160 Learned Hall, Lawrence, KS 66045, U.S.A. E-mail: ylkx7@ku.edu

²Lecturer, Department of Construction and Real Estate, School of Management, Harbin Institute of Technology, Harbin, China. E-mail: chengfeifei@hit.edu.cn

³Associate Professor, Department of Civil, Environmental and Architectural Engineering, The University of Kansas, 1530 W. 15th Street, 2150 Learned Hall Lawrence, KS 66045, U.S.A. Phone: (785) 864-2991; E-mail: ybai@ku.edu

ABSTRACT

Truck-related crashes contribute to a significant percentage of vehicle crashes in the work zones, which often result in injuries and fatalities. To mitigate the risk of truck-related crashes and develop effective safety countermeasures, a study on truck-related crashes between 2000 and 2008 in Kansas highway work zones was conducted. Results of the study indicated that about half of truck drivers were at fault and were responsible for the fatal crashes in the work zones; straight following was the maneuver most truck drivers took before the crash happened; the rear-end crash was the dominant type for fatal, injury and property damage only crashes; and more than half of the fatal crashes occurred on straight and level highway work zones. Based on the study results, safety countermeasures that focus on mitigating the severity of truck-related crashes in the work zones were recommended in terms of work zone traffic control and public education.

INTRODUCTION

Work zone safety has become more challenging because of increasing travel demand and the aging highway system in the United States. Nationwide, there are more maintenance and rehabilitation projects on the highway system. At the same time, the system needs to be utilized to transport people and goods safely. Great efforts have been devoted to improve work zone traffic safety and mobility. The recent Safe, Accountable, Flexible, Efficient Transportation Equity Act: A Legacy for Users (SAFETEA-LU) included a number of provisions emphasizing highway work zone safety and other work zone-related issues. The Federal Highway Administration (FHWA) and the American Association of State Highway and Transportation Officials (AASHTO) have played leading roles on this issue and have developed practical highway work zone safety guides and programs. In addition to the legislative emphasis on work zone safety, a myriad of studies have been published to reveal the safety issues in the work zones and to propose safety countermeasures for mitigating the risks and reducing the numbers of crashes.

Truck-related crashes contribute to a significant percentage of motor vehicle crashes in work zones, which often result in injuries and fatalities. Several studies

have pointed out that truck-related crashes had a higher crash rate and were more severe than other crashes in work zones. Investigating the factors that influence the severity level of crashes will lead to the discovery of knowledge that could benefit the development of safety countermeasures that reduce the instances of high-severity crashes (Li and Bai, 2008a). This paper provides insights of truck-related work zone crashes that could be used to develop effective traffic control measurements with the purposes to reduce the number of truck-related crashes and mitigate the severity of crashes.

LITERATURE REVIEW

The information from the Fatality Analysis Reporting System shows that there were 50,430 fatal crashes in 2008, 8.1% (4,066) of them were large truck related, 37.8% (19,072) were light truck related. Here a light truck is referred to a truck of 10,000 pounds gross vehicle weight or less; a large truck is over 10,000 pounds gross vehicle weight (FARS, 2008). Some researchers had investigated and analyzed truck-related crashes in the work zones using various data sources and techniques.

Benekohal et al. conducted a statewide opinion survey of 930 semitrailer drivers in Illinois in 1993. They found that about 90 percent of truck drivers consider traveling through work zones to be more hazardous than non work zone areas (Benekohal et al., 1995). In another paper, Benekohal and Shim pointed out that, in terms of vehicle miles traveled (VMT), fatal crash rates for large trucks had been consistently higher than the rates for passenger cars; semitrailer trucks were underrepresented in the property damage only (PDO) and injury crashes but overrepresented in fatal crashes (Benekohal and Shim, 1999).

Meyers compared truck and passenger-car crash rates from 1976 to 1978 at 34 limited-access facilities (21 toll expressways and turnpikes, and 13 bridges and tunnels). He found that fatal, injury, and overall expressway crash rates for heavy trucks exceeded that of passenger cars (Meyers 1981). Garber and Joshua (1989) found 75% of all large-truck crashes and 91% of large-truck fatal crashes were attributed to driver-related errors. Hall and Lorenz (1989) found that in New Mexico the number and rate of truck-related crashes increased during the construction season. Richard and Faulkner (1981), Pigman and Agent (1990), Ha and Nemeth (1995), Daniel et al. (2000), Schrock et al. (2004), and Li and Bai (2008b) pointed out the disproportionate of large trucks involved in severe crashes (fatal and injury). Bezwada and Dissanayake (2009) pointed out that truck driver might face many challenges while traversing on Interstate or state highways at high speeds, at intersections, or while taking turns to have control over the vehicle because the physical dimension of a truck creates the blind spots.

In summary, since 1981, several research projects have been conducted to reveal the characteristics of truck-related crashes in highway work zones. Most studies conveyed that the crash rate and severity of truck-related crashes were higher than other types of crashes in work zones. However, some issues are still on debate such as which one is majority between "truck striking" and "truck struck;" what kind of factors have different impact on the crash severity level. Therefore, studying the characteristics of truck crashes becomes the crucial step towards the identification of work zone safety deficiencies.

OBJECTIVE AND SCOPE

The primary objectives of this research include: 1) to investigate the characteristics of fatal, injury, and PDO truck-related crashes in work zones, and 2) to determine if there are differences between fatal and injury crashes, fatal and PDO crashes, and injury and PDO crashes through characteristics comparison. The scope of this research is limited to the truck-related crashes between 2000 and 2008 in Kansas highway work zones. The crashes reports used in this study were provided by the Kansas Department of Transportation (KDOT) which documented descriptive data on date, drivers, vehicle, roadway, environmental conditions, and crash type. For this project, a truck means a vehicle whose gross weight is greater than 10,000 pounds. Kansas had 35 fatal, 374 injury, and 1,541 PDO truck-related crashes from 2000 to 2008 in highway work zones. It would be time-consuming yet not statistically meaningful to compile and analyze the entire PDO dataset. Therefore, a sample size of 380 was determined for the PDO crashes based on the method of Thompson (2006).

DATA ANALYSIS

The truck-related crashes in highway work zones were first analyzed separately based on severity level. Then, the authors compared the characteristics among fatal, injury, and PDO crashes. For three types of crashes, frequency analysis was utilized to discover the basic characteristics based on single-variable frequencies. Table 1 presents the most frequent observations for these three severity level crashes.

Drivers, Climatic and Environment Information

Male drivers are majority drivers of these three different crashes in highway work zones. As shown in Table 1, all truck drivers in fatal crashes were male, and there were 96% and 97% percents of male drivers in injury and PDO crashes, respectively. This does not mean that the male truck drivers are more susceptible to the crashes in work zones, the composition of truck drivers in U.S. maybe the reason for this phenomenon.

Drivers between 35-44 years old were in 43% of the fatal work zone crashes. The same age group involved 25% of PDO crashes. Drivers between 45-54 years old involved in 26% of injury crashes. 57% of truck drivers were at fault when the fatal crashes occurred in work zones, 63% of them were at fault when injury and PDO crashes happened. Figure 1 illustrates the three severity level crashes distribution over all driver age (at fault and not at fault) and Figure 2 presents the age distribution of truck drivers who were at fault.

Most of the truck-related crashes occurred when the weather and road surface conditions were actually favorable as indicated in Table 1. About 31% of fatal crashes occurred when there were poor light conditions such like dawn, dark with or without street lights. The poor light conditions affected the injury and PDO crashes less compared with fatal crashes, 23% of injury crashes occurred with poor light condition and 18% of PDO crashes happened under poor light condition. Dark without street lights is the most frequent factor among poor light conditions for fatal and injury crashes.

Table 1 Frequent Observation for Fatal, Injury and PDO Crash Variables

Variable	Most Frequent Observations		
	Fatal Crashes	Injury Crashes	PDO Crashes
Information of Truck Drivers			
Gender	Male (100%)	Male (96%)	Male (97%)
Age	35-44 (43%)	45-54 (26%)	35-44 (25%)
Driver Factor	No human error (43%)	No human error (37%)	No human error (37%)
Crash Time Information			
Time	10:00am-4:00pm (46%)	10:00am-4:00pm (46%)	10:00am-4:00pm (50%)
Day	Monday (26%)	Tuesday (20%)	Monday (22%)
Month	June (20%)	September (15%)	July (14%)
Climatic and Environment Information			
Light Condition	Daylight (69%)	Daylight (77%)	Daylight (82%)
Weather Condition	Good (94%)	Good (90%)	Good (91%)
Road Surface Condition	Dry (94%)	Dry (86%)	Dry (88%)
Crash Information			
Truck Maneuver	Straight/following road (74%)	Straight/following road (64%)	Straight/following road (54%)
Crash Type	Rear-end (31%)	Rear-end (37%)	Rear-end (22%)
Vehicle Type	Truck-vehicle (74)	Truck-vehicle (64%)	Truck-vehicle (63%)
No. of Vehicles	Two (60%)	Two (60%)	Two (68%)
Road Conditions			
Road Class	Other freeways & expressways (80%)	Interstate highway (43%)	Interstate highway (35%)
Road Character	Straight and level (54%)	Straight and level (58%)	Straight and level (66%)
Number of Lanes	Two-lane (63%)	Four-lane (51%)	Two-lane (46%)
Speed Limit (mph)	65 (57%)	65 (25%)	55 (20%)
Crash Location	Non-intersection (74%)	Non-intersection (63%)	Non-intersection (60%)
Surface Type	Blacktop (71%)	Blacktop (59%)	Blacktop (58%)
Road Special Feature	None (83%)	None (82%)	None (79%)
Area Information	Rural (86%)	Rural (52%)	Urban (59%)
Traffic Control	Center/edge lines (43%)	Center/edge lines (54%)	Center/edge lines (45%)
Contributing Factor			
Pedestrian Factor	No	Inattention (0.5%)	No
Environment Factor	No	Rain, mist, or drizzle (2.4%)	Animal (3.7%)
Vehicle Factor	No	Brakes (1.6%)	Cargo (2.9%)

Crash Information and Driver Fault

Crash information indicated that straight following was the maneuver most truck drivers took before the crash happened. Rear-end crash was the dominant type of fatal, injury, and PDO crashes. About 31% of fatal crashes were rear-end, followed by angle side (23%) and head on (17%). When compared with injury and PDO crashes, there was a significant percent difference of head on type which accounts for 2% for injury crashes and only 0.5% for PDO crashes as shown in Figure 3. Rear-end, angle side and head on account for 71% of fatal crashes which means the impact

point of crashes is critical in the truck-related work zone crashes. Because the rear-end crash is the dominance type for all crashes, it is necessary to reduce the speed variance in work zones. In addition, to reduce the severity of the crashes, more space for trucks are needed when traversing in work zones which can prevent head-on and angle-side crashes.

When identifying the truck drivers' fault in the crashes, about 43% of truck drivers are passive which means they were stroke by other vehicles in fatal crashes. Each of inattention driving and "disregarded traffic signs, signals, or markings" contributed 17% of fatal crashes. Among 37% of trucks stroke by other vehicles in injury crashes, inattention driving was the major fault of truck drivers which accounted for 21% and followed by "too fast for conditions" (10%). In addition, inattention driving contributed to 29% of PDO crashes. Figure 4 shows crash distribution by driver fault.

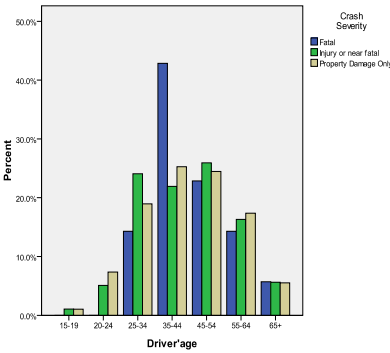


Fig. 1. Age distribution of all truck drivers

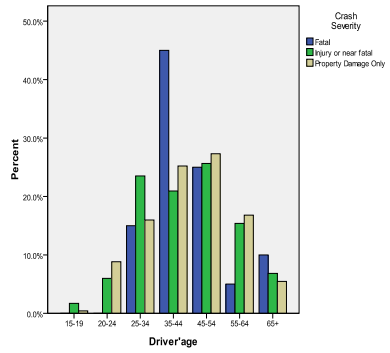


Fig. 2. Age distribution of truck drivers at fault

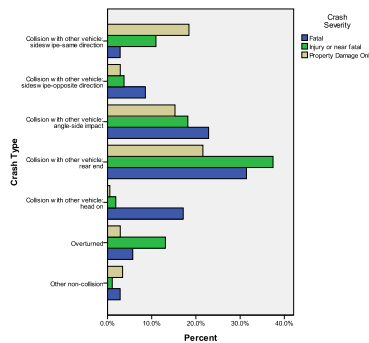


Fig. 3. Crash distributions by crash types

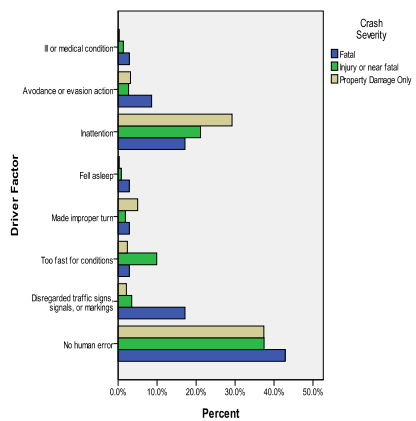


Fig. 4. Crash distributions by driver fault

Independence analysis

During the data compiling process, some data are sorted as ordinal variables like severity level and age; some are sorted as nominal variables such as gender of driver, time of crashes, and light condition; and others are kept as original format like speed limit and number of vehicles in crashes. For categorical variables, the Pearson Chi-square test and Likelihood-ratio test were used to test the dependent variable (severity) and potential independent variables. The Pearson chi-square statistic used for testing is

$$X^2 = \sum \frac{(n_{ij} - \mu_{ij})^2}{\mu_{ij}} \quad (1)$$

This statistic takes its minimum value of zero when all $n_{ij} = \mu_{ij}$. For a fixed sample size, greater differences $\{n_{ij} - \mu_{ij}\}$ produce larger X^2 values. Here, n_{ij} and μ_{ij} mean the observed frequency and expect frequency for each cell of contingency table. Each explanatory variable was paired with dependent variable (severity level), the Pearson Chi-square Test and Likelihood Ratio Test was used for the independence of each pair. Table 2 shows the results of independence test. The variables: Light Condition, Vehicle Maneuver, Crash Type, Number of Vehicles, Speed Limit, Area Information, and Traffic Control were the variables which have correlation with severity of crashes at 95% confidence level, which means the changes of these variables affect the crash severity.

Table 2 Independence Test of Variables

Variable	Statistic	Value	Degree of Freedom	Significance (2-sided)
Light Condition	Pearson Chi-Square	18.589	8	0.017
	Likelihood Ratio	19.546		0.012
Vehicle Maneuver	Pearson Chi-Square	92.241	30	0.000
	Likelihood Ratio	84.469		0.000
Crash Type	Pearson Chi-Square	181.841	28	0.000
	Likelihood Ratio	173.353		0.000
Number of Vehicles	Pearson Chi-Square	92.575	12	0.000
	Likelihood Ratio	63.394		0.000
Speed Limit	Pearson Chi-Square	76.423	22	0.000
	Likelihood Ratio	80.114		0.000
Area Information	Pearson Chi-Square	30.130	2	0.000
	Likelihood Ratio	32.121		0.000
Traffic Control	Pearson Chi-Square	81.980	20	0.000
	Likelihood Ratio	80.942		0.000

CONCLUSIONS AND RECOMMENDATIONS

The characteristics of truck-related fatal, injury, and PDO crashes in Kansas work zones were investigated systematically. The frequency analysis and tests of independence were utilized for identifying the factors that have impact on crash severity level. The study discovered that 38% of truck drivers were not responsible for the crashes in work zones. Within the fatal crashes, 53% of truck drivers were at

fault and were responsible for the crashes. The truck drivers with age between 35 and 44 were the most susceptible group since they accounted for 43% of fatal crashes. The authors found that the truck-related crashes took place when the weather and road surface conditions were favorable. Straight following was the maneuver most truck drivers took before the crash happened. Rear-end crash was dominant type of fatal, injury, and PDO crashes. Rural highways with the 65 mph speed limit had the highest proportion of fatal truck-related crashes. More than half of the fatal crashes occurred on straight and level highway work zones. Based on the results of independence tests, the factors such as light condition, vehicle maneuver, crash type, number of vehicles, speed limit, area information, and traffic control could affect the severity level of a crash.

Improvement of traffic control is the most direct method to reduce highway work zone crashes. More effective and sufficient work zone traffic controls should be installed. In particular, there is an urgent need to develop speed control methods that can be strictly enforced in the work zones. Illumination or highly retro-reflective devices should be installed in the work zones that stay set up at night. Devices such as transverse markings or temporary raised pavement markers in the advance warning areas may be used to alert inattentive travelers of the upcoming work zones. Installation of median separators is necessary in some work zones with high risk of head-on crashes. Lower speed limits should be considered in work zones with complex highway geometric alignments. Special traffic control strategies need to be developed to guide trucks passing the work zones. In addition, the authors suggest the launch of driver-oriented education programs in order to raise awareness on highway work zone hazards. The fact that a major cause of most crashes was human errors also indicates the urgency for developing effective training programs to educate the traveling public.

Some sections of the State of Kansas Motor Vehicle Crash Report need to be modified to better facilitate work zone crash investigation. For instance, the traffic control devices listed on the report do not include temporary traffic control devices such as channelizing devices and temporary lighting devices that are commonly used in work zones. As a result, crash investigators (police) usually either classify those temporary work zone traffic control devices as “other” or do not record them. Revisions might also be considered for other sections such as pedestrian identification (regular pedestrian or construction worker), and detailed crash locations within work zones (advance warning area, transition area, activity area, or termination area). Descriptions of the work zone including the construction work types and construction activities at the crash scene should be also included in the crash reports.

ACKNOWLEDGMENTS

The authors recognize that support for this research was provided by a grant from the U.S. Department of Transportation, University Transportation Centers Program to the Mid-America Transportation Center, at the University of Nebraska-Lincoln. The authors would also like to thank the Kansas Department of Transportation for providing truck-related work zone crashes reports.

REFERENCE

- Benekohal, R. and Shim, E. (1999). "Multivariate analysis of truck drivers' assessment of work zone safety." *Journal of Transportation Engineering*, Vol. 125, No, 5, 398-406.
- Benekohal, R., Shim, E. and Resende, P. (1995). "Truck drivers' concerns in work zones: travel characteristics and accident experiences." *Journal of Transportation Research Record*, No. 1509, 55-64.
- Bezwada, N. and Dissanayake, S. (2009). *Characteristics of fatal truck crashes in the United States*, Proceedings of the 2009 Mid-Continent Transportation Research Symposium. Ames, Iowa.
- Daniel, J., Dixon, K. and Jared, D. (2000). "Analysis of fatal crashes in Georgia work zones." *Journal of Transportation Research Record*, No. 1715, 18-23.
- FARS (2008). "Vehicles Involved in Fatal Crashes by Vehicle Type – State: USA, Year: 2008." <http://www-fars.nhtsa.dot.gov/Vehicles/VehiclesAllVehicles.aspx>. Accessed on April 5th, 2010.
- Garber, N. and Joshua, S. (1989). "Traffic and geometric characteristics affecting the involvement of large trucks in accidents." Final Report for Project VTRC 90-R2, Virginia Transportation Research Council, University of Virginia, Charlottesville, Virginia.
- Ha, T. and Nemeth, Z. (1995). "Detailed study of accident experience in construction and maintenance zones." *Journal of Transportation Research Record*, No. 1509, 38-45.
- Hall, J. and Lorenz, V. (1989). "Characteristics of construction-zone accidents." *Journal of Transportation Research Record*, No. 1230, 20-27.
- Li, Y. and Bai, Y. (2008a). *Fatal and Injury Crash Characteristics in Highway Work Zones*, in Proceedings of the 2008 TRB Annual Meeting, Washington, D.C.
- Li, Y. and Bai, Y. (2008b). "Comparison of characteristics between fatal and injury accidents in the highway construction zones." *Safety Science*, 46(4), 646-660.
- Meyers, W. (1981). "Comparison of Truck and Passenger-Car Accident Rates on Limited Access Facilities." *Journal of Transportation Research Record*, No. 808, 48-55.
- Pigman, J. and Agent, K. (1990). "Highway accidents in construction and maintenance work zones." *Journal of Transportation Research Record*, No. 1270, 12-21.
- Richards, S. and Faulkner, M. (1981). "An evaluation of work zone traffic accidents occurring on Texas highways in 1977." Final report for Project FHWA-TX-81-263, Texas Transportation Institute, College Station, Texas.
- Schrock, D. S., Ullman, G. L., Cothron, A. S., Kraus, E., and Voigt, A. P. (2004). "An Analysis of Fatal Work Zone Crashes in Texas." Final Report for Project FHWA/TX-05/0-4028-1, Texas Transportation Institute, College Station, Texas.
- Thompson, S. K. (2006). *Sampling*, 2nd Edition, John Willy & Sons Inc., New York City, New York.

Evaluation on Effectiveness of Sideview Video Systems to Reduce Transit Bus Side Crashes

Pei-Sung Lin, Ph.D., P.E., PTOE¹, Achilleas Kourtellis, Ph.D.², Chanyoung Lee, Ph.D., PTP, AICP³

¹Program Director, ITS, Traffic Operations and Safety Program, Center for Urban Transportation Research (CUTR), University of South Florida, 4202 E. Fowler Ave., CUT 100, Tampa, FL 33620; PH: (813) 974-4910; FAX: (813) 974-5168; Email: lin@cutr.usf.edu

²Research Associate, ITS, Traffic Operations and Safety Program, Center for Urban Transportation Research (CUTR), University of South Florida, 4202 E. Fowler Ave., CUT 100, Tampa, FL 33620; PH: (813) 974-8073; FAX: (813) 974-5168; Email: kourtellis@cutr.usf.edu

³Senior Research Associate, ITS, Traffic Operations and Safety Program, Center for Urban Transportation Research (CUTR), University of South Florida, 4202 E. Fowler Ave., CUT 100, Tampa, FL 33620; PH: (813) 974-5168; FAX: (813) 974-5168; Email: cylee@cutr.usf.edu

ABSTRACT

The camera-based system has great potential to reduce transit bus side crashes. This paper evaluated the effectiveness of sideview video systems to reduce transit bus side crashes through measuring the reduction of blind zones, and analyzing the results of controlled driving tests and driver surveys using sideview video systems. The result from measurements of blind zone reduction showed that the sideview video systems with a regular angle lens can reduce about 64 percent of the blind zones of a flat mirror system. It can reduce about 43 percent of blind zones of a common combined flat and convex mirror system. The result of the controlled driving test from 28 bus drivers was positive on distance/depth perception and lane change maneuvers using sideview video systems. The driver survey results also confirmed that bus drivers participating in the study valued the benefits of sideview video systems.

INTRODUCTION

Background. Transit bus side crashes occur for a number of reasons. Some of them include driver misjudgment, driver inattention, side blind zones, and other drivers' actions. The only device available to the driver for the purpose of side and rear view are sideview or rearview mirrors. Transit buses, as well as most commercial vehicles, do not have an inside rearview mirror because they usually do not have a rear window or the rear window is too far to provide the driver with useful view information. The primary use of the sideview mirrors is to help the driver with

surveillance of the surroundings of the vehicle while driving, especially in lane change and parking maneuvers.

Mirror-based systems have evolved over the years because of the need to provide a better view to the driver and now include more than one mirror with different magnifications. However, current mirror-based systems have several limitations. First, they do not cover adequate area to the side of the vehicle, thus leaving what are referred to as “blind zones.” Second, they are less effective during adverse weather, such as rain or fog. And finally, they are required to be large in size and extend out of the vehicle perimeter in order to provide the necessary view to the driver. Since transit buses come very close to the edge of the pavement to pick up standing pedestrians and passengers, a mirror that extends out of the bus footprint is not desirable. There have been reported cases where a pedestrian was struck by the mirror from a passing bus. In addition to the small number of crashes, research has shown that up to 94 percent of sideswipe and mirror crashes are not reported in Florida’s state crash database because there is no police report (Sando 2009). This shows a large under-representation of less severe crashes. Research has been conducted in previous years on systems to help address the issues of mirrors and side crashes. Different technologically-advanced systems have been proposed to help the driver detect and avoid objects next to the bus.

Transit bus side collision causes. According to data obtained from the Federal Transit Administration’s (FTA) 2002 National Transit Database (NTD), nearly 46 percent of bus accidents occur on the left or right side of the bus, compared to 25 percent occurring at the front of the bus and 19 percent occurring at the rear of the bus (Rephlo 2008). According to the Traffic Safety Facts reports from 1999-2003, an average of 40 fatalities and 18,430 injuries of bus occupants occurred per year (NHTSA 2009). Reported property damage costs range from \$3,660 per incident for sideswipe collisions to nearly \$13,085 for collisions with fixed objects. These collisions impact the availability of buses for revenue operations, add to the cost of providing transit services, and can have a negative effect on public perception of transit. For these reasons, FTA began working with the transit industry, researchers, and private vendors in 1998 to support the development and study of a Side Object Detection System (SODS) for transit buses.

According to Dunn et al., the sideswipe collisions of transit buses with other vehicles account for 33 percent of total crashes (Dunn 2007). Angle and sideswipe crashes caused a total of 44 percent of crashes. The data from the Florida Crash Analysis Reporting (CAR) System were analyzed for the time period 2003–2006 with the purpose of studying bus lane changing maneuvers and characteristics. The crashes where the bus was at fault have remained consistent over the years, with an average of 2,489 annual bus at-fault crashes. Side collisions include many categories of crashes. It was identified that side crashes with the potential to be avoided included mainly lane change maneuvers and turning maneuvers. Sideview mirrors are used by drivers mainly while changing lanes and making turns. Specifically, drivers perform lane changing maneuvers primarily based on the information obtained from both sideview mirrors. Sideswipe crashes are on the rise, mostly due to improper lane changes for years 2003-2006. One of the major causes of improper lane change

crashes is the side blind zone caused by the mirror's limited view. In addition, some rear end, turn, and angle crashes are caused by the blind zone. Table 1 shows that improper lane changing was a major contributing cause and accounted for about 65 percent of lane change crashes.

Table 1. Contributing Cause in Bus at-fault Lane Change Crashes

Contributing Cause	2003	2004	2005	2006	Total
No Improper Driving/Act	2.17%	1.75%	3.57%	2.41%	2.54%
Careless Driving	15.22%	12.28%	18.57%	15.66%	15.63%
Failed to Yield	6.52%	7.02%	6.43%	6.63%	6.64%
Improper Lane Change	66.30%	65.79%	64.29%	63.25%	64.65%
Improper Passing	2.17%	0.00%	0.71%	1.81%	1.17%
All Other	7.61%	13.16%	6.43%	10.24%	9.38%
Total	100%	100%	100%	100%	100%

Based on the descriptions in the long form reports, there are two kinds of limited view situations. One is that the driver did not see the other vehicle/object because it was located in the blind zone. The other is when the driver did not have the complete view due to weather conditions such as moisture on glass, rain, fog, and darkness, or being careless in noticing a bicyclist driving around the bus.

A number of in-vehicle technologies have been developed to mitigate transit bus collisions of all types. In 2008, the following systems were available for transit buses on experimental basis: Forward Collision Warning System (FCWS), Rear Collision Warning System (RCWS), Side Object Detection System (SODS), Forward Object Detection System (FODS), Rear Object Detection System (RODS), Lane Departure Warning System (LDWS), and Pedestrian Detection System (PDS). One of the causes of side crashes of transit buses is the side blind spot. When the bus operator cannot see far enough next to the vehicle, it can cause collisions, especially during turning and lane changing maneuvers. Since the technologies are fairly new and have no history of use, their effectiveness can only be estimated. A research study showed investigation of the potential of the technologies in avoiding collisions (Dunn 2007). Expert panels were created to review a number of documented crash reports and ranked the systems they thought could help the avoidance of a crash. In the study an average of 29 percent of the reviewed crashes were deemed "avoidable" using the systems above. All warning or detection systems were based on ultrasonic, radar or video sensors. During pilot studies, the systems were deemed not ready for safe operation on transit buses due to many false alarms and inadequate detections.

COMPARISON OF MIRRORS AND CAMERA SYSTEM

Measurement of blind zone reduction. The methodology used in this study for measuring the blind zones of the buses was straightforward. A bus driver of average height (5'10") sat in the driver's seat and adjusted the mirrors for his height. A research team member located outside of the bus carried a white plastic pole, and the two coordinated with two-way radios. The team member located outside walked along the sides of the bus until the driver could not see the plastic pole any longer.

The location of this point in regards to the bus was recorded. The same procedure was performed for all types of buses and side blind zones. Figure 1 shows the blind zones in shaded areas of a typical low floor transit bus. In addition, using three-dimensional software, the blind zones were projected for the volume of area next to the bus.

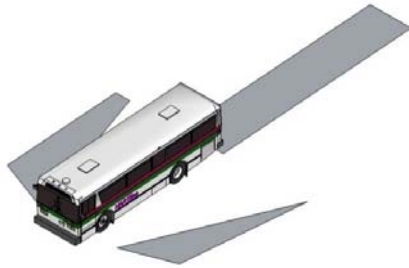


Figure 1. View of blind zones for a bus.

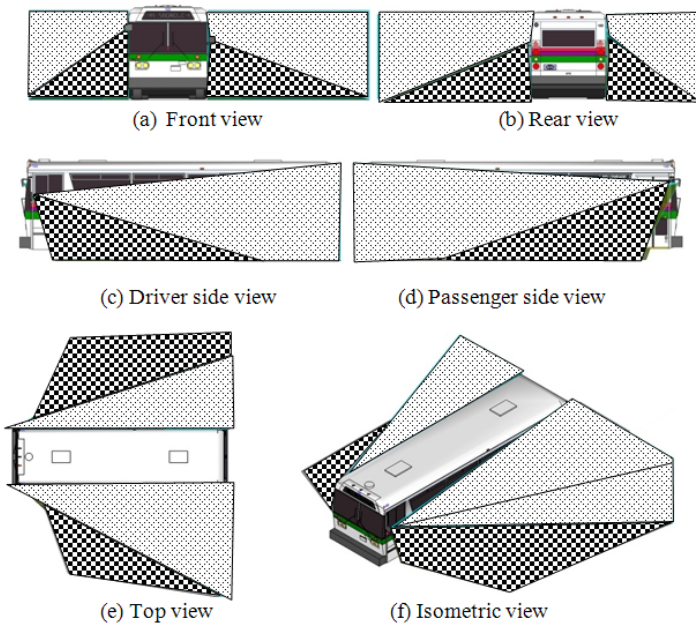


Figure 2. Views of a transit bus with mirror blind zones.

Figure 2 shows a transit bus ULF type in all views. Figure 2(a) shows the front view with the two zones; the dotted pattern on the figure is the area covered by the mirrors and the checkered pattern is the area that still remains blind to the driver. Figure 2(b) shows the rear of the bus with the same two zones. Figure 2(c) shows the

driver side of the bus with the same two zones. Figure 2(d) shows the passenger side of the bus with the two zones. Figure 2(e) shows the top view and blind zones together with the visible zones. Finally, Figure 2(f) shows the isometric view of a bus with the three areas. As seen in Figures 2(c) and 2(d), the driver has low blind zones next to the vehicle.

The resulting blind zone measurements indicate that the camera-based sideview video system can further reduce the blind zones of transit buses which currently use the combination of flat and convex mirror systems. The camera-based video sideview system with a regular-angle lens (no distorted image) can reduce about 64 percent of the blind zones of a flat mirror system along. It can reduce about 43 percent of blind zones of a common combined flat and convex mirror system. Using the wide-angle lens, the blind zones on the both sides of transit buses can be completely eliminated.

CONTROLLED DRIVING TESTS

One of the methods used to evaluate a safety enhancement device is to perform a driving test under controlled conditions, in order to collect certain data pertaining to the use of the system by drivers and its effectiveness on the safety aspects tested. A driving test requires drivers from the relevant population (in this case, transit bus drivers) driving a bus equipped with the safety enhancement device (in this case, the sideview video system) performing certain maneuvers designed to test different aspects of the system. To determine if the drivers can drive the bus with the proposed sideview video system, a controlled driving test was used to assess if the drivers could adapt to the system, and perform basic maneuvers required in everyday driving. Also, the test was used to assure that the drivers could use such a video system and perceive distance and depth relatively correctly (the main functions of the mirrors). In addition, the test was used to obtain feedback from the drivers on the system's effectiveness and capability in identifying potentially hazardous situations they cannot identify with the mirrors.

Test design. The test consisted of three parts: 1) Pre-maneuver driving course 2) Distance/depth perception exercise under static conditions 3) Driving maneuvers under dynamic conditions. *The pre-maneuver course* consisted of a closed loop course. Drivers were provided with a limited time to experience the sideview video system and use it before they performed the driving maneuvers. This allowed for some learning and exposure time. The course consisted of some left and right turns and a lane change maneuver. *Distance/depth perception under static conditions* incorporated a test of the perception of drivers with the mirrors and sideview video system when the bus was not moving. Perceiving the distances correctly is the key to ensuring safe operation of the vehicle. The drivers were asked to estimate how far a person was standing to the left rear or right rear of the bus. The test hypothesis was that the drivers would identify similar distances for the person's position using the mirrors and the sideview video system. *The driving maneuver under dynamic conditions* was a distance perception test, which tested the distance perception of drivers when the bus was moving. These maneuvers were called "lane change maneuvers" but did not actually require the drivers to change lanes. As described in

the driver packet given to the drivers, two different maneuvers were used. The first was a maneuver capturing the minimum distance between bus and vehicle in an eminent lane change, and the second was a maneuver to show the limitations of the FOV of the mirrors and the advantage of the FOV of the sideview video system.

Data Collection. The data collected during the test were in three forms: 1) responses from drivers to survey questions before and after they completed the maneuvers, 2) distance information collected by research staff during the distance perception test, and 3) video recorded during the lane change maneuvers. For the video data collection, the bus was equipped with a Data Acquisition System (DAS) to record multiple video cameras simultaneously and store the video data for later analysis. During the test, there were two side cameras, one rearview camera and one camera aimed at the driver's face to observe behavior. Also connected to the DAS there was a push button for drivers to press to indicate the last moment they would change lanes for the lane change maneuver. Figure 3 shows the equipment used.

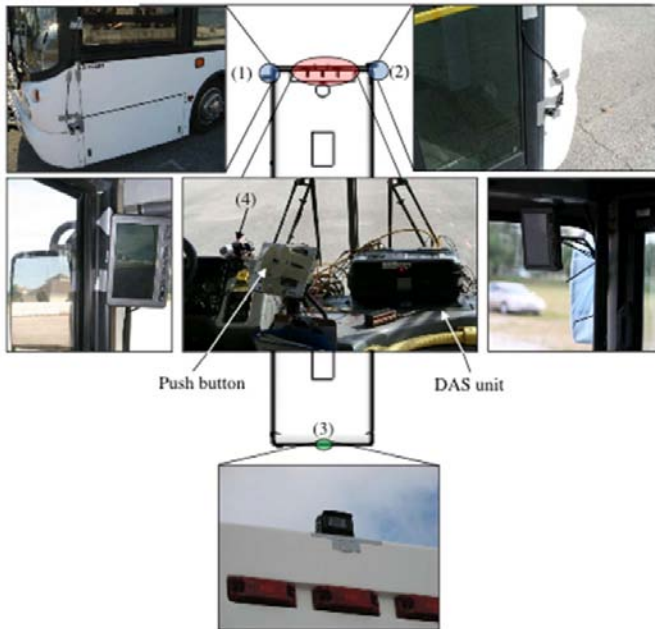


Figure 3. Left (1) and right (2) side cameras, left and right side monitors, DAS unit and push button, rearview camera (3) and driver camera (4).

All of the video collected from the cameras during the driving test was later reviewed using software that multiplexes the videos together in one screen. A screenshot from the software screen is shown in Figure 4. The top two images are the left- and right-side cameras, the left bottom image is from the rearview camera, and the right bottom image is from the driver camera, showing that the driver has pressed

the button and the LED has lit. A virtual scale was superimposed on the rear view image (lower left image on Figure 4) used to calculate the distance of the vehicle location behind the bus when the drivers pressed the button.



Figure 4. Screenshot from the software used for video analysis.

RESULTS OF DRIVING TESTS

The results of the test were very positive towards the sideview system. During the static distance perception test, the 28 participating drivers were able to perceive distances similarly using the mirrors and the sideview video system. Since the hypothesis was to test if drivers can perceive distances similarly to mirrors using the sideview system, this test confirmed the hypothesis.

During the lane change maneuvers, drivers were asked to say when was the last moment they would change lanes in front of an oncoming vehicle to the left or right lanes next to the bus. This provided researchers with the minimum distance between vehicle and bus using the mirrors and camera system. This distance was tested for difference. On average, using the camera system, the drivers said they would change lanes in front of the vehicle when it was located 8.87m (4.4m standard deviation) on the left and 9.54m (5.1m standard deviation) on the right lane of the bus. Using the mirrors, the distance was 9.50m (4.1m standard deviation) on the left and 10.40m (4.6m standard deviation) on the right. The max difference was 1.53m. The statistical analysis showed that, overall, using the sideview video system the drivers can perceive distance similar to the mirrors while the bus is in motion.

During the lane change maneuvers, the drivers were also able to identify the side blind zones of the bus and understand that the wide field of view of the cameras - which had a horizontal 100 degrees of view - can eliminate the side blind zones

completely. This was evident in the replies from the driver survey they completed after the test which showed that the majority of drivers agreed that the system can increase bus safety by providing a better side view, thus eliminating blind zones.

CONCLUSIONS

The study was designed to evaluate the effectiveness of camera-based systems to reduce transit bus side crashes through measuring the reduction of blind zones and analyzing the results of controlled driving tests using sideview video system. Based on the evaluation results of this study, the following conclusions were reached:

- In comparison with the sensor-based systems, camera-based systems provide an image to the driver that is simpler to process and requires less time. Available sensor-based systems have been evaluated in the past, and detection reliability and false alarms were the major concerns of the past studies.
- The side blind zones that exist due to the mirrors' inability to cover the area were greatly reduced or eliminated when using the sideview video system with wide-angle cameras. Volumetric measurements of the field of view from this study showed that the sideview video system provided greater coverage than the mirrors. The bus drivers could see at least two lanes next to the bus, providing them with the capability to avoid a potential sideswipe crash during a lane change maneuver.
- In this study, the sideview video system was used in driving tests under controlled conditions to analyze the system's effectiveness. The drivers were able to adapt to the system and perceive distances similar to mirrors. This result shows that drivers can potentially drive a bus equipped with the system in the future.
- Driver surveys provided valuable feedback on the system. The majority of the participating drivers in this study stated that they liked the sideview video system but were not confident about replacing the mirrors with the system used in the controlled driving test without further enhancement.
- The sideview video systems have minor limitations in certain lighting conditions, which can be further improved in the future. Also, the size and location of the monitors can vary, providing an optimum viewing experience.

REFERENCE

- Dunn, T., Laver, R., Skorupski, D., and Zyrowski, D. (2007). "Assessing the Business Case for Integrated Collision Avoidance Systems on Transit Buses." Publication FTA-OMB No. 0704-0188. FTA, U.S. Department of Transportation.
- National Highway Traffic Safety Administration (NHTSA). (2009) Traffic Safety Facts Reports 2003-2006. <http://www.nhtsa.dot.gov/> (Nov. 10, 2009).
- Rephlo, J., Miller, S., Haas, R., Saporta, H., Stock, D., Miller, D., Feast, L., and Brown, B. (2008). "*Side* Object Detection System Evaluation: Final Evaluation Report." Contract DTFH61-02-C-00061. ITS Joint Program Office, U.S. Department of Transportation.
- Sando, T., Mbatta, G., Chimba, D., and Moses, R. (2009). "The Influence of Narrower Lanes on Bus Sideswipe Crashes." TRB Annual Meeting 2009 Compendium of Papers DVD. Transportation Research Board of the National Academies, Washington D.C.

A Study of Steady State for Distance Headway

Chen, Hsueh-Heng¹ and Lin, Tsung-Chin²

¹Assistant Researcher, International Division, Chung-Hua Institution for Economic Research, Taipei, Taiwan, R.O.C. ; email: k32180918@gmail.com

²Traffic Engineer, T.Y.Lin International Taiwan, RM, 1202 NO.136 SEC. 3, JEN-AI ROAD, TAIPEI, 10657, TAIWAN, R.O.C. ; email: tclin@tylin.com.tw

ABSTRACT

Generally speaking, traffic headway comprises distance headway and time headway, which varies according to velocity and acceleration. Distance headway is a part of the traffic follow model as an expression of the stimulus-response factor. A more responsive driver accelerates and decelerates more frequently in response to the vehicle in front, thereby reducing the capacity of the traffic lane. This study attempts to calculate the distance headway in both the Macro Traffic Model and the Micro Traffic Model, and thus determine a steady state for the distance headway. The research results show that the Macro Traffic Model reaches Steady State at 20-23 seconds and the Micro Traffic Model reaches Steady State at 19-23 seconds. This research can be applied to traffic planning, calculation of crossroad traffic saturation rates, or in traffic simulation applications.

INTRODUCTION

Generally speaking, traffic headway comprises distance headway and time headway, which varies according to velocity and acceleration. Distance Headway is the distance between two vehicles front-to-back in traffic, while Time Headway is the time difference between two vehicles passing a single point. In traditional traffic engineering, the calculation of saturation flow rate is dependent on the distance factor, while the traffic engineer will also take the distance factor into consideration to determine the capacity of the traffic lane (LUO et al., 2001). However, traffic planning of the Distance Headway and Time Headway is often based solely on the experience of the planning engineer.

Distance Headway is a part of the traffic-following model as an expression of the stimulus-response factor, where the basic expression takes the form: Response = Responsiveness \times Stimulus (LI et al., 2005). A more responsive driver accelerates and decelerates more frequently in response to the vehicle in front, thereby reducing the capacity of the traffic lane. Thus, the present research focuses on discussion of Distance Headway based on the Macro Traffic Model and Micro Traffic Model. At the same time, this study uses the Cascaded Fuzzy Inference System to model the vehicles in traffic flow and to derive a Steady State of the Distance Headway. The study results can be applied to traffic lane capacity, crossroad saturation flow rate, or delays in travel time (Chen, 2011).

BACKGROUND

Micro Traffic Model

The Micro Traffic Model is based on the analysis of a single vehicle's behavior in relation to other vehicles, with a focus on the parameters of expected velocity, distance, relative velocity, and driver response time. Steady State of the Micro Traffic Model is determined by the corresponding velocity, lane capacity, and length of traffic under various congestion levels. Furthermore, vehicle behavior is not only affected by the leading vehicle but also by traffic control signals.

The majority of Micro Traffic Models focus on discussion of the Car-following Theory which assumes that a vehicle in motion will maintain a certain safe distance from the vehicle in front, a theory first developed during the 1950s and proposed by Reuschel (1950) and Pipes (1953). The three types of car-following models commonly used are:

- (1) Four Major Restrictions: Proposed by Russell & Harold in 1963, where a vehicle in motion is governed by four restrictions to maintain a minimum safe distance from the vehicles at the front and rear: Spacing Restriction, Acceleration Restriction, Stopping Restriction, and Turning Restriction. These four restrictions dictate the distance a vehicle can be moved within a unit time, thus generating the new vehicle coordinates.
- (2) Stimulus-Response Formula (May 1990): Proposed by General Motors on the test track, where the stimulus-response formula ($\text{Response} = \text{Responsiveness} \times \text{Stimulus}$) is the GM 5th Model.
- (3) Behavior Threshold (Leutzbach, 1988): Hoefs & Wiedemann proposed that the single set of parameters in the stimulus-response formula cannot sufficiently reflect the complexity of a driver's behavior. Thus, the concept of psychological and physical headway should be introduced into the traffic model. This model categorizes the traffic condition as three reaction zones: The first is the no reaction zone, where the driver is not influenced by the vehicle in front; second is the perceptive reaction zone, where the rear vehicle, while approaching the front vehicle, will usually speedup when the distance is perceived to be too large; third is the unconscious reaction zone, where the rear vehicle, when following the leading vehicle too closely, will typically fluctuate in velocity to maintain a safe distance.

Most discussion of the Micro Traffic Model adopts the programming and computer simulation method to collect traffic related data and recreate traffic conditions. The event scanning method is based on event occurrences and the time scanning method is based on unit time updates. Key observation on individual operation of each vehicle combines different models for processing, but such a model is more complex and processing memory-intensive. Thus, large-scale traffic networks cannot be easily modeled and simulated.

FRESIM Traffic Simulation

FRESIM simulation software (Rakha & Crowther, 2003), developed by the University of Pittsburgh, integrates the vehicle velocity and Distance Headway into the model simulation, as shown in (1). The Steady State condition occurs at the moment the velocity of the front vehicle matches the velocity of the rear vehicle,

wherein the third term in (1) equals zero and can be written as (2).

$$h = h_j + c_3u + bc_3\Delta u^2 \dots\dots\dots(1)$$

$$h = h_j + c_3u \dots\dots\dots(2)$$

where

h: Distance Headway between front and rear vehicle

h_j: Distance Headway in Congested Density

c₃: Responsiveness Factor of the driver

b: When the velocity of the rear vehicle is greater than the front, b=0.1; otherwise 0

Δu: Velocity Difference

u_f: Free Flow Rate

INTEGRATION Traffic Simulation

INTEGRATION simulation software (Rakha & Crowther, 2003), developed by Van Aerde (1995), Van Aerde and Rakha (1995), integrates the Greenshield and Pipes into a single model, as shown in (3). The first two terms are linearly correlated, and the third term uses the Pipes model.

$$h = c_1 + c_3u + \frac{c_2}{u_f - u} \dots\dots\dots(3)$$

where

C1, C2, C3: Distance Headway parameters

u_f: free flow rate

u_c: velocity under saturation flow rate

q_c: saturation flow rate

k_j: congestion density

Macro Traffic Model

Macro traffic theory treats vehicle behavior as a type of flow phenomenon. Earlier studies used aerial imaging photography to observe traffic flow and overall vehicle behavior. Then, qualitative description of traffic flow would used to correlate the flow density and velocity. This method is, however, not economically viable and thus not widely applicable. In order to construct such a traffic model, the relevant data must still be collected, such as Greenshields' (1934) observation of a two-lane highway in Ohio State which included a total of seven observation points and established the linear relationship between density and velocity.

In the early 1960s, traffic studies started to use the input-output method, calculating the correlation between density and velocity by measuring the distance and time relationship between the input point and output point. As this method is only suitable for single traffic lane with no vehicles overtaking, it is not widely applicable. On the other hand, an expression for the density using flow rate and velocity is as shown in (4)

$$q = ku \dots\dots\dots(4)$$

Macro Traffic Model – Mathematical Regression

This method observes and fits the flow rate, density, and velocity data to a curve for obtaining an expression, resulting in the Single-Regime Model and Multi-Regime Model. The former is a continuous curve as shown in studies by Greenshields, Greenberg, Underwood, Northwestern University, and Pipes-Munjial models (Chakrobarty, 2006); the latter estimates the curve with multiple sections as shown in studies by Edie and Northwestern University.

Cascaded Fuzzy Inference System

According to cascaded fuzzy inference system (Mar & Lin, 2005), this study simulated human decision making by fuzzy theory. The flowchart of cascaded fuzzy inference system is shown as Fig 1. The architecture of the model can be divided into velocity fuzzy controller stage and acceleration fuzzy controller stage.

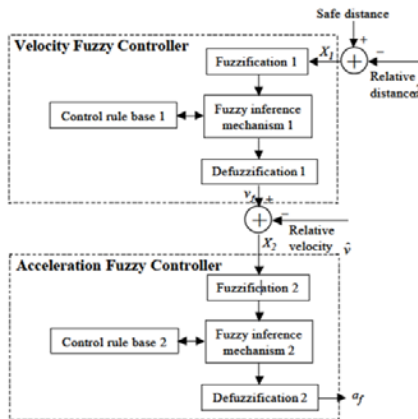


Figure 1. Flowchart of cascaded fuzzy inference system

Velocity Fuzzy Controller

The input value of this stage is based on difference between the distance between the front and rear vehicles and the safe distance. It has fuzzy processing by 11 control rule base, and defuzzification by weighted average method. Output value is the speed difference should be kept under the front and rear vehicles. The relevant parameters are listed in Table 1.

Acceleration Fuzzy Controller

The input value of this stage is based on the output value of velocity fuzzy controller and the difference between the speed between the front and rear vehicles. It has fuzzy processing by 3 control rule base, and defuzzification by weighted average method. The relevant parameters are listed in Table 1.

Table 1. Parameter Description (Cascaded Fuzzy Inference System)

	velocity fuzzy controller	acceleration fuzzy controller
Input value	X_1 =The distance between the front and rear vehicle-safe following distance	X_2 =The difference between the speed between the front and rear vehicle-current difference of speed
Fuzzy rules	IF X_1 is m_{1i} THEN Y_{1i} is C_{1i} , $i = 1, \dots, 10$ $C_1 = (-52.49, -41.99, -31.49, -21.00, -10.50, 0, 21.00, 10.50, 31.49, 41.99, 52.49)$	IF X_2 is m_{2i} THEN Y_{2i} is C_{2i} , $i = 1, 2$ $C_2 = (-13.67, 0, 5.47)$
defuzzification	$v_f = \frac{\sum_{i=0}^{10} \mu_{1i} \cdot Y_{1i}}{\sum_{i=0}^{10} \mu_{1i}} , i = 0, 1, \dots, 10$	$a_f = \frac{\sum_{i=0}^2 \mu_{2i} \cdot Y_{2i}}{\sum_{i=0}^2 \mu_{2i}} , i = 0, 1, 2$

Table 2. Parameter Description

Symbol(Parameters)	Assumption	Description
k_j	100veh/km (0.03veh/ft)	Congestion Density
g_c	1920veh/lane	Saturation Flow Rate
u_f	90km/hr (81ft/sec)	Free Flow Rate
h_j	33ft/veh	Distance Headway with Congestion Density
u_c	40.5ft/sec (assuming Greenshield)	Velocity with Saturation Flow Rate

Table 3. Distance Headway Equation

	FRESIM	$h_j + c_3u$
Micro Traffic Model	INTEGRATION	$c_1 + c_3u + \frac{c_2}{u_f - u}$
	Fuzzy Forbes	$1.5[\dot{x}_i(t)] + 20$
	Greenshield	$\frac{u_f}{k_j} \times \frac{1}{(u_f - u)}$
	Greenberg	$e^{\frac{u}{u_c}} / k_j$
Macro Traffic Model	Underwood's	$\frac{1}{k_o \ln(\frac{u}{u_f})}$
	Pipe's	$k_o \sqrt{-2 \ln(\frac{u}{u_f})}$

CASE DESCRIPTION

Consider an initial Distance Headway of 25ft between the front and rear vehicles, where the front vehicle is accelerating at 3.3ft/s^2 to a velocity of 30mph. After maintaining that speed for 10 seconds, the front vehicle decelerates at 4.6ft/s^2 (May, 1990). The rear vehicle follows the front vehicle with GM3. The relevant parameters are listed in Table 2.

COMPARISON

Steady State Comparison of Macro Traffic Model

Based on Table 3, the Distance Headway calculated in this study for Pipes, Greenshield, Greenberg, and Underwood's is as shown in Fig 2. The simulated time in this research was 33 seconds. The results show that at 20-23 seconds, the Distance Headway reaches a Steady State between 0.85ft ~ -0.94ft.

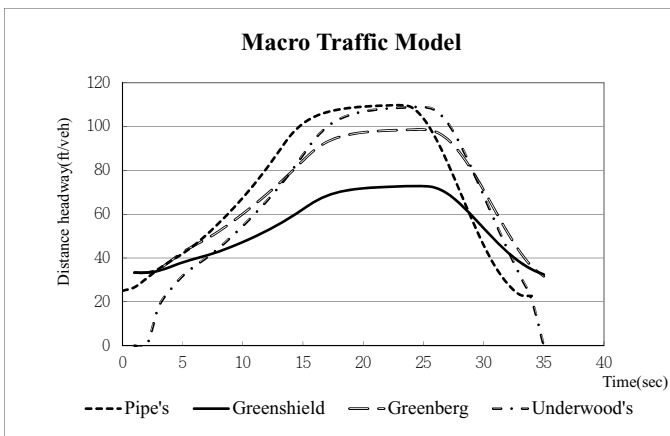


Figure 2. Macro Traffic Model Steady State

Steady State Comparison of Micro Traffic Model

Based on Table 3, the Distance Headway calculated in this study for FRESIM, INTEGRATION, Forbes, and Cascaded Fuzzy Inference System is as shown in Fig 3. The simulated time in this research was 33 seconds. The results show that at 19-23 seconds, the Distance Headway reaches a Steady State between 0.78ft ~ -0.04ft.

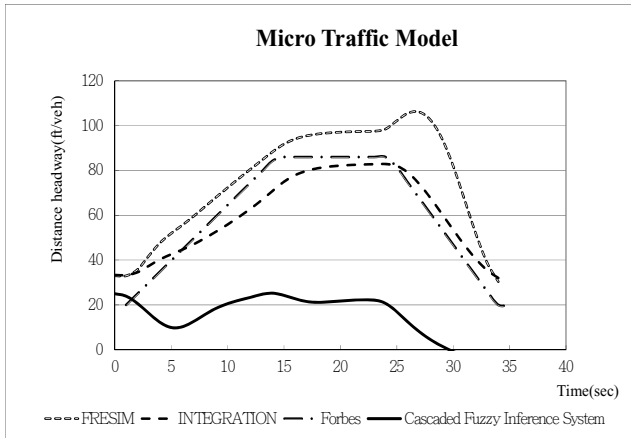


Figure 3. Micro Traffic Model Steady State

CONCLUSION

The study explored the Steady State of Distance Headway for the Macro Traffic Model and Micro Traffic Model respectively. The research results show that the Macro Traffic Model reaches Steady State at 20-23 seconds and the Micro Traffic Model reaches Steady State at 19-23 seconds. Regardless of the Macro or Micro Traffic Models, the Distance Headway is minimal when adopting the Car-following Theory. This research can be applied to traffic planning, calculation of crossroad traffic saturation, or in traffic simulation applications.

REFERENCES

- LUO, X., DU, J. Y., HUO, Y. M. (2001). "Study on the Distribution Patterns of Time Headway of Vehicles." *Journal of Southwest Jiaotong University*, 36(2).
- LI, X., MO, H., DENG, L. (2005). "Research on headway based on the car-following model." *China Traffic Research and Develop.*
- Rakha, H., Crowther, B. (2003). "Comparison and calibration of FRESIM and INTEGRATION steady-state car-following behavior." *Transportation Research Part A*, No. 37, pp. 1-27.
- Chakroborty, P. (2006). "Models of vehicular traffic: An engineering perspective." *Physica A*, No. 372, pp. 151-161.
- May, A. D. (1990). "Traffic Flow Fundamentals." *Prentice-Hall Inc*, New Jersey.
- Mar, J., Lin, H. T. (2005). "A car-following collision prevention control device based on the cascaded fuzzy inference system." *Fuzzy Sets and Systems*, NO. 150, pp.457-473.
- Chen, H. H. (2011). "A Study of Application Traffic Simulation Model in Route Planning." *Journal of Transportation System Engineering and Information Technology* (in press).

Determining Drivers' Acceptance of Using Graphics on Portable Changeable Message Signs in Highway Work Zones

Yilei Huang¹ and Yong Bai²

¹Ph.D. Candidate, Department of Civil, Environmental and Architectural Engineering, the University of Kansas, 1530 W. 15th Street, 2150 Learned Hall, Lawrence, KS 66045 (corresponding author). Phone: (785) 840-8386; E-mail: yileiku@gmail.com.

²Ph.D., P.E., F. ASCE, Associate Professor, Department of Civil, Environmental and Architectural Engineering, the University of Kansas, 1530 W. 15th Street, 2150 Learned Hall, Lawrence, KS 66045. Phone: (785) 864-2991; Fax: (785) 864-5631; E-mail: ybai@ku.edu.

ABSTRACT

Portable changeable message signs (PCMSs) have been employed in highway work zones for decades. Results of previous research indicated that the traditional text-based PCMSs had several limitations. The advanced sign technology has now allowed the use of graphics on PCMSs, and many researchers have studied drivers' responses to graphics on PCMSs using driving simulators. This study employed driver surveys in the real-world traffic conditions to determine drivers' acceptance of using graphics on PCMSs in highway work zones. The results of driver surveys revealed that more than 87% of drivers correctly understood the work zone and flagger graphics, and over 72% of drivers believed the graphics drew their attention more to the traffic conditions. The results also showed that the majority of drivers preferred to see graphics displayed on PCMSs. This study provided valuable knowledge to government agencies and the transportation industry on how to regulate and use graphics on PCMSs in highway work zones.

INTRODUCTION

The aging U.S. highway system has led to an increasing number of highway work zones in recent years, which inevitably disrupt regular traffic flows, result in traffic delays, and lead to safety concerns. According to the National Highway Traffic Safety Administration, the number of annual work zone fatalities has increased by about 34% in the past decade compared with annual fatalities from 1982 to 1999. To improve highway work zone safety, government agencies, the transportation industry, and interested individuals have conducted numerous studies on various work zone temporary traffic control (TTC) methods and devices, one of which is the portable changeable message sign (PCMS). A PCMS is an innovative TTC device which is capable of displaying a variety of messages to inform motorists of unusual driving conditions (FHWA, 2003).

The traditional type of PCMS is text-based and has been in use for decades. Many recent studies (Wang et al., 2007; Ullman et al., 2009), however, pointed out that using text messages on PCMSs has several limitations, such as confusing drivers and delaying their responses during driving, being difficult to read for elderly drivers and non-English-speaking drivers, difficult to see under adverse viewing conditions, and having a short range of legibility. As sign technology advances, the full-matrix PCMS has made it possible to display graphics to drivers. Graphic messages on PCMSs could likely overcome some of these limitations, particularly in complicated driving conditions such as work zones (Ullman et al., 2009). Although the advantages of graphic messages were realized, their use on PCMSs is still new in the U.S.

BACKGROUND

Research on drivers' understanding of graphics displayed on PCMSs started as early as in the 1980s. Riemersma et al. (1982) studied several graphics adapted from European static sign symbols, and discovered that the graphics for roadwork, congestion, slippery road, and two-way traffic were highly recognized, but the graphics for crash, skidding danger and reduced visibility due to rain or snow were less acceptable. Knoblauch et al. (1995) evaluated the graphics for congestion and reduced lanes displayed on a PCMS, and found that most drivers correctly interpreted these two graphics during daylight conditions within 400 ft, but less than half could correctly interpret the graphics from more than 570 ft. Luoma and Rama (2001) evaluated drivers' understanding of graphics displayed on PCMSs, and concluded that graphics for slippery road, congestion, and crash were most understood in European countries.

In the recent decade, with the help of advanced technology, many researchers have employed driving simulators to study drivers' responses to graphics on PCMSs in laboratory environments. Wang et al. (2007) assessed the effects of adding graphics to PCMSs using a driving simulator, and concluded that most people preferred graphic messages to text messages, and graphic messages were responded to significantly faster than text messages, particularly for elderly drivers and non-native drivers. Ullman et al. (2009) studied drivers' understanding of the work zone graphic using laboratory instruments, and revealed that while both text and symbol representations of roadwork were well understood by over 80% of the participants, the roadwork symbol was better understood than text by the Spanish-speaking participants and should be used in graphic designs.

Simulation studies in laboratory environments, however, have some limitations. Their results only provided participants' message reading performance in optimal circumstances. In the real-world driving situation, on the other hand, drivers have to pay attention to many other tasks, such as lane keeping, speed controlling, and car following. To overcome the limitations of simulation studies, this study employed driver surveys in the real-world traffic conditions to determine drivers' acceptance of using graphics on PCMSs in the upstream of one-lane two-way rural highway work zones.

DESIGN OF DRIVER SURVEYS

A full-matrix PCMS was programmed to display two text messages and four graphics. The text messages were WORKZONE AHEAD SLOWDOWN and FLAGGER AHD PREP TO STOP (flagger ahead prepare to stop), as illustrated in Figure 1. The graphics included three work zone graphics, which were designed similar to the W21-1 sign specified by the Manual on Uniform Traffic Control Devices (MUTCD), as shown in Figure 2, and one flagger graphic, which was designed similar to the W20-7 sign specified by the MUTCD, as displayed in Figure 3.



Work Zone Text Message

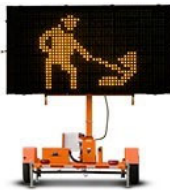


Flagger Text Message

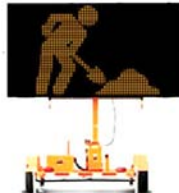
Figure 1. Text Messages on PCMS



W21-1 Sign



Work Zone Graphic One



Work Zone Graphic Two

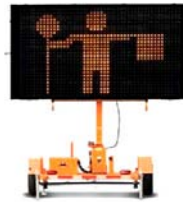


Work Zone Graphic Three

Figure 2. Work Zone Graphics in MUTCD and on PCMS



W20-7 Sign



Flagger Graphic

Figure 3. Flagger Graphic in MUTCD and on PCMS

Using these two text messages and four graphics, four PCMS conditions were set up, which were Work Zone PCMS One (see Figure 4), Work Zone PCMS Two (see Figure 5), Work Zone PCMS Three (see Figure 6), and Flagger PCMS (see Figure 7). Each of the PCMSs had two phases, one displaying a text message and the other displaying a graphic, and it took three seconds to switch from one phase to the other. The PCMSs were placed 575 ft upstream of the beginning of the work zone, which was defined by the W20-1 sign ROAD WORK AHEAD.



Figure 4. Work Zone PCMS One



Figure 5. Work Zone PCMS Two



Figure 6. Work Zone PCMS Three



Figure 7. Flagger PCMS

Driver surveys were conducted in two work zones in Kansas, one located on K-13 between K-16 and US-24, the other on US-75 between Burlington, KS and I-35. The construction projects were paving operations to rehabilitate the roadway surface. When construction operations were underway, the two-lane highway was converted to a one-lane, two-way work zone. A flagger was used at each end of the work zone for traffic control, and a pilot car was employed to guide through traffic. All passing vehicles had to stop before the flagger and wait for the pilot car, which typically took 10 to 15 minutes. Driver surveys were conducted at the flagger locations during drivers' waiting time without interrupting traffic and causing further traffic delay. A single survey took up to three minutes in most cases.

Two survey questionnaires were designed to determine drivers' acceptance of the graphics displayed on the three Work Zone PCMSs and the Flagger PCMS. Each questionnaire contained four multiple-choice questions. Question 1 aimed to evaluate drivers' recognition of the graphics displayed on PCMSs; question 2 aimed to evaluate drivers' understanding of the four graphics; question 3 aimed to determine the effectiveness of the four graphics in drawing drivers' attention to the traffic conditions; and question 4 aimed to determine drivers' preferences to message format displayed on PCMSs. Below is an example of a questionnaire used for the Work Zone PCMSs.

1. Did you see a **graphic** displayed on the Portable Changeable Message Sign when you were approaching the work zone?
 - Yes No
2. How did you interpret the meaning of this graphic?
 - Work zone/Work zone ahead/Someone working Get confused
 - Don't know Other
3. Did you think that the graphic drew your attention more to the work zone traffic conditions?
 - Yes No Don't know
4. Do you prefer the warning signs to be displayed in the graphical format or text format?
 - Text format Text and graphic format Graphic format
 - No difference Don't care Don't know Other

RESULTS OF DRIVER SURVEYS

A total of 578 valid questionnaires were collected from the driver surveys, including 156 for Work Zone PCMS One, 149 for Work Zone PCMS Two, 149 for Work Zone PCMS Three, and 124 for Flagger PCMS.

Drivers’ answers to question 1 are presented in Table 1. 96% of drivers (150 out of 156) saw the graphic on Work Zone PCMS One; 93% of drivers (139 out of 149) saw the graphic on Work Zone PCMS Two; 94% of drivers (140 out of 149) saw the graphic on Work Zone PCMS Three; and all drivers (124 out of 124) saw the graphic on Flagger PCMS. The remaining three questions were answered by the drivers who saw the graphics on the PCMSs.

Table 1. Drivers’ Recognition of Graphics on PCMS

Drivers’ Answer	Work Zone One		Work Zone Two		Work Zone Three		Flagger	
	No.	%	No.	%	No.	%	No.	%
Yes	150	96%	139	93%	140	94%	124	100%
No	6	4%	10	7%	9	6%	0	0%
Total	156		149		149		124	

Drivers’ understanding of the work zone and flagger graphics on PCMSs is shown in Table 2. While all drivers correctly understood the flagger graphic and the work zone graphics two and three, 87% of drivers (130 out of 150) successfully interpreted the work zone graphic one. The other 13% of drivers either misunderstood this work zone graphic or had no idea about its meaning.

Table 2. Drivers’ Understanding of Graphics on PCMS

Drivers’ Answer	Work Zone One		Work Zone Two		Work Zone Three		Flagger	
	No.	%	No.	%	No.	%	No.	%
Work Zone/Flagger	130	87%	139	100%	140	100%	124	100%
Confused	13	9%	0	0%	0	0%	0	0%
Don’t Know	7	4%	0	0%	0	0%	0	0%
Total	150		139		140		124	

Table 3 presents the effectiveness of the four graphics displayed on PCMSs in drawing drivers’ attention to the traffic conditions. When the work zone graphic one was displayed on PCMS, 72% of drivers thought it could draw more of their attention to the traffic conditions in the work zone. The work zone graphic two and the flagger graphic gained the highest percentage of drivers’ attention, at around 90%. 83% of drivers paid more attention to the work zone traffic conditions after they saw the work zone graphic two displayed on PCMS. The 87% of understanding rate of the work zone graphic one could possibly explain the least effectiveness among the four graphics in drawing drivers’ attention to the traffic conditions in the work zone.

The survey results of drivers’ preferences to message format on PCMSs are presented in Table 4. When the work zone graphic one was displayed on PCMS, around a quarter of drivers preferred the text format, the text and graphic format, and

the graphic format, respectively. When the work zone graphic two was displayed on PCMS, the percentage of drivers who preferred the text format decreased to 11%, while the percentage of drivers who chose the text and graphic format and the graphic format increased to 32% and 36%, respectively. When drivers saw the work zone graphic three displayed on PCMS, the percentage of drivers who liked the text format declined to 8%, and the percentage of drivers who chose the text and graphic format and the graphic format changed to 36% and 28%, respectively. When the flagger graphic was displayed on PCMS, only 3% of drivers preferred to see the message in text format, whereas 19% of drivers liked the text and graphic format and over half of drivers chose the graphic format. Between 14% and 19% of drivers did not think there was any difference between these message formats. It is clear that up to a quarter of drivers liked to see text messages on PCMSs, while between 52% and 71% of drivers preferred to see graphics displayed on PCMSs.

Table 3. Effectiveness of Graphics on PCMSs in Drawing Drivers' Attention

Drivers' Answer	Work Zone One		Work Zone Two		Work Zone Three		Flagger	
	No.	%	No.	%	No.	%	No.	%
Yes	108	72%	124	89%	116	83%	112	90%
No	42	28%	15	11%	24	17%	12	10%
Total	150		139		140		124	

Table 4. Drivers' Preferences to Message Format on PCMS

Drivers' Answer	Work Zone One		Work Zone Two		Work Zone Three		Flagger	
	No.	%	No.	%	No.	%	No.	%
Text	37	25%	15	11%	11	8%	4	3%
Text and Graphic	41	27%	44	32%	51	36%	24	19%
Graphic	38	25%	50	36%	39	28%	64	52%
No Difference	23	15%	20	14%	20	14%	24	19%
Don't Care	8	4%	10	7%	19	14%	7	6%
Don't Know	3	2%	0	0%	0	0%	1	1%
Total	150		139		140		124	

DISCUSSION AND CONCLUSIONS

Through the surveys, many drivers expressed their opinions on using graphics on PCMSs. The majority of drivers preferred graphics because the large graphics were able to "catch their eyes" from far away. Most drivers liked the flagger graphic because they were able to understand it on their first sight "without thinking." On the other hand, some drivers questioned the work zone graphic one, complaining that they were confused about its meaning. The confusions made these drivers think while driving, which was likely the reason why they did not like the work zone graphic one displayed on PCMS. Therefore, graphics have to be comprehensively examined by transportation authorities to make sure they can convey a clear and understandable meaning before being displayed on PCMSs.

As the U.S. highway system ages, the reconstruction and maintenance operations have led to an increasing number of highway work zones, which have created safety concerns. To improve highway work zone safety, various TTC devices

have been developed and employed, one of which is the PCMS. The traditional text-based PCMS, however, has been found to have several limitations in recent studies, such as confusing drivers and delaying their responses during driving, being difficult to read for elderly drivers and non-English-speaking drivers, difficult to see under adverse viewing conditions, and having a short range of legibility. The advanced sign technology has now allowed the use of graphics on PCMSs, and many researchers have studied drivers' responses to graphics on PCMSs using driving simulators in laboratory environments.

This study employed driver surveys in the real-world traffic conditions to determine drivers' acceptance of using graphics on PCMSs in the upstream of one-lane two-way rural highway work zones. Two text messages and four graphics, including three work zone graphics and one flagger graphic, were displayed on a PCMS which was placed 575 ft upstream of the beginning of a work zone to evaluate drivers' responses to these graphics. The results of driver surveys revealed that all drivers correctly understood the flagger graphic and the work zone graphics two and three, while 87% of drivers successfully interpreted the work zone graphic one. Over 72% of drivers believed the graphics displayed on PCMSs drew their attention more to the work zone traffic conditions. The results also showed that between 52% and 71% of drivers preferred to see graphics displayed on PCMSs. The results of this study provided valuable knowledge to government agencies and the transportation industry on how to regulate and use graphics on PCMSs in highway work zones.

REFERENCES

- Federal Highway Administration (FHWA). (2003). *Portable changeable message sign handbook*. Report No. FHWA-RD-03-066, U.S. DOT, Washington, D.C.
- Knoblauch, R., Mitzburg, M., Seifert, R., McGee, H., and Daily, K. (1995). *Uniform traffic control and warning messages for portable changeable message signs*. Report No. FHWA-RD-95-171, Washington, D.C.
- Luoma, J. and Rama, P. (2001). "Comprehension of pictographs for variable message signs." *Traffic Engineering and Control*, 42(2), pp. 53-58.
- Riemersma, J. B. J., Hazel, A. T. van de, Buist, M., and Moraal, J. (1982). *Design and evaluation of pictograms adopted for a matrix panel*. Report No. IZF 1982 C-25, Institute for Perception, Richmond, Virginia.
- Ullman, B. R., Trout, N. D., and Dudek, C. L. (2009). *Use of symbols and graphics on dynamic message signs*. Report No. FHWA/TX-08/0-5256-1, Texas Transportation Institute, College Station, Texas.
- Wang, J. H., Hesar, S. G., and Collyer, C. E. (2007). "Adding graphics to dynamic message sign messages." *Transportation Research Record: Journal of the Transportation Research Board*, No. 2018, pp. 63-71.

Transportation Infrastructure Disaster Impact and Lessons Learned after Typhoon MORAKOT

Min-Cheng Teng¹, Jau-Lang Su², Shen-Wen Chien³

¹ National Science & Technology Center for Disaster Reduction, 9F., No. 200, Sec.3, Beixin Rd., Xindian District, New Taipei City 23143, Taiwan, R.O.C. PH(886) 281958642; Fax (886) 289127766; Email: jack@ncdr.nat.gov.tw

² National Science & Technology Center for Disaster Reduction, 9F., No. 200, Sec.3, Beixin Rd., Xindian District, New Taipei City 23143, Taiwan, R.O.C. PH(886) 281958642; Fax (886) 289127766; Email: jlsu@ncdr.nat.gov.tw

³ National Science & Technology Center for Disaster Reduction, 9F., No. 200, Sec.3, Beixin Rd., Xindian District, New Taipei City 23143, Taiwan, R.O.C. PH(886) 281958642; Fax (886) 289127766; Email: una179@mail.cpu.edu.tw

ABSTRACT

The extreme event of natural disaster has had a serious significant impact on transportation infrastructure in recent years. The management financial resources are to have some criteria to show the current condition of infrastructure based on the results from inspection databases. Highway systems are very important to transportation infrastructure, and the highway system in Taiwan is vulnerable to earthquake and typhoon. Vulnerability of a transportation infrastructure system is the susceptibility to incidents that can result in a considerable reduction in transportation network serviceability. Because the major rainfall of Typhoon MORAKOT was focused in mountainous area, most of highway system destroyed was in this mountainous area as well. For example, more than 600 kilometers of highway length and 196 bridges failed or were closed as a result of Typhoon MORAKOT. In addition, the main causes of infrastructure damage were heavy and long periods of precipitation, floods, and upstream watershed debris-flow.

In this paper, according to the Typhoon MORAKOT experience learning, we described the impact and assessment of its region of influence in terms of their susceptibility to and the consequences of typhoon occurrences. In addition, a lesson is learned from this study regarding the key issues arising after Typhoon MORAKOT.

INTRODUCTION

Typhoon MORAKOT invaded Taiwan during August 6th to August 10th, 2009. Southwestern airflow with strong downpour were induced by the typhoon, and the major rainfall was distributed in the mountain area of Chiayi, Tainan, Kaohsiun,g and Pingtung Counties. Particularly, the Ali Mt. meteorological station, in Chiayi County, recorded the rainfall accumulated up to 3,600mm. Typhoon MORAKOT resulted in at least 675 deaths, and also brought large-scaled deep slides and 46 major debris-flow disasters, including Hsiaolin Village case, and destroyed six major road systems of more than 600 kilometers of highway length, and left 196 bridges damaged. The total loss sustained was over 16.4 billion NTD; the budget of reconstruction is over 100 billion NTD. The total budget of reconstruction the affected provincial road system requires over 60 million NTD (Wu, 2010). In terms of the reconstruction of infrastructure, projects such as the Alishan Highway, Jia-shian Bridge, Liou-guei Bridge, and eight loop railway tracks were restored by the end of December, 2009 (Morakot Post-Disaster Reconstruction Council).

Highway systems are an important channel for transportation and livelihood activities of populations. Therefore, when a highway system is damaged by disaster it will create a major impact on post-disaster communications and emergency relief, and will also affect disaster relief efforts. On August 8th, 2009, Typhoon MORAKOT caused major casualties and had significant impact on Taiwan. The Typhoon MORAKOT Post-Disaster Road System Emergency Repair and Reconstruction Project of the Ministry of Transportation and Communication reveals that highway-related disasters in Taiwan are mainly caused by typhoons and downpours (Ministry of Transportation and Communication, 2009).

Cross-river bridges are often damaged due to foundation scouring (Melville, 2000); the scour exposure can cause the traditionally designed pile type to be easy to break. The highway system in Taiwan is vulnerable to earthquake and runoff scour. In particular, there are the known collapse cases of Houfeng (Jian-Hao Hong, 2011) and Shuanyuan bridges. Therefore, the problem of bridge foundation scouring should be taken into consideration in addition to bridge structural damages.

Transportation infrastructure's failure at a time of natural disaster may cause interruption of government and business operations, formation of a cascade effect, and a serious impact on emergency response, economic development and social confidence. Protecting and ensuring the resiliency of the transportation infrastructure

of Taiwan is essential. Furthermore, in developing countries such as China and India, protecting such infrastructure has had a major effect on the implementation of sustainable infrastructure development projects in recent years (Liyin Shen, 2011).

To avoid the impact from typhoons on transportation infrastructure in Taiwan, this study focuses on the impact on typhoon-prone areas in terms of their susceptibility to and the consequences of typhoon occurrences. In addition, a lesson is learned from this study regarding the key issues arising after Typhoon MORAKOT.

STATISTICS OF EFFECTS AND ANALYSIS OF CAUSES OF TYPHOON MORAKOT

History of bridges damaged by typhoons

Statistics from 1972 to 2009 show that 838 bridges were damaged by typhoons and downpours. In 2004, 193 bridges were damaged, followed by 149, 143, 86, and 60 in 2008, 2009, 2005, and 2006, respectively, as shown in Figure 1. Figure 1 indicates the first, second, and third most serious typhoon damage occurred in 2009, 2004 and 2008, respectively. In 2009, 196 bridges were damaged when they were hit by typhoon MORAKOT, a figure which makes up 23.4% of the total historical damages from disasters, as shown in Figure 2.

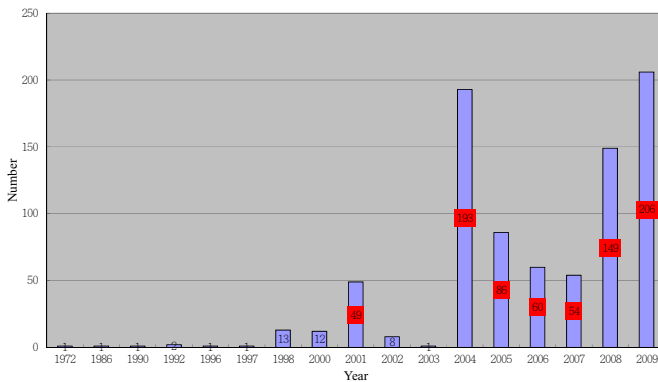


Figure 1. Total historical cases of bridge damage (1972-2009)

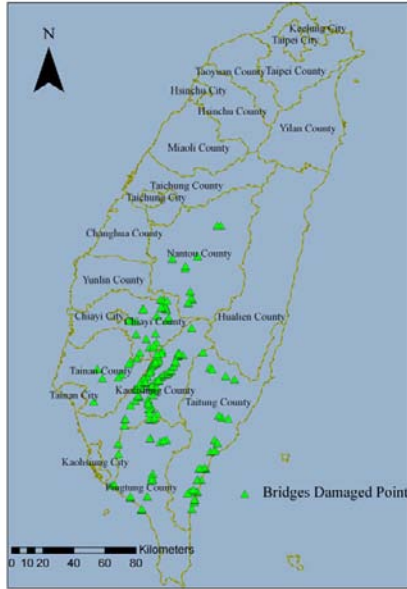


Figure 2. Bridge points damaged by Typhoon MORAKOT

2.2 Statistics of Typhoon MORAKOT bridge damage

Typhoon MORAKOT made landfall in Taiwan from August 6th to August 10th, 2010. The accumulated rainfall was mainly concentrated in mountainous areas of Chiayi, Tainan, and Kaohsiung-Pingtung. Regarding the highway losses due to Typhoon MORAKOT, it is preliminarily estimated that the cost of recovery and reconstruction may reach 18.1 billion NTD (Wu, 2010).

According to the disaster investigation team for disaster information (Chen et al., 2010), the statistics of bridge damage caused by Typhoon MORAKOT indicated that bridge damage mainly occurred in 6 counties and cities. The damage and statistics of 196 damaged bridges in various counties and cities are as shown in Figure 3. Statistical analysis found that bridge damage points under the jurisdiction of local governments (110 cases, 56%) were greater than those under the jurisdiction of the Directorate General of Highways (86 cases, 44%).

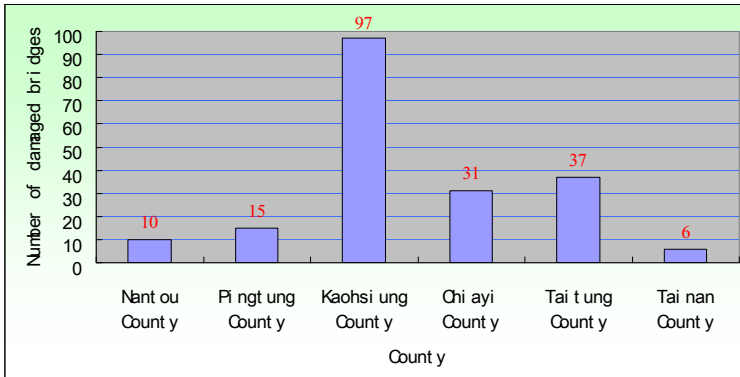


Figure 3. Number of bridges damaged by Typhoon MORAKOT, by county

2.3 Analysis of bridge disaster caused by Typhoon MORAKOT

(1) Precipitation analysis

The heavy and long period precipitation is one of the main causes of the large-scale disaster, because the total accumulated precipitation exceeded the engineering protection design limit. The total accumulated precipitation for the five-day period of Typhoon MORAKOT, with the highest total accumulated precipitation recorded at Alishan Precipitation Station, was 3,060mm. Table 1 shows the top ten towns, cities, and watersheds in terms of precipitation during the typhoon, which shows severely affected areas having the highest precipitation of over 2,000mm.

Table 1. Top 10 cities in terms of total accumulated precipitation due to Typhoon MORAKOT

Station	Accumulated Precipitation(mm)	Watershed	Administrative Area
Alishan	3,060	Tsengwen River	Alishan Township, Chiayi County
Weilaoshan	2,910	Gaoping River	Sandimen Township, Pingtung County
Fengqiuhu	2,863	Bajhang River	Jhuci Township, Chiayi County
Yuyoushan	2,823	Gaoping River	Taoyuan Township, Kaohsiung County

Xiana	2,747	Gaoping River	Taoyuan Township, Kaohsiung County
Shipanlong	2,706	Bajhang River	Jhuci Township, Chiayi County
Nantienci	2,694	Gaoping River	Taoyuan Township, Kaohsiung County
Little Guanshan	2,485	Gaoping River	Taoyuan Township, Kaohsiung County
Laitou	2,408	Tsengwen River	Alishan Township, Chiayi County
Sinfa	2,356	Gaoping River	Liugui Township, Kaohsiung County

Data source: Central Weather Bureau, Taiwan (R.O.C.)

(2) Caused analysis of bridge disaster

All the damaged bridges are classified according to their failure types, including whole bridge flow-away, abutment ruin, pile or foundation distortion, girder distortion, and others. The relevant classification and statistics are as shown in Figure 4. As shown in Figure 4, the bridge destroy type that occurred the most frequently was whole bridge flow-away, with 62 cases (49.2%). Damaged bridges on the rivers of the downstream areas were mainly due to the flooding beyond the design standards of the bridges or the impact of debris or driftwood from upstream.

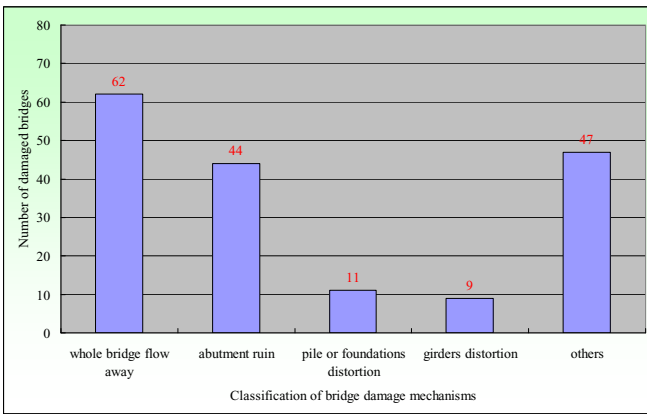


Figure 4. Classification of bridges’ damage mechanisms by Typhoon MORAKOT

DISCUSSION

The heavy and long period of precipitation is one of the large-scale disasters' main causes, because the total accumulated precipitation exceeded the engineering protection design limit.

3.1 Transportation Infrastructure Disaster Impact

(1) Post-disaster rapid assessment method

Typhoon MORAKOT brought large-scale deep slides, 46 major debris-flow disasters and destroyed six major road systems. In view of the numerous infrastructures damaged, it is difficult to easily and rapidly assess the safety and reconstruction priorities of infrastructure of different watersheds across different counties and cities. Therefore, developing a bridge post-disaster rapid assessment method is necessary.

(2) Vulnerability of transportation infrastructure

Vulnerability is divided into various dimensions including physical, social, economic and environmental factors (UN/ISDR, 2004). It is important to find the transportation network system with highest vulnerability via vulnerability assessment, and vulnerable factors should be divided into physical, economic, social and environmental factors. Besides, according to the historical damage records analysis, that could sort the disaster hot spots out for disaster mitigation.

3.2 Transportation Infrastructure key issues from Typhoon MORAKOT

(1) Emphasis on land conservation and reconstruction

The recovery and reconstruction work should be based on land conservation and reconstruction from a comprehensive perspective. Regarding the reconstruction of transportation infrastructure, of particular importance based on the above concept is the recovery and reconstruction of highways in environmentally sensitive areas.

(2) Disaster risk management

Disaster risk assessment should consider post-disaster characteristics learned from Typhoon MORAKOT. This study suggests that future risk management research topics focus on the following: establishing impact assessments, establishing risk assessment analysis methods, and establishing risk management and early stage warning systems.

(3) Special Act and funding

In order to cope with duly to help proceed with Post-Typhoon Morakot and reconstruction tasks in a safe, effective and prompt manner, an enacted Special Act is necessary. Special Act and funding of 116 billion NTD that made the reconstruction

for Post-Typhoon Morakot Disaster Reconstruction (Morakot Post-Disaster Reconstruction Council).

CONCLUSIONS AND LESSONS LEARNED

Based on the previous description, the situation of the transportation system damaged during Typhoon MORAKOT is more important than before. In view of the damage characteristics, the Typhoon MORAKOT post-disaster experience provides several learning follow-up topics, as follows:

(1) Research on river upstream mechanisms and prevention

The floods or debris flows and driftwood would cause failure to the transportation infrastructure. Therefore, in the future there must be a focus on river upstream damage mechanisms, and prevention and reconstruction should take the site into consideration.

(2) Historical damage hot spots

According to the historical bridge damage points, many damage hot spots are similar to those caused by MORAKOT. Hence, the illustrated locations of historical damage may be hot spots in the future.

(4) Early warning system

Because the bridge early warning information and emergency response measures gain more attention gradually, integration of monitoring information in order to sustain the real time monitoring system and supporting decision making is necessary.

REFERENCES

- Chen, L. C. et al. (2010). "Disaster Survey and Analysis of Typhoon MORAKOT." *National Science Committee of the Executive Yuan*.
- Hong J. H. et al. (2011). "Case Study: Houfeng Bridge Failure in Taiwan." *J. of Hydraulic Engineering* doi:10.1061/(ASCE)HY.1943-7900.0000430.
- Melville, B. W., and Coleman, S. E. (2000). "BRIDGE SCOUR." *Water Resources Publications, LLC*.
- Ministry of Transportation and Communication, MOTC (2009). "Typhoon MORAKOT Post-disaster Highway System Emergency Repair and Reconstruction Project".
- Morakot Post-Disaster Reconstruction Council, Executive Yuan, <http://88flood.www.gov.tw/eng/index.php>

- Shen L. et al. (2011). "Key Assessment Indicators for the Sustainability of Infrastructure Projects." *J. Constr. Eng. Manage.* 137, 441; doi:10.1061/(ASCE)
- United Nations, International Strategy for Disaster Reduction (UN/ISDR) (2004). "Living with Risk: A Global Review of Disaster Reduction Initiatives." *United Nations Publication, Geneva.*
- Wu, M. F. et al. (2010). "Typhoon MORAKOT Rescue and Reconstruction Record." *Directorate General of Highways, MOTC.*

Reliability Analysis of Highway Evacuation Network Post-Earthquake Disaster

Yang Sai-ni¹, Zhang Xue-chi¹, Ye Jia-yuan¹, Wu Jian-lin²

¹ State Key Laboratory of Earth Surface Processes and Resource Ecology, Beijing Normal University, Beijing 100875; PH: (086)-10-58800181; Email: yangsaini@bnu.edu.cn

² Institute of Building Energy Efficiency, China Academy of Building Research, Beijing 100013; PH: (086)-10-64517181; Email: wu.jianlin@gmail.com

ABSTRACT

In countries with high population density, evacuating large amount of people in a short time post-disaster is a critical challenge for emergency response agencies. This paper analyzes the reliability of highway evacuation network post earthquake disaster. The capacity of road segment after disasters is modeled as discrete probability function. A modified stochastic flow algorithm based on k-shortest path algorithm is proposed to calculate the possibility of transporting given number of people in pre-defined time window on potentially damaged highway network. Northeast Sichuan is used as case study site and real world data is collected to develop multiple scenarios in order to test the proposed methodology. The results show that the reliability of evacuation network is highly sensitive to the tightness of evacuation time window and the damage probability of critical road segment. The proposed methodology illustrates prominent potential of application in regional emergency planning and risk assessment. (147 words)

BACKGROUND

Many regions prone to earthquake disasters are heavily populated, especially in pan-pacific seismic circum belt. For massive earthquakes, transporting large amount of people from the stricken area to shelters in a short time post-quake is a tough task for emergency response agencies.

Highway system is the major transportation mode for evacuation, though it is subject to various damages caused by earthquake disaster and its secondary disasters. After a massive earthquake, the population needs to be evacuated varies from thousands to millions. Besides the people evacuation, the demands for relief supply and medical evacuation are enormous. It is necessary to apply strict traffic control to ensure efficient emergency logistics, though it is difficult to implement full traffic control on the entire network. Therefore, how to select the evacuation corridor is critical to improve the efficiency of evacuation, and evaluate the reliability of highway evacuation network can help relevant agencies analyze regional risk and

provide efficient support for decision making.

Network reliability has two dimensions: connectivity of a network and performance reliability (Michael G.H. Bell, 2000; M. Sanchez-Silva et al., 2005). For connectivity of a network, various researches have been done, such as network analysis based on routing and rerouting concepts after failure (Sanso B., 1991), connectivity analysis of degradable transportation network (Iida and Wakabayashi, 1989; Du and Nicholson, 1997), robustness analysis of gas networks (Rui Carvalho, 2009) and assessment of availability of an operational s-t path (Timothy C. Matisziw and Alan T. Murray, 2009). However, there are many circumstances that state of the network link is not under a binary distribution (0, 1). Instead, the reliability of the network link can be multi-state, and the regional or global network performance is affected by a number of factors. For example, the performance of the transportation network would be related to stochastic capacity of link (Yi-Kuei Lin, 2003, 2011), which is affected by accessibility of infrastructure, and the behavioral of users (Michael G.H. Bell, 2000). How to build an evaluation model for a multistate network becomes a key issue. Some algorithms have been proposed to evaluate multistate network (Ming J. Zuo et al, 2007; Xumei Chen et al., 2009; Hehong Fang and Xiaohan Sun, 2010; Yi-Kuei Lin, Cheng-Ta Yeh, 2011).

The evaluation of performance reliability for transportation network becomes extremely significant post-emergency (e.g. earthquake, attack of terrorism and fire), because the network reliability directly determines the life security of people who are urged be transported to the safe region. Some researchers have been studying how to evaluate inter-building evacuation network and determine the optimal evacuation route (G.Q. Gu et al. 2005; Wang JH et al. 2007). Considering the response of evacuees under emergency, Weiwei Wu et al. (2008) provided an evaluation model for stochastic moving network in which people move in stochastic direction when faced with emergency. Moreover, emergency sometimes could also result in some unexpected deficiency in the evacuation network, such as road capacity and ITS management failure (Shebang K and Nassiri H, 2008). Taking uncertainty of road capacity into account, Yazici A. et al. (2010) proposed an analytical system-optimal dynamic traffic assignment model and ManWo Ng. et al. (2010) presented a CTM-based model to plan the evacuation route, considering the evacuee amount to be uncertain. Post-earthquake, there are many uncertainties in the process of evacuation, such as secondary disasters, ITS failures. Besides, few related work has been done on multi-multi evacuation network.

In this paper, a reliability evaluation method is proposed for a multi-origin to multi-destination evacuation network. And both of the stochastic road capacity and uncertainty of secondary disasters are taken into account. A case study of Sichuan Province has been tested and indicates the potential of the proposed evaluation method.

PROBLEM STATEMENT

In a highway network $N(n, a)$, each segment (arc or node) has a given discrete probability mass function of states (e.g. no damage, partially or completely damaged). The capacity of each segment (the maximum flow passing the segment per unit time) has multiple levels between 0 and its full capacity. The entire region is composed by belts and each belt represents the area with certain seismic intensity, as shown in Figure 1. Assume the population (D) in inner belts need to be transported to outer belts in a given time window (T). The reliability of this highway evacuation network is the probability that the demands at origins (o_i) can be successfully transported to destinations (d_i) by minimal path in time T . And the minimal path is a sequence of arcs from origin to destination, which contains no cycle.

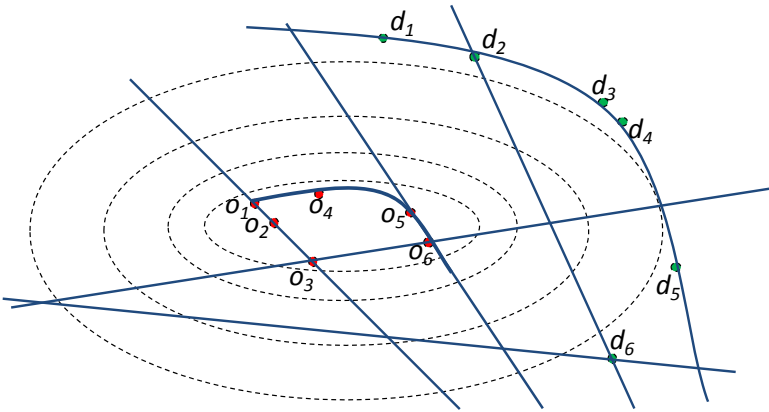


Figure 1. Illustration of highway evacuation network.

The following assumptions are made for simplification:

1. All the population of a town is concentrated at the town center, which is the origin of evacuation.
2. All the demand has access to the highway evacuation network (no isolated population).
3. All evacuation traffic will use the evacuation corridor.
4. Assume the road has strict traffic control and can fully use their available capacity for evacuation when it is selected as corridor.

METHODOLOGY

To calculate the reliability of this highway evacuation network, we design the following methodology framework as shown in Figure 2. This approach is composed by three parts: segment reliability evaluation, path reliability evaluation and network

reliability evaluation. Segment evaluation is based upon the hazard impact analysis of earthquake on piece-wise highway infrastructure. Path evaluation examines all lower boundary points for (D, T) . Network evaluation is the composition of all lower points and inclusion and exclusion method is performed.

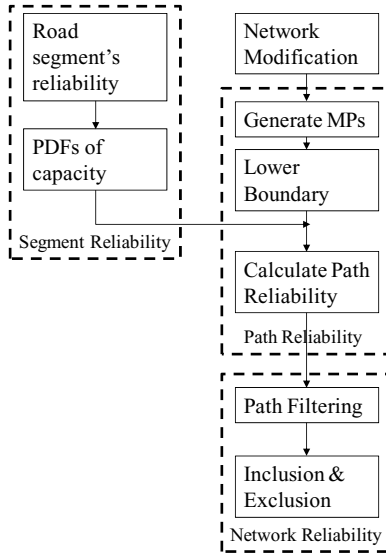


Figure 2. Framework of proposed method.

The detailed steps of the proposed methodology are as follows:

- Step 0 (Network modification): Link all origins (town centers) to a super source and link all destinations (shelters) to a super sink with capacity equal to infinite and arc length equal to zero.
- Step 1 (Find maximal capacity for minimum path P_i): Find all minimum paths using k-shortest path algorithm. For each minimum path $P_i = \{a_{i1}, a_{i2}, \dots, a_{in_i}\}$, find the minimal capacity c_i of components on P_i . c_i is the bottleneck of path c_i and it is the possible maximum population that can be sent through P_i in a unit time.
- Step 2 (Generate all lower boundary points for (D, T)): Find the minimal capacity vector $X_i = \{x_{i1}, x_{i2}, \dots, x_{in_i}\}$. If $\frac{D}{T} > c_i$, then X_i does not exist. Otherwise,

$$x_{ik} = \begin{cases} c_i & \forall k \in P_i, \\ 0 & \text{else.} \end{cases} \tag{1}$$

- Step 3 (Reliability evaluation): If X_i exists, then $B_i = \{X | X > X_i\}$. Otherwise, B_i

$=\varnothing$. Select $M_i = \{B_i \mid \Pr(B_i) > \tau, \text{ for all } i\}$, where τ is a pre-selected threshold .

The system reliability $R_{D,T}$ is $\Pr\{\cup M_i\}$.

In this approach, all lower boundary points for (D, T) can be generated by step 1 and step 2 by alternating the algorithm proposed by *Yi-Kuei Lin(2003)*. To calculate system reliability, the exact solution of inclusion and exclusion method requires the calculation of all possible combinations of set M , and the complexity of this calculation is $O(2^m)$, where m is the size of set for inclusion and exclusion algorithm. To insure reasonable calculation time, all the paths with path reliability greater than some pre-defined threshold τ are selected in the calculation of inclusion and exclusion algorithm. In our case study, the difference of reliability calculated by approximation method and exact method is within 2% of the exact solutions by selecting $\tau=0.01$, while the computational time is much smaller.

CASE STUDY

The northeast part of Sichuan is selected as the case study area and the seismic map for Wenchuan earthquake is used, as shown in Figure 3. All the population in area with seismic intensity IX or above needs to be transported to areas with seismic intensity VI or below. To estimate the damage of highway system caused by earthquake, a software named EQGIS is developed. By inputting the earthquake information, the software can report the potential damage for highway infrastructures, such as road segment, tunnels and bridges, and the stochastic highway evacuation network can be generated. An example output is shown in Table 1. The damage of infrastructures is estimated with known methodologies (*FEMA, 2003*) and modifications.

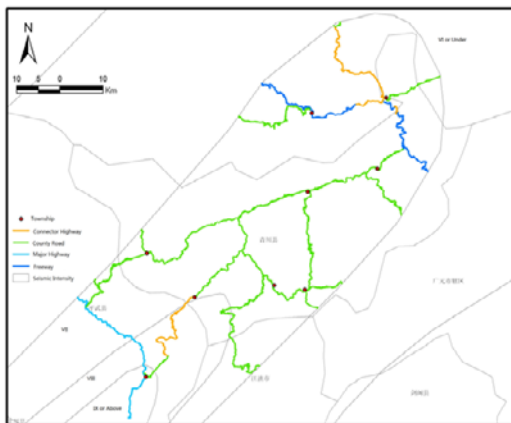


Figure 3 Study area and real world road network.

Table 1 Examples of Network Damage Estimation

Segment ID	Class	Start Point	End Point	No Damage	Medium Damage	Complete Damage
S105	County Road	8	5	0.5	0.4	0.1
FuGao Road	Connector Highway	6	5	0	0.5	0.5
...

Using the algorithm described above, we estimate the network reliability of evacuating 252342 people in 1 hour, 2 hours, ..., 47 hours, and 48 hours (as shown in Figure 4) with and without landslide hazard concern. These results show the substantial difference of network reliability with and without landslide concern. When T=5 hours, the network reliability without landslide concern equals to 1, while the network reliability with landslide concern is 0 for the same T. For network reliability with landslide concern, there are significant jumps at T=9 hours, T=20 hours. The significant difference between these two types of scenarios is because the landslide risk dramatically decreases the reliability of some critical segments. For example, arcs (23, 24) are two segments on a freeway, which are part of the critical path, their probability of no damage decreases from 0.9 to 0.1 when considering landslide risk. This change dramatically reduces the path reliability and the network reliability.

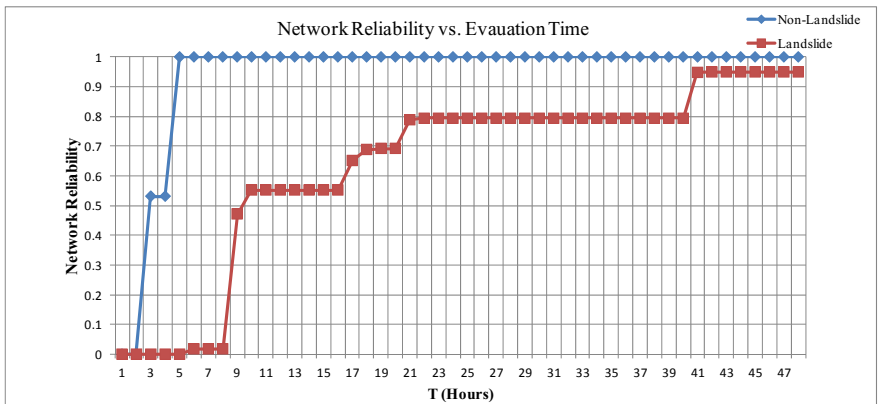


Figure 4 Network reliabilities for various time windows.

DISCUSSION AND CONCLUSION

In regions with high population density, evacuating large amount of people in a given time is a critical challenge for emergency response agencies. In this study, the reliability of evacuation highway network post-earthquake disaster is modeled as a stochastic network flow problem and a approach based on k-shortest path algorithm proposed to calculate the probability of successfully transporting evacuees in given time window. The capacity of road segment after disasters is described as discrete probability function. Northeast Sichuan is used as case study site and real world data is collected to develop multiple scenarios in order to test the proposed methodology.

The results show that the reliability of evacuation network is highly sensitive to the tightness of evacuation time window. The secondary disaster risk dramatically reduces the network reliability since the reliability of critical road segment decreases. By this method, it is possible to evaluate the regional risk of disaster emergency response. At the same time, a detailed solution analysis can help the transportation department to identify the critical road segments which need to be less prone to disaster damage. The proposed methodology illustrates prominent potential of application in regional emergency planning and risk assessment.

ACKNOWLEDGEMENT

This research is sponsored by the Ministry of Science and Technology of People's Republic of China (Project #2012CB955402, the State Key Laboratory of Earth Surface Processes and Resource Ecology Team-Built Project, and the Integrated Risk Governance – Models and Modeling Project (2010DFB20880).

REFERENCE

- Du, Z.P. and A.J. Nicholson. (1997) "Degradable transportation systems: sensitivity and reliability analysis". *Transportation Research B*, 31, 225-237.
- Chu, G.Q., T. Chen, Z.H. Sun, J.H. Sun. (2005) "Probabilistic risk assessment for evacuees in building fires". *Building and Environment*; 42; 1283-1290.
- Fan, Hehong and Xiaohan Sun. (2010) "A multi-state reliability evaluation model for P2P networks". *Reliability Engineering and System Safety*; 95; 402-411.
- Iida Y. and Wakabayashi H. (1989) "An approximation method of terminal reliability of road network using partial minimal path and cut set". In *Proceedings of the Fifth World Conference*, vol. IV. Yokohama, Japan, pp. 367-380
- Ng, ManWo, Travis Waller. (2010). "Reliable evacuation planning via demand inflation and supply deflation". *Transportation Research Part E*; 46; 1086-1094.
- Bell, M. G.H. (2000) "A game theory approach to measuring the performance reliability of transport networks" *Transportation Research Part B*, 34, 533-545.
- Zuo, Ming J., Zhigang Tian and Hong-Zhong Huang. (2007) "An efficient method for

- reliability evaluation of multistate networks given all minimal path vectors”. IEE Transactions; 39; 811-817.
- Sanchez-Silva, M., M. Daniels, G. Lleras, D. Patino. (2005) “A transport network reliability model for the efficient assignment of resources” *Transportation Research Part B*, 39, 47-63.
- Carvaho, R., Lubos Buzna, et al. (2009) “Robustness of trans-European gas networks”. *Physical review E* 80, 016206.
- Sanso, B. and F. Soumis (1991) “Communication and transportation network reliability using routing models”. *IEEE transactions on Reliability*; 40; 29-38.
- Timothy, C. M. and A. T. Murray. (2009) “Modeling s-t path availability to support disaster vulnerability assessment of network infrastructure”. *Computers & Operations Research*, 36, 16-26.
- Wang, JH, Lu SX, Wang DR, Zhang XL, Feng L. (2007) “Risk analysis of evacuation under building fire based on point estimate method”. *Advances in Intelligent System Research*; 2; 312-316.
- Wu, Wei-wei, Angelika Ning, Xuan-xi Ning. (2008) “Evaluation of the reliability of transport networks based on the stochastic flow moving objects”. *Reliability Engineering and System Safety*; 93; 816-822
- Chen, Xumei, Lei Yu, Yushi Zhang, Jifu Guo. (2009) “Analyzing urban bus service reliability at the stop, route, and network levels”. *Transportation Research Part A*; 43; 722-734.
- Yazici, A and K. Ozbay. (2010). “Evacuation Network Modeling via Dynamic Traffic Assignment with Probabilistic Demand and Capacity Constraints”. *Transportation Research Record*; 2196; 11-20.
- Lin, Yi-Kuei. (2003) “Extend the quickest path problem to the system reliability evaluation for a stochastic-flow network”. *Computers & Operations Research*, 30, 567-575.
- Lin, Yi-Kuei. (2011) “Performance evaluation for a transportation system in stochastic case” *Computers & Operations Research*. IN PRESS.
- Lin, Yi-Kuei and Cheng-Ta Yeh. (2011) “Maximal network reliability for a stochastic power transmission network”. *Reliability Engineering and System Safety*; 96; 1332-1339.
- FEMA. (2003) “HAZUS-MH MR3 Technical Manual”. Chapter7.

The Comprehensive Evaluation Model for Earthquake Emergency Shelter

Huan. Cheng¹ and X. K. Yang²

¹ Transportation Research Center, Beijing University of Technology, 100124, No.100 Ping Le Yuan, Chao Yang District, Beijing, China; PH (010)67396182; FAX (010)67391509; email: chenghuan1010@hotmail.com.

² Transportation Research Center, Beijing University of Technology, 100124, No.100 Ping Le Yuan, Chao Yang District, Beijing, China; PH (010)67391678; FAX (010)67391509; email: xiaokuan@hotmail.com.

ABSTRACT

The most important thing facing all levels of government after earthquake is to do everything possible to rescue injured people and evacuate those who are in the dangerous area to the safe places as soon as possible. What kinds of shelters are selected to be appropriate as earthquake shelters? This is an issue emergency management agencies have to deal with. For this reason it is necessary to set an evaluation model for earthquake emergency shelter (EES) so as to provide ground for decision making in the selection of earthquake emergency shelters. The objective of this study focuses on establishing a comprehensive evaluation model for the selection of earthquake emergency shelters. A total of three evaluation indicators are picked up: capacity of shelter, quality of facility, and accessibility. The definitions and quantitative calculation procedure of these indicators are elaborated. The weight of each indicator is estimated based on Analytic Hierarchy Process (AHP). A case study is also conducted to substantiate the validity and usefulness of the model. The result of this study can provide technical support in the selection of shelters for earthquake.

INTRODUCTION

Earthquake brings about more devastating damages for cities as compared to other disasters. Serious earthquakes usually cause family to lose their loved ones, huge economic losses, interruption of water supply, blackout, paralysis of transportation system, and chaos of social and economic life.

There are many seismic belts in China. The data from report show that there are 23 provincial capitals and 2/3 cities with population more than 1 million lie in 7-intensity earthquake belt (Lin, C.Y. 2010). Recent years,

earthquakes have already caused great damages to cities. For example, the earthquake in Wenchuan (Sichuan province of China) in 2008 claimed more than 80,000 lives and the economic loss was estimated over twenty billion US dollars.

After earthquake it is necessary to evacuate people who are in dangerous area to a relatively safe place with all kinds of necessary provisions, such as medical care facilities, lighting, public toilets, drinking water and food. This place is defined in this study as Earthquake Emergency Shelter (EES). EES is a place that can provide a safe place for the evacuees and meet the basic needs of life and emergency rescue after careful planning, construction and management (Qi, Y., 2005). Selection for EES is significant for emergency rescue and reconstruction after the shock (Xiu, J.G., 2001). However, how to choose the appropriate shelters after earthquake becomes an issue facing decision makers. It is crucial to conduct comprehensive evaluation for shelters so as to provide basis for decision making in the selection of EES. It will be beneficial for enhancing the planning and construction of EES and for improving the comprehensive emergency response ability of cities.

OBJECTIVES OF THE STUDY

Earthquake emergency shelter (EES) plays a very important role in earthquake emergency evacuation and rescue management. However, at present decision-making on the selection of earthquake shelters is usually arbitrary without appropriate methodology. The existing public parks and open spaces are generally chosen as earthquake shelters in the city of Beijing, without conducting technical analysis. To overcome this deficiency it is necessary to set principles of selection and build comprehensive evaluation model to minimize the arbitrariness.

It is evident that the selection of earthquake shelter is quite different from that of other disasters. Generally speaking earthquake shelter is featured with longer time of stay and daily necessity such as drinking water, food, medical care. As a result, the choice of emergency shelters should be made according to the particular requirement.

In this paper, a comprehensive evaluation model for the selection of EES is proposed. The objective of this study is to select appropriate and reasonable indicators for EES in the comprehensive manner. The model can be used for disaster officials to select suitable shelters for earthquake emergency purpose.

LITERATURE REVIEW

In her analysis of the critical affecting factors on disaster response ability of city, Wang Xia (Wang, X., 2009) divides the emergency process into three stages and proposes 23 assessment indexes to assess the disaster response ability

of cities. A comprehensive evaluation model over city's disaster response ability is built based on AHP.

Wu Zongzhi et al. conduct researches on evaluating emergency adaptation ability of shelter (Wu, Z.Z., 2005). He selects 18 assessment indexes from planning, internal hardware and outward software environment.

Bao Shengping carries out a study on adaptation assessment of urban refuge in Taiwan (Bao, S.P., 2005). He uses grey correlation analysis theory to do adaptation assessment for shelters and uses Jiayi city in Taiwan as an example.

Chen Sudan et al. analyze the security of shelters in Taiyuan city Shanxi province (Chen, S.D., 2006). In his opinion, there are two important safety factors that affect the safety and reliability of emergency evacuation and rescue significantly: geological factor and public facility factor.

Zhou Xiaomeng et al. study the layout optimization of shelter and propose network optimization model (Zhou, X.M., 2006). The principles of how to determine the number and capacity of shelters are given in this study.

Ye Mingwu et al. perform research on refuge accessibility of park in Shanghai based on GIS (Ye, M.W., 2008). Based on the theory of space accessibility and refuge request of disaster prevention, using ArcGIS technology, a quantitative study on the balance relationship between the existing service of emergency refuge of inner-city parks and refuge demand of residents in Shanghai is conducted.

METHODOLOGY

To evaluate EES in a comprehensive and relatively objective way it is crucial to pick up evaluation indicators among many available candidates. The selection of indicators is in accord to the following principles. First, the number of indicator should be as few as possible. Second, indicators should be independent with each other. Third, indicators should be quantifiable in estimation.

Based on the three principles and the specific demand of earthquake emergency three assessment indexes are selected. They are capacity of shelter, quality of facility and accessibility of shelter.

Interpretations of selected indicator

Capacity of shelter (B_1): Compared to other natural disasters, there will be much higher evacuation demand for earthquake emergency. As a safe refuge for people to get away from danger and wait for rescue, the EES must be large enough to accommodate as many people as possible. The larger the shelter is, the stronger emergency response ability is. Through literature review, it is found that capacity is an indispensable factor that must be considered in the study of

emergency shelter planning and deployment.

Quality of facility (B_2): Quality of facility is determined by three factors: provision of daily necessities, communication service and medical care facilities. The provision of daily necessities concerns with the supply of drinking water, food, tents and toilets. Communication service mainly encompasses deployment of guiding signs, emergency power supply facilities and communication facilities such as telephones and radios etc. With regard to the medical care the shelter should provide necessary medicines, equipments and facilities to conduct medical treatment and operation. It should be noted that daily necessity (C_2), communication service (C_3) and medical care facility (C_4) are difficult to quantitatively estimate. Questionnaire survey and scoring by professionals are combined to measure these indicators as substitutes.

Accessibility of shelter (B_3): Accessibility of shelter refers to the easiness for an emergency vehicle getting to the shelter from the affected area. The accessibility is associated with the distance from the affected place to shelter (C_5), number of connection of shelter to roadways (C_6) and category of highway connecting to shelter (C_7). Lessons have been learned from Wenchuan earthquake that due to the landslide blocking the roadway called “life-saving line” the rescue team couldn’t access ruined area to find survivors. This demonstrates how important of accessibility of shelter is in life-saving activity.

Definitions and calculations of the selected indicators

Capacity of shelter: Capacity is defined as the largest number of evacuees that an EES can accommodate. It is determined by the available refuge area of shelter and average refuge area per person. In order to ensure certain level of service quality, the average refuge area for each evacuee is taken as 3 m^2 . The formula for shelter capacity is given in equation 1. In the formula, the shelter’s available refuge area is 70% discounted, in order to leave some cushions to offset inaccuracy in number of evacuees in the prediction.

$$C = \frac{S \times 70\%}{3\text{m}^2} = \frac{(\text{available area} - \text{water area}) \times 70\%}{3\text{m}^2} \quad (1)$$

Where, C -Capacity of shelter;

S -Available refuge area (m^2). It is calculated by subtracting water area from the total available area.

Inside central city of Beijing, there are 30 shelters that were chosen as emergency shelters by 2010. In the study, we choose these 30 shelters to conduct capacity analysis. After data analysis, distribution of capacity of these shelters is shown in Figure 1. The 85th percentile and 50th percentile data are selected as threshold value and the capacity of shelter can be converted into standard score according to the threshold value. The score converting result is indicated in Table 1.

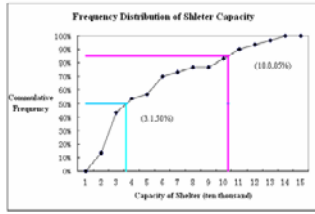


Figure 1. Frequency distribution for capacity of the 30 shelters.

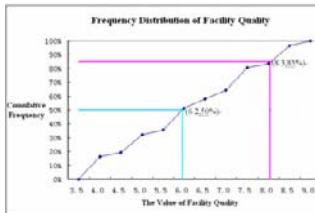


Figure 2. Frequency distribution for facility quality of 30 shelters.

Table 1. Standard Score for Capacity.

Capacity (C) (10^4)	≤ 3	(3,10)	≥ 10
Score of Capacity (C_s)	[0,50]	(50,80)	[80,100]

Quality of facility: In this study, quality of facility within EES is determined by provision of daily necessity, communication service, and medical care facility. Because it is hard to calculate these indexes quantitatively, professionals scoring method is used to measure these indexes. The evaluation results for quality of facility can be obtained by multiplying score of each sub-indicator given by each expert with corresponding weight. The calculation formula is shown in equation 2.

$$Q = x_2O_2 + x_3O_3 + x_4O_4 \tag{2}$$

Where, Q -Evaluation score for quality of facility of EES;

O_2, O_3, O_4 - Score given by expert for daily necessity, communication service and medical care facility of EES, $0 \leq O_2 \leq 10$;

x_2, x_3, x_4 -Weight for daily necessity, communication service and medical care facility, $x_2+x_3+x_4=1$.

The evaluation value of quality can be converted into standard value. The threshold value for ranking is determined using the same method as applied for shelter capacity. The distribution of facility quality of these thirty shelters is given in Figure 2 and the conversion result is shown in Table 2

Table 2. Standard Score for Facility Quality.

Quality of Facility (Q)	≤6	(6,8)	≥8
Standard Score (Q_s)	[0,50]	(50,80)	[80,100]

Accessibility of shelter: Accessibility of shelter is inversely proportional to evacuation distance that is proportional to the number of accesses and category of connecting roads. The calculation formula for accessibility is shown in equation 3.

$$A = \frac{\sum_{i=1}^n k \times D_i}{l}$$

(3)

Where, *A*-Accessibility of shelter;

n-Number of accesses of shelter;

l-Evacuation distance between affected place and shelter, (km);

D_i-Conversion value for road classification of road connecting to *i*th access;

k-Number of roads connecting to *i*th access.

The conversion value for road classification (*D*) referred in equation 3 is given in Table 3.

Table3. Conversion Value of Highway Category.

Highway Category	Freeway/ expressway	Major/ minor Road	Local street
Conversion Value <i>D</i>	3	2.5	2

After calculating accessibility of shelter, the value of accessibility can be converted into standard value. The threshold value for ranking is determined using the similar method as that for shelter capacity. The distribution of accessibility of these thirty shelters is given in Figure 3 and the conversion standard is shown in Table 4.

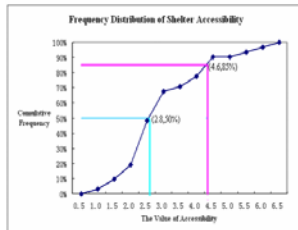


Figure 3. Frequency distribution for accessibility of 30 shelters.



Figure 4. Location of the 30 shelters.

Table 4. Standard Score for Accessibility.

Accessibility (A)	≤ 2.8	(2.8,4.6)	≥ 4.6
Stand Score of Accessibility (C_s)	[0,50]	(50,80)	[80,100]

Weight calculation of indicator

Analytic Hierarchy Process (AHP) theory is used to calculate the weight for each indicator. The procedure for weight calculating is summarized as following.

First, assess the relative importance among different indexes that belong to the same criterion layer and then structure the comparison matrix. Then, based on the comparison matrix, calculate ranking weight for each index using square root method and conduct consistency test for comparison matrix.

In the study, in order to calculate the value of x_2, x_3, x_4 mentioned in equation 2 and the ranking weight of capacity (B_1), quality of facility (B_2) and accessibility (B_3), two comparison matrix are needed and they are structured by expert scoring method.

Thirty experts are invited in the study to structure the comparison matrix, including traffic engineers, safety engineers, road and bridge designers and transportation professors. Based on the comparison matrix given by different expert, the final comparison matrix is obtained using group decision method. On the basis of the final comparison matrix, the value of x_2, x_3, x_4 and ranking weight p_1, p_2, p_3 for B_1, B_2 and B_3 are calculated as well as consistency test for comparison matrix is conducted. The final calculation results are

$$X = (x_2, x_3, x_4) = (0.598, 0.174, 0.228)$$

$$P = (p_1, p_2, p_3) = (0.500, 0.235, 0.265)$$

Model build-up

Based on the special demand of earthquake emergency, three assessment indicators are selected and they are calculated quantitatively. The ranking weight for each indicator is calculated using AHP theory. On the basis of all these analyses, the comprehensive evaluation model for EES is established using linear weighted theory. The model is shown in equation 4.

$$Z = p_1 C_s + p_2 Q_s + p_3 A_s \tag{4}$$

Where, Z —Comprehensive score of shelter, $0 \leq Z \leq 100$;

C_s —Standard score of capacity of shelter, $0 \leq C_s \leq 100$;

Q_s —Standard score of quality of facility of shelter, $0 \leq Q_s \leq 100$

A_s —Standard score of accessibility of shelter, $0 \leq A_s \leq 100$.

p_1, p_2, p_3 —The ranking weight for capacity of shelter, quality of facility, accessibility of shelter, $p_1 + p_2 + p_3 = 1$.

Based on the calculated score, relatively objective evaluation upon comprehensive response ability of shelter can be carried out. Emergency officials can select EES according to the standard and advice designed in Table 5. If the evaluation score is between 80 and 100, it means the comprehensive emergency response ability of shelter is excellent and the shelter can be selected. If the score is between 60 and 80, it means the comprehensive emergency response ability of shelter is good and the shelter can be used for earthquake emergency. When the score is between 40 and 60, it means the shelter is not very suitable for earthquake emergency; but if shelters with score higher than 60 can not meet the evacuation demand, the shelter can also be selected. If the score is lower than 40, the shelter can not be selected as EES. In a word, in the selection, shelter with higher comprehensive score has higher likelihood to be chosen.

Table 5 Level of service of EES

Condition Level	Evaluation Score	Comments for selection
A	(80,100]	Preferred
B	(60,80]	Good
C	(40,60]	Pending
D	≤ 40	Reject

CASE STUDY

In the study, thirty shelters mentioned above are taken as examples to apply the comprehensive evaluation model. Distribution of the thirty shelters inside Beijing is shown in Figure 4. Field survey for these shelters was conducted. Because of the limit of paper, all survey data are not listed.

According to the survey data, we calculate capacity and accessibility of each shelter using equation 1 and 3. At the same time, thirty professionals are invited to evaluate the quality of facility. Then we convert the value of capacity, accessibility and quality of facility into standard value according to the threshold value proposed in the study. Finally, we calculate the comprehensive evaluation value of each shelter using equation 4. Shelter with the high score should be considered first during decision process for EES choice.

It can be seen from Table 6 that the emergency response ability of the first three shelters is excellent and they can be selected for EES. Emergency response ability of shelters from the 4th to 13th is good and these shelters can be selected as EES according to the specific evacuation demand. Shelters from 14th to 23th are not very suitable for earthquake emergency, and are staying at the pending status. The remaining shelters can not be chosen as EES because the score is lower than 40.

Table 6. The Comprehensive Evaluation Result for These Thirty Shelters.

Ranking	NO.	Name	C	C _s	Q	Q _s	A	A _s	Z
1	21	D.P. Park	9	84	8.58	82	2.02	86	84.06
2	14	Y.D.D. Park	15.7	100	5.92	50	4.31	76	81.89
3	3	M.D.R. Garden	13.3	92	6.46	60	4.62	81	81.57
4	2	S.C. Open Space	12.3	88	3.61	36	6.21	95	77.64
5	7	M.C.Q. Park	6	70	7.47	73	4.50	83	74.15
6	5	H.C. Park	4.5	65	6.79	65	5.83	92	72.16
7	17	C.Y. Park	11.5	86	8.01	80	2.09	38	71.87
8	23	C.C. Gym	5	60	8.45	81	3.64	75	68.91
9	26	G.J.S. Garden	10.6	84	4.89	45	2.90	55	67.15
10	19	H.D. Park	9.3	78	6.62	60	2.24	40	63.70
11	27	B.H. Square	10	80	4.59	43	2.50	47	62.56
12	15	T.Y.G. Park	8.6	76	5.74	48	2.76	50	62.53
13	1	F.Y. Park	4.7	65	7.09	67	2.25	46	60.44
14	25	W.Q. Park	2.5	40	8.29	81	1.12	66	56.53
15	24	D.S Park	4	45	7.61	75	2.05	59	55.76
16	20	M.D. Park	4.3	58	7.08	67	2.19	40	55.35
17	4	D.T. Park	2.7	50	7.08	69	2.24	45	53.14
18	18	J.T. Open Space	6.4	70	3.61	34	1.63	30	50.94
19	12	F.Y. Park	2.2	35	6.35	56	4.38	76	50.80
20	13	W.S. Park	2.1	35	6.25	52	4.33	76	49.86
21	30	Olympic Park	2	32	8.09	82	2.76	50	48.52
22	29	Y'an Park	2.8	48	4.88	44	2.44	43	45.74
23	22	Y.G. Park	2.6	45	7.43	73	1.07	20	44.96

Note: In the study, Dongcheng District (marked in Figure 4) is the assumed evacuation area to calculate accessibility of the thirty shelters.

CONCLUSION AND FURTHER STUDY

The major work carried out in the study is summarized as following.

(1) Three assessment indicators are selected. Weight for each indicator is calculated based on the Analysis Hierarchy Process (AHP)

(2).The comprehensive evaluation model is built up using linear

weighted theory. Beside, a recommended table of level of service of EES is given.

(3)Thirty existing shelters that have already been constructed as emergency shelters in Beijing are selected as samples to apply and test the comprehensive evaluation model.

Compared to the previous studies, the selected assessment indicators are more objective and detailed. The specific demand of earthquake emergency and effect caused by traffic on emergency response ability of shelters are considered during indicator selection. A recommended table of level of service of EES is given, which can guide the emergency officials to select the suitable shelters for earthquake emergency. The evaluation result can provide technical support for emergency officials to select suitable shelters for earthquake emergency evacuation and rescue as well as reduce the arbitrary determination and subjectivity during the decision-making process. It will improve the existing shelters and guide the construction and planning of shelters in the future.

However, it is a preliminary study. Although some positive results have been obtained from this study, there is still room for improvement. In order to determine the ranking weight of each indicator, thirty experts including traffic engineers, safety engineers, road and bridge designers and transportation professors are invited to structure the comparison matrix. The number of experts in the study is not adequate. It is suggested that more experts be invited so as to establish more scientific and reasonable evaluation model.

REFERENCES

- Bao, S.P.(2005). "Study on Adaptation Assessment of Urban Refuge – Taking Jiayi City as an Example".*Taiwan Guoli University*.
- Lin, C.Y.(2010). "Research on Key Technologies of Decision Support System for Emergency Traffic Guarantee in Disaster." Jilin University.
- Qi, Y.(2005). "The Planning and Construction of Emergency Shelter in Beijing. Disaster" *Reduction in China*, Vol. 3, pp. 33-36.
- The 11th Professional Meeting of Seismological Society of China. (2006). Study on the Safety of Earthquake Emergency Evacuation and Shelter in Taiyuan. Chen, S.D., Zhang X.F., and Wang L.
- Wang, X., and Wu S.H.(2009). "An Evaluation on Urban Emergency Response Capability against Disaster Based on AHP-Method". *Shanxi Energy and Conservation*, Vol. 52, pp. 42-46.
- Wu, Z.Z., Huang D.J., Cai S.J., Jiang Z.G.(2005). "On assessment method to emergency shelter adaptation by using the statistic theory for fuzzy centralization". *Journal of Safety and Environment*, Vol. 5, No. 6, , pp. 100-103.
- Xiu, J.G.(2001). "Quakeproof, disaster reducing and community building. Cityand

Disaster”.*Reducing*, Vol. 8, pp. 16~18.

Zhou, X.M., Liu M., and Wang Y.(2006). “Emergency shelter amount confirm and location optimized”. *Journal of Safety and Environment*. Vol. 6, , pp. 118-121.

Key Concepts in the Development of a Transit Safety Management System

Dennis Y. N. Li

MetroSolutions Limited, Suite 1202, Pacific Plaza, 410 Des Voeux Road West, Hong Kong; PH: (852) 3421-1791; FAX: (852) 3186-2992; Email: dennis_li@metrosolutions.com.hk

ABSTRACT

The year 2011 saw a number of high profile incidents involving railways in China. While every railway is unique, there are some universal concepts in modern safety management. This paper aims to share some of the basic concepts involved in the development of a modern railway throughout its life cycle. The key concepts are: safety management as sound investment, top down approach, safety is everybody's responsibility, risk-based allocation of safety resources, continuous improvement, no heroics and team from others.

BACKGROUND

Traditionally, safety management for a public transport system is based on two key concepts, viz. statutory compliance and statistics oriented. The former is mandatory and the second is self-motivated. While these two key approaches are very useful, they do have their short-comings.

Many countries have developed comprehensive laws, rules, regulations and codes of practices governing industrial activities. There is some universal understanding of good practices concerning manual lifting, confined space working, asbestos handling, etc. However, these provisions are good for a production-line environment, but not so much applicable to a public transit environment where passengers also play a part in the production process. Examples of these passenger activities include boarding and alighting of vehicles, movements along lifts and escalators, activation of emergency facilities and use of the fare collection system.

Many operators also keep detailed statistics which are often classified into fatal accidents, major accidents, minor accidents, major property damage and minor property damage. However, statistics only cover events that have actually occurred but they do not tell potential problems (such as a major design fault) or near misses. Safety statistics are reactive, not proactive.

Modern safety management for transit operation calls for a risk-based approach. It is characterized by being

- Systematic
- Logical

- Proactive
- Risk-based and
- Traceable.

The adoption of this new approach calls for a change in the mindset for many decision-makers. This paper covers the changes in the Chinese mindset that would be required in the development of a risk-based safety management system for the Greater China Area.

CONCEPT 1 – IT IS AN INVESTMENT THAT PAYS

Many operators see safety as an expense item in the profit and loss account. Like all other expense items, it should be as low as possible. When the statistics look good, e.g. a low accident rate, then there is scope for further cost reduction. To make things worse, some operators resort to some cost-cutting measures which effectively compromise the overall safety performance. This may not have any immediate effect, but the risk associated with the cost-cutting measure may be increased substantially and the result is a situation whereby a major accident is just waiting to happen.

It may be seen from one perspective that safety management measures costs money, but accidents will cost more. Accidents entail both financial and social costs. On the financial side, it involves:

- Property damage
- Personal injury and payout
- Lawsuits and compensation
- Productivity loss
- System down time
- Cost of ratification
- Negative publicity and hence loss of competitive edge
- Negative impact on morale
- Loss of goodwill, resulting in loss of patronage and hence revenue
- High insurance premium
- Pressure from government and watchdog organizations

On the social costs side, it involves:

- Personal pain and loss to those involved
- Grief to family
- System down time causing passenger inconvenience and putting the strain on other operators or systems
- Loss of business and hence potential unemployment

Public transit derives its advantage from economies of scale. As mass carriers, the potential loss in event of an accident is much higher. On the positive side, as insurance companies nowadays adopt a risk-based approach to determine the insurance premium, it is possible to have reduction in insurance premium if some

positive safety measures are adopted. This has happened in the Hong Kong MTR whereby the insurance companies agreed to lower the premium upon the promulgation of its safety management system.

CONCEPT 2 – TOP DOWN APPROACH

Geert Hofstede, in his study of cross culture management around the world, used four cultural dimensions to compare people from different cultures. One of the major dimensions was power distance. He noticed a particularly wide power distance between the top and the bottom among Asians, in particular Japanese and Chinese. While there is nothing right or wrong about power distance, it must be pointed out that to be effective, high level commitment is important. High level commitment means more than a written safety management policy by the Chairman or Chief Executive Officer, it means that the top management is prepared to allocate resources for the implementation of the safety management system.

Top management also has two powerful tools to make a safety management system successful. One is the creation of a safety awareness culture, and the other is the effective communication of the safety message to all levels within the organization.

CONCEPT 3 – SAFETY IS EVERYBODY’S RESPONSIBILITY

Despite the resources, safety is not achieved merely by the establishment of a Safety Management Department, nor the promulgation of a safety manual. It is also not achieved by inspectors nor auditors who could only play the roles of watchdogs. Safety is only achieved by the concerted efforts of everyone within the organization. Management may buy a safety helmet, management may issue instructions that helmets should be used in certain areas, inspectors may do spot checks to ensure people wear them when required, but a helmet is only useful when the worker puts it on every time he goes to work without the need of any supervision.

To ensure that everybody understands his safety obligations, safety responsibilities statements may be issued to all front line staff, and their adherence to safety is part of the appraisal process.

CONCEPT 4 - RISK-BASED ALLOCATION

The reality is that there is never sufficient resource. No prudent manager can afford to address all safety issues in one go. The list of improvement is always very long and every department is jockeying for more funding to improve safety. To ensure that resources are allocated on a logical basis, some form of prioritization is in place to ensure that money is spent on items that pose the higher risks.

To be useful, risks have to be quantified. Risk may be defined as a function of probability (the likelihood of occurrence) and consequence (the severity of the damage). In essence,

$$\text{Risk} = \text{Probability} \times \text{Consequence}$$

The action triggers may be defined by a risk control matrix, which ranks the probability on one side, and the consequence on that other. A generic matrix is shown below:

Table 1. A Generic Matrix

Probability	Impact		
	High	Medium	Low
High	Extreme	High	Medium
Medium	High	Medium	Low
Low	Medium	Low	Minimal

All risks facing the transit operator have to be:

- Identified
- Registered
- Assessed
- Classified
- Allocated an owner to monitor the situation and to propose and implement mitigation measures
- Mitigated
- Evaluated for effectiveness

A central risk register which tracks the process for all these identified risks shall be maintained and reviewed from time to time so that top management is assured that all risk items are properly managed.

CONCEPT 5 – CONTINUOUS IMPROVEMENTS BASED ON ALARP PRINCIPLE

Based on the generic risk control matrix, it is the top priority to address the high probability-high impact items. Action is then followed by items falling into the high probability- medium impact or medium probability-high impact. The good news is – the 80/20 principle applies. In other words, usually it is possible to resolve 80% of the problem by using only 20% of the efforts.

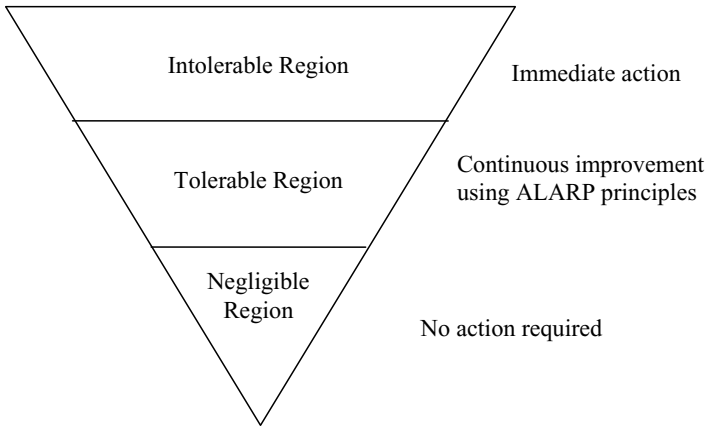


Figure 1. The Generic Risk Control Matrix

The question is how about the remainder of the risks. The above risk pyramid shows that risks may be broadly classified into three regions. Once the safety management is established and implemented, most of the risks in the intolerable region should be eliminated. This leaves the day to day work on continuous improvement to address the risks in the tolerable region. It is recommended that these risks should be addressed as far as possible, based on the As Low As Practicably Possible (ALARP) principle. In essence, the ALARP principle dictates that the cost of mitigation must not exceed that of the consequence.

CONCEPT 6 – LEARN FROM OTHERS

There is a saying – a good woodcutter has only one scar. The first cut will ensure he remembers safety for the rest of his life, and he will never repeat the same mistake again.

We all make mistakes. But the important thing is we have to learn from the mistakes. Not only must we learn from our own mistakes, we must also learn from other's mistakes as well. Of course, we also have to learn good practices from others as well.

We now live in a globalised world. There are international benchmarking organizations which can identify international good practices for its members to learn and consider if they want to adopt these good practices themselves. There are also international organizations such as UITP or ICTPA which create a platform for companies or people interact with each other so as to share information and exchange ideas.

CONCEPT 7 – NO HEROICS

We survive because we fear. Safety is just some simple acts that we do day in, day out. There is nothing specular or heroic about safety performance. As long as people stay vigilant, safety is achieved.

CONCLUSION

Every transit system is unique and calls for a different safety management system. In the Greater China Area, the key to success is top level commitment. With sufficient resources and strong communication, a systematic and logical safety management system may be developed to help the transit operator to achieve safety at reasonable expenses.

Application of Variable Weight Grey Clustering Method in Tunnel Collapse Risk Evaluation

Zhenyu YI

Senior Engineer, Registered Transportation Engineer, Hunan Provincial Communications Planning, Survey & Design Institute, Changsha 410008, China; PH (0083)-13973163427; email: yic2@163.com

ABSTRACT

Bases on the analyses of different factors contributing to tunnel collapse, this paper established a tunnel collapse risk evaluation model utilizing variable weight grey clustering method. To account for the significant variation of dimensions of each variable in the tunnel collapse model, empirical coefficients are introduced to modify each variable. The analysis shows that the updated variable weight grey clustering method is suitable for tunnel collapse risk evaluation in different locations, and is a usable tool to estimate risk level of tunnel construction.

INTRODUCTION

Variable weight grey clustering method, based on the grey systems theory originally proposed by Professor Deng (Deng 1982, 1983), is a new method aimed at studying problems with insufficient data points and large uncertainty (Liu 1989, 2010). The studying objects, typically known as gray clustering, has two different types: grey incidence clustering and grey whitenization weight function clustering. Grey incidence clustering is mostly used for the categorizing of objects within similar class in order to simplify a complex system, and is not suitable for risk evaluation. In contrast, grey whitenization weight function clustering is mainly used to check whether the observed objects belong to different pre-set types such that they can be treated differently. This method can be used for risk evaluation.

In tunnel construction, collapse of tunnel is possible during and after tunnel excavation, evenly after shoring and lining. Factors contributing to tunnel collapse generally include geological factor, design issue, construction error, and knowledge factor. Tunnel collapse not only delays construction schedule, increases project cost, but also causes life safety hazard to the construction personnel. As such, risk evaluation of tunnel collapse is very important. Difficulties for tunnel collapse risk evaluation come from many uncertainty factors and incomplete data base. In order to overcome these difficulties this paper establishes a variable weight grey clustering model , and utilizes it for the tunnel collapse risk evaluation during design phase.

FACTORS CONTRIBUTING TO TUNNEL COLLAPSE

During Tunnel excavation, due to earth pressure and stress redistribution around the opening, cracks could form in the surrounding weak rock, existing bedding and joints could become loosen and open. As a result, rock and soil fall off into the opening, typically called collapse. Collapse sequence is roughly as follows: 1)

Excavation; 2) plastic deformation of surrounding rock; 3) excessive deformation of supporting structure; 4) local damage of supporting structure; 5) instability of supporting structure and surrounding rock; followed by 6) tunnel collapse.

According to Guidelines for Highway bridges and tunnels risk assessment (Ministry of transport, 2011) and previous engineering practice, factors contributing to tunnel collapse can be roughly categorized as the following six areas as shown in Table 1:

- (1) Tunnel surrounding rock classification. The higher the class level of surrounding rock is, the greater the risk will be.
- (2) Geological structure. The more bedding and joint surrounding rock has, the greater the risk will be.
- (3) Tunnel depth (m). Shallower the tunnel depth is, easier the tunnel could collapse.
- (4) Cross-section dimensions of tunnel excavation. The larger the cross-section is, the greater the risk will be.
- (5) Strength of supporting and pre-supporting structure. The weaker these structures are, the greater the risk will be.
- (6) Construction Scheme. An imperfect construction scheme will more likely cause a tunnel to collapse.

Table 1: Tunnel Collapse Risk Evaluation Matrix

clustering indexes with grey classification	ID	1(Class I risk level)	2 (Class II risk level)	3 (Class III risk level)	4 (Class IV risk level)
1. surrounding rock classification	X1	<2	3	4	>5
2. Geological structure	X2	No hazardous configuration , 1	Potential landside risk, 2	Mixed Zone , 3	Fracture Zone, >4
3. Tunnel depth / diameter ratio (m/m)	X3	>2	2~1	1.5~0.5	<0.5
4. Tunnel Cross-section dimensions (m2)	X4	<50	50~150	100~200	>200
5. Strength of supporting and pre-supporting structure	X5	Large strength , 1	Relatively large strength , 2	Relatively weak strength , 3	Weak strength , > 4
6. Construction Scheme Design	X6	Very reasonable , 1	reasonable , 2	fair , 3	Not reasonable, >4

VARIABLE WEIGHT GREY CLUSTERING MODEL FOR TUNNEL COLLAPSE

When using variable weight grey clustering method to analyze the risk of tunnel collapse, as the first step a grey clustering model needs to be established, the factors contributing to tunnel collapse are treated as clustering indexes with grey classification, and the evaluation function for each clustering needs to be set up. Based on risk assessment guidelines (Ministry of transport, 2011), the risk level for tunnel collapse can be divided into four levels: I to IV. Correspondingly, when establishing grey evaluation model, four grey class is set up, i.e. $K=1,2,3,4$.

Treating the six main factors affecting tunnel collapse as six clustering indexes, $j=1$ to 6, and choosing each tunnel sector which needs collapse risk evaluation as the cluster objective, $i=1,2..n$, the tunnel collapse risk evaluation matrix can be set up as shown in Table 1.

Based on previous study, the value range of each clustering mark can be set up as shown in Table 2.

Table 2: Value Range of Each Clustering Mark

Clustering mark	X1	X2	X3	X4	X5	X6
Minimum	1	0	3	0	0	0
Maximum	8	5	0	300	6	7

WHITENIZATION WEIGHT FUNCTION OF EACH CLUSTERING MARK

The whitenization weight function for each clustering mark used for tunnel collapse risk analysis can be established based on triangle whiten function and principal rules of upper and lower limits for weight function, together with parameters given in Table 1.

Using whitenization weight function expression given in Liu (2010) together with data given in Tables 1 and 2, previous real tunnel collapse cases can be analyzed to reach the whiten weight function for each clustering indexes for tunnel collapse evaluation, $f_j^k(x)$, which is suitable for area studied.

The whiten weight function, $f_j^k(x)$, indicates the value of whitenization weight function of grey class, k , for clustering index, j , corresponding to an observation value of x . For example, $f_6^3(2)$ is the whitenization weight function value of grey class 3 (Level III risk) corresponding to clustering index 6 (construction scheme design) with an observation value of 2 (reasonable) .

Using the methods discussed above, the whitenization weight function of each clustering mark for tunnel collapse risk evaluation can be summarized as follows:

- (1) Four whitenization weight function of surrounding rock classification :

$$f_1^1(x) = \begin{cases} 1, & x \in [0,2] \\ 0, & x \notin [0,4] \\ \frac{4-x}{4-2}, & x \in [2,4] \end{cases} \quad (1)$$

$$f_1^2(x) = \begin{cases} \frac{x}{3}, & x \in [0,3] \\ 0.2, & x \notin [0,5] \\ \frac{5-x}{5-3}, & x \in [3,5] \end{cases} \quad (2)$$

$$f_1^3(x) = \begin{cases} \frac{x}{4}, & x \in [0,4] \\ 0.2, & x \notin [0,8] \\ \frac{8-x}{8-4}, & x \in [4,8] \end{cases} \quad (3)$$

$$f_1^4(x) = \begin{cases} 0, & x < 3 \\ \frac{x-3}{5-3}, & x \in [3,5] \\ 1, & x > 5 \end{cases} \quad (4)$$

(2) Four whitenization weight function of geological structure :

$$f_2^1(x) = \begin{cases} 1, & x \in [0,1] \\ 0, & x \notin [0,3] \\ \frac{3-x}{3-1}, & x \in [1,3] \end{cases} \quad (5)$$

$$f_2^2(x) = \begin{cases} \frac{x}{2}, & x \in [0,2] \\ 0.2, & x \notin [0,4] \\ \frac{4-x}{4-2}, & x \in [2,4] \end{cases} \quad (6)$$

$$f_2^3(x) = \begin{cases} \frac{x}{3}, & x \in [0,3] \\ 0.2, & x \notin [0,5] \\ \frac{5-x}{5-3}, & x \in [3,5] \end{cases} \quad (7)$$

$$f_2^4(x) = \begin{cases} 0, & x < 2 \\ \frac{x-2}{4-2}, & x \in [2,4] \\ 1, & x > 4 \end{cases} \quad (8)$$

(3) Four whitenization weight function of ratio between tunnel depth and diameter :

$$f_3^1(x) = \begin{cases} 0, & x < 1 \\ \frac{x-1}{2-1}, & x \in [1,2] \\ 1, & x > 2 \end{cases} \quad (9)$$

$$f_3^2(x) = \begin{cases} \frac{x}{1.5}, & x \in [0,1.5] \\ 0.2, & x \notin [0,3] \\ \frac{3-x}{3-1.5}, & x \in [1.5,3] \end{cases} \quad (10)$$

$$f_3^3(x) = \begin{cases} \frac{x}{2}, & x \in [0,1] \\ 0.2, & x \notin [0,2] \\ \frac{2-x}{2-1}, & x \in [1,2] \end{cases} \quad (11)$$

$$f_3^4(x) = \begin{cases} 1, & x < 0.5 \\ \frac{1.5-x}{1.5-0.5}, & x \in [0.5,1.5] \\ 0, & x > 1.5 \end{cases} \quad (12)$$

(4) Four whitenization weight function of tunnel Cross-section dimensions :

$$f_4^1(x) = \begin{cases} 1, & x \in [0,50] \\ 0, & x \notin [0,150] \\ \frac{150-x}{150-50}, & x \in [50,150] \end{cases} \quad (13)$$

$$f_4^2(x) = \begin{cases} \frac{x}{100}, & x \in [0,100] \\ 0, & x \notin [0,200] \\ \frac{200-x}{200-100}, & x \in [100,200] \end{cases} \quad (14)$$

$$f_4^3(x) = \begin{cases} \frac{x-50}{150-50}, & x \in [50,150] \\ 0, & x \notin [50,300] \\ \frac{300-x}{300-150}, & x \in [150,300] \end{cases} \quad (15)$$

$$f_4^4(x) = \begin{cases} 0, & x < 100 \\ \frac{x-100}{200-100}, & x \in [100,200] \\ 1, & x > 200 \end{cases} \quad (16)$$

(5) Four whitenization weight function of supporting and pre-supporting structure strength :

$$f_5^1(x) = \begin{cases} 1, & x \in [0,1] \\ 0, & x \notin [0,3] \\ \frac{3-x}{3-1}, & x \in [1,3] \end{cases} \quad (17)$$

$$f_5^2(x) = \begin{cases} \frac{x}{2}, & x \in [0,2] \\ 0, & x \notin [0,4] \\ \frac{4-x}{4-2}, & x \in [2,4] \end{cases} \quad (18)$$

$$f_5^3(x) = \begin{cases} \frac{x}{3}, & x \in [0,3] \\ 0, & x \notin [0,6] \\ \frac{6-x}{6-3}, & x \in [3,6] \end{cases} \quad (19)$$

$$f_5^4(x) = \begin{cases} 0, & x < 2 \\ \frac{x-3}{4-3}, & x \in [3,4] \\ 1, & x > 4 \end{cases} \quad (20)$$

(6) Four whitenization weight function of construction scheme design:

$$f_6^1(x) = \begin{cases} 1, & x \in [0,1] \\ 0, & x \notin [0,3] \\ \frac{3-x}{3-1}, & x \in [1,3] \end{cases} \quad (21)$$

$$f_6^2(x) = \begin{cases} \frac{x}{2}, & x \in [0,2] \\ 0, & x \notin [0,4] \\ \frac{4-x}{4-2}, & x \in [2,4] \end{cases} \quad (22)$$

$$f_6^3(x) = \begin{cases} \frac{x}{3}, & x \in [0,3] \\ 0, & x \notin [0,7] \\ \frac{7-x}{7-3}, & x \in [3,7] \end{cases} \quad (23)$$

$$f_6^4(x) = \begin{cases} 0, & x < 2 \\ \frac{x-3}{4-3}, & x \in [3,4] \\ 1, & x > 4 \end{cases} \quad (24)$$

WEIGHT FUNCTION FOR EACH RISK FACTOR AND RISK EVALUATION

Variable weight grey clustering model is suitable for problems with clustering indexes with similar properties and dimensions. When the dimensions of clustering indexes vary significantly, and/or the sample numbers of each clustering mark vary significantly, Variable weight grey clustering model should not be used without modification (Liu 2010). In the case of tunnel collapse model, since the dimensions of each clustering mark do vary a lot, empirical coefficient is introduced into the

model, as shown in Table 3. After the modification, each clustering mark can be considered dimensionless, and can be further used for the calculation of grey clustering coefficient.

In particular, the significance of each factor contributing to tunnel collapse might vary in different cases. Considering this variation, a weight factor, ω_j , is introduced to modify each clustering index. The value of ω_j could be recommended by experts based on analyses of previous tunnel collapse cases in local area.

Table 3: Empirical Coefficient for Each Clustering Index in Tunnel Collapse Evaluation

Clustering Indexes	ID	Empirical Coefficient
1. surrounding rock classification	X1	1
2. Geological structure	X2	1
3. Tunnel depth / diameter (m/m)	X3	2
4. Tunnel Cross-section dimensions (m2)	X4	0.02
5. Strength of supporting and pre-supporting structure	X5	1
6. Construction Scheme Design	X6	1

Assuming λ_j^k is the limit value of clustering index, j grey class, k , which can be obtained from multiplying values in Table 1 by the empirical coefficient given by Table 3; then assuming x_{ij} is the observation value of clustering index, j grey class, k , η_j^k is the weight function of clustering index, j grey class, k , and $f_j^k(\bullet)$ is the whiten weight function for clustering index, j grey class, k , we have (Liu 2010) :

$$\eta_j^k = \frac{\omega_j \lambda_j^k}{\sum_{j=1}^m \omega_j \lambda_j^k} \tag{25}$$

$$\sigma_i^k = \sum_{j=1}^m f_j^k(x_{ij}) \cdot \eta_j^k \tag{26}$$

which is the grey clustering coefficient for clustering index, j grey class, k ;
and

$$\sigma_i = (\sigma_i^1, \sigma_i^2, \dots, \sigma_i^s) = \left(\sum_{j=1}^m f_j^1(x_{ij}) \cdot \eta_j^1, \sum_{j=1}^m f_j^2(x_{ij}) \cdot \eta_j^2, \dots, \sum_{j=1}^m f_j^s(x_{ij}) \cdot \eta_j^s \right) \tag{27}$$

is the the clustering coefficient vector for clustering index i .

And we have clustering coefficient matrix as follows:

$$\Sigma = (\sigma_i^k) = \begin{bmatrix} \sigma_1^1 & \sigma_1^2 & \dots & \sigma_1^s \\ \sigma_2^1 & \sigma_2^2 & \dots & \sigma_2^s \\ \dots & \dots & \dots & \dots \\ \sigma_n^1 & \sigma_n^2 & \dots & \sigma_n^s \end{bmatrix} \tag{28}$$

Utilizing $\max_{1 \leq k \leq s} \{\sigma_i^k\} = \sigma_i^{k^*}$, the grey class of clustering objective i is then k^* .

K decides the corresponding tunnel collapse risk level.

CASE STUDY

According to geo-technical reports and design documentations for a tunnel construction, there are four sectors need tunnel collapse risk evaluation. The observation value of each clustering mark is listed in Table 4.

Table4: Observation Value of Clustering Indexes for a Tunnel Construction

Cluster objectives	1. k125+245 ~350	2. k125+500 ~600	3. k126+080 ~100	4. k126+850 ~950
surrounding rock classification	5	5	4	4
Geological structure	4	5	3	2
Tunnel depth / diameter ratio	20	2	1	10
Tunnel Cross-section dimensions	100	105	95	97
Strength of supporting and pre-supporting structure	1	2	2	3
Construction Scheme Design	2	1	3	1

Based on existing tunnel collapse cases in similar conditions, Experts recommended an appropriate weight factor for each cluster mark as given in Table 5.

Table 5: Experts Recommended Weight Factor for Each Clustering Indexes

Clustering Indexes	ID	Weight factor ω_j
1. surrounding rock classification	X1	1
2. Geological structure	X2	1.5
3. Tunnel depth / diameter (m/m)	X3	0.8
4. Tunnel Cross-section dimensions	X4	1.3

(m2)		
5.Strength of supporting and pre-supporting structure	X5	1.8
6.Construction Scheme Design	X6	2.0

Using Equation 25 and data give in Table 5, the weight function for 4 grey classes, η_j^k , for each clustering index, can be calculated as in Table 6.

Table 6: Weight Function for Each Grey Class of Each Clustering Index

Clustering index	η_j^1	η_j^2	η_j^3	η_j^4
X1	0.16949	0.16129	0.15748	0.15528
X2	0.12712	0.16129	0.17717	0.18634
X3	0.27119	0.12903	0.06299	0.02484
X4	0.11017	0.13978	0.15354	0.16149
X5	0.15254	0.19355	0.21260	0.22360
X6	0.16949	0.21505	0.23622	0.24845

Then, based on equations 1 to 24, the value of each whiten function can be calculated. After that, using equation 26 to calculate clustering coefficient for each grey class of each clustering index, and using equations 27 and 28 to calculate clustering coefficients matrix. The results are listed in table 7.

Table 7: Clustering Coefficients and Results for Different Cluster Objectives

Cluster Objective	Class I risk level	Class II risk level	Class III risk level	Class IV risk level	Grey Class
1.k125+245~350	0.37712	0.73118	0.57480	0.19876	2
2.k125+500~600	0.76695	0.38344	0.35039	0.15528	1
3.k126+080~100	0.13686	0.72957	0.84469	0.30745	3
4.k126+850~950	0.56263	0.65602	0.65169	0.18944	2

From the above table it can be seen that the grey class of risk level for tunnel sector k126 +080 ~ 100 is 3, which corresponds to a grade III collapse risk. It has the highest risk possibility in all the tunnel sectors evaluated. Based on this estimate, it is suggested that the shoring design and construction scheme for this tunnel sector shall be adjusted. In addition, during construction phase, the tunnel designer shall pay attention to any anomalies occurred during construction as well as estimated collapse possibility, adjust its design in time to ensure the safety of the construction. Meanwhile, the construction contractor shall develop his own tunnel collapse emergency plan to reduce its damage and hazard to construction personnel to a

minimum degree in case the collapse occurs.

CONCLUSIONS

Large cross-section and relatively flat opening profile leads to high level risks inherited in highway tunnel construction, including tunnel collapse. In this paper, Variable Weight Grey Clustering Method is utilized for tunnel collapse risk evaluation. It shows that this method can be effectively employed to reduce risk of tunnel collapse.

It needs to be pointed out the factors contributing to tunnel collapse might vary for tunnels in different locations. Therefore, when establishing variable weight grey clustering model for tunnel collapse, extensive study and data collection of previous existing tunnel collapse are needed. From these data, a vital portion of the variable weight grey clustering model, the weight factor based on previous experience, could be built. Otherwise, the analysis results from this method will not be reliable.

REFERENCES

- Deng J., Control Problems of Grey systems. Systems and Control Letters, Vol.1, No.5, March 1982.
- Deng, J., Fundamentals of Grey System, National defense industrial Press, BeiJing, P.R. China , 1985
- Liu, S. , On Perron-Frobenius Theorem of Grey Nonnegative Matrix , The Journal of Grey System, 1989: Vol.1, No.2, pg157- 166
- Liu S., Grey System Theory and its Application, Science Press, BeiJing, P.R. China 2010
- Ministry of transport of the People's Republic of China, Guidelines for Highway bridges and tunnels risk assessment, 2011

Analysis of Influence upon the Beijing-Tianjin Intercity High Speed Railway by a Subway Shield Tunnel Crossing below

Gancheng XU¹, Chengxue LI¹ and Houyu WANG¹

¹The Air Force Engineering Design & Research Institute, China. E-mail: Xugancheng_xgc @163.com

ABSTRACT

This paper chooses the section between the stations of Majiapu Donglu and Yongdingmenwai Dajie on Beijing subway line 14 as the object, adopting a method of numerical simulation to analyze the function of grouting reinforcement in control of deformation of the earth surface while a shield tunnel crosses below the Beijing-Tianjin intercity high speed railway. A 3D numerical model is made to simulate the construction process of a shield tunnel crossing below a high speed railway with a top speed of 350km/h and the requirement of a differential settlement of less than 5mm between the two rails. The calculation result indicates that grouting reinforcement to the stratum of a certain extension of the crossing section can effectively control the settlement of the existing railway caused by shield tunneling so as to ensure safety operation of the railway. And the behind-segment grouting parameters and soil compartment pressure in the shield structure gained in the study can be instructional for further design and construction of tunnels.

FOREWARD

Beijing subway line14 starts in the west from Dahuichang Donglu, Changxindian to the west of Fengtai River, running through Yongding River and turning northeast along the Beijing-Shijiazhuang Freeway, then crossing below the Freeway and turning east, entering into Beijing South Railway Station by way of Caihuying Qiao and extending eastward to Xidawang Lu, and then turning north to Chaoyang Park, running northeast across the 4th Ring Road and entering Jiuxian Qiao area and at last coming to Laiguangying.

As a first-run section of the whole project of Line 14, the railway between the stations of Majiapu Donglu and Yongdingmenwai Dajie shall cross the Beijing-Tianjin intercity high speed railway in the shape of a small radius curve. The Beijing-Tianjin intercity high speed railway, which is the first one in the country, has a top speed of 350km/h. Both the left line and the right line of the shield structure will cross below the railway in two times while ensuring absolute safety of the operation of the railway.

The construction of shield crossing, as a source of super risk, is a joint action of multiple uncertain factors. A tunnel crossing below a railway may cause deformation of the track which will not only increase the impact between wheels and rails, but also aggravate damage to the bedding and structure of the track and bring severe effect on the safety of railway operation. At present, there are two measures adopted to ensure safe operation of existing railway: one is to reinforce the

foundation including grouting reinforcement, etc.; the other is to strictly control the construction parameters of shield tunneling so as to decrease disturb to the stratum. This paper chooses the above-mentioned section on Line 14 as the object, adopting a method of numerical simulation to analyze the function of grouting reinforcement in control of deformation of the earth surface while a shield tunnel crosses below an existing railway. The study can serve as a reference for further design and construction of similar projects.

INTRODUCTIN

The section of the shield structure starts from Majiapu Donglu Station and turns east, crossing Zhonghaiziyu Park, going east along the programmed Songlin Nanjie, and turns south at the east side of the Park, crossing the Beijing-Tianjin intercity high speed railway, and joins to Yongdingmenwai Dajie Station at the south side of the road. There are two curves (350m, 300m) on the route and the buried depth of rails are within the extent of 19.8m ~ 19.0 ~ 21.7m. The starting well of the shield structure will be at the west end of Yongdingmenwai Dajie Station, while the receiving well at the east end of Majiapu Donglu Station.

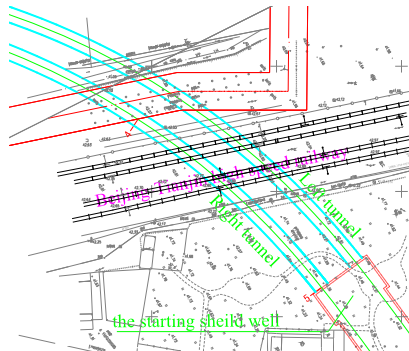


Fig.1 Plane relationship of the positions of the subway route and the intercity railway

At the location of the subway mileage K20+420~K20+445, the route goes slantwise down at an angle of 56° crossing below the Beijing-Tianjin high speed railway. The downward route of the subway is a small radius curve (300m) which is only 46m away from the starting well. Figure 1 shows the relationship of the planimetric positions of the subway route and the intercity railway.

Hydrogeological Condition

This section of the project is located at the lower part of the Yongding River diluvial sector. The landform mainly belongs to plain of the 4th Diluvial Epoch with obvious Epoch 4 deposition rhythm. The stratum has been formed by the alternative depositing of clay, silty soil, sand soil and gravel soil. The gravel soil gradually becomes thinner from west to east, and the buried depth of base rock is larger than 50m.

Within the surveying zone there are mainly perched water, phreatic water and confined water. The perched water is mainly in the layers of artificial fill, silty soil and sand soil, and has the characters of distribution uneven, water level discontinuous and with big variation. The phreatic water is mainly gained from lateral runoff, together with atmosphere precipitation and the vertical infiltration of perched water. The phreatic water drains in two ways: into lateral runoff and downward to be confined water. Confined water is mainly in the layers of sand soil, pudding stones and pebbles, among which there are several water insulation layers of clay.

NUMERICAL MODEL

Range of simulation and calculation parameters

The numerical model chooses a length of 60m along the subway route and a depth of 20m below the sector structure. From the experience of construction of shield-structure correlative stratum in Beijing or other domestic areas, the settlement groove of shield structure construction is about 15~20m in width, so the simulation chooses 18m at the two sides outside the tunnel structure, which is 3 times of the diameter of the hole. The level of track of this section is about 19.9m, the buried depth of the structural soleplate is about 23.5m, and the distance is 22m from the foundation of the intercity railway straightly above the tunnel to the longitudinal edge of model.

The FLAC3D numerical model is shown in Fig. 2 as follows. The earth body structure chooses the Mol-coulomb model inside the FLAC3D. On the basis of the geological survey report (“Survey Report on the Rock & Earth Work of the 02 Contract Section of Beijing Subway Line 14 Project”), the numerical model chooses values for the layer distribution and the mechanical parameters of the earth body as those shown in the following Table 1.

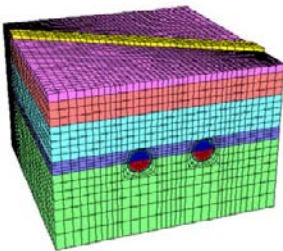


Fig.2 Numerical model

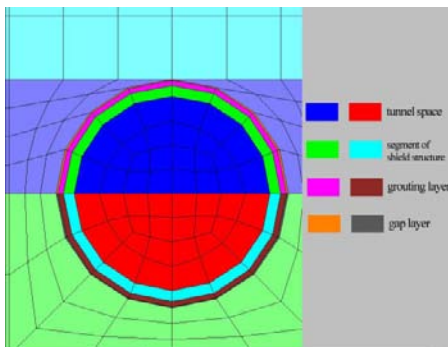
Table 1 Mechanical indexes of the earth layers

Layer	Thickness (m)	Weight (kN/m ³)	Flexibility modulus (MPa)	Poisson ratio	Adhesive power (kPa)	Friction angle (°)
silty clay plain fill	2	18.9	5	0.3	6	10
silty clay	6	19.7	7	0.3	30	15
silty sand	9	19.9	25	0.25	0	30
silty clay	3.2	19.7	7	0.3	30	15
silty soil	4.5	19.8	20	0.3	8	25
pebbles	15.5	22.0	45	0.2	0	40

Simulation of Shield Structure

Three annular entity units of different thickness are specially founded to simulate the construction process of shield tunneling, respectively used as segments of the shield structure, the grouted layer behind the tube wall, and the gap layer caused by over excavation (See in Fig. 3).

Among which, the tube wall is 300mm thick, the grouted layer 150mm. And the thickness of the gap layer is 20mm on the top and bottom of the grouted layer to simulate the over excavation since the outside diameter of the cutter is larger than that of the shield structure, while it is 50mm on the left and right sides of the grouted layer to simulate the over excavation owing to tunnel curve. And the grouted layer unit between the excavation side and the shield tail is used as the shell of the shield machine in order to simulate the propelling of the machine in the tunnel.

**Fig.3 Layers of the shield simulation**

Simulation of the Construction Process of Shield Tunnelling

Method of Simulation of the Shield Tunnelling Construction

Apply restrictions to the sides and bottom of the model from normal direction to make it balanceable in the actions of dead weight or train load (considered as static

load with a value of 30kPa) and generating an initial stress field; and conduct the simulation the construction process of shield tunneling after clearing the node displacement.

First, simulate the process of entering of the shield machine into the hole. The length of the shield machine chooses 8.4m to match the setting of length of the unit grid in the longitudinal direction of the tunnel; and in the process of the simulation, the shield machine will move forward at each step a distance of 1.2m which is the width of a segment ring. It is realized through the following steps:

- Excavate an soil body of tunnel with the length of a width of a segment, including the pre-defined tunnel soil body, segment ring, grouting layer and gap layer;
- Endow the gap layer unit with mechanical parameters far less than those of the surrounding earth body so as to simulate the space around the shield machine caused by over excavation;
- Endow the grouting layer unit with mechanical parameters of the shield shell to simulate the supporting function of the shield machine itself to the surrounding earth body;
- Apply a pressure of a soil compartment on the excavation face so as to keep it stable and balanceable;
- Run the command “solve” to start calculation.

Following these steps, go on with the next step forward of the shield structure until the whole structure entering into the tunnel.

Since the whole shield structure enters into the earth body, every step of the following excavation calculation should be based upon not only the above shell simulation, but also the simulation of installation of segments at the tail of the shield structure and grouting behind the segments. In order to reflect the induration of the grouting material, the grouting layer is endowed with two kinds of property: (1) low rigid grouting material before freezing, whose flexibility modulus equals to the grouting pressure; (2) grouting material after freezing. The simulation of this period of construction takes the steps as follows:

- Set the newly excavated section of grouting layer as the shell;
- Change the material property of the unit of the last section of grouting layer as that of the grouting material before freezing, and meanwhile, set the sheet layer unit closest to the interior of this section of grouting layer as the segment of the shield structure.

Repeat steps 1 and 2 until the pre-freezing grouting material reaches a width of three segment rings; set the first ring of low rigid grouting material as that after freezing, which means that the induration of the grouting material is supposed to be lagged by three segment rings. The segment of the shield structure, the grouting layer and the gap layer are all simulated with flexible material. And the calculation parameters are chosen as shown in Table 2

Table 2 Calculation Parameters of the Model

Material	Flexibility modulus (MPa)	Poisson ratio
Segment	34500	0.25
Grouting layer after freezing	150	0.25
Gap layer	0.0067	0.3

Simulation of the Construction Process and Results of the Calculation

The Jing-jin intercity train has a top speed of 350km/h, requiring a differential settlement of less than 5mm between the two rails. It belongs to the source of risk of super grade and therefore brings forward higher requirements for the construction of the crossing-below section of the subway. The method of grouting reinforcement to the stratum of this section is adopted so as to ensure that the subway construction has no effects upon the normal and safe operation of the intercity railway.

The extension of stratum for reinforcement includes: a width of a single diameter of the hole on the two sides of the tunnel structure of the section; and a depth within the scope from the bottom plate of the tunnel structure to 12m above the structural ceiling plate. And the flexibility modulus of the earth body of the reinforced stratum is chosen as 150MPa.

Fig. 4 is the contour of settlement of the stratum after the run through of the left line. It shows that the settlement value is 14.29mm at the vault of the tunnel, and the maximum value of surface settlement is 5.01mm appearing just above the tunnel.

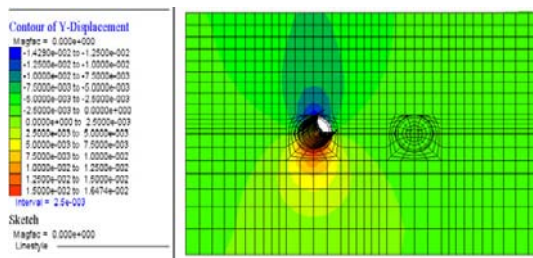


Fig.4 Contour of settlement after the left line runs through

Fig. 5 is the contour of settlement of the stratum after the run through of the right line. The calculation result shows that the settlement values at the vaults of the left and the right line of the tunnel are respectively 17.18mm and 16.73mm, while the maximum value of surface settlement reaches 8.57mm appearing at the position of the symmetrical surface of the two tunnels.

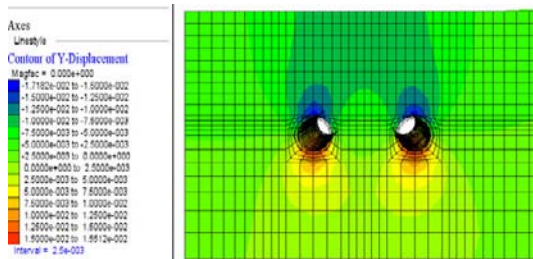


Fig.5 Contour of settlement after the two lines run through

The settlement of the railroad foundation just above the tunnel caused by the construction is basically proportional. Fig. 6 is the curve of settlement of the midpoint of the railroad foundation just above the left line of the tunnel (called “point A”) along with the driving of the excavation face. It shows that, during the construction of the left line, the value of settlement of point A increases quickly along with the approaching of the excavation surface and then tends stable as the excavation surface crosses below the point and drives forward; while during the construction of the right line, there is still a certain additional settlement at point A, since the settlement caused by the construction of the right line accounts 34% of the total volume of settlement.

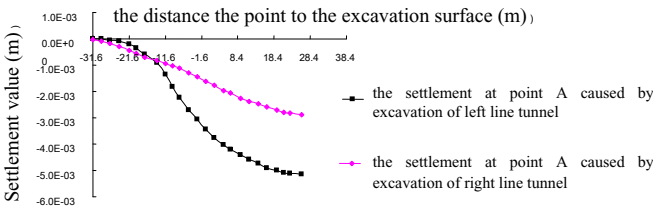


Fig. 6 Curve of settlement of Point A

Fig.7 is the curve of settlement trough of the railroad foundation after the completion of construction of the two lines, showing that the maximum settlement reaches 8.57mm at the position of the symmetrical surface of the two tunnels; and the settlement of the railroad foundation above the left and right line of the tunnel is respectively 8.03mm and 7.86mm.

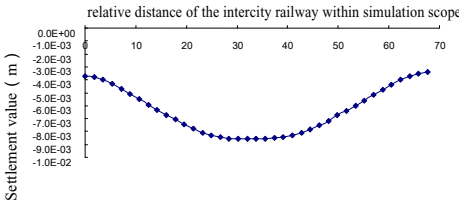


Fig.7 Curve of settlement trough

Thereafter, choose parameters of the original stratum to do the similar numerical simulation of the construction process and get the contour of stratum displacement after the completion of the two lines of tunnels as shown in Fig. 8. And after the construction of the shield structure, the settlement of the railroad foundation above the left and right line of the tunnel is respectively 26.9mm and 25.9mm. It can be seen from comparison with the calculation results in the conditions of reinforcement that grouting reinforcement is obviously effective on settlement control.

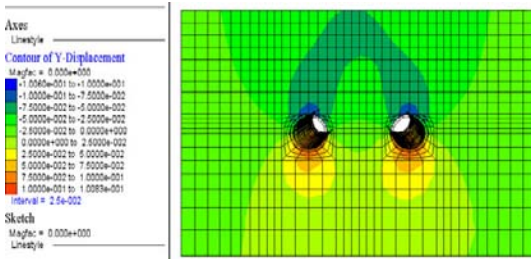


Fig.8 Contour of settlement after two lines run through

CONCLUSIONS

The result of the numerical simulation shows that:

- The stratum deformation caused by shield construction has obvious 3D character. The stratum displacement varies a lot in vertical and horizontal directions at different positions along the tunnel axis.
- Over excavation due to the curve of the route may cause obvious settlement of earth surface and horizontal displacement of the earth body around the tunnel.
- With other factors unchanged, the value of earth surface gets the lowest when the soil compartment pressure is close to the original stress of the stratum; it will cause sinkage of the surface in front of the excavation surface when the soil compartment pressure is less than the original stress of the stratum; while it will cause rise of the surface when the soil compartment pressure is larger than the original stress of the stratum; and it will cause settlement of surface behind the excavation surface whether when the soil compartment pressure is larger or less than the original stress of the stratum.
- The value of surface settlement is inversely proportional to the pressure of grouting, meaning that the value of surface settlement will get lower while the pressure of grouting goes higher.

Against the above-mentioned problems, it is suggested to adopt the following measures in the construction of the shield tunneling:

- Grouting reinforcement to the earth body above the tunnel is effective upon controlling surface settlement. In order to ensure safe operation of the intercity railway, grouting reinforcement should be conducted ahead to the stratum within the affected extent in construction. Choosing of grouting parameters should be based upon the site test to ensure that the flexibility modulus of the earth body is not less than 150MPa after grouting reinforcement.
- The soil compartment pressure should be set the value of the side pressure of the stratum during construction so as not to affect the driving speed while decreasing surface settlement. Meanwhile, in the process of shield driving, the grouting pressure should be taken as a main parameter which should be controlled during construction in order to avoid over settlement or rise of the earth surface.
- Enhance supervision and take control of the driving speed of the shield.. Communicate with the designing and construction organizations when larger deformation occurs and adjust construction parameters.

REFERERNCES

- LI Lin, “Shield Structure Tunnel Construction in Soft Ground[J]”, *Urban Mass Transit*, No. 3, 2005, pp. 50-55.(in Chinese)
- BAI Tinghui, “The Protection Technique During Passing of Shield Through the Operating Metro Tunnel[J]”, *Underground Space*, Vol. 19, No. 4, 1999, pp. 311-316.(in Chinese)
- Peck R B, “Deep Excavations and Tunneling in Soft Ground[A]”, *Proceedings of 7th International Conference on Soil Mechanics and Foundation Engineering[C]*, Mexico City: *State of the Art Report*, 1969, pp. 225-290.

Design of the SR522 Snohomish River Bridge under Multiple Hazards

Hongzhi Zhang, Ph.D., PE

WSDOT/Bridge and Structures Office, Linderson Way SE, Tumwater, WA 98501,
USA, PH (360) 705-7171, Fax (360) 705-6814, Email: zhangho@wsdot.wa.gov

The Snohomish River Bridge is an 1800 foot (one foot equals to approximately 0.3048 meter) long 40 foot wide curved steel plate girder bridge. The bridge has nine piers, including two end piers and seven intermediate piers. Three piers are located in the river and four are located in the flood plain.

The pier arrangement is very similar to the existing bridge that is located immediately to the south of the new bridge (see Figure 1).



Figure 1 Existing Snohomish River Bridge

The hydraulic study¹ indicated that the 600 foot wide river which is currently flowing between Piers 2 and 4 may migrate to any location in the flood plain. Potential river migration may wash away up to 27.5 feet of soil from the river bottom and local scour may wash away an additional 24 feet of soil near the piers. And if all of the piers were not placed parallel to the assumed river flow direction, the scour depth could double. The design had to make the bearing of all the intermediate piers parallel to the flow direction, with a resulting skew angle of 35 degrees for Piers 2 to 5, and gradually increasing up to 51degrees for Piers 6 to Pier 8. The two end piers retained their original alignment (See Figure 2&3).

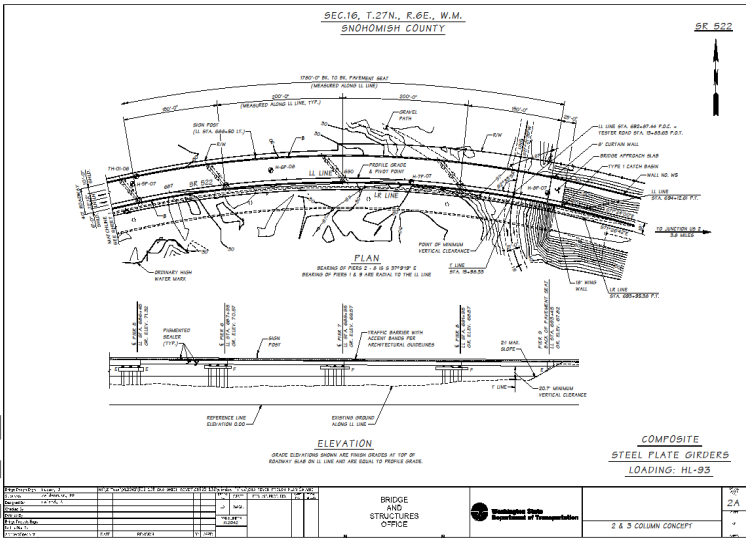
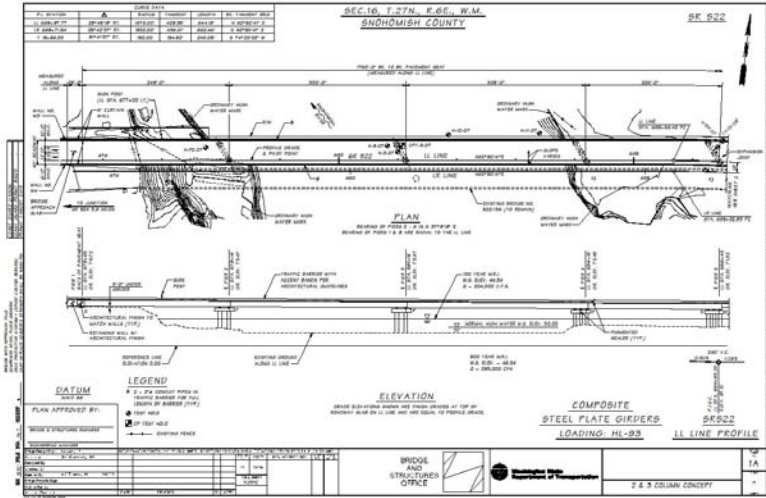


Figure 2&3 Layout of the Snohomish River Bridge

The geotechnical report² also identified multiple liquefiable soil layers at every pier locations, a soft clay layer approximately 130 feet below ground surface, with artesian water below the clay layer at Piers 6 to 9. Therefore, the shafts could not be

founded deeper than approximately 100 feet beneath the current ground surface. The foundation design was then modified from single 12 foot shafts (recommended in preliminary design) to two or three ten foot diameter shafts at each intermediate pier. Because of the AASHTO³ group reduction factor (0.77 for 3D spacing and 0.54 for 2D), the vertical resistance of the shaft foundation were far below the demands.

Under these special circumstances, the decision was made to modify the AASHTO group reduction factors for the vertical resistance capacity to 1.0 for 3D shaft spacing and 0.9 for 2D shaft spacing. The proposed change of group reduction factor was proposed to AASHTO and was accepted by AASHTO in May of 2011 under the condition that temporary casing must be used during the shaft excavation.

A total of 19 ten foot diameter shafts will be installed at the seven intermediate piers and at least two intermediate piers, Pier 7&8, will require base grouting (tip grouting), even with the modified group reduction factors (see Figure 4). This would be the first highway bridge design in Washington State using the base grouting (tip grouting) technique to increase the vertical bearing capacity of the drilled shafts. Ground improvements were also required at Pier 9.



Figure 4 Tip Grout (Base Grout) for Pier 7 & 8 (the existing bridge is on the left)

Originally, this project was designed using the 2009 AASHTO Guide Specifications for LRFD Seismic Bridge Design⁴. The seismic spectrum for the period of 0.2 second

and 1.0 second are 0.96g and 0.5g respectively for a 5% exceedance in 50 years event (975 years return period, see Figure 5).

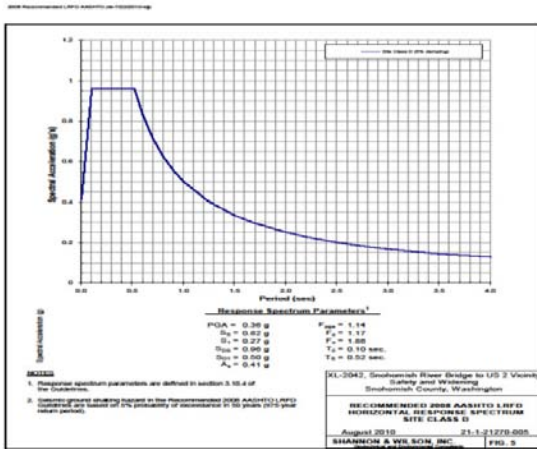


Figure 5 Seismic Response Spectrums for the Snohomish River Bridge

The LRFD Bridge design is based on the probability of the loads and the resistances. However, each of the applied loads may be studied and summarized with a conservative assumption to cover the worst case scenario. In reality, the worst case scenario of two or more hazards occurring simultaneously should have a very low probability. Under the multiple hazards, if the worst case scenario of all hazards are superimposed and then applied to a bridge at the same time without any justifications, the bridge design could be too conservative and the bridge construction would be too expensive.

The current AASHTO does not have a clear policy toward the multiple hazards and therefore, a reduction factor of 0.25 of local scour was superimposed and applied to the seismic design of the Snohomish River Bridge if soil liquefaction was also considered.

Since the bridge site is located in the high seismic zone, the “Displacement Based Seismic Design” or “Performance Based Seismic Design” was utilized. According to the AASHTO Guide Specifications for LRFD Seismic Bridge Design, 2009, the column should be designed using Strength and Service Limit States as the first step. The structure is then analyzed with seismic loads to determine the demand of the displacements.

Finally, a “Pushover Analysis” is required to check the displacement capacity of the column. If a local or global instability occurs before the column displacement reaches displacement demand that was calculated by the spectrum analysis, the column has to be redesigned.

If the displacement of the columns in Pushover analysis reaches the displacement demand, a Ductility Factor, μ_D , will then be calculated at the same time to compare with the requirements in the AASHTO Guideline.

If column displacement capacity (from the Pushover analysis) is adequate, the AASHTO Guideline requires an amplification factor of 1.2 be applied to the plastic moment of the column for the design of the members connecting with the column (so called “protected members”, e.g. cross beam on the top of the column and the foundation at the bottom of the column) because the connecting members will be designed in the elastic range. An additional amplification factor of 1.25 shall be applied to the drilled shaft design to cover the uncertainty of the surrounding soil.

According to WSDOT practice, large drilled shafts are usually three feet larger in diameter than the column they support, in order to meet construction tolerances in the overlapping zone of the two rebar cages. In normal circumstances, the shaft design should have the minimum ratio of longitudinal reinforcement (0.75% A_g ratio of longitudinal reinforcing for drilled shaft is the minimum requirement at WSDOT⁵).

However, if the top 30 to 40 feet of surrounding soil of a shaft is very poor soil or liquefiable soil, the plastic hinge moment of the column could develop a huge flexural and shear demand on the shaft and create serious challenges for the shaft design.

The Snohomish River Bridge was designed twice, the first time by following the AASHTO Seismic Bridge Design Guideline and the second time by using seismic isolation bearings.

With the reduction factor of 0.25 for the local scour depth, the top $27.5 + 0.25 \times 24 = 34.5$ feet of soil surrounding the shafts was assumed being washed away in the seismic design of the bridge.

By applying the plastic moment and associated shear of the six and a half foot in diameter column on the top of the shaft, the shafts had to be designed with 3% longitudinal reinforcement for flexural and three I-shaped structural steel members for shear (see Figure 6). The construction cost would be very high and the heavy rebar cages would create constructability problems, especially for the piers in the middle of the river (constructed from work bridges).

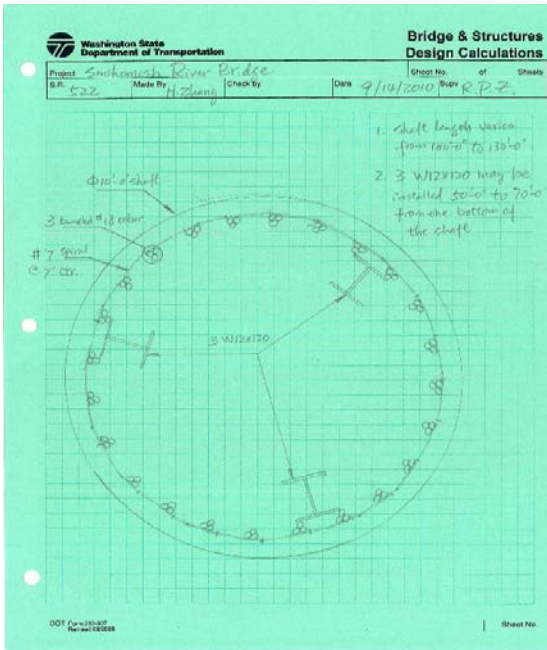


Figure 6 Section of the Ten Foot Shaft Design

For the second time of the design, the Friction Pendulum Isolation Bearing was selected over the disc bearing to reduce the lateral seismic force. According to the “Guide Specifications for Seismic Isolation Design, Third Edition – July 2010”⁶, the substructure would have essentially elastic response in a design level earthquake (meaning no post-earthquake repair is required, theoretically).

A few years ago, the Friction Pendulum Isolation Bearing had a top and bottom concaved steel plates. A slider was inserted between the two concaved plates and could slide in 2D on the surface of the plates during a strong earthquake. In recent years, the bearing was modified by adding a smaller slider inside of the larger slider (see Figure 7) to dissipate more seismic energy. It’s called Triple Friction Pendulum Bearing.

By using Triple Friction Pendulum Bearings on the Snohomish River Bridge, the maximum lateral seismic load that can be transferred from the superstructure to the substructure is reduced to about 10% of the Dead Load of the superstructure. It was

the first time that the isolation designed was used on the design of a new highway bridge in Washington State.

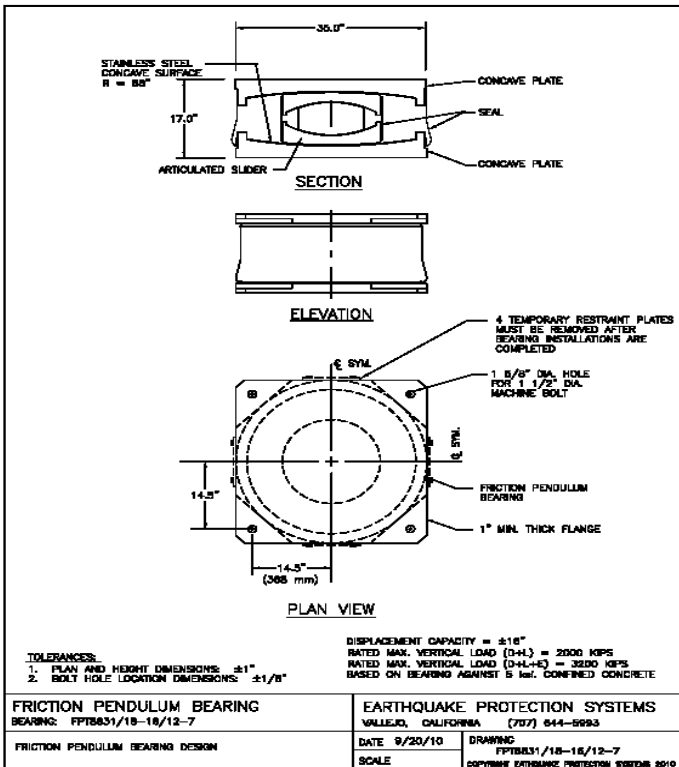


Figure 7 Triple Friction Pendulum Isolation Bearing

With the Friction Pendulum Isolation Bearing, the longitudinal reinforcement ratio in the drilled shafts was reduced to 1% for Piers 2 & 3 and to 0.8% for Piers 4 to 8. The shear reinforcement was also greatly reduced. This represents more than two million pounds of structural steel and steel reinforcement reductions. The total length of the drilled shafts was also reduced. The total net saving is estimated for a minimum of \$2,000,000, approximately 10% of the total construction cost of the bridge. The much lighter rebar cages for the drilled shafts will greatly improve the constructability of the drilled shafts and better fit the very tight fish window for in-water pier constructions.

The construction of the SR522 Snohomish River Bridge was awarded in the summer of 2011. Currently, the contractor is working on the installations of the drilled shafts with oscillator (see Figure 8), because of the potential existence of large size boulders in the vicinity of the bridge site. It will take two years to complete the construction of the substructure. The bridge construction will be completed in 2013.



Figure 8 Oscillator was setup for the drilled shaft constructions

Model Test Studies on Ground Subsidence and Cracks Induced by Tunneling in Weak Rock Mass with High Water Content

Wei, X.¹ and Wang, G.²

¹School of Civil Engineering, Southwest Jiaotong University, P.O. Box 610031, Chengdu, P.R. China; email: weixinghl@163.com

²Ertan Hydropower Development Company, P.O. Box 610051, Chengdu, P.R. China; email: wanggang@ehdc.com.cn

ABSTRACT

Tunneling in weak rock mass with high water content may cause large ground movements and cracks, which may cause heavy damage to adjacent buildings and overlying facilities. During the construction of Beigang Tunnel, a railway tunnel buried in highly fractured and completely weathered rock mass rich in groundwater, serious collapse occurred. Taking the Beigang Tunnel as a prototype, model tests were conducted to study the pattern and law of ground subsidence and cracks when tunneling in weak rock mass. It was found that (1) water flow, which induced soil erosion, took the main responsibility for the tunnel's collapse, (2) before the appearance of the cracks, the distribution of surface settlements at the transverse section can be well described by Peck's Normal Probability Curve, (3) collapse happened first at the top of the tunnel and then developed upwards to form an arch shaped bearing structure; (4) the two largest cracks on the ground surface occurred at the early stage of collapse and were located on the either side of the tunnel axis, and settlements and cracks on ground surface developed mainly in the region between the two largest cracks.

INTRODUCTION

Large ground movements and surface settlements induced by tunneling in saturated weak rocks and soft soils have been often reported in China, such as Beigang tunnel (Zhou, 2007), Gangcheng tunnel (Hou, 2009), Tianjin subway tunnels (Jia et al., 2006), and Guangzhou subway tunnels (Yuan, 2003). In these events, the low strength of surrounding rocks and soils and the richness of the soil in groundwater were found to be the two main factors resulting in the collapse of the tunnels.

It is very important for a designer to predict the magnitude of the deformation and damage pattern of a tunnel. Peck (1969) first proposed a Normal Probability Curve (NPC) to describe the shape of a transverse surface settlement trough over a tunnel. The NPC was validated to be suitable for describing transverse surface settlement of a tunnel by model tests, numerical simulations, and field observations (O'Reilly and New,

1982; Lee et al., 1999; Zhou and Pu, 2002; Sterpi and Cividini, 2004; and Qi et al., 2006).

The influence of water on tunneling, especially water infiltration into the tunnel, has seldom been taken into consideration in previous studies. Water may spout out and carry a lot of soil away, so the collapse could be more serious and the damage mechanism may become more complicated. In the presented study, model tests on a practical tunnel, which was collapsed during construction, were conducted to study the damage patterns, the laws of deformations, and ground cracks during tunneling in high water content weak rock, with special emphasis on water infiltration.

COLLAPSES OF BEIGANG TUNNEL

Beigang Tunnel, a railway tunnel, is 2130m long, and is located between Wuzhou city and Cenxi city. The mileage of the tunnel is from DK462 km+235 m to DK464 km+366 m. The maximum and minimum buried depth of the tunnel is 80m and 2m respectively. The largest excavation profile of the tunnel is 9.59 m in height and 7.36 m in width. In some construction sites, the rocks around the tunnel are highly fractured and weathered. The geology conditions along the tunnel axis direction are shown in Figure 1. Abundant groundwater was found during geology exploration.

During the Beigang tunnel excavation, a series of damage phenomena occurred such as sudden and large deformation of surrounding rocks, wall rock collapse, and a large amount of water and soil infiltration, groundwater falling down, fountain drain up and ground surface settlements and cracks. Several sites, where serious damage had occurred, are illustrated in Figure 1 (denoted by dots). For example, at the site between DK 462 km + 527 m to DK 462 km + 537 m, several streams of water jetted out from the tunnel wall and digging face, and the rocks around turned into slush and were carried away by water. Three obvious cracks were found on the ground surface above the site. The biggest width of the three cracks reached 5 cm. At the site between DK463 km + 215 m to DK463 km + 220 m, the total water flow was about 5000 m³/d. The tunnel collapsed upwards progressively, and at last a hole 6m in diameter was formed at the ground surface.

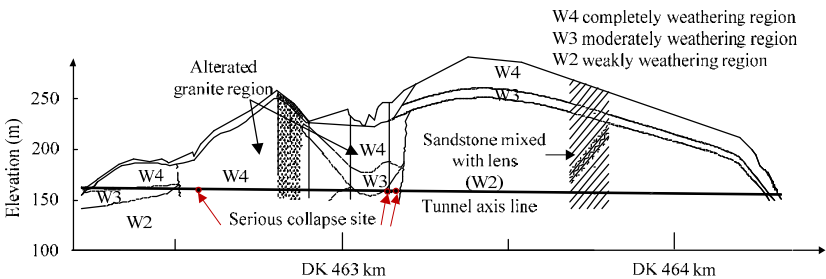


Figure 1. Geological and geographical profile of Beigang tunnel along its axis

DESIGN OF MODEL TEST

The section at DK 462 km + 530 m of the Beigang tunnel was taken as the prototype for the model test. The buried depth at this section is about 55 m. The geologic survey shows that the tunnel here is below the groundwater table, and the surrounding rocks could be assumed to be saturated. Geometry scale and similitude law. The ratio of the geometry of the model to the original is 1/100. The buried depth of the tunnel in the model is 55 cm, and the excavation profile of the model tunnel is 10 cm in height and 8 cm in width. Figure 2 shows a schematic view of model container box. The model container box is 100 cm high, 120 cm long and 50 cm wide. The frame of the box is made up by four I steel pillars and engaged by four U steel beams in each side. The front and back side panels of the box are made of glass, 2 cm thick, so the transverse deformation of the model can be seen and recorded during the whole test process. A circular window of 120 mm diameter is opened for excavation on the front glass panel, as shown in Figure 2.

Based on the law of similitude derived from test requirements and dimensional analysis, if a quantity possesses a dimension of length, its ratio will be equal to the geometrical ratio coefficient K_L ; if a quantity possesses a stress dimension, its ratio will be equal to the stress ratio coefficient K_σ ; if the quantity is dimensionless, the ratio will be equal to 1. The similitude ratio of the quantities of the model and the original can be written as follows:

$$K_b=K_h=K_w=K_L; K_{qu}=K_E=K_c=K_\sigma; K_\varepsilon=K_\mu=K_\varphi=1 \quad (1)$$

Where K_b , K_h and K_w are, respectively, the ratios of width, height, and displacement of the model to the original; K_{qu} , K_E and K_c are, respectively, the ratios of compressive strength, modulus of deformation, and cohesion of the model to the original; K_ε , K_μ and K_φ are, respectively, the ratio of the strain, Poisson's Ratio, and the angle of internal friction of the model to the original. In this model test, the geometrical ratio coefficient and stress ratio coefficient are all 1/100.

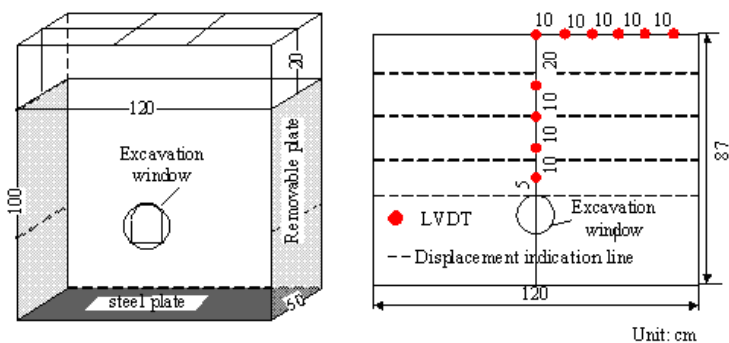


Figure 2. Illustration of model test frame and measure system

Model tests scheme. How to simulate the water infiltration is the key problem of the model test. A scheme of two stages was adopted to realize the purpose.

First stage: The model material was deposited in low water content, and then the tunnel was excavated. In the first stage, the model material had high strength with low water content, so the tunnel wall would keep stable after excavation. The total height of the soil bed in the model was 87cm, as depicted in Figure 4. The bed is filled by layers. The placement height of each layer is about 12cm, and corresponding height after compaction is about 10cm. Full-face method was adopted in the excavation of the tunnel. The total excavation length is 50cm, and was divided into five segments of 10cm length. A time interval of 20 minutes was left between the first and second segments for recording and observation of the change of the model during the first segment.

Second stage: A certain amount of water was added from the surface of the model to reproduce the water infiltration and the collapse of the tunnel. Before adding water, it was determined whether the tunnel and surrounding rocks were stable or unstable. If the surrounding rocks were stable, then 30 kg water was slowly poured into the contained box. The water added then seeped into the soil from the surface and flowed out through the crown and side walls of the tunnel. The surrounding soil became saturated, and its strength decreased. Due to the decrease of the strength of the surrounding soil and the water infiltration, the tunnel collapsed in this step.

Selection of model material. The surrounding rock mass is very heterogeneous and is mainly composed of two kinds of rocks. The samples of the two kinds of rocks were taken from the field and studied carefully in the laboratory. It was found that the mineral composition and material parameters of different kinds of rocks are quite different. Furthermore, the composition and parameters of the rocks are quite different from site to site. The completely weathered altered sandstone can be categorized into clayey sands and its parameters were obtained from triaxial tests. The completely weathered granite can be categorized into gravels and its parameters were obtained from large scale direct shear test. It was found that even for the same soil, the parameters of the tests are divergent, so a range of the parameter was given in Table 1.

Table 1. Material parameter in prototype system and model system

material	Unit weight (kN/m ³)	Void ratio	Water content	Cohesion (kPa)	Friction angle (°)
weathered sandstone	16.5-18.5	1.42-1.80	70-120%	70-120	21-31
weathered granite	18.5-20	0.84-0.99	45-70%	120-180	27-35
Mixture 1	16.4	0.9	20%	10	33
Mixture 2	18.5	0.9	35%	1.4	27

The rock mass around the tunnel was simplified to be homogenous in the model test. The model materials were supposed to be a mixture of coarse sand, fine sand, clay and water. The clay part of the mixture was obtained from the sample of completely weathered adulterated sandstone by sieving and milling. The strength parameters, cohesion c and friction angle φ of the model material, which must follow the similitude law listed in Equations 1, 2, and 3, are the most important criteria for determination of the mix proportion of the model material. A series of material tests in laboratory were carried out for the mixtures composed of the above soils with different proportions.

Two mixtures of different proportions, named Mixture 1 and Mixture 2 in Table 2, were found to be acceptable for the model material in the two stages of model tests respectively. The two mixtures have same solid parts: coarse sand 80%, fine sand 15%, and clay 5%. The different is the water content; Mixture 1 is unsaturated with water content of 20%, while Mixture 2 is saturated with water content of 35%. Their material properties are listed in Table 1.

Mixture 1 was used as model material in the first stage. It should be pointed out that the mandatory similitude relationship between model material and its prototype material is not satisfied in the first stage. But the deformation progress in the first stage can be taken as a good reference to compare it with the following stage. At the second stage, while water was added to the model, the water content of the model material increased, and then the model material turned into Mixture 2. Therefore, the similitude relationship of the strength parameters between the model and the original are nearly satisfied. At the second stage, damage phenomena such as sudden large deformation, water burst and tunnel wall collapse which occurred in Beigang Tunnel would be reproduced in the model test.

Measure system. The deformation in both stages was recorded and measured by displacement transducers and digital photos. Linear variable differential transducers (LVDT) and photogrammetry techniques were used to get the displacement of the model. The LVDTs and displacement indication lines for photogrammetry are shown in Figure 2. The LVDTs were placed along the model centerline and ground surface of the middle transverse section. The displacement indication lines were set on the front face of the model; a set of reference lines were drawn on the glass to mark the initial positions. The image of the model during the whole test process was recorded by a camera through the glass panes at the front and back of the model. The displacement distribution of the model can be obtained by comparing the difference between the indication lines and reference lines through image processing techniques.

TEST RESULT AND ANALYSIS

First stage. Figure 3 gives the distribution of the surface subsidence of the model on the middle transverse section and the internal displacement of the surrounding soil along the centerline of the tunnel in the five excavation steps. It can be seen from Figure 3 that at the 1st and 2nd steps of excavation, the tunnel was stable, and the surface settlement and internal displacement at these two steps was relatively small. During the 3rd step, the LVDT at 5 cm above the tunnel measured an obviously sudden settlement. At the 4th step, the LVDT at 5 cm above the tunnel fell down, and a local collapse around the middle section above the tunnel occurred. After the 5th step, the excavation finished, a small amount of water flowed out from the tunnel, lasting for about 20 minutes. When the flow stopped, no further displacement or collapse developed.

The Normal Probability Curve describing the settlements on the ground surface caused by tunneling suggested by Peck (1969) was written as follows:

$$s(y) = s_{\max} \exp\left(\frac{-y^2}{2i^2}\right) \quad (2)$$

in which $s(y)$ is the settlement at the distance of y ; y is the distance from the tunnel center line; s_{max} is the maximum surface settlement at the point above the tunnel center line; i is the horizontal distance from the tunnel center line to the point of inflection on the settlement curve.

The comparison between the theory settlement curves and measured data is shown in Figure 4. A good accordance between the theory curves (O'Reilly and New, 1982) and the model test results was found. The displacement indication lines show that the settlement of surrounding soil at different depths had a very similar shape. The value of i decreases and the value of s_{max} increases separately with the increase in depth.

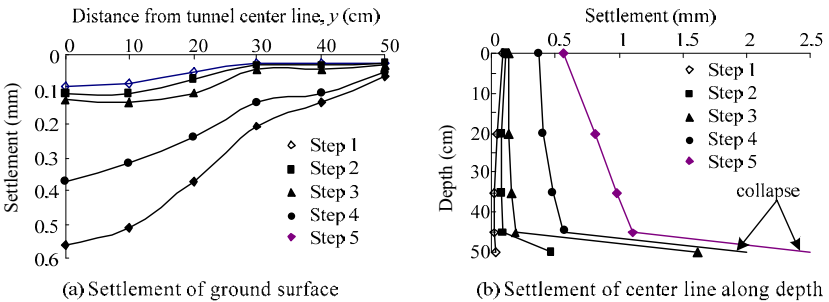


Figure 3. Settlement of ground surface and center line along depth

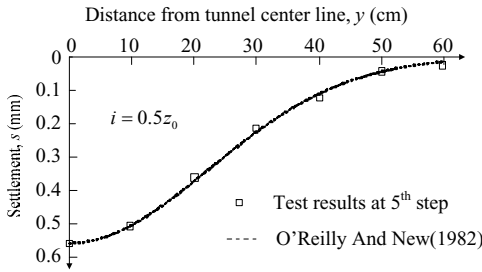


Figure 4. Comparison between test data and theory curve

Second stage. The surface of the tunnel became wet 20 minutes after watering, and water flowed slowly into the tunnel. The settlements developed more quickly than before and collapse occurred above the tunnel in small scope. The flow became muddy about 25 to 30 minutes later after watering, and the soil around the tunnel was carried out by the water flow.

30 minutes later after watering, large scope collapse occurred suddenly. A block of soil dropped down from the top of the tunnel and filled in the tunnel. A cavern was generated above the original tunnel, and some cracks appeared both inside the ground and on the surface. The caverns are arch-shaped bearing structures. Figure 5(a) gives a sketch of the collapse profile and cracks of the model at that time. There were two

large cracks (named as main cracks to distinguish them from other cracks) on the ground surface located on the each side of the tunnel axis respectively. Other cracks were almost located within the region between the two main cracks. The distance from left main crack to the tunnel axis is about 31 cm; the distance from right main crack to the tunnel axis is about 24 cm.

35 minutes after watering, the water flow turned into debris flow. Due to the erosion of the surrounding rocks, the cracks inside and on the surface of the ground developed quickly. The two main cracks became deeper and wider, and several small cracks occurred on the ground between the two main cracks. The settlement of the region between the two main cracks developed more quickly than that out of this region. The cavern became larger and all the LVDTs inside the strata were dropped down and out of work.

The obvious debris flow and serious collapse lasted for about 25 minutes; then, the flow became smaller and collapse stopped. 3 hours later after watering, no water flow or debris flow could be observed. Figure 5(b) gives the collapse profile and cracks of the model at that time. The cavern above the original tunnel developed upwards and its top face was very near the ground surface. The cavern's diameter is 27 cm, and the distance between the top face of the cavern and the ground surface is 14 cm. The biggest width of the main cracks is 0.4 cm, and the biggest depth of the main cracks is 12 cm.

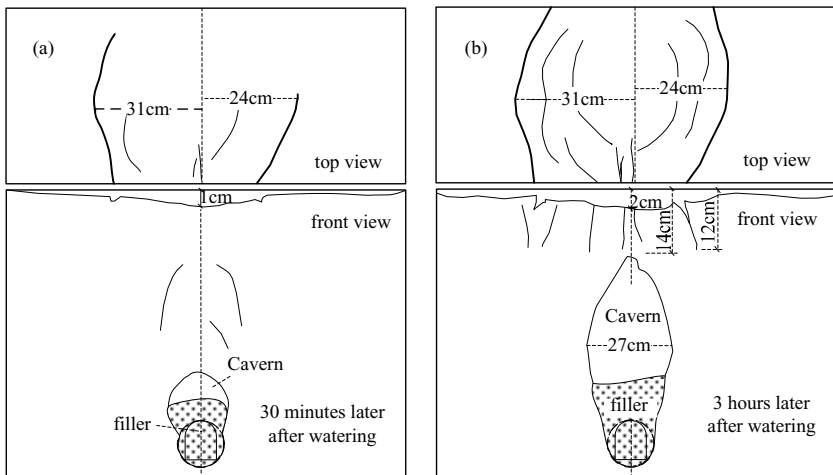


Figure 5. Sketch of the model 30 minutes and 3 hours later after watering

The damage phenomena after watering are very similar to those which took place in the Beigang Tunnel; therefore, the collapse phenomena of the Beigang tunnel were reproduced in the model to some extent.

Based on the collapse characteristics observed in the model test, besides the weak surrounding rock mass, large water infiltration may be the main factor resulting in the collapse of the Beigang Tunnel. The water flow carried out a lot of soil particles, and the surrounding rock mass became loose and full of cracks. Due to larger void ratio

and internal cracks, the seepage velocity increased and the problem of flow became more serious. The strength of the surrounding rock mass lessened as a result of mass loss, so the tunnel collapsed.

CONCLUSION

Taking the Beigang tunnel as a prototype, model tests were conducted to investigate the deformation, cracks and collapse pattern of surrounding rock mass when tunneling in weak rock with high water content. Similar damage phenomena of the Beigang tunnel were reproduced in the model test. The following conclusions can be drawn from the analysis:

- 1) Water infiltration, which induced soil erosion and decreased the strength of the surrounding soils, was mainly responsible for the tunnel's collapse.
- 2) The distribution of surface settlements at the transverse section before surface cracks appeared can be described well by Peck's Normal Probability Curve.
- 3) Two main cracks, the two deepest and widest cracks, appearing on the ground surface in the early stages of collapse were located on the each side of the tunnel axis respectively. The settlements and cracks on ground surface developed mainly in the region between the two largest cracks. During tunneling, this region should be carefully monitored, and once the cracks occur on the ground, proper measures must be taken in order to control the collapse of the tunnel.

ACKNOWLEDGEMENTS

This research was financially supported by the National Basic Research Program of China, No. 2010CB732103.

REFERENCES

- Hou, J. H. (2009). "Treatment of the collapse of Gangcheng tunnel of Taiyuan." *Journal of Railway Engineering Society*, 10, 74-78.
- Jia, J. B., Jiao, C. and Fan P. (2006). "Analysis on ground surface deformation induced by undercutting under shallow overburden in Tianjin Metro." *Tunnel Construction*, 1, 18-20.
- Lee, C. J., Wu, B. R. and Chiou, S. Y. (1999). "Soil movements around a tunnel in soft soils." *Proc. Natl. Sci. Counc. ROC*, 2, 235-247.
- O'Reilly, M. P. and New, B. M. (1982) "Settlements above tunnels in the United Kingdom-their magnitude and prediction." *Tunneling*, 179-185.
- Peck, R. B. (1969). "Deep excavations and tunneling in soft ground." *Proceedings of the 7th International Conference on Soil Mechanics and Foundation Engineering, state-of-the-art Volume*, 225-290. Mexico City, Mexico.
- Qi, H. T., Gao, B. and Ma, J. L. (2006). "Centrifugal model test for ground surface subsidence caused by metro tunneling in saturated soft clay strata." *Journal of Southwest Jiaotong University*, 2, 184-189.

- Sterpi, D. and Cividini, A. (2004). "A physical and numerical investigation on the stability of shallow tunnels in strain softening media." *Rock Mechanics and Rock Engineering*, 4, 277- 298.
- Yuan Q. (2003). "Analysis of the reason and control of ground settlement of subway at Guangzhou Subway No. 2 line Kecun contact line fork." *Journal of Shijiazhuang Railway Institute*, 7, 19-22.
- Zhou, X. W. and Pu, J. L. (2002). "Centrifuge model test on ground settlement induced by tunneling in sandy soil." *Soil Mechanics*, 5, 559-563.
- Zhou, Y. F. (2007). "The discussion of construction method on Beigang tunnel crossing-over weak-fracture zone." *Shanxi Architecture*. 19, 313-314.

Application of Story Isolation Technique in the Seismic Reduction of Integrated Building-Bridge Station

Guo, W.¹, Yu, Z.² and Zhang, H.S.³

¹ Lecturer, School of Civil Engineering, Central South University, Hunan 410075, China;
email: wei.guo.86@gmail.com

² Professor, School of Civil Engineering, Central South University, Hunan 410075, China;
email: zhwyu@mail.csu.edu.cn

³ Postgraduate student, School of Civil Engineering, Central South University, Hunan 410075, China;
email: zhanghuashuai222@163.com

ABSTRACT

As a novel structure, the integrated building-bridge station has appeared in the high speed railway construction of China, which is of great significant to ensure the seismic safety of the new structure in an earthquake. Meanwhile, the isolation technique which is an important passive control strategy has also been widely used in both buildings and bridges. Based on these, an intensive study of the story isolation technique is carried out in this paper which is to investigate the isolation technique's feasibility and effect on the integrated building-bridge station. Firstly, given the special characteristics of structure and isolation devices which are usually installed on the connection positions between the building and bridge, the numerical model is established considering the dynamic coupling effect. As earthquake ground motion is practically a random process, an accurate and efficient stochastic expression is derived based on the pseudo-excitation method and complex mode technique. Then a rational and effective optimization strategy is proposed to achieve the appropriate setting of the isolation devices. Finally, a numerical example is given to investigate the story isolation technique's application in the integrated building-bridge station by utilizing the stochastic analysis method and optimization strategy proposed in this paper.

INTRODUCTION

Regarded as an important public structure and transportation hub, the safety issue of the integrated building-bridge station in an earthquake is of great significance, and it is necessary to perform seismic control design for such structures. Currently the most common and widespread application of vibration control strategy in seismic control is isolation design, which includes base isolation and story isolation. The isolation technique is usually applied to lower buildings, which has been proved to be very effective by the scholars all over the world in their research (Zhou, 1997; Liu, 2004; Skinner and Robinson, 1993; Naeim and Kelly, 1993; Kelly, 1997) which has been developed systematically, and some correlative research achievements have already been applied to engineering. Therefore, for the integrated building-bridge station, how to introduce the isolation technique in construction and achieve the appropriate parameter setting to reduce vibration in an earthquake has considerable

significance. Liu et al. (2008) pointed out that it is impossible to achieve cooperative vibration control by installing the appropriate set isolation devices on the connection part of building and bridge in their research work about the seismic design of integrated building-bridge stations based on the translational single-DOF model and time history analysis, and Fang (2004) studied the isolation application in the sub-frame and mega-frame structures. His theoretical model is similar to the integrated building-bridge station.

Based on the statement above, the multi-DOF numerical model of the integrated building-bridge station which takes into account the coupling effect between the building and bridge is established in this paper. Considering the earthquake ground motion as a random process, the accurate and efficient stochastic calculation expression is also derived based on the complex mode theory and pseudo excitation method (Lin and Zhang, 2004). In fact the parameter optimization of isolation devices applied in the integrated building-bridge station is a multi-objective problem, so the parameter field method is introduced in this paper to appropriately determine the optimal setting of isolation devices and corresponding vibration reduction effect. Finally, a numerical example is given to investigate the working mechanism and the damping effect of the story isolation technology applied in the integrated building-bridge station.

STORY ISOLATION MODEL

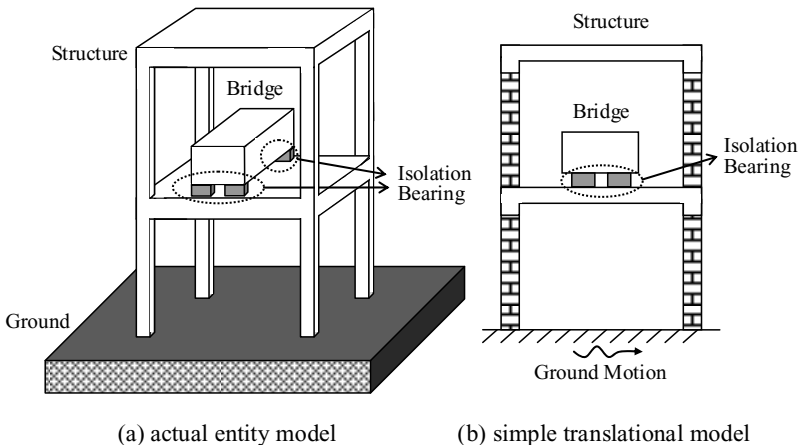


Figure 1. Schematic diagram of integrated building-bridge station with isolation devices

Figure 1 gives the schematic diagram of setting isolation devices in the bottom of the bridge structure, in which Figure 1(a) describes the entity model and Figure 1(b) is an simplified model of the integrated building-bridge station. Based on such a model, the dynamic equilibrium equation of multi-DOF model can be established as follows:

$$M_s \ddot{U}_s + C_s \dot{U}_s + K_s U_s = -M_s E_s \ddot{u}_g + E_b F_b, \quad m_b \ddot{u}_b + F_b' = -m_b \ddot{u}_g \tag{1a,b}$$

in which M_s , C_s and K_s are the mass, damping and stiffness matrices of n DOF building respectively; $U_s = [u_{s1}, u_{s2}, \dots, u_{sn}]^T$ is the displacement vector of the building relative to the ground; m_b is the mass of bridge; u_b is the displacement vector of the bridge relative to the building; \ddot{u}_g is the acceleration of the ground; E_s represents the position vector of the earthquake force; E_b represents the position vector of the force F_b ; F_b is the external force on the building provided by the bridge; $-F_b'$ is the external force on the bridge provided by the building; $F_b = F_b' = c_b \dot{u}_b + k_b u_b$; $c_b = 2m_b \omega_b \xi_b$, $k_b = m_b \omega_b^2$ are the damping coefficient and stiffness coefficient of the isolation devices, respectively; ω_b and ξ_b are the circular frequency and damping ratio, respectively. Based on equation (1), the dynamic equilibrium equation of integrated building-bridge station can be obtained:

$$M\ddot{U} + C\dot{U} + KU = -ME\ddot{u}_g \tag{2}$$

in which, $M = \begin{bmatrix} M_s & 0_{n \times 1} \\ 0_{n \times 1} & m_b \end{bmatrix}$, $C = \begin{bmatrix} C_s + C_s^{(b)} & C_{sb} \\ C_{bs} & c_b \end{bmatrix}$ and $K = \begin{bmatrix} K_s + K_s^{(b)} & K_{sb} \\ K_{bs} & k_b \end{bmatrix}$ are the mass, damping and stiffness matrices of the integrated building-bridge station respectively, and the total DOF of the structure is $n+1$; C_s , K_s , c_b and k_b have been defined above; C_{sb} , C_{bs} , K_{sb} and K_{bs} are the coupled damping and stiffness matrices associated with both the building and the bridge; $C_s^{(b)}$ and $K_s^{(b)}$ represent the force on the building reacted from the bridge; $U = [U_s^T, u_b]^T$ is the displacement vector relative to the ground; $E = [E_s^T, 1]^T$ is the vector of earthquake force position.

Since the isolation devices are set on the bottom of bridge, the integrated building-bridge station has non-proportional damping characteristic. So, in order to realize decoupling calculation the state vector method and complex mode theory are generally adopted. Firstly define the state vector:

$$\bar{U} = [\dot{U} \quad U]^T \tag{3}$$

Introduce the equation $M\dot{U} - M\dot{U} = 0$; the state equation can be established as follows:

$$A\dot{\bar{U}} + B\bar{U} = -A\bar{E}\ddot{u}_g \tag{4}$$

in which $A = \begin{bmatrix} 0 & M \\ M & C \end{bmatrix}$, $B = \begin{bmatrix} -M & 0 \\ 0 & K \end{bmatrix}$, $\bar{E} = \begin{bmatrix} E \\ 0_{(n+1) \times 1} \end{bmatrix}$. For the under-damped model described by equation (4), there exists $n+1$ groups of eigenvalue and eigenvector, which are conjugate with each other in one certain group. Then the following equation can be given:

$$B\Phi_i = -\eta_i A\Phi_i \tag{5}$$

in which $\Phi_i = \begin{bmatrix} \eta_i \varphi_i \\ \varphi_i \end{bmatrix}$, $\varphi_i = \varphi_{iR} + r\varphi_{iI}$, $\eta_i = -\eta_{iR} + r\eta_{iI} = -\xi_i \omega_i + r\omega_i \sqrt{1 - \xi_i^2}$, $r = \sqrt{-1}$, $i = 1 \sim n+1$. There exist generalized orthogonality relationship for different eigenvectors, and utilizing the relationship the circular frequency ω_i and damping ration ξ_i are:

$$\omega_i^2 = \frac{(\boldsymbol{\varphi}_i^*)^T \mathbf{K} \boldsymbol{\varphi}_i}{(\boldsymbol{\varphi}_i^*)^T \mathbf{M} \boldsymbol{\varphi}_i}, \quad 2\xi_i \omega_i = \frac{(\boldsymbol{\varphi}_i^*)^T \mathbf{C} \boldsymbol{\varphi}_i}{(\boldsymbol{\varphi}_i^*)^T \mathbf{M} \boldsymbol{\varphi}_i} \tag{6}$$

in which superscripts * denote the conjugate complex. Using the $2(n+1)$ complete orthonormal eigenvectors, the response of the integrated building-bridge station is expressed as:

$$\mathbf{U} = \sum_{i=1}^{2(n+1)} \boldsymbol{\varphi}_i Q_i \tag{7}$$

in which Q_i is the number i generalized displacement response of the structure. Substituting equation (7) into equation (4), and pre-multiplying by $\boldsymbol{\varphi}_i^T$, one can get:

$$\ddot{Q}_i - \eta_i Q_i = -\mu_i \ddot{u}_g \tag{8}$$

in which $\eta_i = -\frac{\boldsymbol{\varphi}_i^T \mathbf{B} \boldsymbol{\varphi}_i}{\boldsymbol{\varphi}_i^T \mathbf{A} \boldsymbol{\varphi}_i}$, $\mu_i = \frac{\boldsymbol{\varphi}_i^T \mathbf{R} \bar{\mathbf{E}}}{\boldsymbol{\varphi}_i^T \mathbf{A} \boldsymbol{\varphi}_i}$. Meanwhile, define q_i as the response of the following model:

$$\ddot{q}_i + 2\xi_i \omega_i \dot{q}_i + \omega_i^2 q_i = -\ddot{u}_g \tag{9}$$

As is shows in Zhou and Yu (2006), by orthogonality of modes and matrix transformation the structural response can easily be obtained:

$$\mathbf{U} = \sum_{i=1}^{n+1} [\mathbf{X}_i q_i + \mathbf{Y}_i \dot{q}_i] \tag{10}$$

in which , $\mathbf{X}_i = \frac{2}{a_i^2 + b_i^2} \left[(\xi_i p_i + \sqrt{1 - \xi_i^2} w_i) \boldsymbol{\varphi}_{iR} + (\xi_i w_i - \sqrt{1 - \xi_i^2} p_i) \boldsymbol{\varphi}_{iI} \right] \omega_i$,

$$\mathbf{Y}_i = \frac{2}{a_i^2 + b_i^2} (p_i \boldsymbol{\varphi}_{iR} + w_i \boldsymbol{\varphi}_{iI}), \quad a_i = -2\eta_{iR} (\boldsymbol{\varphi}_{iR}^T \mathbf{M} \boldsymbol{\varphi}_{iR} - \boldsymbol{\varphi}_{iI}^T \mathbf{M} \boldsymbol{\varphi}_{iI}) - 4\eta_{iI} \boldsymbol{\varphi}_{iR}^T \mathbf{M} \boldsymbol{\varphi}_{iI} + \boldsymbol{\varphi}_{iR}^T \mathbf{C} \boldsymbol{\varphi}_{iR} - \boldsymbol{\varphi}_{iI}^T \mathbf{C} \boldsymbol{\varphi}_{iI},$$

$$b_i = 2\eta_{iI} (\boldsymbol{\varphi}_{iR}^T \mathbf{M} \boldsymbol{\varphi}_{iR} - \boldsymbol{\varphi}_{iI}^T \mathbf{M} \boldsymbol{\varphi}_{iI}) - 4\eta_{iR} \boldsymbol{\varphi}_{iR}^T \mathbf{M} \boldsymbol{\varphi}_{iI} + 2\boldsymbol{\varphi}_{iR}^T \mathbf{C} \boldsymbol{\varphi}_{iI}, \quad p_i = a_i c_i + b_i d_i, \quad w_i = b_i c_i - a_i d_i,$$

$$c_i = \boldsymbol{\varphi}_{iR}^T \mathbf{M} \mathbf{E}, \quad d_i = \boldsymbol{\varphi}_{iI}^T \mathbf{M} \mathbf{E}.$$

STOCHASTIC ANALYSIS

In order to resolve the low calculation efficiency of the conventional stochastic method, Lin proposed a pseudo-excitation method (Lin and Zhang, 2004), in which the seismic random input is converted to be the sinusoidal form to simplify the theoretical derivation and improve the computational efficiency. Firstly, the ground motion is converted into sinusoidal input:

$$\ddot{u}_g(t) = \sqrt{S_{\ddot{u}_g}(\omega)} e^{r\omega t}, \quad r = \sqrt{-1}. \tag{11}$$

in which $S_{\ddot{u}_g}(\omega)$ is the power spectral density function. Generally, the method is also applicable for a non-stationary earthquake, and then the power spectral density function varies with time and can be written as $\sqrt{S_{\ddot{u}_g}(\omega, t)}$. Considering the huge computation quantity of the matrix operation, the decoupling computation method utilizing complex mode theory will be introduced in this paper. From derivation above it can be known that the pseudo response of the model described by equation (9) can be written as:

$$q_i = H_i \ddot{u}_g(t) = H_i \sqrt{S_{\ddot{u}_g}(\omega)} e^{r\omega t} \tag{12}$$

in which $H_i = -\frac{1}{\omega_i^2 - \omega^2 + 2r\zeta_i\omega}$, $i = 1 \sim n+1$. Introducing equation (12) into equation (10), the pseudo response can be obtained:

$$U = \sum_{i=1}^{n+1} (X_i q_i + Y_i \dot{q}_i) = \left[\sum_{i=1}^{n+1} (X_i + r\omega Y_i) H_i \right] \sqrt{S_{\ddot{u}_g}(\omega)} e^{r\omega t} \tag{13}$$

According to the pseudo excitation method, the power spectrum density function matrix of structural response can be expressed as:

$$S_U = U^* U^T \tag{14}$$

If only the l th floor response of the building is concerned (usually the top floor displacement), the pseudo response is given by:

$$u_{sl} = \sum_{i=1}^{n+1} (X_{i,l} q_i + Y_{i,l} \dot{q}_i) = \left[\sum_{i=1}^{n+1} (X_{i,l} + r\omega Y_{i,l}) H_i \right] \sqrt{S_{\ddot{u}_g}(\omega)} e^{r\omega t} \tag{15}$$

in which, $X_{i,l}$ is the l th element of vector X_i and $Y_{i,l}$ is the l th element of vector Y_i . Suppose the bridge is supported on the a th floor of building; we can get:

$$u_b = u_b - u_{sa} \tag{16a}$$

$$u_b = \sum_{i=1}^{n+1} (X_{i,n+1} q_i + Y_{i,n+1} \dot{q}_i) = \left[\sum_{i=1}^{n+1} (X_{i,n+1} + r\omega Y_{i,n+1}) H_i \right] \sqrt{S_{\ddot{u}_g}(\omega)} e^{r\omega t} \tag{16b}$$

$$u_{sa} = \sum_{i=1}^{n+1} (X_{i,a} q_i + Y_{i,a} \dot{q}_i) = \left[\sum_{i=1}^{n+1} (X_{i,a} + r\omega Y_{i,a}) H_i \right] \sqrt{S_{\ddot{u}_g}(\omega)} e^{r\omega t} \tag{16c}$$

in which, $X_{i,n+1}$ and $X_{i,a}$ are the $(n+1)$ th and a th element of vector X_i , $Y_{i,n+1}$ and $Y_{i,a}$ are the $(n+1)$ th and a th element of vector Y_i , respectively. The control indexes of the integrated building-bridge station in the earthquake are: $u_{control} = [u_{sl}, \dots, u_{sm}, u_b]$, in which u_{sl} and u_{sm} are the l th and m th displacement of building relative to the ground respectively. In the stochastic analysis, power spectrum density function and square average value are usually adopted, and the square average value can be given as follows:

$$S_{u_l} = u_{sl}^* u_{sl}, \dots, S_{u_m} = u_{sm}^* u_{sm}, \quad S_{u_b} = u_b^* u_b, \tag{17a}$$

$$\sigma_{u_l}^2 = \int_{-\infty}^{\infty} S_{u_l} d\omega, \dots, \sigma_{u_m}^2 = \int_{-\infty}^{\infty} S_{u_m} d\omega, \quad \sigma_{u_b}^2 = \int_{-\infty}^{\infty} S_{u_b} d\omega \tag{17b}$$

OPTIMIZATION STRATEGY

Some researchers proposed parameter field optimization strategy (Fang, 2004), and in this paper the strategy is used to achieve an appropriate parameter optimization of the isolation devices in the integrated building-bridge station. Combined with the special structural characteristics, the optimization strategy can be expressed as follows:

$$\Omega = \{(\omega_b, \xi_b) | R^1 / [R^1] \leq 1, \dots, R^s / [R^s] \leq 1, R^{s+1} / [R^{s+1}] \leq 1\} \tag{18}$$

in which Ω is the parameter field; (ω_b, ξ_b) are the isolation device parameters which would be optimized; R^1, \dots, R^s are the response quantities of building which need to be controlled; R^{s+1} is the response quantities of bridge which need to be controlled; $[R^1], \dots, [R^s], [R^{s+1}]$ are the permissible limits of response quantities. In view of the

above, the control indexes are $\mathbf{u}_{control} = [u_{sl}, \dots, u_{sm}, u_{b'}]$, $R^1 = u_{sl}, \dots, R^s = u_{sm}, R^{s+1} = u_{b'}$.

NUMERICAL STUDY

In this section, a simple analysis model is used to investigate the derived stochastic calculation expression and to validate the optimization strategy. As shown in Figure 2, the structure model is assumed to be a 4-story building, whose 2nd floor supports the bridge structure. The parameters are set as: $m_{s1} = m_{s2} = m_{s3} = m_{s4} = 4 \times 10^5 \text{ kg}$, $k_{s1} = k_{s2} = k_{s3} = k_{s4} = 1 \times 10^9 \text{ N/m}$. The Rayleigh damping is adopted, and a 5% damping ratio is considered for first and 2nd mode of the structure. From the discussion above, the damping ratio of isolation devices on the bottom of bridge does not need optimization, and the stiffness characteristic $k_b = m_b \omega_b^2$ is the optimization factor. The stochastic model of ground motion, the Kanai-Tajimi model, is adopted here, which can be described as:

$$S_{\ddot{u}_g} = \frac{\omega_g^4 + (2\zeta_g \omega_g \omega)^2}{(\omega_g^2 - \omega^2)^2 + (2\zeta_g \omega_g \omega)^2} S_0 \quad (22)$$

in which $\omega_g = 13.96 \text{ rad.s}^{-1}$ and $\zeta_g = 0.72$ are the circular frequency and damping ratio of soil, which correspond to the site type 1 and classification of the earthquake 3 as has been defined in code GB50011-2001 in China. The seismic intensity is assumed to be $S_0 = 0.0006 \text{ m/s}^3$.

Because the vibration control strategy is story isolation, the optimization objective should take into account the lower floor response u_{s2} . First of all, initialize the response of no isolation situation corresponding to the setting that $\xi_b = 0.05$, $\omega_b = \omega_{s1}$, in which ω_{s1} is the circular frequency of first mode of building. Assume the initial response to be $u_{s2,0}$, $u_{s4,0}$ and $u_{b',0}$. The aim of setting isolation devices is not only to reduce the response of the building but also to reduce the response of the bridge. As the damping ratio is assumed to be $\xi_b = 0.2$, the parameter ω_b changing, and the normalized optimization index then can be written as:

$$\bar{\mathbf{u}}_{control} = [u_{s2}/u_{s2,0}, u_{s4}/u_{s4,0}, u_{b'}/u_{b',0}]$$

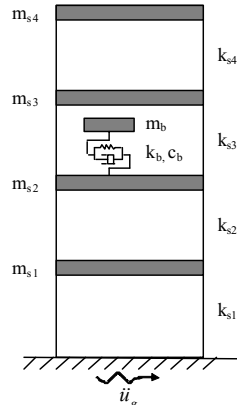


Figure 2. Model of the integrated building-bridge station structure-bridge

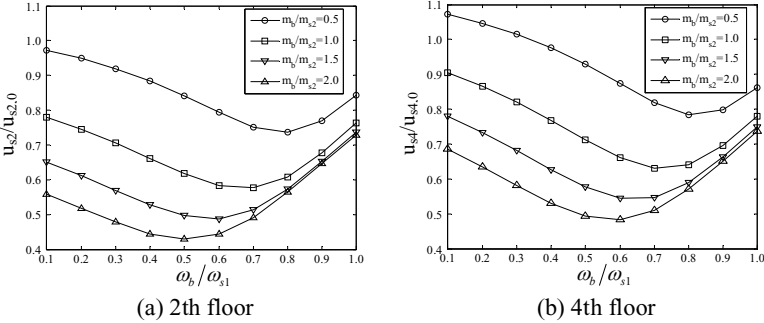


FIG.3. Effect of stiffness characteristic of isolation devices on the relative displacement of structure

Figure 3 shows variety of responses of building with changing of the parameters of the isolation devices, from which it can be seen that in order to reduce the response of building the parameters of isolation devices should be appropriate set. Also it shows that there exists an optimal value of stiffness characteristic. Moreover, the effect of vibration control is obviously better as the mass of the bridge increases. However, the work mechanism of the large mass tuned mass damper (TMD), which depends mainly on the damping force but also upon turning frequency, is different from the small mass TMD. Just as is shown in the Figure 3, the optimal frequency will deviate from the turning frequency with the increase of mass of bridge, and the optimal region of stiffness characteristic distributes as $0.4\omega_{s1} \sim 0.8\omega_{s1}$.

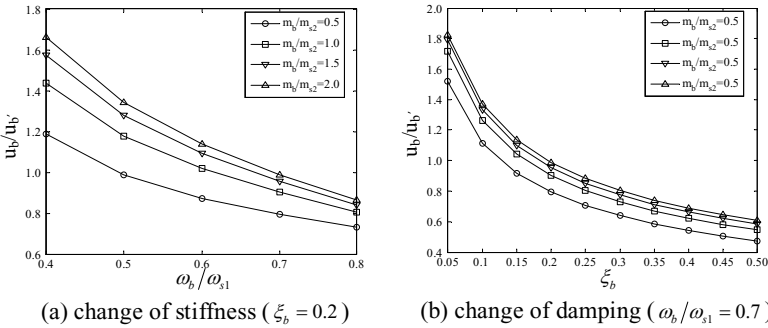


FIG.4. Effect of stiffness and damping characteristics of isolation devices on the displacement of bridge relative to structure

Figure 4 gives the response variation of the bridge along with the change of stiffness and damping characteristics of isolation devices. Figure 4(a) shows that while the damping ratio of isolation devices remains stable, the response of the bridge relative to the building would increase as the stiffness decreases, the change trend of

which is consistent with our intuitive understanding. Figure 4(b) reveals that increasing the damping ratio of isolation devices can effectively reduce the displacement of the bridge relative to the building. In summary, the optimal design of parameters of isolation devices can be divided into two steps: (1) Gain an equivalent linear damping ratio of isolation devices, and optimize the stiffness parameter according to the proposed method in this paper to achieve vibration reduction; (2) Examine whether the response of the bridge can meet the permissible limit value. If it does satisfy, stop the calculation, and the parameters' values are optimal; if not, then correct the damping ratio, and repeat step (1).

CONCLUSIONS

In this paper, the story isolation technique applied in the integrated building-bridge station has been investigated intensively. Some valuable conclusions can be given:

- (1) Installing the isolation devices on the connection parts of building and bridge, the optimal setting, could effectively reduce the response of building and bridge according to the strategy introduced in this paper.
- (2) The damping ratio of isolation devices doesn't need optimization and can be directly set to be the upper limit value. Accordingly, in order to control the bridge's displacement relative to the building and reduce the building's response relative to the ground, only the stiffness characteristics need to be optimized to provide appropriate feedback force.

ACKNOWLEDGMENTS

The authors appreciate the support of the National Natural Science Foundation of China (No.50938008,51108466), the National Science Foundation for Post-Doctoral Scientists of China (No.20110491277), the Science Foundation for Post-Doctoral Scientists of Central South University, the Freedom Explore Program of Central South University, the Scientific Research Foundation of Central South University.

REFERENCES

- Fang, L. (2004). "Vibration control mechanism and experimental research of multifunctional vibration-absorption megaframe structure under earthquake." *Southeast University*, Nanjing, 2004. (in Chinese)
- Feng, D.M., He, W.F., Yang, Y.Q. and Liu, W.G. (2008). "Numerical response analysis and shaking table tests for bridge and building complex structural system (Part I: complex structure dynamic test research)." *14th WCEE.*, October 12-17, 2008, Beijing, China.
- Kelly, J.M. (1997). "Earthquake resistant design with rubber (Second Edition)." *Springer Verlag London Limited*, UK, 1997.
- Lin, J.H. and Zhang, Y.H. (2004). "Pseudo-Excitation Method of Random Vibration." *Science Press*, Beijing. (in Chinese)

- Liu, W.G. (2004). "Mechanics properties of rubber bearings and earthquake response analysis of isolated structure." *Beijing University of Technology.*, 2004. (in Chinese)
- Liu, W.G., Yang, Q.R., Hua, L. and He, W.F. (2008). "Numerical response analysis and shaking table tests for bridge and building complex structural system (Part II: parameter optimum and earthquake response analysis)." *14th WCEE.*, October 12-17, 2008, Beijing, China.
- Naeim, F. and Kelly, J.M. (1993). "Design of seismic isolated structures." *John Wiley & Sons, Inc.*, UK, 1999 .
- Skinner, R.L. and Robinson, W.H. (1993). "An introduction to seismic isolation." *John Wiley & Sons*, UK, 1993.
- Zhou, F.L. (1997). "Seismic control of engineering structure." *Earthquake Press*, Beijing, 1997. (in Chinese)
- Zhou, X.Y. and Yu, R.F. (2006). "CCQC method for seismic response of non-classically damped linear system based on code response spectra." *Engineering Mechanics.*, Vol. 23(2): 10-17. (in Chinese)

Network Arches: The World's Lightest Arch Bridges

Per Tveit

Dr.ing. Docent Emeritus, Agder University, PO-Box 509, N-4898 Grimstad, Norway. E-mail: per.tveit@uia.no; Phones: Home: +47 370 44 036; Office: +47 37 23 32 36; Cell phone: +47 909 86 507; Fax: +47 372 53 031

Summary

Network arches have a tensile and a compressive flange with a web consisting of crossing hangers. Some of the hangers cross each other twice. The network can be seen as a very light, simply supported beam. There is little bending. There is a lot of tension in tie and hangers. The arches are well supported by hangers and wind bracing. Thus the buckling strength of the arch is high as long as few hangers relax. That is easiest to prevent when a concrete tie gives extra weight in the tie.

The optimal shape of network arches is discussed. In two lane and two track network arches the biggest bending in the tie is usually the transverse bending half way between the arches. The optimal shape of network arches is discussed at length. The axial force between the ends of the arches is best taken by prestressing cables.

Pontoons or big cranes can move a network arch to the pillars after it have been built somewhere else. The weight to be moved is much lighter if it consists of the structural steel, plus a temporary lower cord that can carry the casting of the concrete tie. This steel skeleton can also be built on ice in the winter and be lifted onto the pillars. The concrete tie can be cast in the spring.

The author came to think of the network arch when he was doing his master thesis in 1955. Till now around 100 network arches have been built in over 20 countries. There is a lot of information on network arches attached to the author's home page <http://home.uia.no/pert> and in Tveit (2008).

Brandanger Bridge



Figure 1. The Brandanger Bridge in western Norway was opened in 2010. Span 220 m.

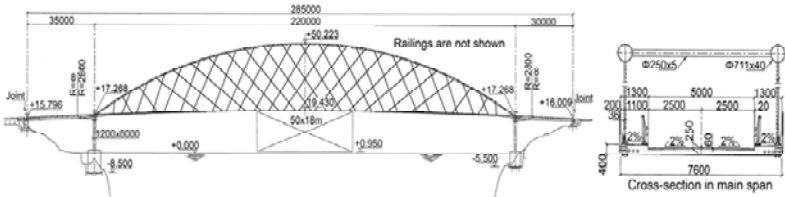


Figure 2. Final design of Brandanger Bridge

The main span weighs 1862 t. It was built on a flat area 5 km from the bridge. It was lifted to the site by two big floating cranes. The continuity in the three spans is not necessary, but in bridges for high speed trains it would have been a good idea. It would have reduced the bumps in the track. Larsen and Jakobsen (2011).

If we define the slenderness of an arch bridge as the span divided by the sum of the heights of arch and tie, the slenderness of the Brandanger Bridge is $220 / (0.711 + 0.4) = 198$. The bridge will probably be the world's most slender arch bridge for very many years to come. When a long span is needed, the arch will normally have more than one lane. Then the arch will be heavier and thicker.

Optimal Design of Network Arches

A network arch is much like a simply supported beam. The arch is the compression zone. The tie is the tension zone. The hangers are a very light web. Most of the shear force is carried to the supports by the vertical component of the axial forces in the arches. The hangers distribute the loads between the chords in such a way that the chords get little bending. Schanack and Brunn (2009) and (2009a).

The arch should be a circle or an ellipse, but never a parabola. The circle is the simplest, but the ellipse shortens the length of the wind portal and gives constant axial force in a longer part of the arch. If the arches are universal columns, the lower parts of the wind portal should have steel plates on top.

When there are two lanes or two railway tracks between the arches, the transversal bending is bigger than the longitudinal bending. The tie should be a concrete slab with small edge beams with room for prestressing cables. The prestressing cables take the axial force in the tie. For everyday loads, there is a lot of longitudinal prestressing in the tie. Pedestrians and cyclists should be outside the arches. Schanack (2009) gives advice on buckling in the arch.

If wider lanes are needed, the concrete slab can be made of concrete with higher strength. Sometimes too big deflections might be counteracted by transversal strands of fibre-reinforced polymer threads under the tie. In wider slab transversal prestressing could be used. In that case, varying the stress in some of the prestressing cables could be used to keep an optimal deflection.

Aesthetics of Optimal Network Arches

Slender network arches look good. You can concentrate on the network arch or the countryside behind it, but you cannot concentrate on both at the same time. Therefore it is an advantage that the network arch covers little of the landscape behind it. The rise of an optimal network arch is normally between 0.15 and 0.2 of the span. The rise is normally smaller in Europe than in the USA.

Fig. 3 shows the author's first bridge before the final painting. The architect recommended that the red colour of the bridge should be kept, but the author did not dare to do this and let the bridge be painted grey. When seeing Chinese arch bridges that were painted red, the author understood that the architect had been right.



Figure 3. The author's first network arch at Steinkjer

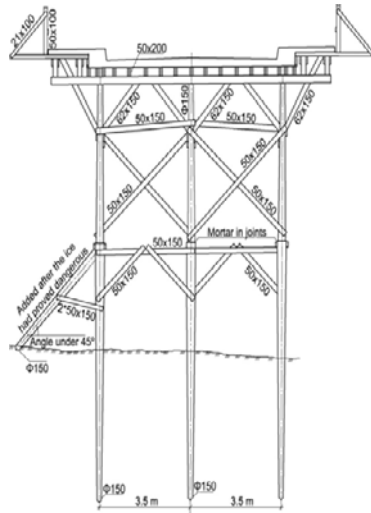


Figure 4. Scaffold for the erection of the network arch at Steinkjer

Erection of the Author's First Network Arch

The structure was supposed to be erected before the winter set in, but the delivery of steel was delayed and a big flood pushed ice toward the scaffold and almost removed it. Deflections in the concrete tie were considerable. However the scaffold was repaired and the bridge was saved and is now in good shape.

Influence Lines for the Author's First Network Arch

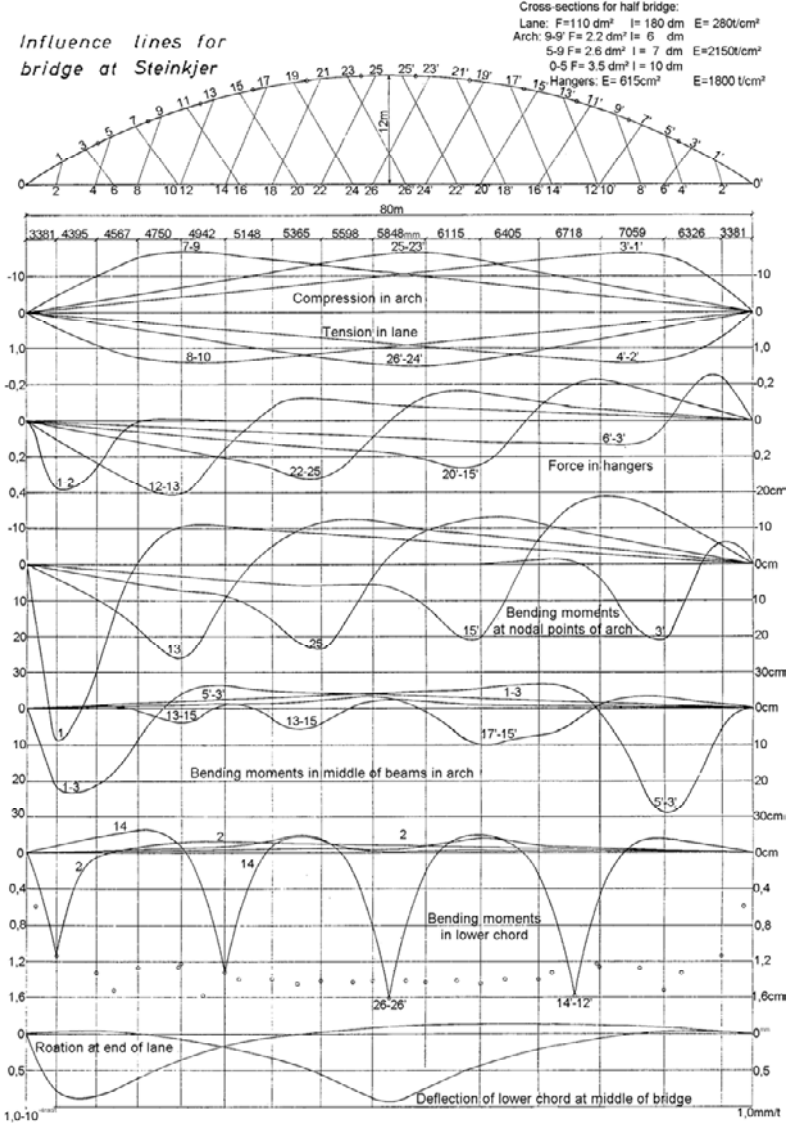


Figure 5. Influence lines for the network arch at Steinkjer in Norway (Opened 1963)

Steel Weight in Optimal Network Arches

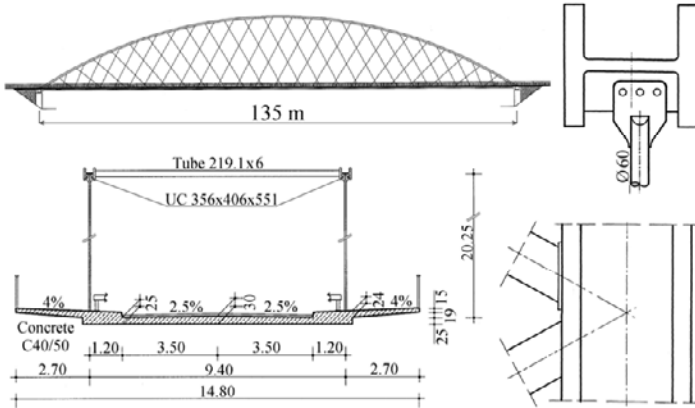


Figure 6. A network arch between two Norwegian islands

A good example of an optimal network arch is shown in fig. 6. It was designed by two students from TU-Dresden. Teich and Wendelin 2001. They did their master’s thesis with the author in Norway. One of the students, Stephan Teich, will defend his doctoral thesis on network arches in 2012. In fig. 7 the steel weight of the network arch in fig. 6 is compared to the steel weight in German arch bridges with vertical hangers. The spans and the years when the bridges were built are indicated. N means that there is no wind bracing. S means that the arches slope towards each other.

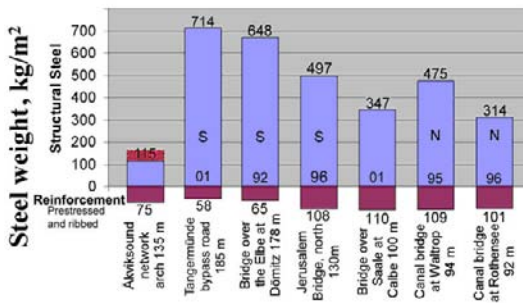


Figure 7. Comparison of steel weights in some arch bridges

The German bridges have steel beams in the tie. Still the network arch use about the same amount of reinforcement without steel beams in the tie. Part of the reason for this is the high amount of minimum reinforcement that is needed in the concrete on top of the elongating steel beams. The cracks over elongated beams give higher maintenance costs. A temporary tie for the Åkvik Sound network arch (dotted area) would weigh 45 kg/m².

An Economic Method for the Erection of the Loftesnes Network Arch in Norway

It was very costly to use the floating cranes that moved the Brandanger Bridge in fig. 1. Methods will be shown for moving the Loftesnes Bridge by means of much smaller cranes or by pontoons.

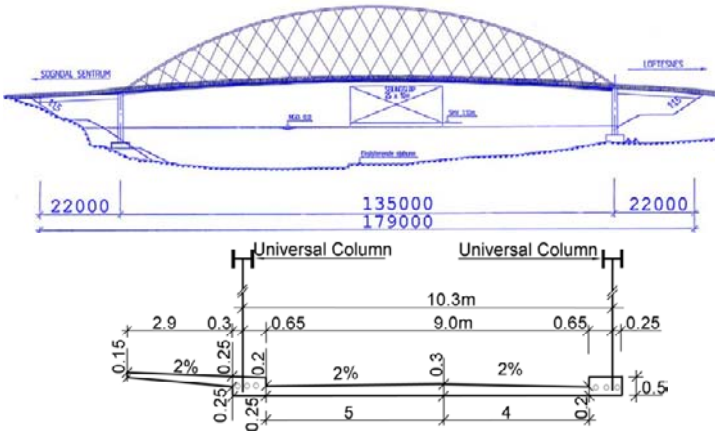


Figure 8. The suggested Loftesnes Bridge in western Norway

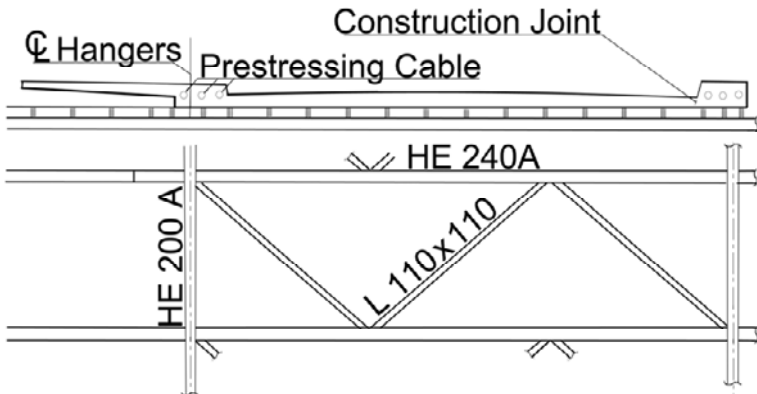


Figure 9. Temporary lower chord for the Loftesnes Bridge

The main spans of the Loftesnes and the Brandanger Bridge both weigh 1862 tonnes. Hiring the floating cranes for moving the Loftesnes Bridge would be costly. Instead we could move a steel skeleton consisting of arches, hangers and a

temporary lower chord made of steel. The skeleton could be lifted by two cranes lifting around 150 tonnes each.

In many cases it might be economical to put in the wooden form and some of the reinforcement before the skeleton was lifted on to the pillars. If all the reinforcement was put in, the weight to be lifted could be around 500 tonnes. If small concrete beams are cast at each end of the span, the lift would be around 530 tonnes.

When the skeleton is on the pillars, the concrete edge beams are cast first starting from both ends to avoid relaxation of the hangers. The lane is cast last. With small alterations the temporary lower chord could be used over and over again in network arches of varying width and length.

Moving Network Arches by Means of Pontoons

In lakes, canals and inland rivers big floating cranes might not be available. Then the steel skeleton, described in the previous section, might be erected on one of the side spans or ramps leading up to the network arch..

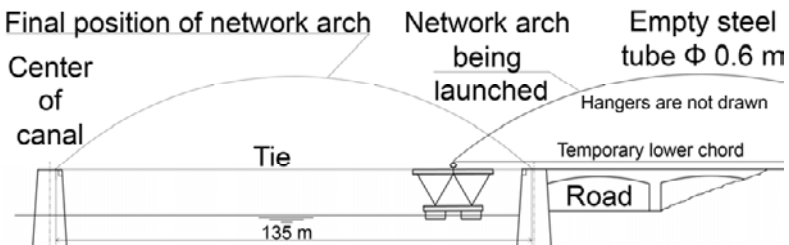


Figure 10. Moving a skeleton of a network arch by means of a pontoon

Summing up Advantages of the Network Arch

General: Since the advantages of network arches are so great, there is no need to exaggerate. Network arches are well suited for railway bridges, but even better suited for road bridges. If the ties are made of concrete, around 70% of the structural steel can be saved. If the tie is made of steel, around 30% of the steel can be saved. The slim tie is an advantage if the traffic over the bridge has to be lifted to let traffic pass under the bridge.

Structural: All members efficiently carry forces that cannot be avoided in any simply supported beam. If a network arch has less than 15m between the planes of the arches, the tie can be a concrete slab with small edge beams with room for prestressing cables. If the span of this slab is more than 10 m, transversal prestress should be considered.

Tension is predominant in tie and hangers. All hangers can have the same cross-section and nearly the same force. H-beams like universal columns or American wide flange beams with horizontal webs can be used in arches. They have a favourable stiffness distribution. Network arches have very small bending moments in the chords. Schanack and Brunn (2009) and (2009)a convincingly explain why the network is more efficient than arch bridges with vertical hangers.

Erection: Erection can be done using a temporary lower chord which combined with the structural steel has the strength and stiffness to carry the casting of the concrete tie. Other efficient methods of erection are available.

Aesthetics: A well designed network arch is likely to remain the world's most slender arch bridge. The slim chords are pleasing to the eye and do not hide the landscape and cityscape that is behind.

Foundations: Lightness and vertical reactions give savings in the substructure. Network arches are not sensitive to uneven settlements in the foundations.

Earthquake: High strength and low weight give the network arch good resistance to earthquake.

Upkeep: Most concrete parts need more maintenance than a concrete slab with a slight prestress. Network arches with concrete ties have small steel surfaces, thus they need little corrosion protection.

References

- Brunn, B. and Schanack, F. (2003) "Calculation of a double track railway network arch bridge applying the European standards" Graduation thesis at TU-Dresden. August 2003. 320 pages. A revised version of this thesis can be found at <http://home.uia.no/pert> under the button "Masters Theses".
- Larsen, R.M Jakobsen, S. E (2010) Brandanger Bridge A light and slender network arch IABSE-IASS 2011. London Symposium Report. p. 334. ISBN: 978-0-7079-7122-3
- Schanack. F. (2009) "Berechnung der Knicklast in Bogenebene von Netzwerkbögen" (Calculation of the Buckling Load in the Plane of the Arches in Network Arches.) Bautechnik, Heft 5, Ernst & Sohn, Berlin.
- Schanack, F. and Brunn, B. (2009) „Analysis of the structural performance of network arch bridges.“ The Indian Concrete Journal. January 2009. pp. 7-13.
- Schanack, F. and Brunn, B. (2009)a "Netzgenerierung von Netzwerkbogenbrücken " (Creation of Nets of Hangers in Network Arches.) Stahlbau, Heft 7 2009, Ernst & Sohn, Berlin.
- Teich , S. and Wendelin, S. (2001) „Vergleichsrechnung einer Netzwerkbogenbrücke unter Einsatz des Europäischen Normenkonzepts.“ (In German). Graduation thesis at TU-Dresden. August 2001. 300 pages. A revised version of this thesis can be found at <http://home.uia.no/pert> under the button "Masters Theses".
- Tveit, P. (2008) "About The Network Arch". <http://elearning-iabse/120>

Seismic Failure Analysis of Huilan Flyover in Wenchuan Earthquake

MENG Jie¹, ZHANG Jiandong², and LIU Zhao³

¹T. Y. Lin. International Engineering Consulting Co., Ltd, Chongqing 401121, China.
Tel: (86)02367033084; E-mail: mengjie@tylin.com.cn

²Jiang Su Transportation Research Institute Co., Ltd, Nanjing, Jiangsu 210096, China

³School of Civil Engineering, Southeast University, Nanjing, Jiangsu 210096, China.
E-mail: mr.liuzhao@seu.edu.cn

ABSTRACT

The devastating Wenchuan earthquake caused substantial flexural failure to Huilan flyover, located in Mianzhu of Sichuan, China. Based on the investigation of bridge damage, three-dimensional mathematical models suitable for eigenvalue analysis and non-linear time-history dynamic analysis are presented. In nonlinear time-history analysis, elasto-plastic mathematical model, effect of pounding and effect of slippage of bearing are studied by sensitivity analysis. Finally, the causations of seismic failure are concluded.

Huilan flyover is located at Huilan Avenue in Mianzhu city and crosses several railway tracks. Four circular concrete ramps flank on both ends of main flyover structures, as shown in Fig. 1.

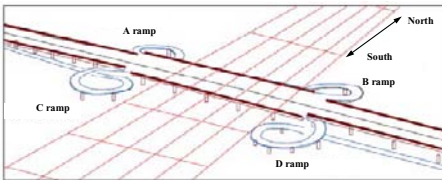


Fig. 1. General layout of Huilan flyover



Fig. 2. Plastic failure at top zone of columns

During the devastating Wenchuan earthquake, significant plastic failure occurred (Fig. 2). After the earthquake, qualitative analysis is given by many researchers based on field reconnaissance (Liu 2009, Sun 2009). The radii of these curved ramps are uniformly small, which are quite vulnerable in earthquake, so it seems that more researches about curved bridge with small radius are necessary for design work in the future. Qualitative and quantitative analysis subject to those curved ramps are carried out in this article; finally, the causations of seismic failure are concluded.

INTRODUCTION

The Huilan flyover consist of four circular, continuous, reinforced concrete ramps, with a radius of 20.25m and a uniform span of 16m. The curved ramps, with a 4.5m wide and 0.95m high box gird, are supported on single-column bents with circular columns 0.8m in diameter; the columns are connected with oversized pile 1.2m in diameter. And the connections, between the top of column and the soffit of girder, are either constructed with moment-resisting connection or bearing supported connection. The detail of supporting forms and seismic failure distribution can be seen in Fig. 3. A, C ramps and B, D ramps have the same structure form, but different failure mode, after earthquake.

EARTHQUAKE INPUT

Qingping seismic observation station, with a distance of 25km, is the nearest one to Huilan flyover. The time history records for Wenchuan earthquake from Qingping station are available for seismic analysis (Fig. 4).

The time history records of earthquake indicating the duration time for earthquake is about 160s; with highly intensity ground motion in time interval of 30~60s. The peak ground acceleration (PGA) values for EW and NS horizontal component, which is about 824gal and 803gal (1gal=1mm/s²) respectively, are closed. The PGA value for UD vertical component, which is the least one, is about 623gal.

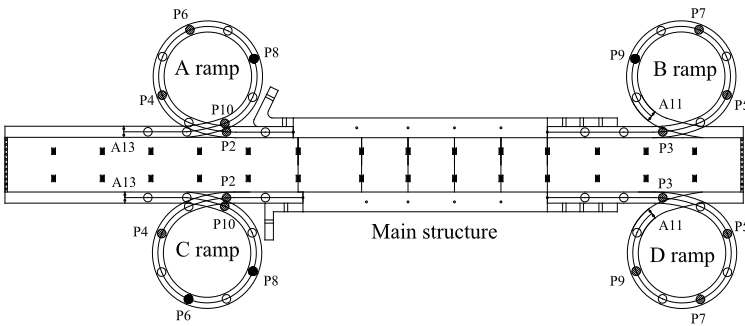


Fig. 3. Connection form detail and plastic failure distribution of Huilan Flyover
 (○ represent bearings support column; ⊗ represent column with moment-resisting connection; ● represent column with plastic failure)

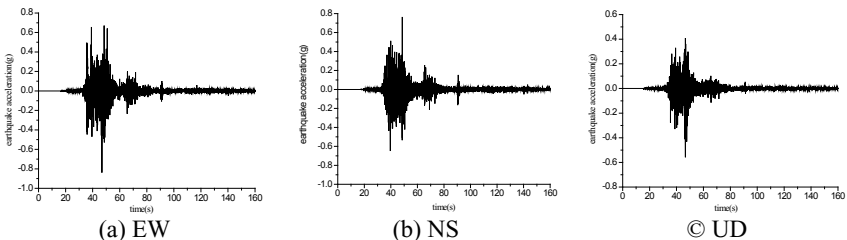


Fig. 4. Time history records for Wenchuan earthquake from Qingping station

BRIDGE ANALYSIS MODEL

Considering the seismic damage trends of four ramps are similar (Fig. 3), it is reasonable to choose model A ramp as typical case for study. In three dimensional mathematical model (Fig. 5), soil-foundation-structure interaction is included by using Winkler spring model (Priesley et al. 1996).

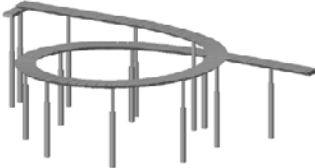


Fig. 5. Analysis model of A ramp

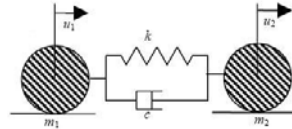


Fig. 6. Kelvin impact model

Boundary pounding model

Due to different dynamic characteristic between ramps and main structures, seismic pounding happened at adjacent boundary and expansion joints locations. Kelvin impact model (Li 2008, Kim and Shinozuka 2003, Kim et al. 2006), with a linear spring element to represent pounding force and a damping element to represent energy loss, has been well applied to approach the real seismic pounding effect, as shown in Fig. 6. Then the pounding force F_{ab} between m_a and m_b can be expressed as follows:

$$F_{ab} = K_{ab}\Delta_{ab} + C_{ab}\dot{\Delta}_{ab} \tag{1}$$

$$\Delta_{ab} = / u_a - u_b / - d_{ab} \geq 0 \tag{2}$$

where the u_a and u_b = absolute displacement of mass m_a and m_b ; the d_{ab} = gap between mass m_a and m_b . The stiffness of the spring is typically large and highly uncertain due to the unknown geometry of the impact surfaces, uncertain material properties under impact loadings, and variable impact velocities, etc. The stiffness of the spring in this study is determined by a sensitivity study. The damping constant which determines the amount of energy dissipated is obtained by following relationship (Anagnopoulos 1995, Kim et al. 2000):

$$C_{ab} = 2\xi\sqrt{K_{ab} m_a m_b / (m_a + m_b)} \tag{3}$$

where ξ is the damping ratio and is assumed to be 5%.

Bearing slippage model

Stainless steel-PTFE bearing are used as sliding bearing in Huilan flyover to allow thermal movements. In the nonlinear analysis, rigid-plastic model (Fan et al. 2003) can be used to represent the sliding bearing, as shown in Fig. 7, where the F_{max} =maximal friction force; X_y =initial sliding movement and is assumed to be 2mm.

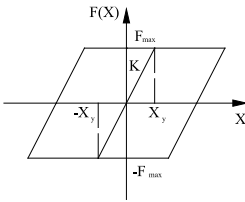


Fig. 7. Model for bearing slippage

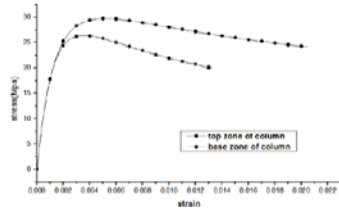


Fig. 8. Mander's model for confined concrete

Model for plastic hinge

The most promising models for the nonlinear analysis of reinforced concrete members are, presently, flexibility-based fiber elements. In these models the element is subdivided into longitudinal fibers. The constitutive relation of the section is derived by integration of the response of the fibers, which follows the uniaxial stress-strain relation of the particular material. In the following analysis, Hognestad's model is used for unconfined concrete, Mander's model for confined concrete (Fig. 8) and Menegotto-Pinto's model for steel bars; the detail parameter for each models can be got in references (Meng 2010).

EIGENVALUE ANALYSIS

The distribution of structure mass and stiffness can be reflected through eigenvalue analysis. Fig. 9 shows the key modes for A ramp of Huilan flyover.

The connections between superstructure and column are constructed with a moment-resisting connection or with a bearing support. As ignoring the stiffness of the column with bearing support, the dynamic characteristic is mainly affected by the stiffness of column with moment-resisting connection. Overall, the higher column dominates the lower order mode; on the contrary, the lower column dominates the higher order mode.

In Wenchuan earthquake, the ramps suffered severe damage. As shown in Fig. 3, plastic failure had been seen in P8 column at A ramp, P9 column at B ramp and P6, P8 columns at C ramp; seismic damage appeared mainly at lower columns location; the damaged column's height is around 4m; from the eigenvalue analysis, the lower columns dominates the higher order mode, with shorter vibration period, and bears more seismic shear force.

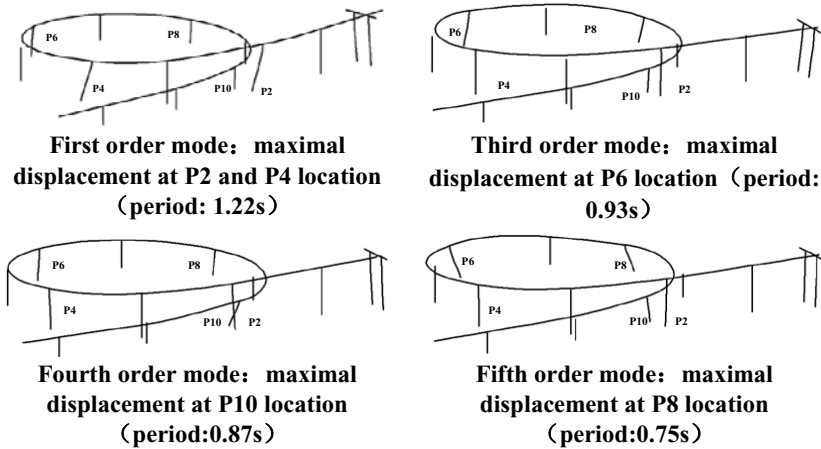


Fig. 9. Key modes

(P2, P4, P6, P8 and P10 are the columns with moment-resisting connection.)

NON-LINEAR TIME-HISTORY ANALYSIS

Vulnerable position deduction

The ramps substructure consists of single column bents with circular columns 0.8m in diameter. The columns are connected with oversized pile 1.2m in diameter; with the pile moment capacity increased, the plastic hinge may occur at the bottom of column. At the same time, the columns with moment-resisting connection may have hinge at the top of columns. Thereby, fiber elements are putted in the top and bottom zone of columns in the analysis model.

The transverse reinforcement layers were uniform 20cm in the columns, only placed relatively close at 10cm along the bottom zone. Clearly, confinement of concrete is improved in the bottom zone of columns compared to the top zone, which means the top zone may be more vulnerable in the earthquake, as shown Fig. 8.

Seismic force effect analysis

Moment–curvature analysis is used to predict the expected ultimate moment and curvature values at plastic zone. Under axial force of dead load, the moment-curvature analysis for top-zone and base-zone are shown in Fig. 10 and Fig. 11, respectively.

The PGA records from Qingping seismic observation station seems too large to real condition. For the purpose to approach the real effect of structure, several cases of time-history analysis are carried out. The details for different case are shown in table 1.

Through the case study of time history analysis (Fig. 12 and Fig. 13), some conclusion are drawn:

1) As the value of pounding force is hard to calculate, sensitivity analysis is conducted. The moment of top columns are hardly affected by the stiffness of

pounding force, as shown in Fig. 14. That is because the pounding force is not always happening and it can only affects the nearby; the pounding force time history at expansion joints is shown in Fig. 15. In case1 and case2, the moment values for top and base section of column are accord with the conclusion from the sensitivity analysis; So, in the case study, the error brought by fixing pounding stiffness = 10^6 kN/m is favorable.

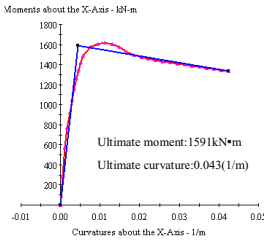


Fig. 10. Moment-curvature curves for top zone

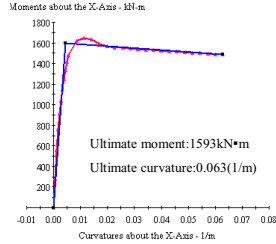


Fig. 11. Moment-curvature curves for base zone

Table 1. Case Study of Time-history Analysis

Analysis method	Reduction coefficient for earthquake intensity	Pounding effect	Bearing slippage effect	Material nonlinearity	Remarks
Case 1	0.2	×	×	×	Basic case
Case 2	0.2	√	×	×	Pounding effect evaluation
Case 3	0.2	×	√	×	Bearing slippage effect evaluation
Case 4	0.2	×	×	√	Material nonlinearity effect evaluation
Case 5	0.2	√	√	√	Ground motion density evaluation
Case 6	0.4	√	√	√	
Case 7	0.6	√	√	√	
Case 8	0.8	√	√	√	
Case 9	1.0	√	√	√	

Note: In the case study, the stiffness of pounding force = 10^6 kN/m; the friction coefficient = 0.05.

2) In case3, as the bearing slippage effect is included in the calculation, the columns with bearing participate in withstanding the ground motion, the distribution of earthquake induced shear force is changed and the earthquake effect for columns with moment-resisting connection is reduced. That is why the distribution of moment for each column with moment-resisting connection in case1 and case2 is different.

3) In case4, the distribution of moment for each columns with moment-resisting connection in case1 and case4 is consistent; But the values in case4 is reduced because of the considering of material nonlinearity.

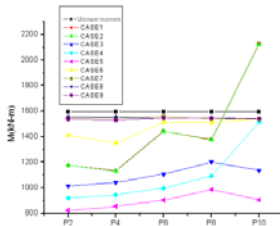


Fig. 12. The moment of top column section under different cases

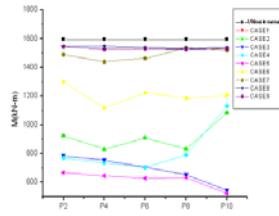


Fig. 13. The moment of base column section under different cases

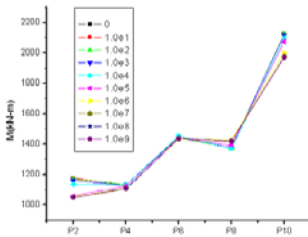


Fig. 14. The moment of top column section under different pounding stiffness

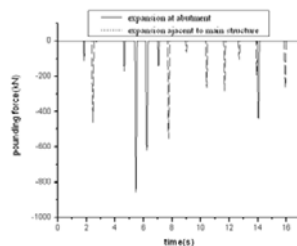


Fig. 15. time-history of pounding force at expansion joints

4) From case5 to case9, the force effect of columns is increasing following the increasing of density of ground motion imported in calculation model. In case5 and case6, not all columns reach the ultimate moment. On the contrary, all the columns reach the ultimate moment and form plastic hinge in case7 to case9. After the plastic hinge forms, the columns reach the ultimate capacity, relying on the deformation to dissipating earthquake energy.

Plastic deformation analysis

From the force effect analysis, it is known that plastic hinge forms in case7 to case9, and the column reach the ultimate force capacity; then the member inelastic rotation and ductility capacity is of great interest. Principle curvature is used for assessing the member inelastic rotation, which could be expressed as follows:

$$\varphi_i = \sqrt{\varphi_{it}^2 + \varphi_{ir}^2} \tag{4}$$

where φ_i represent principle curvature at time $t=i$; φ_{it} represent tangential curvature along axes of ramps at time $t=i$; φ_{ir} represent radial curvature along axes

of ramps at time $t=i$. Thus, the maximal principle curvature φ_{max} along the time history can be used to assessment the inelastic rotational capacity.

Fig. 16 and Fig. 17 show the maximal principle curvature for top and base section of columns with moment-resisting connection respectively, from case7 to case9. In case7 (Reduction coefficient for earthquake intensity:0.6), only the φ_{max} of top section for P8 column exceed the ultimate curvature achieved from the moment–curvature analysis (see Fig. 16), which means the plastic failure occurs at top zone of P8 columns; that coincides with the real failure condition. Contrarily, in case8 and case9, the top zone of each column exceeds the ultimate curvature and plastic failure happened, which is different to real condition; the same trend can be seen in the base section of columns (see Fig. 17). So the deduction that real PGA of ground motion at Huilan flyover is about 0.6 times (about 500gal) of the one recorded in Qingping seismic observation station is reasonable.

The friction coefficient of PTFE on stainless steel is about 0.02 to 0.03 (depending on possible lubrication) for very low slip rates, such as in the case of temperature or creep movements, but it is much higher and dependent on pressure and sliding velocities at typical earthquake velocities. For typical earthquakes velocities and typical pressure for bridge bearings, the friction coefficient ranges from about 0.10 to 0.15 or more for un-lubricated bearings. As shown in force effect analysis, the friction coefficient of sliding bearings will change the distribution of seismic shear force for each column, so the sensitivity analysis for different friction coefficient is necessary.

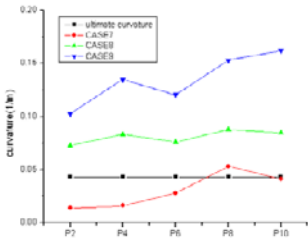


Fig. 16. Maximal principle curvature for top section of columns, from case7 to case9

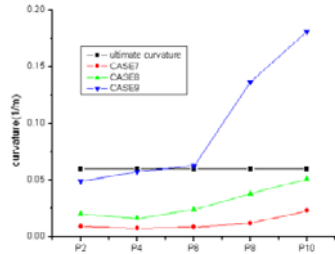


Fig. 17. Maximal principle curvature for base section of columns, from case7 to case9

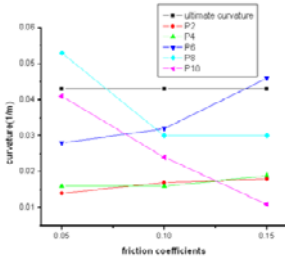


Fig. 18. Maximal principle curvature for top section of columns, under different friction coefficient

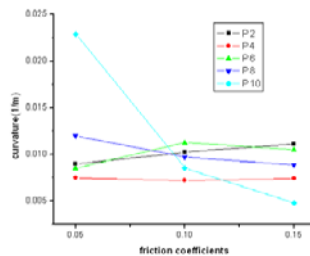


Fig. 19. Maximal principle curvature for base section of columns, under different friction coefficient

Fig. 18 shows the maximal principle curvature for top section of columns with moment-resisting connection, under different friction coefficient. As the friction coefficient increases, the value of plastic rotation for P2, P4 and P6 increases, but the value for P8 and P10 decreases. When the friction coefficient equals 0.05, plastic failure occurs at P8 column location only, which coincides with the real failure mode. When the friction coefficient equals 0.1, no plastic failure happens. When the friction coefficient equals 0.15, the plastic failure occurs at P6 column location instead of P8.

Fig. 19 shows the maximal principle curvature for base section of columns with moment-resisting connection, under different friction coefficient. As the friction coefficient increases, the trends for plastic rotation are same as the top zone of columns. But the value of plastic rotation remains at low level, so the base zone of columns are all in safe.

From the analysis hereinbefore, the bearing friction coefficient will change the distribution of seismic shear force in each columns, which means different bearing friction coefficient will lead to different failure mode for ramps of Huilan flyover.

SEISMIC FAILURE ANALYSIS

(1) During the devastating Wenchuan earthquake, significant plastic failure occurred in the circular concrete ramps flank on both ends of main flyover structures. Plastic failure had been seen in P8 columns at A ramp, and P9 column at B ramp, and P6, P8 columns at C ramp. Seismic damage appeared mainly at lower columns; the damaged column's height is around 4m; from the eigenvalue analysis, the lower columns dominate the higher order mode, with shorter vibration period, and bear more shear force.

(2) Through investigation of the original design for Huilan flyover, it is found that the transverse reinforcement layers were uniform 20cm in the columns, only placed relatively close at 10cm along the bottom zone. Clearly, lack of confinement in the top zone (potential plastic hinge zone) is the main reason for concrete crush failure in the top connecting joints of columns.

(3) Through several case studies using nonlinear time history analysis, some conclusion can be drawn as follows: firstly, the PGA at Huilan flyover is 500gal around. Secondly, the connections between superstructure and column are constructed with a moment-resisting connection or with a bearing support; in three-dimensional analysis model, considering the columns with bearing support participating in bearing seismic shear force or not is directly related to the distribution of shear force among each column; and different bearing friction coefficient will lead to different failure mode for ramps, thus that is why A and C ramp have same structure form, but different failure mode after Wenchuan earthquake.

REFERENCES

- Anagnopoulos, S.A. (1995). "Earthquake Induced Pounding; State of the Art." **Tenth European Conference on Earthquake Engineering** pp. 897-905.
- Fan, L., Ni, L., and Li, J. (2003). "Dynamic Characteristic Analysis of Laminated Rubber Bearing Sliding under Earthquake." **China Journal of Highway and Transport** 2003.10.16(4), pp. 30-35.
- Kim, S.H., Lee, S.W., and Mha H.S. (2000). "Dynamic Behaviors of Bridges

- Considering Pounding and Friction Effects under Seismic Excitations.” **Structural Engineering and Mechanics** 20(6): 621-33.
- Kim, S.H. and Shinozuka, M. (2003). “Effects of Seismically Induced Pounding at Expansion Joist of Concrete Bridges.” **Journal of Engineering Mechanics** 129(11): 1225-1234.
- Kim, S.H., Mha, H.S., and Lee, S.W. (2006). “Effects of Bearing Damage upon Seismic Behaviors of a Multi-span Girder Bridge.” **Engineering Structures** (28): 1071-1080.
- Li, Z. (2008). “Equivalent Kelvin Impact Model for Pounding Analysis of Bridges during Earthquake.” **Engineering Mechanics**, 2008.4.25(4), pp. 128-133.
- Liu, Z. (2009). “Reconnaissance and Preliminary Observations of Bridge Damage in the Great Wenchuan Earthquake, China.” **Structure Engineering International** 2009.3, pp. 277-282.
- Meng, J. (2010). **Seismic Damage Analysis of Huilan Flyover in Wenchuan Earthquake and Research on Seismic Design of Curved Bridges**. Master Thesis. Southeast University.
- Priesley, M.J.N., Seible, F., and Calvi, G.M. (1996). **Seismic Design and Retrofit of Bridges** A Wiley-Interscience Publication.
- Sun, Z. (2009). “Damage Investigation of Huilan Interchange in Mianzu after Wenchuan Earthquake.” **Journal of Earthquake Engineering and Engineering Vibration** 2009.8.29(4), pp. 132~138.

Fatigue Considerations in Design of Cable-stayed Road-rail Bridges with Orthotropic Steel Deck

Xiaohu Chen, Delan Yin, Yaping Lai, and Xiaofei Liu

T.Y. Lin International Engineering Consulting (China) Co., Ltd, 6 Furong Road, New North Zone, Chongqing, China 401121

ABSTRACT

With China's nationwide development of urban rail transit, several dual purpose road-rail major bridges have been or are being built in metropolitan areas and many more are yet to come. Most of these major bridges will be cable-stayed long-span structures with orthotropic steel deck. However, it has been lack of well recognized criteria and code specifications to fully accommodate their design process. Furthermore, fatigue considerations have not been clearly addressed in many cases because of the complexity to determine both fatigue load and resistance. Taking one such bridge currently under construction as an example, this paper proposes a practical fatigue design approach for dual purpose cable-stayed steel bridges by combining results from fatigue load definition, fatigue detail categorization, global and local structural analysis, fatigue strength determination, and its comparison to European standards.

BACKGROUND

Urban rail transit has been under rapid development in China for the last decade. Before 2000, urban rail transit only existed in three metropolitan cities: Beijing, Shanghai, and Guangzhou. By 2010, the total in service length of rail transit routes has reached 1400 kilometers. Moreover, additional 2700 kilometers are planned to be built in 28 cities in the next five years. In metropolitan areas where big river runs through, such as Shanghai in East China and Chongqing in West China, construction of long-span bridges may be in necessity to fulfill both transportation and navigation needs. Because the resource of suitable river-crossing bridge sites is rather limited in terms of geological and hydrological conditions, a long-span bridge allowing for both roadway and rail traffic is highly desirable where rail transit applies. A major bridge with dual road-rail function is also more cost effective than two separated bridges provided transportation planning is adequately considered.

During the past a few years several dual purpose road-rail major bridges have been built or are currently under construction. Among them two are worth mention: The Caiyuanba Yangtze River Bridge in Chongqing, and the Second Minpu Bridge in Shanghai. The Caiyuanba Yangtze River Bridge (see Figure 1) is a steel tied-arch bridge with a main span of 420 meters. The main girder of the bridge is a combined steel truss-orthotropic steel deck structure which carries six lanes of roadway on its upper deck as well as double-line light rails on its lower deck. The Second Minpu

Bridge (see Figure 1) is the 9th Huangpu River crossing but the first to carry dual traffic. It is a single pylon cable-stayed bridge with a main span of 251 meters. The structural type of the main girder is also a steel truss girder with orthotropic steel plate on both upper and lower decks, very similar to the Caiyuanba Yangtze River Bridge.



Figure 1. Caiyuanba Yangtze River Bridge (left) and Second Minpu Bridge (right)

Rail transit service requires much higher structural rigidity than roadway traffic, which may control the design of a dual function bridge. In this sense, arch bridge and cable-stayed bridge are more desirable structural types for long-span rail bridges than girder bridge or suspension bridge. Moreover, cable-stayed bridge will be more favorable in most cases because of its relative lower cost and shorter construction period.

CABLE-STAYED ROAD-RAIL BRIDGE WITH ORTHOTROPIC STEEL DECK

It has been lack of well recognized criteria and code specifications to fully accommodate the design process of cable-stayed or any type of long-span dual purpose road-rail bridges. In China two design codes are separated and serve independently for design of highway bridge and railway bridge. Nor much international standard can be relied on. For example, the deduction factor is not specified when combining of truck load and rail vehicle. It has to be included in special design provisions for each bridge along with many other definitions otherwise ambiguous.

Furthermore, fatigue considerations have not been clearly addressed because of the complexity to determine both fatigue load and resistance. Combined structure of steel truss and double decks of orthotropic steel plate has been the common choice for the main girder of cable-stayed road-rail bridges, in which the lower steel deck not only improves the bridge's torsion resistance, but also serves as the platform for rail tracks. However, this combination introduces more issues to fatigue design of orthotropic steel plates. For the upper deck, fatigue is induced by truck wheel load as well as by stay cable force, while for the lower deck, it is induced by rail vehicle wheel load. In the same time, acting as part of the main girder, both orthotropic plates

at top and bottom also bears fatigue load for global structure of the bridge.

Taking one such bridge currently under construction as an example, the remaining part of this paper discusses a practical fatigue design approach for dual purpose cable-stayed steel bridges by combining results from fatigue load definition, fatigue detail categorization, global and local structural analysis, fatigue strength determination, and its comparison to European standards.

A CABLE-STAYED ROAD-RAIL BRIDGE UNDER CONSTRUCTION

The Dongshuimen Yangtze River Bridge (see Figure 2) is a cable-stayed bridge located in Chongqing City, which is known as “Bridge Capital” of China. The bridge crosses the Yangtze River with a main span of 445 meters and a total length of 858 meters, carrying four lanes of highway traffic as well as double-line urban rails. It has twin pylons of 110 meters above the deck and one single cable plane with 9 pairs of stay cable at each pylon.

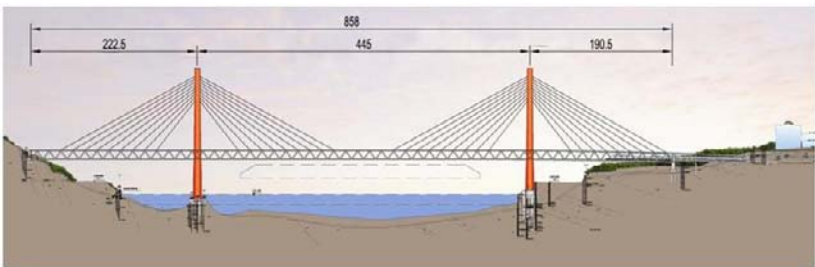


Figure 2. Rendering of Dongshuimen Yangtze River Bridge (m)

The main girder of the bridge (see Figure 3) is composed of a steel truss and double decks of orthotropic steel plate. The steel truss is 13 meters deep and 15 meters wide. The thickness of the orthotropic steel deck is 16 mm.

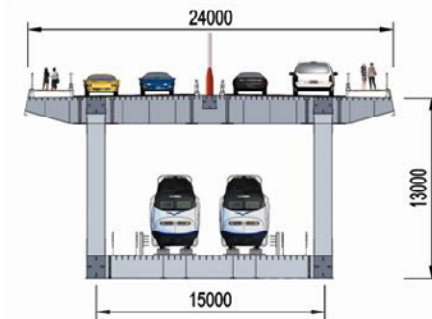


Figure 3. Cross section of main girder (mm)

The Dongshuimen Yangtze River Bridge has been under construction since December 2009. The construction is expected to be completed by 2013.

DEFINITION OF FATIGUE LOADS

Due to lack of predicted highway traffic data, in many cases it is impractical to define the load spectrum of fatigue trucks for a particular bridge. The more realistic way is to use a single equivalent fatigue truck. The steel highway bridge design code (China DOT, 2009) specifies the equivalent fatigue truck (see Figure 4), which is very similar to what has been presented in the Eurocode 1 (BSI 2003).

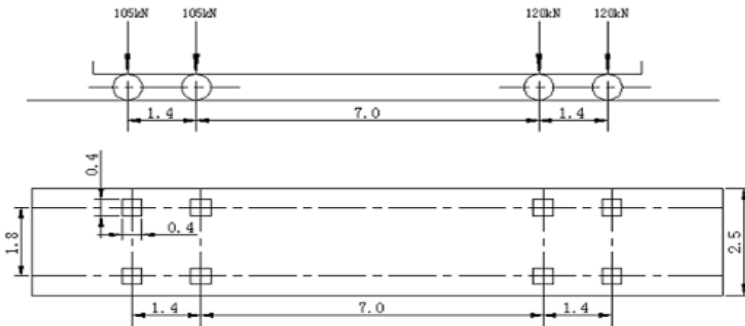


Figure 4. Plan and elevation of equivalent fatigue truck (m)

On the other hand the fatigue load of rail vehicle is identical to its global loading condition. In this case one rail vehicle consists of six rail cars. Each single rail car (see Figure 5) has four axle loads of 140 kN for a total weight of 560 kN. The effect of rail fatigue load to the upper steel deck is reflected through the stay cable force.

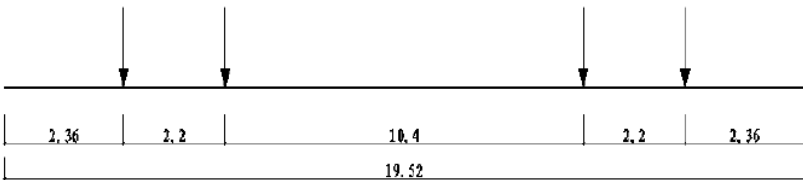


Figure 5. Layout of axle loads of single rail car (m)

FATIGUE DETAIL CATEGORIZATION

For design of steel structure, critical fatigue details have to be thoroughly identified for each welding or bolting connection. The design fatigue strength is then determined by categorizing each detail to an equivalent type specified in design specification.

The Eurocode 3 (BSI 2005, 2006) has the most comprehensive fatigue detail categories and is adopted in defining fatigue details in design of the Dongshuimen Yangtze River Bridge. Eight critical fatigue details (see Figure 6) are identified through this step for the upper deck as well as the stay cable anchorage.

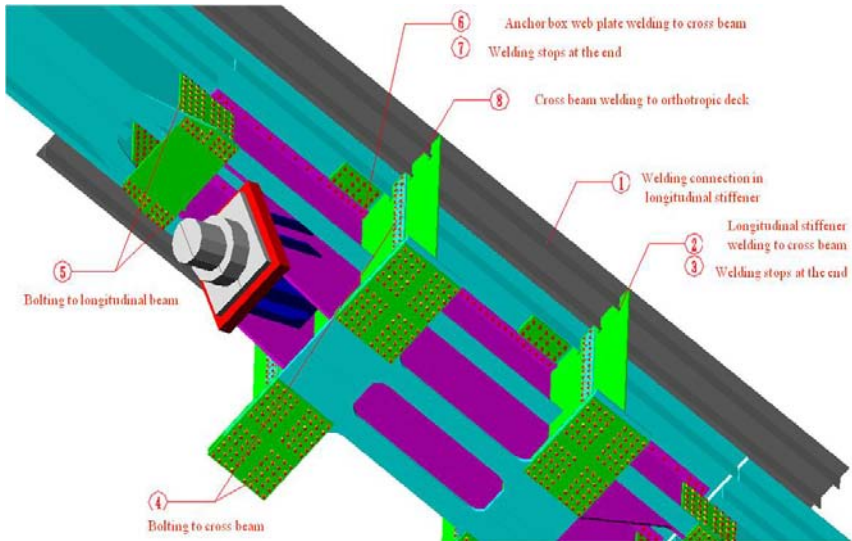


Figure 6. Fatigue details in upper deck and stay cable anchorage

GLOBAL AND LOCAL ANALYSIS

The fatigue problem in orthotropic steel plate is induced by combination of global loading and local wheel loading.

The upper and lower steel decks, the steel truss consisting of top and bottom chords as well as diagonal web members, and transverse diaphragms and secondary crossbeams together form the main framework (see Figure 7) to carry global roadway and rail loads.

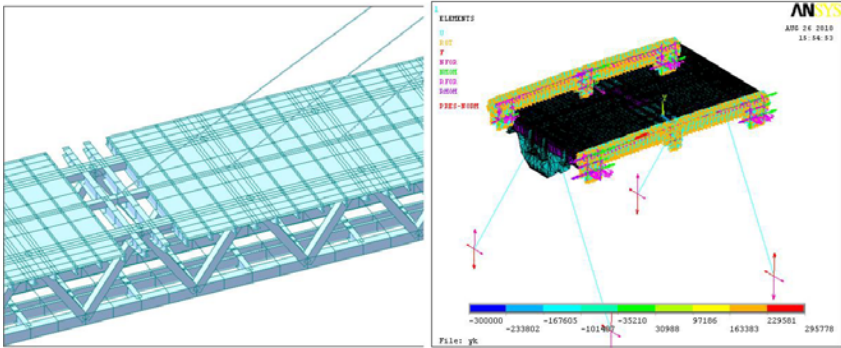


Figure 7. Global analysis model (left) and local analysis model for upper deck

The maximum global fatigue stress $\Delta\sigma$ at top and bottom of the upper steel deck (see Figure 8) is 31.9MPa and 49.2 MPa, respectively, which is well under the allowable fatigue stress of grade 345 steel. So design of the orthotropic plate is not controlled by fatigue.

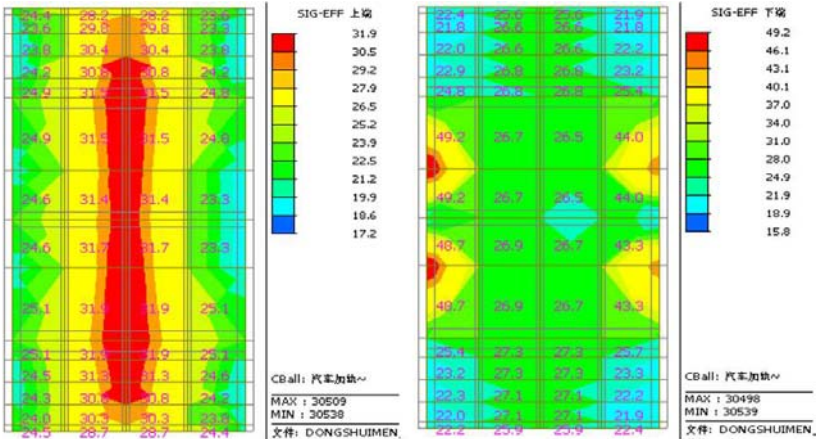


Figure 8. Global fatigue stress at top (left) and bottom (right) of upper deck

The local analysis model is composed of three 16 meters-long girder segments for a total length of 48 meters. For the upper deck (see Figure 7) wheel load is applied directly on top of orthotropic steel plate neglecting the stress dispersion by the pavement. While for the lower deck the stress dispersion by the concrete ballast bed is considered because of its significant thickness. The stay cable force due to live load is applied simultaneously with wheel loads.

The fatigue stress distribution at the detail of anchorage web plate welding to transverse diaphragm is shown in Figure 9. The maximum stress range is used to compare with the corresponding fatigue strength defined in the Eurocode for this detail as well as for other critical detail previously identified.

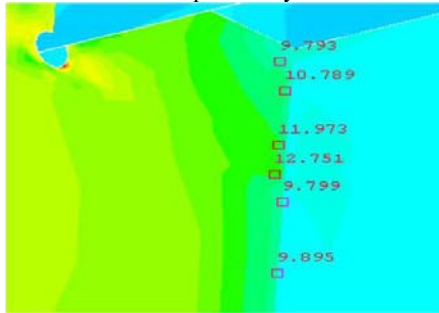


Figure 9. Fatigue stress distribution at anchorage web plate welding to diaphragm

ASSESSMENT OF FATIGUE DETAILS

In past designs for the equivalent fatigue truck used the fatigue strength is usually determined at the 2 million cycles, which is corresponding to a traffic volume of 2 million annually. In most cases this appears low, with 5 million loading cycles mark now commonly recognized as the threshold not to require a traffic volume check. Furthermore, the life-time loading cycles of rail fatigue vehicle can be accurately predicted. Assuming the rail transit service operates 16 hours daily running every 3 minutes during 8 peak hours and every 5 minutes during non-peak hours, the total number of rail loading cycles would be 18.7 million during the bridge's design life of 100 years. With consciousness to many cracking problems in orthotropic steel plate bridges, 20 million loading cycles are taken for both truck and rail fatigue loads to determine the fatigue strength with the Eurocode 3 (see Figure 10) so appropriate assessment on design details can be performed.

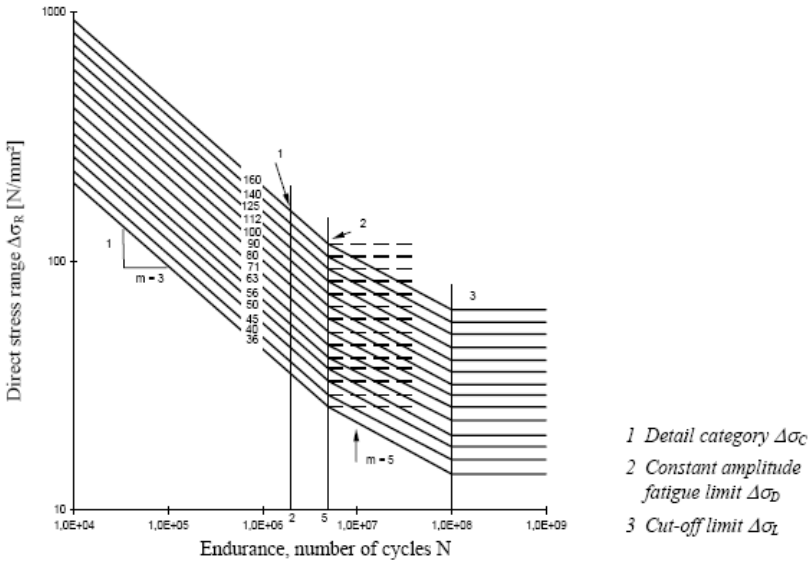


Figure 10. Fatigue strength determination with Eurocode 3

The calculated fatigue stress and corresponding allowable stress for upper deck details are listed in Table 1, where the numbers in the first column are corresponding to the numbering in Figure 6. The results show that these critical details have adequate fatigue strength in duration of 20 million cycles of combined truck and rail vehicle loadings. The calculated fatigue stress for details in the lower deck turns out to be far less than the allowable so fatigue does not control its design. This is largely because the local stress has been dispersed through the ballast bed before it is transferred to the orthotropic steel plate.

Table 1. Assessment of Fatigue Details in Upper Deck

Fatigue Detail	Calculated Stress Range (MPa)	Eurocode 3 Allowable Stress (MPa)	Number of Cycles, N
□	31.3	62.5	20 million
②③	19.8	31.3	20 million
④⑤	7.3	62.5	20 million
⑥⑦	12.8	44.7	20 million
⑧	16.6	39.6	20 million

CONCLUSION

Taking one bridge as example, this paper illustrates a practical and adequate process for fatigue design of cable-stayed road-rail bridge with orthotropic steel decks. With growing development of urban rail transit in China, more major dual function bridges are yet to come. In lack of uniform standard, this approach provides reference to future projects in addressing fatigue design issues.

REFERENCES

- China Department of Transportation (2009). *Design Specifications for Steel Highway Bridges*, JTG/T D64-2009, Tentative Version.
- British Standards Institution (2003). *Eurocode 1: Actions on structures — Part 2: Traffic loads on bridges*, BS EN 1991-2:2003.
- British Standards Institution (2005). *Eurocode 3: Design of steel structures — Part 1-9: Fatigue*, BS EN 1993-1-9:2005.
- British Standards Institution (2006). *Eurocode 3: Design of steel structures — Part 1-1: General rules and rules for buildings*, BS EN 1993-1-1:2006.

Waterproofing Solutions for Metro Tunnels

Francis Lung, Ph.D.

Deputy Chairman & CEO, Hydrotech International, Australia. E-mail: francis.lung@hydro-usl.com

ABSTRACT

Almost all underground structures suffer from water leakage problems. Traditional methods using injection for waterproofing in underground metro tunnels can only reduce large water leakages; they are not effective in preventing water from seeping into the tunnel. In addition, traditional injection methods cannot prevent reinforcing steel corrosion in concrete structures. The reinforcing steel can expand by twice its original volume after reacting with water and oxygen in producing ferric hydroxide. This phenomenon causes deterioration and spalling of concrete cover around the reinforcing steel. If this problem is not attended to, the longer-term structural integrity of the tunnel will be impaired. An innovative solution making use of the electro-osmosis theory has been devised and implemented in London Underground and the MTR in Hong Kong. It is an effective way of keeping underground structures dry, and at the same time, protecting the structural integrity of reinforced concrete. This paper discusses how the electro-osmosis theory can be applied to these structures and examples demonstrating how the technology can be applied in real situations.

INTRODUCTION

Water has a habit of getting into basements and tunnels through concrete walls. The problem with water ingress is that water acts as the catalyst for corrosion to reinforcing steel inside concrete. Indeed, the corrosion rate of wet concrete is approximately 30 times that of dry concrete. The picture below shows the typical appearance after long periods of water ingress where calcification on the wall can be clearly seen due to dissolved chloride carried to the wall surface by water.

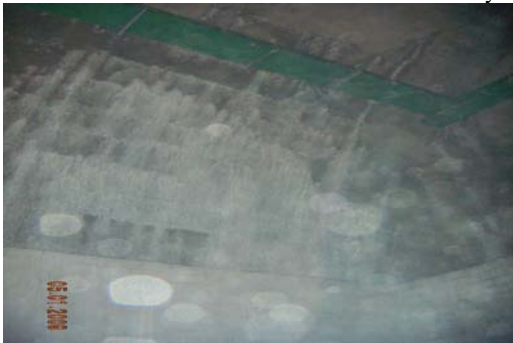


Figure 1. Concrete wall calcification from water ingress

The traditional approach for waterproofing concrete has been by adopting methods to prevent water getting through; this has been done by putting a membrane or coating layer mainly on the external surfaces.

Membranes, tanking, and surface coatings are invariably thin sections and rely heavily on the skill of the applicator to ensure integrity. When barrier systems fail, the causes of failure may be due to bad jointing, pin holing, and damage during back-filling operations; or, they may simply come down to poor workmanship. In most cases failure is on the wrong side of the structure which makes repair almost impossible, as water tends to travel behind membranes with water ingress being seen on the structure far away from the actual point of damage to the barrier system. The tendency is to accept that the structure will inevitably leak and to provide a drained cavity system inside the structure. Another way is to take the remedial measure of sealing the cracks by injecting polyurethane or epoxy into the concrete body when leaks occur as demonstrated in the Figure 2. However, injection is unlikely to be a permanent solution because concrete has a natural affinity for water. According to the concrete water absorption test under BS1881, Part 222, one cubic meter of good quality dry concrete can absorb 60 litres of water in 30 minutes. Water will inevitably find its way to other areas of the concrete structure despite the fact that the injection method can seal the large cracks.



Figure 2. Concrete Wall Calcification from Water Ingress & Polyurethane Injection

CAPILLARY ABSORPTION IN CONCRETE

In fact, the main mechanism for water absorption in concrete is small capillary tubes in the concrete structure. Capillaries are formed during the hardening of concrete. As excess water slowly dries, it leaves tiny passages in the concrete structure (Figure 3).

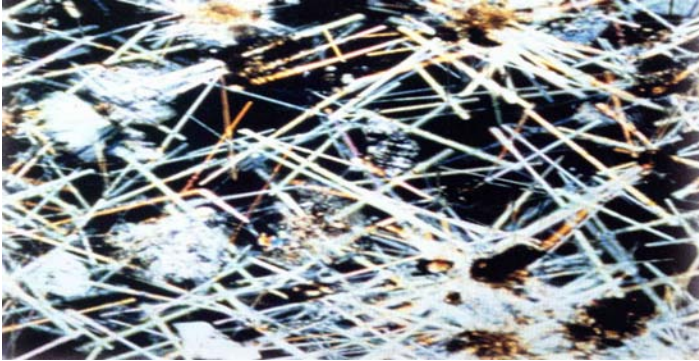


Figure 3. Microscopic view-Capillary tubes in concrete (4000x magnification)

Dr. Andrew Butler, Transport Research Laboratory (TRL), has shown in his paper 'Capillary absorption by concrete'¹ that the speed of water penetration into concrete through capillary absorption is in the order of a million times faster than permeability.

Reuss first discovered the electro-osmosis phenomenon in 1809, observing that water could be forced through a clay-water system when an external electric field was applied to soil. Actually, water flow is initiated by the movement of positively charged ions (cations) present in the fluid of clay pores or similar structures such as concrete, resulting in the water surrounding the cations moving with them.

Electro-osmotic systems for waterproofing masonry walls started in Europe in the 1960s. The main use at that time was for the prevention of rising damp from masonry through capillary action by applying a steady "positive" direct current at the point where the damp course was installed. However, rapid corrosion on the cathode was observed.

The corrosion problem can be resolved by incorporating a pulsating electric current consisting of a few positive voltage pulses on the concrete, followed by a negative pulse and a period of rest when no voltage is applied. The pulse interval for the positive voltage pulse is longer than the negative voltage in order to ensure that water flows in one direction in the capillary channels. Assuming the outer wall of the concrete is exposed to water, applying positive electrical pulses to the inner wall will cause cations (e.g. Ca^+) and associated water molecules to move to the outer wall against the hydraulic pressure gradient and prevent water penetration into the concrete structure. Experiments have shown that the hydraulic pressure gradient resistance can be as high as 60 barg (or 600 meters pressure head). Hydrotech's proprietary technology, the MPS® System (Multi-Pulse Sequencing), is currently being used by Hydrotech International to dry out internal surfaces of concrete walls in tunnels and building basements in projects around the world. Figure 4 shows diagrammatically how the MPS® System works.

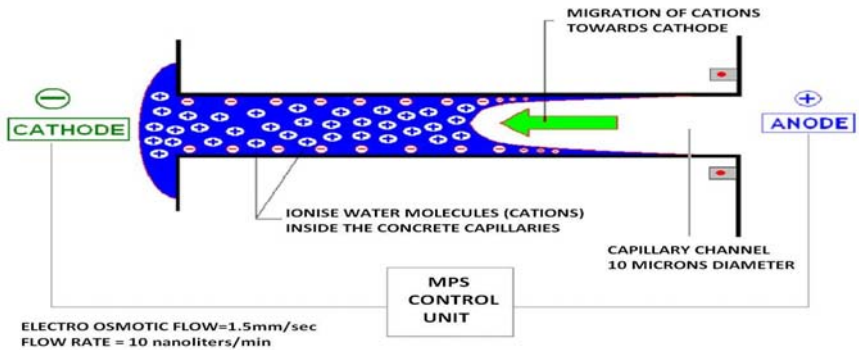


Figure 4. Electro-osmotic process in a capillary tube

ADVANTAGES OF THE MPS® SYSTEM

Unlike membrane or coating waterproofing technologies, which provide a passive barrier to prevent water ingress, the MPS® System produces an electromagnetic barrier that actively prevents water molecules from penetrating through the concrete structure. This active method of water prevention has the following advantages over membrane or coating type installations:

1. It dries out masonry and concrete within a sub-structure. This is particularly important in concrete, as the corrosion rate in wet concrete is approximately 30 times higher than in dry conditions; this will prolong the life of the concrete structure;³
2. It stops efflorescence, which is a whitish, powdery deposit on concrete structure surfaces;
3. It reduces buildup of mold, fungi, micro-organisms and other bacteria elements; this is particularly important when health and hygiene are key design considerations;
4. As air quality is playing an increasingly important role in underground railway systems, the MPS® System helps improve air quality within the underground tunnel; and
5. Energy consumption for MPS® installations is typically very low, equivalent to the energy cost of an electric light bulb.

Because of these advantages, electro-osmosis is ideally suited in underground structures where water ingress is constantly an issue, especially when it is hard to identify the source of water.

INSTALLATION AND CHARACTERISTICS OF MPS® SYSTEM

Installation of the MPS® system is relatively simple. There are essentially four steps and these are illustrated in the diagrams below.



Step 1: Cut grooves of 2 cm x 1 cm and fit titanium wires into the grooves.



Step 2: Put conductive grout on the grooves to hold titanium wires in place.



Step 3: Insert the cathode on the outside wall to complete the electric circuit



Step 4: Connect the electric circuit to the control box to start the electro-osmosis operation

Figure 5. Installation of MPS® System

According to British Standard BS6150, concrete is considered to be damp in a wall where relative humidity stays at 90%-100%. If the relative humidity is below 75%, the concrete is considered to be dry. If the wall relative humidity is between 75% and 90%, the concrete is considered to be drying.

Typically, it takes two to three months for the MPS® system to work through and dry the concrete structure. The following graph demonstrates the characteristics of the drying process by the MPS® system.

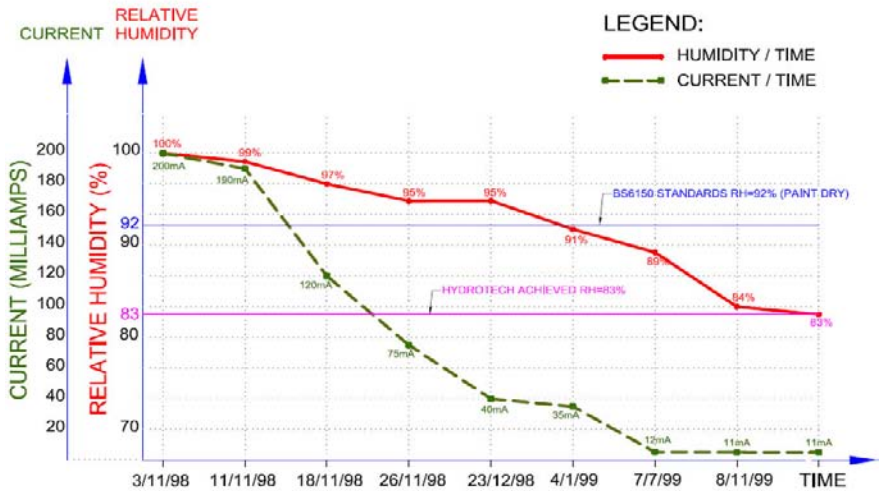


Figure 6. Relationship between Relative Humidity and MPS® System Current during drying process

The graph shows that the MPS® system automatically controls the electric current to be delivered into the concrete structure. The electric current is higher when the wall is wet, and, as the wall dries, the current decreases accordingly. In this case, the system took approximately 2 months before the wall surface reached paint dry status (92% relative humidity). It then took a further 6 months to reach the eventual wall dryness in the project.

EXAMPLES OF UNDERGROUND INSTALLATIONS

London Underground – Walthamstow Station

Walthamstow is a London Underground station that has been in operation since 1894. It had been suffering from water ingress problem for a long time and many methods had been used to prevent the water ingress problem; they were all ineffective. The MPS® system was installed on the inner walls of the station in 2006. Following the installation, and in order to ensure the system worked properly, the system was placed under observation for a period of two years. On 17 April 2008, the London Underground issued the trial completion certificate for the successful operation of the MPS® system and is still found to be one of the most effective systems in the prevention of water ingress today. A similar electro-osmosis technology is currently being adopted by the US Army Corps of Engineers to prevent ground water intrusion into military bunkers and underground ammunition storage facilities.



Figure 7: MPS® Installation Pictures for Walthamstow Underground Station

Hong Kong MTR – Central Subway at Hong Kong Station

There is a pedestrian walkway linking the Central and Hong Kong Stations in the Hong Kong MTR system. In 2000, MPS® was installed on the subway to prevent water ingress into the station. In addition to the prevention of water ingress, MTR finds the installation effective in maintaining good air quality, and there is no mold in areas where MPS® has been installed. In 2008, MTR issued a satisfaction certificate noting that MPS® was also effective in protecting the artwork in that subway.



Figure 8. MPS® Installation at MTR Central to Hong Kong Station pedestrian walkway

CONCLUSIONS

This paper demonstrates that the MPS® system is an effective alternative method in controlling water ingress problems with the added benefits of extending the life of the concrete and improving the air quality of underground structures. Applications in station boxes are particularly useful as air quality is an increasing concern of metro passengers.

REFERENCES

- Butler, A. (1998) "Capillary Absorption by Concrete," Transport Research Laboratories, UK.
- Crow, D.R. (1974). "Principles and Application of Electrochemistry," Chapman and Hall, London.
- Marshall, O.S., Hock, V.F. (2009). "Dehumidification for Enhancement of Electro-osmotic Pulse Technology in Underground Storage Facilities," DoD Corrosion Conference, US.

Experimental Study of the bearing capacity of double CFST member

Zhongfu XIANG¹ and Yang YU¹

¹ School of Civil Engineering and Architecture, Chongqing Jiaotong University, Chongqing 400074, China

ABSTRACT

In this article, the bearing capacity of double CFST (concrete filled steel tube) members is analyzed and simulated tested, aim at SFST member sections which is composed by coating steel tube covered outside conventional CFST with the stress state that inner CFST have initial stress, this article puts forward the ultimate bearing capacity calculation formula. It has a positive reference value for double CFST arch ring reinforcement design of this kind.

INTRODUCTION

In recent years, CFST (concrete filled steel tube) arch bridge is rapid developed in China, more than 300 seats of long-span CFST arch bridge are built, including the largest span bridge “Chongqing Wushan Yangtze River” of its kind in the world. As the time since CFST structure applied on bridge is not long, and its reinforcement research is very little. In view of the needs of arch ring reinforcing design with the method of coating concrete in the CFST arch ring, and on the basis of existing research results, this article conducts an experimental study on bearing capacity and calculation method of double steel tube concrete component in the condition that the inner CFST have initial stress.

BEARING CAPACITY CALCULATION FORMULA

According to CECS28:90, single steel tube bearing capacity formula is as follow:

$$N_u = f_c A_c (1 + \xi + \sqrt{\xi}) \quad (1)$$

In the formula: $\xi = f_y A_s / f_c A_c$

As shown in Figure 1, according to the characteristics of double CFST member, its bearing capacity can calculated with the formula as below:

$$N_u = f_{co} A_{co} (1 + \xi_o + \sqrt{\xi_o}) + f_{ci} A_{ci} (1 + \xi_i + \sqrt{\beta(1 + \xi_o) + \xi_i}) \quad (2)$$

In the formula : $\beta = \frac{(d_2 - 2t_2)^2 - d_1^2}{(d_1 - 2t_1)^2}$

Through the aforementioned formulas, this article analyzes and brings forward bearing capacity calculation formula as below for the double CFST member (as Figure 1) with coating concrete outside the exiting CFST section in the condition that the inner CFST has initial stress.

$$N_u = f_{co} A_{co} (1 + \xi_o + \sqrt{\xi_o + \kappa_p}) + f_{ci} A_{ci} (1 + \xi_i + \sqrt{\beta(1 + \xi_o) + \xi_i} - \frac{d_2 - d_1}{d_1} \kappa_p) \quad (3)$$

In the formula: $\lambda = \frac{P}{Af_{sc}}$ (Inner CFST initial stress coefficient)

A — The whole area of inner CFST; $A = A_i + A_s$

f_{sc} — Compressive strength of mixed material.

$$\kappa_p = 0.9998 - 0.1669\lambda - 0.2924\lambda^2$$

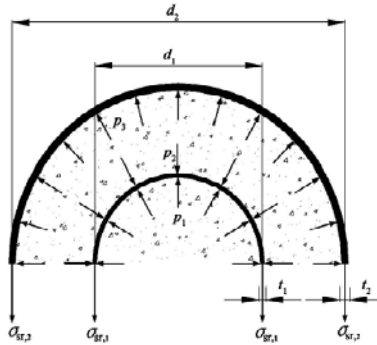


Figure 1 Double CFST member section and stress state

Table 1 lists the bearing capacity calculation results comparison between conventional CFST member and double CFST member proposed in this article.

Table 1 Calculation of bearing capacity of specimen table

Specimen Numbers	Steel tube(mm)	Equivalent single steel tube sections (mm)	Conventional CFST bearing capacity calculated value(kN)	Double CFST bearing capacity calculated value(kN)
SM1	$\phi 325 \times 8 + \phi 219 \times 6$	$\phi 325 \times 8.9$	5864.94	7455.77
SM2	$\phi 325 \times 8 + \phi 219 \times 6$	$\phi 325 \times 8.9$	5864.94	7455.77
SM3	$\phi 325 \times 8 + \phi 219 \times 6$	$\phi 325 \times 8.9$	5864.94	7455.77

According to the data above, conclusion is drawn that coating CFST improves the ultimate bearing capacity of conventional CFST members.

SIMULATED EXPERIMENT

Specimens

External steel tube uses 325 mm Outer diameter and 8mm wall thickness Q235 seamless steel tube. Internal steel tube uses 219 mm outer diameter and 6mm wall thickness Q235 seamless steel tube. In consideration of the technical economy and material ductility performance, take C40 concrete as tube filler. In order to simulate the stress state that all the inner CFST have initial stress (that is exactly the arch ring stress state of already built CFST arch bridge), it is need to prestress the inner CFST.3 groups of

the same specimens are produced in this experiment and the production is as follow: Processing interior and exterior steel tube→Pouring inner CFST concrete→Maintenance→Prestressing inner CFST concrete (as shown in Figure 2)→Coating exterior steel tube→Pouring concrete between interior and exterior steel tube→Forming double CFST specimens whose stress state is that whole inner CFST have initial stress.



Figure 2 Tension within the steel strand

Specimens' Measuring-point arrangement

In the quarter, 1/2, 3/4 place of the specimens along the longitudinal direction, four impedance resistance strain gauges are attached every 90 degrees along the radial direction to measure the longitudinal and radial strain. Meanwhile, a certain amount of displacement gauges are set outside the specimens along the longitudinal direction to measure the total longitudinal deformation. To obtain information of the lateral bending deflection in the middle of specimens, displacement gauges are placed at both ends and the middle. The specific measuring-point arrangement is as shown in Figure 3 and Figure 4.

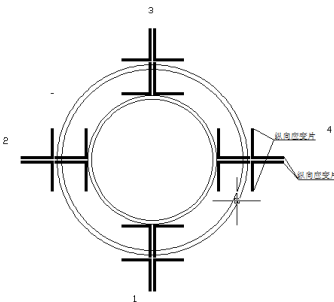


Figure 3 Distribution of the strain gauges

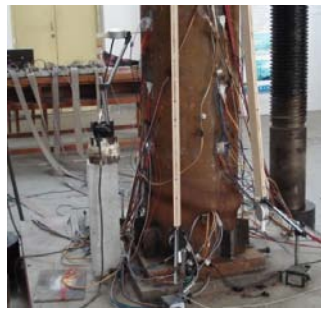


Figure 4 Layout of dial indicator

Loading Procedure

When load is less than 6% of the expected ultimate bearing capacity, load is applied at an increment of 500 kN, then at a increment of 250 kN until the specimens is broken.

Experiment Phenomenon Description

When load reached the point of yielding, slip lines appeared in part of the wall of the steel tube, the slip lines crossed the longitudinal axle line in ± 45 degrees, which were slim and less in number. First, slip lines appears in part area, it indicated that the specimen has already entered the plastic deformation stage in these region. In the test specimen loading process, with the continued increase in external load, the shear slip line became more in number and coarser in linear, gradually covered the full area of tube wall, this phenomenon showed that the whole specimen has entered the plastic deformation stage, and then the convex phenomenon was produced in the region earliest share slip lines appeared, in theory specimen entered the stage of destruction. In the loading process, when load reached the ultimate load, specimen were not immediately destroyed.its bearing capacity would not increase, but the deformation were still increasing, and part bloating phenomenon appeared in the middle or end of the test steel tube, eventually specimen produced larger deformation, namely distinct diagonal share failure surface formed when it entered destruction state, this finally cause specimen to the ultimate load. Then bearing capacity reduced slowly, while the strain increased rapidly, and apparent bearing capacity slip area emerged. After slight decrease in bearing capacity, due to the load redistribution led, the surface oxide layer on steel tube begun to fall off followed by the emergence of shear slip lines, and the larger load was, the obvious shed phenomenon performed.

Early in the process, longitudinal deformation and overall shape of specimen change little. It's basically in elastic stress stage, specimen expanded uniformly in the longitudinal, increased 5mm in average. As applied load gradually increased, specimen deformation began to present an irregular phenomenon, especially at the ends of the specimen, very apparent convex phenomenon appeared because of that the cover plate restrained the radial deformation of specimen.these phenomenons emerged on SM1 are shown as Figure 5 and Figure 6 in detail.



Figure 5 Specimen 1 damaged state diagram



Figure 6 Ends convexity and welding line shed diagram

According to destruction phenomenon of the specimen 1, we can find the reasons. The first, the internal poured concrete of CFST is not dense; the second, external steel tube is shorter than internal steel tube, so in theory external steel tube is in the stress state first. For more accurate analysis, external steel tube and internal steel tube should in the same plane, so welding a Welding block ($40 \times 100 \times 20$) with external steel tube (Figure 7), and do the axial compressive experiment of specimen 2 and specimen 3, Figure 8 and Figure 9 show steel tube shape which in limit state.



Figure 7 CFST specimen after welding



Figure 8 Specimen 2 of the failure modes diagram

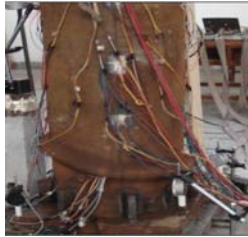


Figure 9 Specimen 3 failure modes diagram

Experiment Result

We can find that the end of specimen bulge outward apparently in Figure 8 and Figure 9, it leads to Overall buckling failure. Experiment result shows that: Local initial buckling load of specimens is 2700kN, when specimen 1 loads 6800kN, specimen 2 loads 7340kN, specimen 3 loads 6130kN, specimens cannot continue to load. Experiment load readings drop off, deformation continued to develop, it shows that these loads are ultimate loads.

Comparison of Calculated Value and Experimental Value

The comparison of calculated value and experimental value shows in Table 2.

Table 2 Comparison of calculated value and experimental value

Specimen number	Steel tube (mm)	Steel ratio	Diameter ratio	Ultimate capacity (experimental value)	Calculated value	Error (%)
SM1	$\phi 325 \times 8 + \phi 219 \times 6$	0.11	0.674	6800	7455.77	9.8
SM2	$\phi 325 \times 8 + \phi 219 \times 6$	0.11	0.674	7340	7455.77	1
SM3	$\phi 325 \times 8 + \phi 219 \times 6$	0.11	0.674	6130	7455.77	21

So, bearing capacity calculation formula of double steel tube concrete component in the condition that the inner CFST have initial stress is feasible. In Table 2, calculated value is a little bigger than experimental value, the reason is: when the strand tensioned , the inner concrete of steel tube is not dense; when pour concrete of external steel tube, the space between external steel tube and internal steel tube is small, the concrete is not dense and shrinkage and creep of concrete lead ultimate capacity to reduce. Specimen machining accuracy may lead ultimate capacity to reduce.

CONCLUSION

This paper, based on existing research of CFST, proposed bearing capacity calculation formula of double steel tube concrete component in the condition that the inner CFST have initial stress, and verified by experiments. Research results have

reference value in reinforcement and design of CFST Arch Bridge.

REFERENCES

- Chen, B.C. (2007). Concrete-filled Steel Tubular Structures [M]. Beijing: China Communications Press.
- Han, L.H. (2004). Concrete filled steel tubular structures from theory to practice [D]. Beijing: Science Press.
- Jiang, H., Zuo, J., and Cheng, W.R. (2006). Experimental Study of Concrete-filled Double Steel Tubular Short Columns Subjected to Axial Compression Load [J]. Earthquake Resistant Engineering and Retrofitting.
- Li, G.X., Cheng, W.R. (2006). Experimental Study of Concrete-filled Double Steel Tubular Short Columns Subjected to Axial Compression Load [J]. Journal of Southeast University.
- Li, Y.F. (2003). Experimental Research of the Concrete Filled Steel Tube Column Subjected to Axial Compression [D]. Xi'an University of Architecture and Technology.
- Zhong, S.T. (2003). Concrete-filled Steel Tubular Structures [M]. Beijing: Tsinghua University Press.
- Zhong, S.T. and Zha, X.X. (1997). Research of the Influence of Initial Stress in Steel Tube on Load Carrying Capacity for Concrete Filled Steel Tubular (CFST) Members. Journal of Harbin University of Civil Engineering and Architecture (3), 13-22.

Seismic Design of Dillon Road Grade Separation Bridge

Jian Lan, P.E.

Transportation Engineer, California Department of Transportation, 464 West 4th Street, San Bernardino, CA 92401; E-mail: Jian_Lan@dot.ca.gov

ABSTRACT

Dillon Road Grade Separation Bridge is just 2.2 miles away from the San Andreas Fault. San Andreas is the most famous fault in the world. It is a continental fault between North American Tectonic Plate and the Pacific Tectonic Plate. Its notoriety comes partly from the disastrous 1906 San Francisco earthquake, but rather more importantly because it passes through California. Dillon Road Grade Separation Bridge is in the City of Coachella. It carries Dillon Road over State Route 111 and Union Pacific Rail Road. This paper presents the seismic design of Dillon Road Grade Separation Bridge and discusses the design philosophy, criteria and approach for bridge at high seismic intensity area. The author shares his hand-on experiences on seismic design. It includes know-how on designing an effective seismic resistance system to reduce the displacement demand. Hence, the construction cost is reduced and the bridge's seismic safety is improved.

Introduction

The Dillon Road Grade Separation Bridge (The Bridge) is in the City of Coachella. It carries Dillon Road over State Route 111 (Grapefruit Boulevard) and two pairs of railroad tracks of Union Pacific. The design challenge comes from its vicinity to San Andreas Fault. The distance from the bridge to the San Andreas Fault is only 2.2 miles (See Figure 1. Project Location Map). San Andreas Fault is a continental fault between North American Tectonic Plate and the Pacific Tectonic Plate. It is the most famous fault in the world. It passes through California from north to south, and then enters Mexico. It caused the disastrous 1906 San Francisco earthquake. The motion of the fault is right-lateral strike-slip (horizontal motion). California experiences frequent earthquakes from minor to major scale due to the movement of these two tectonic plates. The San Andreas Fault had experienced massive earthquakes in 1857 at its central section and in 1906 at its northern segment (the 1906 San Francisco earthquake), but the southern section of the fault has not seen a similar rupture in at least 325 years. Unfortunately, the Bridge is within that section and just 2.2 miles away from the San Andreas Fault.

The Bridge has two spans with a total span of 295'-4". See the elevation view in Figure 2. An Acceleration Response Spectrum (ARS) is developed with the

consideration of the near-fault effect. See Figure 3. The peak rock acceleration is 0.6g (g is the gravity acceleration). The response acceleration can be as high as 1.6g.

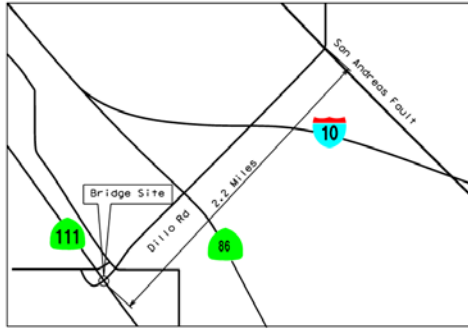


Figure 1. Project location map

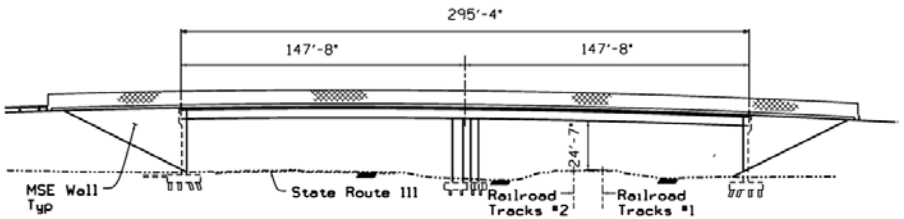


Figure 2. Elevation view of the bridge

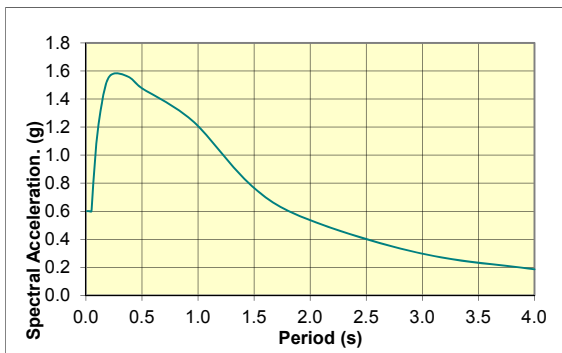


Figure 3. Acceleration response spectrum

Design Philosophy

The Bridge is at a high seismic intensity area. In the forthcoming mode analysis of the Bridge, we will find the period of the first mode is 1.45 seconds. Its corresponding response acceleration is 0.8g. It is not economically feasible to design a bridge which is intact at such a great seismic force. The intactness of a bridge means that it acts within elastic range. The displacement of bridge is totally recoverable by itself. The strains of its structural members have not reached the yield limit.

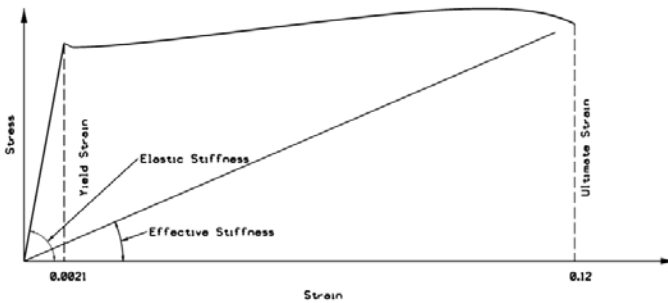


Figure 4. Steel stress and strain curve

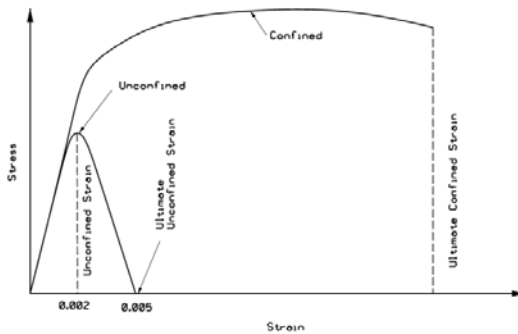


Figure 5. Concrete stress and strain curve

Figure 4 shows the stress and strain curve of reinforcement steel. The yield tensile strain is about 0.0021. The ultimate tensile strain is about 0.12. (The ultimate tensile strain varies with the size of the reinforcement steel. 0.12 is for bar #10 and smaller.) After the yielding, the reinforcement steel can sustain fifty-time more strain without losing its strength. In order to make best use of the material to design an economical bridge, the design shall go beyond the elastic range and go into the plastic range of

reinforcement bar. Furthermore, the effective (secant) stiffness at plastic range is much less than the elastic stiffness. $T = 2\pi \sqrt{\frac{m}{k}}$, (T = period, m = mass, k = stiffness). The smaller stiffness results in a longer period. As we can see in the response acceleration spectrum, longer period has lower response acceleration. The seismic load is lower when the structure goes into plastic range.

Reinforcement concrete is made of reinforcement steel and concrete. The reinforcement steel can sustain large plastic stain without rupture. On the contrary, the concrete can't sustain large strain. When the unconfined concrete reaches its compressive stress, its corresponding compressive strain is 0.002. Then, its stress starts to fall while its stain is reaching to the spalling strain 0.005. In order to mobilize the plastic strain capacity of reinforcement steel, the strain capacity of concrete shall be increased accordingly. The way is to well-confine the concrete. Recent studies show that if the concrete is well-confined, its ultimate compressive strain can be increased by 16 folds. See Figure 5 for the Concrete Stress Strain Curve. The methods to confine the concrete are tight-spaced stirrup, steel casing, and etc.

By utilizing the material to the plastic strain range, the plastic strain is no longer recoverable. At major earthquake, the structure will have non-recoverable displacement. But the structure shall be designed not to fail or collapse. The human being's life shall not be lost. This design idea is more economical and hence practical at high seismic intensity area. Based on the design idea, the philosophy for bridge design at high seismic intensity area is:

“No (or minimal) damage at minor earthquake; Repairable at moderate earthquake; No fatality at major earthquake.”

To implement the philosophy, the design concept for bridge is “strong deck, weak column”, which is on contrary to “strong column, weak deck” for building design. Even at a major earthquake, the deck will maintain its integrity and drivability so that the motorists do not face a deformed deck surface. In another word, the deck is designed within elastic range while the column is designed into plastic range at a major earthquake attack. The column absorbs and dissipates the seismic energy; so, the deck is protected.

Design Method – Displacement-based Design

Force-based design was used for seismic design in California. It applies a seismic load on the structure. Then the load is treated in the same way as the other static loads. Studies find that this approach does not reflect the seismic behavior of the structure. It has the following flaws:

- It seriously underestimates the seismic deflection at high seismic intensity area. It causes unseating and pounding. The unseating is that the superstructure displaces more than the seat width at the abutment or bent. The superstructure slides off the seat and falls down. The pounding is that two adjacent superstructures pound to each other at seismic event. The reason is that the displacements of the

superstructures are underestimated at design and the space between the superstructures is not designed wide enough.

- It seriously underestimates the seismic force. For example, design for lateral force equivalent to 6% to 15% of gravity load was used in the past. Now, it is understood that elastic response levels may exceed 100% of gravity load. In the forthcoming paragraph, for this bridge design, we will see the response acceleration is 0.8g for the first mode shape and 0.9g for the second mode shape. The underestimated seismic force level caused wrong moment shape of combined seismic load and gravity load, even wrong moment sign. Accordingly, the reinforcement steel is placed at the wrong side of structure. Fortunately, this underestimation of seismic load is compensated by the conservative nature of elastic design method somehow. Otherwise, the force-based elastic design would cause much more seismic failures.
- It can't consider the inelastic structural actions and associated ductility, which are crucial to the survival of inelastic system under severe seismic response. Thus critical potential hinge locations were not detailed to sustain large plastic deformation without strength degradation.

At the plastic range, microscopically, the strain increases but the stress does not increase correspondingly; macroscopically, the displacement increases but the force does not increase correspondingly. The force-based design can't reflect the structural behavior at plastic range. However, the plastic strain can be converted into displacement. Hence, the displacement-based design is introduced.

Same as the force-based design, the displacement design is to achieve:

$$\text{Capacity} \geq \text{Demand}$$

The difference is that the capacity and demand are in the term of displacement, not force. They are called displacement capacity and displacement demand.

Conceptual Seismic Design of the Bridge

The goal of the seismic design is very simple: to reduce the displacement demand and increase the displacement capacity.

In order to reduce the displacement demand, first, the bridge shall have balanced stiffness and mass distribution. Irregular geometry causes irregular seismic behaviors, for example, rotation, which increases the displacement demand. Hence, the Bridge is designed to have two equal spans, 147'-8" each.

Second, the bridge shall have effective seismic-resistant system.

Longitudinally, the most effective seismic resistance is the passive soil press at the end of superstructure. When the seismic load pushes the superstructure toward the abutment, the end of the super structure pushes the soil and mobilizes the passive soil pressure. The passive soil press is close to the resultant seismic force elevationwise. It is the most effective way to counteract the seismic force and reduce the displacement

demand. The passive soil press is the multiplication of the end area and the passive soil pressure. The most effective way to increase the passive soil press is to enlarge the end area of the superstructure by a drop-down design. See Figure 6, Longitudinal Seismic Resistant System.

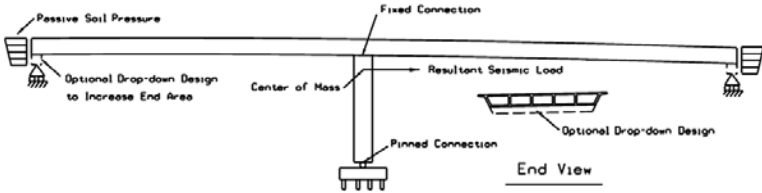


Figure 6. Longitudinal seismic resistance system

Another option to reduce the displacement demand is to have fixed connection between column and footing. But it is not as effective as the passive soil press at the superstructure end. Furthermore, the fixed connection transfers moment to foundation. It causes uneven load distribution among the piles, which is not an effective foundation design. This option is not chosen for the design.

Transversely, the seismic load is carried by the frame of bent cap beam and columns. The frame action provides seismic resistance.

The displacement capacity is determined by the ductility of the columns. In order to obtain a good ductility, the column shall be well-confined by stirrups. A slender column has better ductility and better displacement capacity. The rigidity of the bent can be compensated by increasing the number of columns. In the design, three columns are proposed with a diameter of 5'-6" each.

Displacement Demand

The displacement demand for the Bridge is calculated by SAP 2000. In modeling the Bridge, as aforesaid, the effective stiffness is used instead of the elastic stiffness of the structural members. Table 1 summarizes the first four mode shapes. Figure 7 shows the first mode shape.

Table 1. Mode Shapes of the Bridge

Mode Shape	Vibration Description	Period	Response Acceleration (g)
First	Mainly Longitudinal	1.45	0.8
Second	Mainly Lateral	1.35	0.9
Third	Mainly Vertical	0.51	1.45
Fourth	Combined Vertical and Lateral	0.14	0.8

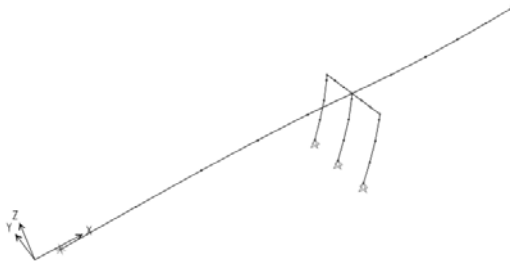


Figure 7. The first mode shape

Displacement Capacity

The displacement capacity is calculated by push-over analysis. The push-over analysis applies a series of incremental force to the structure till the structure is pushed over to collapse. The ultimate displacement capacity is obtained therefore.

The push-over analysis for this bridge is implemented by two computer programs, XSection and WFrame.

Xsection only generates the ultimate curvature of a column. Transversely, the bridge has a frame of bent cap beam and three columns. WFrame consider the frame action and overturning effect. It applies a series of incremental lateral load to the frame and models the lateral “collapse” process. The longitudinal reinforcement and lateral stirrup is designed by iteration of these two programs.

Table 2 summarizes the push-over analysis. The displacement capacity is compared with displacement demand. The capacity is higher than the demand. The column’s Demand Displacement Ductility and Displacement Ductility Capacity are listed as well. They meet the requirements by Seismic Design Criteria.

Other Seismic Designs

The other major seismic designs for the bridge include the following:

- Overstrength design for superstructure. Overstrength design refers to the special seismic design limit. The material’s strength used is higher than its yield strength. The design goes beyond (over) the yield strength. Hence, it is called overstrength design.
- Superstructure joint design. The joint between the superstructure and the column needs to transmit the overstrength moment and shear when the plastic hinge is forming at the columns. Special reinforcement detailing is designed for the joint.
- Vertical acceleration design.
- Abutment seat width and shear key design.
- The pile foundation seismic design.

Table 2. Summary of Push-over Analysis

Bent	Direction	Yield Displacement, Δ_y	Ultimate Displacement Capacity, Δ_u	Demand Displacement [From SAP2000]	Demand Displ. Ductility, $\mu_D = \Delta_D / \Delta_y$	Capacity Displ. Ductility, $\mu_C = \Delta_C / \Delta_y$	D/C Ratio = Δ_D / Δ_C
		[in]	[in]	[in]			
COL	Long	5.38	23.14	22	4.13	4.30	0.96
	Tran	4.58	20.00	19	4.07	4.36	0.93

Conclusion

At high seismic intensity area, the displacement-based design approach shall be used to design the bridge instead of the force-based design. It makes use of the material's capacity beyond the yield limit and produces a more economical solution. Because it captures the inelastic structural behavior at major earthquake, it also produces a safer solution.

Acknowledgement

The author thanks Mohan Char, Vice President of AECOM, for his help on this paper.

References

- Our Earth (2010). "San Andreas Fault."
<http://destroyedworlds.blogspot.com/2010/01/san-andreas-in-danger.html>
 (Jan. 26, 2010)
- Earth System Southwest (2005). "Preliminary Geotechnical Design Memorandum for Dillon Road/Avenue 48 Grade Separation." Jan. 11, 2005.
- M.J.N. Priestley, et al (1996). Seismic Design and Retrofit of Bridges, John Wiley and Sons, New York.
- California Department of Transportation (2006). "Seismic Design Criteria." Version 1.4.

A Study on Application of Resin Composite Sleeper in Design of Long-span Rail Bridges

An-shuang LIU¹, Delan Yin¹, and Guoxiang Liu¹

¹ T.Y. Lin International Engineering Consulting, Chongqing, China. E-mail: liuas@tylin.com.cn

ABSTRACT

Located in the center of Chongqing City, both Dongshuimen Yangtze River Bridge and Qiansimen Jianling River Bridge are cable-stayed bridges and are designed to allow for dual highway and rail traffic. To better meet the bridges' stiffness requirements, a comparison study is carried out between resin composite sleeper and ballasted track in their structural characteristics as well as their performance on construction, maintenance, operation, cost effectiveness and environmental impact. Analytical results show that resin composite sleeper functions properly when applied to these bridges. This study provides valuable references to design of long-span rail bridges, especially when reduction of superimposed dead load becomes desirable.

PROJECT OVERVIEW

Project Background

The Dongshuimen Yangtze River Bridge and the Qiansimen Jianling River Bridge is next to the Dongshuimen Gate and Qiansimen Gate on the Yuzhong Peninsular, respectively. The Danzishi region, Jiefangbei CBD and Jiangbeicheng region, which are cradles of the Chongqing City, are connected by these two bridges.



Figure 1.1 Plan of geographic location of the project

Structure characteristics of the bridges

The Dongshuimen Bridge and the Qiansimen Bridge, both as part of the Chongqing Rail Transit Line 6 First-stage Project, is collectively known as the Twin River Bridge. The span layouts of the bridge are as follow:

The Dongshuimen Bridge is a double pylon, single plan, partially cable stayed bridge with the main span layout of $222.5\text{m}+445\text{m}+190.5\text{m}=858\text{m}$ and a 96m approach in the Yuzhong District. The span layout of the bridge is shown in Figure 1.2-1.

The Qiansimen Bridge is a single pylon, single plan, partially cable stayed bridge with the main span layout of $88\text{m}+312\text{m}+240\text{m}+80=720\text{m}$. The span layout of the bridge

is shown in Figure 1.2-2.

Both bridges are rail-cum-road bridges with upper and lower deck. The upper deck supports four traffic lanes and sidewalks while the lower deck carries transit tracks for two way light rail. The cross section is shown in Figure 1.2-3.

Because of the flexible, long span structure of the Twin River Bridge, relative large deflection and relative large rotation at girder ends under train load influence the mechanical state in the fastener at the girder end and influence the safety and smoothness of the running, large elongation and shortening of the bridge under temperature action cause uneven spacing between the fasteners at the girder ends, which cause large interaction between the girder and the track, and finally influence the strength and stability of the seamless line. Therefore the structural characteristics, such as “long span, large deflection and large rotation” of the Twin Bridge shall be considered in the scheme of the track.

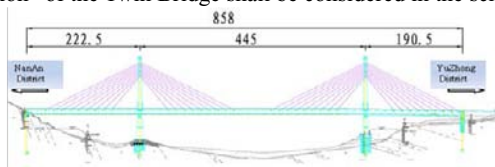


Figure 1.2-1 Elevation layout of the Dongshuimen Yangzi River Bridge

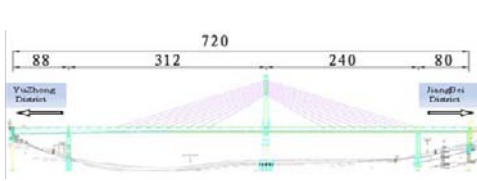


Figure 1.2-2 Elevation layout of the Qiansimen Jialing River Bridge

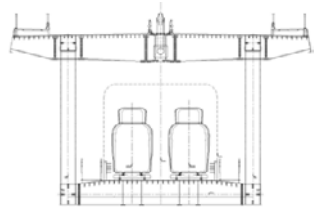


Figure 1.2-3 Cross section of standard section of girder in the Twin River Bridge

Boundary condition of the alignment

Plane condition: a circular curve with 2000m radius and 26.823m length is set between K12+866.924~K12+893.746 in the Nan'an District near the Dongshuimen Bridge, each end of the circular curve connects to a 30m transition curve; a circular curve with 500m radius and 52.165m length is set between K13+742.903~K13+795.068 in the Yuzhong District, each end of the circular curve connects to a 60m transition curve. The main bridge of the Qiansimen Bridge is along the straight alignment, with better plane condition.

Vertical profile condition: due to the requirements of stations at both ends of the bridge and requirements of navigation, long ramps are with both bridges. For the Dongshuimen Bridge, there is a 700m ramp with near-level grade and a 340m ramp with up-grade of 20.5% slope, a circular vertical curve with 5000m radii is placed at K13+350. For the Qiansimen Bridge, there is a 400m ramp with up-grade of 23.7% slope and a 700m ramp with near-level grade, a circular vertical curve with 5000m radii is placed at K14+600.

BALLASTED TRACK AND RESIN SLEEPER

The time for maintenance of track can't be long due to massive traffic flow of urban transit rail, therefore the track shall be designed to reduce maintenance work. Two schemes of track: ballasted track and light track with the resin sleeper are introduced as below:

Ballasted track

The ballasted track is composed of steel rail, fastener, anti-derailment safety system, prestressed concrete sleeper, ballast and concrete ballast channel slab, as shown in Figure 2.1 Cross section of ballasted track. The superimposed dead load from the track is 152.8kN/m.

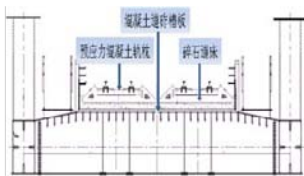


Figure 2.1 Cross section of ballasted track

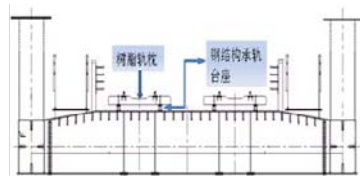


Figure 2.2 Cross section of light resin track

Light resin track with the resin sleeper

The light track with the resin sleeper is composed of steel rail, fastener, anti-derailment safety system, resin sleeper, steel bearing set, and etc. as shown in Figure 2.2 Cross section of light resin track. The superimposed dead load from the track is 40kN/m.

SPECIAL TOPIC ON TECHNICAL FEASIBILITY OF THE RESIN SLEEPER

The resin sleeper is made of a composite material synthesized from long glass fiber and rigid polyurethane, the material is called FFU (Fiber Reinforced Formed Urethane). The synthetic resin (FFU) looks like timber but has advantages of modern synthetic material. Products with various dimensions can be made of this material. The products made of the synthetic resin can be drilled or cut by traditional fabricating machinery for timber. Another advantage of the synthetic resin is the small coefficient of thermal expansion and low thermal conductivity. Considering the characteristics of the Twin River Bridge, such as “long span, large deflection, large rotation, large thermal deformation and long ramp”, the discussion of resin sleeper in terms of selection of fastener type; influence of displacement at the end of girder on mechanical state of fastener; influence of rotation at the end of girder and influence of faulting of girder ends are discussed as below:

Selection of fastener type

K type fastener is widely used with the unballasted deck on the steel railway bridge in China. To reduce the longitudinal force in the seamless rail and to reduce the relative displacement between the rail and the sleeper, the K type fastener is arranged alternately with tight fastener and non-tight fastener. For the tight fastener, rail clip is tightened to the rail flange; while for the non-tight fastener, a spacer with proper thickness underneath the rail clip doesn't allow tightening the clip to the rail flange, a 0.5mm~1mm clearance is reserved between the rail clip and the top surface of the rail flange.

K type fastener and elastic rod fastener are widely used with the resin sleeper in other countries, as shown in Figure 3.1-1, these two type fastener are belong to separate rail fastener, the elastic part is either clip or rod to fasten the rail.

K type fastener

Rubber tie plate between steel rail and iron tie plate is not needed for the K type fastener; a plastic tie plate is placed under the iron tie plate instead. Under normal condition, the thickness of the plastic tie plate is 4mm. When necessary, uplifting tie plate with proper thickness can be put under the iron tie plate. But the allowable uplifting value for the K type fastener is small. Large uplifting value puts the screw spike in poor mechanical state, the iron tie plate is subject to transverse movement under train load, which makes it difficult to keep the rail in position. The thickness of packing of sleeper can be adjusted if the uplifting is large. The schematic diagram of K type fastener is shown in Figure 3.1-2.



Figure 3.1-1 K type fastener and elastic rod fastener on the resin sleeper of the Shinkansen Japan

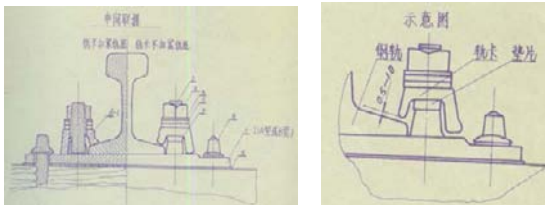


Figure 3.1-2 Schematic diagram of K type fastener

Wood sleeper is generally equipped with K type fastener for railway bridge with unballasted deck in China. The main problems in the K type fastener in application over many years are in tie plate, hanging plate, skewed bridge sleeper, rail creep. The problems are characterized by:

- (1)The spike is loose due to hammer hitting screw spike, K type tie plate and hanging plate.
- (2)The iron tie plate is broken due to the uneven sleeper surface, inverted rail cant, gap between rail component and tie plate.
- (3)The sleeper ponding underneath the iron tie plate due to no sealing or improper sealing with putty on the holes of the K type tie plate.
- (4)The sleeper on bridge is skewed or torn due to large torque in T-shape bolt.
- (5)Because the structural strength differs between track components, the gap is often found in the transition section between general iron tie plate and K type tie plate.
- (6)Steel rail creep is due to either insufficient torque in T-shape bolt or loss of spike

force in the spike hole.

Because of the larger pullout resistance of the spike in the resin sleeper and the improved evenness of sleeper surface due to easy fabrication of resin material, it is expected to eliminate the above mentioned problems when the resin sleeper is equipped with the K type fasteners. It is shown from Japan's experiences that problems, such as torn sleeper, eaten tie plate or projected spike doesn't occur when the resin sleeper is equipped with the K type fasteners. The Japan's experience demonstrates that the K type fastener works well with the resin sleeper.

Elastic rod fastener

Other countries have accumulated experience in applying the elastic rod fastener on the resin sleeper. Compared with K type fastener, the elastic rod fastener is pressed onto steel rail by elastic force, which makes it easy to maintain the rail condition. It's also possible to place the elastic tie plate underneath the rail to decrease the stiffness of the rail.

Currently there is no mature elastic rod fastener that can be equipped with the resin sleeper in China. It is possible to develop the elastic rod fastener based on the research and development of the fastener used with unballasted track. The features of the new fastener as below:

- (1) Composite rubber tie plate underneath the rail decreases the whole stiffness of the rail;
- (2) The fastener has certain uplifting capacity. If needed, the tie plate for uplifting can be placed underneath the rail, which makes it easy to maintain.
- (3) The clip force is only 4kN, the smaller force decreases the longitudinal resistance in the fastener and decreases the interaction between rails on the bridge.

Force analysis of influence of girder end displacement on fastener

Model

Due to temperature fluctuation, train load, foundation settlement, subgrade settlement, and etc. of the bridge, the girder end displacement, including vertical displacement and rotation, has certain influence on track system and cause deformation and additional stress in the rail. The girder end displacement forces each node in the fastener system to move. The model is shown in Figure 3.2.1.



Figure 3.2.1 Model

Influence of girder end rotation

As to the elastic rod fastener, when the rotation at girder end increases from 1mrad to 4mrad, the corresponding maximum tensile force in the fastener increases from -8.63kN to -20.87kN, the corresponding maximum compressive force in the fastener increases from 18.87kN to 67.67kN, the maximum compressive force obviously increases faster than the tensile force. When the rotation at girder end increases from -1mrad to -3mrad, the corresponding maximum tensile force in the fastener increases from -12.48kN to -21.36kN; the corresponding maximum compressive force in the fastener increases from

5.99kN to 13.17kN, the maximum tensile force obviously increases faster than the compressive force.

When the rotation value at girder end is positive, the relations between the maximum compressive and tensile force in the fastener and the rotation are basically the same as those of the elastic rod fastener, the maximum compressive and tensile forces are a little larger than those of the elastic rod fastener. While the rotation value at girder end is negative, the relations between the maximum compressive and tensile force in the fastener and the rotation are markedly different from those of the elastic rod fastener, the maximum compressive and tensile forces are much larger than those of the elastic rod fastener. When the rotation at girder end is -3mrad, the maximum tensile force in the K type fastener reaches -75.11kN. Figure 3.2.2 shows the influence of different fastener type on the maximum tensile force in the fastener when rotation at girder end varies from -3/1000 to 4/1000.

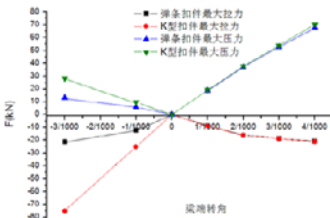


Figure 3.2.2 Influence of different fastener type on the tensile force in the fastener for rotation at girder end varies from -3/1000 to 4/1000

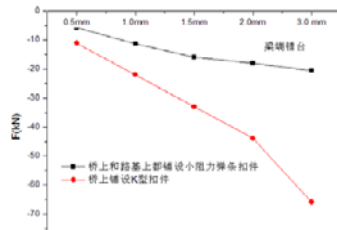


Figure 3.2.3 Influence of different fastener type on the tensile force in the fastener for faulting at girder end varies from 0.5mm to 3mm

Influence of faulting of girder end

The vertical force in the fastener induced by the faulting of girder end varies with different fault and different type of fastener. The value of force is related to the vertical stiffness of the fastener. The vertical force is larger in the K type fastener due to its larger vertical stiffness. Figure 3.2.3 shows Influence of different fastener type on the tensile force in the fastener for faulting at girder end varies from 0.5mm to 3mm.

Elongation or shortening of the girder in the long ramp

Conditions for calculation: the girder in the long ramp of the Qiansimen Bridge in the Yuzhong District is modeled, translation and rotation at the end of girder occur at the same time; the force in the K type fastener is calculated. Temperature fluctuation in the girder is 25°C, the slope of the ramp is 30%. The maximum vertical tensile force is -0.49kN and the maximum vertical compressive force is 0.47kN in the fastener, respectively. The influence of the elongation or shortening of the ramp bridge on the vertical force of the fastener and on the vertical displacement of the rail is small.

Calculation of longitudinal force

Principle of calculation

The model and method for the calculation of longitudinal force in the seamless rail on the bridge is based on the principle of interaction between girder and rail: With the displacement of the girder due to temperature changes or train load, the sleeper and the fas-

tener are driven by the bridge deck, and the longitudinal force is applied to the rail by the fastener. The rail apply the reaction with the same value but with the opposite direction on the bridge, this reaction is transferred through the girder and the supports, and finally applies on the abutment, at the same time the reaction also cause additional longitudinal force and additional longitudinal displacement in the rail. The girder-rail interaction model is shown in Figure 3.4.1, the reaction force between the girder and rail per unit length is the longitudinal resistance for rail. The longitudinal force applied on the rail when train is in braking or in traction is the braking force on rail p_u , the force is related to the train traction load, axial load, coefficient of adhesion between wheel and rail and train speed. K is the longitudinal horizontal linear stiffness of pier/abutment and it can be defined as the longitudinal force that causes unit displacement on top of the bearing pad on the pier/abutment.

With large temperature fluctuation in the Twin River Bridge, the interaction between the girder and rail, and the elongation or shortening in the rail is large without the expansion device. The elongation or shortening in the rail is markedly decreased with the help of the expansion device.

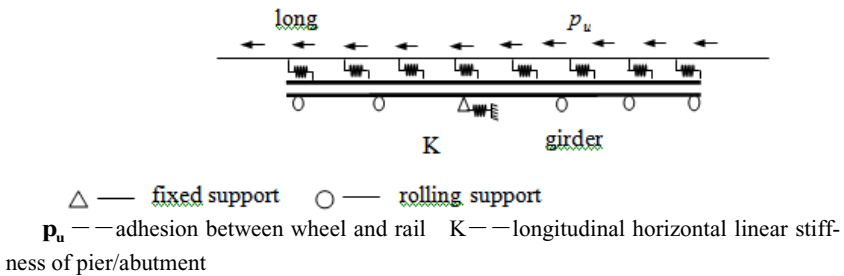


Figure 3.4.1 Girder-rail interaction model

Calculation result of longitudinal force

The calculation result of the longitudinal force in the Dongshuimen Bridge is shown in Table 3.4.2-1.

Table 3.4.2-1 Summary of longitudinal force in the Dongshuimen Bridge

	Constant resistance model			Nonlinear resistance model		
	Force due to elongation or shortening	Bending force	Braking force	Force due to elongation or shortening	Bending force	Braking force
Max. tensile force in the rail(kN)	378.00	244.59	53.75	120.33	81.78	40.89
Max. compressive force in the rail (kN)	-479.9	-369.03	-57.11	-479.73	-153.39	-40.75

The calculation result of the longitudinal force in the Qiansimen Bridge is shown in Table 3.4.2-2.

Table 3.4.2-2 Summary of longitudinal force in the Qiansimen Bridge

	w/o expansion joint			w/ expansion joint		
	Force due to elongation or shortening	Bending force	Braking force	Force due to elongation or shortening	Bending force	Braking force
Max. tensile force in the rail(kN)	618.5	236.1	45.66	120.33	116.87	43.04
Max. compressive force in the rail (kN)	-479.5	-260.6	-45.6	-479.7	-119.4	-42.82

Table 4.1 Comparison between the ballasted track and the light track with the resin sleeper

Scheme Indicator	Ballasted track	Light track with resin sleeper
Self-weight	152.8KN	40KN
Stability	Longitudinal and transverse resistance can't be guaranteed	Large longitudinal and transverse resistance
Adaptability to alignment	Good adaptability to various alignment and track	Achieve the alignment and rail protection through good workability of the resin sleeper, sleeper wedge, and adjustment ability of the fastener
Adaptability to bridge deformation	<ol style="list-style-type: none"> 1. The expansion and contraction device at girder end is needed; 2. Ballast channel length shall be limited or the linkage shall be strengthened to allow the bridge deformation; 3. The sleeper displacement disturbs the ballast due to the rotation at girder end, which affects the alignment stability. 	<ol style="list-style-type: none"> 1. The expansion and contraction device at girder end is needed; 2. The influence of the bridge deformation on the single sleeper can be omitted; 3. Special fastener is needed at girder end.
Link to bridge deck	Ballast channel is needed and shear stud shall be installed between the ballast channel and the deck	Bolt connection is needed, bolt connection on unballasted deck can be used as reference
Complexity of construction	The construction of ballast channel is complex, track-laying technology for the ballasted track is mature	Complex due to positioning and connection of each sleeper
Efficiency of construction	Long curing time for the ballast channel	Low efficiency due to positioning and connection of each sleeper
Work load	large	small
Adjustability of track geometry	Easy to lift and lining the track to recover track geometry	Easy to adjust a single sleeper through reposition or adjust block
Check and maintain the deck	difficult	easy
Plan for maintenance	<ol style="list-style-type: none"> 1. Sleeper: replacement; 2. Ballast bed: tamping, cleaning and replacement; 3. Ballast channel: repair for the channel is needed if the crack width is over the limit, which greatly dis- 	<ol style="list-style-type: none"> 1. Sleeper: repairing or replacement 2. Bolt can be easily and separately replaced if the connection fails

		turbs the alignment and takes long time to repair.	
Operability	Ability to keep the smoothness of alignment	Recovery of track geometry is often needed which greatly disturbs the alignment	After the construction is completed, the smoothness of the alignment can be guaranteed for long time
	Influence on the operation	Often disturbs the alignment and therefore greatly influence the operation	Small impact on other alignment when in maintenance
Environmental performance	Aesthetics	good	better
	Reduction of vibration and noise	The ballast has certain elastic modulus, reduction of vibration and noise can be achieved with the ballast pad	Noise is high with no sound-absorbing material. High-elastic pad can be used on bridge to reduce the vibration and noise
General requirement		Rotation at girder end $\leq 3.0\%$ Faulting of girder end ≤ 2 mm Stiffness $\geq 1/600$	Rotation at girder end $\leq 3.0\%$ Faulting of girder end ≤ 1.5 mm Stiffness $\geq 1/600$

CONCLUSION

The great difference between the superimposed dead load of the ballasted track and the light track with resin sleeper has greatly effects on the structure and investment. Based on the principle of "safety, adaptability, economy, and aesthetics" of the structure, two schemes of the track system are compared in terms of the structure characteristics, constructability, maintainability, operationability and environmental performance, as shown in Table 4.1. Both the ballasted track and track with the resin sleeper have good adaptability to the bridge. But the large self-weight of the ballasted track will markedly increase the project investment and has adverse effect of recurrent maintenance. In sum, the track with resin sleeper is suitable for the super long span bridge with its good economic effect and good adaptability to the environment.

Research on the Technique of Utilizing River Sludge as Road Fill

Fanyi Bai¹, Haiyun Song², Lei Cao³, and Baowei Zhang⁴

^{1,2,3,4}Tianjin Haishun Traffic Engineering Design Co., LTD, Tianjin, China; PH: (+86)13702172991; FAX: (+86)022-23537273; email: baifanyi1@vip.sina.com

ABSTRACT

Based on the comprehensive treatment project of Dagu Drainage River, this paper proposes the reutilization of river sludge in roadbed filling to realize their recycling and harmless treatment and presents the first domestic classification standard of sludge utilization in accordance with relative state road and environment standards. The author carried out indoor tests and field construction tests of material performance after mixing sludge with lime, powder of building debris and lime slag respectively. These tests showed that all performance indexes of the sludge mixings meet the requirement of road specification, the limits of relative state standards and test requirements for heavy metals content and Extraction toxicity (ET).

INTRODUCTION

River sludge is formed when small clay mineral particles under the force of electrostatic interaction and molecular attraction deposit in the slow moving water body such as rivers or lakes in the form of flocculation and cellular structure (Y. Heng, 2009) mingled with domestic waste and construction waste and containing a lot of methane, poisonous and smelly gases and even contaminants such as heavy metals. It has difficult engineering properties, high water and toxic content. Its strength can hardly be improved through dewatering consolidation due to the small size of the particles, high clay particle and organic content and low permeability coefficient. Therefore, it is very hard for the sludge to be utilized directly. Currently most of the dredged river bottom sludge in our country is disposed at the landfills thus inevitably causing the pollution in the disposal areas or the waste of land resources (C. Zhang, 2007). Improper disposal of river sludge can easily cause secondary pollution affecting the life and work of the people who live around. With the increasing amount of the sludge each year, the landfill has already become inadequate to the disposal problem of the dredged river sludge. Facing the ever worsening water environment, voice about improvement and rehabilitation of the water bodies has become more and more resonant.

With high-speed development of the Tianjin's economy, the infrastructure of Tianjin especially the transportation infrastructure is developed very rapidly and a large amount of fill dirt is needed each year. These fill materials are mostly dug out from the farmland, which damaged the local environment. Utilizing the meliorated dredged sludge as a kind of soil resources in the road embankment construction can not only satisfy the demand for earth in road construction but also reduce the abandoned dredged sludge to solve the issue of environment pollution on the disposal land. No recycling and harmless utilization of the dredged sludge has become the

major factor that limits and restricts the development of the local economy of some places and thus has to be solved. From the statistics, the total amount of the sludge generated from the major draining rivers reaches 5.2 million cubic meters; just Dagu Drainage River alone can generate 1.2 million cubic meters of sludge.

The major issues in utilizing sludge as road fill material for embankment are as follows:

- The water content of river sludge can reach 50%-60%, thus long dewatering time is needed. It is necessary for the sludge to be put in the storage yard for more than 2 months in the process of natural decantation, then after being tedded 3-4 times it will satisfy the water content requirement as road fill material.

- High content of contaminants especially heavy metals and other toxic materials in river sludge that will damage the surrounding environment much limits the range of its application. Therefore contamination of the neighbouring environment along the road with sludge as fill material has to be avoided.

- Poor engineering property stability of the sludge due to the alteration of sludge density and structural state caused by the decomposition of the organic matter contained can lead to excessive compression deformation of the embankment and reduce the shear strength and bearing capacity.

CATEGORIZATION OF RIVER SLUDGE

Based on the analysis of the chemical properties and physical composition the classification method and standard have been proposed. The classification standard is basically in accordance with the follows.

- 'Specifications for Design of Highway Subgrades' (JTG D30-2004) gives requirements on the maximum particle size, minimum strength, liquid and plastic limit and content of other impurities.

- 'Control Standards for Pollutants in Sludges from Agriculture Use' (GB4284-84) gives the specification on content of pollutants such as heavy metals.

- 'Identification Standard for Hazardous Wastes Identification for Extraction Toxicity' (GB5085.3-2007) gives the relevant requirements on the extraction toxicity of the heavy metals.

River sludge can be divided into 3 types. The detailed classification is as follows.

Type I sludge. This type of sludge can be utilized directly without any special treatment requirement (e.g. for dangerous wastes). It has the similar properties to sandy soil in silt type, composition, grain size distribution, soil and mechanical characteristics, contaminants content etc. that complies with the criteria for fill materials used in road embankment construction. So it can be used directly and no serious environmental pollution will happen during the construction and usage of the roads. It also has the ability to foresee any threat of environmental damage.

Type II sludge. This type of sludge cannot be used as fill material for road construction by just reducing the water content. Other processes such as drying, sieving and blending with lime, construction wastes, waste incinerator bottom ash or other materials are also needed for the sludge to be used after treatment. No serious

environmental pollution will happen during the construction and usage of the road. It also has the ability to predict any threat of environmental damage.

Type III sludge. This type of sludge has the problems of complicated composition, unsatisfied engineering properties for construction criteria, environment pollution, and unpredictable threat to the environment, among others. Treatment is very difficult and expensive. The content of heavy metals or extraction toxicity surpasses the standard in relevant specification, or it falls into the category of other strictly forbidden dangerous wastes. So it is not recommended to be reused.

Table 1. Detail Index Table for Different Types of Sludges

Type	Particle diameter	Mechanical properties	Composition	Heavy metal	Extraction properties
Type I (Can be used directly)	Even, compact, PD<100mm: can be used for roadbed, PD<150mm: can be used for road foundation.	Liquid limit≤50%, plastic index≤26. Compactness and expansion rate etc. all satisfy specifications.	No turf, household waste, root stump and humus etc. with organic content ≤10%	Satisfy the criteria of 2 times bound value in 'Control Standards for Pollutants in Sludges from Agriculture Use' (GB4284-84)	Satisfy the criteria in 'Identification Standard for Hazardous Wastes Identification for Extraction Toxicity' (GB5085.3-2007)
Type II (Use after treatment)	Even, compact, PD<100mm: can be used for roadbed, PD<150mm: can be used for road foundation.	After treatment, liquid limit≤50%, plastic index≤26. Compactness and expansion rate etc. all satisfy specifications.	Contain a few impurities, but easy to be rid of. After treatment, organic matter content≤10% and stable.	Satisfy the criteria of 2 times bound value in 'Control Standards for Pollutants in Sludges from Agriculture Use' (GB4284-84) after treatment.	Satisfy the criteria in 'Identification Standard for Hazardous Wastes Identification for Extraction Toxicity' (GB5085.3-2007) after treatment.
Type III (Not recommended)	Difficult to crash, maximum PD>150mm	After treatment, liquid limit > 50%, plastic index > 26. Compactness and expansion rate etc. do not satisfy specifications.	Contain a lot of turf, household wastes, tree roots, humus etc. After treatment, organic matter content still>30% and also unstable.	Not satisfy the criteria of 2 times bound value in 'Control Standards for Pollutants in Sludges from Agriculture Use' (GB4284-84) after treatment.	Not satisfy the criteria in 'Identification Standard for Hazardous Wastes Identification for Extraction Toxicity' both before and after treatment. (GB5085.3-2007)

Through the comparison between the analysis of physical properties and heavy metal composition of sludge dredged from Dagou Drainage River and the classification standard, we can tell that Dagou River sludges have the process

characteristics of small grain size, low sand content, high plasticity, higher desiccation sensitivity and shrink ratio, and ease in drying. Meanwhile, they also have the features of uneven distribution of heavy metal content and higher content of some heavy metals. In general, Dagou river sludges can be categorized as Type II sludge, so they can be used as the application materials for transport engineering.

MATERIAL CHARACTERISTICS OF RIVER CHANNEL SLUDGES

- River channel deposits settle out of slow-moving or standing water, with natural water content being higher than liquid limit and natural void ratio above 1.5. It is very complex uneven clayey soil consisting of organic residue, inorganic particles, bacteria bodies and colloids with high compressibility; it has a large void ratio and low bearing capacity.

- There is a lot of organic matter, accounting for about 6%-21%. Humus in silty soil makes up 50%-90% of the total organic matter content, while humic acids account for 60% of the total humus content, which causes the sludges to have higher water capacity and plasticity, a bigger expansion rate and lower permeability.

Inherent drawbacks of sludges as fill material for road embankment construction:

- High natural water content. The natural water content of the dredged sludge can reach as high as 55%, or even higher, in the shape of mud with almost no strength. Though the water content can drop to about 43% after a short period of drainage in the stock bank, dredged sludge can still hardly be used in road construction.

- Low bearing capacity. The CBR value of the sludge is 2.9%. It cannot satisfy the criteria of road construction with such a low bearing capacity.

- High organic matter content. The organic matter content is about 6%-12%, affecting the acidity of the soil. On the other hand, the oxidation of organic matter also affects the long term stability of the soil body. The organic matter content of the Dagou Drainage River sludges at landfill is 9.8%.

TREATMENT TECHNIQUE FOR RIVER CHANNEL SLUDGES

Different treatment measures can be taken for sludge with low and intermediate water content and high water content, as river channel sludge has a large water content variation range.

Sludges with intermediate and low water content (<40%) can be treated using quicklime and construction wastes.

Sludges with high water content ($\geq 40\%$) can be treated jointly with lime and incinerator slag.

Sludges have been taken from the Qingninghou country landfill and the Dagou River Drainage drainage River site respectively and have undergone the indoor heavy compaction test, liquid and plastic limits tests, and CBR test. The details are as follows.

(1) Treatment with lime: With the increase of blended lime ratio, the liquid and plastic limits of the mixed sludge will rise; meanwhile, the bearing capacity will also increase significantly. This means that the engineering properties of sludge material solidified with lime can be changed to satisfy the criteria for fill material to be used in road embankment construction.

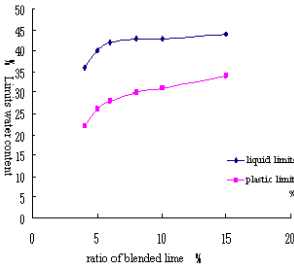


Figure 1. Relationship between liquid, plastic limits and ratio of blended lime

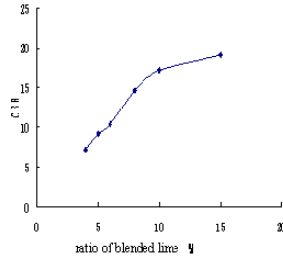


Figure 2. Relationship between CBR and ratio of blended lime

(2) Treatment with construction wastes : So-called construction wastes are defined as the granular or powder materials obtained by grinding waste concrete blocks, bricks, and stones. Addition of construction wastes decreases the liquid limit of river sludge and the plastic limit of the combination will rise with the increased percentage of blended construction wastes. With the rising of the blended construction waste quantity, the CBR of the sludge will increase first then decrease, with the peak appearing at 35% of blended construction wastes. So by choosing the proper construction waste blending ratio, the engineering properties of sludge material can be effectively changed to satisfy the criteria for fill material to be used in road embankment construction.

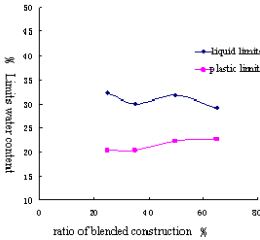


Figure 3. Relationship between liquid, plastic limits and ratio of blended construction wastes

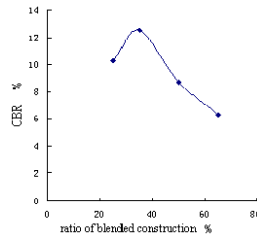


Figure 4. Relationship between CBR and ratio of blended construction wastes

(3) Treatment with quicklime and slag : River sludges with high water content need a treatment method that can both rapidly reduce the water content and effectively increase the bearing capacity. Municipal waste incinerator slag has low water content, and good water absorption capacity also contains a lot of active effective elements, which can significantly improve its bearing capacity. If the waste incinerator slag is used jointly with quicklime, the water content of the sludges can be effectively reduced; meanwhile, the physical and chemical reaction between lime, slag, and sludges can improve the sludges' bearing capacity.

In this experiment, the mixing ratio of lime is fixed at 6% and the mixing ratios of slag are set at 12%, 24%, and 48% in order to find how the mixing ratio of slag affects the strength of the composite. It can be observed that the liquid limit and

plastic limit of sludge composite drops when the mixing ratio of waste incinerator slag increases, and the bearing capacity of the composite is improved significantly. Expansion after saturation is not obvious. It shows that when the mixing ratio of lime is fixed at 6%, blending a certain amount of waste incinerator slag can effectively change the engineering properties of the sludge material to satisfy the criteria needed for a fill material in road embankment construction.

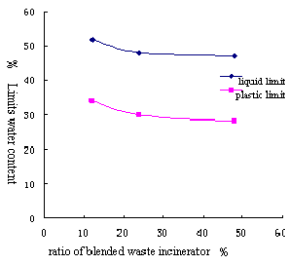


Figure 5. Relationship between liquid, plastic limits and ratio of blended waste incinerator slag

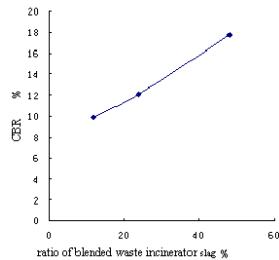


Figure 6. Relationship between CBR and ratio of blended waste incinerator slag

MECHANICAL ANALYSIS

Finite element analysis software is used in this paper to analyse the deformation difference of the road surface under the weight of standard axle load BZZ-100 between using subbase ash as base course and using treated sludge as base course in order to measure the influence of using river channel sludge as fill material for road embankment construction upon the level of vehicle safety during the operation period of the road.

From simulation and calculation, settlement of road surface structure will happen along the z direction (down vertically). When filled with 20cm 8% subbase ash base course material the maximum settlement appears at the center of the vehicle wheel with a maximum value of 0.665cm; when the base course material is replaced by treated sludge, the maximum settlement also appears at the center of the vehicle wheel with a maximum value of about 0.6688cm.

It can be observed from the calculation above that replacing the base course layer with a treated sludge layer in a roadbed does not greatly affect the pavement condition; in fact, there is only a small increase of 0.0038cm for the maximum settlement. There is no apparent change in the level of vehicle safety on the road due to the replacement of the base course with a treated sludge layer.

Test road project : A Grade 2 highway to be reconstructed in the Dagang District to be reconstructed was selected as a real project test road with roadbed width of 18m, pavement width of 15m, and 4 four lanes on dual direction in both directions. 2 Two segments of the base courses with length of 100m and width of 9m were chosen. Due to the lack of waste incinerator slag, we only replaced the original subbase ash base course layer with quicklime- treated sludge and construction waste - treated sludge. 1.0m thick clay was also laid around the sludge layer to reduce the possible impact of any extraction from the sludge layer on the surrounding environment.

Sludges used are from Qingninghou landfill, so the sludges have been deposited for a while with sludge grain size <50mm, 32.2% water content, 57.2% liquid limit, plastic index of 23.4, and organic matter content of 23.4. Heavy metal content and extraction test all satisfy the specifications.

The ILiquid & and plastic limits test, standard compaction test, and CBR test have all been performedbeen taken respectively. It can be observed based on the on-site testing results that all property indexes of the test road can meet the specifications, as shown in Table 2 below.

Table 2. Property Indexes of Sludge after Treatment

Mixed amount (%)	Liquid limit (%)	Plastic limit (%)	Plastic index	Maximum dry density (%)	Optimal moisture content (%)	CBR	Expansion (%)	Degree of compaction (%)
Lime 6%	42.9	27.1	15.8	1.675	19.0	8.8	1.1	95.2
Construction wastes 35%	32.8	20.6	12.2	1.762	18.0	10.6	1.9	96.2



Figure 7. Photos of construction site

Environmental assessment of road embankment with sludges as fill material : Due to the serious heavy metal pollution of some parts of the Dagu River, and also the consideration thatbecause sludges will be used as fill material in road embankment construction, special attention is given to the extraction property of the pollutants, and (especially the extraction property of the pollutants) the extraction tests for original sludges, mixed sludge materials and soil surrounding the test part of road embankment have been taken.

Table 3. Extraction Test Results

Test sample	Test item	Test place	Test standard
original sludge	8 heavy metals including: Cadmium, Chromium, Zinc, Mercury, Copper, Manganese, Lead, Nickel	indoors	1. 'Identification Standard for Hazardous Wastes Identification for Extraction Toxicity' (GB5085.3-2007)
6% lime treated sludge composite 35% construction waste treated sludge composite		outdoors	
Soil surrounding the embankment with sludge as fill material		Construction site	2. 'Solid waste-Extraction procedure for leaching toxicity-Sulphuric acid & nitric acid method' (HJ/T299-2007)

The trial road was finished in 2009 and has been in use through winter and rainy season. The Tianjin environment monitoring center was invited to do an environmental test and the heavy metal analysis for the surrounding environment of the trial road in June 2010. Sampling point distribution is shown in Figure 8 below.

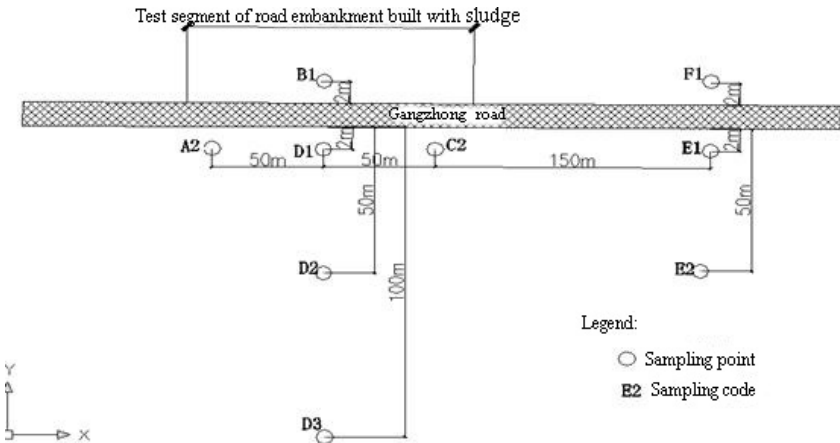


Figure 8. Soil sampling point distribution of test road

The test results show that there is not much discrepancy in the content of heavy metals between the soil surrounding the embankment built using sludges as fill material and the soil surrounding the embankment built with the traditional materials.

Table 4. Heavy Metal Test Results for Soil Surrounding Test Embankment

Test item	Test result mg/kg (dry basis)	Analysis method	Standards	Standard limit value (1 grade)mg/kg (dry basis)
Lead	23.27	Atomic absorption method	GB/T17141-1997	35
Cadmium	0.115	Atomic absorption method	GB/T17141-1997	0.20
Zinc	49.92	Atomic absorption method	GB/T17141-1997	100
Manganese	532.2	Atomic absorption method	GB/T17141-1997	-
Chromium	55.87	Atomic absorption method	HJ491-2009	90
Copper	18	Atomic absorption method	GB/T17141-1997	35
Nickel	25.17	Atomic absorption method	GB/T17141-1997	40
Mercury	0.0094	Atomic fluorescence method	'Water and Waste Water Monitoring Method' Version 4,2002	0.15

Firstly, we for the first propose that sludges have to be categorized according to the engineering properties such as organic matter content, particle size, liquid and plastic limits and hazardous material content etc., and that they should be to exploited them in different applications based on their categories. Secondly, it has been proved through experiments that sludges treated using lime, construction wastes and lime together with waste incinerator slag, with a mixing ratios derived from a serial series of experiments of road usage properties such as liquid plastic limits, CBR etc., can achieve the property requirement for fill material in road embankment construction, and all the experiments have been successful. Finally, after analysis of a sample of the soil surrounding the test segment, it is found that there is no significant increase of heavy metal content in the soil surrounding the test road segment that adopts treated sludge as fill material in the construction of road embankment and that the amount of heavy metal in the surrounding soil entirely conforms to the bound requirement of Grade 1 level in “Soil Environment Quality Standard” (GB15618-1995).

The test method used in this paper with its merits including its of high digest volume of sludge and rapid and easy execution process etc. provides a solution to problems of land occupancy and impact on the local environment caused by land filling the sludges from river dredging. It also solves the problems of large quantity earth taking, soil damage and resource waste for the sake of obtaining roadbed fill material. Especially In particular, the mixture of sludges with construction wastes realizes the purposes goals of ‘treating wastes with wastes’ and ‘double wastes turn into treasure’ and provides an important development idea and a path to a low carbon, energy saving and environmentally friendly recycling economy with a good economic benefit and a huge social benefit as well.

REFERENCES

- Heng, Y. (2009). *Study on Road Performance and Filling Technology of Solidified Muddy Soil by Fly-Ash*. Ph.D. thesis, Shanghai Jiaotong University.
- Zhang, C. (2007). *Study of Dredged Sludges Solidification Mechanism Based on Water Transfer Model*. Ph.D. Thesis, Hohai University.

The Key Technology for Construction Quality Control of Cement Emulsified Asphalt Mortar of CRTS Ballastless Slab Track for High-speed Railway

Liangwei Lou¹ Yan Cheng² Changhua Zhu¹ and Xinhua Zhong¹

¹Railway Engineering Research Institute, China Academy of Railway Science, No.2, Daliushu Road, Haidian District, Beijing, China; PH(86-10)51849535; FAX(86-10)51874253; E-mail: louliangwei@163.com

²Nanjing-Hangzhou railway Co., Ltd, No.166, Tianmushan Road, Xihu District, Hangzhou, Zhejiang, China; PH(86-571)56722252; FAX(86-571)56732832; E-mail: shtljcy@163.com

Abstract

CRTSII ballastless slab track used in high-speed railway was originated from B(o)gle slab track system of Germany. Cement emulsified asphalt mortar (CEAM) layer, as one of the three core technologies of CRTS ballastless slab track, has been playing a significantly important role in the track structure. Combined with engineering practice of CEAM layer used in the ballastless slab track for the Beijing-Shanghai high-speed railway and the Shanghai-Hangzhou high-speed railway, the effects of raw materials, mix proportion design and key processes, such as wetting, edge banding, grouting and curing on construction quality were analyzed in this paper. Furthermore, the key technologies of construction quality control were mainly expounded in different construction stages, and the quality control measures were also proposed, correspondingly.

Introduction

CEAM layer, which is the main part of CRTSII ballastless slab track structure, functions as adjustment, filling, supporting, force bearing and transferring, as well as providing appropriate elasticity and toughness to the track (see Figure 1). While CEAM is high sensitive to environment because of its complicated composition, and this can contribute to difficulty in construction (Zeng, Zheng, and Wen, 2009). Thus, it is quite important to control the construction quality of CEAM so that it could achieve the structure functions and the operating requirements of ballastless slab track.

Based on the weak link of construction quality control, the key points for quality control of CEAM are presented, through the analysis of raw materials, mortar mix proportion, key technology as well as quality inspection, and so on.

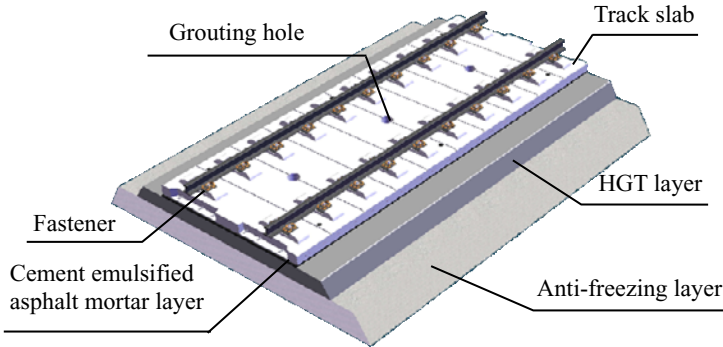


Figure 1. The structure of CRTSII ballastless slab track on subgrade

Material Quality Control

The quality of raw materials has a great influence on performance and construction quality of CEAM. To ensure the service performance and structure durability, serious measures should be taken to control the quality of raw materials.

Technical requirements

CEAM is a multi-component and multi-phase material, which requires better dispersion, stability and compatibility (China Academy of Railway Sciences, 2007). To achieve the above requirements, the following aspects should be considered :

(1) Emulsified asphalt is the main liquid component of CEAM, with fine cementation and toughening effect. In addition to the conventional indexes mentioned in the criterion, the adaptability between emulsified asphalt and cement must be paid more attention (Liu, and Liu, 2007).

(2) Dry-mixed mortar has played an important role in the overall performance of CEAM. Considering the large shrinkage during setting and hardening period, the dry-mixed mortar should provide certain expansion for CEAM. Therefore, in order to ensure the volume stability, the expansion ratio must cause enough attention. In many engineering applications, the expansion ratio of dry-mixed mortar would reach 1.0 ~ 3.0%, for achieving the expansion ratio of CEAM in the rang of 0 ~ 2.0%, ultimately.

It is also observed that the grain grading and the maximum particle size of dry-mixed mortar will greatly affect the CEAM in terms of workability, compressive/flexural strength and elastic modulus. It has been demonstrated that the segregation of mortar would be much easier when the grain becomes coarse gradually,

and vice versa, the strength and elastic modulus can be apt to decrease.

(3) For the difference of seasonal construction, the components of raw materials need to be adjusted in advance according to recommended technical requirements, especially for the dry-mixed mortar and superplasticizer.

Transportation and storage

The quality of raw materials is easily affected by transportation distance, storage time, and storage environment including ambient temperature and ambient humidity. Several points for attention in usage that must be considered are thus:

(1) Special storage tank is suitable for emulsified asphalt by means of the automatic temperature control device and stirring device in that the temperature is the most important influence factor for emulsified asphalt.

(2) Besides the temperature, another significant factor that influences the properties of dry-mixed mortar is ambient humidity. During the transportation and storage, dry-mixed mortar must be prevented from being moistened in case the latent danger of large early-stage shrinkage after grouting.

(3) Raw materials are stored separately by different batches, and also followed by the principle of first in and first out.

(4) However, it should be borne in mind that the storage temperature of raw material must be controlled in the range of 5 ~ 30□.

Mix Proportion Design

Recommended mix proportion

For meeting the structure function of filling layer, it is quite necessary to design the mix proportion of CEAM seriously. The recommended parameters of mix proportion are given in Table 1, and the acceptable properties of fresh CEAM have also been listed in table 2, accordingly.

Table 1. Recommended mix proportion (kg/m³)

Component	Emulsified asphalt	Dry-mixed mortar	Water	Superplasticizer	Defoamer
Reference value	250 ~ 280	1460 ~ 1500	120 ~ 160	1.0 ~ 10	≤1.2

Table 2. Recommended properties of fresh mortar

Detection index	Temperature(°C)	Slump flow (mm)	Fluidity (s)	Bulk density (kg/m ³)	Air content (%)
Reference value	5 ~ 30	280 ~ 310	90 ~ 120	1860 ~ 1940	4 ~ 7

Adjustment of mix proportion

Based on the laboratory study, the mix proportion should be adjusted through the way of changing types and compositions of raw materials, technology and parameters of mixing, which is dependent on raw materials, equipment type,

construction environment, and so on. Additionally, the final results will be always determined by technological test and type inspections.

As mentioned above, the properties of CEAM is susceptible to the temperature. In this case, the parameters of mix proportion and material composition should be modified in time, along with the temperature variation of environment, raw materials and fresh mortar. Appropriate adjustment method and adjustment range have been given in table 3, in which the type and amount of superplasticizer should be adjusted primarily when the ambient temperature varies.

Table 3. Adjustment method and range.

Ambient temperature	Emulsified asphalt	Dry-mixed mortar	Superplasticizer	Defoamer	Water
Low 5–10°C	Decrease 10–15 kg/m ³	Winter formula	Early-strength 2–5 kg/m ³	0.6–1.2 kg/m ³	±5 kg/m ³
Normal 15–25°C	Medium	Common formula	Standard 4–6 kg/m ³	0.4–0.6 kg/m ³	±5 kg/m ³
High 30–40°C	Increase 10–15 kg/m ³	Summer formula	Retarding 5–8 kg/m ³	0.2–0.4 kg/m ³	±10 kg/m ³

Construction of CEAM

Technological test

For obtaining stable quality, advanced process, reliable equipment and professional constructors, the mix proportion, mixing technology, grouting technology, personnel organization, and emergency plan must be determined through technological test before the practical application. Up to recently, the practice shows that the construction units should attach importance to technological test, summarized from the Beijing-Shanghai high-speed railway and the Shanghai-Hangzhou high-speed railway.

Construction technology control

Each link of construction will be associated with the mechanical properties, durability and service life of CEAM at different degree. In order to ensure the construction quality, the construction process must be in-control. More specifically, key process needs monitoring and special-personnel examination.

(1) Wetting: Wetting of support layer and track slab is one of the key processes in the construction of CEAM. Further emphasis should be put on wetting support layer due to its high porosity. Specific engineering practice indicates that the quality defects of mortar caused by incorrect wetting are most common (see Fig. 2).

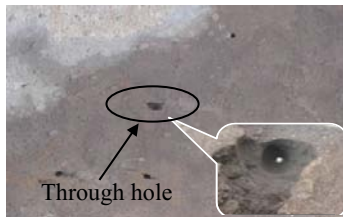


Figure 2. Typical quality defects caused by incorrect wetting

To avoid these problems, three available principles should be followed: (a) multi-wetting, (b) rather wet than dry, and (3) immediate coverage. Firstly, the support layer and track slab must be washed down completely and wet until saturated using hydraulic giant. Secondly, water accumulation must be removed before edge banding using earthwork cloth or blower. Prior to grouting, the humidity of concrete surface of support layer needs to be checked again. Suitable water supplement such as fogging and misting remains to be carried out when the humidity decreases greatly. At last, the stress should be laid on coverage in time to keep the humidity of chamber filled by CEAM later. Above all, time interval from wetting to grouting should be within 2 ~ 3 hours in summer and 3 ~ 5 hours in winter, respectively.

(2) Compaction device: An important remaining question to consider is what a suitable compaction device is that the track slab can be fixed firmly. The main function of compaction device is to maintain the geometric position of track slab after grouting. The three key points to focus on are: (a) the depth of planting bar; (b) the quantity of compaction; (c) the location of compaction. Figure 3 shows one of optimal types of compaction device commonly used in construction.

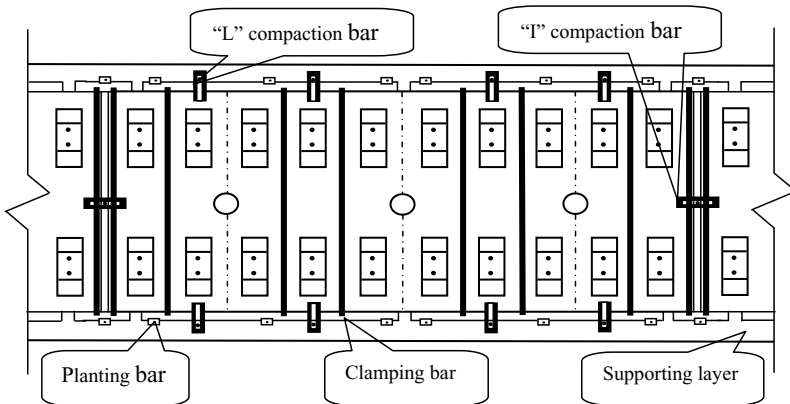


Figure 3. Compaction device

(3) Edge banding and discharge port arrangement: More recently, a new method performed by using angle steel and breathable multilayer film has had widely application in edge banding, which has the advantages followed as high construction efficiency, good exhaust effect, easy to wetting and less impact on fine tuning, compared with cement mortar or wood formwork (see Figure 4). There are several precautions could be presented: (a) the track slab has been fixed completely by compaction device before edge banding; (b) the size of angle steel must so match with multilayer breathable film that it can closely attach to slab and support layer; and (c) as illustrated in figure 3, the longitudinal and vertical force lade on angle steel ought to be appropriate without serious knock during the banding.

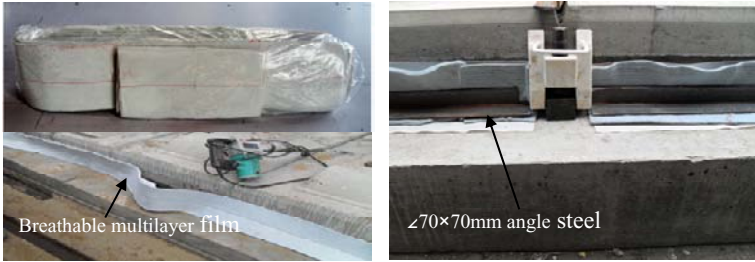


Figure 4. Edge banding

The arrangement of discharge port is important as well. The quantity of discharge ports is no less than 10 on tangent sections, and 6 on curve sections, respectively. To serve its purpose of full exhaust, discharge port requires symmetrical distribution on tangent sections. Moreover, the angle between discharge port and support layer is about 15° , which can effectively solve the problem of excessive bubble on mortar surface (see Figure 5).

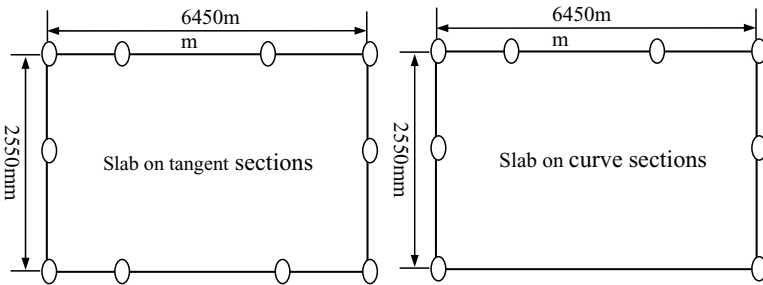


Figure 5. Discharge port arrangement

(4) Grouting: In practice, it is well recognized that grouting is a major premise, and also great responsible for the quality of CEAM. For the stable and controllable quality, the grouting technology is not allowed to be changed once it is to be decided. Grouting time and grouting speed, as the two main parameters, will influence each other, but each has the different requirements. It will definitely increase grouting pressure, exhaust resistance, as well as a higher demand on edge banding if grouting time is short, namely the speed is faster. Contrarily, it is likely to lead to the segregation of mortar owing to stratified flow, and even not completely filled (see Figure 6). Generally speaking, the grouting time with 4 ~ 6 minutes would be fine on tangent sections, and 5 ~ 8 minutes on curve sections, respectively. Meanwhile, combined with flow track under the track slab, grouting speed prefers to be uniform.

Anyway, it should be never interrupted in the whole process of grouting.



Fig. 6. Segregation of mortar



Fig. 7. Exhaust and grouting funnel

Figure 7 clearly shows a special exhaust and grouting funnel used in practical engineering. It can keep the grouting speed uniform, control the grouting time, and enhance the exhaust effect.

(5) Curing: Different from concrete curing, proper curing for CEAM is much more important to ensure that they meet their design function and life requirements. For that purpose, a strict restriction on curing has been taken after finishing grouting immediately, not only curing temperature and humidity, but also curing time. Traditional curing, for example, sprinkling and coverage using earthwork cloth, has been verified not enough, especially in summer or winter. As a result, such a curing can lead to strength reduction of CEAM, and even a large shrinkage crack between track slab and mortar. In view of this, breathable multilayer film should not be removed at least 7 days, which acts as heat-preservation and moisture-preservation material and plays a great role in curing. Once the breathable multilayer film had been removed, the exposed mortar should be sprayed a special curing agent for mortar, or bonded with water-saving curing film without frequently sprinkling and much labor.

Quality inspection and acceptance

The quality inspection of CEAM has three main points:

(1) Establishing and improving quality assurance system, and perfecting construction quality inspection and acceptance regulations (Republic of China Ministry of Railways, 2008).

(2) Strengthening the construction of field laboratory of CEAM, emphasizing on-site tracing monitoring, as well as improving the technical level of the qualified inspection personnel, and strengthening personnel training.

(3) Strengthening type inspection, site acceptance and daily inspection of raw materials. In the daily inspection, the indexes of fresh mortar such as slump flow, fluidity, air content, temperature must be strictly monitored.

Summary

CEAM is a new structural material with fully independent intellectual property right, through the re-innovation of the ballastless slab track in China. For its highlight features, how to develop a correct and comprehensive construction strategy, involving technology management and quality control measures is definitely a fundamental, but important task for ensuring the engineering quality. It can be very helpful not only by fully using the scientific research achievements and technical force of the scientific research units, but also by giving play to the experiences of design unit, construction unit and supervision unit. In this way, the expected object of zero-defect in engineering quality can be attained finally.

References

- China Academy of Railway Sciences. (2007). "Stage experimental study on CEAM used in CRTSIIballastless slab track in severe cold area."=na Academy of Railway Sciences, Beijing.
- Liu, S. A., and Liu, D. H. (2007). "Analysis of knotty problems in CEAM." China Railway 17 Bureau Group Co., LTD, Taiyuan.
- Republic of China Ministry of Railways. (2008). Technology base [2008] 74, "Tentative technical pecification for cement asphalt mortar in CRTS□ ballastless slab track of passenger dedicated railway." China Railway Press, Beijing.
- Zeng, Z., Zheng, X. G., and Wen, Z. C. (2009). "Construction technique of cement-emulsified-bitumen mortar used in CRTSII-type ballastless slab track." 2009 (9): 97-100.

Preliminary Analysis of AASHO Road Test Rigid Pavement Data Using Linear Mixed-Effects Models

H. W. Ker¹, Y. H. Lee², T. C. Huang², and K. Lin²

¹ Department of International Trade, Chihlee Institute of Technology, #313, Sec. 1, Wen-Hwa Rd., Pan-Chiao District, New Taipei City, Taiwan 220; PH: (886-2) 2257-6167 ext 1683; E-mail: hker@mail.chihlee.edu.tw

² Department of Civil Engineering, Tamkang University, E732, #151 Ying-Chuan Rd., Tamsui District, New Taipei City, Taiwan 251; PH/FAX: (886-2) 2623-2408; E-mail: yinghaur@mail.tku.edu.tw

ABSTRACT

Pavement performance data is a very common example of multilevel data. While analyzing this type of data using conventional regression techniques, the normality assumptions with random errors and constant variance were often violated. Because of its hierarchical data structure, multilevel data are often analyzed using Linear Mixed-Effects (LME) models. The exploratory analysis, statistical modeling, and the examination of model-fit of LME models are more complicated than those of standard multiple regressions. A systematic modeling approach using visual-graphical techniques and LME models was proposed and demonstrated using the original AASHO road test rigid pavement data. The proposed LME modeling process including selecting a preliminary mean structure, selecting a random structure, selecting a residual covariance structure, model reduction, and examining the model fit will be further discussed in this paper.

INTRODUCTION

Longitudinal data are used in the research on growth, development, and change. Multivariate analysis of variance (MANOVA), repeated measures ANOVA, and standard multiple regression methods have historically been the most widely used tools for analyzing longitudinal data. Linear Mixed-Effects (LME) models are an alternative for analyzing longitudinal data. These models can be applied to data where the number and the spacing of occasions vary across individuals and the number of occasions is large. LME models can also be used for continuous time. LME models are more flexible than MANOVA in that they do not require an equal number of occasions for all individuals or even the same occasions. Moreover, varied covariance structures can be imposed on the residuals based on the nature of the data. Thus, LME models are well suited for longitudinal data that have variable occasion time, unbalanced data structure, and constrained covariance model for residual errors.

A systematic modeling approach using visual-graphical techniques and LME models was proposed and demonstrated using the original AASHO road test rigid pavement data [HRB, 1962]. The proposed approach includes characterizing the growth patterns at both group and individual levels, identifying the important predictors and unusual subjects, choosing suitable statistical models, selecting

random-effects structures, suggesting possible residuals covariance models, and examining the model-fits [Ker, 2002; Lee & Ker, 2008; 2009].

DATA DESCRIPTION AND REEVALUATION OF THE EXISTING MODEL

The AASHO road test was a large-scale highway research project conducted near Ottawa, Illinois from 1958 to 1960, and has had by far the largest impact on the history of pavement performance analysis. The test consisted of 6 loops, numbered 1 through 6. Each loop was a segment of a four-lane divided highway and centerlines divided the pavements into inner and outer lanes, called lane 1 and lane 2. Pavement designs varied from section to section. The axle loads on each loop and lane can be found elsewhere. All sections had been subjected to almost the same number of axle load applications on any given date. Pavement performance data was collected based on the trend of the pavement serviceability index at 2-week interval. The last day of each 2-week period was called an "index day." Index days were numbered sequentially from 1 (November 3, 1958) to 55 (November 30, 1960) [HRB, 1962; Huang, 2004]. Empirical relationships between pavement thickness, load magnitude, axle type, accumulated axle load applications, and performance trends for both flexible and rigid pavements were developed after the completion of the road test. Several combinations of certain rules, mathematical transformations, analyses of variance, graphs, and linear regression techniques were utilized to develop such empirical relationships.

During the road test, it was found that the damage rate was relatively constant in both winter and spring for concrete pavements. Therefore, unlike flexible pavements, the load applications (W) of rigid pavements were not adjusted by "seasonal weighting function." Only the serviceability records of 3.5, 3.0, 2.5, 2.0, and 1.5 were used for the regression model. A load equivalence factor was then established to convert different configurations of load applications to standard 18-kip equivalent single-axle loads (ESAL). This ESAL concept has been adopted internationally since then. The well-known original rigid pavement design equation is as follows:

$$\log(ESAL) = 7.35 * \log(D + 1) - 0.06 + \frac{\log[(4.5 - PSI)/(4.5 - 1.5)]}{1.0 + 1.624 * 10^{-7} / (D + 1)^{8.46}} \quad (1)$$

To serve the needs of predicting pavement serviceability index (PSI) after certain load applications on a given section, it is not uncommon that engineers would rearrange the original rigid pavement equation into the following form:

$$PSI = 4.5 - 3.0 * 10^{\left[\frac{1.624 * 10^7}{(D+1)^{8.46}} \right] * [\log(ESAL) - 7.35 * \log(D+1) + 0.06]} \quad (2)$$

Lee [1993] has pointed out that a regression model is very different from a mathematical equation in that the latter one may be transformed or rearranged in various forms without losing its generality. On the other hand, the prediction of a transformed or rearranged regression will not have the same degree of accuracy as the original one. Various forms of the original rigid pavement equation were used to predict $\log(W)$, W , and PSI using the same set of data from which the original equation was developed. The regression statistics are summarized as follows:

1. Prediction of $\log(W)$: $R^2=0.659$, $SEE=0.136$, $N=371$
2. Prediction of W : $R^2=0.498$, $SEE=201600$, $N=371$

3. Prediction of PSI: $R^2=0.032$, $SEE=0.702$, $N=316$

Figure 1 shows the predicted versus actual W and PSI values. Apparently, the error variance increases when the predicted number of load repetitions (W) increases. Note that PSI ranges from 0 to 5 (0-1 for very poor; 1-2 for poor; 2-3 for fair; 3-4 for good; and 4-5 for very good conditions). D is the slab thickness (in.); R^2 is the coefficient of determination; SEE stands for the standard error of estimates; and N is the number of observations. Only 316 data points were used for the PSI prediction since some data having predicted PSI values less than zero were excluded. Banan and Hjelmstad [1996] also indicated that the existing AASHO model does not represent the observed road test serviceability trends well.

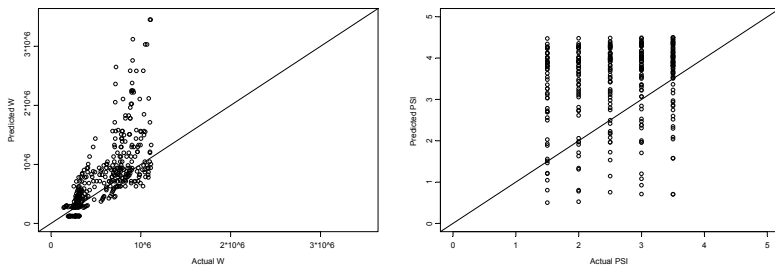


Figure 1. Predicted versus actual W and PSI values.

As pavement design evolves from traditional empirically based methods toward mechanistic-empirical, the ESAL concept used for traffic loads estimation is no longer adopted in the recommended Mechanistic-Empirical Pavement Design Guide (MEPDG) [ARA, Inc., 2004], although many researchers have argued that it is urgently in need of reconsideration [HRB, 1962; Lee, 1993; Ker et al., 2008].

Furthermore, additional serviceability records at 11, 22, 33, 44, and 55 index days were also obtained from the original report [HRB, 1962]. Both datasets were merged together providing at least 5 and at most 10 data points for each design section for the subsequent analysis. The combined dataset consists of 1546 data points. The raw “unweighted” traffic data were adopted to avoid the undesirable complication of the “weighted” applications. Several climatic variables including temperature, freezing index, and average monthly freeze-thaw cycles (FT) were also retrieved from the Long-Term Pavement Performance (LTPP) database [FHWA, 2004] to incorporate the test site climatic effects into the modeling process.

LINEAR MIXED-EFFECTS MODELING APPROACH

After extensive exploratory analyses have been conducted to characterize the growth patterns at both group and individual levels, identify the important predictors and unusual subjects, and choose suitable statistical models. The following modeling approach which is generally applicable to modeling multilevel longitudinal data with a large number of time points was adopted. The model building procedures including the selection of a preliminary mean structure, the selection of a random structure, the selection of a residual covariance structure, model reduction, and the examination of

the model fit are subsequently illustrated.

Selecting a Preliminary Mean Structure

Covariance structures are used to model variation that cannot be explained by fixed effects and depend highly on the mean structures. The first step to model building is to remove the systematic part and remove this so that the variation can be examined. The dataset includes the following explanatory variables: thick, substhck, uwtappl, FT. In which, thick is slab thickness (in.); substhck is subbase thickness (in.); uwtappl is unweighted applications (millions), and FT stands for monthly freeze-thaw cycles.

A model containing all main effects, and all the two-way, three-way interaction terms was first investigated. This model (called model-1) has the form, where β_{0i} is level-1 intercept; β_{1i} to β_{9i} are level-1 regression coefficients; and r_{ii} is the residual error term:

$$\begin{aligned} \overline{PSI}_{ii} = & \beta_{0i} + \beta_{1i}(\text{thick})_{ii} + \beta_{2i}(\text{substhck})_{ii} + \beta_{3i}(\text{uwtappl})_{ii} + \beta_{4i}(\text{uwtappl})_{ii}^2 + \beta_{5i}(\text{FT})_{ii} \\ & + \beta_{6i}(\text{thick})_{ii}(\text{substhck})_{ii} + \beta_{7i}(\text{thick})_{ii}(\text{uwtappl})_{ii} + \beta_{8i}(\text{substhck})_{ii}(\text{uwtappl})_{ii} \\ & + \beta_{9i}(\text{thick})_{ii}(\text{substhck})_{ii}(\text{uwtappl})_{ii} + r_{ii} \end{aligned} \quad (3)$$

Selecting a Preliminary Random Structure

The second step is to select a set of random effects in the covariance structure. An appropriately specified covariance structure is helpful in interpreting the random variation in the data, achieving the efficiency of estimation, as well as obtaining valid inferences of the parameters in the mean structure of the model. In longitudinal studies, the same subject is repeatedly measured over time. The data collected from longitudinal study is a collection of correlated data. The within-subject errors are often heteroscedastic (i.e., having unequal variance), correlated, or both.

Exploring preliminary random-effects structure

A useful tool to explore the random-effects structure is to remove the mean structure from the data and use ordinary least square (OLS) residuals to check the need for a linear mixed-effects model and decide which time-varying covariate should be included in the random structure. The boxplot of residuals by subject corresponding to the fit of a single linear regression by using the same form of the preliminary level-1 model was conducted. This is the case when grouping structure is ignored from the hierarchy of data. Since the residuals are not centered around zero, there are considerable differences in the magnitudes of residuals among subjects. This indicates the need for subject effects, which is precisely the motivation for using linear mixed-effects model. Separate linear regression models were employed to fit each subject to explore the potential linear relationship.

Selecting a variance-covariance structure for random effects

Three possible variance-covariance structures including general positive definite (unstructured), diagonal, and block-diagonal based on different assumptions were investigated. General positive-definite is a general covariance matrix parameterized directly in terms of variances and covariances. Diagonal covariance structure is used when random-effects are assumed independent. Block-diagonal matrix is employed when it is assumed that different sets of random effects have different variances.

Table 1 displays the model comparison of these three models. The unstructured model has the smallest absolute value of log-likelihood among them. The likelihood ratio test for unstructured model versus diagonal model is 38.81 with p-value less than 0.0001. Thus, unstructured variance-covariance model will be used hereafter.

Table 1. Model Comparison Using Three Variance-Covariance Structures.

Model	df	Akaike Information Criterion (AIC)	Bayesian Information Criterion (BIC)	Log-Likelihood (logLik)	Test	L.Ratio	p-value
(1) Unstr	26	3083.87	3222.80	-1515.94			
(2) Diag	16	3102.69	3188.18	-1535.34	1 vs.2	38.81	<0.0001
(3) Bk-diag	13	3153.26	3222.72	-1563.63	2 vs.3	56.57	<0.0001

The random effects of the preliminary level-2 model include intercept, *uwtappl*, quadratic term of *uwtappl*, and *FT*. The variance-covariance structure is a general positive-definite matrix. Putting the preliminary level-1 and level-2 models together, the preliminary linear-mixed-effects model is then, where γ_{00} to γ_{90} are level-2 regression coefficients or the “fixed effects”; u_{0i} , to u_{4i} are level-2 random effects associated with level-1 intercept and slopes:

$$\begin{aligned}
 \overline{PSI}_{ii} = & \gamma_{00} + \gamma_{10}(thick)_{ii} + \gamma_{20}(subasthk)_{ii} + \gamma_{30}(uwtappl)_{ii} + \gamma_{40}(uwtappl)_{ii}^2 + \gamma_{50}(FT)_{ii} \\
 & + \gamma_{60}(thick * subasthk)_{ii} + \gamma_{70}(thick * uwtappl)_{ii} + \gamma_{80}(subasthk * uwtappl)_{ii} \\
 & + \gamma_{90}(thick * subasthk * uwtappl)_{ii} + u_{0i} + u_{1i}(thick)_{ii} + u_{2i}(subasthk)_{ii} \\
 & + u_{3i}(uwtappl)_{ii} + u_{4i}(uwtappl)_{ii}^2 + r_{ii}
 \end{aligned}
 \tag{4}$$

Selecting a Residual Covariance Structure

The absolute value of log-likelihood for this heteroscedastic model is 1319.78. The need of heteroscedastic model can be formally checked by using the likelihood ratio test, which is summarized in Table 2. The small p-value indicates that the heteroscedastic model explains the data significantly better than homoscedastic model.

Table 2. Comparison of Heteroscedastic and Homoscedastic Models.

Model	Df	AIC	BIC	logLik	L.Ratio	p-value
Homoscedastic	26	3083.87	3222.80	-1515.94		
Heteroscedastic	33	2705.55	2881.89	-1319.78	392.32	□0.0001

Modeling dependence

Correlation structures are used to model dependence among the within-subject errors. Autoregressive model with order of 1, called AR(1), is the simplest and one of the most useful models [Pinherio & Bates, 2000]. The autocorrelation function (ACF), which begins autocorrelation at lag 1 and then declines geometrically, for AR(1) is particularly simple. Autocorrelation functions for autoregressive model of order greater than one are typically oscillating or sinusoidal functions and tend to damp out with increasing lag [Pindyck & Rubinfeld, 1998].

Thus, AR(1) may be adequate to model the dependency of the within-subject errors. The absolute value of log-likelihood for this heteroscedastic AR(1) model is 995.18. The estimated single correlation parameter ϕ is 0.39. The heteroscedastic

model (corresponding to $\phi = 0$) is nested within the heteroscedastic AR(1) model.

Likewise, the need of heteroscedastic AR(1) model can be checked using likelihood ratio test as given in Table 3. The small p-value indicates that the heteroscedastic AR(1) model explains the data significantly better than heteroscedastic model, suggesting that within-group serial correlation is present in the data.

Table 3. Comparison of Heteroscedastic and Heteroscedastic AR(1) Models.

Model	df	AIC	BIC	LogLik	L.Ratio	p-value
Heteroscedastic	33	2705.55	2881.89	-1319.78		
Heteroscedastic AR(1)	34	2058.35	2240.03	-995.18	649.20	< 0.0001

Reduction of random effects

As suggested by Morrell, Pearson, and Brant [1997], the matrix of known covariates should not have polynomial effect if not all hierarchically inferior terms are included. The same rule applies to interaction terms. Hence, significance tests for higher-order random effects should be performed first. Table 4 shows the models and the associated maximum log-likelihood values. The small p-value indicates that the preliminary random-effects structure (Model 1) explains the data significantly better than the others. A large p-value of 0.89 indicates that the reduction of random effects in subasthk is needed. The random effects (Model 4) included in the preliminary random-effects structure are: intercept, thick, uwtappl, and uwtappl².

Table 4. Comparison of Different Random-Effects Models.

Model	df	AIC	BIC	logLik	Test	L.Ratio	p-value
(1) Intercept, thick, subasthk, uwtappl, uwtappl ²	34	2058.35	2240.03	-995.18			
(2) Intercept, thick, subasthk, uwtappl	29	2367.78	2522.74	-1054.89	1 vs 2	219.43	<0.0001
(3) Intercept, subasthk, uwtappl, uwtappl ²	29	2117.96	2272.92	-1029.98	1 vs 3	69.61	<0.0001
(4) Intercept, thick, uwtappl, uwtappl ²	29	2049.97	2204.93	-995.99	1 vs 4	1.620	0.89

Reduction of fixed effects

An adequate and appropriately specified random-effects structure implies efficient model-based inferences for the fixed effects. When considering the reduction of fixed effects, one model is nested within the other model and the random-effects structures are the same for the full and the reduced models. Likelihood ratio tests are appropriate for the model comparison. The parameter estimates, estimated standard errors, t-statistics and p-values for the fixed effects of the heteroscedastic AR(1) model are revisited. The heteroscedastic AR(1) model can be reduced to a more parsimonious model due to the existence of some insignificant parameter estimates. The reduction of fixed effects starts with removing the parameters with largest p-values, insignificant terms, and combining the parameters not changing significantly. These processes are repeated until no important terms have been left out of the model.

Preliminary LME Model

A preliminary linear mixed-effects model is listed in Table 5. The fixed-effects structures of the model contain significant treatment effects for thick, uwtappl, uwtappl², and thick*uwtappl. The positive parameter estimates for thick, indicates that higher mean PSI values tend to occur on thicker pavements. The parameter estimate of uwtappl is negative indicating that lower PSI values for higher load applications. Furthermore, the preliminary LME model also indicates that: Thicker pavements have much less variations as compared to thinner pavements. For example, the standard deviation of 12.5-in. concrete pavements is only about 22.1% of those of 5-in concrete pavements. There exists dependency in within-subject errors. The estimated single correlation parameter for the AR(1) model is 0.39.

Table 5. A Preliminary LME Model.

Random Effects					
	Intercept	thick	uwtappl	uwtappl ²	Residual
Standard Deviation	0.627	0.124	1.166	0.486	0.628
Fixed Effects					
Parameter	Value	Std.Error	df	t-value	p-value
(Intercept)	3.559	0.227	1532	15.702	< 0.0001
thick	0.132	0.042	1532	3.156	0.0016
uwtappl	-4.265	0.452	1532	-9.440	< 0.0001
(uwtappl) ²	1.002	0.226	1532	4.434	< 0.0001
thick*uwtappl	0.336	0.027	1532	12.650	< 0.0001

Note: (a) Model fit: AIC=2049.839, BIC=2178.081, logLik=-1000.919 (b) Correlation structure: AR(1); parameter estimate(s): Phi=0.39 (c) Variance function structure: for different standard deviations per stratum (thick= 5, 2.5, 3.5, 6.5, 8, 9.5, 11, 12.5 in.), the parameter estimates are: 1, 0.877, 1.031, 1.104, 0.182, 0.602, 0.966, 0.221.

Examination of the model fit

A plot of the population predictions (fixed), within-group predictions (Subject), and observed values versus time for the preliminary LME model by subjects was made. Population predictions are obtained by setting random-effects to zero whereas within-group predictions use estimated random effects. The prediction line of the within-group predictions follows the observed values more closely indicating the preliminary LME model provides better explanation to the data. The goodness of fit of the preliminary LME model is shown in Figure 2.

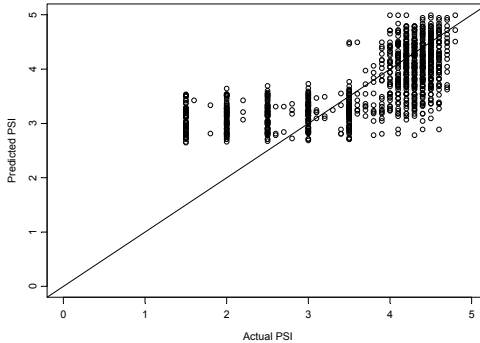


Figure 2. Goodness of the fit of the preliminary LME model.

CONCLUSIONS

A systematic modeling approach using visual-graphical techniques and LME models which is generally applicable to modeling multilevel longitudinal data with a large number of time points was proposed in this paper. The original AASHO road test rigid pavement data was used to illustrate the proposed modeling approach. A preliminary LME model for PSI prediction was developed. The positive parameter estimates for slab thickness indicates that higher mean PSI values tend to occur on thicker pavements. The parameter estimate of unweighted applications is negative indicating that lower PSI values for higher load applications. The prediction line of the within-group predictions (Subject) follows the observed values more closely than that of the population predictions (fixed) indicating the preliminary LME model provides better explanation to the data.

REFERENCES

- ARA, Inc. (2004). *Guide for mechanistic-empirical design of new and rehabilitated pavement structure*. NCHRP 1-37A Report, Transportation Research Board, National Research Council, Washington, D. C.
- Banan, M. R., and Hjelmstad K. D. (1996). Neural Networks and AASHO Road Test. *Journal of Transportation Engineering, ASCE*, 122(5), pp. 358-366.
- FHWA (Federal Highway Administration) (2004). *Long-Term Pavement Performance Information Management System: Pavement Performance Database Users Reference Guide*. Publication No. FHWA-RD-03-088.
- Highway Research Board (HRB) (1962). *The AASHO road test, Report 5, Pavement Research, Special Report 61E*. Publication No. 954, National Research Council, Washington, D.C., 1962.
- Huang, Y. H. (2004). *Pavement analysis and design*, 2nd ed., Pearson New Jersey: Education, Inc.
- Ker, H. W. (2002). *Application of regression spline in multilevel longitudinal modeling*, Ph.D. Dissertation, University of Illinois, Urbana, Illinois, 2002.
- Ker, H. W., Lee, Y. H., and Wu, P. H. (2008). "Development of fatigue cracking performance prediction models for flexible pavements using LTPP database."

- Journal of Transportation Engineering, ASCE, 134(11)*, pp. 477-482.
- Lee, Y. H. (1993). *Development of pavement prediction models*, Ph.D. Dissertation, University of Illinois, Urbana, Illinois.
- Lee, Y. H., and Ker, H. W. (2008). *Reevaluation and application of the AASHTO mechanistic-empirical pavement design guide, Phase I*, Summary Report, NSC96-2211-E-032-036, National Science Council, Taiwan. (In Chinese)
- Lee, Y. H., and Ker, H. W. (2009). *Reevaluation and application of the AASHTO mechanistic-empirical pavement design guide, Phase II*, NSC97-2221-E-032-034, Summary Report, National Science Council, Taiwan, 2009. (In Chinese)
- Morrell, C. H., Pearson, J. D., and Brant, L. J. (1997). "Linear transformations of linear mixed-effects models." *The American Statistician*, 51, pp. 338-343.
- Pindyck, R.S., and Rubinfeld, D. L. (1998). *Econometric models and economic forecasts*, 4th ed. New York: McGraw-Hill, Inc.
- Pinheiro, J. C., and Bates, D. M. (2000). *Mixed-effects models in S and S-plus*, New York: Springer-Verlag.

Research on Strength Developing Procedure of Epoxy Asphalt Mixture

L. L. Chen¹, Z. D. Qian², and C. L. Jiang³

¹ Intelligent Transport System Research Center, Southeast University, Nanjing 210096, China; PH: (86)13813896903; E-mail: chenleilei@seu.edu.cn

² Intelligent Transport System Research Center, Southeast University, Nanjing 210096, China; PH & FAX: 86-25-83792868; E-mail: qianzd@seu.edu.cn

³ T.Y.Lin International Engineering Consulting Co., Ltd., Chongqing 401121, China; PH: (86)15023670158; E-mail: jcdragon123@163.com

ABSTRACT

Epoxy asphalt mixture (EAM) is a thermosetting material, and its strength develop law depends not only on temperature, but also on curing time, while the strengths of most other asphalt mixtures are only a function of temperature. This complication in the strength developing procedure of EAM has brought many difficulties to its construction. To find a better way to approach the construction of EAM, the strength developing procedure of EAM was studied. Firstly, the viscosities of epoxy asphalt binder (EAB) in different temperatures were tested to investigate the viscosity developing law of EAB. Secondly, a thermokinetic analysis was conducted based on the differential scanning calorimetry (DSC) test to establish a curing model of EAB. Thirdly, the performance of EAM under different curing times and at different temperatures is studied to investigate the strength developing law of EAM. The test results indicated that the optimum viscosity range for EAM construction is from 1000mPa·s to 3000mPa·s, and the optimum laboratorial curing condition is 5 hours at 130°C. Finally, a curing model of EAB was established and verified on the basis of the test results.

INTRODUCTION

Epoxy asphalt mixture (EAM), mixed by thermosetting epoxy asphalt binder (EAB) and high quality aggregate, has been extensively used in China (Gaul R, 2009). It is widely acknowledged that the thermosetting nature of epoxy asphalt binder has contributed significantly to the good performance of EAM; for example, it exhibits good resistance to fatigue and permanent deformation (Huang W, 2003). This is because the curing reaction can transform the epoxy resin contained in the EAB into plastic or rubber by a cross-linking process and subsequently links the molecular chains into a rigid, 3-D structure (Milton, 2000). However, as an irreversible process, the curing reaction brings complications to EAM construction control. These complications have always been a challenge in the application of EAM.

Like thermoplastic material, the performance of EAM depends on curing time and temperature. According to the construction experience of EAM, for a certain temperature there are two key time points for EAM, the reserved time and the curing time. The reserved time is defined as the time from the mix of asphalt and aggregate to the compaction of the mixture; an optimum reserved time will lead to the best performance of EAM. The length of curing time will significantly affect the performance of the EAM. Both of the two times can be determined from the strength developing law of EAM. Therefore, to make construction control easier, the strength developing procedure of EAM needs to be studied.

There have been many studies examining the strength mechanism of paving materials. The Transportation Materials Research Center (TMRC) of the Michigan Technological University has researched the strength mechanism of asphalt mixtures using the finite element and discrete element methods (Dai Q, 2007; You Z, 2007; Dai Q, 2006), Ranja Bandyopadhyay (Ranja Bandyopadhyay, 2007) and Martin H. Sadd (M.H. Sadd, 2005) have also investigated the strength formation of asphalt mixtures from a microscopic view. However, this research all focuses on thermoplastic material such as HMA; few studies are conducted on the thermosetting material. The Intelligent Transportation System Research Center of Southeast University has conducted a number of studies on EAM in recent years (Qian, 2011; Chen, 2010); nevertheless, most of the research focuses on the performances of EAM after curing. Few studies about the curing procedure of EAM can be found.

In this paper, an experimental program is performed to investigate the strength developing law of EAM. First, a viscosity test was performed on EAM to determine a suitable viscosity range for construction. Secondly, a differential scanning calorimetry (DSC) test was conducted to establish a curing model of EAM. Thirdly, the performances of the EAM under different curing time are studied to investigate the strength developing law of EAM. At last, a curing model of EAM was established and verified based on the laboratory tests.

EXPERIMENTAL STUDIES

Materials and specimens

Materials Preparation. The binder used in the test was 2910-type local epoxy asphalt, which was composed of two components marked as A and B. Component A was the epoxy resin and component B consisted of petroleum asphalt and a curing agent. The basic information of the material is given in Table 1.

Specimen Preparation. Considering the convenience of the specimen shaping, the Marshall test is adopted to investigate the performance of EAM. Marshall stabilities and air voids are two main indices in practical EAM construction. Based on the Marshall mixture design procedure, a 6.5% binder content is determined as the optimum asphalt content, the Marshall mixtures are shaped using impact compaction method, and five replicates are prepared for each testing.

Table 1. Technical Index of 2910-Type Local Epoxy Asphalt

Technical Indexes	Measured Value	Criteria	Test Method
Modulus (MPa)	100:290	100:290	
Tensile strength (MPa, 23°C)	3.26	≥2.0	ASTM D 638
Elongation at break (% , 23°C)	242	≥200	ASTM D 638
Flow rate (mm/min)	110	≥50	JTJ052-2000

Viscosity test of EAB

The viscosity of EAB is an important index in the curing reaction of EAM. In this paper, 110°C, 115°C, 120°C, 125°C and 130°C are selected as test temperatures according to the practical construction temperatures. The viscosity of EAB is measured using a Brookfield rotational dial viscometer with a rotating speed of 100 rpm (29⁷). The viscosity-time curves of EAB in different temperatures are shown in Figure 1. As shown, the viscosity of EAB increased with as the reaction time increased, and the viscosity increased slowly at the beginning of the test, while it increased faster and faster as time passed.

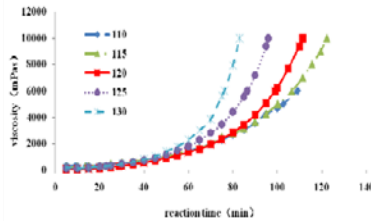


Figure 1. Viscosity-time curve of EAB

It can be also observed that before the viscosity of EAB reaches 1000mPa·s, the viscosity grows slowly. This low viscosity of EAB is not good for the shaping of the mixture. On the other hand, after the viscosity of EAB rises to 3000mPa·s, the viscosity grows rapidly. This rapid growth of the viscosity will result in an inhomogeneous compacting of EAM. So, it can be indicated that the suitable viscosity range for EAM construction is about 1000mPa·s to 3000mPa·s.

Differential Scanning Calorimetry (DSC) test of EAB

The DSC test is a thermo-analytical technique, in which the difference in the amount of heat required to increase the temperature of a sample and reference is measured as a function of temperature (O'Neill M, 1964). In this paper, the DSC test was conducted for the establishment of the EAB curing model using the simultaneous thermal analyzer STA 449 C Jupiter ®. A pretext was used to connect the thermo gravimetric analyzer (TGA) and the differential thermal analyzer (DTA); thus the thermo gravimetric TG and DSC curves can be obtained simultaneously.

During the test, the component A and B of the epoxy asphalt used in the test were placed separately before testing and then were mixed carefully. With the selected heating rates of +5K/min, +10K/min and +20K/min, three replicates were prepared for each heating rate. The TG and DSC curves were recorded as shown in Figure 2, which will be analyzed later for the calculation of the thermokinetic parameters in the reaction model of EAB.

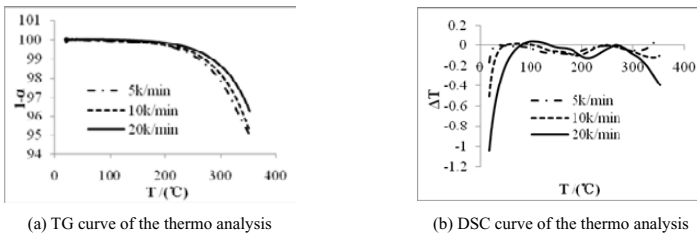


Figure 2. Simultaneous thermal analysis curves of EAM

Strength Test of EAM

The Marshall mixtures are shaped in the same condition at temperature 120°C and reserved time 50min. Then part of the specimens were curing at the temperatures of 120°C, 125°C and 130°C respectively, in accordance with the mixing temperature, while the other ones are curing at room temperature at about 15°C to simulate the actual condition of EAM construction.

The EAM stability test results for different curing times are shown in Figure 4. It can be seen from Figure 3(a) that the stability grows as curing time increases until it achieves the maximum value. It also can be seen that it takes less time to get to the peak value when the curing temperature is higher. Considered the time savings, 5 hours at 130°C is the optimum laboratorial curing condition. From Figure 3(b), it can be observed that the curing process at room temperature is much slower than in laboratorial conditions; under this circumstance, it takes about 40 days for EAM to reach 40kN, which is the requirement for the EAC pavement open to traffic.

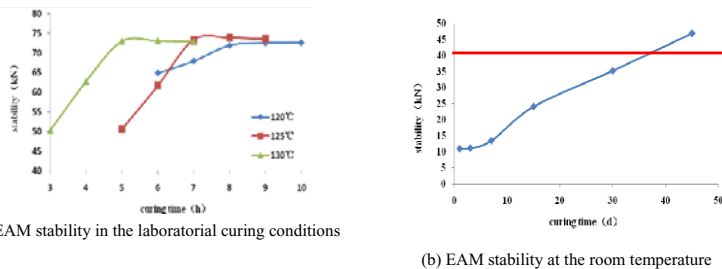


Figure 3. Experimental results of study on the curing time

CURING MODEL OF EAB

Model design

The thermosetting property of EAM comes from the curing reaction of EAB. Therefore, the curing model of EAM was established, based upon a thermokinetic analysis. In this paper, the reaction process was assumed to depend upon two individual parameters as the reaction conversion degree α ($0 \leq \alpha \leq 1$) and the reaction time t . Thus the kinetic function $f(\alpha)$ can be described as:

$$\frac{d\alpha}{dt} = f(\alpha)k(T) \tag{1}$$

where $k(T)$ is the reaction rate that is a function of the absolute temperature T .

Let β denote the heating rate and assume that there is a linear relationship between temperature and time; then β can be represented as dT / dt . Based on this, Equation 1 can be rewritten as:

$$\frac{d\alpha}{dT} = \frac{1}{\beta} f(\alpha)k(T) \tag{2}$$

For the reaction rate $k(T)$, many formulas have been given since the last decade, among which the Arrhenius equation is well accepted (Mianowski A, 2003) and is adopted in this study. The Arrhenius equation is a simple but remarkably accurate formula for the temperature dependence of the reaction rate, and can be represented as:

$$k(T) = A \exp(-E/RT) \tag{3}$$

where A and E are the pre-exponential factor and activation energy, respectively, and considered to be independent of T , while R is the gas constant, known as $8.314 \text{ J} \square \text{K}^{-1} \square \text{mol}^{-1}$. When Equation 3 is substituted into Equation 2, Equation 2 can be rewritten as:

$$\frac{d\alpha}{dT} = \frac{A}{\beta} \exp\left(\frac{-E}{RT}\right) f(\alpha) \tag{4}$$

Where A , E and $f(\alpha)$ are three main components in the thermokinetic analysis.

Model Solution

Equation 4 can be solved through the well-known Kissinger Law (Kissinger HE, 1957), in which $f(\alpha)$ can be assumed as $f(\alpha) = (1-\alpha)^n$, where n , the reaction order, is 0, 1, 2, 3, or a fraction.

By taking a differentiate treatment to both sides of the equation, Equation 4 can be written as:

$$\frac{d}{dt} \left[\frac{d\alpha}{dT} \right] = \frac{d\alpha}{dT} \left[\frac{E}{RT^2} \frac{dT}{dt} - An(1-\alpha)^{n-1} e^{-E/RT} \right] \tag{5}$$

In Equation 6, the parameters can be acquired through the DSC test. In a DSC curve, the maximum reaction rate always reaches at the temperature peak T_p , i.e.,

$\frac{d}{dt} \left[\frac{d\alpha}{dT} \right] = 0$. By taking logarithm, Equation 6 can be transformed to:

$$\ln \frac{\beta}{T_{max}^2} = \ln \frac{nAR}{E} + (n-1)\ln(1-\alpha_{max}) - \frac{E}{RT_{max}} \tag{6}$$

As seen in Equation 6, it is found that two different heating rates β_1 and β_2 will correspond to two different maximum temperatures; by making a subtraction, we get:

$$\ln \frac{\beta_1 T_{max2}^2}{\beta_2 T_{max1}^2} - (n-1)\ln \frac{(1-\alpha_{max1})}{(1-\alpha_{max2})} = \frac{E}{R} \cdot \frac{T_{max1} - T_{max2}}{T_{max1} T_{max2}} \tag{7}$$

In Equation 7, since β , T_{max} and α_{max} are all known quantities in the DSC test, the activation energy E can be obtained. Consequently, the pre-exponential factor A can be estimated.

The model parameters can be obtained from the TG-DSC simultaneous thermal analysis curve at the heating rates of 5K/min, 10K/min, and 20K/min. Take the TG-DSC simultaneous thermal analysis curve at the heating rate of 5K/min as an example, as shown in Figure 4; the parameters at the different predetermined heating rates are summarized in Table 2.

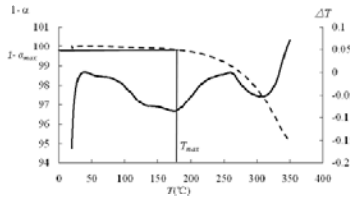


Figure 4. Simultaneous thermal analysis curves of the heating rate of 5K/min

Table 2. Parameters of Epoxy Asphalt in the Curing Reaction

Heating rate $\beta/(K \cdot \text{min}^{-1})$	Temperature peak T_{max}/K	Reaction degree $1-\alpha/\%$	Temperature differential $\Delta T/(mw/mg)$
5	447.76	0.9982	-0.0856
10	465.86	0.9978	-0.1018
20	485.16	0.9981	-0.1278

With the model parameters available, Equation (7) can be used to compute the activate energy E of the EAM when the reaction order is determined. As known, the reaction order n ranges from 0 to 3; therefore, a trial method was used to calculate the activate energy E . The calculated results show that the mean value of E is 59.2kJ/mol. Consequently, the optimal value of the reaction order n is 1.5 and the pre-exponential factor A is 1.588×10^4 .

Based on the type II kinetic equation, integral can be taken on Equation (6) :

$$\int_0^\alpha \frac{d\alpha}{(1-\alpha)^n} = A \exp(-E/RT) \cdot t \tag{8}$$

By solving Equation (8), the reaction convert degree α can be represented as a function of the reaction temperature T and the reaction time t in the form of:

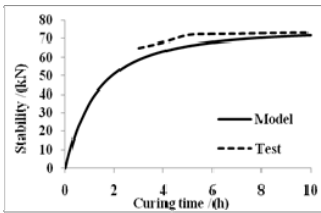
$$\alpha = 1 - [1 + (n - 1) \cdot A \cdot \exp(-E/RT) \cdot t]^{\frac{1}{n}}$$

where $A=1.588 \times 10^4$, $E=5.92 \times 10^4$ and $n=1.5$, so the final curing reaction model of EAM is established as:

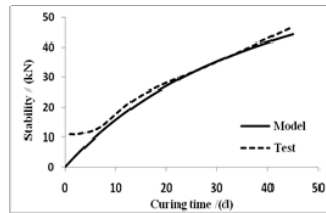
$$\alpha = 1 - [1 + 7.94 \times 10^3 \cdot \exp(\frac{-7.12 \times 10^3}{T}) \cdot t]^2$$

Model Validation

As seen in the established curing reaction model of EAB, the convert degree α is a function of the reaction temperature and the reaction time. In most cases, EAM is cured at a determined temperature; thus, the curing degree can be simplified as a function of time. This can be used for figuring out the strength developing law of the EAM at a determined curing temperature. For instance, the strength developing law at 15°C and 120°C were simulated by the proposed model and compared to the laboratory tests result, as shown in Figure 5. It can be seen in Figure 5(a) that the peak value of the EAM is about 75kN. Therefore the predicted strengths from the model are all based upon the final strength of 75kN.



(a) EAM stability at 120°C



(b) EAM stability at 15°C

Figure 5. Comparison between the simulation and the test results of EAM strength

It can be seen that the Marshall stability of the EAM generated by the proposed model is close to the laboratory test results, especially in the later stage of the curing reaction. This can be explained by the strength formation of the EAM. The strength of the EAM was formed from not only the adherence of the binder, but also the embedment of the aggregate. The strength of EAM mainly comes from the aggregate at the early stage of the curing reaction, while the strength of the epoxy asphalt binder may become the major source as the reaction continues. The results also indicated that it is reasonable to assume a linear relationship between the strength of EAM and the curing reaction convert degree at the later stage of the curing reaction.

The proposed model can be used to predict the EAM strength in EAM construction. For example, as shown in Figure 5(b), the model implies that 37 days are required for EAM to attain the stability of 40kN, nearly the same as the test

result. In construction engineering, some adjustments should be made to the predicted results in accordance with the factual curing temperature.

RESULTS AND CONCLUSIONS

The strength developing procedure of EAM was studied in this paper; some conclusions were drawn as follows:

- The viscosity of EAB grows slowly before 1000mpa·s and grows rapidly after 3000mpa·s, the optimum construction viscosity is the range between these two values.
- The strength of EAM developed faster in a higher temperature, the optimum laboratory curing condition for EAM is curing 5h at 130°C.
- The curing reaction model for the epoxy asphalt binder uses the Kissinger law, and the parameters of the model were calibrated through the DSC test.
- The model was proved to be valid and effective using the strength test data of EAM. It can be used to predict the strength of the EAM.

REFERENCES

- Bandyopadhyaya, R, et. al. (2007). "Numerical simulation of mechanical behavior of asphalt mix". *Constr Build Mater*, Vol. 23, pp.1-8.
- Chen, L.L. and Qian, Z.D. (2010). "Experimental study on dynamic modulus of thermosetting epoxy asphalt mixture for steel deck pavement", *J. Southeast univ.(English Ed.)* 26 (1), 112-116.
- Dai, Q., You, Z., and Sadd, M.H. (2006). "A Micromechanical Visco-elastoplastic Model for Asphalt Mixture", *Geotechnical Special Publication: Asphalt Concrete: Simulation, Modeling, and Experimental Characterization, ASCE*, pp. 12-20.
- Dai, Q. and You, Z. (2007). "Prediction of Creep Stiffness of Asphalt Mixture with Micromechanical Finite Element and Discrete Element Models", *J Eng. Mech., ASCE*, Vol. 133 No.2, pp. 163-173.
- Gaul, R. (2009) "A Long Life Pavement for Orthotropic Bridge Decks in China" *Proceedings of Selected Papers from the GeoHunan International Conference.*
- Huang, W., Qian, Z.D. et. al (2003). "Epoxy asphalt concrete paving on the deck of long-span steel bridges". *Chin. Sci. Bull.*, 48(21): 2391- 2394.
- Kissinger, H.E. (1957). "Reaction Kinetics in Differential Thermal Analysis." *Anal Chem.* 29: 1702-1706.
- Mianowski, A. (2003). "The Kissinger Law and Isokinetic Effect. Part I: Most common solutions of thermokinetic equations". *J. Therm. Anal. Calorim.* 74: 953-973.
- Milton, K. T838 "Design and Manufacture with Polymers: Introduction to Polymers," The Open University (UK), 2000, pp. 9.

- M.H., Sadd and Dai, Q. "A comparison of micro-mechanical modeling of asphalt materials using finite elements and doublet mechanics". *Mech. Mater.* Vol. 37, 2005, pp. 641–662.
- O'Neill, M. J. (1964) "The Analysis of a Temperature-Controlled Scanning Calorimeter" *Anal Chem.* 36: 1238-1245.
- Qian, Z.D., Chen, L.L. (2011) "Performance evaluation of a lightweight epoxy asphalt mixture for bascule bridge pavements" *Constr Build Mater*, 25(7), 3117-22.
- You, Z., Dai, Q. (2007) "A Review of Advances in Micromechanical Modeling of Aggregate - Aggregate Interaction in Asphalt Mixture". *Can. J. Civ. Eng.* 34(2), 239-252.

Research on Flexural Strength of Asphalt Mixture in Cold Highlands

Wei Youpo^{1,2}, Song Yunxiang¹, and Li Yumei¹

¹Henan Transportation Research Institute CO. LTD, Zhengzhou, 450006, China.

Phone : 18790268096; E-mail: wyp@hntri.com

²Key Laboratory for Special Area Highway Engineering, Ministry of Education, Chang'an University, Xi'an, 710064, China

ABSTRACT

The cracking of asphalt pavement caused by temperature changes is one of the main problems in cold highlands where climate characteristics include a low average temperature and a large variation in temperature. Temperature contraction cracking has a greater relation to the flexural strength of asphalt mixture. The effects of the temperature, nominal maximum size of aggregate and the asphalt-aggregate ratio on flexural strength are investigated in the laboratory combining with the climate features of cold areas. The results show that there are two strategic points, -10°C and 15°C , in the curve of the flexural tensile strength under the five kinds of temperatures. The flexural tensile strength of AC-13 is greater than that of AC-16 at lower temperatures. The asphalt-aggregate ratio is given for the maximum flexural strength of 6.0%-7.0%. The extent of influence on flexural strength is analyzed by variance analysis, revealing that temperature and asphalt-aggregate ratio have a highly significant influence on flexural strength of asphalt mixture. Regression analysis is conducted for the results using a binary quadratic model. The yield for temperature and asphalt-aggregate ratio can be described well by the model.

INTRODUCTION

Low-temperature cracking of asphalt pavement has occurred throughout cold areas both here and abroad. The reason why low-temperature cracking of asphalt pavement is particularly harsh in cold highlands is because of a Climate characteristic in which average temperatures are low and temperature variation is extreme. It is a common pavement distress in our country's northern region and is harmful to road quality and service life (Ma, 2007; Hu, Ma, Zhang, & Ding, 2007). Cracking is one of the major failure modes of bituminous pavement in cold areas. Apart from the special climate of the northern region, the reasons the cracks occur is closely related to the characteristics of road material. The objective of this study is to evaluate the tensile strength and bending strength of asphalt mixtures under

different temperatures utilizing the constant loading speed bending test which is used at home and abroad for the special climate of the northern region. The study includes complications such as the temperature, nominal maximum size of aggregate, and the asphalt-aggregate ratio, and describes the effects of these factors on the curved characteristic of asphalt mixture (Ma, Fu, & Zhang, 2008).

MATERIALS AND EXPERIMENTS

SBR modified asphalt, which is used in cold areas, was supplied by the construction site of Qinghai-Tibet Highway and the result of asphalt parameters was shown in Table 1. The aggregates for this study were sampled from the Qinghai-Tibet Area, with the main constituents of lime-stone rocks. The same aggregate source, gradation and asphalt binder were used for all mixtures. The mineral aggregate gradation was designed following the intermediate gradation of AC-16 and AC-13 in the dense-graded bituminous mixture design method (Table 2).

Table 1. Test Result of Asphalt Parameters

Test Description	SBR Modified Asphalt
Penetration at (25) 100σ 5s 0.1mm	123
Softening Point R&BC °C Min	46.0
Ductility 5cm/min at 15°C cm Min	>150
Solubility in Trichlorethylene % Min	99.6
Density g·cm ⁻³ Min	0.9988
Flash Point Clevel Open Cup °C Min	>260
Rtftot Oven Mass Loss % Max	0.2
Heating Test163°C Penetration At 25% °C % Min	0.61
85 Mins Ductility 5cm/minAT5°C cm	69

Table 2. Aggregate Gradations of Asphalt Mixture

Gradation Types	Through the percentage %										
	19	16	13.2	9.5	4.75	2.36	1.18	0.6	0.3	0.15	0.075
AC-13	100	100	95	76.5	53	37	26.5	19	13.5	10	6
AC-16	100	97	83	68	53	42	30	22	16	11	5

Bearing special climate and traffic conditions, and combining with the actual project, the optimum binder content of 6.5 percent was determined by the Marshall Method. Flexural testing was carried out for the specimens, shaped by Marshall Test, with binder contents of 5.5, 6.0, 6.5, 7.0, and 7.5 percent under the temperatures of -20 °C, -10 °C, 0 °C, 15 °C, 20 °C. The electronic hydraulic universal material testing machine was adopted, acquiring data automatically. The environmental chamber, with a precision of ±0.1 °C, was used as a temperature control unit for the specific temperatures.

RESEARCH PROCEDURE

Temperature

Flexural testing was carried out for SBR modified AC-16 asphalt mixture in the five temperatures (Figure 1). The flexural strength of asphalt mixture changes in parabolic shape with the rising of temperature for the five asphalt-aggregate ratios. The flexural strength reaches a maximum at about -10°C . According to the peak point temperature and the rate of temperature, the curve can be divided into three parts which are less than -10°C , -10°C - 15°C and more than 15°C . The flexural strength increases as temperature rises, when temperature is below -10°C . The strength rapidly decreases within the range of $-10^{\circ}\text{C} \sim 15^{\circ}\text{C}$, while the rate of decreases slows when the temperature above 15°C .

The brittle temperature has appeared to be about 10°C for the slow loading rate and low temperature. At higher temperatures than that, flexural strength becomes larger with temperature, while at lower temperatures than that the strength decreases (Zhou, 2007; Li, 2005). The reducing rate of flexural strength slows for the viscoelastic asphalt when the asphalt rheology increases above 15°C .

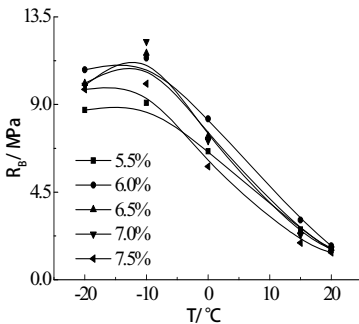


Figure 1. Relationship between flexural strength and temperature

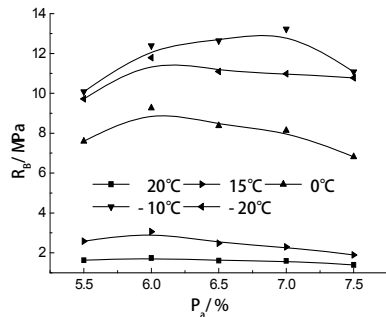


Figure 2. Relationship between flexural strength and asphalt-aggregate ratio

Asphalt-aggregate ratio

Figure 2 shows the comparison of flexural strength for the five asphalt-aggregate ratios. Experimental data show that the asphalt-aggregate ratio has a great effect on strength. The flexural strength of the asphalt mixture changes in parabolic shape with the rising of asphalt-aggregate ratios for the five temperatures. There is existing maximum flexural strength between 6.0%-7.0%. The existing research material draws similar conclusions. Value rationality of asphalt-aggregate ratio is verified.

The flexural strength of the asphalt mixture not only depends on viscosity of binder and the rapping which is produced by interaction of asphalt and aggregates, but also relies on cohesion from free asphalt. At the low temperature, the film thickness wrapped with the surface of aggregate increases with the rising of asphalt binder. The asphalt has two rules including bonding among binder and aggregates and lubrication in favor of moving of aggregates in asphalt mixture (Wang & Li, 2008; Li, 2008). With the growth of asphalt, film thickness become thicker and movement among aggregates enhances. When the asphalt is enough to form a thin film asphalt binder and fully rap on the aggregate surface, the flexural strength reaches maximum. With the increase of the asphalt-aggregate ratio, the asphalt appears excessive and aggregates are pushed. Too much asphalt becomes lubrication, and in favor of moving of aggregates in asphalt mixture, the force of the asphalt mixture lessens. Optimal asphalt content range appears for the maximum flexural strength with the effect of temperature (Hao & Zhang, 2000).

Table 3. Flexural Strength of Two Kinds of Nominal Maximum Size

Flexural strength Mpa	20°C	15°C	0°C	-10°C	-20°C
AC-16	1.61	2.48	7.38	11.64	10.09
AC-13	1.72	2.44	8.56	12.87	12.43

Table 3 shows that the nominal maximum size has great effect on flexural strength. According to the strength, the change of strength can be divided into two parts which are less than 0°C and above 0°C. The flexural strength of two kinds of asphalt mixture is similar when the temperature is higher than 0°C, while the flexural tensile strength of AC-13 is greater than that of AC-16 at lower temperatures.

ANOVA OF INFLUENTIAL FACTORS`

In order to further verify conclusion reliability, variance analysis was made on the results using SPSS. The major influential factors were screened out and the test result optimized. Three factors were temperature (A), asphalt-aggregate ratio (B) and maximum normal size (C). The calculation results follow in Tables 4 and 5.

Table 4. ANOVA of Flexural Strength

Origin	Sum of squares	Degree of freedom	Mean square deviation	F-Value
A	356.81	4	89.1909	FA=241.44
B	6.96	4	1.74019	FB=4.71
Error	5.91	16	0.36941	
Sum	369.63	24		

Given the level of significance $\alpha = 5\%$ and 1% , $F_{0.05} (4, 16) = 3.01$, $F_{0.01} (4, 16) = 4.77$, $F_A > 4.77$, $F_B > 4.77$, based on the results of variance analysis, temperature and asphalt-aggregate ratio has a highly significant influence on flexural strength of asphalt mixture.

Table 5. ANOVA of Flexural Strength

Origin	Sum of squares	Degree of freedom	Mean square deviation	F-Value
A	191.41	4	47.851	FA=102.03
C	2.32	1	2.323	FB=4.95
Error	1.87	4	0.469	
Sum	195.60	9		

Given the level of significance $\alpha = 10\%$, 5% and 1% , $F_{0.01}(4, 9) = 6.42$, $F_{0.05}(1, 9) = 5.12$, $F_{0.1}(1, 9) = 3.36$, $FA > 6.42$, $5.12 > FB > 3.36$, based on the results of variance analysis, temperature has a highly significant influence on flexural strength of asphalt mixture, and asphalt-aggregate ratio, the influence of which was lower than temperature, has obvious effects on flexural strength.

RELATIONSHIP BETWEEN INFLUENCE FACTORS AND FLEXURAL STRENGTH

In order to analyze the impact of asphalt-aggregate ratio and maximum normal size on flexural strength, the Origin analytical procedure was adopted. Regression analysis was conducted for the results by using binary quadratic model. The yield for temperature and asphalt-aggregate ratio can be described well by the model (Formula 1 and Figure 3). The coefficient and the correlation coefficient of the formula are shown in Table 6.

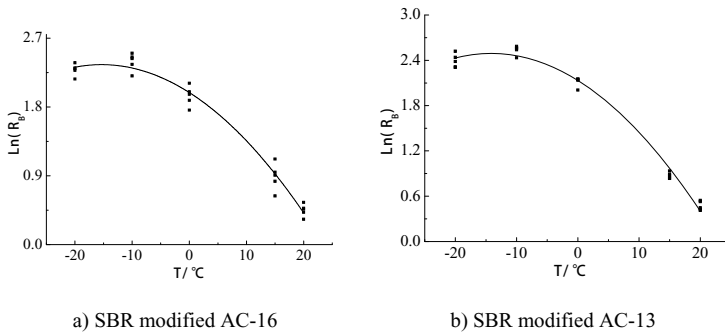


Figure 5. Relationship between flexural strength and temperature

$$\ln(RB) = a + b \times T + c \times T^2$$

Where:

RB= Mpa flexural strength

T= °C temperature

a、 b、 c= fitting factor

Table 6. Coefficient and Related Coefficient of SBR Modified AC-16 and AC-13

Mixture Types	Coefficient	The Relationship between Coefficient Ratio	Related Coefficient
SBR	a	$-7.10424+2.88816 \times Pa-0.22642 \times Pa^2$	0.7951
Modified AC-13	b	$-0.01824-0.00452 \times Pa$	0.9880
SBR	a	$0.00858-0.00323 \times Pa-0.0025 \times Pa^2$	0.8152
Modified AC-13	b	$0.2564+0.5962 \times Pa-0.046 \times Pa^2$	0.7619
SBR	a	$-0.01158-0.003 \times Pa-2.27408 \times Pa^2$	0.7825
Modified AC-13	b	$0.0205-0.002 \times Pa+0.0014 \times Pa^2$	0.7611

CONCLUSION

(1) The brittle temperature has appeared about 10°C . At higher temperatures than this, flexural strength became larger as temperature increased, while at temperatures lower than this, strength decreased. Combining with the local unique climatic condition, the importance of flexural strength at 10°C should be taken seriously in a perennially frozen soil zone; structural design of asphalt pavement in this area and cracking resistance of asphalt mixture at low temperatures has improved.

(2) The laws between flexural strength of asphalt mixture and asphalt-aggregate ratio were studied. It is reasonable to choose an asphalt-aggregate ratio in the range of 6.0% to 7.0%. When flexural strength asphalt mixture with different maximum normal size is compared, the flexural tensile strength of AC-13 is found to be greater than that of AC-16 at lower temperatures.

(3) The influence of temperature, maximum normal size and asphalt-aggregate ratio on flexural strength was studied through the use of variance analysis. Temperature and asphalt-aggregate ratio had a highly significant influence on flexural strength of the asphalt mixture; maximum normal size also had an effect on flexural strength of the asphalt mixture.

(4) Regression analysis was conducted for the results by using a binary quadratic model. The yield for temperature and asphalt-aggregate ratio can be described well by the model.

REFERENCES

- Hao, Pei-wen, Zhang, Deng-liang. (2000) "Evaluation Method for Low Temperature Anti-cracking Performance of Asphalt Mixture" J, (5):63-67.
- Hu, Dong-Xia, M,a Biao, Zhang, Yi, Ding, Lan. (2007) "Application of Fibers-reinforced Asphalt Mixture in Permafrost Area, " J. Highway, (7):81-84.

- Li, Xue. (2005) "Investigation of the Fracture Resistance of Asphalt Mixtures at Low Temperatures With a Semi Circular Bend (SBC) Test," D. University of Minnesota, 43-44.
- Li, Zhi-dong. (2008) "Study on Design Method of Asphalt Mixture Proportion for the Permafrost Area" J. Highway, (1): 125-127.
- Ma, Biao. (2006) "Study of Asphalt Pavement Material Composing and Structure Design for the Permafrost Area" D. Chang'an University. (in Chinese)
- Ma, Jun-yi, Fu, Jin, Zhang, Jin-zhao. (2008) "The Popularization and Application of the Scientific Research Achievements in the Reconstruction Project of Qinghai-Tibet Highway," J. Journal of Highway and Transportation Research and Development, (9): 287-290.
- Wang, Shuang-jie, Li, Zhu-long. (2008) "Research on Highway Construction Technology in the Permafrost Region of China," J. Journal of Highway and Transportation Research and Development, 25(1): 1-9.
- Zhou, Lian. (2007) "Temperature design of asphalt pavement pavement at cold area," J. Journal of Chang'an University (Natural Science Edition), 27(5): 40-43.

Long-Life Pavement Design and Construction – A Case Study

George Wang¹, Yuhong Wang², Russell Thompson³ and Yong Han Ahn¹

¹East Carolina University, Department of Construction Management, Greenville, NC 27858. Ph: (252)737-1887; Fax: (252)328-1165; E-mail: wangg@ecu.edu

²Hong Kong Polytechnic University, Hung Hom, Kowloon, Hong Kong. Ph: (852) 2766-4489; E-mail: ceyhwang@polyu.edu.hk

³Monash University, Clayton, Victoria, Australia 3800. Ph: (613)9905-1850; E-mail: russell.thompson@monash.edu

ABSTRACT

Over the past 20 years, China's transportation infrastructure has developed rapidly. To date, more than 40,000 kilometers expressway have been built and opened to traffic, ranking second in the world. In the meantime, short service life and early failure of the highway pavement have become one of major concerns. This may be contributed by the poorly designed semi-rigid pavement structure and heavily overloaded vehicles. In more recent years, some long-life pavement structures have been designed and constructed. This paper discusses the design and construction of an expressway long-life flexible pavement structure in China. The project involved is a new 26.78 kilometer, Da'an to Jiliao Section in Henan Province, of the Erliahaote to Guangzhou Expressway. The pavement had been designed as a semi-rigid structure which was later replaced by the new long-life flexible pavement structure in order to introduce this pavement technology as a cost-effective alternative to current semi-rigid or rigid pavement technology in China. Technical services provided through integrated technology transfer activities have presented a model for future expressway projects an option, and made the long-life flexible pavement structure the leading edge of national practice.

INTRODUCTION

In more recent years, there are several long-life pavement structures have been designed and constructed in China. Comprehensive technical services were requested by a local highway authority to provide design and construction quality control and assurance services for an expressway long-life flexible pavement structure for the Da'an to Jiliao Section, in Henan Province, of the Erliahaote to Guangzhou Expressway. The project involved was the new 26.78 kilometer, Da'an to Jiliao Section in Henan Province, of the Erliahaote to Guangzhou Expressway. This Expressway Section had a design speed of 100 km/hour and includes twin tunnels (12.5 meter width, 2.1 kilometer length), many culverts, small bridges, and one large, low-level bridge (840 meter length). The width of the expressway (road base is 26 meters (two 0.75 meter soil shoulders, two 3.0 meter emergency stopping zones, four 3.75 meter driving lanes, two 0.5 meter left side edges, and a 2.0 meter median). The original proposed semi-rigid asphalt pavement design was 4 cm PM

Asphalt concrete (Type AC-13C), over 6 cm PM asphalt concrete (Type AC-20C), over 8 cm asphalt concrete (Type AC-25C), over 0.6 cm modified asphalt slurry seal, over 18 cm cement/fly-ash stabilized crushed stone base (4:10:86), over 30 cm (two 15 cm lifts) cement/fly-ash stabilized sand and gravel subbase, and an average fill (embankment) height of 4.5 meters.

From the initial site visit observation and discussions, and the cut/embankment geotechnical evaluations provided, it was clear that the site was geologically quite complex: considerable poor, low-lying soils (~ km 0 to 2, fairly good soil conditions and ~ km 2 to 10, poor soil conditions with some expansive clay and generally shallow groundwater), rising to foothills which will be a major source of fill; then hilly (~ km 13 to 16, with twin tunnels); low-lying soils again (~ km 16 to 18, with land acquisition still in progress); the 840 meter length bridge (~ km 20); and then foothills again with deep soil deposits (~ km 20 to 27). The strength, California Bearing Ratio (CBR) and construction quality of the embankment fills, which formed the subgrade for the pavement structure, will be very important to the satisfactory performance of any expressway semi-rigid asphalt pavement or long-life flexible (asphalt) pavement at this site.

The local highway authority proposed changing the original semi-rigid asphalt pavement structure (design) for the entire length of the project. It was intended to adopt a long-life flexible (asphalt) pavement structure (design) for the project, in order to introduce this pavement technology as a cost-effective alternative to current semi-rigid or rigid pavement technology. The comprehensive technical services for the project was provided through integrated technology transfer cooperation with expressway, so that the long-life flexible (asphalt) pavement structure (design) will be at the leading edge of national and international practice and provide a model for future expressway projects. It has been demonstrated or will be reflected in the continuing performance long-life flexible pavement quality and life-cycle cost advantages.

BACKGROUND INFORMATION ON LONG-LIFE PAVEMENT

According to 1990 European asphalt study tour (FHWA/AASHTO/NAPA), long-life flexible pavement is not a new concept; it has been widely used in Europe. New technologies have contributed to the development of long-life pavement, which include new mix designs, Stone Mastic Asphalt (SMA), for instance; porous asphalt and high-tech surface treatments; new attitudes toward quality and longevity in pavements - 'perpetual' pavement; SHRP activities, Superpave (construction equipment, April 1997), AASHTO 93 - pavement structure - serviceability and fatigue (if checked), AASHTO 2002 (mechanistic) fostering in the US and Canada, which are straight forward to implement.

International experience - International technical literature has presented long-life asphalt pavements (LLAP) and distress type(s) newly identified in recent years, such as top-down cracking (TDC) in the US (Myers, 2002). International practical experience, French, Belgian and UK, for instance, indicates the deterioration of thick, well-constructed, asphalt concrete pavements is not generally structural, and that the deterioration generally starts at the surface as cracking, i.e., TDC and surface course

asphalt concrete rutting, i.e., non-structural deterioration. This implies that a properly designed flexible pavement built with appropriate strength and quality will remain structurally serviceable for a lengthy design life, i.e., a LLAP, 50, or more, years design life, provided a pavement management strategy/system (PMS) and maintenance management systems (MMS) is implemented to ensure that systematic maintenance, pavement preservation such as crack sealing and surface course HMA renewal, 3 to 4 cm, on about a 20 year cycle, typically, which is adopted to detect/monitor and mitigate non-structural deterioration (cracks and rutting) before it impacts on structural performance (2,3,4). Good pavement foundations (strong, drained, stable and consistent) are essential to preclude distresses that originate deep within the pavement structure (Newcomb, 2003).

Chinese expressway practice - Large scale of expressway, especially flexible (asphalt) expressway construction in China started in the late 1980's. For the last two decades, over 40,000 kilometers expressway have been constructed. Majority of the expressway is semi-rigid structure plus overwhelming overloaded vehicles. This has been a direct or indirect cause for early failure of many expressways in China. The forms of early distresses are various. Fig. 1 shows typical distress in fairly new expressway pavement. Fig. 2 shows typical overloaded truck with poor axle and tire distribution of loadings.



Fig. 1 Cracking of relatively new semi-rigid asphalt pavement in Hohhot, Inner Mongolia, transverse thermal crack with top down cracking in wheel path



Fig. 2 Typical heavily overloaded truck with poor axle and tire distribution of loadings

PAVEMENT STRUCTURE DESIGN

The project earthwork had started in spring 2006 when the long-life pavement structure design was proposed. The long-life flexible (asphalt) pavement structure design, and associated technology, mitigation of TDC for instance, involved the following work meeting the components completion timeline, particularly subgrade, base and subbase, pavement surface, and warranty period. The design of recommended long-life flexible (asphalt) pavement structure(s) in accordance with the "Design of Long-Life Flexible Pavements", "AASHTO 2002 for Asphalt Pavement Design", and "Material Properties", including assistance with site CBR, Falling Weight Deflectometer (FWD) and Dynamic Cone Penetrometer (DCP) testing and characterization of representative subgrade soil (fill) samples, granular materials, and asphalt concrete. The activities followed by preliminary design(s), materials characterization, final design(s), complete life-cycle performance and life-cycle cost analysis comparisons of the recommended long-life flexible (asphalt) pavement structure(s) and current semi-rigid asphalt pavement structure including a value engineering comparison.

In the meantime, to ensure the quality of construction, materials performance requirements (subgrade, subbase, base, and asphalt concrete) and relevant end-result materials and construction specifications (End-Results Specifications (ERS)), quality (flexible pavement materials and construction) verification procedures for the project (contractors/subcontractors/material suppliers' responsibility for quality control (QC), with local authority responsible for quality assurance (QA) were developed subsequently. Preliminary and final quality assurance requirements report was prepared. The pavement performance will monitored during the warranty period, to prepare the end-of-construction performance report and end-of-warranty period performance report with recommendations for any necessary remedial work and/or future mitigation maintenance activities.

Pre-Design Evaluation - The pavement design methodology used for the Da'an to Jiliao long-life pavement design consisted of the following: (i) review of project preliminary semi-rigid pavement design, and related documentation, including geotechnical, traffic information, pavement maintenance, rehabilitation and construction unit prices and supplemented by the author's previous major pavement design experience; (ii) determination of ESALs using the project preliminary design for semi-rigid pavement, supplemented by traffic data for existing 'similar' expressways; (iii) review and recommendations of pavement design parameters, including pavement layer structural, and drainage coefficients; (iv) development of preliminary pavement designs using the AASHTO Guide for the Design of Pavement Structure, 1993, supplemented by the author's previous pavement design experience; (v) overstressing evaluation (high loadings of heavy vehicles) using the Shell Bituminous Structures Analysis in Roads (BISAR) software; and also review of the Specifications for the Design of Asphalt Pavement Highways (JTG D50-2006), the Chinese national flexible pavement design method. Fig. 3 presents the situation of subgrade and tunnel construction when the pavement design, i.e. long-life flexible pavement designs, amendment was developed.



FIGURE 3. Subgrade preparation and compaction in December 2006 (left). South entrance of one of the twin tunnels in December 2006 (right).

Traffic Considerations - ESALs were determined using the project preliminary design for semi-rigid pavement traffic information, supplemented by traffic data for existing ‘similar’ expressways. Based on the Specifications for the Design of Asphalt Pavement Highways (JTG D50-2006), Paragraph 3.1, standard Axle Load and Design Traffic Volume, the typical axle is the BZZ-100 (single axle on dual tires), with a standard load of 100 kN, tire pressure of 0.70 MPa, single wheel contact diameter (circular contact area) of 213 mm, and distance from the center points between dual tires of 320 mm ($1.5 \times$ diameter). The standard axle load was adjusted to include allowable overloading (up to 150 kN (50% overload) is permitted). The estimation of traffic loads is a critical pavement design input, and for this reason most recent commercial vehicle traffic and axel loading data was used for the pavement designs.

The traffic volumes and traffic composition provided by the local highway authority were as follows:

Total traffic volume (in):	220,000/month	7,000/day;
Total traffic volume (out):	210,000/month	6,900/day;
Traffic composition: 32% trucks, 30% of which are overloaded		

The Equivalent Axle Loads (EALs) for 15, 20, 25, 30, 40 and 50 years were calculated using the data from the project preliminary semi-rigid pavement design report, including EALs per day (based on deflection 4602 EALs/day and based on tensile strain 3812 EALs/day) and project traffic growth estimates. After Year 25, it was assumed there would be zero percent growth in EALs as new lanes are installed and new regulations enforced (more modern trucks and reduced axles loading/overload control, for instance). For the analysis, three scenarios were considered to maintain reasonable capacity for future traffic growth: A – future lane construction (4 lanes to 6 lanes) in Year 15; B – in Year 20; and C – in Year 30. A factor of 4.6 was used to convert the EAL’s (100 kN) into ESAL’s (80kN). This factor was calculated assuming a blend of loaded and unloaded trucks, and 30 percent of the vehicles overloaded (> 100 kN, up to 50%, 150 kN) and typical truck factors.

Materials Properties - Pavement structure designs were developed using AASHTO 93 design method, using parameters specified by AASHTO 93 and supplemented with the author’s previous design parameters. Two conditions were modeled in order to reflect the quality of materials and construction (good and standard). In addition,

three types of subgrade performance (resilient modulus) were considered (Good, Fair and Poor).

Preliminary Pavement Designs - As indicated, preliminary pavement designs were completed using the AASHTO 93 design method. A total six systems (runs) were completed for each analysis period (15, 30, 40 and 50 years) to compare the influence of quality construction, materials and subgrade on the resulting pavement structures, and to select the most appropriate design. The preliminary designs are presented in Table 3. An overstressing evaluation (high loading of heavy vehicles) was completed using the Shell Oil Company BISAR program. A four-layer system was used in the analysis (HMA, Granular Base/Subbase, Selected Subgrade Material and Subgrade (Fill)). The load used in this analysis was the standard axle BZZ-100 load (single axle on dual tires) of 100 kN (150 kN for an overloaded truck). The tire pressure was assumed to be 0.70 MPa, with a circular contact area. The strains were calculated at the bottom of the hot-mix asphalt layer and at the top of the subgrade (fill).

FINAL PAVEMENT STRUCTURAL SELECTION AND COST COMPARISON

Table 1 provides the final design selection for Da'an to Jiliao Section long-life flexible pavement design compared with the previous semi-rigid pavement design.

Table 1. Long-life pavements structure with the original semi-rigid pavement design

	Current Design Period 15 Year Design	Concession Period 30 Year Design	Long-Life 50 Year Design
High Stability HMA	19 cm*	24 cm*	30 cm*
Crushed Rock Base	20 cm	20 cm	20 cm
Crushed Rock Subbase	40 cm	40 cm	40 cm
Sand and Gravel Select Subgrade Material	80 cm	80 cm	80 cm
Geotextile	Geotextile	Geotextile	Geotextile
Embankment Fill/Cut Road Bed	Fill/Cut	Fill/Cut	Fill/Cut

Notes:

* The total thickness of the HMA can probably be reduced by 2 to 4 cm with high quality materials/construction and care taken to deal with potential top-down cracking. The HMA surface course (wearing course) should incorporate SBS modified asphalt binder. The HMA lower course (bottom course) should be somewhat 'rich' in asphalt binder and also incorporate SBS modified asphalt binder. The HMA must incorporate an anti-stripping additive (typically one percent hydrated lime).

CONSTRUCTION

The final design amendment was approved in February 2007, and implemented immediately into the construction. Construction quality management

services further were provided to ensure the quality of construction. Hydrated lime surface treatment was used to reduce asphalt pavement temperature (black body absorption in Figure 4).



Fig. 4 APA Asphalt Concrete Testing (Left). Hydrated Lime Surface Treatment To Reduce Asphalt Pavement Temperature (Right)

Normally design-build projects essentially place all pavement performance responsibility directly on the contractors, through the initial five year maintenance requirement plus additional five year guarantee against defects. New technologies were employed during the long-life flexible pavement design and construction stages. These included, but not limited, the project (FWD, conventional and portable) testing; Asphalt Pavement Analyzer (APA) verification testing (Figure 5); Impact-Echo Equipment; DCP testing. FWD is very effective for checking that the design strengths are being achieved. Satisfactory and consistent FWD deflection levels indicate that the horizontal tensile strains (ϵ_h) at the bottom of the HMA, and vertical compressive strains (strains (ϵ_v)) at the top of the subgrade, will meet design requirement in terms of HMA fatigue endurance and pavement structural rutting resistance respectively. Figure 5 presents FWD and Impact-Echo testing.



Fig. 5 Portable FWD was used to determine the M_r directly on the surface of the granular base, granular subbase or subgrade during construction (left). Field testing of asphalt concrete pavement with impact-echo equipment to determine cracking and interface conditions (right)



Fig. 6 Asphalt paving in summer 2008



Fig. 7 The 26.78 km long Da'an to Jilao expressway long-life flexible pavement was completed and opened at the end of November 2008

Figs. 6 and 7 present the construction of asphalt layer and the views at the completion of construction.

CONCLUSION

This subject expressway section is located an important component of the national key trunk expressway system, i.e. 13 vertical and 15 horizontal expressway system. It is also the 4th vertical trunk expressway in Henan province, (Henan has five vertical, four horizontal expressways and six corridors highway plan). It is the major expressway in northwestern Henan. The total investment is ¥1.206444 billion yuan RMB (~\$ 180 million USD). When the long-life pavement design amendment was proposed, the construction preparation had started, which include by-passage, resident offices, central laboratory, earthwork. Materials testing, mix designs, surveying, construction plan for road bed, bridges and culverts had been approved. Concrete beam plants were being established. Three bid sections have started to produce concrete beams. By the mid December 2006, the completed construction work included: 1.56 million cubic meters of surface soil removal; 60,000 cubic meters of back fill; 381,000 cubic meters of cut; 107.4 meters of culverts, 44 culvert, two precast beams, and 277 meters of tunnel advancement.

The goal of the design amendment was to optimize the pavement design, determine the best type of pavement structure, improve the construction quality, build a high quality, economical long-life expressway. The design, construction and the short term performance have proved the advantages of the long-life flexible pavement over semi-rigid pavement. Technical services provided through integrated technology transfer activities have presented a model for future expressway projects an option in China, and made the long-life flexible pavement structure the leading edge of national highway transportation practice.

REFERENCES

- FP2 (2002). A Pocket Guide to Asphalt Pavement Preservation. Foundation for Pavement Preservation. FP2/FHWA.
- Myers, L.A. and Roque, R. (2002). Top-Down Crack Propagating in Bituminous Pavements and Implications for Pavement Management. Asphalt Paving Technology 2002. Journal of the Asphalt Paving Technologists, Vol. 71, AAPT, 2002.
- Newcomb, D. (2003). Perpetual Pavements and Pyramids Have a Lot in Common, both need a Perpetual Foundation. Hot Mix Asphalt Technology, March/April 2003.
- Shahin, M.Y. (1998). Pavement Management for Airports, Roads, and Parking Lots. Kluwer Academic Publishers, Norwell, Massachusetts, Third printing 1998.
- TRB (2001). Perpetual Bituminous Pavements. TRB Committee on General Issues in Asphalt Technology. Transportation Research Circular 503, TRB, 2001.

A Rational Approach for Estimating the Resilient Modulus of Constructed Granular Subgrade Materials

W. Virgil Ping¹, M.ASCE, and Biqing Sheng²

¹ Professor, Department of Civil and Environmental Engineering, FAM-FSU College of Engineering, Florida State University, 2525 Pottsdamer Street, Tallahassee, FL 32310, USA; PH (850) 410-6129; FAX (850) 410-6142; email: ping@eng.fsu.edu

² Research Associate, Department of Civil and Environmental Engineering, FAM-FSU College of Engineering, Florida State University, 2525 Pottsdamer Street, Tallahassee, FL 32310, USA; PH (850) 410-6217; FAX (850) 410-6142; email: shengbi@eng.fsu.edu

ABSTRACT

The resilient modulus is an essential engineering property for determining the stress-strain characteristics of pavement structures subjected to traffic loadings. Due to the complexity, labor intensiveness, and time consuming in conducting resilient modulus measurements in laboratory, it is necessary to establish a rational approach for estimating the resilient modulus of subgrade materials after compaction. This paper presents an extensive study to estimate the resilient modulus from basic soil properties for two common types of granular subgrade soil in Florida: fine sand (A-3 soil), and silty/clayey sand (A-2-4 soil). Laboratory triaxial tests were conducted to measure the resilient modulus values of constructed granular subgrades at different conditions. Correlation models were developed for different types of soil from experimental results. The estimated resilient modulus values from the correlation models were generally within a range of +/- 20% of the measured resilient modulus values from laboratory triaxial tests. This approach for estimating the resilient modulus of subgrades could be utilized in the mechanistic-empirical pavement design guide to better evaluate the resilient modulus of constructed subgrade materials.

INTRODUCTION

The resilient modulus is an essential engineering property for determining the stress-strain characteristics of pavement structures subjected to traffic loadings. The AASHTO 1993 Guide for Design of Pavement Structures (AASHTO 1993) incorporated the resilient modulus of component materials into the design process. In recent years, considerable attention has been given to the development of mechanistic-empirical approach for design and evaluation of pavements (AASHTO 2008). Both the AASHTO 1993 Guide and the mechanistic based design methods use the resilient modulus of each pavement layer in the design process.

Due to the complexity, labor intensiveness, and time consuming in conducting resilient modulus measurements in laboratory, it is necessary to establish a rational approach for estimating the resilient modulus of subgrade materials after compaction. Most of recent research studies were conducted to predict or estimate the subgrade

resilient modulus (Mohammad et al. 1999, Rahim & George 2002, Elias & Titi 2006, Malla & Joshi 2007, El-Badawy et al. 2011, Nazzal & Mohammad 2010). In Florida, several major research projects were conducted to study the resilient modulus characteristics of constructed Florida pavement subgrade soils (Ping & Ge 1997, Ping & Yang 1998, Ping & Yang 2005, Ping et al. 2001, Ping et al. 2002, Ping et al. 2003). Comparative studies were performed to evaluate the resilient modulus from laboratory cyclic triaxial tests and field experimental studies. In view of the complexity and difficulty in conducting the resilient modulus measurement, a resilient modulus database program was developed to catalog available resilient modulus test results and to evaluate the subgrade resilient modulus for facilitating the pavement design. An extended study was also conducted to correlate resilient modulus with basic physical properties of the soil (Ping & Ling 2006).

This paper presents an extensive study performed to evaluate the compacted subgrade resilient modulus from laboratory cyclic triaxial tests. A resilient modulus database was established to develop the resilient modulus correlation models for two types of granular subgrades that are commonly used in Florida: fine sand (A-3 soil) and silty/clayey sand (A-2-4 soil). The experimental program is briefly described as follows.

EXPERIMENTAL PROGRAM

Laboratory experimental program was conducted on selected soils obtained from seven districts of the Florida Department of Transportation (FDOT) around the state. Laboratory resilient modulus tests were conducted on the selected soils using the AASHTO T307-99 test method (AASHTO 2003) and AASHTO T 292-91I test method (AASHTO 1991).

Test materials. Representative soil materials were obtained from the FDOT districts. The soil materials primarily consisted of A-3 soils and A-2-4 soils. A summary of the tested soil materials is presented in Table 1 for information.

Resilient modulus testing program. The AASHTO T307-99 test procedure was adopted for the resilient modulus test program. This test method was considered an improvement to the AASHTO T292-91I and T294-92 test methods (AASHTO 1992). The major components of the testing setup include a closed-loop servo-hydraulic loading system, digital controller, workstation computer, triaxial cell, and linear variable differential transducer (LVDT) deformation measurements system. To obtain more reliable test results, a deviation from the AASHTO T307-99 test procedure was made by using the internally mounted LVDTs for the vertical full-length measurements instead of using the external LVDTs as specified in the standard AASHTO T307-99 test method. The test setup is illustrated in Figure 1.

Table 1. Summary of physical properties of tested soil materials

Soil Sample Number	Max. dry unit weight	Moisture content	CBR*	Percent fines	Plasticity index	Percent clay	Classification	Soil type**
	pcf	%		%		%		
A24-1	120.2	10	113	17.3	NP	12	A-2-4	2
A24-2	128.4	8.6	106	24	5	6	A-2-4	2
A24-3	116.4	13.3	86	20.4	NP	18	A-2-4	2
A24-4	118.2	9.2	66	15.2	NP	4	A-2-4	2
A24-5	110.7	13.3	68	30	NP	6	A-2-4	2
A24-6	113.2	13.2	94	17.9	NP	9	A-2-4	2
A24-7	112.8	12.8	101	12.2	NP	9	A-2-4	2
A3-1	111.2	12	29	6	NP	-	A-3	2
A3-2	105.8	16.3	26	5	NP	3	A-3	2
A3-3	107.9	12.1	28	7.8	NP	-	A-3	2
A3-4	104.9	14.7	22.4	2	NP	2	A-3	2
A3-5	105.1	13.2	14	3.7	NP	-	A-3	2
A3-6	106.1	13.3	14	3.4	NP	0.5	A-3	2
A3-7	108.1	13.2	28	4.1	NP	-	A-3	2
A3-8	115.4	11.5	72	10.3	NP	-	A-3	2
A3-9	118.8	10	68	2.9	NP	-	A-3	1
A3-10	107.7	12.4	19	4.7	NP	3.5	A-3	2
A3-11	104.4	12.6	17	2.2	NP	-	A-3	2

*CBR: the CBR is converted from LBR (Limerock Bearing Ratio). The LBR test is a modified California Bearing Ratio (CBR) test. Numerically, the CBR can be related to the LBR through the formula, $LBR = 1.25 \text{ CBR}$.

**Type 1 soil: All untreated subgrade soils which meet the criteria of less than 70 percent passing the 2.00-mm (No. 10) sieve, and which have plasticity index of 10 or less.

**Type 2 soil: All untreated soils not meeting the criteria for Type 1 soils.

Note: $1.0 \text{ pcf} = 0.16 \text{ kN/m}^3$

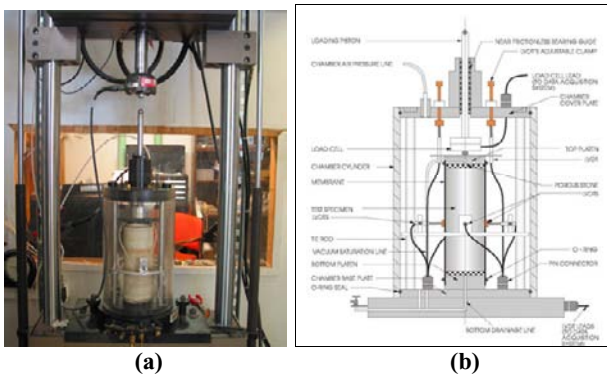


Figure 1. Laboratory Resilient Modulus Measurement:
(a) Test Setup; (b) Schematic of Triaxial Cell

EXPERIMENTAL RESULTS

In actual field conditions, the confining pressure at subgrade layers was found to be approximately 2 psi (13.8 kPa). Therefore, the resilient modulus value at 2 psi (13.8 kPa) confining pressure was selected to represent the resilient modulus of the constructed subgrade material. For each soil, the resilient modulus test results under the condition of optimum moisture content and maximum wet unit weight as specified in the AASHTO T307-99 test procedure were selected and the corresponding resilient modulus values were averaged to represent the average resilient modulus value at its optimum compacted condition. The T307-99 resilient modulus test data and the T292-91I test results were integrated together for further analysis. Two types of soils, namely A-3 and A-2-4, were selected to be representative of the typical subgrade soils in Florida. A summary of the detailed resilient modulus test results may be found elsewhere (Ping & Ling 2006).

DEVELOPMENT OF RESILIENT MODULUS CORRELATION MODELS

In the past, most of the resilient modulus estimation models were developed for fine grain soils. For coarse grain or granular soils, the primary influencing factors are the soil type, the gradation, the percent of fines and clay content, the degree of saturation, the compaction condition, and the confining pressure (Rada & Witczak 1981, Zaman et al. 1994). In this study, eight influencing parameters were available for selection in the resilient modulus database: moisture content, dry unit weight, percent of fines, percent of clay content, CBR, coefficient of curvature (C_C), uniformity coefficient (C_U), and permeability. Statistical methods were employed to perform the multiple regression analysis (McClave & Sincich 2000). The eight parameters were evaluated employing the stepwise multiple regression with the criteria of $\alpha = 0.05$ to obtain a useful subset of the predictors. The regression analyses were performed using the statistical software R (Ugarte et al. 2008) to correlate the soils physical properties with the resilient modulus.

Three stepwise regression models were considered for the A-3 soils, the A-2-4 soils, and the A-3 and A-2-4 soils, respectively. The model variables were selected according to the importance of the influencing parameters as indicated by the stepwise analysis and the experimental results. The logarithm value of the full-length resilient modulus measurements under the stress state of 2 psi (13.8 kPa) confining stress and 6 psi (41.3 kPa) deviator stress was chosen as the model response. The usability of the model was then checked through the analysis of a variance F-test.

Resilient modulus correlation model for A-3 soils. By adding and removing predictors from the stepwise analysis, the final correlation model was obtained based on the coefficient of curvature (C_C), uniformity coefficient (C_U), and permeability (k). The model had an R-squared value of 0.8931 and a p-value of 5.122e-10, and was considered to be a statistically useful model. The selected correlation equation is presented as follows:

$$\ln(Mr) = 4.977 - 0.548C_C + 0.139C_U - 105.05k \quad (1)$$

where Mr = Resilient Modulus in MPa @ 2 psi (13.8 kPa) confining pressure
 C_C = Coefficient of Curvature
 C_U = Uniformity Coefficient
 k = Coefficient of Permeability (cm/s)

Resilient modulus correlation model for A-2-4 soils. Backward stepwise regression analysis was used to study the correlation model for A-2-4 soils. At the end of the stepwise analysis, coefficient of curvature (C_C), uniformity coefficient (C_U), and moisture content were chosen for the regression model since their p-values were all lower than 0.05 criteria. The final regression model resulted in an R-squared value of 0.4573 and a p-value of 5.748e-6. Therefore, it appears that this regression model should be considered as a useful model for the constructed A-2-4 soils. The selected correlation equation is shown as follows:

$$\ln(Mr) = 5.145 - 0.0439C_C + 0.0097C_U - 0.0478MC \quad (2)$$

where Mr = Resilient Modulus in MPa @ 2 psi (13.8 kPa) confining pressure
 C_C = Coefficient of Curvature
 C_U = Uniformity Coefficient
 MC = Gravimetric Moisture Content (%)

Resilient modulus correlation model for A-3 and A-2-4 soils. After a couple of trials, the regression analysis used the predictors from both the A-3 and A-2-4 correlation models. The results showed an R-square value of 0.3726, a p-value of 4.247e-9, and an F-value of 18.03, which is greater than the required F value (2.715) to reject the null hypothesis based on the 0.05 of alpha value. This correlation model was accepted as a suitable one for the constructed A-3 and A-2-4 soils. The correlation equation is shown as follows:

$$\ln(Mr) = 4.945 - 0.0523C_C + 0.0114C_U - 0.0284MC \quad (3)$$

where Mr = Resilient Modulus in MPa @ 2 psi (13.8 kPa) confining pressure
 C_C = Coefficient of Curvature
 C_U = Uniformity Coefficient
 MC = Gravimetric Moisture Content (%)

EVALUATION OF RESILIENT MODULUS CORRELATION MODELS

The proposed correlation models were examined to evaluate the performance. The comparative ratios of the estimated resilient modulus over laboratory measured resilient modulus versus the laboratory measured resilient modulus for the three proposed models were evaluated. It was observed that most values of the comparative ratio were within the range of 0.8 to 1.2, which indicated that the proposed

correlation models would achieve a reasonably estimated resilient modulus value within an error of $\pm 20\%$.

The correlation model for the A-3 soils had a confidence level higher than 90%, while the corresponded R-squared value of this model was 0.89. The data were more scattered for the A-2-4 soils as well as for the A-2-4 and A-3 soils since the R-squared values of these two models were relatively lower than the R-squared values of the A-3 soils model. The reason is that moisture content was chosen as a parameter for the correlation models of A-2-4 soils. The performance of correlation model for the A-3 and A-2-4 soils is shown in Figure 2. In order to achieve a higher confidence level ($>90\%$) for the other correlation models, the estimated resilient modulus value might be adjusted to compensate for the regression error with a 20% reduction from the proposed models.

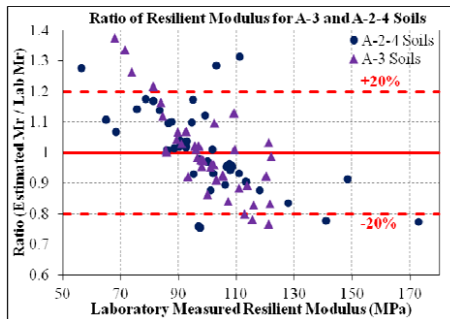


Figure 2. Performance of Correlation Model for A-3 and A-2-4 Soils

CONCLUSIONS

Several major laboratory experimental studies were performed to evaluate the resilient modulus characteristics of two types of commonly available pavement subgrade soils in Florida: fine sand (A-3 soil) and silty/clayey sand (A-2-4 soil). A resilient modulus database was established to catalog the compacted subgrade resilient modulus under different soil physical properties. The resilient modulus test results showed that the soil physical properties, such as moisture content, dry unit weight, and percent of fines, had more significant effects on the resilient modulus of A-2-4 soils than the resilient modulus of A-3 soils.

Based on the resilient modulus database, three resilient modulus correlation models were proposed for the A-3 soils, the A-2-4 soils, and the A-3 and A-2-4 soils, respectively. The correlation model for the A-3 soils showed that the resilient modulus was directly related to the coefficient of curvature, uniformity coefficient, and permeability. The resilient modulus was related to the coefficient of curvature, uniformity coefficient, and moisture content in the correlation model for the A-2-4 soils and the correlation model for the A-3 and A-2-4 soils. The proposed correlation models would achieve a reasonably estimated resilient modulus value within an error of $\pm 20\%$, which provided a rational approach for estimating the resilient modulus of constructed Florida subgrade materials. The regression analyses indicated that a

safety factor should be applied to adjust the estimated resilient modulus for practical applications. A resilient modulus value with 20% lower than the estimated value from the proposed correlation model should be considered for estimating the resilient modulus of constructed subgrade materials for the pavement design applications.

ACKNOWLEDGEMENTS

Funding for this research was provided by the Florida Department of Transportation (FDOT) and Federal Highway Administration (FHWA) through the FDOT Research Center. The strong support from the FDOT managers, Bruce Dietrich, David Horhota, and Emmanuel Uwaibi, are gratefully acknowledged. The opinions, findings, and conclusions expressed in this paper are those of the authors and not necessary those of the sponsors.

REFERENCES

- AASHTO. (1991). *Interim Method of Test for Resilient Modulus of Subgrade Soils and Untreated Base/Subbase Materials*. AASHTO Designation: T292-91I, Washington, D.C.
- AASHTO. (1992). *Standard Method of Test for Resilient Modulus of Unbound Granular Base/Subbase Materials and Subgrade Soil*. SHRP Protocol P46, AASHTO Designation: T294-92, Washington, D.C.
- AASHTO. (1993). *Guide for Design of Pavement Structures*. Volume I & II, Joint Force on Pavements, Highway Sub-committee on Design, Washington D.C.
- AASHTO. (2008). *Mechanistic-Empirical Pavement Design Guide, Interim Edition: A Manual of Practice*. Washington D.C., 2008.
- AASHTO. (2003). *Standard Method of Test for Determining the Resilient Modulus of Soils and Aggregate Materials*. AASHTO Designation: T307-99, Washington D.C.
- El-Badawy, S. M., Bayomy, F. M., and Miller, S. M. (2011). “**Prediction of the Subgrade Resilient Modulus for the Implementation of the MEPDG in Idaho.**” *Geo-Frontiers 2011: Advances in Geotechnical Engineering – Proceedings of the Geo-Frontiers 2011 Conference, Geotechnical Special Publication, No. 211 GSP, 4762-4772*.
- Elias, M. B., and Titi, H. H. (2006). “Evaluation of Resilient Modulus Model Parameters for Mechanistic-Empirical Pavement Design.” *Transportation Research Record: Journal of the Transportation Research Board*, No. 1967, Transportation Research Board of the National Academies, Washington, D.C., 89-100.
- Malla, R. B., and Joshi, S. (2007). “Resilient Modulus Prediction Models Based on Analysis of LTPP Data for Subgrade Soils and Experimental Verification.” *Journal of Transportation Engineering*, ASCE, 133(9), 491-504.
- McClave, J. T., and Sincich, T. (2000). *Statistics*, Eighth Edition. Prentice-Hall Inc., Upper Saddle River, NJ.
- Mohammad, L. N., and Huang, B., Puppala, A. J., and Allen, A. (1999). “Regression Model for Resilient Modulus for Subgrade Soils.” *Transportation Research*

- Record: Journal of the Transportation Research Board*, No. 1687, Transportation Research Board of the National Academies, Washington, D.C., 47-54.
- Nazzal, M. D., and Mohammad, L. N. (2010). "Estimation of Resilient Modulus of Subgrade Soils Using Falling Weight Deflectometer." *Transportation Research Record: Journal of the Transportation Research Board*, No. 2186, Washington, D.C., 1-10.
- Ping, W. V., and Ge, L. (1997). "Field Verification of Laboratory Resilient Modulus Measurements on Subgrade Soils." *Transportation Research Record: Journal of the Transportation Research Board*, No. 1577, Transportation Research Board of the National Academies, Washington, D.C., 53-61.
- Ping, W. V., and Yang, Z. (1998). "Experimental Verification of Resilient Deformation for Granular Subgrades." *Transportation Research Record: Journal of the transportation Research Board*, No. 1639, Transportation Research Board of the National Academies, Washington, D.C., 12-22.
- Ping, W. V., Yang, Z., Liu, C., and Dietrich, B. (2001). "Measuring Resilient Modulus of Granular Materials in Flexible Pavements." *Transportation Research Record: Journal of the Transportation Research Board*, No. 1778, Transportation Research Board of the National Academies, Washington, D.C., 81-90.
- Ping, W. V., Yang, Z., and Gao, Z. (2002). "Field and Laboratory Determination of Granular Subgrade Moduli." *Journal of Performance of Constructed Facilities*, ASCE, 16(4), 149-159.
- Ping, W. V., Xiong, W., and Gao, Z. (2003). *Implementing Resilient Modulus Test for Design of Pavement Structures in Florida*. Research Report FL/DOT/RMC/BC-352-6(F), Florida Department of Transportation, Tallahassee, FL.
- Ping, W. V., and Yang, Z. (2005). *Development of an Automated Procedure for Implementing Resilient Modulus Test for Design of pavement Structures in Florida*. Research Report FL/DOT/RMC/BC-352-11, Florida Department of Transportation, Tallahassee, FL.
- Ping, W. V., and Ling, C. (2006). *Enhancement of Resilient Modulus Data for Design of Pavement Structures in Florida*. Research Report FL/DOT/RMC/BD-543-4, Florida Department of Transportation, Tallahassee, FL.
- Rada, C., and Witzcak, W. M. (1981). "Comprehensive Evaluation of Laboratory Resilient Moduli Results for Granular Material." *Transportation Research Record: Journal of the Transportation Research Board*, No. 810, Transportation Research Board of the National Academies, Washington, D.C.
- Rahim, A. M., and George, K. P. (2002). "Automated Dynamic Cone Penetrometer for Subgrade Resilient Modulus Characterization." *Transportation Research Record: Journal of the Transportation Research Board*, No. 1806, Transportation Research Board of the National Academies, Washington, D.C., 70-77.
- Ugarte, M. D., Militino, A. F., and Arnholt, A. T. (2008). *Probability and Statistics with R*. Chapman & Hall, Boca Raton, FL.
- Zaman, M. M., Chen, D. H., and Laguros, J. G. (1994). "Resilient Moduli of Granular Materials." *Journal of Transportation Engineering*, ASCE, 120(6), 967-988.

The Effect of Groundwater Base Clearance on Constructability of Florida Pavements

W. Virgil Ping¹, M.ASCE, and Biqing Sheng²

¹ Professor, Department of Civil and Environmental Engineering, FAM-FSU College of Engineering, Florida State University, 2525 Pottsdamer Street, Tallahassee, FL 32310, USA; PH (850) 410-6129; FAX (850) 410-6142; email: ping@eng.fsu.edu

² Research Associate, Department of Civil and Environmental Engineering, FAM-FSU College of Engineering, Florida State University, 2525 Pottsdamer Street, Tallahassee, FL 32310, USA; PH (850) 410-6217; FAX (850) 410-6142; email: shengbi@eng.fsu.edu

ABSTRACT

In highway construction, loose roadbed and subgrade soils must be compacted to improve their strength characteristics for the long-term pavement performance. Groundwater base clearance, which is defined as the clearance between the groundwater level and pavement base layer within a pavement system, becomes an important factor during the pavement construction. When an adequate groundwater base clearance is not provided, difficulties in constructing the pavement sublayers are often encountered. This paper presents an experimental study of the constructability of compacting pavement sublayer under various levels of groundwater base clearance. A full-scale test-pit program and a field experimental program were conducted to evaluate the constructability of pavement compaction in Florida. Both static and dynamic compaction methods were evaluated. The experimental results indicated that constructability of the granular pavement sublayer was not a problem where the groundwater base clearance was at least about 2 – 3 feet (0.60 - 0.91 m). To ensure constructability, a minimum of 3-foot (0.91 m) groundwater base clearance would be suggested for the pavement design and construction.

INTRODUCTION

Constructability, which is defined as the optimum use of construction knowledge and experience in planning, design, procurement, and field operations to achieve the overall project objectives, has been widely used as a design consideration in highway construction projects (CII 1986). In highway construction, loose roadbed and subgrade soils must be compacted to increase the strength characteristics of soils, thereby increasing the bearing capacity of the pavement constructed above them. Compaction also decreases the undesirable settlement of pavement structure and increase the stability of embankment slopes. However, roadway grades sometimes do not allow for much groundwater base clearance between the groundwater level and pavement base layer within a pavement system due to various reasons. Most past researches (Barber and Sawyer 1952, Cedergren 1974, Moulton, 1980, Ridgeway

1982) have focused on the needed clearance between the base and the groundwater table to ensure long-term performance of the pavement section. When an adequate separation is not provided between the compacted sublayer and the groundwater table, difficulties in constructing the pavement sublayer are often encountered (Ping et al. 2005). Furthermore, the high groundwater table will also reduce the resilient modulus characteristics of the subgrade soils (Ping et al. 2008, Ping et al. 2010). These constructability problems are sometimes so severe, work must be stopped and the project redesigned during construction. In addition, the constructability problems usually result in large claims and delays in highway construction projects.

This paper presents an experimental study to evaluate the constructability of the pavement sublayer for different types of soil material under various levels of groundwater base clearance according to construction specifications. A full-scale laboratory experimental program and a field experimental program were conducted to evaluate the constructability of the pavement sublayer in Florida. Two large test pits were set up in the laboratory to simulate the field conditions of compacting pavement sublayer under high levels of groundwater table. A field test site was also selected to evaluate the constructability problems under actual field conditions. The laboratory and field experimental programs are described as follows.

LABORATORY EXPERIMENTAL PROGRAM

Test-Pit System. A full-scale laboratory experimental program was initiated to evaluate the constructability of subbase (stabilized subgrade) layers in two large test pits. The test pit is a controlled environment structure where soil or recycled materials can be constructed as a model pavement and evaluated. The test pit is a 7.31 m (24 ft.) by 2.74 m (9 ft.) by 2.13 m (7 ft.) deep reinforced concrete structure that is surrounded by a sump with an interconnecting channel system for controlling the water table (Figure 1a). The materials in the test pit are consisted of four layers. The bottom layer is composed of a bed of 0.23 m (9 in.) river gravel layer. A builder's sand layer with depth of 0.23 m (9 in.) is set upon the river gravel and separated by a permeable filter fabric. Both layers are composed of well absorbent materials and located on the interconnecting water channel system to facilitate the upward percolation of groundwater. For this study, a 0.9 m (36 in.) subgrade (embankment) layer was placed in 0.3 m (12 in.) lifts on the builder's sand layer and compacted to 100% of the maximum standard Proctor density. On top of the subgrade (embankment) soil was the 0.3 m (12 in.) subbase (stabilized subgrade) layer for evaluation (Figure 1b).

Test Materials. The materials under evaluation in this research study are listed in Table 1. The tested soils were selected and believed to represent the most commonly used pavement materials as subbase (stabilized subgrade) and subgrade (embankment) materials in Florida.

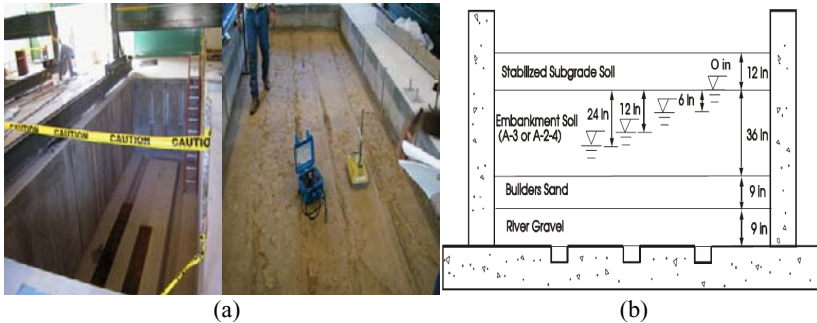


Figure 1. The Test-Pit System: (a) Overview of Test Pit; (b) Schematic Diagram of Test Pit.

Table 1. Engineering Properties of Tested Soil Materials

	Soil Type	Percent Passing No. 200 Sieve (%)	Standard Proctor Density (pcf*)	Maximum Dry Density (pcf)	Optimum Moisture Content (%)	LBR**
Embankment Soils	A-2-4	12	108.8	-	12.2	-
	A-3	5	110.8	-	10.9	-
Stabilized Subgrade Soils	A-2-4	12	-	110.2	12.7	44
	A-3	12	-	110.8	12.5	39

* 1 pcf = 0.1571 kN/m³

** LBR: Limerock Bearing Ratio = 1.25 × CBR (California Bearing Ratio)

Water Levels. Five different water level conditions were used for this study. For the first three water level conditions, the water levels were raised to 0.6 m (24 in.), 0.3 m (12 in.), and 0.15 m (6 in.) below the interface of the embankment (subgrade) layer and the stabilized subgrade (subbase) layer. For the fourth water level condition, the water level was first raised to top of the embankment (subgrade) material. Then, the water level was drained down to 0.15 m (6 in.) below the top of the embankment (subgrade) material. For the fifth water level condition, the water level was further drained down to 0.3 m (12 in.) below the top of the embankment (subgrade).

Compaction Techniques. The tested subgrade soils were compacted by two types of compactors, i.e., static and dynamic compactors, to simulate the field compactive efforts. The main characteristics of the compactors used in the test pit are summarized in Table 2. The compactive energy was represented by “cover”, which meant the compactor was moved back and forth on the subgrade soil for a complete cover. The dry unit weight (density) of the compacted subgrade soil was measured by the nuclear gauge method. The desired dry densities for the subgrade soils were 98% of the maximum modified Proctor density (FDOT 1999).

Experimental Procedure. Two embankment (subgrade) soils, an A-3 soil and an A-2-4 soil were separately placed and compacted at three 0.3 m (12 in.) lifts in the two

test pits. Each lift was compacted to 100% of the maximum dry density as determined by the standard Proctor test. The second stage of the experimental program involved the water table adjustment and monitoring of the capillary action taking place in the embankment soils. After the water table in the test pits was set to one of the five desired levels, the capillary rise was monitored in the embankment soils. The subgrade soils were placed and compacted after the capillary rise action in the embankment soils had been stabilized. The third stage of the test involved compaction of the subgrade soils. The compactive energy was measured simply by the “covers”. After the subgrade soils were compacted for a certain number of covers, the wet density and moisture content of the subgrade soils were measured to check the results. The compaction would come to a halt when the desired density was achieved. Depending on the test results, a decision could be made when the required density could not be achieved under the circumstance. For each of the five desired water level conditions, the subgrade soil was excavated after the third stage of the test. A new subgrade soil was subsequently placed after the water table adjustment and stabilization to start another cycle of the compaction test.

Table 2. Compactors Used in the Test Pit Program

Type	Brand	Model	Comp. Depth (in)	Oper. Size (in)	Oper. Weight (lbs)	Center Force (lbs)
Vibratory Plate	Wacker	BPU 3345A	-28	35 x 23.6	636	7,550
Vibratory Sheepsfoot	Rammer	P33 HMR	N/A	33 (Drum)	3,175	15,975
Vibratory	Gardener	Plus 716	-8	4.0 x 8.0 (tire)	139	N/A
Static Smooth Drum	Wacker	RD880	N/A	36 (Drum)	2,430	3,000

FIELD EXPERIMENTAL PROGRAM

A field site was selected, and field tests were carried out to simulate full-size-field compaction and to verify the laboratory constructability experimental results. The selection of the field test site took into considerations of the availability of a high groundwater table, the type of embankment and stabilized subgrade materials, and the accessibility for field operations.

The field test took place at Lake Worth site in West Palm Beach, Florida (Figure 2). The groundwater level was at 1.5 m (5 ft.) below the ground surface and at 0.3 m (12 in.) below the embankment surface after excavation (Figure 2). The embankment material was an A-3 soil with a wet unit weight of 124.9 pcf and in-situ moisture content 14.5% prior to the testing. The test bed was very firm with no problem of carrying a heavy field compactor. An A-3 material was also used for the stabilized subgrade layer. The modified Proctor maximum dry unit weight of the A-3 subgrade was 113 pcf. The modified optimum moisture content was 8.7%, and the LBR was 53. A BOMAG BM-213D-3 vibratory compactor (with an operating weight of 16,850 lbs.) was used for the field compaction. The field test program was conducted in the following sequence:

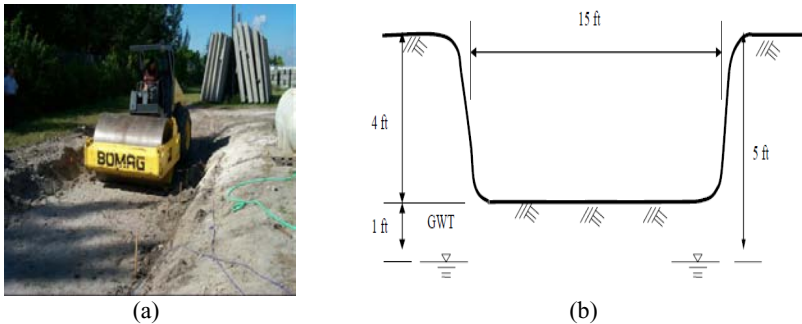


Figure 2. Field Test System: (a) Overview of Field Test; (b) Schematic Sketch of Field Test

- Case 1: Groundwater level at 0.3 m (12 in.) below the top of the embankment
 Case 2: Groundwater level at 0.45 m (18 in.) below the top of the embankment
 Case 3: Groundwater level at 0.15 m (6 in.) below the top of the embankment
 Case 4: Groundwater level at 0.3 m (12 in.) below the top of the embankment
 Case 5: Groundwater level at 0 m (0 in.) below the top of the embankment

EXPERIMENTAL RESULTS

Laboratory Experimental Results. The laboratory experimental results were presented and analyzed to evaluate the constructability of stabilized subgrade layers under high water levels in the test pit. The relationship between the degree of compaction, i.e., the measured dry density divided by the maximum dry density determined from modified Proctor test, and the number of compaction covers could be interpreted to evaluate whether the desired 98% degree of compaction had been achieved after a sufficient number of compaction covers. The experimental test results are summarized according to the five different levels of high water table in Table 3.

Field Experimental Results. The field test was used to calibrate or check the laboratory compaction results. Various water level conditions were simulated under field compaction including the groundwater levels at 18 in. (0.45 m), 12 in. (0.3 m), 6 in. (0.15 m), and 0 in. (0 m) below the top of embankment layer. Although the drawdown condition was simulated based on the laboratory results, the drawdown condition was not evaluated in the field due to physical limitations. The field test was limited to one type of A-3 soil. The field test results were summarized in Table 4.

Table 3. Summary of Laboratory Test-Pit Test Results

Condition	Groundwater level (below the top of Embankment Layer)	Soil Type		Be able to reach 98% degree of compaction
		Embank- ment	Subgrade	
1	24 in.	A-3	A-2-4	Yes
1	24 in.	A-3	A-2-4 + Limerock	Yes
1	24 in.	A-2-4	A-2-4	Yes
1	24 in.	A-2-4	A-2-4 + Limerock	Yes
2	12 in.	A-3	A-2-4	Yes
2	12 in.	A-3	A-2-4 + Limerock	Yes
2	12 in.	A-2-4	A-2-4	Yes
2	12 in.	A-2-4	A-2-4 + Limerock	Yes
3	6 in.	A-3	A-2-4	Yes
3	6 in.	A-3	A-2-4 + Limerock	Yes
3	6 in.	A-2-4	A-2-4	Yes
3	6 in.	A-2-4	A-2-4 + Limerock	Yes
4	6 in. (Drained)	A-3	A-2-4	No
4	6 in. (Drained)	A-3	A-2-4 + Limerock	No
5	12 in. (Drained)	A-3	A-2-4	Yes
5	12 in. (Drained)	A-3	A-2-4 + Limerock	Yes

Table 4. Summary of Field Compaction Test Results

Groundwater level (below the bottom of loose material)	Thickness of Stabilized Subgrade	Thickness of loose A-3 material	Be able to reach to 98% degree of compaction
18 in.	6 in.	16 in.	Yes
12 in.	0 in.	16 in.	Yes
6 in.	0 in.	16 in.	No
18 in.	12 in.	6 in.	No
0 in.	0 in.	15 in.	No

ANALYSIS OF EXPERIMENTAL RESULTS

Based on the test-pit experimental results, both the A-3 and A-2-4 embankment soils were shown to have very similar performance. According to the test results shown in Table 3, water level Condition 1, which is a commonly used clearance by designers, was only studied in the test-pit program. Proper compaction could be achieved under this water condition for both subgrade soils and on both embankment soils. The water level at 0.3 m (12 in.) below the top of embankment layer was studied in Condition 2 (undrained) and Condition 5 (drained). Under Condition 2, adequate compaction was obtained for both subgrade soils on both A-3 and A-2-4 embankment soils. Only A-3 embankment soils were evaluated for Condition 5. It was shown that adequate compaction was obtained for both subgrade soils. The water level at 0.15 m (6 in.) below the top of embankment layer was evaluated in Condition 3 (undrained) and Condition 4 (drained). It was found that adequate compaction was only obtained for the undrained condition. Based on the test-pit results, the groundwater level should not be less than 0.3 m (12 in.) below the top of embankment layer to ensure a proper compaction of subgrade layers. In case of a drained or drawdown condition under construction, the groundwater table should be

lowered to a level of at least 0.3 m (12 in.) below the top of the interface for facilitating the compaction of subgrade layers.

According to the field experimental results presented in Table 4, the A-3 subgrade soil could be constructed according to the specifications under the water level conditions at least 18 in. (0.45 m) below the top of embankment layer. Under this condition, the desired 98% degree of compaction was achieved using either the static or the vibratory compaction. When the groundwater level was raised to 12 in. (0.3 m) below the top of embankment, the desired 98% degree of compaction could not be achieved using the vibratory compaction, although using the static compaction was adequate to achieve the desired compaction. When the groundwater level was further raised to 6 in. (0.15 m) below the top of embankment, either the static or the vibratory compaction could not achieve the desired 98% degree of compaction. Adequate compaction was not possible for the groundwater level right at the surface of the embankment. Following the field experimental results, the groundwater level should not be less than 12 in. (0.3 m) below the top of embankment layer to ensure a good constructability of stabilized subgrade layers. In case of a drawdown condition in the field, the groundwater table should be lowered to a level of at least 18 in. (0.45 m) below the top of the embankment to facilitate an adequate compaction of stabilized subgrade layers.

The laboratory test-pit test results were validated by field compaction test results. The in-situ moisture content of subgrade soil was critical to successful compaction and to achieve the specified density. Both the test-pit test results and the field results showed that water level at 0.3 m (12 in.) below the top of embankment layer was the critical water table level to obtain the desired degree of compaction, while only static compaction was adequate for field test. In case of a drained condition, the groundwater level should be lowered to at least 0.45 m (18 in.) below the top of embankment layer. Therefore, a water level at 0.45 m (18 in.) to 0.6 m (24 in.) below the top of embankment layer, which means 0.75 m to 0.90 m base clearance when 0.3 m stabilized subgrade is used, would be an optimum level to ensure the constructability for the highway construction.

CONCLUSIONS

A full-scale laboratory test-pit experimental program and a field experimental program were carried out to evaluate the effect of groundwater base clearance on the constructability of stabilized subgrade (subbase) layer. It was found that the in-situ moisture content of the subgrade soils was critical to successful compaction and to achieve the specified density. The A-3 and A-2-4 soils showed similar performances as an embankment (roadbed) soil based on the test-pit experimental results. The groundwater level should not be less than 0.3 m (12 in.) below the top of embankment layer to ensure a proper compaction of stabilized subgrade layers. Field test results showed that constructability of the subgrade soils was not a problem by either static or dynamic compaction when the groundwater table was about 18 in. (0.45 m) below the top of embankment layer. When the groundwater level was 12 in. (0.3 m) below the top of embankment layer, only the static compaction could be used to reach the desired 98% degree of compaction. Furthermore, Static compaction was

more effective for compacting subgrade layers under high groundwater condition. In case of a drained or drawdown condition under construction, the groundwater table should be lowered to a level of at least 0.6 m (24 in.) below the top of embankment layer for facilitating the compaction of subgrade layers. To optimize the performance of pavement subbase, it is suggested that 3 ft. (0.9 m) groundwater base clearance is used to improve the constructability of stabilized subgrade layer in Florida.

ACKNOWLEDGEMENTS

Funding for this research was provided by the Florida Department of Transportation (FDOT) and Federal Highway Administration (FHWA) through the FDOT Research Center. The strong support from the FDOT managers, Bruce Dietrich, David Horhota, and Emmanuel Uwaibi, are gratefully acknowledged. The opinions, findings, and conclusions expressed in this paper are those of the authors and not necessary those of the sponsors.

REFERENCES

- Barber, E. S., and Sawyer, C. L. (1952). "Highway Subdrainage." *Highway Research Board Proceedings*, 642-666.
- Cedergren, H. R. (1974) *Drainage of Highway and Airfield Pavements*. John Wiley & Sons, New York.
- Construction Industry Institute (CII). (1986) *Constructability: A Primer*. Publication 3-1. University of Texas at Austin, Austin, TX.
- Florida Department of Transportation (FDOT). (1999). *Standard Specifications for Road and Bridge Construction*, Tallahassee, Florida.
- Moulton, L. K. (1980) *Highway Subdrainage Design*. Report No. FHWA-TS-80-224. Federal Highway Administration.
- Ping, W. V., Lan, J., and Yang, Z. (2005) *Constructability of Stabilized Subgrade Layer under High Groundwater Table*. Publication FDOT BC-352-7, Florida Department of Transportation, Tallahassee, FL.
- Ping, W. V., Ling, C. C., Zhang, C., Liu, H., and Lan, J. (2008) *Design Highwater Clearances for Highway Pavements*. Publication FDOT BD-543-13, Florida Department of Transportation, Tallahassee, FL.
- Ping, W. V., Sheng, B., Ling, C. C., Dietrich, B., and Horhota, D. (2010). "Influence of Base Clearance on Subgrade Resilient Modulus of Florida Roadway Pavements." *Transportation Research Record*, No. 2154, 176-186.
- Ridgeway, H. H. *Pavement Subsurface Drainage Systems*. Synthesis of Highway Practice 96, Transportation Research Board, Washington, D.C.

Effect of Polymer Binder Content on Fracture Mechanics Properties of Hot Mix Asphalt Concrete

W. Virgil Ping¹, M.ASCE, and Yuan Xiao²

¹Professor, Department of Civil and Environmental Engineering, FAM-FSU College of Engineering, Florida State University, 2525 Pottsdamer Street, Tallahassee, FL 32310, USA; PH 1-850-410-6129, FAX 1-850-410-6142; e-mail: ping@eng.fsu.edu

²Former Graduate Research Assistant, Department of Civil and Environmental Engineering, FAM-FSU College of Engineering, Florida State University, 2525 Pottsdamer Street, Tallahassee, FL 32310, USA; e-mail: xiaoyu@eng.fsu.edu

ABSTRACT

Asphalt binder is one of the key factors that influence the engineering properties of hot mix asphalt (HMA) concrete. Many research studies suggest that the Styrene-Butadiene-Styrene (SBS) polymer is a promising modifier to improve the asphalt binder, and hence benefit the HMA viscoelastic properties. The specific beneficial characteristics and appropriate polymer concentration need to be evaluated. This paper presents an experimental program based on the fracture mechanics framework to evaluate the effect of SBS polymer-modified binder concentration on engineering properties of HMA concrete mixtures. Two standard Superpave control mixes with the base asphalt (PG 67-22) which is commonly used in Florida were selected. Each control mix design was modified to three SBS polymer content levels (3.0%, 4.5%, and 6.0%). Three types of Indirect Diametral Tension (IDT) test, i.e., the resilient modulus test, the creep compliance test, and the tensile strength test, were performed to determine the fracture mechanics properties of polymer-modified asphalt (PMA) specimens at three temperature levels: -10, 5, and 25°C (14, 41, and 77°F). The test results indicated that the SBS polymer-modified asphalt binder improved the fracture mechanics behavior of asphalt mixtures comprehensively. Excessive amount of polymer content might improve the stiffness, creep, and failure strain properties at low temperatures; however, its effect on the PMA resilient modulus at high temperatures is not always favorable.

INTRODUCTION

Over the past 20 years in the United States, efforts dedicated to the research and application of asphalt modifiers have greatly increased due to the fact that many regular asphalt binders are not qualified for the design requirements that exist in areas with extreme climate conditions. Many state highway agencies in the US use styrene-butadiene-styrene (SBS) polymer-modified asphalt binders in the HMA mixtures in an effort to enhance the engineering properties of asphalt concrete mixtures. Recent research studies have attempted to establish a relationship between the SBS polymer concentration and the chemical and mechanical characteristics of asphalt binders (Bahia et al., 1995; Chen et al., 2002). More research studies were performed to investigate the relationship between the SBS polymer content and polymer-modified HMA mechanical properties (King et al., 1993; Lundstrom and Isacson, 2004). The

findings implied that the effects of polymer modifier concentration on HMA are complex depending on the specific composition of the blend.

Asphalt binders modified with about 3% SBS polymer have been used by many state agencies as an effective way of treating the Superpave mixtures. Earlier research studies showed that modifiers with high percentage of SBS polymer may cause phase separation between base asphalt binder and polymer (Lu et al., 1999). It would be advisable to evaluate the performance of actual HMA mixtures produced with modified asphalt binder. The fracture mechanics approach has been proposed and studied extensively (Roque et al., 2002 & 2004). It has been verified by some field sections and cores related to the top-down cracking mode of failure in Florida. The fracture mechanics framework appeared to be capable of distinguishing the performance of HMA pavement structures and thus was adopted as a basis to evaluate the engineering properties of polymer-modified HMA mixtures in this study.

The objective of this paper is to present and discuss the results of experiments conducted in laboratory using the three Superpave indirect diametral tension (IDT) tests on selected asphalt concrete mixtures with different levels of SBS polymer content. The effect of SBS polymer-modified binder on the engineering properties of HMA mixtures is evaluated by analyzing the fracture mechanics properties obtained from the tests. The experimental program involved two standard mix designs (a granite mix and a limestone mix) as control mixes. Each of the two Superpave control mixes was modified using three levels of SBS polymer-modified asphalt (PMA). All specimens were prepared at targeted optimum air voids of 4%. The laboratory experimental program is described as follows.

EXPERIMENTAL PROGRAM

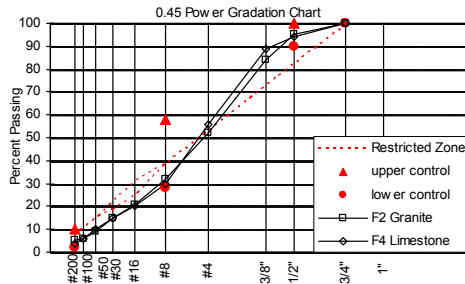
Test Material and Mix Design. One Georgia granite mix (SP 04-3034A, TL-D, Ga553), referred to as “F2C,” and one South Florida limestone mix (LD 02-2529A, TL-D, SFL), designated as “F4C,” were selected as the control mixes for the tests. The two Superpave mix designs are commonly used in Florida and were known to perform well in the field. The unmodified asphalt PG 67-22 (AC-30) was selected as the base asphalt. Three levels of SBS polymer-modified asphalt (PMA) at 3.0%, 4.5%, and 6.0% were produced and used in the SBS effects study. The mixtures are listed in Table 1 and the aggregate gradations for granite mixes and limestone mixes are displayed in Figure 1. Table 2 presents a summary of the volumetric properties of all mixtures, where G_{mm} is maximum specific gravity, G_{mb} is bulk specific gravity, and $VTM(V_a)$ is air voids.

Table 1. Summary of Mixtures and SBS Polymer Modifications

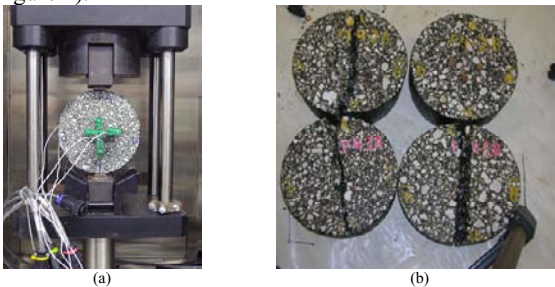
Control Mixes	F2C (Ga553)			F4C (SFL)		
Base Asphalt	PG 67-22			PG 67-22		
PMA Mixes	F2P1	F2P2	F2P3	F4P1	F4P2	F4P3
SBS Polymer Content	3.0%	4.5%	6.0%	3.0%	4.5%	6.0%

Table 2. Volumetric Properties of Test Mixtures

Mix	F2C	F2P1	F2P2	F2P3	F4C	F4P1	F4P2	F4P3
G_{mm}	2.589	2.573	2.573	2.573	2.253	2.253	2.253	2.253
G_{mb}	2.479	2.472	2.463	2.479	2.173	2.179	2.130	2.187
VTM (V_a)	4.3%	3.9%	4.3%	3.7%	3.5%	3.3%	5.4%	3.0%

**Figure 1. Gradation Curves for F2 and F4 Mixtures**

Specimen Preparation. The specimen preparation for the IDT tests was based on the findings from the NCHRP Project 1-28A, “Harmonized Test Methods for Laboratory Determination of Resilient Modulus for Flexible Pavement Design”. The resilient modulus test, the creep compliance test, and the tensile strength test were all performed on the 150 mm (5.9 in) in diameter by 63 mm (2.5 in) in thickness test specimens (Figure 2).

**Figure 2. (a) Indirect Diametral Tension Test Setup, and (b) Specimen Fails After Tensile Strength Test**

Fracture Mechanics Test Procedures. The fracture mechanics framework consists of three tests based on the Superpave indirect diametral tension (IDT) test (Roque et al., 1997): the resilient modulus test, creep compliance test, and tensile strength test. Typically, the IDT resilient modulus test is defined as a repetitive 0.1-second haversine load followed by a 0.9-second rest period, continued at 1 Hz intervals, along the vertical diametral plane of a cylindrical specimen of the asphalt concrete mixture [Figure 2(a)]. The creep compliance is determined by applying a static compressive load of fixed magnitude along the diametral axis of a cylindrical specimen. The resulting horizontal and vertical deformations measured near the

center of the specimen are used to calculate tensile creep compliance as a function of time. The tensile strength is determined by loading the specimen along its diametral axis at a fixed deformation rate until failure occurs [Figure 2(b)]. The concepts of dissipated creep strain energy (DCSE) threshold and fracture energy (FE) threshold were introduced as the key elements in defining the cracking mechanism of HMA concrete, which can be used to evaluate fracture characteristics of pavement structure. The work that led to the development of the HMA fracture mechanics framework was based solely on Superpave IDT test results (Roque et al., 2002 & 2004). For each mixture, eight IDT specimens were produced. At least three specimens were tested to determine the average resilient modulus and creep compliance values and two specimens were tested for determining the tensile strength of each mixture. The aforementioned test procedures were followed for conducting the three IDT tests of this study. The tests were performed at temperatures of -10, 5, and 25°C. The resilient modulus and creep compliance tests began with the lowest temperature and proceeded to the highest.

EXPERIMENTAL RESULTS

Resilient Modulus Test Results. The measurement and analysis procedures developed by Roque et al. (1997) were used for the IDT data reduction. This method modified the LVDT mounting system and took the specimen bulging effect into account through three-dimensional finite element analysis. A series of correction factors were developed to adjust stresses and deformations obtained with the modified measurement system. The resilient modulus and Poisson's ratio are calculated using the following equations:

$$M_R = \frac{P \times GL}{\Delta H \times t \times D \times C_{C MPL}} \quad C_{C MPL} = 0.6354 \times (X/Y)^{-1} - 0.332$$

$$\nu = -0.1 + 1.480 \times (X/Y)^2 - 0.778 \times (t/D)^2 \times (X/Y)^2$$

Where M_R =Resilient Modulus, P =Maximum Load, GL =Gage Length, ΔH =Horizontal Deformation, t =Thickness, D =Diameter, $C_{C MPL}$ =Non-dimensional Factor, ν =Poisson's Ratio, and (X/Y) =Ratio of Horizontal to Vertical Deformation. The average resilient modulus values and Poisson's ratios are summarized in Table 3.

Table 3. Summary of Resilient Modulus Test Results

Mixture	M_R (GPa) at Temperature Level			Poisson's Ratio		
	-10°C	5°C	25°C	-10°C	5°C	25°C
F2C	28.15	18.25	5.53	0.35	0.36	0.44
F2P1	26.61	18.86	5.24	0.33	0.34	0.37
F2P2	24.49	16.39	4.29	0.35	0.35	0.31
F2P3	22.45	13.57	3.06	0.31	0.29	0.29
F4C	20.61	12.90	4.22	0.35	0.32	0.45
F4P1	18.91	11.98	3.78	0.27	0.36	0.35
F4P2	16.14	10.57	4.04	0.26	0.27	0.39
F4P3	14.01	7.26	1.99	0.33	0.39	0.30

Figures 3(a) and 3(b) show comparisons of resilient modulus values at various temperature levels for the SBS polymer-modified asphalt mixes of the F2 and F4

series, respectively. The resilient modulus values of PMA mixtures are less than those of control mixtures and an increment of SBS polymer content lowers the resilient modulus magnitude. The only exception is that the M_R of F2P1 at 5°C is a little higher than the F2 control. In general the PMA mixtures tend to keep the same stiffness levels as the mixtures with base asphalt, and an optimum SBS content may exist within the 3% to 6% range depending on the practical mixing and distribution conditions of materials.

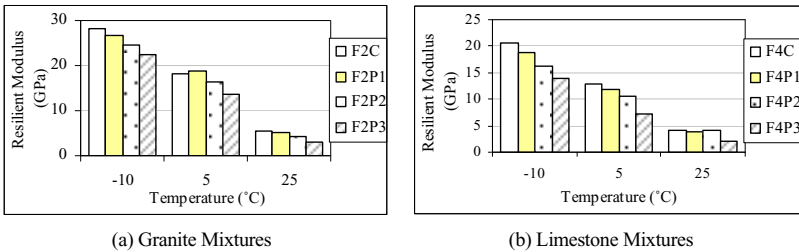


Figure 3. Comparison of Resilient Modulus Values

Creep Compliance Test Results. Creep compliance is a function of time-dependent strain (ϵ_t) divided by constraint stress (σ). Once the resilient modulus test was completed, the creep test was conducted by applying a static load on the specimen for 100 seconds. Similar to the M_R test, the horizontal strain was limited from 150 to 300 micro-strains at 100 seconds to avoid excessive permanent deformation. The creep compliance is calculated by:

$$D(t) = \frac{\Delta H \times t \times D \times C_{CAPL}}{P \times GL}$$

where $D(t)$ is the creep compliance at time t with a unit of 1/GPa, other parameters are the same as defined in the resilient modulus equations. The creep compliance test results were analyzed using the power law relationship presented by Roque et al. (1997) since it was shown that the parameters obtained from this model are fairly accurate indicators for the viscous response and rutting performance of HMA mixtures: $D(t) = D_0 + D_1 t^m$. Table 4 shows the regression coefficients D_1 and m for all mixes. The creep compliance master curves are shown in Figure 4 and 5.

Table 4. Regression Coefficients of Creep Compliance Power Model

	F2C	F2P1	F2P2	F2P3	F4C	F4P1	F4P2	F4P3
D_1 (1/GPa)	0.012	0.011	0.014	0.034	0.013	0.016	0.015	0.017
M	0.360	0.413	0.365	0.279	0.369	0.353	0.365	0.318

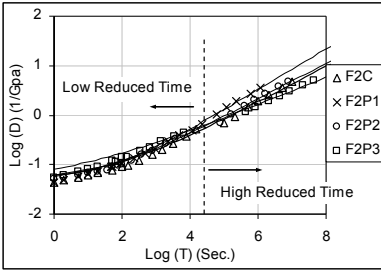


Figure 4. Creep Compliance Master Curves for Granite Mixtures

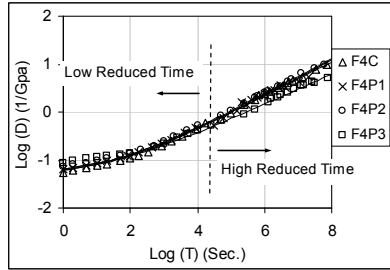


Figure 5. Creep Compliance Master Curves for Limestone Mixtures

As demonstrated in the figures, at low reduced time of about 0 to 104.4 seconds, the PMA mixtures are all more compliant than the control mixes. This means that the polymer modifier makes the HMA more ductile at low temperatures which would be beneficial to the reduction of thermal cracking. At high reduced time, the master curves come across each other and the PMA mixture master curves tend to go below the control ones, indicating that the PMA mixes are stiffer and more resistant to rutting at high temperatures.

Tensile Strength Test Results. The tensile strength test is a destructive test. The tensile strength test and the M_R test were used to determine asphalt mixture fracture mechanics properties which included the tensile strength (St or TS), fracture energy (FE), elastic energy (EE), dissipated creep strain energy (DCSE), and failure strain (FS). The procedures used to calculate these limits are presented in the following equations (Roque et al., 1997):

$$S_t = \frac{2P(C_{SX})}{\pi \cdot t \cdot D} = \frac{2P \cdot (0.948 - 0.01114 \cdot (t/D) - 0.2693 \cdot \nu + 1.436 \cdot (t/D) \cdot \nu)}{\pi \cdot t \cdot D}$$

$$FE = \int_0^{S_t} \sigma \cdot d\varepsilon \quad EE = \frac{1}{2} \cdot \varepsilon_{EE} \cdot S_t = \frac{(S_t)^2}{2 \cdot M_R} \quad DCSE = FE - EE$$

where C_{SX} is the stress correction factor. All fracture mechanics parameters obtained from the tensile strength test were calculated and summarized in Table 5.

Table 5. Tensile Strength Test Results and Fracture Mechanics Parameters

Temp. (°C)	F2 Control			F2P1 (3.0%)			F2P2 (4.5%)			F2P3 (6.0%)		
	-10	5	25	-10	5	25	-10	5	25	-10	5	25
EE (KPa)	0.45	0.27	0.07	0.30	0.50	0.15	0.41	0.20	0.46	0.42	0.19	0.15
DCSE (KPa)	2.37	5.16	3.37	1.99	6.93	3.14	2.58	5.06	4.73	3.12	7.27	3.76
FE (KPa)	2.82	5.43	3.44	2.29	7.43	3.29	3.00	5.25	5.19	3.53	7.46	3.91
TS (MPa)	5.04	3.11	0.90	3.88	4.33	1.23	4.44	2.52	1.99	4.33	2.25	0.96
FS (10^{-3})	0.86	4.35	5.56	0.77	2.28	3.73	3.04	2.64	3.30	1.66	5.90	5.29
Temp. (°C)	F4 Control			F4P1 (3.0%)			F4P2 (4.5%)			F4P3 (6.0%)		
	-10	5	25	-10	5	25	-10	5	25	-10	5	25
EE (KPa)	0.41	0.49	0.11	0.52	0.48	0.10	0.67	0.47	0.15	0.68	0.31	0.13
DCSE (KPa)	1.69	4.57	3.86	2.44	5.76	4.18	1.85	5.83	3.20	8.09	6.38	4.80
FE (KPa)	2.11	5.06	3.98	2.96	6.24	4.31	2.52	6.29	3.35	8.77	6.69	4.92
TS (MPa)	4.10	3.57	0.98	4.42	3.38	0.85	4.62	3.14	1.09	4.36	2.12	0.71
FS (10^{-3})	0.86	1.95	9.85	1.09	2.50	6.25	0.89	2.62	4.08	3.10	4.24	11.1

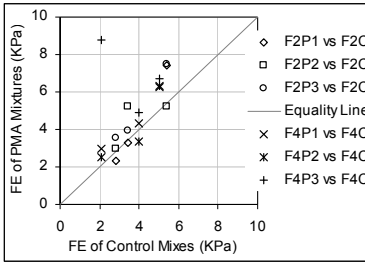


Figure 6. Comparison of Fracture Energy between Control and PMA Mixtures

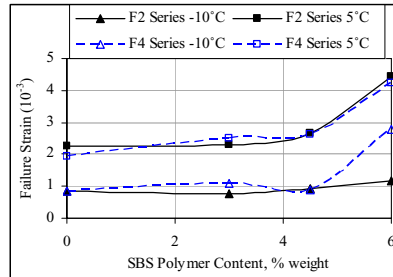


Figure 7. Relationship of Failure Strain and SBS Polymer Content

Compared to the tensile strength of control mixes, PMA mixtures with SBS polymer did not seem to critically affect the HMA tensile strength. The comparison of fracture energy (FE) values between control and PMA mixtures are shown in Figure 6. Most of the data points fall above the line of equality indicating that the SBS polymer tends to increase the fracture energy and hence improve the fatigue cracking performance of HMA mixes. However, no specific relationship was observed between the fracture energy and the SBS polymer content. At temperature of 25°C, the PMA mixtures exhibit complicated behavior related to failure strains, probably due to the enhanced viscous effect of the polymer-modified binder, which makes the mixture properties more dependent on the overall particle distributions of the SBS polymer, the asphalt, and the aggregate. At low testing temperatures (-10°C and 5°C), it was found that the failure strain of PMA mixtures tended to increase with an increase of SBS polymer content, as shown in Figure 7.

DISCUSSION ON EFFECT OF SBS POLYMER MODIFIED BINDER

The SBS polymer-modified asphalt binder was found to be beneficial to the HMA mixtures in terms of fracture mechanics properties. The SBS polymer improved the stiffness behavior of asphalt mixtures. The SBS polymer-modified binder made the PMA mixtures less stiff than control mixes with unmodified asphalt binder at low-to-mid range temperature levels (-10°C and 5°C). The resilient modulus values of PMA mixtures decreased with an increase of SBS polymer content for the concentration range tested. These observations were analogous with the results reported by other research studies (Collins et al., 1991; Chen et al., 2002) on polymer-modified binders and PMA mixtures. The analysis on resilient modulus results based on this study indicated that when SBS polymer is used in the HMA mixtures, although increasing the SBS polymer content will always improve pavement low temperature performance, limiting the concentration within an optimal range is especially important at high service temperatures. The SBS polymer also helped the HMA mixtures obtain an upgraded creep performance. The PMA mixtures were more compliant than the control mixes with unmodified asphalt binders at the low temperature level (-10°C). At a specific temperature level, a higher SBS polymer

concentration generally resulted in higher creep compliance values. These effects should lead to improved resistance to rutting and thermal cracking of HMA mixtures. In addition, the SBS polymer modifier improved the asphalt mixture fracture properties. The indirect tensile strength test showed that the SBS polymer did not significantly affect HMA tensile strength at low temperature levels (at around 0°C). However, the SBS polymer generally increased the fracture energy and the creep strain energy which are indicators of mixtures' resistance to fatigue cracking. At low temperatures (-10°C and 5°C), the failure strain of PMA mixtures tended to increase with an increase of SBS polymer content. These performances provided further justification to the benefits of using polymer-modified binder, documented by other researchers in the past (Kennedy et al., 1992; King et al., 1993).

CONCLUSIONS

The SBS polymer modifier made the HMA mixture softer and more ductile. It did not critically affect the HMA tensile strength. However, it tended to increase the fracture energy limit, and hence would improve the fatigue cracking performance of HMA mixtures. The failure strain of PMA mixtures tended to increase with an increase of SBS polymer content. These findings are in agreement with the theoretical suppositions and other practical studies. Further, the effect of SBS concentration for PMA mixtures appears to be related to the findings for SBS modified asphalt binders reported by other researchers. An effective SBS polymer content appeared to exist between 3.0% and 6.0% depending on the actual conditions of mixture production. An excessive polymer content might improve the stiffness, creep, and failure strain behavior at low temperatures; however, its effect on the PMA resilient modulus property at high temperatures is not always favorable, due to a combined performance of mixing and distribution of SBS polymer modifier, base asphalt binder, and aggregate. The optimum SBS polymer content specification should be based on a scale of practical evaluation of modified HMA mixture performance.

REFERENCES

- Bahia, H.U. and D.A. Anderson (1995) "Strategic Highway Research Program Binder Rheological Parameters: Background and Comparison with Conventional Properties", Transportation Research Record: Journal of the Transportation Research Board, No. 1488, Washington, D.C, 32-39.
- Chen, J., M. Liao and M. Shiah (2002) "Asphalt Modified by Styrene-Butadiene-Styrene Triblock Copolymer: Morphology and Model", Journal of Materials in Civil Engineering, ASCE, May/June, 224-229.
- Collins, J.H., M.G. Bouldin, R. Gellens and A. Berker (1991) "Improved Performance of Paving Asphalts by Polymer Modifications", Proceedings of the Association of Asphalt Paving Technologists, Vol. 60, 43-79.
- Kennedy, T.W., H. Torshizi and D. Jones IV (1992) <<Mix Design Procedures and Considerations for Polymer-Modified Asphalt Compatibility and Stability>>, Center for Transportation Research, Research Report 492-1F, Project 3-9-87/1-492, The University of Texas at Austin.

- King, G.N., H.W. King, O. Harders, W. Arand and P. Planche (1993) "Influence of Asphalt Grade and Polymer Concentration on the Low Temperature Performance of Polymer Modified Asphalt", Proceedings of the Association of Asphalt Paving Technologists, Vol. 62, 1-22.
- Lu, X., U. Isacson and J. Ekblad (1999) "Phase Separation of SBS Polymer Modified Bitumens", Journal of Materials in Civil Engineering, Vol. 11, No. 1, ASCE, 51-57.
- Lundstrom, R. and U. Isacson (2004) "Linear Viscoelastic and Fatigue Characteristics of Styrene-Butadiene-Styrene Modified Asphalt Mixtures", Journal of Materials in Civil Engineering, Vol. 16, No. 6, ASCE, November/December, 629-638.
- Roque, R., W.G. Buttlar, B.E. Ruth, M. Tia, S.W. Dickison, and B. Reid (1997) <<Evaluation of SHRP Indirect Tension Tester to Mitigate Cracking in Asphalt Pavement and Overlays>>, Final Report Contract No. B-9885, Florida Department of Transportation, Tallahassee, Florida, 364 p.
- Roque, R., B. Birgisson, B. Sangpetnam, and Z. Zhang (2002) "Hot Mix Asphalt Fracture Mechanics: A Fundamental Crack Growth Law for Asphalt Mixtures", Journal of the Association of Asphalt Paving Technologists, Vol. 71, 816-828.
- Roque, R., B. Birgisson, C. Drakos, and B. Dietrich (2004) "Development and Field Evaluation of Energy-Based Criteria for Top-down Cracking Performance of Hot Mix Asphalt", Journal of the Association of Asphalt Paving Technologists, Vol.73, 229-260.

Pavement Noise Investigation in North Carolina

George C. Wang¹

¹Department of Construction Management, East Carolina University, Greenville, NC 27858-4353; PH (252) 737-1887; FAX (252) 318-1365; email: wangg@ecu.edu

ABSTRACT

This paper presents the findings on pavement noise on various types of pavements in North Carolina (NC) by using an On-Board Sound Intensity (OBSI) method. As a competitive alternative for noise mitigation, quieter pavement may provide advantages that noise barriers do not have, or to where sound barriers are not suited. The first step in developing quieter pavement is identifying the noise levels of different types of highway pavements. To reach the ultimate goals of quieter pavement development, this research has focused on the most imperative task, i.e., to measure the noise levels of different types of pavements. Pavement noise levels of 61 highway sites including 153 test sections around 30 counties for nine types of pavements across North Carolina have been investigated. Quiet pavement(s) has been identified.

INTRODUCTION

In 1976, the US Congress passed legislation requiring the states to provide mitigation for highway noise as a part of all federal-aid new highway projects and it is mandatory to consider noise abatement as part of the highway construction if a traffic noise impact is expected to occur. Traditionally, construction of noise barriers is the most common method of traffic noise abatement. The design goal for traffic noise barriers is to provide an 8 dB(A) noise level reduction in equivalent traffic noise levels for the “first row” of noise-sensitive receptors near or adjacent to the highway facility. However, there are limitations to build noise barriers, including high cost, unsuitability for some locations, and noise reflections or echoes may occur for two or more opposing or parallel barriers. Traffic noise is a combination of the noises produced by engines, exhaust, tires and aerodynamic noise. Research revealed that tire-pavement noise is the dominant component of traffic noise. Tire-pavement noise is defined as the noise emitted from a rolling tire as a result of the interaction between the tire and road surface (Sandberg 2002). To improve the noise level of road pavement, it is critical to accurately measure tire-pavement noise level of different types of pavements, which includes (i) the selection of the appropriate measuring methods and procedures to capture tire-pavement noise at the source, (ii) the selection of appropriate procedures that should exclude interfering factors during data collection, and (iii) proper data analysis to provide pertinent direction in developing quieter pavement.

OBSI EQUIPMENT AND PRE-MEASURING PREPARATION

On-board sound intensity method. The On-Board Sound Intensity Method (OBSI) was developed by GM for tire sound research. The OBSI measurement hardware consists of a probe (microphone pair) held next to the tire-pavement contact patch by a fixture attached to the wheel studs of the test tire-wheel. The microphone is cabled to the interior of the vehicle where the signals are simultaneously captured on a recorder and processed by a real time-analyzer. The specially tuned microphone only picks up the noise of the tire-pavement interface, noise from other sources such as wind or other vehicles does not intervene.

Tire-pavement noise measuring equipment. OBSI system was selected for the tire-pavement noise data collection. The specific set up included a Brüel & Kjær (B & K) 3050-A-040- PULSE® LAN-XI 51.2kHz 4ch input mini-frame. A Uniroyal standard reference testing tire (SRTT) P225 60R16 97S test tire was used. The test vehicle is 2008 Chevrolet Impala LS. The setup of the two pairs of microphones and test vehicle are shown in Figures 1 and 2. The entire OBSI system was established at East Carolina University (ECU) located in Greenville, NC.



Figure 1. Microphones with windscreens, mounting fixture and cables (Left)

Figure 2. OBSI test vehicle and microphone mounting system (Right)

Validation of equipment and data. Field trial measuring was conducted to verify the stability of the fixture with microphones, preamps, probes, and cables connected to the analyzer and to conduct OBSI data collection with all standard settings for practice purposes. The trial test also validated the equipment and data collected during the trial test.

OBSI Rodeo. To evaluate the system established before the systematic data collection, an OBSI national rodeo was conducted. FHWA Volpe Research Center, East Carolina University, Rutgers University and Illingworth & Rodkin, Inc. (I&R) participated in the rodeo. The test sections of the rodeo included in the rodeo were located to the north and east of Elkin, NC, on US 21 Bypass, Interstate I-77, and State Route 268 Bypass. The test circuit defined a loop about 6½ miles in length with a typical transit time of 7 minutes. Within the loop, 12 test sections were defined on both hot mix asphalt (HMA) and Portland cement concrete (PCC). Physical inspections, verification and calibration of the hardware and software were made before the rodeo. Throughout the rodeo, the run-to-run variation in overall A-

weighted OBSI level for each team was low. The average variation was 0.2 to 0.3 dBA for each of the teams with standard deviations about those averages of only 0.1 to 0.2 dBA. Comparison of the overall OBSI levels for the four participants, as measured initially for the first testing indicated the average difference between teams on each of the pavements was 1.2 dBA with a standard deviation of 0.5 dBA. The difference in levels for the individual sites spans from 0.3 dBA at Site 3 to 2.3 dBA at Site 5A. Figure 3 presents a comparison of sound intensity data for 12 pavement sites during the 2010 OBSI rodeo. A comparison indicates that the ECU OBSI performed well and the data was close to the mean of the data from all teams in the overall 12 sites testing. The rodeo results indicated that the OBSI system and data collection process used in North Carolina was valid. After the rodeo, a systematic OBSI data collection was continued.

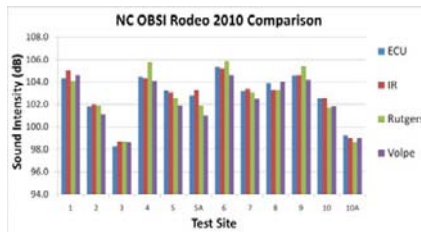


Figure 3. A Comparison of OBSI data for 12 pavement sites in the OBSI rodeo

Tire-pavement noise data collection. Nine types of pavements on 61 highway sites and 153 test sections in 30 counties were investigated. Table 1 presents the pavement types which were investigated.

Table 1. Pavement types investigated

Typical asphalt pavement					Special pavement				
SF9.5A	S9.5A	S9.5B	S9.5C	S9.5D	S12.5D	OGFC	UTBWC	DGCP	

Test procedures. Prior to each data collection, procedures were strictly followed including: (i) Check the test sections laid out prior to the test; (ii) Calibrate the microphones prior to and after the test on each day; (iii) Check cold tire inflation pressure; (iv) Conduct warm-up runs for the SRTT for 10 miles (16 km); (v) Record environmental conditions, including temperature (air, pavement and tire) and air pressure.

Test section selection. Prior to each test, a visual site survey was conducted of the geometric shapes in the pavement and pavement surface characteristics to ensure that the pavement surface was smooth, with no aggregate segregation, no patches and potholes and no cracks or other surface defects of any type. During the site visit, a 440 ft. (135 m) test section was selected with approximately 1,000 ft. (305 m) before and after the test section. Table 2 presents the selection criteria for the test sections. The pre-test visit and pre-selected test sections made the OBSI data collection

efficient and safer. The typical pavement types found in North Carolina for this study were mainly those surface courses with 20 years of design life, and with various traffic volumes: < 0.3 million Equivalent Single Axle Loads (ESALs) (SF9.5A, S9.5A); 0.3 to 3 million ESALs (S9.5B); 3 to 30 million ESALs (S9.5C); > 3 million ESALs (S9.5D, S12.5D). The pavements tested also included newly resurfaced surface courses. Surface treated pavements are not commonly used in North Carolina, and were not tested. The asphalt pavements were located in approximately 30 counties across North Carolina and included eight different types of asphalt pavements, which were SF9.5A, S9.5A, S9.5B, S9.5C, S9.5D, S12.5C, S12.5D, open grade friction course (OGFC), and ultrathin bonded wearing course (UTBWC). The selected pavements were 1 to 3 years old for better comparison purposes.

RESULTS AND FINDINGS

Dense graded friction course. SF9.5A and S9.5A are dense graded surface courses used on low volume roads in North Carolina. Compared to S9.5A, SF9.5A is more commonly used. The average sound intensity for SF9.5A was 99.1 dBA, which was the second lowest out of the nine pavements investigated in the project, including both asphalt and concrete pavements. S9.5A is also a surface course which is used on very low volume roads in North Carolina, but it is not as commonly used in NC as SF9.5A currently. The average of sound intensity levels for S9.5A is 99.1 dBA which is the same as SF9.5A. S9.5B is a surface course used in North Carolina, which carries average daily traffic (ADT) approximately 0.3 to 3.0 million ESALS. Although this is the lowest among the data collected, it is very close to other dense graded surface courses. S9.5C is an HMA surface course used in North Carolina. The average of sound intensity levels for S9.5C is 99.3 dBA. S9.5D is a surface course used in North Carolina for high volume roads. The average of sound intensity levels for S9.5D is 99.5 dBA. S12.5D is a dense graded surface course used on high volume roads in North Carolina and the average daily traffic (ADT) is larger than 30 million ESALS. The average sound intensity level for S12.5D is 99.7 dBA. It was found that the six typical dense graded friction courses tested, i.e. S9.5A, S9.5B, S9.5C, S9.5D, SF9.5A, and S12.5D, had very close sound intensity tire-pavement noise levels. The lowest average number is 98.4 dBA for S9.5B, while the highest is 99.7 dBA for S12.5D. This indicates the difference of the sound intensity among the typical asphalt pavements in North Carolina is very low, which is 1.3 dBA based on the OBSI data obtained.

Open graded friction course. Open Graded Friction Course (OGFC) is a surface course commonly used in North Carolina. Various OGFC have been used since 1950 in different parts of the US to improve the frictional resistance of asphalt pavements. However, the experience of states with this kind of mix has been widely varied. While many states have reported good performance, many other states have stopped using OGFC due to low durability or loss of the voids (Smith 1992). However, many improvements have been made during the last few years in the way OGFCs are designed and constructed. The average of sound intensity levels for OGFC is 103.2 dBA. It was found that the OGFC tested in the project had the highest measured noise level with an average sound intensity of 103.2 dBA. This number is slightly

higher than the average of OGFC reported in some states. However, there can be various reasons.

Ultrathin bonded wearing course. Use of an ultra-thin bonded wearing course (UTBWC) is reported on as a pavement preservation strategy for jointed plain concrete pavements. UTBWC is a special treatment surface course recently used in North Carolina. Construction of UTBWC is the application of a warm polymer modified emulsion membrane followed immediately with an ultra-thin wearing course. Hot mix asphalt composed of about 6% asphalt binder of PG 70-28. Depending on the 3/8 inch gap graded coarse aggregate in the mix, the binder content slightly varied from 6% binder content to meet the mix design. UTBWC can be used on both urban and rural sections. One of the benefits of the UTBWC is that the elevation change is small, typically 5/8 inch. Expenses associated with thick overlays, such as adjustments to signs, guardrails, bridge clearances, and shoulders are minimized. The effectiveness of the UTBWC in improving ride quality and extending pavement life is evaluated for five projects (Corley-Lay and Martin 2005). The two highway sites (I-95) were two years old when tested. The average OBSI level is 101.8 dBA, from 101.2 to 102.5 dBA. This is in the higher levels of the OBSI levels of the pavements investigated in the project. However, this is an acceptable level for thin overlays.

Diamond ground concrete pavement. Diamond grinding was typically used for restoring profile or making concrete pavement smoother. A typical surface texture resulting from diamond grinding is shown in Figure 4. It is reported that diamond grinding can produce the smoothest and quietest surfaces while also enhancing the friction characteristics. A typical diamond grinding pavement after trafficking might have a “ridge” height of 1 - 2 mm and is separated by 1/16 to 1/8 inch grooves. Diamond Ground Concrete Pavement (DGCP) is a surface course used in North Carolina. The overall average OBSI level of the concrete is 102.8 dBA, from 100.8 to 104.9 dBA. This range is in the lower level as compared with other data from different states. The detailed texture needs further investigated from the construction plan to verify the reason.

Table 2. Pavement test section selection criteria

Pavement condition category	Visual observation
Pavement Surface Characteristics	Smooth, no transverse or longitudinal cracks observed
Materials Properties	No surface segregation and asphalt bleeding observed
Geometry	Straight driving lane, no uphill, downhill, for approximately 1500 ft. (428 m), (440 ft. or 135 m for test section for 60 mph)

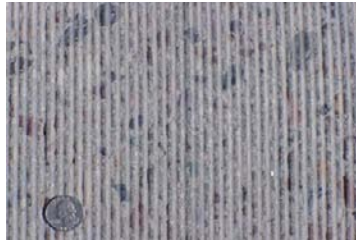


Figure 4. Atypical diamond ground surface

Effect of Driving Speed on the Sound Intensity Tire-Pavement Noise Level

Two test sites were selected to verify the effect of driving speed on sound intensity levels. Fig. 6 presents a view of the NC 11 southbound site tested to verify the effect of driving speed on the sound intensity. Two linear equations which are almost perfectly fitted were found during the test. For NC 11 Southbound lane and NC 43 Northbound lane, the relationships between driving speed (X) and noise level (Y) are given by the following equations:

$$Y = 0.3024 X + 79.895, R^2 = 0.9940$$

$$Y = 0.3324 X + 78.501, R^2 = 0.9913$$

This finding is similar to the reports in other literature (Donavan and Lodico 2009). From the two equations in Section 4.2.9, the slopes of linear equations are 0.30 and 0.33 respectively, it indicated that if driving speed is reduced by 10 mph (16km/h), the sound intensity can drop 3.0 to 3.3 dBA. This may be a factor to consider reducing traffic noise in populated urban areas. Figure 10 presents ranges of sound intensity levels for nine types of pavements. Figure 11 presents the sound intensity with two standard deviation spread.



Figure 5. A Site view of NC 11 southbound

CONCLUSIONS

The OBSI system established has been proved to be valid by internal, external verifications and calibrations, and also by the OBSI rodeo. The OBSI system meets the requirements for OBSI measurements and future needs. The OBSI equipment represents a unique and updated version of similar equipment in the nation and the world. The assessment of tire-pavement noise levels at the source is necessary to adequately identify and develop quieter pavement types. The OBSI method allows researchers to quickly measure and compare pavement acoustics in great detail and

has proven to be a reliable method for tire-pavement noise measurement throughout this project. For quieter (or louder) pavement identification and quieter pavement development purposes, a reliable standard measuring method should be identified and maintained so that the data can be compared nationally and internationally. The OBSI method can be used for general OBSI data collection to enhance the tire-pavement noise database in NC and to increase the sample sizes of each type of pavement. The equipment is also a power tool to conduct research and investigate various influencing factors that affect tire-pavement noise, which include the effects of temperature, moisture, vehicle driving speed, weight of vehicle, and age of pavement. It can be used to map tire-pavement noise distributions in densely populated or noise sensitive areas for traffic noise management purpose. With this equipment, agencies can perform tire-pavement noise investigations and research in a similar manner with other agencies and be able to share data with other agencies.

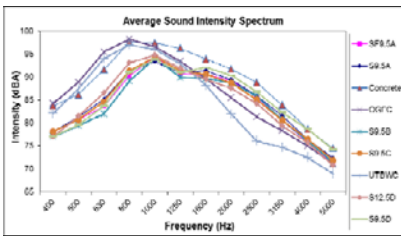


Figure 6. Average of sound intensity spectrum for nine types of pavements

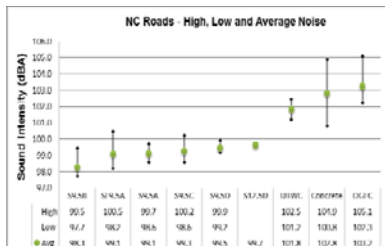


Figure 7. Ranges of sound intensity levels for nine types of pavements

Dense graded friction course. Six types of typical (dense graded) asphalt pavement surfaces have been investigated for tire-pavement noise levels. The six typical pavements cover from very low volume traffic to very high volume traffic. The results of OBSI data indicate that the tire-pavement noise levels of these six types of pavements are in a lower range, from 98.2 to 99.6 dBA, comparing with other dense graded surface friction courses in other states. The difference between the lowest (S9.5B) and highest (S12.5D) is 1.4 dBA. The pavement selected for this project is approximately 1 to 3.5 years old (2.5 years difference). Research by others for the OBSI values changes due to the age of the pavements indicate that for a three year difference, the OBSI value changes in the ranges of between -0.6 dBA to +2.0 dBA (positive sign means the OBSI values increase with longer life). In the research conducted by Colorado for 34 pavements, the maximum OBSI change in three years was 2.6 dBA (Rasmussen 2011). Therefore, for the eight asphalt pavements investigated in this project, the age difference, i.e. approximately 2.5 years can be one of the reasons that contribute to the OBSI difference (1.4 dBA) between the lowest and highest noise levels.

Open Grade Friction Course. Eleven sites were tested for OGFC. The average of the sound intensity value was 103.2 dBA (102.3 to 105.1 dBA). This result indicated that the OGFC tested in the project had 3.6 dBA differences (higher). This is somewhat different from the reports from other states. This may come from the

following reasons, (i) the mix designs of OGFC can be very different, for instance, in Washington State, most of the OGFCs contain asphalt rubber and SBS modified asphalt binder; (ii) the age of the OGFC investigated in this project is approximately four years or older which may cause a couple of decibels loss; (iii) the detailed mix design, and other parameters of the OGFCs, especially aggregate characteristics is not clear and there is no comparison among the OGFCs at this stage. Therefore, more information is needed to identify the cause of the higher noise level of OGFC in the highways tested.

Ultra-thin Bonded Wearing Course (UTBWC). OBSI data was collected for UTBWC in Cumberland and Harnett Counties on Highway I-95. The pavement was two years old when tested. The average noise level was 101.8 dBA, from 101.2 to 102.5 dBA. This was on the higher side of the pavements investigated in the project. The reasons for this may come from (i) the conditions and type of old pavement overlaid was unknown; (ii) the gap graded, angular coarse particles (no fine aggregate) may cause higher noise level. There is not much literature regarding tire-pavement noise level for UTBWC. Further research on UTBWC mix designs is needed to improve the pavement noise level for UTBWC.

Concrete Pavement. OBSI data were collected on US 1 in Wake County, I-77 in Yadkin County, I-73 and I-85 near Greensboro. The overall average OBSI level is 102.8 dBA, from 100.8 to 104.9 dBA. Seven sites on I-73 were tested and the values ranged from 100.8 to 105.6 dBA; three sites were tested on I-85, the values ranged from 104.8 to 105.4 dBA. However, the overall average, 102.8 dBA, is a promising number compared to those of concrete pavement from some other states.

REFERENCE

- Sandburg, U., and Ejsmont, J. (2002). Tyre-road noise reference book. Informex, Harg, Sweden.
- Rasmussen, R. (2011). Tire-pavement and environmental traffic noise research study. the Colorado Department of Transportation, DTD Applied Research and Innovation Branch.
- Smith, H., (1992). Performance characteristics of open graded friction courses. In NCHRP Synthesis of Highway Practice 180, TRB Annual meeting, Washington, D.C.
- Corley-Lay, J. and Mastin J. (2005). Ultrathin bonded wearing course as pavement preservation treatment for jointed concrete pavements. Transportation Journal of the Transportation Research Board, 2005: 0361-1981.

Precast Prestressed Concrete Pavement Construction

Luh-Maan Chang¹ and Yu-Tzu Chen²

¹ Professor, Department of Civil Engineering, National Taiwan University, Taiwan.
E-mail: luhchang@ntu.edu.tw; Phone: (02)-3366-4269; Fax: (02)-2366-1640

² Adjunct Faculty, Construction Management, Goodwin College of Professional Studies,
Drexel University, Philadelphia, USA. E-mail: yc445@drexel.edu

Abstract

To minimize the effects of traffic congestions, a method with the speedy construction and lower user impact cost is needed. This paper introduces a relatively new pavement construction method lately developed in United States. The method is called Precast Prestressed Concrete Pavement (PPCP.) PPCP sustains a life-cycle pavement construction project. The state-of-the-art of the PPCP method will be reviewed and compared. Their design concepts, field installation procedures, merits, pitfalls will be discussed. With all the comparative advantages and disadvantages, PPCP is comparatively sustainable. It is inevitable that PPCP will be a vital option for roadway construction in the near future.

Introduction

It is well known that the closure of roadways for new pavement, overlays, or removal and replacement applications constantly causes traffic congestions. Congestions not only cause delays, and increase of accidents and user costs, but also, increase the fuel consumption and environmental pollution that are not sustainable.

To minimize the frequency of new pavement, overlays, removal, and/or replacement applications, to expedite the pavement construction process, to mitigate the effects of traffic delays and to reduce the impact on environment, the U.S. Federal Highway Administration (FHWA) has sponsored many US Departments of Transportation (DOTs) to experiment the use of precast Prestressed concrete pavement (PPCP) method for expediting the construction of Portland Cement Concrete (PCC) pavements.

Objective

Precast Prestressed Concrete Pavement (PPCP) method has been experimented in the US since early 2000's. It demonstrates advantages over conventional cast-in-place concrete pavement construction due to its speed of construction, saving in user cost, and sustainability. The objective of this paper is to introduce the

state-of-the-art PPCP method recently developed in United States. The paper will begin with a brief review on the design concepts and field installation procedures of PPCP. And then, its advantages and disadvantages will be discussed in detail.

Precast Prestressed Concrete Pavement

Precast Prestressed concrete pavement (PPCP) can be defined as “a pavement in which a permanent and essentially horizontal compressive stress has been introduced prior to the application of live load”, according to the AASHTO Subcommittee on Prestressed Concrete Pavement of the Committee on Rigid Pavement Design.

The basic concept of PPCP involves with a series of individual precast panels that are longitudinally post-tensioned together after laid on site along the traffic direction. During fabrication, pretension is made in the transverse direction. Ducts for longitudinal post-tensioning are imbedded into each of the panels as well as the expansion joints.

The 1st PPCP pioneer project was conducted by Texas Department of Transportation (TxDOT) in 2001. TxDOT’s PPCP demonstration project in Georgetown, Texas, was completed on the frontage road of the US Interstate Highway 35. The total length of the precast pavement was 700 m (2,300 ft) on the both sides of a bridge. Construction cost including panel fabrication, delivery, and field installation is around \$204/m² (\$19/ft²). The basic schematic drawings for PPCP are shown in the Figures 1 and 2.

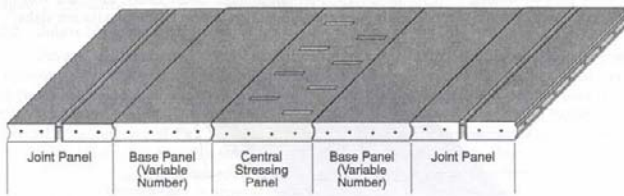


Figure 1. Assembly of Panels for Precast Pavement (Merritt et al. 2002)

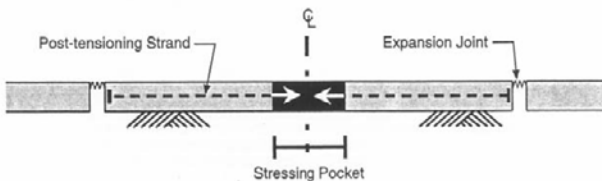


Figure 2. Concept of Central Stressing (Merritt et al. 2002)

Assembly of Precast Panels

The assembly of the above precast panels starts with a joint panel at the end of the slab. The base panels will be placed, followed by the central stressing panel as shown in Figure 1. Numbers of base panels can be designed to be assembled between joint panel and central stressing panel based on the designated condition. The strands are inserted into the ducts through central stressing pockets, apply post-tension and anchored by spring-loaded and self-locked anchors in the joint panels. The strands are then post tensioned from the stressing pockets of the central stressed panel as shown in Figure 2. After post-tensioning, the tendons are grouted in the ducts, the stressing pockets are filled with fast-setting concrete. Sealants are then injected into the joints between each of the panels (Chang et al. 2004; Merritt et al. 2002; and Merritt et al. 2002). The Figure 3 demonstrates the example of the assembling procedures used in the CaDOT's PPCP demonstration project-I-10 HOV Widening Project between Baldwin Avenue and I-605.

Advantages and Disadvantages of Using PPCP

Advantages

Speedy Construction

Since extra time is not required for the concrete to reach sufficient strength before opening to traffic, as with conventional, the roadway can be open for traffic almost right after placement.

Better Quality Control

The panels can be precast in the factory or some place near the field and then transported to the construction site. Better quality is possible because of thermal and acoustical control for PPCP's plant-fabrication. This may lead to less required maintenance and longer pavement life than conventional pavements.

Year Round Construction

PPCP can be constructed "unseen" (casting and curing the slab in site or at the factory) and in all kinds of weather. Overnight or weekend construction is possible for precast concrete. All year round construction is possible with PPCP method.

Lower User Cost

User costs are the costs incurred by the users of the roadway due to the presence of construction activities, such as increased fuel consumption and lost work time. Shortening the period of time roadways are closed for construction will lead to roadway user cost savings.

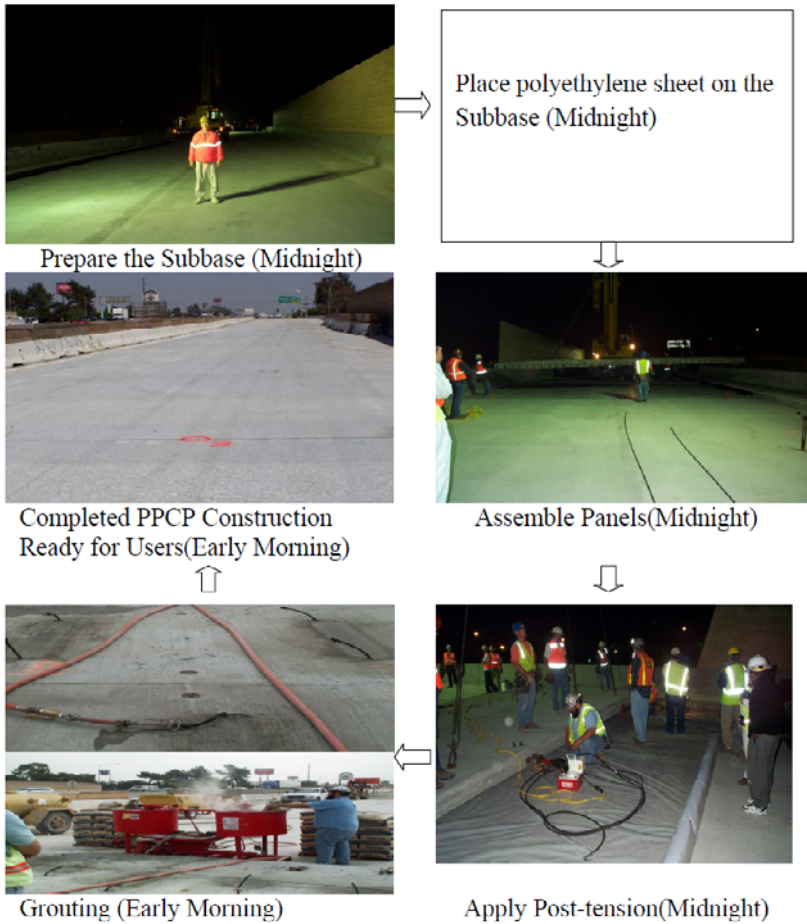


Figure 3. The Construction Process of CaDOT's Demonstration Project

Disadvantages

Five PPCP demonstration projects have been constructed. They are: 1) along the frontage road of I-35 at the George Town, Texas in 2001, 2) along I-10 at El Monte, California in 2004, 3) along the northbound I-57 near Sileston, Missouri in 2005, 4) on SR 60 near Shelton, Iowa in 2006, and 5) at the intersection of route 869 and route 40 of Delaware in 2009.

Although the US Federal Highway Administration (FHWA) partners with State highway agencies, industry, and academia for providing helpful tools for use in

materials selection, mixture proportioning, and the design, construction, and rehabilitation of PPCP (Issa et al., 1998). However, the lack of long term experiments for solidly proving theories and easily applied design and construction procedures have been major obstacles to its application.

The other disadvantages could be generally summarized as below: (Chang et al. 2004; Merritt et al. 2002)

1) Ride Quality

PPCP has higher average International Roughness Index (IRI) than normally required correction for conventional concrete pavement. Leveling course is 5.08 cm (2 inches) asphalt. It is hard to be even and may cause fractures

2) Cost

The total cost of the Georgetown PPCP, including the panels' fabrication, base preparation, and construction, was approximately \$203/m² (\$19/ft²). The cost is significantly higher than expected for an equivalent 355 mm CRCP \$36-\$48/ m² (\$3.34-4.59/ft²).

3) Complexity

PPCP is still relatively new. Parties involved were not familiar with precast paving techniques yet.

4) New Construction Equipments needed

New construction equipment may be necessary for precast concrete construction projects. The system requires larger and longer size form and heavier cranes.

5) Surface

Leveling course: 5.08 cm (2 inches) asphalt leveling course is hard to be even and may cause fractures

Design Factors

The major design factors include the following (Cable 1985):

Foundation Strength

The stress in a PCP for a given load is inversely proportional to the strength of the supporting foundation and the ability of the PCP to withstand repetitive loads in proportion to the strength of the supporting foundation. Usually, PCP has 200 psi or higher modules of subgrade reaction.

PCP Thickness

Factors affecting the design of PCP thickness include foundation strength, concrete strength, and magnitude of pre-stress, and expected traffic loads. PCP

thickness has been determined more on the basis of providing the minimum allowable concrete cover on the pre-stressing tendons than on the basis of load-carrying consideration. This procedure has resulted in thickness of PCP on the order of 10 to 15 cm (4 to 6 inches).

Slab Length

The two main factors which must be balanced when selecting the optimum slab length for PCP are:

- a) The prestress force required to overcome the frictional restraint between the subgrade and the slab, and to provide the desired minimum compressive stress at the midlength of the slab, is proportional to the slab length. The cost associated with providing this prestress force is, in turn, proportional to the magnitude of the required force.
- b) The number of and total cost for transverse joints is inversely proportional to the slab length. (Total cost should include initial cost and maintenance cost over the life of the facility, since transverse joints are the largest maintenance item for a pavement.)

Slab Width

Slab width refers to the distance between the two exterior longitudinal free edges of the completed pavement and does not refer to the distance between intermediate inactive longitudinal construction joints.

In many instances it is not feasible to construct the full width of either a new pavement or an overlay on an existing pavement in a single operation and, as a result, the pavement must be constructed in two or more successive, contiguous longitudinal strips. Construction joints must be provided between adjacent pavement strips with this type of construction. This type of construction is necessary due to equipment limitation and accommodating public and construction traffic.

Summary

The paper briefly reviewed the Precast Post-tensioned Concrete Panel. Its strengths and weaknesses were addressed and their implementation procedures were demonstrated in detail.

PPCP was originally developed for longer and continuous paving in Texas. Comparing with conventional cast-in-place concrete pavement methods, PPCP has a higher construction cost (First Cost) and currently the industry is still not very familiar with this new method. Nevertheless, PPCP possesses many advantages that precast concrete construction has. The speedy pace of the precast concrete construction results in less traffic congestion, pollution and delays, and lowers the user costs significantly. In addition, the precasting quality is under better controlled environment.

Moreover, because the post-tensioned force exerts compression on the tensioned side of precast concrete panel and tightens certain degree of cracks, it leads to a more durable concrete. And PPCP requires less maintenance and less frequency for new pavement, overlays, removal, and/or replacement applications. In addition to the additional compressive force, PPCP reduces the thickness of the pavement slab and corresponding materials for concrete.

It is predictable that PPCP will become a popular method for pavement construction, particularly, in the areas with heavy traffic. The strength of PPCP by using less energy and generating less pollution is sustainable.

References

- Cable, N. D., McCullough, B. F., and Burns, N. H. (1985). "New Concepts in Prestressed Concrete Pavement," Research Report 401-2, December, Center for Transportation Research, the University of Texas at Austin.
- Chang, Luh-Maan, Lee, S., and Chen, Yu-Tzu, (2004). "Using Pre-cast Concrete Pavement Under Severe Congested Traffic Condition," The Proceedings of the 4th International Conference on Concrete Under Severe Conditions of Environment and Loading. CONSEC04, Seoul National University, and Korea Concrete Institute, Seoul, Korea, June 27-July , pp. 1580-1587.
- Issa, M. A., Yousif, A. A., Issa, M. A., Kasper, I. I., and Khayyat, S. Y. (1998). "Analysis of Full Depth Precast Concrete Bridge Deck Panels," *PCI Journal*, Jan/Feb , pp. 74-85.
- LePree, J. (2002) "Taking a Toll," *Precast Solutions*, pp10~12.
- Lin, T. Y., and Burns, N. H., (1981) *Design of Prestressed Concrete Structures*, 3rd ed., John Wiley and Sons, Inc., pp. 1-30.
- Merritt, D. K., McCullough, B. F., and Burns, N. H. (2001). "Feasibility of Using Precast Concrete Panels to Expedite Construction on Portland Cement Concrete Pavements," Paper No. 01-2904, Transportation Research Board, 80th Annual Meeting, January 7-11, Washington, D.C, Transportation Research Record 1761, pp. 3-9.
- Merritt, D. K., McCullough, F. B., and Burns, N. H., (2002) "*Texas Tests Precast for Speed and Usability*", US department of Transportation, Federal Highway Administration, July/August , Vol.66, No.1.
- Merritt, D. K., McCullough, B. F., Burns, N. H., and Schindler, A. K. (2002) "The Feasibility of Using Precast Concrete Panels to Expedite Highway Pavement Construction," Research Report 1517-1, February, Center for Transportation Research, The University of Texas at Austin.

- Merritt, D. and Tayabji, S. (2009) "Precast Prestressed Concrete Pavement for Reconstruction and Rehabilitation of Existing Pavements", January, U.S. Department of Transportation, Federal Highway Administration
- PCI Concrete Handbook Committee, (1999). *PCI Design Handbook*, 5th Edition, pp.1-3
- Wilde, W. J., Waalkes, S., and Harrison, R. (1999). *Life Cycle Cost Analysis of Portland Cement Concrete Pavements*, Research Report 1739-1, Center for Transportation Research, The University of Texas at Austin, September, pp. 65-95.

Performances of Vibro Compaction Gravel-Concrete Composite Pile

G.Q. Kong

Assistant Professor, Key Laboratory for Ministry of Education for Geomechanics and Embankment Engineering, Geotechnical Research Institute, Hohai University, Xikang Road No.1, Nanjing, Jiangsu P.R. China 210098. E-mail: gqkong1@163.com

ABSTRACT

A new pile, vibro compaction gravel-concrete composite pile (referred to as GCP) is developed. The principle, construction method, quality assurance (QA) and quality control (QC) of gravel-concrete composite pile are briefly introduced. Simple calculation models of gravel-concrete composite pile embedded in soft soils are built by FLAC^{3D} and LPILE software, and models of conventional concrete pile and gravel pile with the same volumes are also built for comparative analysis. The performances on vertical compressive load, uplift load, and lateral load capacities are comparatively analyzed and discussed. Then the parameter study on the proportion of gravel materials in the whole gravel-concrete composite pile is carried out. The results show that the gravel-concrete composite pile is a cost-effective pile, which can improve bearing capacity effectively.

INTRODUCTION

Many railways, highways, and high buildings have been constructed over soft soils, wherein problems such as lack of foundation bearing capacity and large post-construction settlement are very common. Pile foundation or pile-supported embankments are widely used to facilitate rapid construction of foundations on soft soils due to the anticipated benefits such as savings in construction time and cost when compared to other traditional soft soil improvement methods. At present, pile can be identified into two types: one is flexible piles, such as stone columns, deep cement mixing (DCM) piles, geosynthetic-encased stone columns, and cement fly-ash gravel (CFG) piles; the other one is rigid piles, such as driven precast concrete piles or cast-in-place piles. The use of flexible pile type tends to be relatively low cost but may suffer large post-construction settlement; on the other hand, the use of rigid pile type may be more costly but yield relatively less post-construction settlement. In an effort to develop economical pile systems for supporting embankments on soft clays, the combinations of CFG pile, DCM pile and lime columns are used for soft soil ground improvement. This system consists of installing different pile types with different diameters and lengths to support the embankment fill and to mobilize the strength and stiffness of the soil at shallow depths. Field tests or numerical simulations on foundation systems using a combination of different piles were carried out. This treatment method is cost-effective, while its construction method is too complex, and

different pile type constructions will be influenced by each other during pile driving.

In some conditions, using only flexible pile does not meet design requirements, while using only rigid pile may cause design waste. However, there has never been a description of a construction method on flexible-rigid composited on one pile, until now. Hence, in this paper, a new pile, vibro compaction gravel-concrete composite pile (referred to as GCP), is developed (China patent: CN 101781888 A). The principle, construction method, quality assurance (QA) and quality control (QC) of GCP is briefly introduced. Simple calculation models of GCP embedded on soft soils are built by FLAC^{3D} and LPILE software, and models of conventional gravel pile, and concrete pile with the same volumes are also built for comparative analysis. The performance in vertical compressive/uplift load capacity, and lateral load capacity are comparatively analyzed and discussed. Then, the parameter study on the proportion of gravel materials in the whole gravel-concrete composite pile is carried out.

GCP TECHNIQUES INTRODUCTION

Principles

For conventional gravel piles, the settlement of pile top is large under vertical load, and the lateral load capacity is little under lateral load. For conventional concrete pile, the settlement of the pile top is small under vertical load, and critical pile length exists when it is under lateral load, which means that if the pile length is too long, it becomes useless for lateral bearing capacity. At the same time, use of flexible pile type tends to be relatively low cost, and the use of rigid pile type tends to relatively lessen post-construction settlement and lateral bearing capacity. For a certain site conditions, using whole gravel pile may not meet design requirements, while using whole concrete pile may cause design waste. Base on these, vibro compaction gravel-concrete composite pile, using a flexible and rigid pile part in one pile, was developed. For this new pile type, the vertical and lateral load capacities are in the acceptable range while the cost is lower, which means that GCP is one of the most cost-effective piles compared with conventional concrete pile with the same volume of usage. GCPs usually have diameters of 0.5 m-1.0 m, and the maximum depth of piles can normally reach 25 m for soft ground treatment.

Construction Method

GCP construction process combines driving, excavating, and casting in one operation, which improves construction efficiency. The annular casing is closed ended by cutting shoes (valve pile tip). The schematic diagram of construction technology of GCP was shown in Figure 1. The construction procedures for GCP can be described as follows: (1) the vibratory pile driver was connected to the steel casing by a flange; the steel casing was connected with the cutting pile shoe. It was determined that the plane's angle between the oriented perpendicular and ground was less than 1.5%, and the deviation of practical holes centered with that of the designed was less than 50 mm. Then, the pile model was driven into soils together with a pile shoe to the designed depth by driving machine, as shown in Figures 1(a) and (b). 1-min vibrations were used

for each 0.5 m sink. (2) A certain amount of gravel was put into the pile model, as shown in Figure 1(c). (3) The pile model withdrew with the vibrations, as shown in Figure 1(d). Processes (2) and (3) were repeated until the gravel pile reached the design length. (4) A certain amount of concrete was put into the pile model, and the pile model withdrew with the vibrations, as shown in Figures 1(e) and (f). In order to improve the quality of the constructed piles, the withdrawing rate of casing should be controlled within 0.5 to 0.8 m/min under soft soil layers, 1.0 to 1.4 m/min under loose to medium-loose sand layers, less than 1.0 m/min on the junction of hard and soft soils, and 10 s vibrating should be carried out in this position. 1 min vibration should be used for each 1.0 m of distance.

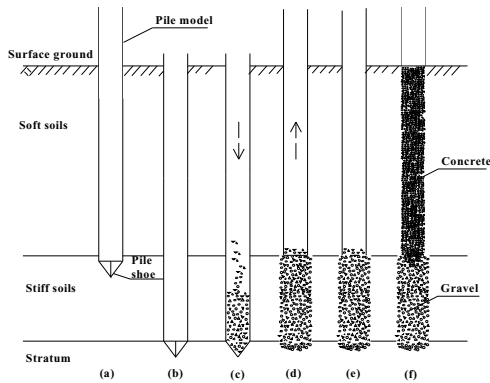


Figure 1. Schematic diagram of construction technology for vibro compaction gravel-concrete composite pile.

Quality Assurance and Quality Control

Compared with conventional DCM piles, the quality of GCP can be improved and the quality check of the constructed piles can also be executed easily in the field. High quality cast-in-place GCP is achieved due to the use of the steel casings as a form, which prevents necking and bulging of the poured concrete. The use of steel casing also enables the volumes of concrete and gravel required to form a pile to be estimated accurately. The quality of the cast-in-place GCPs after their formation in the ground can be checked by three different methods: (1) static pile load testing, (2) low-strain integrity testing, and (3) monitoring of the amount of concrete poured during concreting. The ratio of the actual concrete volume versus the theoretical volume could be used as an indicator of the quality of constructed GCP.

COMPARATIVE ANALYSIS

Soil Site Description

Hangzhou-Qiandaohu highway project, located in the north of Zhejiang province, China, is one of the key projects in Zhejiang Province. The total length of the

highway is about 120 km, and the width of the embankment is about 26 m. The designed driving speed is 100 km/h. Most of the embankments were constructed over deep soft soils with a high underground water table. Most of the soft soils are saturated mud clay mixed with silt sand. The site physical and mechanical index properties are shown in Table 1. Pile-support embankment was used for soft ground treatment.

Table 1. Soil physical and mechanical index properties at Hangzhou-Qiandaohu road, Zhejiang Province, China.

Materials	Thickness (m)	Unit Weight (kN/m ³)	Water Content (%)	Compression Modulus (MPa)	CU Test		Undrained confined strength (kPa)
					c_{cu} (kPa)	ϕ_{cu} (°)	
Silty clay	1.60	18.90	32.70	8.89	9.00	28.50	11.01
Mud clay	1.92	19.30	27.60	11.62	5.00	30.50	11.87
Clay	1.93	19.30	27.60	11.62	5.00	30.50	17.04
	2.40	19.50	28.50	10.80	3.50	31.50	22.08
	2.40	19.50	28.50	10.80	3.50	31.50	28.79
Silty sand	1.30	18.90	34.20	7.67	5.00	23.50	30.31
Silty clay	2.10	17.60	45.20	2.60	16.80	12.00	32.88
	2.20	17.60	45.20	2.60	16.80	12.00	35.62
	2.20	17.60	45.20	2.60	16.80	12.00	38.43
	2.20	17.60	45.20	2.60	16.80	12.00	41.24
	2.00	17.70	29.60	3.32	24.70	13.50	54.95
Silty clay	2.00	17.70	29.60	3.32	24.70	13.50	57.79
	2.00	17.70	29.60	3.32	24.70	13.50	60.64
	2.50	20.10	26.20	5.79	38.80	18.20	101.81

Model Built and Parameters Selections

Three different piles (conventional gravel pile, concrete pile, and GCP) with the same volume usage were chosen for comparative analysis. Each pile under vertical compressive load, uplift load, and lateral load is carried out. Model pile embedded in viscous soils (shown in Table 1) under vertical load, with pile length h , pile diameter D , equal 15 m, and 0.8 m, respectively, was built by using FLAC^{3D} software. Owing to symmetry, only a quarter of the whole mesh was used in the 3D simulation. In the geometric model, typical finite difference meshes and model size are shown in Figure 2. For GCP, the lengths of gravel and concrete equal 4 m, and 11 m, respectively. The modulus of gravel pile and concrete pile equal 250 MPa, and 25 GPa, respectively. Soil material properties used in the analysis are shown in Table 1. Pile is modeled as isotropic elastic model. The soil is modeled on the Mohr-Coulomb model. The interface of pile-soil is modeled as Coulomb sliding model with k_n and k_s , assumed as 1.0×10^7 kPa/m. The cohesion c_a and internal friction angle ϕ of the pile-soil interface are assumed as those of soils. The upper boundary condition is assumed as free boundary, while the side boundary condition is assumed to a level direction sliding support. The bottom boundary condition is assumed as a vertical direction sliding support. Groundwater table is assumed on the ground surface. Model piles embedded

in viscous soils under lateral load are carried out by the p - y method through LPILE software. In order to improve calculation accuracy, each soil layer were divided into smaller thicknesses which were less than 3 m thickness for LPILE software input. Suppose that the pressure of pile axial force is positive, while tension is negative; the downward displacement of pile is positive, while upward displacement of pile is negative.

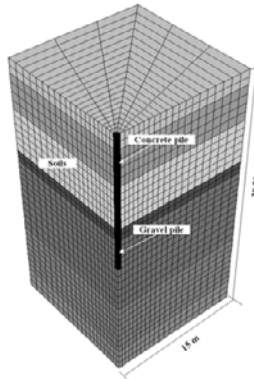


Figure 2. Geometric model, model size, and typical meshes for gravel-concrete composite pile (1/4).

Comparative Analysis Results

Figure 3 shows the curves of pile head vertical compressive/uplift load versus displacement, and lateral load versus deflection for each pile type. It shows that the displacement of GCP is a little larger than that of conventional concrete pile, while much smaller than that of conventional gravel pile under the same vertical load, which means that the vertical bearing capacity of GCP is a little smaller than that of concrete pile, while much larger than that of gravel pile. When the pile is under lateral load, the lateral bearing capacity of GCP is similar to that of concrete pile, and much larger than that of gravel pile. Figure 3(a) shows that the vertical compressive load bearing capacities of GCP, concrete pile, and gravel pile equal 2721 kN, 3000 kN, and 916 kN, respectively. It means that vertical compressive load bearing capacity of GCP is nearly 90.7 % of that of concrete pile, while it is nearly 3.0 times of that of gravel pile with the same volumes. Figure 3(b) shows that the vertical uplift load bearing capacities of GCP, concrete pile, and gravel pile equal 2500 kN, 2000 kN, and 790 kN, respectively. It means that the vertical compressive load bearing capacity of GCP is nearly 80.0 % of that of concrete pile, while it is nearly 2.5 times of that of gravel pile with the same volumes. Figure 3(c) shows that the lateral load bearing capacity of GCP is nearly 99.9 % of that of concrete pile, while it is nearly 4.9 times of that of gravel pile with the same volume.

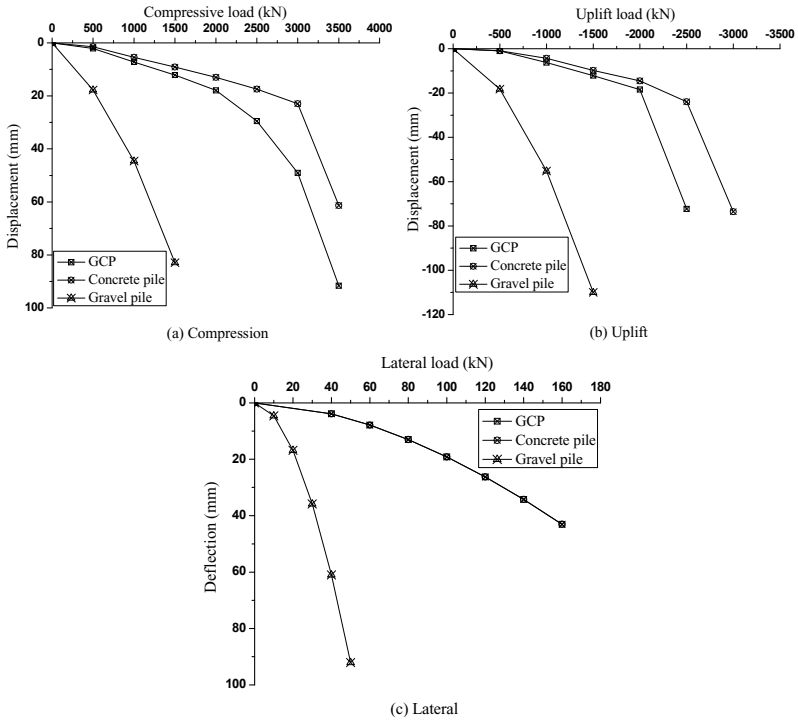


Figure 3. Comparative curves of pile head load versus displacement for GCP, concrete pile, and gravel pile: (a) compression; (b) uplift; (c) lateral.

Parametric Study of Composite Ratio

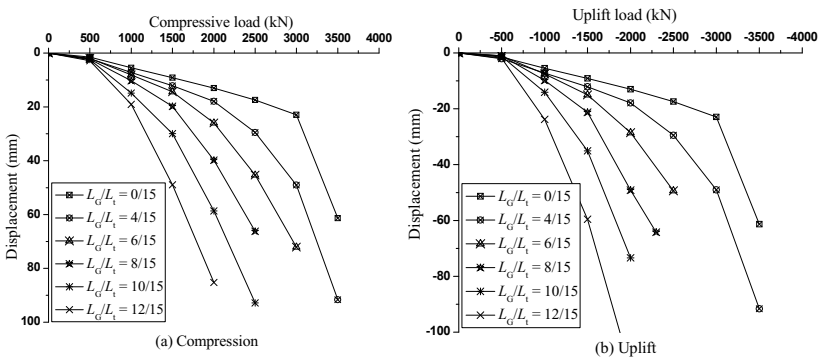


Figure 4. Comparative curves of vertical load versus displacement for GCP under different composite ratio: (a) compression; (b) uplift.

Figure 4 shows the curves of pile head vertical compressive/uplift load versus displacement of GCP with different composite ratio, which is defined as the proportion of gravel materials in the whole GCP. It shows that the vertical bearing capacity of GCP increases as composite ratio decreases. Figure 5(a) shows the curves of pile head lateral load versus deflection of GCP with a different composite ratio. It shows that the deflections of GCP are increased with composite ratio increasing, while the change is minor when composite ratio is less than 6/15. Figure 5(b) shows the curves of deflection distribution along pile depth of GCP with a different composite ratio. When pile depth is larger than 9 m, the deflection distribution is nearly similar. It is because that critical pile length exists when piles are under lateral load.

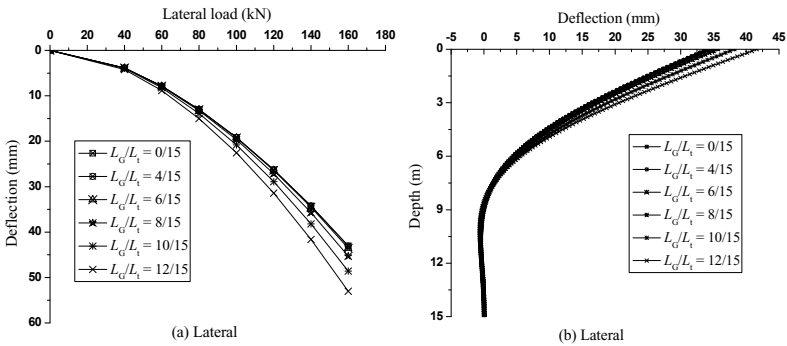


Figure 5. Comparative curves of (a) lateral load versus deflection, (b) deflection distribution along pile depth for GCP under different composite ratio.

CONCLUSIONS

A brief introduction to the GCP principle, construction method, and QA/QC is given in this paper. Based on the studies comparing bearing capacity and composite ratio of GCP with those of conventional concrete pile and gravel pile, some major conclusions may be drawn from these results as follows:

(1) Gravel-concrete composite pile is one of the most cost-effective piles. In this case, when compared with conventional gravel pile, the vertical compressive, uplift, and lateral bearing capacity of GCP with 4/15 composite ratio can be improved nearly 3.0 times, 2.5 times, and 4.9 times, respectively.

(2) The vertical (both compressive and uplift) and lateral bearing capacities of GCP increase as composite ratio decreases. In this soil site condition, when composite ratio is less than 6/15, the lateral bearing capacities are nearly the same because critical pile length exists.

ACKNOWLEDGMENTS

The author acknowledges financial support from the National Science Foundation of China (No. 51008116).

REFERENCES

- Kong, G. Q., Ding, X. M., Chen, Y. M. and Yang, G. (2010). "Methods for one vibro compaction gravel - concrete composite pile." C.N. Patent 101781888 A.
- Itasca, (2000). Fast Lagrangian Analysis of Continua in 3-Dimensions, version 3.0, manual, Itasca, Minnesota.
- Liu, H. L., Chu, J., and Deng, A. (2009a). "Use of large-diameter, cast-in situ concrete pipe piles for embankment over soft clay." *Can. Geotech. J.*, 46(7), 915-927.
- Matlock, H. (1970). "Correlations for design of laterally loaded piles in soft clay." *Proc., 2nd Offshore Technology Conf., Houston*, 577-594.
- Reese, L. C., Wang, S. T., Isenhower, W. M., Arrellaga, J. A., and Hendrix, J. (2004). *User's manual of LPILE plus 5.0 for windows*, Ensoft, Inc., Austin, Tex.
- Reese, L. C., and Welch, R. C. (1975). "Lateral loading of deep foundations in stiff clay." *J. Geotech. Eng. Div.*, 101(7), 633-649.

Time-Frequency Analysis of Seismic Response of a High Steep Hill with Two Side Slopes when Subjected to Ground Shaking by using HHT

Yang Changwei¹, Zhang Jianjing², Fan Gang³, Huang Zhiyi⁴, and Zhang Cheng⁵

^{1,2,3,4,5}Department of Civil Engineering, Southwest Jiaotong University, Chengdu, China, 610031. Phone: 0086-28-87601117; FAX: 0086-28-87601117; E-mail: yangchangwei56@163.com

ABSTRACT

In this paper, a high steep hill with two side slopes near National Road 213 is used as a prototype. A full process from initial deformation to sliding of the slope during ground shaking is simulated by a new discrete element method CDEM. First, we compare simulation results with those from a shaking table test, verifying that our simulation is reliable. Then seismic responses of the slope are re-analyzed by a new time-frequency analysis method HHT. The results: before the sliding of slope occurs, amplifications of the acceleration in the slope are the most prominent while both instantaneous frequency of the acceleration in the slope wash-sliding bed structural plane and natural frequency of the slope wash are close to each other. Meanwhile, the instantaneous frequencies of the acceleration in the slope wash are in a limited range, but those reduce suddenly after the sliding of slope wash occurs. The starting time of sliding and the arrival time of peak value of the instantaneous energy are synchronous, or the former lags behind the latter slightly. With respect to input seismic wave, regardless of whether it occurs on the steep slope, on the gentle slope, or inside the slope, the peak value of instantaneous energy amplifies as the elevation increases. Generally speaking, amplification of the peak value of instantaneous energy in a vertical direction > that of instantaneous energy in a horizontal direction, and amplification of the peak value of instantaneous energy on a steep slope > that on a gentle slope > that inside the slope.

INTRODUCTION

On May 12, 2008, the Great Earthquake of M_S 8.0 struck Wenchuan, Sichuan Province in China and caused a lot of geohazards such as collapse, landslide, and debris flow. Since that time, the geohazards induced by the earthquake have been widely studied by experts and scholars because of their powerful destruction. Among the geohazards, landslide is one of the most frequently researched (2003). On the sliding mechanism of landslides induced by earthquakes, there are many exciting

results. For examples, Cao (2011) simulated the whole process of initial deformation and subsequent movements of the slope wash by using discrete element software UDEC. Zhang (1993) thought that the impact of the earthquake on the slope stability come from two different aspects: the cumulative effect and the triggering effect. Cui (2010) thought that the time difference produces a coupling effect which considered the regionalism and the space heterogeneity of triggering the initial collapse of the slope. Wu (1995) analyzed the sliding mechanism of landslides induced by the earthquake with the spectral analysis method. Jin (2011) found that the predominant frequency of seismic waves had a remarkable effect on the dynamic responses of slope.

From the above results on seismic responses of a high steep hill, it is known that most researchers in their studies have mainly concentrated their attention on two fields: first, analyses have been done in the time domain alone, which considers the dynamic responses of peak values and time-history curves of acceleration, velocity, and displacement in the time domain; second, analyses have been done within the frequency domain alone, which considers the dynamic responses of Fourier spectrums and energy spectrums of the acceleration and velocity in the frequency domain. However, studies on seismic responses of a high steep hill with two side slopes based on combined time and frequency domains are very few. At the same time, a seismic wave is a complicated and non-stationary signal, whose instantaneous frequency gradually changes with time. Therefore, a study on seismic responses of a high steep hill with two side slopes in combined time and frequency domains is necessary.

Therefore, combined with field investigation results from the “5.12” Wenchuan earthquake, this paper will select the structure type of slope which has seen tremendous destruction in the Wenchuan seismic hazard area. By using the related data from our shaking table test, seismic responses of a high steep hill with two side slopes was analysed in combined time and frequency domains, and by using the Hilbert-Huang transform.

HILBERT-HUANG TRANSFORM

Normally, a non-stationary signal can be decomposed into a series of intrinsic mode function (IMF) components by using ensemble empirical mode decomposition (EEMD) method. The instantaneous frequency of each IMF will be derived by using the Hilbert-Huang transform, and then the Hilbert spectrum will be obtained by integrating all the instantaneous frequency spectrums. The analytical signal, amplitude function, phase function and instantaneous frequency function can be obtained by using the Hilbert-Huang transform. The computational formulas are shown in Eqs.1 to 4.

$$Z(t) = c(t) + jH[c(t)] = a(t)e^{j\Phi(t)} \text{-----(1)} \quad a(t) = \sqrt{c^2(t) + H^2[c(t)]} \text{-----(2)}$$

$$\Phi(t) = \arctan \frac{H[c(t)]}{c(t)} \text{-----(3)} \quad f(t) = \frac{1}{2\pi} \frac{d\Phi(t)}{dt} \text{-----(4)}$$

From the above formulas, it is known that both amplitude and frequency are the function of time. If the amplitude is calculated by using a combined time and frequency domain approach, the Hilbert spectrum can be obtained, as shown in Eq. 5 .The marginal spectrum and the instantaneous frequency spectrum can be obtained by using Equations 6 and 7. The Hilbert spectrum can be obtained by integrating amplitude squared, as shown in Equation 8.

$$H(\omega, t) = \text{Re} \sum_{i=1}^n a_i(t)e^{j\Phi_i(t)} \text{-----(5)} \quad h(\omega) = \int_0^T H(\omega, t)dt \text{-----(6)}$$

$$IE(t) = \int_{\omega} H(\omega, t)dt \text{-----(7)} \quad ES(\omega) = \int_0^T H^2(\omega, t)dt \text{-----(8)}$$

Shaking table test model and numerical model of two-side high steep hill

In order to study the seismic responses of a high steep hill with two side slopes, a shaking table test of the high steep hill with two side slopes was performed by simulating the hill on the left side of National Road 213. The shaking table test model is shown in Figure 1. This model is 1810mm high, 3500mm wide and contains a steep slope and a gentle slope. The angle of the steep slope is 50°-60°, and the angle of the gentle slope is 42°-50°, both of which are used to study the effect of slope angle on the seismic responses of a high steep hill. In order to study the seismic responses of the slope wash at different levels on the high steep hill with two side slopes, the shaking table test model simulates surface soil and the weathered layer generalized as three slope washes, which are located at the bottom, in the middle, and at the foot of slope. In order to study the landslide mechanism of a high steep hill with two side slopes induced by the earthquake, this paper developed a numerical analysis model according to the shaking table test model and a lot of inner and surface monitoring points have been set, which are used to monitor the acceleration, velocity, and displacement time histories of the slope wash and the sliding bed. The three points, B4, B6, and B8, are not only on the shaking table test model, but also on the numerical simulation model, which are used to verify the validity of numerical simulation results. The other monitoring points are additional points in the simulation, as shown in Figure 2.



Figure 1. Shaking table test model

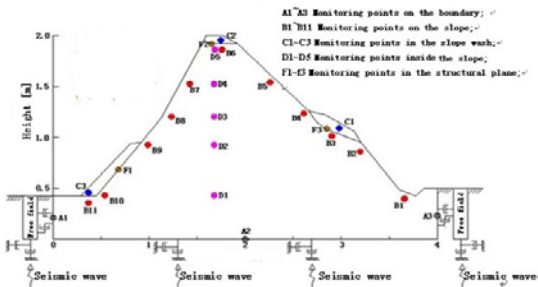


Figure 2. Numerical model and the distribution of monitoring points

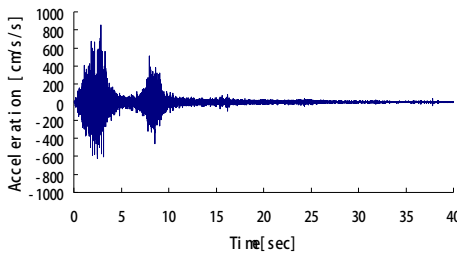
NUMERICAL SIMULATION

Constitutive model and parameters of the material. In dynamic calculation, the rock and soil masses of the slope wash and sliding bed will produce some plastic deformation before the instability of slope occurs. Therefore, both slope wash and sliding bed are modeled by an elastic or visco-elastic constitutive model and the Mohr-Coulomb failure criterion is used. After instability of slope occurs, a rigid constitutive model will be used to model the sliding wash, and for the sliding bed it may produce deformation during the earthquake, so the sliding bed is modeled by elastic-plastic constitutive model and the Mohr-Coulomb failure criterion is used. Because the slope wash-sliding bed structural plane shows some damage, such as slippage and rupture, the structural plane is modeled by a brittle rupture constitutive model and the Mohr-Coulomb failure criterion is used. It is noted that although the slope wash-sliding bed structural plane is complex and with randomness, the random structural plane model of CDEM can solve the above problems. In the random structural plane model, the springs linking structural planes or discrete elements can be calculated by using a node-mixed element model. The relative parameters are shown in Table 1.

Table 1. Physical and Mechanical Parameters of the Slope Wash, Sliding Bed and Structural Plane

Model	Density (KN/m ³)	Cohesion (KPa)	Inner frictional angle (°)	Modulus of elasticity (MPa)	Poisson's ratio
Sliding bed	22	15.6	37.9	75	0.25
Slope wash	21	8.3	28.8	10	0.35
Slope wash -sliding bed structural plane	Normal stiffness	Shear stiffness	Inner frictional angle (°)	Tension	Cohesion
Inside the slope wash	6.0e8 Pa	3.0e8 Pa	32°	4.33 KPa	8.1 KPa
Structural plane(at the foot of the hill)	4.5e9 Pa	2.3e9 Pa	32°	1.21 KPa	2.3 KPa
Structural plane (in the middle of the hill)	4.5e9 Pa	2.3e9 Pa	32°	1.05 KPa	2.3 KPa
Structural plane (at the top of the hill)	6.2e9 Pa	6.2e9 Pa	36°	3.86 KPa	7.2 KPa

Boundary conditions and ground input motion. In dynamic numerical simulation of slope, imposing reasonable artificial boundary conditions and inputting reasonable seismic waves are very important. In order to dissipate reflected seismic waves on boundaries, in this paper absorbing boundary is imposed at the bottom of the model and the free boundary on both sides of the model. Because the calculation results need to make some comparisons with the shaking table test results, this paper selects the input seismic wave which is the same as that of the shaking table test. At the same time, this seismic wave is a compressed wave of the Wolong record. The peak values of the horizontal and vertical waves are 957cm/s/s and 857cm/s/s, and the duration is 40s. The horizontal and vertical time histories are shown in Figures 3 and 4.

**Figure 3. Time-history curve of the horizontal acceleration**

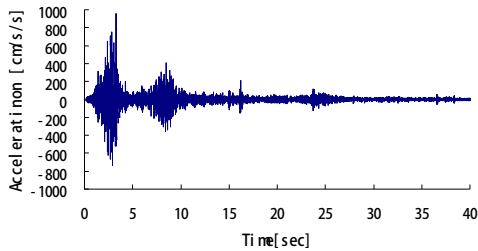


Figure 4. Time-history curve of the vertical acceleration

NUMERICAL SIMULATION RESULTS AND ANALYSIS

Verification of the numerical simulation results. In order to verify the validity of the numerical simulation results, this paper selects three points, B6, B4, and B8, which are used to do a comparison. The simulation results and experimental results are shown in Table 2.

Table 2. Comparison of Peak Ground Accelerations between the Shaking Table Test Results and the Simulation Results

Monitoring points	Simulation results (m/s/s)		Shaking table test results (m/s/s)		Error (%)	
	Horizontal	Vertical	Horizontal	Vertical	Horizontal	Vertical
B4	23.1	21.35	23.843	22.321	-3.11	9.71
B6	27.5	32.5	27.026	30.504	1.75	6.54
B8	22.1	31.2	24.545	30.504	9.96	2.28

Note: In Table 2, Error = (simulation results-experimental results)/experimental results.

Table 2 shows that the maximum errors of the horizontal and vertical accelerations at the three points all are less than 10%; the minimum errors of the horizontal and vertical accelerations are only 1.75% and 2.28%, respectively. The simulation results consist of the shaking table test results. The result verifies that the simulation model is valid and the results are reliable.

Amplification of peak value of the instantaneous energy. In order to study the amplification of the peak value of instantaneous energy along the height of the hill, this paper sets monitoring points B1-B6 on the gentle slope, monitoring points B6-B10 on the steep slope and monitoring points D1-D10 inside of the hill. These monitoring points are used to monitor acceleration. Monitoring point eB6 is at the top of the hill, namely the crossing between the gentle and steep slopes. The acceleration time histories can be transformed into instantaneous energy by using Eq.6, and then the peak value of each instantaneous energy time history is identified and studied.

The calculation results show that the peak value of instantaneous energy is amplified with the increase of elevation, regardless of whether it takes place on the steep slope, on the gentle slope, or inside the slope. The peak values and amplification coefficients of instantaneous energy are shown in Tables 3 and 4.

Table 3. Peak Values and Amplification Coefficients of Instantaneous Energy in the Horizontal Direction

Distance away from the bottom h/m	Steep slope [(m/s ²) ²]		Gentle slope[(m/s ²) ²]		Inside the slope[(m/s ²) ²]	
	Horizontal (No.)	Magnification coefficient	Horizontal (No.)	Magnification coefficient	Horizontal (No.)	Magnification coefficient
1.75	828 (B6)	2.89	821 (B6)	2.87	827 (D5)	2.89
1.35	656 (B7)	2.29	741 (B5)	2.59	706 (D4)	2.47
1.05	666 (B8)	2.33	692 (B4)	2.42	646 (D3)	2.26
0.75	643 (B9)	2.45	652 (B2)	2.28	566 (D2)	1.98
0.25	737 (B10)	2.58	574 (B1)	2.01	494 (D1)	1.73

Table 4. Peak Values and Magnification Coefficients of Instantaneous Energy in the Vertical Direction

Distance away from the bottom h/m	Steep slope [(m/s ²) ²]		Gentle slope[(m/s ²) ²]		Inside the slope[(m/s ²) ²]	
	Vertical (No.)	Magnification coefficient	Vertical (No.)	Magnification coefficient	Vertical (No.)	Magnification coefficient
1.75	913 (B6)	3.81	913 (B6)	3.81	906 (D5)	3.78
1.35	903 (B7)	3.77	819 (B5)	3.42	721 (D4)	3.01
1.05	874 (B8)	3.65	589 (B4)	2.5	563 (D3)	2.35
0.75	815 (B9)	3.40	537 (B2)	2.24	491 (D2)	2.05
0.25	735 (B10)	3.07	455 (B1)	1.90	436 (D1)	1.82

Note: In Tables 3 and 4, the amplification coefficient = the simulation results of peak value of

instantaneous energy/ the peak value of instantaneous energy of the input seismic wave.

Tables 3 and 4 show that the peak values of instantaneous energy in horizontal and vertical directions are amplified with the increase of evaluation on the gentle slope; for example, amplification coefficients of peak value of instantaneous energy in a horizontal direction are within 2.5-3, and in a vertical direction are within 3.0-4.0. Peak values of the instantaneous energy in horizontal and vertical directions are also amplified with the increase of evaluation on the steep slope; for example, the amplification coefficients of peak values of the instantaneous energy in a horizontal direction are within 2.0-3.0, and in a vertical direction are within 1.9-4.0. Peak values of the instantaneous energy in horizontal and vertical directions inside of the hill are amplified with the increase of evaluation; for example, the amplification coefficients of peak values of the instantaneous energy in a horizontal direction are within 1.7-3.0 and in a vertical direction are within 1.8-3.8. Generally speaking, amplification of the peak value of instantaneous energy in a vertical direction > that of the instantaneous energy in a horizontal direction, and amplification of peak value of the instantaneous energy on a steep slope > that on a gentle slope > that inside the slope.

Differences of acceleration responses between slope wash and rock bed. In order to study the differences of acceleration responses between slope wash and sliding bed, this paper sets up three group points, (B6,C2), (B3,C1) and (B11,C3), which are used to monitor the characteristics of seismic wave propagation in the slope wash and sliding bed. Because sliding of soil wash at the middle of the gentle slope and at the foot of the steep slope occur after 3.93s (input acceleration time history), and then the monitoring points lose their working abilities in the following loading process. Therefore, acceleration time histories from 0s-3.5s are selected and used to study the characteristics of seismic responses. Due to the limited length of this paper, only some representative results are selected, which are the horizontal accelerations in the middle of the gentle slope. The researchers then transform them by HHT—Eq.6 and analyze the instantaneous frequency time-history curves.

This paper takes advantage of the Hilbert spectrum to define the instantaneous frequency, as follows:

$$\omega(t) = \max(H(t, \omega))$$

In the above formula, $H(t, \omega)$ is the Hilbert Spectrum corresponding to the original acceleration time-history curve; $\omega(t)$ is the value of ω which can make the instantaneous Hilbert spectrum $H(t, \omega)$ reach the maximum value. So this ω is the predominant frequency of Hilbert spectrum: $H(t, \omega)$.

In Figure 7, the blue shows the contact elements are undamaged, the red shows the contact elements are shear failure, and the green shows the contact elements are the tension failure.

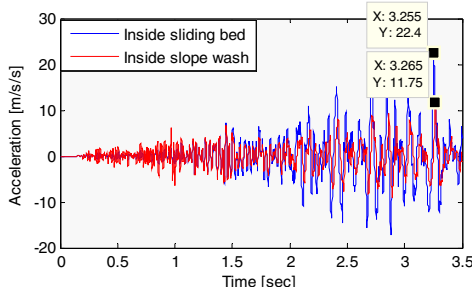


Figure 5. Time history of the horizontal acceleration

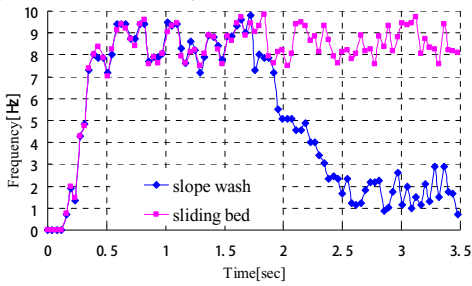


Figure 6. Time history curve of the instantaneous frequency

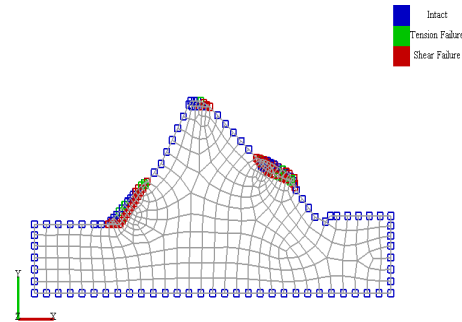


Figure 7. Distribution of the shear failure points

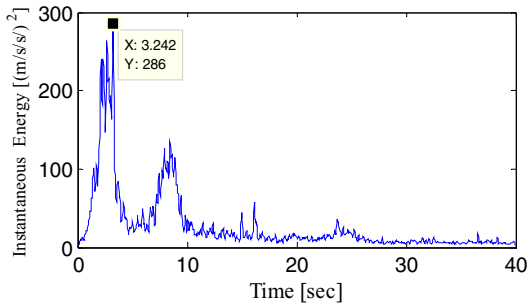


Figure 8. Time-history curve of the input instantaneous and the tension failure points at $T=3.2525s$ energy

Figures 5 and 6 show that there are great differences between the horizontal acceleration responses from the slope wash and from the sliding bed. First, when seismic ground motion intensity is smaller, the horizontal acceleration in the slope wash is greater than that in the sliding bed, and the instantaneous frequencies of the horizontal acceleration in the slope wash and in the sliding bed are in a range of 7Hz-10Hz. The horizontal acceleration in the sliding bed exceeds that in the slope wash with the increase of seismic ground motion intensity. At the same time, the instantaneous frequency of horizontal acceleration in the slope wash gradually decreases and reaches a stable level within 1Hz-3Hz. Second, there are greater differences in the arrival time of the peak values of horizontal acceleration between the slope wash and the sliding bed, and there is some lag in arrival time for the slope wash.

The above-mentioned phenomena may require further explanation: first, at the beginning of the earthquake, seismic ground motion intensity is small, and there are few discontinuous shear failure points. As a result, there is no relative slip between slope wash and sliding bed, and the movements of the slope wash and sliding bed have consistency. As a result, the instantaneous frequency of the acceleration in the slope wash reaches a stable level within 7Hz-10Hz. When seismic waves reach the structural plane, amplification of the peak value of acceleration in the slope wash is produced. Based on the wave propagation theory, this paper gives some possible reasons for the amplification: (1) When seismic waves spread from the sliding bed to the overlaying soil, the reflection waves will produce wave field separation phenomena, such as the P (SV) wave transformed into the SV (P) wave when the P (SV) wave is reflected in the structural plane. The complex seismic wave field is formed by superposition of various types of reflection waves, which leads to the amplification of movements of the overlaying soil. (2) The energy of seismic waves is mainly provided by P wave, SH wave and SV wave, but they all have the characteristic of amplifying movements of the overlaying soil when they propagate

from the sliding bed to the overlaying soil. At the same time, amplifications of the acceleration in the slope wash are the most prominent while both instantaneous frequency of the acceleration in the slope wash-sliding bed structural plane and natural frequency of the slope wash are close to each other. Second, the difference in acceleration between in the slope wash and in the sliding bed increase with the increase of the seismic ground motion intensity, which gives rise to the increase of shear failure points on the structural plane; these failure points gradually link up, and then the shear failure plane is developed. Because of the relative slippage between the slope wash and the sliding bed, the movements of the slope wash and the sliding bed have some nonconformity, and the above wave propagation theory is no longer in force, which then leads to the dissipation of seismic energy at the structural plane. The nonconformity of movements of the slope wash and the sliding bed increases with the increase of relative slippage, which leads to a decrease in the instantaneous frequency of horizontal acceleration in the slope wash and that of the horizontal acceleration in the sliding bed at $T=1.5s-2.5s$, and then reach a stable level within $1Hz-3Hz$. At the same time, the increase of relative slippage causes an increase of dissipation of seismic energy, which then leads to the rapid attenuation of horizontal acceleration in the slope wash, and then the horizontal acceleration in the sliding bed exceeds that in the slope wash.

At last, Figure 7 shows that at $T=3.2525s$, the shear failure points of the slope wash at the foot of the hill have formed the continuous shear failure plane which occurs throughout the whole structural plane of the slope wash. There is some collapse of the slope wash which happens in the middle of the hill. A few of the shear failure points and tension failure points occur in the structural plane at the top of the hill. Therefore, this paper defines that the collapse of the high steep hill with two side slopes has occurred. Figure 8 shows that the arrival time of peak value of the instantaneous energy of the input acceleration is $T=3.242s$, which is basically consistent with the arrival time of the collapse of the high steep hill with two side slopes. The above phenomenon is not only consistent with the results of shaking table test but also consistent with the seismic survey results from the time when the collapse happened during the 5.12 Wenchuan earthquake.

CONCLUSION

Combining with the seismic survey data in the 5.12 Wenchuan Earthquake, this paper used a new discrete element method, CDEM, to study the seismic responses of a high steep hill with two side slopes. The major conclusions are summarized as follows:

First, when the seismic ground motion is small, there is no relative slippage between the slope wash and the sliding bed. The acceleration in the slope wash is greater than that in the sliding bed, and amplifications of the acceleration in the slope wash are the most prominent while both instantaneous frequency of the acceleration

in the slope wash-sliding bed structural plane and natural frequency of the slope wash are close to agreement. At the same time, the instantaneous frequency of the acceleration in the slope wash is in a limited range; when some relative slippages between the slope wash and the sliding bed appear with an increase of the seismic ground motion intensity, the horizontal acceleration in the slope wash increasingly exceeds that in the sliding bed. Meanwhile, the instantaneous frequency of the horizontal acceleration in the slope wash gradually decreases and reaches a stable limit range. Second, the starting time of slope sliding and the arrival time of the peak value of instantaneous energy are synchronous, or the former lags behind the latter slightly. Third, with respect to input seismic wave, regardless of whether it occurs on the steep slope, on the gentle slope, or inside the slope, the peak value of instantaneous energy amplifies as the elevation increases. Generally speaking, amplification of the peak value of instantaneous energy in a vertical direction > that of instantaneous energy in a horizontal direction, and amplification of the peak value of instantaneous energy on a steep slope > that on a gentle slope > that inside the slope.

ACKNOWLEDGEMENTS

Supported by Major Program of National Natural Science Foundation of China (41030742).

REFERENCES

- Cao, Y.B., Dai, F.C., and Xu, C., et. al. (2011). "Discrete Element Simulation of Deformation and Movement Mechanism for Tangjiashan Landslide." *Journal of Rock Mechanics and Engineering*, 30(1), 2878- 2887.
- Cui, F.P, Hu, R.L., and Yin, Y.P. (2009). "Discrete Element Analysis of Collapsing and Sliding Response of Slope Triggered by Time Difference Coupling Effects of P and S Seismic Waves – Taking Tangjiashan Landslide in Beichuan County for Example." *Journal of Rock Mechanics and Engineering*, 29(2), 319-327.
- Hu, G.T. (1995). "Landslide Dynamics." Beijing, *Geological Publishing House*.
- Jin, A.B., Sun, J.H., and Gao, Y.T. (2011). "Numerical modeling on the dominant frequency and its influence factors of slope dynamic response." *Journal of University of Science and Technology Beijing*, 33(3):383-387.
- Li, Z.S. (2003). "The Review of Research on the Seismic Landslide Hazard At Home and Abroad." *Journal of Catastrophology*, 18 (4), 64–70.
- Wu, H.Z. (2010). "Study on Analysis Method for Spectrum of Seismic Landslide." *Ph.D. dissertation*, Wuhan, Institute of Rock and Soil Mechanics Chinese Academy of Sciences.
- Zhang, Z.Y., Wang, S.T., and Wang, L.S. (1993). "Analytical Principle of Engineering Geology." Beijing, Geological Publishing House.

Experimental and Numerical Investigation of the Influence of Dilatancy on a Shallow Anchor Plate in Sand

Jinyuan Liu

Dept of Civil Engineering, Ryerson University, Toronto, Canada

ABSTRACT

This paper presents both experimental and numerical investigations on the influence of soil dilatancy on the behaviour of a shallow anchor plate in sand. A series of scaled model tests are performed to obtain the soil displacement field around an uplifting anchor using an image processing technique. The failure plane is identified by locating the points with maximum shear strain values deduced from the displacement field. The finite element package, Plaxis, is used to perform numerical analyses. The results show that the numerical analyses can simulate the experimental results by varying the angle of dilatancy during shearing. Two distinctively different failure modes are observed in loose and dense sand conditions. A significant compaction is experienced in loose sand to form a bell shaped compaction zone above the anchor plate. In dense sand two shear bands extend outward to the ground surface forming an angle of approximately the dilatancy angle of soil with the vertical.

INTRODUCTION

Anchor plate, as an efficient and reliable anchorage system, has been widely used to resist uplift loads produced by structures, such as transmission towers, offshore platforms, submerged pipelines, and tunnels. With the extensive use of anchors, the understanding of their behaviour has attracted the attentions of researchers for more than half a century. The pullout capacity of an earth anchor plate relies on many factors, including the anchor geometry, the embedded depth, surrounding soil conditions, etc.

Many testing methods have been used to study the behaviour of anchors, including field tests, laboratory tests, numerical analyses, and analytical solutions. The large-scale field tests on foundations for transmission line towers and shafts contributed to the development of early empirical design methods (Sutherland 1988). The scaled model tests have been performed to understand the failure modes of anchors in various anchor and soil conditions (Vesic 1971). Numerical methods including the finite element method (FEM) have also been used in studying anchors in both sand

and clay. For example, Rowe and Davis (1982) used FEM to analyze a strip anchor in sand and found that the dilatancy could significantly influence the ultimate pullout resistance. Sakai and Tanaka (2007) performed FEM analysis of shear band development for a circular anchor in sand. Analytical solutions were also developed to calculate the pullout capacity of the anchor in sand based on equilibrium approach on an assumed failure plane (Meyerhof and Adams 1968).

Among various failure modes, there are mainly three distinctive failure modes proposed by various researchers, as shown in Fig. 1. The first failure surface is a frictional cylinder, as shown in Fig. 1a, which was first proposed by Majer (1955). The second type is a truncated cone, proposed firstly by Mors (1959), extending from the anchor with an apex angle of $90^\circ + \phi$, where ϕ is the friction angle of soil, as shown in Fig. 1b. The third type is a circular surface extending from the edge of the anchor and intersecting the ground surface with an angle of approximately $45^\circ - \phi/2$. Although extensive research has been performed, the discrepancies between the prediction and actual behaviour of an anchor plate are still varying extensively. It is believed that these discrepancies are due to the lack of full understanding of the behaviour of an anchor and the interaction between the anchor and soil during anchor uplifting.

An experimental investigation using digital image correlation (DIC) method is presented in this paper along with a finite element analysis on the behaviour of a shallow anchor plate in sand. Distinctive soil failure modes were observed between loose sand and dense sand.

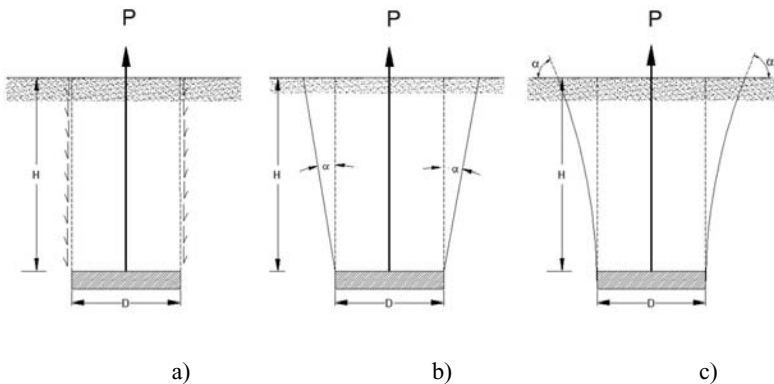


Fig. 1 Three different failure modes of a soil anchor

EXPERIMENTAL PROGRAM

Experimental Set-up

An experimental test set-up was developed in this research, which consisted of a mono complementary metal oxide semiconductor (CMOS) camera, a loading frame, a Plexiglas mould, and a computer. The loading frame consisted of a load cell and a linear variable differential transformer (LVDT). A data acquisition system was developed in-house to acquire load and displacement in the anchor.

The mould had dimensions of 500 mm (length) x 300 mm (width) x 500 mm (depth). A semicircular anchor with a diameter of 50.8 mm and a thickness of 5 mm was used in this study. A 1 m long threaded steel rod with a diameter of 5 mm was used to uplift the anchor. The rod was connected to the load cell before connecting to the loading frame through an adaptor. The anchor was lifted along a guide slot upward by manually rotating the handle.

In order to study the influence from the soil density, two density conditions were tested: 1) loose sand (LS); 2) dense sand (DS). The maximum dry unit weight was determined to be 16.5 kN/m^3 and the minimum unit weight was 13.8 kN/m^3 . Sand with an effective grain size, D_{10} , of 0.56 mm was classified as SP uniformly graded according to the Unified Soil Classification System.

Sample Preparation

The soil density was controlled by pulverization and tamping methods. As for loose samples, the samples are prepared through pulverization, while the dense sample were prepared using pulverization plus tamping in each layer until the design depth was reached. A wide range of anchor embedment depths were used in the tests, which corresponded to an embedment ratio (ER) from 1 to 9. This paper focuses on the shallow anchor case with an ER of 3.

First, the camera was set approximately 300 mm away from the mould with its optical axis perpendicular to the mould. Second, the data acquisition and image capture drivers were activated in the PC. Third, the camera was set in auto mode for data acquisition with a desired frame rate. One frame per second was used in this study. Fourth, the anchor was uplifted by manually rotating the handle while the images and data of loads and displacements were acquired by the computer. The rate of uplifting was controlled at approximately 3 mm/min while load and displacement data acquired through the load cell and the LVDT were saved automatically to the computer. Fifth, the test was terminated until an apparent failure rupture was observed in the sample or no additional loading could be taken by the anchor. Sixth, the images, a log file with time corresponding to each individual image, and the load

and displacement file were transferred to a desired folder in the computer. More details can be found in Liu *et al.* (2011).

Image processing Technique

Digital image correlation (DIC) is a classic pattern recognition technique, where two images are compared to obtain the relative displacement between them. In geotechnical engineering, DIC has been recently used to study soil deformations during shear by many researchers (Gudehus and Nubel 2004). The accuracy of DIC can be improved to the order of $1/10^{\text{th}}$ to $1/20^{\text{th}}$ of a pixel by approximating the discrete cross-correlation peak function with a continuous function and then estimating the peak from the continuous function (Raffel *et al.* 2007).

In this study the PIVview2c software (PIVTEC 2006) was used to calculate soil displacement fields during anchor uplifting. Unless noted, the features used in this research are the following: the initial interrogation window size of 96×96 , the final window size of 32×32 pixels, the step size of 16×16 pixels, the multi-grid interrogation algorithm, the least square Gaussian fit (3×3 points) for sub-pixel estimation.

EXPERIMENTAL RESULT ANALYSES

The Failure Displacement Field

Two images were taken to calculate their relative displacement by DIC. Each image was marked at its corresponding time in the load vs. displacement curves. Figs. 2 shows the calculated soil displacement fields for anchors with the same ER of 3. The background image are images taken at the moment of peak pullout resistances of the anchor.

Two distinctively different displacement fields were observed in the tests between loose sand and dense sand. In loose sand, soil displacement does not extend to the sample surface. Significant deformation occurs within a bulb-shaped influence zone, which extends from the anchor to a distance of about two times its diameter above. A significant compaction was noticed in this influence zone based on the gradient change in soil displacement.

A truncated cone, which resembles the one in Fig. 1b, was observed in dense sand. The middle of the block is fully mobilized and bounded by two shear zones on both sides. The shear zones start at the anchor edges and gradually widened until they reach the soil surface.

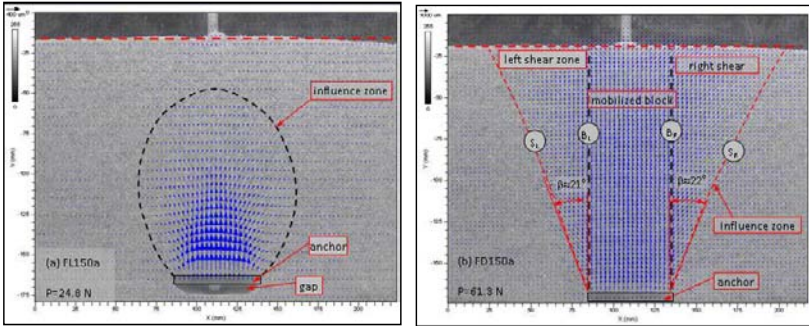


Fig. 2. Soil displacement field at the moment of peak pullout resistance (liu *et al.* 2011)

The Strain Field around an Uplifting Anchor

Strains can be calculated using the predicted displacements per Roscoe *et al.* (1963). The failure plane can be studied approximately by linking the points with maximum shear strain values. The contours of shearing strain field for both loose and dense conditions are shown in Fig. 3. The shearing strain field shows clearly the shearing zones at the right and left edges of anchor plate. The shearing zones begin from the upper edge of the anchor plate and extend outward to the ground surface with an inclination angle of 10° from the vertical.

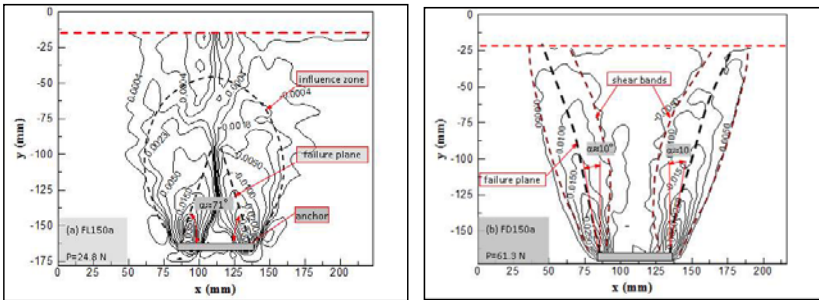


Fig. 3. Shear strain fields at the moment of peak pullout resistance (liu *et al.* 2011)

FINITE ELEMENT ANALYSIS

The FEM is used to investigate the density influence on the behavior of a shallow anchor plate. A 2-D axisymmetrical model is built in Plaxis to analyze the anchor with the ER of 3. The anchor plate is modelled as a 50 cm diameter steel plate with a

thickness of 5 cm. A predefined uniform displacement is applied to the anchor plate to simulate the pullout. The Mohr-Coulomb failure criteria are used to model natural sand while a linear elastic model is used for the anchor plate. In order to evaluate the differences between loose and dense soils, three main parameters are changed between the loose and dense sand conditions: Young's modulus, the angle of friction, ϕ , and the dilatancy angle of soil, ψ . Based on the data from various natural sands (Been & Jefferies 1985), the input parameters of soils, as shown in Table 1, are for the loosest and densest sand conditions normally measured from the laboratory testing.

Table 1. The input parameters in the finite element model

Condition	Failure model	E (MPa)	ϕ ($^{\circ}$)	ψ ($^{\circ}$)
Loose sand	M-C	15	32	0
Dense sand	M-C	50	48	20

NUMERICAL MODELLING RESULT ANALYSES

The Failure Displacement Field

A predefined displacement of 10 mm was used to uplift the anchor plate. The displacement fields for both loose and dense sand conditions are shown in Fig. 4. It can be found the soil movement propagates to the soil surface in dense sand while the soil movement is restrained within the soil mass in loose sand. This is in a good agreement with experimental results, as shown in Fig. 2. The soil displacement patterns are also similar to those measured from experimental tests.

The Shear Strain Field

The shear strain fields for both loose and dense sand conditions are shown in Fig. 5. The shear strain field in loose sand do not indicate a clear failure plane. While in dense sand a clear shear failure plane extends outward from the anchor edge and forms an angle with the vertical. The angle from the vertical is measured at 21° which approximately equals to the dilatancy angle of soil, 20° used in the analysis.

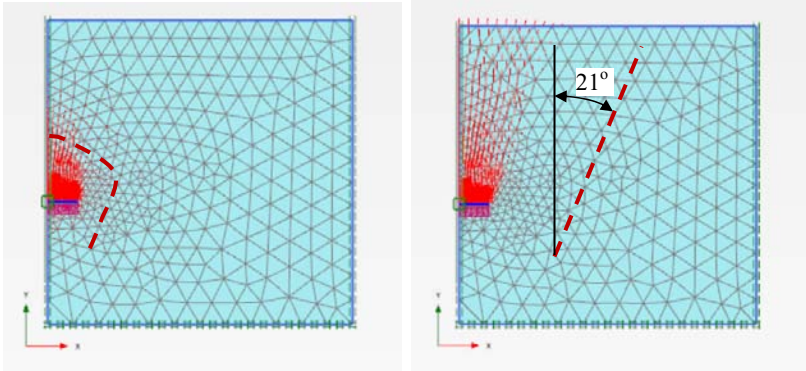


Fig. 4. The displacement fields from FEM. (LHS: loose sand, RHS: dense sand)

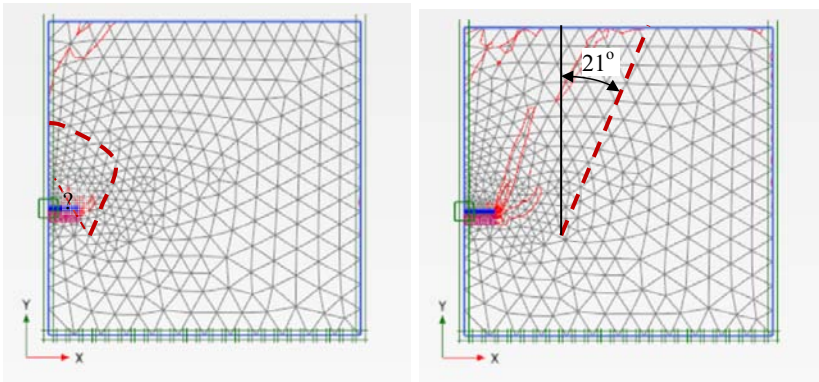


Fig. 5. The shear strain fields from FEM. (LHS: loose sand, RHS: dense sand)

CONCLUSIONS AND DISCUSSIONS

The influence of soil dilatancy on the behavior of a shallow anchor plate is studied through experimental tests using digital image correlation (DIC) method and finite element analysis in this paper. It can be found that the failure plane is significantly influenced by soil density condition. In loose sand, soil experiences a significant compaction process with most soil movement is restrained within the soil mass. While in dense sand a clear failure plane can be identified with shearing bands extending outward from the anchor edge to the ground surface. The failure plane forms an angle with the vertical, which approximately equals to the dilatancy angle of

soil. A failure mode is required to consider the influence of soil density for a better anchor plate design.

ACKNOWLEDGEMENTS

The author acknowledges the financial support of the Seed Fund from Ryerson University and a Discovery Grant No. 355425 from the Natural Sciences and Engineering Research Council (NSERC) of Canada.

REFERENCES

- Been, K. & Jefferies, G. (1985). "A state parameter for sands." *Geotechnique* 35(2), 99-112.
- Gudehus, G. and Nubel, K. 2004. "Evolution of shear bands in sand." *Geotechnique*, 54(3), 187-201.
- Liu, J. Liu, M., and Zhu, Z. (2011). "Sand deformation around an uplifting plate anchor." *Accepted by ASCE, Journal of Geotechnical & Geoenvironmental Engineering*.
- Majer, J. (1955). "Zur berechnung von zugfundamenten." *Osterreichischer Bauzeitschrift*, 10(5), 85-90.
- Meyerhof, G. G., and Adams, J. I. (1968). "The ultimate uplift capacity of foundations." *Canadian Geotechnical Journal*, 5, 225-244.
- Mors, H. (1959), "Behavior of pole foundations under train stresses Das Verhalten von Mastgruendungen bei Zugbeanspruchung." *Bautechnik*, 36(10), 367-378.
- Raffel, M., Willert, C., Wereley, S., and Kompenhas, J. (eds) (2007). *Particle Image Velocimetry: A Practical Guide*. 2nd edition, Springer, pp. 448.
- Roscoe, K., Arthur, J., & James, R. (1963). "The determination of strains in soils by an X-ray method." *Civil Engineering and Public Works Review*, Vol.58, 873-876 and 1009-1012.
- Rowe, R. K., and Davis, E. H. (1982). "the behaviour of anchor plates in sand." *Geotechnique*, 32(1), 25-41.
- Sakai, T., and Tanaka, T. (2007). "Experimental and numerical study of uplift behavior of shallow circular anchor in two-layered sand." *J. of Geotechnical and Geoenvironmental Engineering*, 133(4), 469-477.
- Sutherland, H. B. (1988). "Uplift resistance of soils." *Geotechnique*, 38(4), 493-516.
- Vesic, A. S. (1971). "Breakout resistance of objects embedded in ocean bottom." *American Society of Civil Engineers Proceedings, Journal of the Soil Mechanics and Foundations Division*, 97(9), 1183-1203.

Seismic Analysis of Lateral Loaded Pile under Strong Shaking: A Case Study from the 2008 Wenchuan Earthquake

Zhang Jianjing¹, NIE Chun-Xiao², Liu Qiang³, Yang Changwei⁴

^{1,2,3,4}Southwest Jiaotong University, Chengdu 610031, China. Phone:
0086-28-87601117; FAX: 0086-28-87601117; Email: 657365664@qq.com

ABSTRACT

Lateral loaded pile is a type of retaining structure widely used for stabilizing slope. Although various static design methods for lateral loaded pile are recommended in design codes, few seismic design methods for the pile were developed in the past. In this paper, the deformation and load acted on the lateral loaded piles with 3 degrees of tilt, caused by the ground shaking from the 2008 Wenchuan earthquake, are analysed by using software ABAQUS. To truly obtain the deformation and load of the pile, back-analysis and trial and error approaches are taken and measured pile displacements are used as control criteria. By using the back-analysis, we get the bending moment and shear force of the piles and earth pressure distribution on the piles. When compared with the values recommended from Chinese code, our results show that a seismic coefficient of 0.4 can work very well for evaluating seismic response of the piles subjected to the 2008 Wenchuan earthquake. On this basis, we re-analyze the seismic response of the lateral loaded piles when subjected to $PGA=0.1g$ (7 degrees), $0.3g$ (8 degrees) and $0.4g$ (9 degrees). Results show that a seismic coefficient of 0.3 is suitable for 7 degree, 0.35 for 8 degree, 0.4 for equal to and greater than 9 degree areas. In the paper, some impacted factors for lateral loaded pile design are also studied. Finally, a seismic design method for lateral loaded pile subjected to strong shaking is proposed.

INTRODUCTION

The 2008 Wenchuan earthquake not only caused huge disaster to people in Sichuan province, but also damaged many roadway and railway retaining walls. However, as a type of flexible structure, lateral loaded pile has displayed good seismic performance in the earthquake. But until now, not many studies have been carried out to study its aseismic mechanism and design method. Normally to explore

the aseismic mechanism and design method of a retaining wall, a shaking table test is considered to be better approach; however, the disadvantage of shaking table test is its “size effect.” In order to overcome the size effect a prototypic lateral loaded pile was selected in this paper and back analysis was conducted. The pile selected, located at DK1016+800—DK1016+835 of National Road 213, experienced ground shaking from the 2008 Wenchuan earthquake. To guarantee correction of the results from back analysis, tilt of the pile caused by the earthquake and soil parameters supported by the pile were measured after the earthquake. The tilt of the pile measured is used as a control index for our back analysis. Input ground motion used in the back analysis is an earthquake record recorded in the 2008 Wenchuan earthquake and the record site is close to the construction site of the pile. From the analysis, bending moment and earth pressure on the pile caused by the 2008 Wenchuan earthquake were obtained and aseismic mechanism is recognized. Further, results from our calculations and Chinese code were compared for different seismic intensity areas, and some significant recommendations were proposed for seismic design of lateral loaded pile.

Lateral loaded pile selected

The lateral loaded pile is located at DK1016+800 - DK1016+835 of National Road 213. Here a weathered layer consisting of a mixture of soils and gravels overlays the mountain. After excavation of the road, the weathered layer was tending to slide downward. In order to prevent the slope from sliding, the lateral loaded pile was designed and constructed, and the measurements of the lateral loaded pile are listed in Table 1. At the construction site, the height of the slope over the top of the lateral loaded pile is 71m and the angle of the slope is 41° . After the 2008 Wenchuan earthquake, the lateral loaded pile inclined 3° , creating permanent displacement of about 20cm at the top of the lateral loaded pile, as shown in Figure 1.

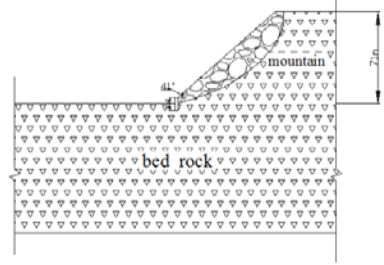
In this paper, the lateral loaded pile was selected as a typical project to carry out our analysis. The analysis is expected to ascertain the damage mechanism and design method of the lateral loaded pile. In the analysis, a unit width is taken out to do seismic response analysis, as shown in Figure 2.

Table 1. Geometry Parameters of the Lateral Loaded Pile

Width of pile (m)	Length of pile (m)	Height of pile (m)	Embedded depth (m)	Distance between two piles (m)
1.5	2.0	10.0	5.0	6.0

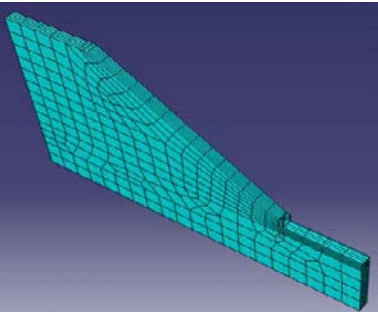


(a) Site of the lateral loaded pile

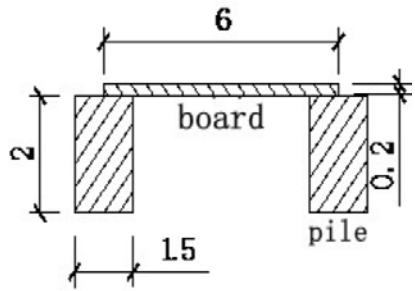


(b) Section of the lateral loaded pile site

Figure 1. Site and section of the lateral loaded pile



(a) Analytical model



(b) Plane of unit calculation width

Figure 2. Analytical model and plane of unit calculation width

Development of numerical analysis model

Soil strength and reinforced concrete parameters. In this paper, soil static and dynamic strength parameters were obtained by using static and dynamic triaxial tests. In the test, the diameter of the sample is $D=61.8\text{mm}$, and test results are shown in Figures 3 and 4. Table 2 gives soil parameters and also includes parameters for reinforced concrete plate and pile.

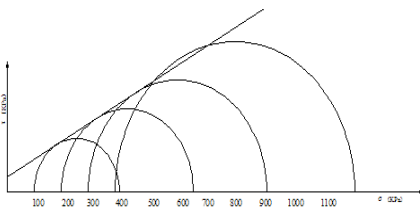


Figure 3. Static strength of accumulation body

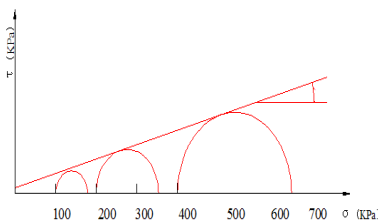


Fig. 4. Dynamic strength of accumulation body

Table 2. Rock, Sheet Pile and Soil Mechanics Parameters

Type	Density / (kN/m ³)	Modulus of elasticity /kpa	Poisson's ratio	Cohesion /kPa	Angle of friction / (°)
Accumulation		3.8*10 ⁴	0.25	25	33
Bedrock	e	2.1*10 ⁷	0.30	50	40
Retaining plate	2.6	2.4*10 ⁷	0.17		
Anti slide pile	2.5	2.4*10 ⁷	0.30		

Material damping. Determining material damping is very important in numerical analysis. A number of types of damping models have been proposed such as Rayleigh damping and composite modal damping. In this paper, the Rayleigh damping model is used. In the Rayleigh damping model, damping matrix [C] is the linear combination of mass matrix [M] and stiffness matrix [K].

$$[C] = \alpha[M] + \beta[K] \quad (1)$$

In Equation 1, α is the mass damping coefficient and β is the stiffness damping coefficient. In this study, a simplified calculation method was used, as shown in Equation 2.

$$\alpha = \xi_1 \omega_1 \quad \beta = \xi_1 / \omega_1 \quad (2)$$

Table 3. Sliding Mass Damping and Vibration Cycle

α	β	Vibration Cycle (s)
0.72	0.005	1.15

Absorbing boundary. In order to dissipate the reflected waves on the boundary, normally absorbing boundary is used. In the paper, viscoelastic boundary is selected and used with the numerical model. The reason for doing so is that it can satisfy the requirements of engineering accuracy and has better frequency stability. Coefficients of viscoelastic boundary are determined by Equations 3 and 4, as shown in Figure 5.

$$K_{BT} = \alpha_T G / R \quad C_{BT} = \rho c_s \quad (3)$$

$$K_{BN} = \alpha_N G / R \quad C_{BN} = \rho c_R \quad (4)$$

where, K_{BN} and K_{BT} are normal stiffness and shear stiffness, C_{BN} and C_{BT} are normal damping coefficient and tangential damping coefficient. The distance from a point source to artificial boundary is R, c_s and c_p are wave velocities of S and P

waves. G is shear modulus and ρ is mass density, α_T and α_N are the tangential and normal viscoelastic artificial boundary correction coefficients, as shown in Table 4.

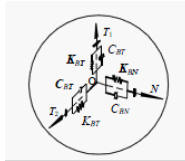
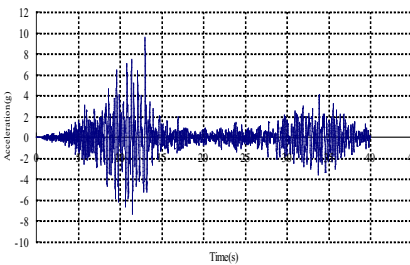


Figure 5. Spring and dash-pot on viscoelastic boundary

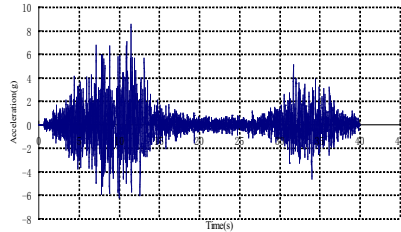
Table 4. Recommended Values of Correction Coefficient

Artificial boundary coefficient	Value range	Recommended coefficient
α_T	1-2.0	1.33
α_N	0.5-1	0.67

Input ground motion. In this paper, the acceleration time history recorded at the Wolong stations was selected. In order to save calculation time, the Wolong record with 40s is selected, because the 40s contain two main acceleration peak values. To reflect the real situation which the lateral loaded pile experienced, the effect of horizontal and vertical accelerations were considered in our analysis. The horizontal and vertical acceleration time histories of the Wolong record are shown in Figure 6.



(a) Horizontal component



(b) Vertical component

Figure 6. Acceleration time histories recorded at the Wolong station

Analysis of results

Results from numerical analysis. The results from numerical analysis show that the permanent displacement calculated at the top of the lateral loaded pile is 20.1 cm, as shown in Figure 7, which is nearly similar to that measured on site. The displacement of the pile in Figure 8 shows that the pile is a nearly rigid body, namely without deformation. From the analysis, bending moment, shear force and earth pressure distribution on pile were also obtained, as shown in Figure 9.

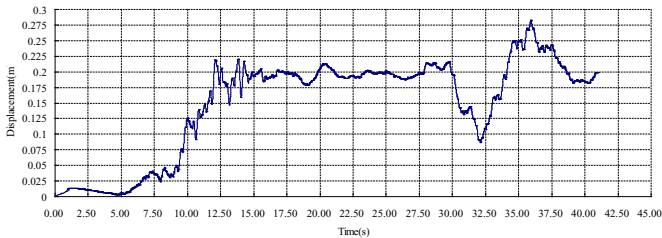


Figure 7. Displacement time history at the top of the pile

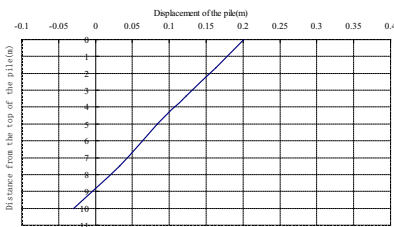


Figure 8. Displacement of the pile

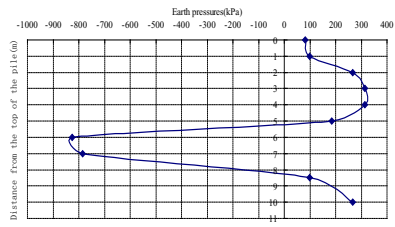


Figure 9. Earth pressure on the pile

Comparison of results from numerical analysis and Chinese design code. In Chinese design code, normally a pseudo-static method is used, rather than acceleration time history analysis. In calculating earth pressure produced by a slope in code, a horizontal acceleration modification coefficient C_z (taking 0.25) is often used. In calculation, inertia force produced by the slope is equal to $0.25 \times$ peak ground acceleration \times the mass of the sliding body. Normally C_z in Chinese design code is taken as a constant (0.25), For a common gravity retaining wall, perhaps taking C_z as a constant is correct, but for a lateral loaded pile, it may not be correct, because the slope behind the pile is high, and so acceleration amplification should be considered.

For the typical pile experienced the 2008 Wenchuan earthquake, the results from numerical analysis are greater than those from Chinese design code ($C_z=0.25$), as shown in Figure 10. Then we set $C_z=0.3, 0.35$ and 0.4 , in the calculation by using

Chinese design code and obtained that if $C_z=0.4$, the results from numerical analysis and Chinese design code are close, as shown in Figures 11 to 13.

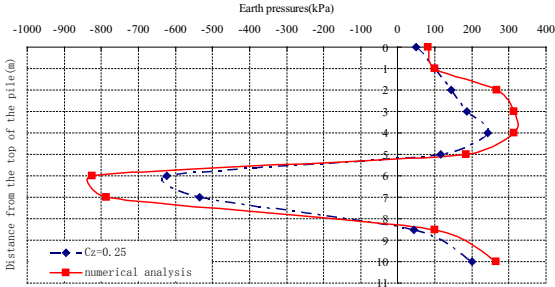


Figure 10. Comparison of earth pressures from numerical analysis and Chinese design code

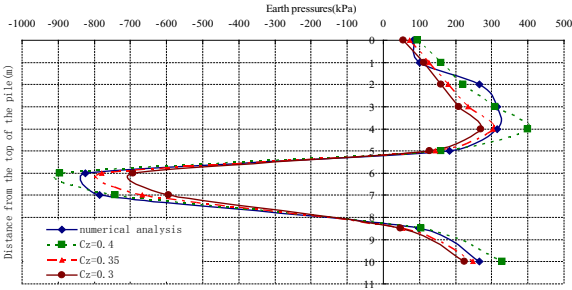


Figure 11. Comparison of earth pressures for numerical analysis and $C_z=0.3, 0.35$ and 0.4

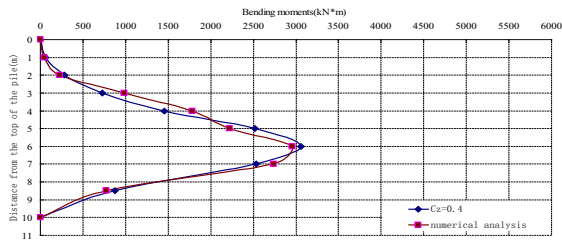


Figure 12. Comparison of bending moments from numerical analysis and $C_z=0.4$

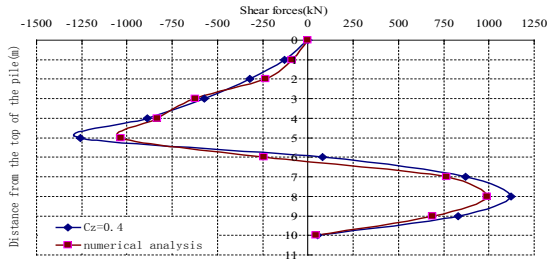


Figure 13. Comparison of shear forces from numerical analysis and $C_z=0.4$

The above results show that if $C_z=0.4$ is used in Chinese design code, the results from numerical analysis and Chinese design code are close for bending moment, shear force and earth pressure of the typical pile which experienced shaking from the 2008 Wenchuan earthquake..

Comparison of results from numerical analysis and Chinese design code for different seismic intensity areas. In order to verify if $C_z=0.25$ in Chinese design code is reasonable for different seismic intensity areas, this paper analyzed seismic response of the lateral loaded pile by using numerical analysis and Chinese design code for seismic intensities of 7^0 (0.1g), 8^0 (0.3g) and 9^0 (0.4g). To get acceleration time histories for seismic intensity of 7^0 (0.1g), 8^0 (0.3g) and 9^0 (0.4g), the horizontal acceleration time history in Figure 6 is scaled to 0.1g (intensity=7), 0.3g (intensity=8), and 0.4g (intensity=9), respectively. The scale factors obtained from the above are used to scale the vertical acceleration time histories. The results from the numerical analysis and Chinese design code are shown in Figures 14 to 16.

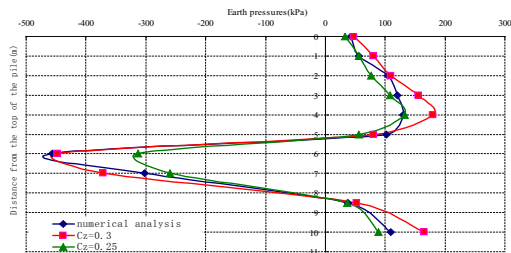


Figure 14. Comparison of earth pressures for numerical analysis and $C_z=0.25$ and 0.3

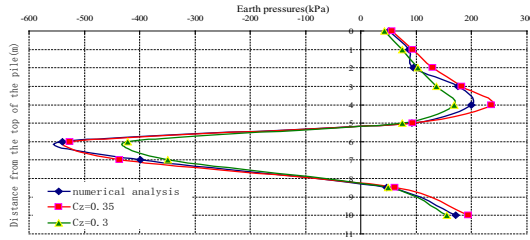


Figure 15. Comparison of earth pressures for numerical analysis and $C_z=0.3$ and 0.35

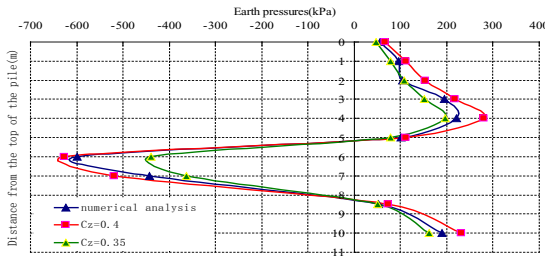


Figure 16. Comparison of earth pressures for numerical analysis and $C_z=0.35$ and 0.4

Figures 14 to 16 show that $C_z=0.3$ is suitable for seismic intensity of 7^0 , 0.35 for 8^0 , 0.4 for equal to and greater than 9^0 . If these horizontal acceleration modification coefficients are used for different intensity areas, safety of engineering design can be improved.

CONCLUSIONS

From the above analysis, some conclusions have been achieved as follows:

1. Results from numerical analysis and Chinese design code show that if $C_z=0.25$ is used, earth pressure is underestimated. Our study shows that $C_z=0.4$ can work well for evaluating seismic response of the pile when subjected to the 2008 Wenchuan earthquake.
2. We analyzed seismic responses of lateral loaded pile in different seismic intensity areas. Our results show that $C_z=0.3$ is suitable for a seismic intensity of 7^0 , 0.35 for 8^0 , 0.4 for equal to and greater than 9^0 . If C_z proposed are used for these seismic intensity areas, safety of engineering design can be guaranteed.
3. Lateral loaded pile displacement time history shows that damage extent of lateral loaded pile accumulates as the shaking time increases. Therefore, we can not

always simply use pseudo-static analysis in place of dynamic time history analysis, because the process may result in an energy accumulation effect.

REFERENCES

- Chen Q, Liu Q, Zhang J, Seismic response analysis of lateral loaded pile based on ABAQUS, Railway Construction, 2011.
- Chen Zhuyi, Soil slope stability analysis—Theory, Methods and Program. China water resources and hydropower press, 2002.
- Jiang DY, Zhu HH, Du YG, Slope stability analysis and protection technique, ChongQin University press, 2005.
- Shi YP, Zhou YR. ABAQUS –A detailed explanation to finite element method. China Machine Press, 2006.
- Geo-Slope International Ltd. SLOPE/W for slope stability analysis [M]. Versions, User's Guide, Canada, 2001.
- Liu L.P. & Jiang, D.Y. Recent advance of slope stability analysis method. Journal of ChongQin University (natural sciences) 2000, 23(3):115-118.
- Wang JC, Chen YK. ABAQUS applications in civil engineering. Zhejiang University press, 2006.
- Zhu YW. ABAQUS and analysis of geotechnical engineering. China books press, 2005.

Numerical modeling of strike-slip fault rupture propagation through soft soil deposit and embankment

Chen Qi¹, Liu Qiang², NIE Chun-Xiao³, Yang Changwei⁴

^{1,2,3,4}School of Civil Engineering, Southwest Jiaotong University, Chengdu 610031, China, P.O. Box.610031, Ph. 0086-28-87601117, FAX. 0086-28-87601117

Email: niechunxiao123@163.com

¹Keylaboratory of High-speed Railway Engineering, Ministry of Education,

P.O. Box.610031, Ph. 0086-28-87601117, FAX. 0086-28-87601117

Email: niechunxiao123@163.com

ABSTRACT

To explore the effect of strike-slip fault rupture propagation through soft soil deposit on embankment deformation, we performed dynamic response analyses by using the software ABAQUS. In the first step of our analysis, we discuss the effect of strike-slip fault rupture direction and velocity on the embankment deformation. The reason behind this is that in most studies fault rupture direction is assumed to be unilateral and its velocity is assumed to be slow, with linear changes occurring with time. As a result, in the study we assume that the fault rupture can unilateral or bilateral, and that the fault rupture velocity changes with time. Results from the analyses show that the ground displacement is greater than the displacement on the top of the embankment regardless of the fault rupture direction and velocity; bilateral fault rupture produces greater embankment displacement than the unilateral fault rupture and an approximately symmetrical embankment deformation shape with respect to the fault location. If the increments of the fault rupture velocity change with the increase of time, the embankment deformation is different. For example, if the increment of the fault rupture velocity reduces with time, the situation shows that the embankment deformation is smaller than if the increments of the fault rupture velocity increase with time. From the study, we also obtained the worst-case fault rupture direction and velocity, which will be of assistance to engineers' design.

INTRODUCTION

Recently, an increasing number of researchers, particularly those from the United States, Japan, and New Zealand have been placing their focus on the effect of fault rupture on structural performance in cases where the structure was built on a fault belt. They have done a significant amount of research including numerical

analysis and creating physical models. China is located between the West Pacific seismic zone and the Mediterranean—the Himalayan seismic zone, which is the most active seismic zone in the world and their tectonic activities are strong. To speed up the economic development in China, some structures such as highway, railway and industrial and civil building have to be built on the fault rupture belt or near it. Therefore the structural performance has become a concern to engineers when the fault ruptures.

This paper explores the effect of fault rupture on embankments built on the fault rupture belt under different conditions, draws conclusions, and makes suggestions that can be utilized in engineering practice.

Dynamic Response Numerical Simulation

Numerical model. The embankment prototype selected in the study is from a high-speed railway, which is 21m high and situated in a valley. The slope of the embankment is separated into three stages and each stage has a different slope. The highest and lowest elevations are at the valley with lengths of 400m, 57m, and 39m. The bottom of the valley consists of a soft soil layer (on the top) and brecciated form. CFG piles are used on the foundation of the embankment. The spacing of the pile is 1.6m, the diameter is 0.5m, and the length is 8.5m. The physical and mechanical parameters used in the paper are listed in Table 1. In the simulation, CFG pile is modeled by using a beam element, and elastic response is assumed; the embankment and foundation are modeled by a solid element and a More-Column model. The numerical embankment models and CFG pile foundation are shown in Figures 1 and 2.

Table 1. physical and mechanical parameters used in the paper

Materials name	Specific weight (KN/m ³)	Elastic modulus (Mpa)	Poisson's ratio	C (Kpa)	φ (°)
CFG piles	23	12000	0.19	-	-
Cushion	21	200	0.2	-	-
Soft soil	18.5	20	0.3	12	8
Silty clay	19	25	0.3	25	16
Breccia	24	1000	0.2	5	40
Fillings	20	150	0.3	10	30

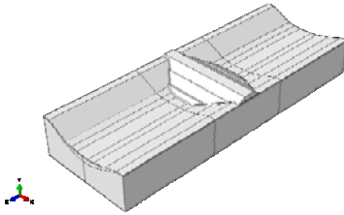


Figure 1. Embankment model

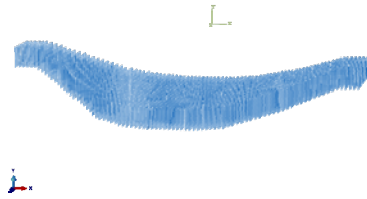


Figure 2. CFG pile foundation

Static analysis

In the static analysis, all horizontal nodes of the foundation's bottom boundary are fixed in the vertical direction, whereas the nodes on the four lateral boundaries of the model are fixed in the horizontal direction. The force of gravity bears its initial impact. The results from the static analysis are shown in Figure 4.

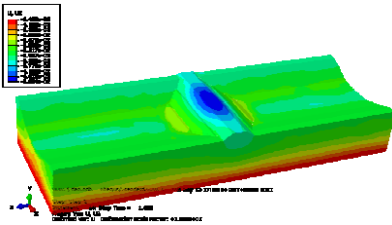


Figure 4. Embankment vertical displacement

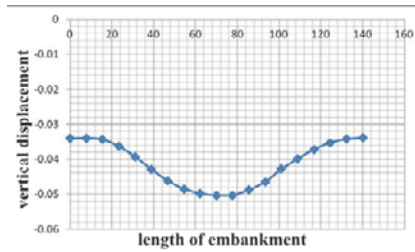


Figure 3. Embankment vertical deformation

The negative value in the figure indicates that the displacement is opposite to the coordinate axis, as shown in Figure 3. The maximum displacement in the vertical direction occurs at the center of the embankment. As the valley and embankment are symmetrical, the displacement is also symmetric relative to the central line. As shown in Figure 4, the maximum deformation of the embankment is 0.05m, while the minimum is 0.034m.

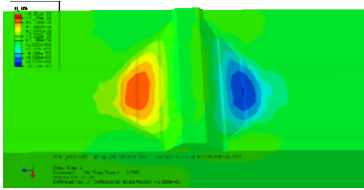


Figure 5. Embankment horizontal deformation figure

The horizontal deformation of the embankment is also symmetric relative to the center of the embankment under gravity force. The maximum horizontal deformation occurs at the slope on the second stage and reaches 8.59mm. Compared with the vertical deformation, the maximum horizontal deformation is much smaller. Both the vertical and horizontal deformations are small under gravity force, so the deformations have little impact on embankment safety.

Fault rupture

Since the rupture direction of the strike-slip fault is across the central line of the embankment at a large angle, a perpendicular angle of 90 degrees is assumed in simulating the fault rupture (Zhao, Li, & Huo, 2007), namely that the fault strikes perpendicular to the central line of the embankment. In the above procedure, the horizontal boundary nodes of the model remain fixed in the vertical direction, whereas a uniform displacement caused by fault rupture is imposed on the front and back boundaries and bottom of the analytical model (Li, Zhao, & Li, 2009). There are two reasons for taking the above assumption: 1) the front and back boundaries are far from the embankment; therefore the displacements on the front and back boundaries do not affect the deformation of the embankment; 2) taking the assumption simplifies our analytical procedure. A similar assumption has been taken by Anastasopoulos and Gazetas (2008) in their study of the effect of fault rupture on ground deformation.

In order to estimate fault rupture displacement for the specific fault, the model developed by Wells and Coppersmith (1994) is used. From the model of Wells and Coppersmith, an average fault rupture displacement of 1m for a magnitude 7 earthquake is obtained. In our analysis, the fault rupture velocity of 1m/s is taken.

To achieve the effects of fault rupture style on embankment deformation, two rupture-styles are discussed. One rupture style is a unilateral fault rupture, and the other is a bilateral fault rupture. Unilateral fault rupture is shown in Figure 6 where fault rupture direction is perpendicular to the central line of the embankment. Half of the foundation is fixed while the other half moves at about 1m at speed of 1m/s (Liv & Hanna, 2004). Bilateral fault rupture is that fault rupture direction is perpendicular to the central line of the embankment. Half of the foundation moves to the front and

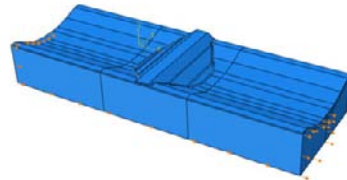


Figure 6. Strike-slip fault rupture loading method

the other half moves to the back at a speed of 0.5m/s in the opposite direction. The working time is 1s.

It is normally assumed that the movement of fault rupture with time is linear; however, this is uncertain. To show the effect of the movement type of the fault on deformation of ground surface and embankment, a curve $Y=X^n$ is taken, where n can take any value. For example, when $n=1$, the movement of fault is linear, and when $n=2$, the movement of the fault is hyperbolic; that is, initially the fault ruptures quickly, and then becomes slow. Here, seven n values are taken and the movement tendencies corresponding to the seven n values are shown in Figure 7.

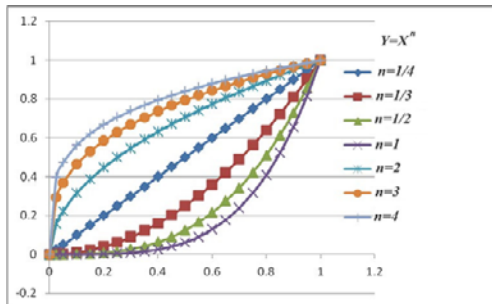


Figure 7. The different ways of loading curve

Results from fault rupture analysis

Unilateral fault rupture. Fault rupture in a horizontal direction will cause great horizontal and vertical displacements at some parts of the embankment. This displacement of the embankment has an immense effect on the safety of operating railroads. Therefore, great attention should be paid to the deformation caused by fault rupture. Figures 8 and 9 show the horizontal and vertical displacements.

Figure 10 illustrates horizontal displacements on the embankment's top surface and on the ground. From Figure 10, it is known at two ends that the horizontal displacements on the embankment's top surface and its ground are almost the same, but at the location of fault rupture the difference in the horizontal displacements on the embankment's top surface and its ground is great. Figure 10 also shows that the slope on the embankment's top surface after the fault rupture is smaller than that on its ground. The result, the fault rupture not causing serious damage, implies that the high embankment can dissipate part of the energy produced by the fault rupture. In Figure 10 the maximum horizontal displacement on the ground is about 0.8m, less than 1.0m (fault ruptures 1.0m in the calculation). The reason for this is that the soft soil layer plays an important role in reducing fault rupture deformation on the ground,

because soft soil layers can also dissipate energy produced by fault rupture.

Figure 11 shows that fault rupture has greater influence on vertical displacement at the embankment's top surface than on the ground. However, compared with the horizontal displacement of the embankment, the effect of the vertical displacement can be neglected.

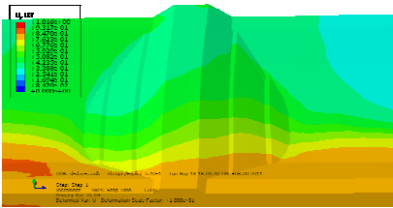


Figure 8. Embankment horizontal displacement

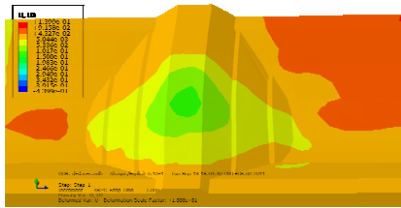


Figure 9. Embankment vertical displacements

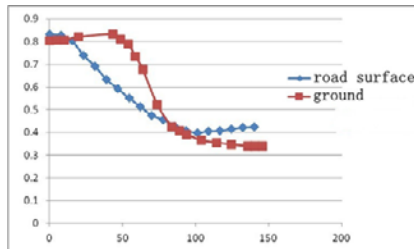


Figure 10. Horizontal displacements

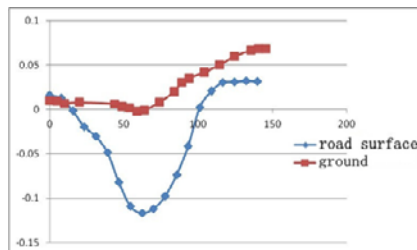


Figure 11. Vertical displacements

Bilateral fault rupture. The results of bilateral fault rupture are shown in Figures 12 and 13. The maximum embankment horizontal displacement is 0.43m, distributing in a symmetrical way. The maximum embankment vertical displacement is -0.145m.

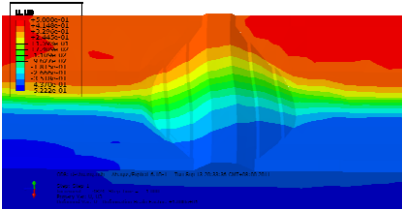


Figure 12. Horizontal displacement of model

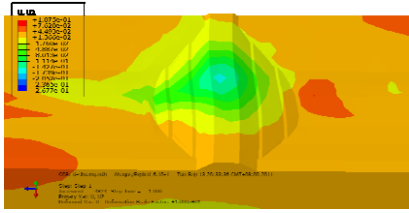


Figure 13. Vertical displacement of model

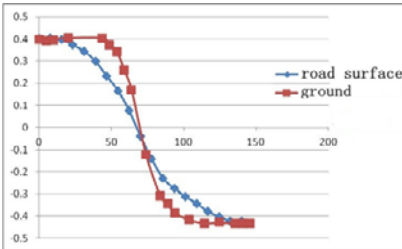


Figure 13. Horizontal displacement curve

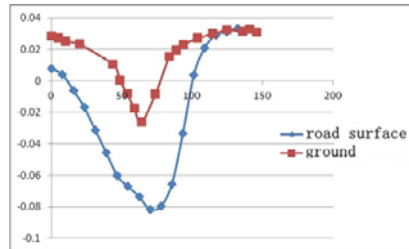


Figure 14. Vertical displacement curve

Figures 12 and 13 show that in the case of bilateral fault rupture, the horizontal displacements of the embankment and ground are also symmetrical, as shown in unilateral fault rupture cases, and the deformation on the embankment's top surface is less severe than that on the ground. This illustrates that a high embankment plays an important role in reducing the horizontal displacement of embankment; because the valley is asymmetrical, the vertical displacement produced the fault rupture is asymmetrical, as shown in Figure 14.

By comparing the results from unilateral and bilateral fault rupture cases, it is found that the differences of horizontal and vertical displacements are great, although overall relative displacements are nearly the same, because a 1.0m unilateral rupture cannot be taken as the sum of two bilateral ruptures of 0.5m in the opposite direction. Unilateral fault rupture affects soils mainly on the side that moves, while bilateral fault rupture affects soils on both sides.

Effect of movement-type fault rupture. The effect of movement-type fault rupture on the displacements of embankment and ground is discussed in this section, as shown in Figure 7. It focuses on the displacement in the horizontal and vertical directions for three cases: 1) reducing the increment of fault rupture velocity with the increase of time, 2) keeping the increment of fault rupture velocity constant with the increase of time, 3) increasing the increment of fault rupture velocity with the increase of time. The comparison of the displacements for Cases 1 and 3 is shown in Figures 15 to 18.

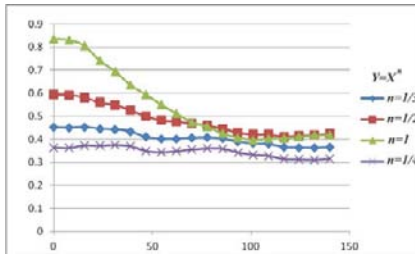


Figure 15. Horizontal displacements for Case 1

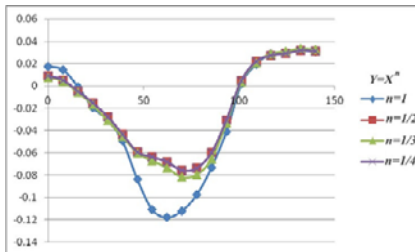


Figure 16. Vertical displacements for Case 1

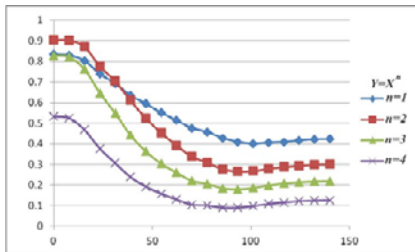


Figure 17. Horizontal displacements for Case 3

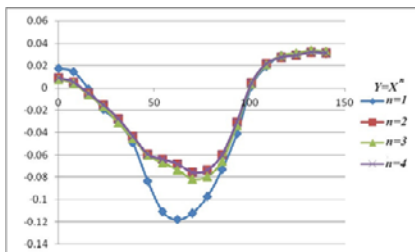


Figure 18. Vertical displacements for Case 3

Figures 16 and 18 show the vertical displacements on the top surface of the embankment for different n values; maximum vertical displacement occurs for $n=1$. Figures 16 and 18 also show that corresponding to $n=2, 3$, and 4 (or $1/2, 1/3$, and $1/4$), the maximum vertical displacements are smaller than they are for $n=1$. If only considering vertical displacement, the worst case is from $n=1$. Figures 15 and 17 show the horizontal displacements on embankment top surfaces for different n values. From Figure 15, it is known that for $n=1$ case, the maximum displacement difference in the range of 150m is produced, and for $n=1/4$ the minimum displacement difference is obtained. Figure 18 illustrates a situation similar to that shown in Figure 15, but the maximum displacement difference is from $n=2$. From the above results, some conclusions for horizontal displacement can be obtained. For example, the movement type of a fault rupture has a significant effect on the horizontal displacement of the embankment, and normally the maximum displacement difference is from $n=1$ or $n=2$. This implies that in practice, $n=1$ can be used as the worst case scenario.

DISCUSSION AND CONCLUSION

Discussion. This paper studies the effect of deformation and displacement on an embankment under the fault rupture, but it does not further discuss how to reduce the damage to the embankment. To do so would be beyond the scope of this paper.

Conclusions. From the above analyses, the following conclusions have been obtained:

1. Results from the analyses show that the horizontal displacement on the ground is greater than the displacement on the top of the embankment regardless of the kind of fault rupture direction and velocity, which shows that embankment plays a role in reducing deformation. Although vertical displacement takes place on top of an embankment, the deformation volume is small; therefore, it has little impact on the safety of the embankment.
2. Although it has the same fault rupture displacement and produces an approximately symmetrical embankment deformation shape, bilateral fault rupture produces greater embankment displacement than that produced by unilateral fault rupture.
3. When the increments of the fault rupture velocity change with time, the embankment deformation is different. If the increment of the fault rupture velocity reduces with time, the embankment deformation is smaller than that which occurs if the increments of the fault rupture velocity increase with time. The faster the increment of the fault rupture velocity decreases with time, the gentler the

deformation becomes. The vertical deformation is almost the same when the rupture velocity increases or decreases with time, but it is greater than when the velocity changes linearly with time.

ACKNOWLEDGEMENTS

Supported by a Major Program of the National Natural Science Foundation of China (41030742); Supported by Technological Research and Development Programs of the Ministry of Railways (2009G010-c).

REFERENCES

- Fei, K., Zhang, J.W. (2010) "Abaqus in Geotechnical Engineering" [M]. Beijing: China WaterPower Press: 44-70 .
- Zhao, L., Li, X.J., and Huo, D. (2007) "Problems of Rupturing Process of Overlaying Soil Due to Fault Dislocation of Bedrock" [J]. Journal of Beijing University of Technology. 33(1): 2-4 .
- Li, X.J., Zhao, L., and Li, Y.Q. (2009)."Simulation of Fault Movement Induced Rupture Process of Overlaying Soil of Bedrock" [J].Chinese Journal of Rock Mechanics and Engineering. 28 (Supp.1): 1-5.
- Anastasopoulos, I., Gazetas, G., Drosos, V. et. al. (2008). "Design of bridges against large tectonic deformation" [J]. Earthquake Engineering and Engineering Vibration. 7(4): 7-9.
- Wells, D.L., Coppersmith, K. J. (1994)."New Empirical Relationships among Magnitude, Rupture Length, Rupture Width, Rupture Area, and Surface Displacement" [J] . Bulletin of the Seismological Seismological. 84(4):11-23.
- Liu, X.Z. , Hama, T.Z. (2004). "Experiments on rupture propagation of active faults in soil" [J] . Chinese J. Geot. Eng . V26(3): 1-3.

Research on Assessment Method of High Large Steeply Inclined and Accumulation Slope Stability in Southeast Region of Chongqing

HUANG Wei¹, FENG Xiao¹, ZHOU Jianting¹, and YANG Guanghui²

¹Civil Engineering and Construction College, Chongqing Jiao Tong University, Chongqing, China, 400074

²Xiu Shan Xian Transit Authority, Chongqing, China, 409912

ABSTRACT

Research on assessment method of highway slope stability becomes more of a concern. The high large steeply inclined and accumulation slope stability in southeast region of Chongqing located in mountain area in Southwest China, where the slope is high and large. The toe of slope is steeply inclined and the slope is mainly composed of loose piles with characteristics of large system, uncertainty and complexity. On the basis of mechanism analysis on this kind of slope, we established a fuzzy comprehensive evaluation mathematic model and ascertained method of some relevant method parameters by the application of mathematic theory. Taking the rocky slope of highway as an example, we provided stability assessment of some sections in 319 national roads in Xiushan County in Chongqing city. This slope is typical located in southeast region of Chongqing, which has special meaning to analyze and evaluate stability on this kind of slope.

INTRODUCTION

Southeast region of Chongqing is located in the southeast of Sichuan basin, at the intersection site on the edge of basin between the Dalou Mountains and the Wulingshan Mountains, including Qianjiang, Shizhu, Pengshui, Youyang and Xiushan Counties. Generally speaking, the terrain in the northern and northeastern parts is shallower than that in the southern and southwestern parts, and the types of landform are complicated in this region. The high large steeply inclined and accumulation slope risk in Southeast region of Chongqing located in mountain area in Southwest China, where the slope is high and large. The toe of slope is steeply inclined and the slope is mainly composed of loose piles with characteristics of large system, uncertainty and complexity.

Many factors are related to the high large steeply inclined and accumulation slope risk in Southeast region of Chongqing, and the effect of the factors has not been quantitative analyzed yet. According to the characteristic of slope stability, using the fuzzy mathematical method to analyze slope stability is more comprehensive on considering factors than conventional methods. The advantages of

this method are combining quantitative analysis and qualitative analysis organically, avoiding a lot of complicated calculations, process of analysis is preciseness and the results are reliable. Analysis theory and research methods on the slope stability mainly contain quantitative analysis, qualitative analysis, and nondeterministic analysis method (Deng et al. 2010).

MAIN CHARACTERISTICS OF SOUTHEAST REGION OF CHONGQING

Southeast region of Chongqing is covered by vegetation soil and its geological conditions are complex (Shen et al. 2005). Highway Slopes mainly are magmatic rock and metamorphic rock, rock mass discontinuity are rough, attitude change greatly. The general features of the high large steeply inclined and accumulation slope are as follow.

Terrain Situation

The topography is complex and the transverse slope is relatively large. The total contour terrain is higher in north and lower in south, which is basically identical with the total pattern of the bottom terrain of the Sichuan basin. Specifically speaking, the terrain is high in the northwest and low in the southwest in the north of Yangtze River while high in the south and low in the north in the south of Yangtze River. With large surface relief, mountains and rivers interlaced, the mountain chains here mainly are from southwest to northeast, and from east to west there are three mountains, such as Mingyue mountain, Tongluo mountain and the East Hot-Spring mountain; Rivers here belong to Yangtze river system, which run through the area diagonally from the southwest to the northeast and the tributaries are various.

Tectonic Landform

Tectonic-denuded landform: the landform of Southeast region belongs to tectonic landform, with the characters of anticlines low mountains and synclines hills are in interval, and the main landform is quaversal fold hilly of tectonic basin.

Piedmont slope accumulation landform: the main geomorphic unit is slide rock skirt formed by sliderock colluvium and proluvial fan and proluvial skirt formed by diluvium.

Karst landform: karst landform here mainly development and distribution in anticlineaxis part formed by limestone and dolomitestratum in T1j and T2l.

Formation Lithology

Surface formation: all are sedimentary strata formed by Triassic period and period afterward. They contain marine deposit formation formed in low-middle Triassic (T1f, T1j, T2l) and continental sedimentary strata formed in T3xj, Jurassic system (J1+2z1, J2s, J2sna and J3p) and Quaternary system. Surface formation in the area lack upper Triassic, Cretaceous system and Tertiary system.

Deep formation: deep formation has been exposed by many well drilling, such as lower Ordovician even Sinian System in a small zone.

In this area, Holocene series mainly are the modern river alluvium and weathered soil (including rockfall sliderock and residual hillside waste); mainly

distributed in the modern river riverbed, floodplain and valley side in the both sides, the bottom part of U—shaped valley, intermontane area, gentle hills and piedmont in low mountain. Its stratum is disconformity.

Geological structures

Tectonic belonging of central south of middle depression area in Sichuan of northwestward in Yangtze para-platform belongs to geotectonic element of a country or region. Tectonic movement is not very strong, with no deep and large fault, the earthquake intensity is about 6 degree or less. The stability of earth crust is relatively better, no more earthquakes appeared.

Hydrogeology condition

Hydrogeology condition in this area is relatively complicated. There are four basic types of groundwater existing form: water in karst region, confined water in sandstone fissure, fissure water in fracture between clay rock and flagstone and pore water in deposit sediment of Quaternary system.

INSTABILITY MECHANISM ANALYSIS ON GANCHUAN SLOPE

The slope in Xiushan County Ganchuan road section of the national road 319 had occurred collapse failure at late August in 2010 under unfavorable natural condition of continuous torrential rain, which led to completely interrupt of the traffic, made it seriously difficult for Xiushan people on day-to-day travel, and caused bad effect in the society.

Instability Mechanism Analysis

According to comprehensive analysis of landslide exploration report in Xiushan County, landslide deformation mainly concentrated on the middle-upper part. Under the effect of continuous torrential rain, block stone and soil mass had been saturated, its dead weight increased, the decline of the binding power between accumulation bodies, shear strength died-off, which led the surface earth-rock to instability state.

Under the effect of surface water and ground water, bed rock fissure water developed, weathered bedrock saturated dead weight increased, the decline of the binding power between accumulation bodies, shear strength died-off, which increased the global instability of the rock.

Rocks here are covered by vegetation soil and geological condition is complex, where the slope is high and large, the toe of slope is steeply inclined and the slope is mainly composed of loose piled. The global stability is under the control of secondary landslide in the lower part, the sliding failure of secondary landslide in the lower part will drag the whole bedrock landslide as shown in Figures 1 and 2 (Li 2008, Chen et al. 2006).



Figure 1. Whole landslide figure



Figure 2. Local landslide figure

Calculation of Ganchuan Slope Stability

According to the practical exploratory data and the geological condition of Southeast region in Chongqing, Calculation of the Stability of Ganchuan Slope is as follow.

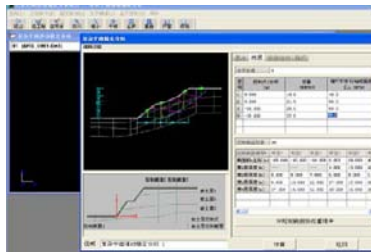


Figure 3. Stability analysis mechanism

1) Selection of calculation method, formula and software

The calculation used Li-cheng, geotechnical analysis of slope stability calculation software, to calculate the slope stability factor and confirm the Most Dangerous Sliding Surface by the combination way of automatic search empirical analysis based on the arc sliding theory and Sweden slice method (shown in Figure 3). The calculation formula is as follow.

$$K_s = \frac{\sum R_i}{\sum T_i}$$

where T_i represent the reaction in the tangential line of sliding surface (kN/m) and R_i represent the skid-resistance of sliding surface (kN/m).

2) Selection of calculation parameters

The calculations results show that the slope is in limit equilibrium state under natural state and emergency capacity is not enough, while saturated it is in unstable state and landslide distribution may occur easily. Table 1 shows the selected parameters.

Table 1. Parameter Selection

Geotechnical Category	Natural Unit Weight (KN/m ³)	Saturation Weight (KN/m ³)	Natural Shear Strength		Saturation Shear Strength	
			Cohesion C (Kpa)	Friction Angle (φ°)	Cohesion C (Kpa)	Friction Angle (φ°)
Plain fill	18.0	19.0	8	20	4	6
Silty clay	19.5	20.5	30	22	20	7
Weathered quartzite	21.0	22.0	30	28	23	21
Strong decomposed quartzite	24.0	25.0	50	38	30	27

FUZZY MATHEMATICS EVALUATION MODEL OF RISK

Cardinal Principle of Fuzzy Mathematics

1) Approximate theory

Cardinal principle of fuzzy mathematics is the main links in analyses large system, uncertainty and complexity system. Its mathematical expression is as follow.

$$B_i = A_i \circ R \tag{3-1}$$

where A_i , and B_i , respectively represent the fuzzy subset of the universe of discourse $V \Delta \{ u, v2...vn \}$ and $\nabla \{ u, v2...vn \}$, R represents the fuzzy relation and “ \circ ” represents operation rules for synthetic method.

2) Determination principle of membership function

In the process of construction of membership function, dialectical unity of subjective and objective must be paid full attention in order to make the membership function constructed reflect the crux of the matter comprehensive and real.

Determination principle of membership function is as follow:

(1) If fuzzy sets reflect common social consciousness, which is in a large number and can be expressed repeat, then fuzzy statistical method is a good idea in seeking membership function.

(2) If fuzzy sets reflect individual consciousness and experience in some particular time segment, then Delphi method can be used in this kind of problem.

(3) If fuzzy sets reflect fuzzy concept had corresponding mature index and generally accepted as reflection of the crux of the matter comprehensive and real, then the index can be used directly or transform the index into membership function by mathematical model.

(4) If it is difficult for some fuzzy concept to write membership function directly, then selection method is a good chose by comparing membership degree of the two elements.

(5) If a fuzzy concept is compounded by several fuzzy factors, then membership function of every fuzzy set can be sought firstly and synthesize the

membership function of the fuzzy concept.

3) Seeking method of A_i in the approximate theory formula $B_i = A_i \circ R$

A_i can be given according to expert experience, which is affected by subjective factors of specialist. To accurate determination A_i , the combination of experience and formula is proposed.

$$(1) \text{ if } \mathbf{a} \leq \mathbf{a}_{\min}, \mathbf{a}_{\min} \in \mathbf{A}_i, \text{ then } \mathbf{A}_i = [1, 0, \dots, 0] \tag{3-2}$$

$$(2) \text{ if } \mathbf{a} \geq \mathbf{a}_{\max}, \mathbf{a}_{\max} \in \mathbf{A}_i, \text{ the } \mathbf{A}_i = [0, 0, \dots, 1] \tag{3-3}$$

$$(3) \text{ if } \mathbf{a}_{\min} < \mathbf{a} < \mathbf{a}_{\max}, \text{ then } \mathbf{A}_i = \mathbf{Max} \left(0, \frac{\Delta - |\mathbf{a}_i - \mathbf{a}|}{\Delta} \right), i = 1, 2, \dots, n. \tag{3-4}$$

Δ represents step.

COMPREHENSIVE EVALUATION

Considering the influencing factors of slope stability are various, multistage comprehensive evaluation model is used to improve the assess accuracy.

1) Factor set X is divided into several subsets: X_1, X_2, \dots, X_s in a certain attributive and meet demand the formula $\bigcup_{i=1}^s X_i = X, X_i \cap X_j = \emptyset (i \neq j), X_i = \{X_{i1}, X_{i2}, \dots, X_{im}\} (i = 1, 2, \dots, s)$

2) Give comprehensive evaluation to each subset X_i in first-order model, assumption evaluation set $Y = \{y_1, y_2, \dots, y_m\}$, weight distribution of each factor in X

is $\mathbf{a}_i = (a_{i1}, a_{i2}, \dots, a_{im})$. And in here the meet $\sum_{i=1}^n a_{ij} = 1$ must be demand, if single

factor evaluation matrix of X is R , then one-level fuzzy multifactor evaluations is $\mathbf{b}_i = \mathbf{a}_i \circ R$

$$= (\mathbf{b}_{i1}, \mathbf{b}_{i2}, \dots, \mathbf{b}_{im}) \quad i = 1, 2, \dots, s.$$

3) If every X_i is seen as a single element and use \mathbf{b}_i as its single factor judge, then single factor evaluation matrix of $X = \{X_1, X_2, \dots, X_s\}$ is R .

$$R = \begin{bmatrix} \mathbf{b}_1 \\ \mathbf{b}_2 \\ \vdots \\ \mathbf{b}_s \end{bmatrix} = (\mathbf{b}_j)_{s \times m} \tag{3-5}$$

As a part of X each X_i , it reflects a certain attribute of X , according to the importance of each factor weight distribution is set as $\mathbf{a} = (a_1^*, a_2^*, \dots, a_s^*)$, then Two-level fuzzy comprehensive assessment is given as $\mathbf{b} = \mathbf{a} \circ R$.

According to the actual conditions of concrete engineering, the iterations are repeated as the above steps until the result of the above fuzzy comprehensive evaluation is obtained satisfactorily.

Selections of Main Influence Factors

Consider the needs of the analytic methods, divided the grade of slope stability into five classes: stable as grade I, basically stable-grade II, latent instability as grade III, unstable grade IV and extremely unstable for grade V.

As geological conditions in Southeast region in Chongqing is complex and the slope has its own characters: the slope is high and large, the toe of slope is steeply inclined and the slope is mainly composed of loose piled; rock mass structural plane is rough, attitude variance is relatively large and vegetation covered seriously. According to the influence extent, we choose fourteen factors as the main influencing factors that affect slope stability and its classification as shown in Table 2.

Table 2. Rating Table of Contributing Factors

Influencing factor		I	II	III	IV	V
seismic factor	maximum scale seismic intensity	<3	3-5	5-7	7-8	>8
	blasting dynamics factor	had no effect	definite influence	slightly influence	relatively strong influence	strong influence
	human factor	had no effect	definite influence	slightly influence	relatively strong influence	strong influence
geological structure and geological processes	initial geostress (MPa)	<2	2-8	8-14	14-20	>20
	slope aspect strata attitude	the most favorable	favorable	general	unfavorable	very dangerous
	Internal friction angle/(o)	>35	35-28	28-21	21-14	<14
	cohesion /(MPa)	>0.25	0.25-0.15	0.15-0.1	0.1-0.05	<0.05
	Ground-water	no ground water	little	some	much	rich
	Lithology	Very good	good	general	poor	Very poor
climatic factors	rainfall /(mm)	<50	50-100	100-150	150-200	>200
	Temperature effect	had no effect	definite influence	slightly influence	relatively strong influence	strong influence

Topography and Geomorphology	terrain	flat	lies between I-III	hilly	lies between III-V	high-steep P
	slope height(m)	<75	75-150	150-225	225-300	>300
	slope angle(o)	<20	20-30	30-40	40-50	>50

Constructing of Membership Function

Constructing of Membership Function of Quantitative Effect Factors

Grade evaluation in Table 2 use the qualitative evaluation standard has not considered the fuzziness of boundaries and the transition state between grades. According to the determination principle of membership function given by HUANG Chongfu (Huang 2008), the paper determine the slope state more accurately by constructing membership function considering the transition state between grades, and rhombus-type membership function is used to construct membership function of quantitative effect factors influence .

Slope angle:

$$U_I(x) = \begin{cases} 1 & x \leq 20 \\ \frac{1}{2} - \frac{1}{2} \sin \frac{\pi}{2.5}(x-21.25) & 20 \leq x \leq 22.5 \\ 0 & x \geq 22.5 \end{cases} \quad (3-12)$$

$$U_{II}(x) = \begin{cases} 0 & x \leq 20 \\ \frac{1}{2} + \frac{1}{2} \sin \frac{\pi}{2.5}(x-21.25) & 20 \leq x \leq 22.5 \\ \frac{1}{2} - \frac{1}{2} \sin \frac{\pi}{2.5}(x-30) & 22.5 \leq x \leq 27.5 \\ 0 & x \geq 32.5 \end{cases} \quad (3-13)$$

$$U_{III}(x) = \begin{cases} 0 & x \leq 27.5 \\ \frac{1}{2} + \frac{1}{2} \sin \frac{\pi}{5}(x-30) & 27.5 \leq x \leq 32.5 \\ \frac{1}{2} - \frac{1}{2} \sin \frac{\pi}{5}(x-40) & 32.5 \leq x \leq 37.5 \\ 0 & x \geq 42.5 \end{cases} \quad (3-14)$$

$$U_{IV}(x) = \begin{cases} 0 & x \leq 37.5 \\ \frac{1}{2} + \frac{1}{2} \sin \frac{\pi}{3.5}(x-40) & 37.5 \leq x \leq 42.5 \\ \frac{1}{2} - \frac{1}{2} \sin \frac{\pi}{3.5}(x-48) & 42.5 \leq x \leq 47.5 \\ 0 & x \geq 50 \end{cases} \quad (3-15)$$

$$U_{V}(x) = \begin{cases} 0 & x \leq 47.5 \\ \frac{1}{2} + \frac{1}{2} \sin \frac{\pi}{2.5}(x-48.75) & 47.5 \leq x \leq 50 \\ 1 & x \geq 50 \end{cases} \quad (3-16)$$

According to the membership function of slope angle membership function curve of the total gradient of slope is obtained as shown in Figure 4.

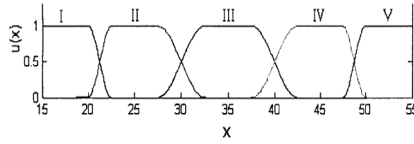


Figure 4. Membership function curve of the total gradient of slope

In the same way, curve of the Slope total height, the Slope total height, the slope internal friction angle, the rock mass cohesion, the initial gestures, the process rainfall and the minimum seismic intensity can be obtained as shown in Figures 5 to 10.

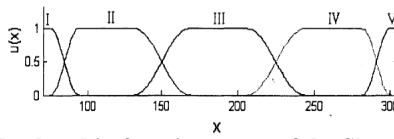


Figure 5. Membership function curve of the Slope total height

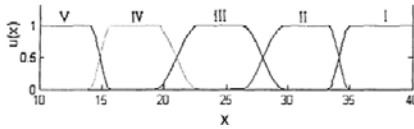


Figure 6. Membership function curve of the slope internal friction angle

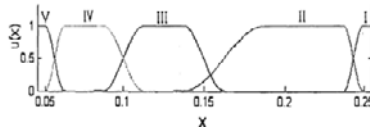


Figure 7. Membership function curve of the rock mass cohesion

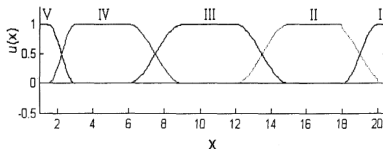


Figure 8. Membership function curve of the initial gestures

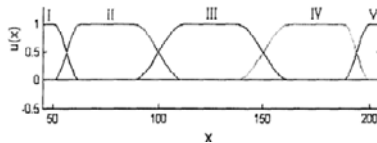


Figure 9. Membership function curve of the process rainfall

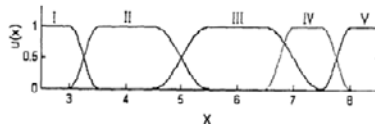


Figure 10. Membership function curve of the minimum seismic intensity

Constructing of Membership Function Qualitative Effect Factors

As for qualitative effect factors, in constructing the membership function, some quantitative disposal should be done in a certain rule. In the paper, divided the influencing factors of slope stability into five classes: very dangerous (10 scores), unfavorable (30 scores), general (65 scores), favorable (85 sores), the most favorable (100 scores); or the influence of effect factors: strong influence (10 scores), relatively strong influence (30 scores), slightly influence (65 scores), definite influence (85 sores), had no effect (100 scores). In the same, trapezoid-type membership function is used to construct membership function.

Membership function curve of terrain, lithology, slopes and strata change shape relationships, groundwater, temperature influence, the blasting motivates factors and human factors are obtained as shown in Figure 11.

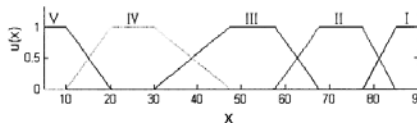


Figure 11. Membership function curve of terrain, litho logy, slopes and strata change shape relationships, groundwater, temperature influence, the blasting motivate factors and human factors

COMPREHENSIVE EVALUATION OF GANCHUAN SLOPE STABILITY

Wight Determination of Effect Factors

The influence to slope stability has the distinction between the primary and the secondary and contribution degree is various, so the Wight must be different for every effect factors. The paper determinate the Wight by using the combination of experience’s scoring and formula given by Huang Chongfu. Then the two-level Wight values of effect factors are obtained in the Table 3 as follow.

Single Factor Evaluation

$$[r_i] = [r_{i1}, r_{i2}, r_{i3}, r_{i4}, r_{i5}] \quad (i = 1, 2, 3,) \tag{3-17}$$

Evaluate the membership function of all the effect factors in the table 3-1 and 4-1 and their fuzzy vector $[r_i] = [r_{i1}, r_{i2}, r_{i3}, r_{i4}, r_{i5}] \quad (i = 1, 2, 3,)$ is proposed.

One-level Fuzzy Multifactor Evaluations

The comprehensive evaluation for every factors and subset $U_k(k=1,2,3,4)$ means that weight vector is provided according to the importance of every factors in

the subset U_k , then evaluation matrix R_k is composed by evaluation results r_i of every single factor and last seek the grade fuzzy vector B_k of corresponding subset by the formula 3-18.

$$B_k = [b_{k1}, b_{k2}, b_{k3}, b_{k4}, b_{k5}] = A_k \circ R_k \tag{3-18}$$

where “o” represent combinatorial operations, common square operator is used in the paper after trial calculation as for there are many kinds of combinatorial operations.

Table 3. Effect of Two-level Factors Weights

Index of Every Effect Factors		Two-level Weight Value of Every Effect Factors	
		Distribute of one-level evaluations value	Distribute of two-level evaluations value
Topography geomorphology (U_1)	slope angle (u11) slope height (u12) terrain (u13)	0.35(a11) 0.35(a12) 0.3(a13)	0.12(a1)
Geological structure and geological processes (U_2)	lithology (u21) slope aspect strata attitude u22) Internal friction angle (u23) cohesion (u24) groundwater (u25) initial geostress (u26)	0.35(a12) 0.12(a22) 0.15(a23) 0.15(a24) 0.15(a25) 0.08(a26)	0.60(a2)
Climatic factors (U_3)	rainfall (u31) temperature effect (u32)	0.85(a31) 0.15(a32)	0.15(a3)
Rest human factors (U_4)	maximum scale seismic intensity (u41) blasting dynamics factor (u42) human factor (u43)	0.30(a41) 0.40(a42) 0.30(a43)	0.13(a4)

Two-level Fuzzy Multifactor Evaluations

Take two-level fuzzy multifactor evaluations considered the four factors subsets (such as topography geomorphology, geological structure and geological processes, climatic factors as four single factors.

$$B = [b_1, b_2, b_3, b_4, b_5] = A \circ R \tag{3-19}$$

Fuzzy Multifactor Evaluations

Single Factor Evaluation

All the single factors are evaluated by the membership function curve above,

and the evaluation results of every single factor are seen in Table 4.

One-level Fuzzy Multifactor Evaluations

The grade fuzzy vector is obtained by taking the multifactor evaluations for every single factor subsets.

$$b_{1,1} = (0 \ 0.318 \ 0.825 \ 0.325 \ 0)$$

$$b_{1,2} = (0 \ 0.212 \ 0.7095 \ 0.525 \ 0)$$

$$b_{1,3} = (0 \ 0.15 \ 0 \ 0.85 \ 0.425)$$

$$b_{1,4} = (0.49 \ 0.36 \ 0.36 \ 0 \ 0)$$

Two-level Fuzzy Multifactor Evaluations

Take two-level fuzzy multifactor evaluations considered the four kinds factors as four single factors.

$$B = (b_1 \ b_2 \ b_3 \ b_4) = AoR$$

$$B = \begin{pmatrix} 0 & 0.318 & 0.825 & 0.325 & 0 \\ 0 & 0.212 & 0.7095 & 0.525 & 0 \\ 0 & 0.15 & 0 & 0.85 & 0.425 \\ 0.49 & 0.36 & 0.36 & 0 & 0 \end{pmatrix}$$

$$= (0.0637 \ 0.235 \ 0.5715 \ 0.4815 \ 0.0632)$$

Table 4. Results of Single Factor Evaluation

single factor	grade membership					
	I	II	III	IV	V	
U ₁	u	0	0.5	0.5	0	0
	u	0	0.4	1	0	0
	u	0	0.5	1	0.5	0
U ₂	u	0	0.4	0.85	0.6	0
	u	0	0	0.8	1	0
	u	0	0	1	0	0
	u	0	0	0.5	0.5	0
	u	0	0	0.5	0.8	0
	u	0	0.9	0.2	0	0
	u	0	0.9	0.2	0	0
U ₃	u	0	0	0	1	0.5
	u	0	1	0	0	0
U ₄	u	0	0.2	0.7	0	0
	u	1	0	0	0	0
	u	0.3	1	0.5	0	0

Analyses on Evaluation Result

According to the principle of the biggest subject, choose the maximum $b_{max} = 0.5715$ in the matrix and its relative stability level is grade III showing that the slope is under potentially steady state.

1. Accumulation slope is composited by sediment formed by rocks upon the

mountain, which is instability and slide under the effect of external force and geological processes such as drastic weathering, erosion action, seismic action and rock fracture.

After the effect of long-term compaction, accretion has a close structure, rocks interdigitate and overlap with each other, rock block gap is filled with sandy loam composited with crushed stone that can not form successive layered structure.

Weak and soft zone is found between accumulation body and bedrock, and the main controlling factors of its deformation failure is the state of substrate interface of falling accumulation that decide its special orientation of the main-phase of sliding surface and its form and range when inability.

2. Mechanism analysis on instability of accumulation slope

Under the complicated environmental condition and structure conditions, instability of accumulation slope is complicated. According to slope structure of accumulation slope and the state of substrate interface, divided the deformation failure form into three kinds: accumulation slope occur overall instability long substrate interface, relatively large-scale latent slump masses exist in accumulation slope and local instability.

Continuous rainfall promotes the form of instability of accumulation slope; destroy the favorable conditions of groundwater drainage with its loose structure and transmission capacity is stronger. So after the accumulation body had been formed, surface water is detained, when absorbed it penetrate into basement of accumulation body and improve the supply condition of groundwater. When a certain scale of accumulation body formed (such as coverage area and stack height), groundwater is supplied and detained favorable leading to the water content increasing.

Under the long-term permeation and invasion effect of rainfall result in intensifies the slide tendency of basal interface, firstly as the combined action of pore water pressure and seepage force, secondly the water soak into the basement, soften and corrosion the medium inside the basal interface under the suffusion erosion that reduce the mechanical strength index of the accumulation body and the basal interface.

CONCLUSION

Research was conducted on assessment method according to the high large steeply inclined and accumulation slope stability in Southeast region in Chongqing. Considering uncertainty of stability analysis on this kind of slope, two-level fuzzy multifactor evaluations is used to analysis the slope stability according to the actual engineering experience and the formula given by Huang Chongfu and combining the slope character (high large steeply inclined and accumulation slope) to determine weights of every effect factor. On the base of structure membership function, take assessment on the slope of Ganchuan sections in 319 National Road in Xiushan County in Chongqing city. Its results coincide with the real state of a slope showing that it is reasonable in Wight distribute of every effect factors, and can be used in the kind of slope in Southeast region of Chongqing.

REFERENCES

- Chen, M., Li, H., and Wang, T. (2006). "The Determination of Nonlinear Membership Function in Fuzzy Comprehensive Evaluation." **Mathematics in Practice and Theory**9: 49-52.
- Deng, Z., Xu, S., and Guo T. (2010). "Summary of Analysis & Assessment Methods of Slope Stability." **Mining Engineering**001 (8): 14-16.
- Feng, S., Sun, S., and Duan, W. (2009). "Application of Fuzzy Mathematics Evaluation Way in Slope Stability." **Safety in Coal Mines**, 40(2): 110-114.
- Huang, C. (2008). "A Basic Model for Assessing Integrated Risk." **Journal of Basic Science and Engineering**16(3).
- Li, R., and Xie, Y. (2009). "Application of Fuzzy Information Analysis Method to Stability Analysis of Highway Landslide." **Subgrade Engineering**1: 145-147.
- Li, W. (2008). "Analysis on Common Failure Mode of Rock Slope." **Friend of Science Amateurs**32: 11-14.
- Shen, L., Liao, J., and Zhang, Y. (2005). "Summary on the Evaluation Methods of Slope Stability." **Mining Research and Development**: 39-42.
- Xie, Q., and Xia, Y. (2003). "Fuzzy Hierarchy Analysis on Decision Making of Rockmass Slope Treatment Based on Entropy Weight." **Chinese Journal of Rock Mechanics and Engineering**(1): 46-53.

Dynamic Response of High-Speed Rail Roadbed under Harmonic Moving Loads

Fu-Chun Xue¹, Liping Yan², Jian-Min Zhang³, and Jian-Lin Ma⁴

¹School of Civil Engineering, Tsinghua University, Haidian District, Beijing 100084, China; PH 86-139-8191-8355; email: ocean2008xfc@163.com

²Los Angeles Department of Water and Power, 111 N. Hope Street, Room 1368, Los Angeles, CA 90012, U.S.A.; PH (714) 414-2905; email: lipingyan.ge@gmail.com

³School of Civil Engineering, Tsinghua University, Haidian District, Beijing 100084, China; PH 86-10-62785593; email: zhangjm@tsinghua.edu.cn

⁴School of Civil Engineering, Southwest Jiaotong University, Chengdu, Sichuan 610031, China; PH 86-139-8002-6902; email: majianlin01@126.com

ABSTRACT

This study was conducted to investigate the dynamic response of a non-ballasted track-subgrade system under the high-speed train moving loads. On the assumption that the stress distribution is uniform under the bottom of the track plate, a complete finite element (FE) model was established for the roadbed-subgrade system with the FE analysis computer software ABAQUS. Using the FE model, numerical analyses were performed with focus on the variations of the system's vibration displacement, velocity, and acceleration under loading of a moving high-speed train. The dynamic responses under different moving speeds were analyzed and compared for a sinusoidal loading with a constant amplitude. The analysis results indicate that the system's dynamic responses increase nonlinearly as the moving speed increases with similar pattern. The findings of this study are useful to the design and construction of high-speed rail roadbeds.

INTRODUCTION

Because of its high speed, comfort, high security and train grid density, high-speed rail has been developed rapidly in China and will be the trend for the rail transit system in the world. The roadbed ground vibrations and the impact on the environment caused by moving train loads have drawn widespread concern and is one of the hot topics in research.

In the current research methods, the track is basically modeled as a beam on elastic (or visco-elastic) roadbed and elasticity theory is used to obtain solutions (e.g. Cai et al. 2008). The load is applied directly on the surface of a half space in some of

the models and to the beams placed on the half space in other models. All the methods are over simplified and thus can not properly reflect the actual situations. Therefore, their applications are limited.

In fact, the non-ballasted track on the roadbed consists of track, the track plate, base plate, surficial layer of roadbed, bottom layer of roadbed, roadbed, and foundation. There are complex contacts among different parts. The propagation of the train-induced vibration is a very complex process. To study this issue, we must establish a more complete model using numerical methods and obtain more realistic results.

FINITE ELEMENT MODEL

Assuming the rail line is in good condition and is in a straight line section, the train load on the track is predominantly a vertical load. The load passes to the track plate and the pressure on the bottom of the plate can be approximated as a uniformly distributed harmonic load. To simplify the analysis, the model consists of support layer, surficial layer of roadbed, bottom layer of roadbed, roadbed, and foundation, not including track plate and rail track to avoid complicated train-track dynamic interaction.

Model description. In the finite element model, the longitudinal length is 50 m, the maximum width is 160 m, and the foundation depth is 50 m. The established model is shown in Figure 1. In analyses using the model, the reduced integration elements C3D8R are adopted and the model has a total of 485,514 nodes and 406,465 elements.

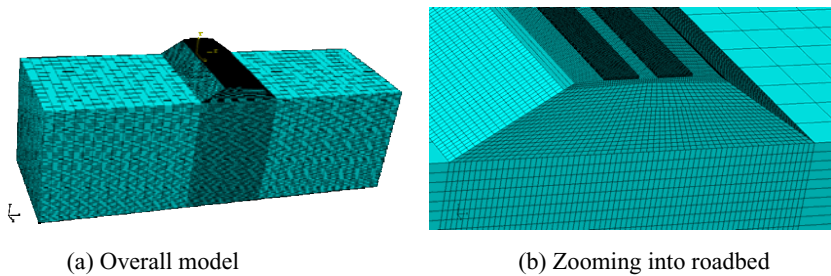


Figure 1. Finite element model.

Model parameters. The Drucker-Prager plasticity model was used for foundation, roadbed, bottom layer of roadbed, and surficial layer of roadbed. The linear elastic model was used for support layer. Table 1 lists the model parameters. In the table, the

modulus is the compression modulus except for the support layer where it is the Young's modulus; and the Raleigh damping is adopted, where damping coefficients α and β are calculated from natural frequency (f) calculated from a modal analysis.

Table 1. Parameters Used in FE Model.

Name	Density (kg/m ³)	Modulus (MPa)	Poisson ration	Internal Friction Angle (°)	Cohesion (kPa)	Damping coefficients	
						α (s ⁻¹)	β (s)
Foundation	1800	50	0.30	22	30	0.4091	0.00567
Roadbed	1850	85	0.28	24	35	0.4091	0.00567
Bottom layer of roadbed	1900	100	0.30	26	45	0.4091	0.00567
Surficial layer of roadbed	1950	190	0.30	28	50	0.2454	0.0034
Base plate (Support layer)	2400	31.5e3	0.15	-	-	0.1227	0.0017

Boundary conditions. In a dynamic analysis, a transmission boundary is needed to simulate infinite domain in a finite model. A transmission boundary can be achieved in two ways: (1) to directly apply springs and dampers in the model boundary with given appropriate parameters; (2) to apply a layer of massless elements on the outside of the model with equivalent parameters calculated by the springs and dampers. The first method was used in the present model.

In addition to the transmitting boundary, the model is also needed to be imposed boundary constraints, i.e., the model bottom that restrains all degrees of freedom and the model, left, right, front, and rear that restrain the normal degree of freedom to the surface located.

Loading. Train loading on the rail roadbed is a one-way stress wave pulse (excitation wave), and the impact and harm to the structure from the low-frequency excitation is greater than from the high-frequency excitation. Theoretical studies have shown that an excitation wave is superposition of harmonic excitation waves (sine or cosine waves) with a number of different frequencies and different amplitudes. The measured dynamic stress on the bottom of ballastless rail plate of the existing high speed rail is approximately 30 kPa (Xue, 2010). Therefore, the amplitude of the sine wave used in the present study is also 30 kPa.

The train load is a moving load, which needs to be generated by an ABAQUS subroutine. The load applied to the bottom of the track plate is a uniform sinusoidal pressure. The sinusoidal load with a frequency of 5 Hz and an amplitude of 30 kPa is shown in Figure 2. The model after application of the load is shown in Figure 3. Analyses of the loading cases are listed in Table 2. Loading time is from 0 to 0.2 s and the total computation time is 0.4 s.

Steps of computation. Prior to the dynamic computation, the construction has

gone through the sequence of constructing roadbed, bottom layer and surficial layer of roadbed, and base plate. Therefore, the corresponding computation steps need to simulate the sequence, as listed in Table 3.

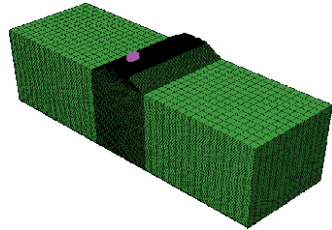
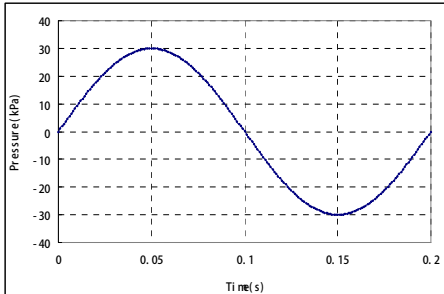


Figure 2. Sinusoidal load with 5 Hz and 30 kPa. Figure 3. Model after loading.

Table 2. Loading Cases.

No.	Loading amplitude (kPa)	Moving speed of loading (km/h)
1	30	108
2	30	200
3	30	300

Table 3. Computation Steps.

Sequence No.	Calculation conditions	Analysis type
1	Generating the initial stress	Implicit static analysis
2	Construction of roadbed	Implicit static analysis
3	Construction of bottom layer of roadbed	Implicit static analysis
4	Construction of surficial layer of roadbed	Implicit static analysis
5	Construction of support plate	Implicit static analysis
6	Modal analysis	Linear perturbation analysis
7	Application of train loading	Put displacements to zero, explicit

Modal analysis. To obtain the system's natural frequency, the modal analysis was performed. The first 100 orders of natural frequency were calculated as follows: $f_1 = 0.94006$ Hz, $f_2 = 0.94127$ Hz, $f_3 = 0.94855$ Hz, ..., $f_{99} = 1.1854$ Hz, $f_{100} = 1.1857$ Hz. They are all around 1 Hz.

ANALYSIS RESULTS AND DISCUSSIONS

To obtain time histories of the model's vibration displacement, velocity and, six representative nodes (shown in Figure 4) are selected for monitoring.

The dynamic response of the entire system was computed under sinusoidal loadings with an amplitude of 30 kPa and moving speeds of 108 km/h, 200 km/h and 300 km/h. The computation duration is two periods, i.e. 0.4 s.

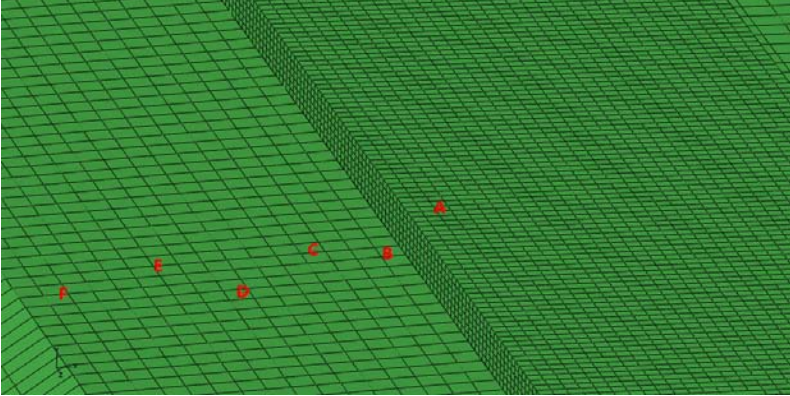


Figure 4. Locations of representative nodes.

Each of computed vibration displacement, velocity and acceleration has three components. Because the train load is mainly a vertical load, the vertical component should be focused on. Therefore, only the vertical components are presented.

Vibration displacement. The results are shown in Figures 5 through 10, where U_y is the vertical component of displacement and a negative value indicates the downward direction. These figures indicate that the node displacements increase approximately linearly during the time from 0 to 0.2 s that is in the forced vibration phase, whereas they increase first and then decrease with some volatility from 0.2 to 0.4s that is in the free vibration phase. The displacement at the end of computation (time = 0.4 s) is not zero because the computation duration is short. It can be expected that the displacement will eventually decay to zero the computation duration is long enough.

Clearly, the displacement at each node increases as the moving speed increases; but it does not meet the simple linear relationship. The maximum elastic dynamic displacement is 0.54 mm.

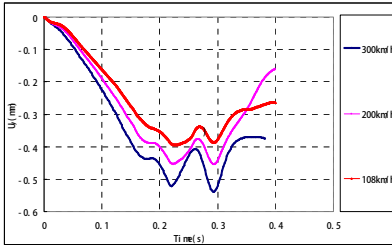


Figure 5. Displacement at Node A.

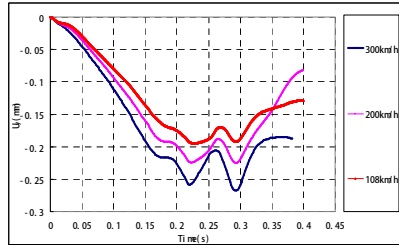


Figure 6. Displacement at Node B.

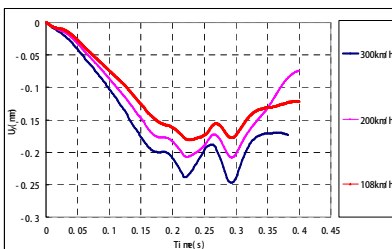


Figure 7. Displacement at Node C.

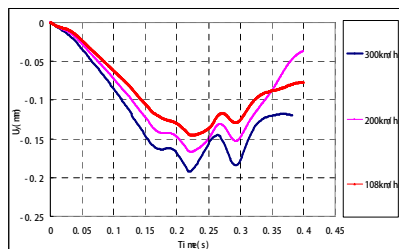


Figure 8. Displacement at Node D.

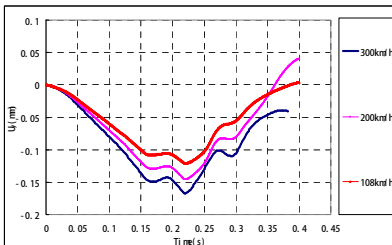


Figure 9. Displacement at Node E.

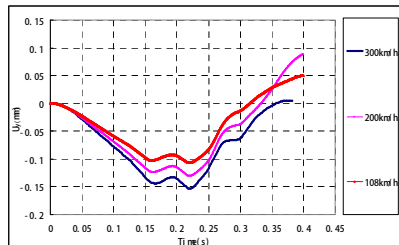


Figure 10. Displacement at Node F.

Vibration velocity and acceleration. The results are shown in Figures 11 through 22, where V_y and A_y are the vertical components of velocity and acceleration. These figures indicate that the vibration velocity and acceleration caused by a moving sinusoidal load do not respond immediately, rather it lags somewhat. This is because the system is nonlinear and contains damping.

Different nodes respond similarly in vibration velocity and acceleration under different moving speeds. The vibration velocity and acceleration gradually reduce as the distance to the loading surface increases. The computed maximum and minimum vibration velocities are 3.3 mm/s and 0.72 mm/s, which are much smaller than the allowable value 30-40 mm/s for a predominant frequency less than 30 Hz (Xue et al. 2010). Therefore, the roadbed of high-speed rail will not be adversely affected. The

computed maximum and minimum vibration accelerations are 3.1 m/s^2 and 0.72 m/s^2 .

In the same location, the vibration velocity and acceleration increase with moving speed's increase. The velocity and acceleration increments when the moving speed increases from 200 km/h to 300 km/h are significantly greater than those when the moving speed increases from 108 km/h to 200 km/h, indicating the system's stronger dynamic response.

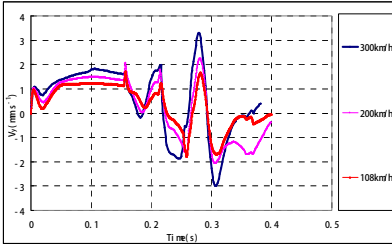


Figure 11. Velocity at Node A.

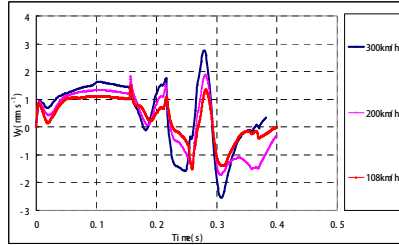


Figure 12. Velocity at Node B.

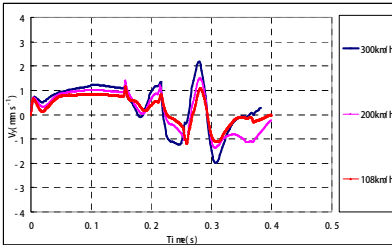


Figure 13. Velocity at Node C.

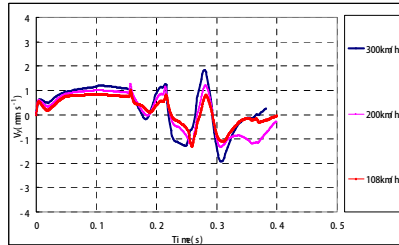


Figure 14. Velocity at Node D.

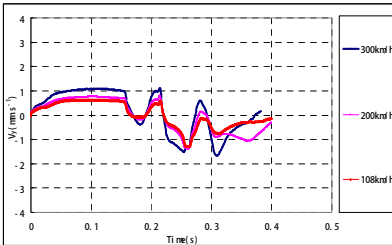


Figure 15. Velocity at Node E.

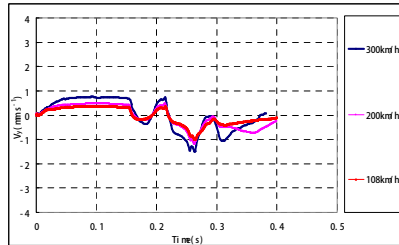


Figure 16. Velocity at Node F.

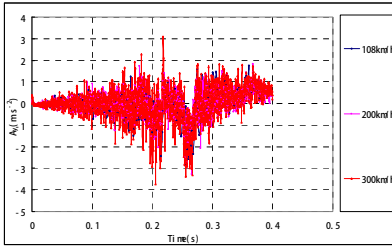


Figure 17. Acceleration at Node A.

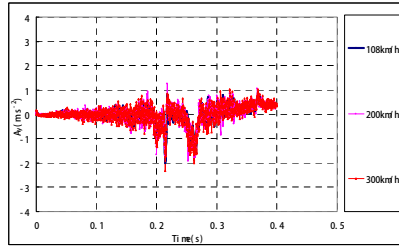


Figure 18. Acceleration at Node B.

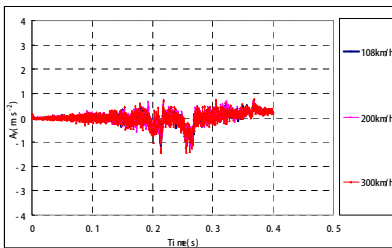


Figure 19. Acceleration at Node C.

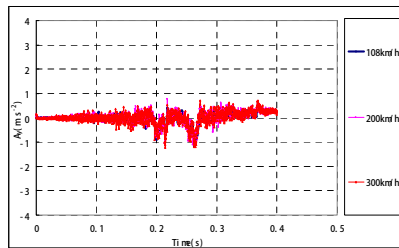


Figure 20. Acceleration at Node D.

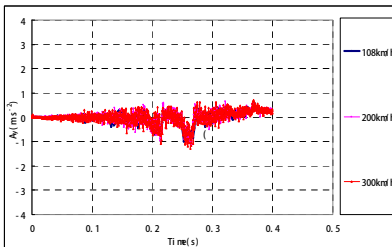


Figure 21. Acceleration at Node E.

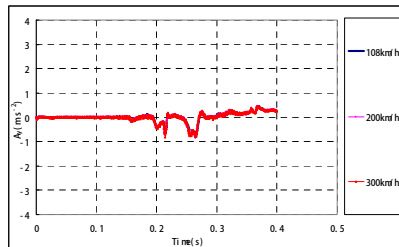


Figure 22. Acceleration at Node F.

CONCLUSIONS

Based on the FE analysis results, the following conclusions are drawn:

1. The vibration displacement, velocity and acceleration respond similarly under loading with different moving speeds.
2. The deformation caused by the moving load is elastic and no cumulative plastic deformation occurs.
3. Under the selected moving load, the system's vibration velocity and acceleration are low, thus the response meets the specifications for a normal working condition.

REFERENCES

- Cai, Y.-Q., Sun, H.-L., and Xu, C.-J. (2008). "Three-dimensional analyses of dynamic responses of track-ground system subjected to a moving train load." *Computers and Structures*, 86, 816–824.
- Xue, F.-C. (2010). Studies on dynamic characteristics of water-rich loess tunnel's foundation base, Southwest Jiaotong University, Chengdu (in Chinese).
- Xue, F.-C. et al. (2010). "Testing on vibration characteristics of a water-rich loess tunnel in a passenger-dedicated line." *J. Vibration and Shock*, 29(2), 202-207 (in Chinese).

Author Index

- Ahn, Yong Han, 573
Au, Vincent, 130
- Bai, Fanyi, 531
Bai, Yong, 146, 363, 386
Ban, Xiaojing, 323
Bencherif, H., 315
Boubakour, F., 315
- Cao, Lei, 531
Chang, C. W., 176
Chang, Luh-Mann, 615
Chang, S. K. Jason, 234
Chen, Chenghui, 217
Chen, Feng, 299
Chen, G. P., 168
Chen, H. H., 176
Chen, Hongyun, 1, 331
Chen, Hsueh-Heng, 379
Chen, L. L., 557
Chen, Qi, 661
Chen, Reh-Lin N., 9
Chen, S. Y., 176
Chen, Xia, 226
Chen, Xiaohu, 490
Chen, Yu-Tzu, 615
Cheng, Feifei, 363
Cheng, Huan, 411
Cheng, Yan, 540
Cheung, William, 110
Chien, Shen-Wen, 394
Chung, C. L., 355
Cong, Cong, 217
Cooke, Keith R., 9
- Duan, Li-ren, 68
- Fabregas, Aldo, 1, 331, 340
Fan, Gang, 631
Feng, Wang Ji, 248
Feng, Xiao, 671
- Gao, Jianjie, 226
Gao, Xingzhong, 55
Geng, Rui, 16
Gong, Bao-jun, 38
Gong, Gui-xiang, 154
Gonzalez-Velez, Enrique, 340
Guan, Jinping, 29
Guo, W., 463
- Hajji, Apif, 138
Hsu, Jiun-Jia, 209
Hu, Wenjun, 184
Hu, Y. C., 168, 176
Huang, Dan, 226
Huang, T. C., 548
Huang, Wei, 671
Huang, Yilei, 386
Huang, Zhiyi, 631
- Jeng, J. Y., 355
Jiang, C. L., 557
Jiang, Ling, 193
Jiang, Shan, 22
Jiang, Yi, 85
- Ker, H. W., 548
Kong, G. Q., 623
Kourtellis, Achilleas, 371
Kuo, P.-H., 282
- Lai, Yaping, 490
Lan, Jian, 514
- Lee, Chanyoung, 371
Lee, June-Shian, 355
Lee, Y. H., 548
Lee, Z. Y., 355
Levine, Carol R., 9
Lewis, Phil, 138
Li, Carmen, 268
Li, Chengxue, 437
Li, Chia-Nung, 160
Li, Dennis Y. N., 422
Li, Shuo, 85
Li, Xue, 348
Li, Yi, 348
Li, Yingfeng, 290
Li, Yue, 363
Li, Yumei, 566
Liang, C., 47
Lin, K., 548
Lin, Pei-Sung, 1, 331, 340, 371
Lin, Tsung-Chin, 379
Lin, W. T., 168
Liu, An-shuang, 522
Liu, Chunxiao, 290
Liu, Cui-lian, 38
Liu, Guoxiang, 522
Liu, Jian-mei, 38
Liu, Jinyuan, 643
Liu, Qiang, 651, 661
Liu, Wei, 226
Liu, Weiming, 22
Liu, Xiaofei, 490
Liu, Zhao, 480
Lou, Liangwei, 540
Lu, Bai-chuan, 348
Lu, Ying-Chih, 119, 234
Lung, Francis, 499
Luo, Jia-an, 154
Luo, Ying, 257

- Ma, Jian-Lin, 685
 Mao, Li-zeng, 68
 Meng, Jie, 480

 Nan, Jin, 60
 Neff, Rita, 146
 Nie, Chun-Xiao, 651, 661

 Ou, Yang-fei, 154

 Ping, W. Virgil, 582, 590, 598

 Qian, Z. D., 557
 Qiao, F., 282

 Ruegg, Steven, 307

 Schonfeld, Paul, 257
 Shen, L. David, 201, 209
 Sheng, Biqing, 582, 590
 Shi, Jing, 101
 Shi, Ling, 22
 Song, Haiyun, 531
 Song, Lijing, 299
 Song, Yunxiang, 566
 Su, Jau-Lang, 394
 Sun, Chuanjiao, 323
 Sun, Mingzheng, 299

 Teng, Min-Cheng, 394
 Thompson, Russell, 573
 Tveit, Per, 472

 Udemezue, Uche, 9

 Wang, G., 454
 Wang, George, 573, 607

 Wang, Houyu, 437
 Wang, N., 47
 Wang, Yuhong, 573
 Wei, X., 454
 Wei, Youpo, 566
 Wen, P. C., 176
 Wu, Jian-lin, 403
 Wu, Zhaozhang, 101

 Xian, Kai, 299
 Xiang, Zhongfu, 507
 Xiao, Yuan, 598
 Xu, Gancheng, 437
 Xu, Jinghua, 307
 Xu, Yongneng, 217
 Xue, Fu-Chun, 685

 Yan, Fu, 274
 Yan, Liping, 685
 Yang, Changwei, 631, 651, 661
 Yang, Guanghuai, 671
 Yang, Sai-ni, 403
 Yang, X. K., 411
 Yang, Y. W., 168
 Ye, Jia-yuan, 403
 Yeh, Chao-Fu, 119
 Yi, Zhenyu, 428
 Yim, William F., 77
 Yin, Delan, 490, 522
 Yu, L., 282
 Yu, Ming, 234
 Yu, Shijun, 193
 Yu, Tiao-lan, 38
 Yu, Yang, 507
 Yu, Z., 463

 Zhang, Baowei, 531
 Zhang, Cheng, 631
 Zhang, H. S., 463
 Zhang, Hongzhi, 446
 Zhang, Jiandong, 480
 Zhang, Jianjing, 631, 651

 Zhang, Jian-Min, 685
 Zhang, Jie, 323
 Zhang, Jun-hong, 154
 Zhang, Xue-chi, 403
 Zhao, Guangyuan, 85
 Zhao, Hongbin, 248
 Zhong, Xinhua, 540
 Zhou, Jianting, 671
 Zhou, Nian, 101
 Zhou, Xizhao, 184
 Zhu, Changhua, 540
 Zhu, Hong-ge, 68
 Zhu, Yandong, 193
 Zou, Xin, 248

Subject Index

- Air transportation, 77
- Airports, 77, 201, 209
- Algeria, 315
- Anchor plate, 643
- Asphalt, 557, 566, 598

- Bicycles, 9
- Bridge design, 446, 463, 472, 490, 507, 514
- Bridges, 446, 463, 472, 490, 507, 514, 522
- Buses, 168, 176, 217, 234, 299, 371

- Carpools, 355
- China, 16, 101, 130, 234, 268
- Computer software, 85
- Concrete, 598, 615, 623
- Construction equipment, 138
- Cracking, 566

- Damage, 480
- Data analysis, 290, 480, 548
- Delay time, 1

- Emissions, 138, 146, 160, 168, 176, 184
- Environmental issues, 38, 138, 146, 160, 531
- Evacuation, 403

- Freight transportation, 146
- Fuel consumption, 138, 168

- Geographic information systems, 290
- Geotechnical design, 623, 631, 643, 651, 661, 671, 685

- High-speed rail service, 193, 248, 268, 463
- Highways, 1, 85, 307, 363, 386, 394, 403, 446, 480, 522, 573, 590, 607, 671
- Human factors, 29, 379

- Infrastructure, 22
- Intelligent systems, 274, 282, 290, 299, 307, 315
- Intermodal transportation, 201
- Intersections, 282, 348

- Models, 160, 176, 184, 193, 217, 257, 379, 411, 428, 454, 548, 582, 661

- Natural disasters, 394, 403, 411, 480
- Noise, 607

- Optimization, 68, 193

- Parking, 130, 217
- Passengers, 248
- Pavement, 531, 540, 548, 557, 566, 573, 582, 590, 598, 607, 615, 623
- Pedestrians, 9, 282
- Performance characteristics, 257
- Planning, 9, 22, 55, 60, 119, 176, 226, 274, 411
- Ports, 38, 47
- Public transportation, 60, 119, 209, 217, 234, 299, 371, 422

- Rail construction, 540
- Rail transportation, 68, 193, 201, 248, 268, 422, 437, 463, 490, 499, 522, 540, 685
- Risk evaluation, 428
- Road construction, 363, 386, 531, 573, 615
- Routes, 355, 403

Seismic design, 631, 651, 661, 671, 685
Signage, 386
Simulation, 631
Soil compaction, 582, 590, 623
Spacing, 379
Subgrades, 582, 685
Subsidence, 454
Subway systems, 299, 437, 499
Sustainable development, 1, 9, 16, 22, 29, 38, 47, 55, 60, 68, 77, 85, 101, 110, 119, 130, 274

Taxis, 257, 315
Tolls, 307
Traffic accidents, 110, 323, 371
Traffic congestion, 55, 68, 307
Traffic flow, 226, 340, 379
Traffic management, 1, 323, 331, 340, 348, 355

Traffic safety, 110, 282, 371
Traffic signals, 331, 340, 348
Traffic speed, 226, 323
Traffic volume, 331
Transportation infrastructure, 394
Transportation management, 422
Transportation networks, 101, 184, 209
Travel time, 193
Trucks, 363
Tunnels, 110, 428, 437, 454, 499

Urban areas, 29, 47, 60, 119, 130, 160, 234, 315, 348
Urban development, 274

Vehicles, 323

Water transportation, 154
Waterproofing, 499